frontiers
RESEARCH TOPICS

RESTING STATE BRAIN ACTIVITY: IMPLICATIONS FOR SYSTEMS NEUROSCIENCE

Hosted by
Vinod Menon and Lucina Q. Uddin

frontiers in
SYSTEMS NEUROSCIENCE

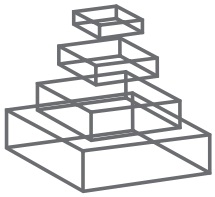

frontiers

Cover image provided by Ibbl sarl, Lausanne CH

ISSN 1664-8714
ISBN 978-2-88919-041-6
DOI 10.3389/978-2-88919-041-6

ABOUT FRONTIERS

Frontiers is more than just an open-access publisher of scholarly articles: it is a pioneering approach to the world of academia, radically improving the way scholarly research is managed. The grand vision of Frontiers is a world where all people have an equal opportunity to seek, share and generate knowledge. Frontiers provides immediate and permanent online open access to all its publications, but this alone is not enough to realize our grand goals.

FRONTIERS JOURNAL SERIES

The Frontiers Journal Series is a multi-tier and interdisciplinary set of open-access, online journals, promising a paradigm shift from the current review, selection and dissemination processes in academic publishing.
All Frontiers journals are driven by researchers for researchers; therefore, they constitute a service to the scholarly community. At the same time, the Frontiers Journal Series operates on a revolutionary invention, the tiered publishing system, initially addressing specific communities of scholars, and gradually climbing up to broader public understanding, thus serving the interests of the lay society, too.

DEDICATION TO QUALITY

Each Frontiers article is a landmark of the highest quality, thanks to genuinely collaborative interactions between authors and review editors, who include some of the world's best academicians. Research must be certified by peers before entering a stream of knowledge that may eventually reach the public - and shape society; therefore, Frontiers only applies the most rigorous and unbiased reviews.
Frontiers revolutionizes research publishing by freely delivering the most outstanding research, evaluated with no bias from both the academic and social point of view.
By applying the most advanced information technologies, Frontiers is catapulting scholarly publishing into a new generation.

WHAT ARE FRONTIERS RESEARCH TOPICS?

Frontiers Research Topics are very popular trademarks of the Frontiers Journals Series: they are collections of at least ten articles, all centered on a particular subject. With their unique mix of varied contributions from Original Research to Review Articles, Frontiers Research Topics unify the most influential researchers, the latest key findings and historical advances in a hot research area!
Find out more on how to host your own Frontiers Research Topic or contribute to one as an author by contacting the Frontiers Editorial Office: researchtopics@frontiersin.org

RESTING STATE BRAIN ACTIVITY: IMPLICATIONS FOR SYSTEMS NEUROSCIENCE

Hosted By
Vinod Menon, Stanford University, USA
Lucina Q. Uddin, Stanford University, USA

Research on resting state brain activity using fMRI offers a novel approach for understanding brain organization at the systems level. Resting state fMRI examines spatial synchronization of intrinsic fluctuations in blood-oxygenation-level-dependent (BOLD) signals arising from neuronal and synaptic activity that is present in the absence of overt cognitive information processing. Since the discovery of coherent spontaneous fluctuations within the somatomotor system (Biswal, et al. 1995), a growing number of studies have shown that many of the brain areas engaged during various cognitive tasks also form coherent large-scale brain networks that can be readily identified using resting state fMRI. These studies are beginning to provide new insights into the functional architecture of the human brain. This Research Topic will synthesize current knowledge about resting state brain activity and discuss their implications for understanding brain function and dysfunction from a systems neuroscience perspective. This topic will also provide perspectives on important conceptual and methodological questions that the field needs to address in the next years. In addition to invited reviews and perspectives, we solicit research articles on theoretical, experimental and clinical questions related to the nature, origins and functions of resting state brain activity.

Table of Contents

05 ***Introduction to Special Topic – Resting-State Brain Activity: Implications for Systems Neuroscience***
Lucina Q. Uddin and Vinod Menon

07 ***Identifying basal ganglia divisions in individuals using resting-state functional connectivity MRI***
Kelly A Barnes, Alexander L Cohen, Jonathan D Power, Steven M Nelson, Yannic B L Dosenbach, Francis M Miezin, Steven E Petersen and Bradley L Schlaggar

17 ***Resting-state functional connectivity differences in premature children***
Eswar Damaraju, John Phillips, Jean R Lowe, Robin Ohls, Vince D Calhoun and Arvind Caprihan

30 ***Maturing thalamocortical functional connectivity across development***
Damien Fair, Deepti Bathula, Kathryn L Mills, Taciana G Costa Dias, Michael S Blythe, Dongyang Zhang, Abraham Z Snyder, Marcus E Raichle, Alex A Stevens, Joel T Nigg and Bonnie J Nagel

40 ***Network scaling effects in graph analytic studies of human resting-state fMRI data***
Alex Fornito, Andrew Zalesky and Edward T Bullmore

56 ***Glutamatergic and Resting-State Functional Connectivity Correlates of Severity in Major Depression – The Role of Pregenual Anterior Cingulate Cortex and Anterior Insula***
Dorothea I. Horn, Chunshui Yu, Johann Steiner, Julia Buchmann, Joern Kaufmann, Annemarie Osoba, Ulf Eckert, Kathrin C. Zierhut, KoljaSchiltz, Huiguang He, Bharat Biswal, Bernhard Bogerts and Martin Walter

66 ***Adolescent Resting State Networks and Their Associations with Schizotypal Trait Expression***
Annalaura Lagioia, Dimitri Van De Ville, Martin Debbané, François Lazeyras and Stephan Eliez

78 ***Functional implications of age differences in motor system connectivity***
Jeanne Langan, Scott Peltier, Jin Bo, Brett W Fling, Robert C Welsh and Rachael D Seidler

89. ***Age-Related Differences in Functional Nodes of the Brain Cortex – A High Model Order Group ICA Study***
Harri Littow, Ahmed Abou Elseoud, Marianne Haapea, MattiIsohanni, Irma Moilanen, Katariina Mankinen, Juha Nikkinen, Jukka Rahko, Heikki Rantala, Jukka Remes, Tuomo Starck, Osmo Tervonen, Juha Veijola, Christian Beckmann and Vesa J. Kiviniemi

100 ***Distinct Superficial and Deep Laminar Domains of Activity in the Visual Cortex During Rest and Stimulation***
Alexander Maier, Geoffrey K. Adams, Christopher Aura and David A. Leopold

111 ***Advances and pitfalls in the analysis and interpretation of resting-state FMRI data***
David M Cole, Stephen M Smith and Christian F Beckmann

126 ***Clinical applications of resting state functional connectivity***
Michael D Fox and Michael Greicius

139 ***The relation of ongoing brain activity, evoked neural responses, and cognition***
Sepideh Sadaghiani, Guido Hesselmann, Karl J Friston and Andreas Kleinschmidt

153 ***Typical and atypical development of functional human brain networks: insights from resting-state fMRI***
Lucina Q Uddin, Kaustubh Supekar and Vinod Menon

165 ***Graph-based network analysis of resting-state functional MRI***
Jinhui Wang, Xinian Zuo and Yong He

179 ***A Novel Model-Free Data Analysis Technique Based on Clustering in a Mutual Information Space: Application to Resting-State fMRI***
Simon Benjaminsson, Peter Fransson and Anders Lansner

187 ***Using coherence to measure regional homogeneity of resting-state fMRI signal***
Dongqiang Liu, Chaogan Yan, Juejing Ren, Li Yao, Vesa J Kiviniemi and Yufeng Zang

196 ***DPARSF: a MATLAB toolbox for "pipeline" data analysis of resting-state fMRI***
Chaogan Yan and Yufeng Zang

203 ***Exploring the electrophysiological correlates of the default-mode network with intracerebral EEG***
Karim Jerbi, Juan R Vidal, Tomas Ossandon, Sarang S Dalal, Julien Jung, Dominique Hoffmann, Lorella Minotti, Olivier Bertrand, Philippe Kahane and Jean-Philippe Lachaux

frontiers in
SYSTEMS NEUROSCIENCE

EDITORIAL
published: 11 August 2010
doi: 10.3389/fnsys.2010.00037

Introduction to special topic – Resting-state brain activity: implications for systems neuroscience

Lucina Q. Uddin[1,2]* and Vinod Menon[1,2,3]**

[1] *Department of Psychiatry and Behavioral Sciences, Stanford University School of Medicine, Stanford, CA, USA*
[2] *Program in Neuroscience, Stanford University School of Medicine, Stanford, CA, USA*
[3] *Department of Neurology and Neurological Sciences, Stanford University School of Medicine, Stanford, CA, USA*
*Correspondence: *lucina@stanford.edu; **menon@stanford.edu*

Research on resting-state brain activity using fMRI offers a novel approach for understanding brain organization at the systems level. Resting-state fMRI (rsfMRI) examines spatial synchronization of intrinsic fluctuations in blood oxygenation level dependent (BOLD) signals arising from neuronal and synaptic activity that is present in the absence of overt cognitive information processing. Since the discovery of coherent spontaneous fluctuations within the somatomotor system (Biswal et al., 1995), a growing number of studies have shown that many of the brain areas engaged during various cognitive tasks also form coherent large-scale brain networks that can be readily identified using rsfMRI (Smith et al., 2009). These studies are beginning to provide new insights into the functional architecture of the human brain. This special topic synthesizes current knowledge about resting-state brain activity and discusses implications for understanding brain function and dysfunction from a systems neuroscience perspective. Reviews written by experts in the field provide perspectives on important conceptual, methodological, and empirical questions that need to be addressed in the next years. Additionally, this collection includes original research articles addressing questions related to the nature, origins, and functions of resting-state brain activity.

The low cognitive demand and relatively short duration of rsfMRI scans make them well suited for studying pediatric and clinical populations with low tolerance for the MRI scanner environment. The review by Uddin et al. (2010) summarizes rsfMRI studies to date in children and adolescents, and describes new insights that have emerged about the typical and atypical development of functional brain networks, a topic also examined in an empirical study by Littow et al. (2010). The review by Fox and Greicius (2010) highlights advantages of examining the resting-state signal for clinical applications and discusses methodological issues that need to be resolved to facilitate translational applications of rsfMRI. A number of important clinical applications are already emerging as emphasized by the studies of functional connectivity in premature children (Damaraju et al., 2010), adolescents with schizotypal traits (Lagioia et al., 2010), major depression (Horn et al., 2010), and aging (Langan et al., 2010). Furthermore, rsfMRI studies in healthy individuals are continuing to provide new insights into cortical and subcortical functional networks and their interconnections with a high degree of specificity, as demonstrated by Barnes et al. (2010) in the basal ganglia and Fair et al. (2010) in the thalamus.

As the neuroimaging field begins to incorporate rsfMRI into its arsenal of tools, increasingly sophisticated methods are being developed to maximize its potential contribution to systems neuroscience. Cole et al. (2010) provide a timely review of current methods and describe their strengths and limitations with respect to analysis and interpretation of rsfMRI data. A number of papers describe new tools and methods that are being developed in the field, as described in the studies by Chao-Gan and Yu-Feng (2010) (Benjaminsson et al., 2010; Liu et al., 2010). Graph theoretical analyses offer insights into brain networks at a global level, as discussed by Fornito et al. (2010) and reviewed by Wang et al. (2010). These methodological and technical advances have paved the way for increasingly sophisticated insights into the topology of human brain networks.

RsfMRI studies would, of course, not be meaningful if they did not have an underlying neurophysiological correlate. The review by Jerbi et al. (2010) emphasizes the links between rsfMRI connectivity and inter-areal synchronization observed with intracranial EEG, and they describe how intracranial EEG studies can provide insights into transient neural processes underlying task-induced deactivation. Maier et al. (2010) take this a step further and describe original research on the laminar pattern of spontaneous activity in primate visual cortex. Their demonstration that functional compartmentalization in superficial and deep layers found during rest, was also preserved when a neuron's receptive field was stimulated during a visual task, suggests that even at this level of brain organization, resting-state activity imposes massive constraints on stimulus processing. Sadaghiani et al. (2010) provide both a theoretical and an experimental perspective on how intrinsic brain activity influences task-evoked activity and perceptual response variability. Clearly, more work is needed to better understand the relationship between resting-state and task-evoked activity. This set of articles suggests that both theoretical and neurophysiological approaches have much to offer in this regard.

The reviews and empirical articles presented in this special topic reveal a complex and rapidly unfolding profile of how the human and primate brain are intrinsically organized. Advances in the field, both methodological and conceptual, will have profound implications for understanding human brain function from a systems neuroscience perspective.

REFERENCES

Barnes, K. A., Cohen, A. L., Power, J. D., Nelson, S. M., Dosenbach, Y. B. L., Miezin, F. M., Petersen, S. E., and Sehlaggar, B. L. (2010). Identifying basal ganglia divisions in individuals using resting state functional connectivity MRI. *Front. Syst. Neurosci.* 4:18. doi:10.3389/fnsys.2010.00018.

Benjaminsson, S., Fransson, P., and Lansner, A. (2010). A novel model-free data analysis technique based on clustering in a mutual information space: application to resting-state fMRI. *Front. Syst. Neurosci.* 4:34. doi:10.3389/fnsys.2010.00034.

Biswal, B., Yetkin, F. Z., Haughton, V. M., and Hyde, J. S. (1995). Functional connectivity in the motor cortex of resting human brain using echo-planar MRI. *Magn. Reson. Med.* 34, 537–541.

Chao-Gan, Y., and Yu-Feng, Z. (2010). DPARSF: a MATLAB toolbox for "pipeline" data analysis of resting-state fMRI. *Front. Syst. Neurosci.* 4:13. doi:10.3389/fnsys.2010.00013.

Cole, D. M., Smith, S. M., and Beckmann, C. F. (2010). Advances and pitfalls in the analysis and interpretation of resting-state FMRI data. *Front. Syst. Neurosci.* 4:8. doi:10.3389/fnsys.2010.00008.

Damaraju, E., Phillips, J., Lowe, J. R., Ohls, R., Calhoun, V. D., and Caprihan, A. (2010). Resting-state functional connectivity differences in premature children. *Front. Syst. Neurosci.* 4:23. doi:10.3389/fnsys.2010.00023.

Fair, D. A., Bathula, D., Mills, K. L., Costa Dias, T. G., Blythe, M. S., Zhang, D., Snyder, A. Z., Raichle, M. E., Stevens, A. A., Nigg, J. T., and Nagel, B. J. (2010). Maturing thalamocortical functional connectivity across development. Front. Syst. Neurosci. 4:10. doi:10.3389/fnsys.2010.00010.

Fornito, A., Zalesky, A., and Bullmore, E. T. (2010). Network scaling effects in graph analytic studies of human resting-state fMRI data. *Front. Syst. Neurosci.* 4:22. doi:10.3389/fnsys.2010.00022.

Fox, M. D., and Greicius, M. (2010). Clinical applications of resting state functional connectivity with functional magnetic resonance imaging (fMRI). *Front. Syst. Neurosci.* 4:19. doi:10.3389/fnsys.2010.00019.

Horn, D. I., Yu, C., Steiner, J., Buchmann, J., Kaufmann, J., Osoba, A., Eckert, U., Zierhut, K., Schiltz, K., He, H., Biswal, B., Bogerts, B., and Walter, M. (2010). Glutamatergic and resting state functional connectivity correlates of severity in major depression – the role of pregenual anterior cingulate cortex and anterior insula. *Front. Syst. Neurosci.* 4:33. doi:10.3389/fnsys.2010.00033.

Jerbi, K., Vidal, J. R., Ossandon, T., Dalal, S. S., Jung, J., Hoffmann, D., Minotti, L., Bertrand, O., Kahane, P., and Lachaux, J.-P. (2010). Exploring the electrophysiological correlates of the default-mode network with intracerebral EEG. *Front. Syst. Neurosci.* 4:27. doi:10.3389/fnsys.2010.00027.

Lagioia, A., Van De Ville, D., Debbané, M., Lazeyras, F., and Eliez, S. (2010). Adolescent resting state networks and their associations to schizotypal trait expression. Front. Syst. Neurosci. 4:35. doi: 10.3389/fnsys.2010.00035.

Langan, J., Peltier, S., Bo, J., Fling, B. W., Welsh, R. C., and Seidler, R. D. (2010). Functional implications of age differences in motor system connectivity. *Front. Syst. Neurosci.* 4:17. doi:10.3389/fnsys.2010.00017.

Littow, H., Elseoud, A. A., Haapea, M., Isohanni, M., Moilanen, I., Mankinen, K., Nikkinen, J., Rahko, J., Rantala, H., Remes, J., Starck, T., Tervonen, O., Veijola, J., Beckmann, C., and Kiviniemi, V. J. (2010). Age-related differences in functional nodes of the brain cortex – a high model order group ICA study. *Front. Syst. Neurosci.* 4:32. doi:10.3389/fnsys.2010.00032.

Liu, D., Chao-Gan, Y., Ren, J., Yao, L., Kiviniemi, V. J., and Yu-Feng, Z. (2010). Using coherence to measure regional homogeneity of resting-state fMRI signal. *Front. Syst. Neurosci.* 4:24. doi:10.3389/fnsys.2010.00024.

Maier, A., Adams, G. K., Aura, C., and Leopold, D. A. (2010). Distinct laminar domains of activity in the visual cortex during rest and stimulation. *Front. Syst. Neurosci.* 4:31. doi:10.3389/fnsys.2010.00031.

Sadaghiani, S., Hesselmann, G., Friston, K. J., and Kleinschmidt, A. (2010). The relation of ongoing brain activity, evoked neural responses, and cognition. *Front. Syst. Neurosci.* 4:20. doi:10.3389/fnsys.2010.00020.

Smith, S. M., Fox, P. T., Miller, K. L., Glahn, D. C., Fox, P. M., Mackay, C. E., Filippini, N., Watkins, K. E., Toro, R., Laird, A. R., and Beckmann, C. F. (2009). Correspondence of the brain's functional architecture during activation and rest. *Proc. Natl. Acad. Sci. U.S.A.* 106, 13040–13045.

Uddin, L. Q., Supekar, K., and Menon, V. (2010). Typical and atypical development of functional human brain networks: insights from resting-state fMRI. *Front. Syst. Neurosci.* 4:21. doi:10.3389/fnsys.2010.00021.

Wang, J., Zuo, X., and He, Y. (2010). Graph-based network analysis of resting-state functional MRI. *Front. Syst. Neurosci.* 4:16. doi:10.3389/fnsys.2010.00016.

Conflict of Interest Statement: The authors declare that the research was conducted in the absence of any commercial or financial relationships that could be construed as a potential conflict of interest.

Received: 27 June 2010; accepted: 05 July 2010; published online: 11 August 2010.
*Citation: Uddin LQ and Menon V (2010) Introduction to special topic–resting-state brain activity: implications for systems neuroscience. Front. Syst. Neurosci. **4**:37. doi: 10.3389/fnsys.2010.00037*

frontiers in
SYSTEMS NEUROSCIENCE

ORIGINAL RESEARCH ARTICLE
published: 10 June 2010
doi: 10.3389/fnsys.2010.00018

Identifying basal ganglia divisions in individuals using resting-state functional connectivity MRI

Kelly Anne Barnes[1]*, Alexander L. Cohen[1], Jonathan D. Power[1], Steven M. Nelson[1], Yannic B. L. Dosenbach[1], Francis M. Miezin[1,2], Steven E. Petersen[1,2,3,4] and Bradley L. Schlaggar[1,2,3,5]

[1] *Department of Neurology, Washington University School of Medicine, St. Louis, MO, USA*
[2] *Department of Radiology, Washington University School of Medicine, St. Louis, MO, USA*
[3] *Department of Psychology, Washington University School of Medicine, St. Louis, MO, USA*
[4] *Department of Anatomy and Neurobiology, Washington University School of Medicine, St. Louis, MO, USA*
[5] *Department of Pediatrics, Washington University School of Medicine, St. Louis, MO, USA*

Edited by:
Lucina Q. Uddin,
Stanford University, USA

Reviewed by:
Adriana Di Martino,
New York University Langone Medical Center, USA
Bogdan Draganski,
University College London, UK

***Correspondence:**
Kelly Anne Barnes,
Department of Neurology, Washington University School of Medicine, 4525 Scott Avenue, Room 2220, St. Louis, MO 63110, USA.
e-mail: barnesk@npg.wustl.edu

Studies in non-human primates and humans reveal that discrete regions (henceforth, "divisions") in the basal ganglia are intricately interconnected with regions in the cerebral cortex. However, divisions within basal ganglia nuclei (e.g., within the caudate) are difficult to identify using structural MRI. Resting-state functional connectivity MRI (rs-fcMRI) can be used to identify putative cerebral cortical functional areas in humans (Cohen et al., 2008). Here, we determine whether rs-fcMRI can be used to identify divisions in individual human adult basal ganglia. Putative basal ganglia divisions were generated by assigning basal ganglia voxels to groups based on the similarity of whole-brain functional connectivity correlation maps using modularity optimization, a network analysis tool. We assessed the validity of this approach by examining the spatial contiguity and location of putative divisions and whether divisions' correlation maps were consistent with previously reported patterns of anatomical and functional connectivity. Spatially constrained divisions consistent with the dorsal caudate, ventral striatum, and dorsal caudal putamen could be identified in each subject. Further, correlation maps associated with putative divisions were consistent with their presumed connectivity. These findings suggest that, as in the cerebral cortex, subcortical divisions can be identified in individuals using rs-fcMRI. Developing and validating these methods should improve the study of brain structure and function, both typical and atypical, by allowing for more precise comparison across individuals.

Keywords: striatum, functional connectivity, graph theory, cortico-basal ganglia loops, connectome

INTRODUCTION

The basal ganglia are subcortical brain structures important for motor, cognitive, and emotional processing (Mink, 1996). The consequences of basal ganglia pathology can be devastating, exemplified by the symptoms of degenerative basal ganglia disorders such as Parkinson's and Huntington's disease. Understanding the location and functional connectivity patterns of basal ganglia divisions would improve cognitive neuroscience investigations. Indeed, methods that could identify putative basal ganglia divisions are needed to test hypotheses about cortical-basal ganglia circuitry in typical development (Rubia et al., 2006), healthy aging (Hedden and Gabrieli, 2004), and disorders (e.g., Parkinson's disease, Huntington's disease, Tourette's syndrome) and are critical for region identification needed to develop more precise models of whole-brain connectivity (Butts, 2009).

There are multiple levels of organization in the basal ganglia. Anatomically, the basal ganglia comprise five gray matter nuclei: the caudate, putamen, globus pallidus, substantia nigra, and subthalamic nucleus. The majority of projections from the cerebral cortex to the basal ganglia terminate in the caudate and putamen, collectively referred to as the striatum. Discrete cerebral cortical regions project to discrete striatal regions that then project, via the thalamus, back to those cortical regions (Alexander et al., 1986). Within the striatum are compartments, termed patches and matrices, that have distinct neurochemical markers and receive projections from different cortical layers (Gerfen, 1989; Graybiel, 1990). Beyond basal ganglia nuclei that can be seen on structural MRI scans, more fine-grained divisions in human basal ganglia, though presumed to exist based on non-human primate and rodent studies, are difficult to identify with current neuroimaging methods.

While historically considered to be a motor structure, the basal ganglia receive cortical projections from all lobes of the cerebral cortex and contribute to both motor and non-motor processing (Mink, 1996). Anatomical tracer studies in non-human primates (Alexander et al., 1986; Middleton and Strick, 2000; Haber, 2003) have documented anatomical connections between the basal ganglia and many regions in the cerebral cortex, including lateral prefrontal, orbitofrontal, anterior cingulate, lateral parietal, motor, premotor, oculomotor, somatosensory, auditory association (superior temporal gyrus), and visual association (inferior temporal gyrus) cortex.

Resting-state functional connectivity MRI (rs-fcMRI) and diffusion tensor imaging (DTI) provide a means to assess functional and anatomical connectivity non-invasively in humans. It is important to note at the outset that these methods yield distinct information about brain connectivity. rs-fcMRI measures correlations in

low-frequency (i.e., <0.1 Hz) spontaneous blood oxygenation level-dependent (BOLD) signal fluctuations (Fox et al., 2005) and may reflect a history of co-activation between regions (Fair et al., 2007; Dosenbach et al., 2008). DTI measures the diffusion of water molecules, which is constrained by the presence of axons, particularly myelinated axons, and provides indices of white matter coherence used to create visualizations of white matter tracts. While there can be overlap in connectivity patterns identified using rs-fcMRI and DTI, functional connectivity has been documented in the absence of anatomical connectivity. For example, seeds placed in voxels corresponding to left and right retinotopic eccentric representations in primary visual cortex exhibit strong functional connectivity with rs-fcMRI, but are not anatomically connected (Vincent et al., 2007). This observation suggests that functional connectivity should not be treated as a measure simply homologous to anatomical connectivity.

Despite fundamental differences in the types of information about brain connectivity that can be gleaned from rs-fcMRI and DTI, these methods converge with evidence from anatomical tracer studies examining cortical-basal ganglia connectivity, revealing significant connectivity between basal ganglia regions and frontal, parietal, and temporal regions. Using rs-fcMRI, dorsal and ventral caudate and putamen regions of interest (ROIs) were shown to have different patterns of functional connectivity with the cerebral cortex (Di Martino et al., 2008; Harrison et al., 2009). Similarly, large-scale cortical ROIs (e.g., prefrontal cortex, parieto–occipital cortex) were shown to have different patterns of partial correlations with the basal ganglia (Zhang et al., 2008). DTI investigations have revealed different anatomical connectivity between basal ganglia divisions and large-scale frontal ROIs (e.g., prefrontal cortex, orbitomedial frontal cortex) (Lehericy et al., 2004; Leh et al., 2007; Draganski et al., 2008). Across these methods, convergent findings regarding patterns of cortical-basal ganglia connectivity have emerged. For example, both rs-fcMRI and DTI respectively reveal functional and anatomical connectivity between dorsal caudate and lateral prefrontal cortex, ventral striatum and orbitofrontal cortex, and dorsal caudal putamen and motor and premotor cortex (Lehericy et al., 2004; Leh et al., 2007; Di Martino et al., 2008; Draganski et al., 2008; Harrison et al., 2009).

Basal ganglia divisions have two properties that would facilitate identification with noninvasive neuroimaging methods: they have different patterns of connectivity with the cerebral cortex and they are spatially constrained (i.e., discrete) entities (Alexander et al., 1986). Thus, it may be possible to identify basal ganglia divisions smaller than nuclei on the basis of their unique patterns of cortical-basal ganglia functional connectivity using rs-fcMRI and community detection algorithms, which are used to identify groupings in networks. rs-fcMRI is sensitive to changes in patterns of functional connectivity across adjacent, proximal (i.e., ~2 cm apart) cortical regions. For example, rs-fcMRI data contained abrupt transitions, consistent with boundaries between putative cortical areas, in the measured similarity of functional connectivity maps generated from seeds placed along a line between supramarginal and angular gyrus regions (Cohen et al., 2008). Rather than simply measure along a single line, rs-fcMRI methods can also be used to sample from a larger structure (e.g., the basal ganglia). By calculating the similarity in whole-brain rs-fcMRI maps generated from each voxel in a structure, we can obtain a matrix of the pairwise similarity relationships between voxels. Similarity matrices can be used to bring recent developments in graph theory, the mathematical description of networks, to bear on our question of identifying divisions in the basal ganglia.

In graph theory parlance, a graph is composed of two elements: nodes, which represent the units of observation in a graph, and edges, which represent the pairwise relationships between nodes. We can thus view our similarity matrix as a network, with voxels as nodes and eta^2 values, a measure of similarity, as edges. Community detection algorithms (e.g., modularity optimization [Newman, 2006] used here) can be applied to cluster the nodes into highly interconnected communities, with relatively few edges between communities. In other words, these algorithms can be viewed as grouping voxels with similar correlation maps. Returning to our question of interest, these groupings can be examined to determine whether they reflect expected divisions within the basal ganglia. If (1) the anatomical loci of modularity optimization groupings is consistent with basal ganglia divisions identified from anatomical studies in non-human primates and rodents and (2) functional connectivity maps generated from the modularity optimization groupings are consistent with presumed patterns of cortical-basal ganglia connectivity, then we will consider these groupings to be putative basal ganglia divisions.

In this paper, we demonstrate that a novel approach to functional mapping that combines rs-fcMRI and modularity optimization analyses can reveal putative basal ganglia divisions in individuals. Our approach identifies putative basal ganglia divisions with reliable patterns of functional connectivity with an amount of data that can be acquired in a single, brief MRI session (i.e., one ~8-min structural scan and three ~5-min scans of relaxed fixation). Remarkably, these results appear to be robust at the individual subject-level.

MATERIALS AND METHODS

SUBJECTS

Two cohorts of healthy young adult subjects were recruited from the Washington University community. Subjects were screened with a self-report questionnaire to ensure that they had no current or previous history of neurological or psychiatric diagnosis. Informed consent was obtained from all subjects, and the study was approved by the Washington University Human Studies Committee. Cohort One consisted of 15 subjects (four males, ages 21–29 years, mean age = 25 years). Cohort Two consisted of 11 subjects (five males, ages 21–27 years, mean age = 25 years). The purpose of examining two cohorts was to test independently the reliability of the results (see Ihnen et al., 2009).

DATA ACQUISITION

Data were acquired on a Siemens 3 Tesla MAGNETOM Trio system (Erlangen, Germany) with a Siemens 12 channel Head Matrix Coil. To help stabilize head position, each subject was fitted with a thermoplastic mask fastened to holders on the head coil. Structural images were obtained using a sagittal magnetization-prepared rapid gradient echo (MP-RAGE) three-dimensional T1-weighted sequence (TE = 3.08 ms, TR (partition) = 2.4 s, TI = 1000 ms, flip angle = 8°, 176 slices with $1 \times 1 \times 1$ mm voxels). Functional images were obtained using a BOLD contrast sensitive gradient echo echo-planar sequence (TE = 27 ms, volume TR = 2.5 s, flip angle = 90°, in-plane resolution

4 × 4 mm). Whole-brain coverage was obtained with 32 contiguous interleaved 4-mm axial slices. Three runs of either 133 (Cohort One) or 132 (Cohort Two) BOLD volumes per run were acquired. Steady state magnetization was assumed after four frames (i.e., 10 s). An auto align pulse sequence protocol provided in the Siemens software was used to align the acquisition slices of the functional scans parallel to the anterior and posterior commissure (AC–PC) plane and centered on the brain. A T2 weighted turbo spin echo structural image (TE = 84 ms, TR = 6.8 s, 32 slices with 1 × 1 × 4 mm voxels) in the same anatomical plane as the BOLD images was also obtained to improve alignment to the atlas.

During functional scans, subjects viewed a centrally presented crosshair that subtended <1 visual degree and were instructed to relax and maintain fixation on the crosshair. The fixation cross was either white on a black background (Cohort One) or black on a white background (Cohort Two).

DATA PRE-PROCESSING

The analysis stream from the present study is depicted in **Figure 1A**. Functional images were first processed to reduce artifacts (Miezin et al., 2000). These steps included: (i) removal of a central spike caused by MR signal offset, (ii) correction of odd versus even slice intensity differences attributable to interleaved acquisition without gaps, (iii) correction for head movement within and across runs, and (iv) intensity normalization to a whole-brain mode value of 1000 for each run. Atlas transformation of the functional data was computed for each individual via the MP-RAGE and T2 weighted scans. Each run was then resampled in atlas space on an isotropic 2-mm grid combining movement correction and atlas transformation (12 parameter affine co-registration) in one interpolation (Lancaster et al., 1995; Snyder, 1996). All subsequent operations were performed on the atlas-transformed volumetric time series.

Several additional pre-processing steps were used to reduce spurious variance (e.g., heart rate and respiration) unlikely to reflect neuronal activation. These steps included: (i) temporal bandpass filtering (0.009 Hz < f < 0.08 Hz) and spatial smoothing (4 mm full width at half maximum), (ii) regression of six parameters obtained by rigid body head motion correction, (iii) regression of the whole-brain signal averaged over the whole brain, (iv) regression of ventricular signal averaged from ventricular ROIs, and (v) regression of white matter signal averaged from white matter ROIs. [Ventricular and white matter ROIs were defined using masks described in Fox et al. (2005) and depicted in Supplemental Figure 1 of Fox et al. (2009)]. Regression of first order derivative terms for the whole brain, ventricular, and white matter signals and any trend term from the movement regressors was also included in the pre-processing.

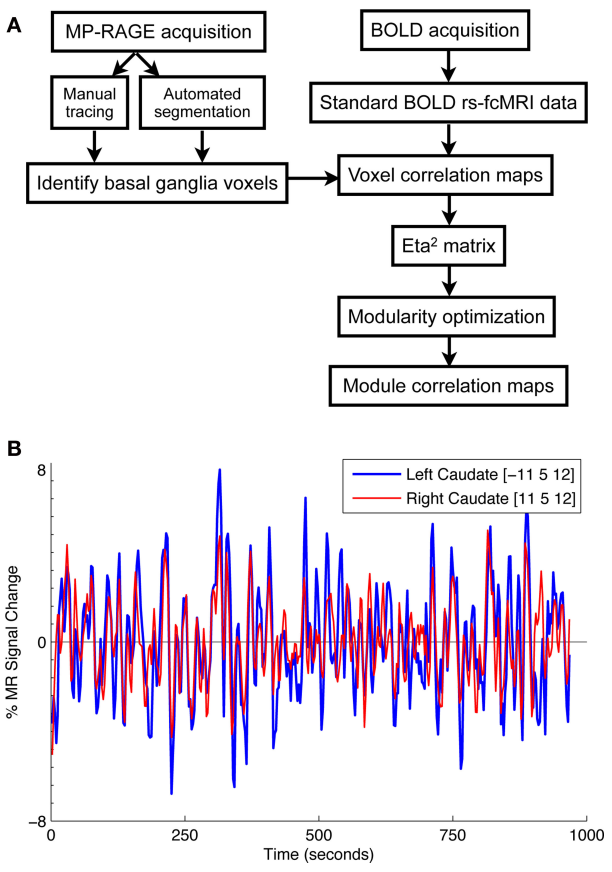

FIGURE 1 | (A) Flowchart of analysis stream. **(B)** Time courses extracted from two basal ganglia voxels ([–11 5 12] and [11 5 12]) are highly correlated (r = 0.70). Time courses such as these were used to generate whole-brain correlation maps for each basal ganglia voxel.

IDENTIFYING THE BASAL GANGLIA

Two methods were used to identify basal ganglia voxels in individual subjects. For Cohort One, the caudate, putamen, and pallidum were manually traced from each subject's MP-RAGE scan. For Cohort Two, the caudate, putamen, and pallidum were identified from each subject's MP-RAGE using FreeSurfer[1], an automated segmentation algorithm (Fischl et al., 2002, 2004). Automated segmentation results for each subject were reviewed as a quality control step. From this point forward, the methods applied to the two cohorts were identical. The purpose of examining two cohorts separately, rather than collapsing cohorts into a single group, was to test independently the reliability of the results.

rs-fcMRI AND MODULARITY OPTIMIZATION ANALYSIS

For each basal ganglia voxel, whole-brain rs-fcMRI correlation maps were generated by correlating each basal ganglia voxel's timecourse with all other voxels in the brain (see **Figure 1B** for example basal ganglia time courses). To quantify the similarity of the whole-brain rs-fcMRI correlation maps, a measure of similarity, eta^2, was computed between each pair of correlation maps for each hemisphere in each subject (see Cohen et al., 2008). Thus, for each hemisphere in each subject, we generated a similarity matrix that could be examined to identify basal ganglia voxels with similar patterns of functional connectivity.

Modularity optimization (Newman, 2006), a network analysis tool, was used to identify basal ganglia voxels with similar patterns of functional connectivity and then to assign voxels, based on their similar patterns of connectivity, to groups termed modules. In graph theory terms, each voxel in each subject's basal ganglia was treated as a node and the similarity (i.e., eta^2) between each

[1]http://surfer.nmr.mgh.harvard.edu.

pair of nodes was treated as an edge. Networks with N nodes were mathematically represented as a $N \times N$ matrix of relationships where cell ij contained the measure of the similarity between node i and node j. Similarity matrices were thresholded such that all cells with values below a certain threshold were set to zero, effectively removing the edges between the nodes. We therefore explored a range of thresholds in our analyses to ensure that our results were not specific to a particular threshold. Modules, our unit of analysis to test for putative divisions within the basal ganglia, were detected with modularity optimization algorithms adopted from Newman (2006) and described in Fair et al. (2009). The modularity (Q) of a given set of module assignments for a graph is a measure of the number of connections found within the assigned modules versus the number predicted in a random graph with equivalent degree distribution. A positive Q indicates that the number of intra-module connections exceeds those predicted statistically. A wide range of Q may be found for a graph, depending on how nodes are assigned to modules. Thus modularity optimization returns the set of node assignments that returns the highest Q, that is, the optimal modular description of the data.

RESULTS

COHORT ONE

Modularity optimization groupings were examined to determine whether they were consistent with putative divisions in the basal ganglia. An eta^2 threshold of 0.85 was selected for the analyses reported below because at this threshold the network was sparse (i.e., edge density < 0.1) but fully connected (i.e., graph connectedness ~1.0) and there was strong community structure (i.e., Q > 0.3) in the network (see **Figure S1** in Supplementary Material).

Modularity optimization generated discrete, contiguous groupings of basal ganglia voxels in locations consistent with presumed basal ganglia divisions (see **Figure 2**, rows 1–3). The number of modules identified for the left ($M = 6.60$, SD = 2.19, range = 3–11) and right ($M = 6.73$, SD = 2.76, range = 3–13) hemispheres did not differ, $p = 0.87$. We focused on identifying and characterizing three modules because at least three modules were generated across subjects in Cohort One.

In each hemisphere for each subject, we identified groupings of basal ganglia voxels that were consistent with the location of the dorsal caudate, the ventral striatum, and the dorsal caudal putamen. Labels were assigned on the basis of stereotactic coordinates reported in prior functional connectivity (Di Martino et al., 2008; Harrison et al., 2009) and functional MRI co-activation (Postuma and Dagher, 2006) studies. The dorsal/ventral distinction for the caudate and putamen was $z = 2$ (i.e., dorsal = $z \geq 2$; ventral = $z \leq 2$). The rostral/caudal distinction for the putamen was $y = 0$. When more than one module met these criterion, the module closest to the coordinates reported in Di Martino et al. (2008) was assigned the particular label (i.e., dorsal caudate, ventral striatum, dorsal caudal putamen). As the spatial extent of each module was not fixed across subjects and hemispheres (it was determined by the number of voxels assigned to a particular grouping using modularity optimization), we sought to determine whether these stereotactic guidelines identified modules in similar locations across subjects. Accordingly, we conducted a conjunction analysis for each label by creating a masked image of that putative division and summing each subject's masked image. This analysis revealed that the spatial location of each putative basal ganglia division overlapped across subjects in anatomical locations consistent with the stereotactic guidelines described above (see **Figure 2**, row 4).

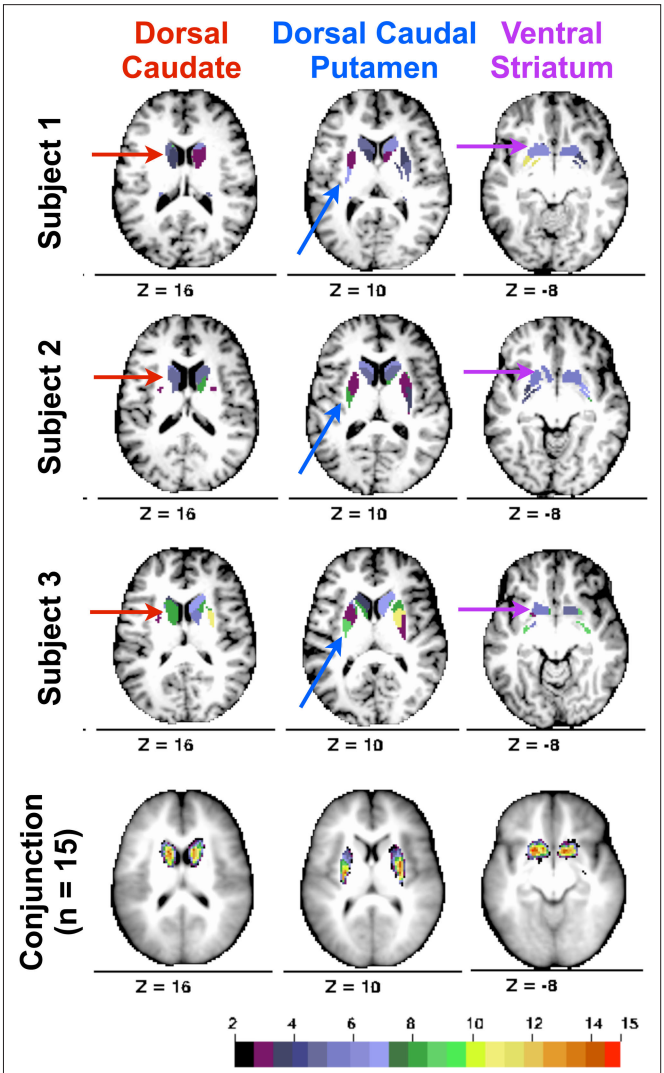

FIGURE 2 | Rows 1–3. From Cohort One, three subjects' basal ganglia voxels colored with respect to modularity optimization groupings (shown on each subject's MP-RAGE; coloring for each hemisphere and each subject is arbitrary). Arrows indicate modules labeled as dorsal caudate (red arrows, $z = 16$), dorsal caudal putamen (blue arrows, $z = 10$), and ventral striatum (purple arrows, $z = -8$). **Row 4**. Conjunction of modules ascribed the same label across Cohort One subjects. Color bar depicts number of subjects with a module assignment at each voxel.

To assess the validity of the modularity optimization results, we examined functional connectivity maps derived from modularity optimization assignments. For each of the three basal ganglia divisions (i.e., the voxels labeled as the putative dorsal caudate, dorsal caudal putamen, and ventral striatum) we generated six whole-brain correlation maps for each subject (three putative divisions × two hemispheres). Each subject's z-transformed whole-brain correlation map was used in a second level random-effects analysis involving one-sample t-tests ($z > 3.00$, $k = 21$,

corresponding to $p < 0.05$, Monte Carlo corrected). The random-effects maps for the left hemisphere (**Figure 3**, row 1) revealed qualitatively distinct patterns of functional connectivity for the putative dorsal caudate, dorsal caudal putamen, and ventral striatum (see **Figure S3** in Supplementary Material, Row 1 for random-effects analyses for putative right basal ganglia divisions.)

Functional connectivity maps from modularity optimization assignments revealed patterns of functional connectivity similar to the previously reported patterns of anatomical and functional connectivity of the dorsal caudate, dorsal caudal putamen, and ventral striatum (see **Figure 3**, row 1; **Table 1**). For example, the dorsal caudate was functionally connected to regions in lateral prefrontal cortex, the dorsal caudal putamen was functionally connected to regions in premotor and motor cortex, and the ventral striatum was functionally connected to regions in orbitofrontal and ventromedial prefrontal cortex.

The three putative basal ganglia divisions had distinct patterns of functional connectivity that were qualitatively reliable across individuals. We generated thresholded ($z > 2.00$), binarized images of individuals' z-transformed correlation maps for the putative left dorsal caudate, left dorsal caudal putamen, and left ventral striatum and summed them to determine whether robust functional connectivity in the random-effects analyses were driven by a handful of the subjects or whether overlapping patterns of functional connectivity could be seen in a majority of subjects. Conjunction analyses for each putative basal ganglia division across all Cohort One subjects revealed that regions of functional connectivity identified in the random-effects analyses seen in individual subjects (see **Figure 4**, rows 1–3) were present in a majority of subjects (see **Figure 4**, row 4). These findings suggest that putative basal ganglia divisions yield patterns of functional connectivity that are reliable at the individual subject-level.

COHORT TWO

We examined a second cohort to assess independently the reliability of our results. First, we examined Cohort Two to test whether we would find similar groupings. As with Cohort One, the number of groupings identified for the left ($M = 6.82$, SD = 2.04, range = 3–10) and right ($M = 9.09$, SD = 5.87, range = 4–21) hemispheres did not differ, $p = 0.25$. Further, the number of groupings identified for each hemisphere did not differ across cohorts (left hemisphere: $p = 0.80$, right hemisphere: $p = 0.18$). Visual inspection of the groupings' locations revealed that modularity optimization

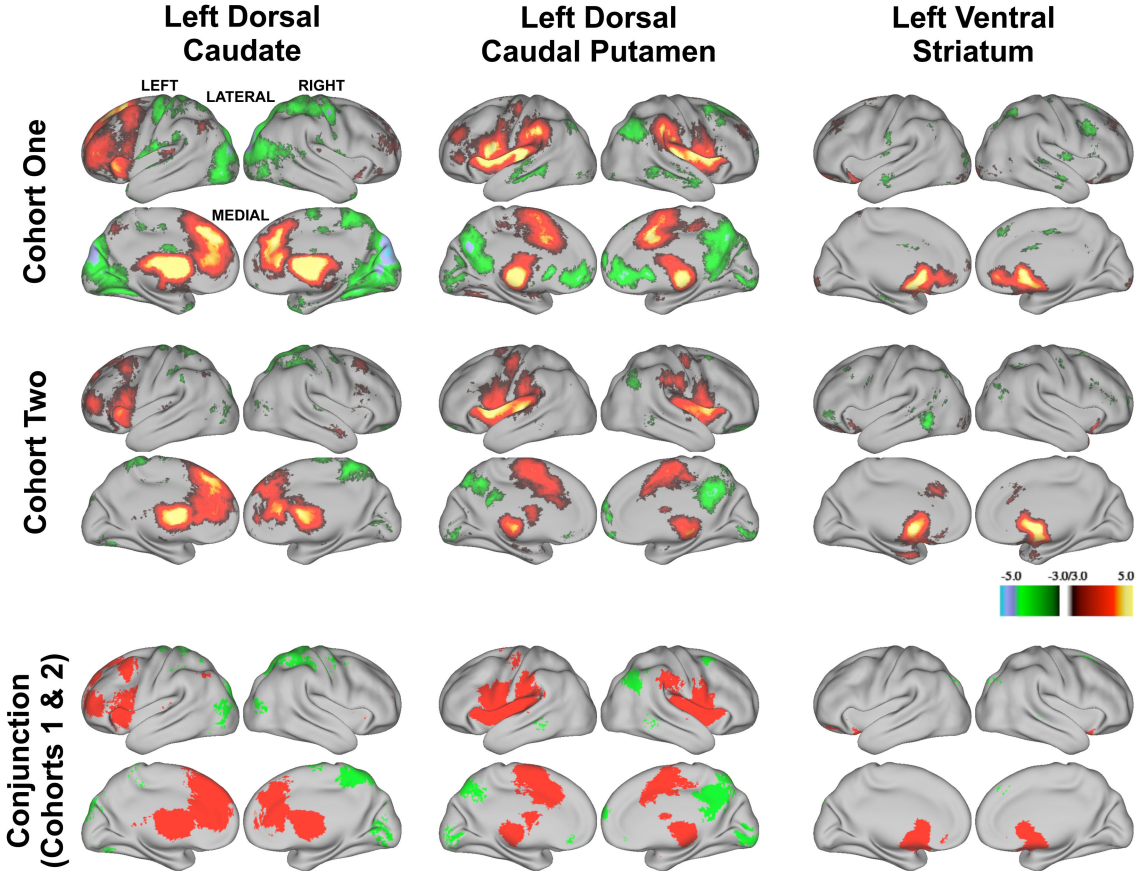

FIGURE 3 | *Z*-transformed rs-fcMRI maps from modularity assignments are statistically reliable within each cohort for the left hemisphere divisions (first and second rows, $z > 3.00$, $k = 21$, corresponding to $p < 0.05$, Monte Carlo corrected) and yield common regions of correlation across cohorts (conjunction analysis, third row). Positive correlations are depicted in warm colors (first two rows) and their overlap is depicted in red in the conjunction analysis (third row). Negative correlations are depicted in cool colors (first two rows) and their overlap is depicted in green in the conjunction analysis (third row).

Table 1 | Brain regions showing significant functional connectivity with putative basal ganglia divisions identified using random-effects one-sample *t*-tests ($z > 3.00$, $k = 21$, corresponding to $p < 0.05$, Monte Carlo corrected).

X	*Y*	*Z*	Hemisphere	Anatomical landmark	*Z*-score
DORSAL CAUDATE: POSITIVE CORRELATIONS					
Subcortical					
–12	8	8	Left	Caudate	7.42
13	10	7	Right	Caudate	7.13
–23	0	10	Left	Putamen	6.49
–6	–5	7	Left	Anterior thalamus	6.33
24	6	–4	Right	Putamen	5.88
6	–5	4	Right	Anterior thalamus	5.29
–30	–17	–4	Left	Putamen	5.08
–17	–14	15	Left	Thalamus	5.08
Frontal					
–7	26	41	Left	Medial frontal gyrus	5.73
–5	45	32	Left	Medial frontal gyrus	5.07
14	30	32	Right	Medial frontal gyrus	5.00
–6	35	11	Left	Cingulate gyrus	4.92
–17	22	58	Left	Superior frontal gyrus	4.91
–37	45	3	Left	Inferior frontal gyrus	4.83
Cerebellar					
22	–81	–27	Right	Cerebellum	5.33
38	–55	–41	Right	Cerebellum	4.88
DORSAL CAUDATE: NEGATIVE CORRELATIONS					
Frontal					
41	–9	47	Right	Precentral gyrus	–5.05
–35	–15	43	Left	Precentral gyrus	–4.86
Occipital					
12	–85	40	Right	Cuneus	–5.71
7	–84	31	Right	Cuneus	–5.41
–16	–88	38	Left	Cuneus	–5.27
4	–90	20	Right	Cuneus	–5.20
22	–54	–7	Right	Lingual gyrus	–4.95
–49	–80	–6	Left	Inferior occipital gyrus	–4.92
–15	–74	3	Left	Lingual gyrus	–4.87
15	–72	34	Right	Cuneus	–4.85
5	–73	4	Right	Lingual gyrus	–4.80
–16	–98	19	Left	Middle occipital gyrus	–4.74
25	–86	23	Right	Middle occipital gyrus	–4.71
–37	–87	25	Left	Middle occipital gyrus	–4.69
–32	–76	–9	Left	Fusiform gyrus	–4.66
DORSAL CAUDAL PUTAMEN: POSITIVE CORRELATIONS					
Subcortical					
–24	–14	7	Left	Putamen	7.47
30	–11	5	Right	Putamen	7.45
–12	–20	5	Left	Thalamus	6.07
12	–17	1	Right	Thalamus	5.67
19	–10	8	Right	Thalamus	5.67
Frontal					
42	8	10	Right	Insula	5.95
–40	7	3	Left	Insula	5.83
–52	3	11	Left	Precentral gyrus	5.72
53	4	11	Right	Precentral gyrus	5.60
9	13	39	Right	Cingulate gyrus	5.53
–43	15	10	Left	Inferior frontal gyrus	5.38
–6	11	34	Left	Cingulate gyrus	5.29
–6	8	56	Left	Pre-supplementary motor area	5.07
Parietal					
66	–35	34	Right	Inferior parietal lobule	5.09
–56	–28	28	Left	Inferior parietal lobule	4.91
DORSAL CAUDAL PUTAMEN: NEGATIVE CORRELATIONS					
Frontal					
5	45	–5	Right	Anterior cingulate cortex	–4.37
–2	45	–14	Left	Ventral anterior cingulate cortex	–4.24
46	24	36	Right	Middle frontal gyrus	–4.16
–13	50	0	Left	Anterior cingulate cortex	–4.12
Parietal					
–1	–71	31	Left	Precuneus	–5.41
5	–76	49	Right	Precuneus	–4.86
8	–64	27	Right	Precuneus	–4.67
42	–72	41	Right	Inferior parietal lobule	–4.66
47	–50	36	Right	Supramarginal gyrus	–4.56
–13	–60	20	Left	Posterior cingulate cortex	–4.55
–7	–50	9	Left	Posterior cingulate cortex	–4.41
11	–50	8	Right	Posterior cingulate cortex	–4.38
8	–41	39	Right	Cingulate gyrus	–4.15
Occipital					
11	–101	–10	Right	Lingual gyrus	–4.25
3	–82	–2	Right	Lingual gyrus	–4.19
VENTRAL STRIATUM: POSITIVE CORRELATIONS					
Subcortical					
–20	12	–11	Left	Ventral striatum	5.90
–8	12	–7	Left	Ventral striatum	5.34
4	13	–4	Right	Ventral striatum	4.99
–12	21	–5	Left	Caudate	4.75
Frontal					
10	42	–8	Right	Ventral anterior cingulate cortex	4.26
–33	38	42	Left	Middle frontal gyrus	3.95
12	30	–9	Right	Ventral anterior cingulate cortex	3.54
–18	36	–14	Left	Ventromedial prefrontal cortex	3.36

X	*Y*	*Z*	Hemisphere	Anatomical landmark	*Z*-score
–19	55	–17	Left	Orbitofrontal cortex	3.32
–3	69	2	Left	Ventromedial prefrontal cortex	3.30
–25	21	–15	Left	Inferior frontal gyrus	3.29
VENTRAL STRIATUM: NEGATIVE CORRELATIONS					
Frontal					
20	19	49	Right	Superior frontal gyrus	–4.51
15	–7	36	Right	Cingulate gyrus	–4.24
10	38	45	Right	Superior frontal gyrus	–3.64
34	14	28	Right	Middle frontal gyrus	–3.57
–19	19	33	Left	Anterior cingulate cortex	–3.44
Parietal					
34	–57	53	Right	Superior parietal lobule	–4.21
12	–44	22	Right	Posterior cingulate cortex	–3.92
55	–10	18	Right	Postcentral gyrus	–3.64
30	–68	44	Right	Inferior parietal lobule	–3.61
Temporal					
–53	–13	–18	Left	Middle temporal gyrus	–4.34
58	–11	–21	Right	Inferior temporal gyrus	–3.87
47	–11	–17	Right	Middle temporal gyrus	–3.76
62	–33	–1	Right	Middle temporal gyrus	–3.53
Occipital					
–33	–87	6	Left	Middle occipital gyrus	–3.64
Cerebellum					
–32	–84	–20	Left	Cerebellum	–3.53

generated discrete, contiguous groups of basal ganglia voxels in locations consistent with presumed basal ganglia divisions (see **Figure S2** in Supplementary Material for representative Cohort Two subjects and conjunction analysis for Cohort Two). Again, we could identify groupings of basal ganglia voxels consistent with the location of the dorsal caudate, the dorsal caudal putamen, and the ventral striatum in each hemisphere and subject.

Next, we examined whether functional connectivity maps derived from modularity optimization assignments were consistent across cohorts. As described above, for each of the three basal ganglia divisions (i.e., the putative dorsal caudate, dorsal caudal putamen, and ventral striatum) we generated six whole-brain correlation maps for each subject (three putative divisions × 2 hemispheres). Each subject's *z*-transformed whole-brain correlation map was used in a second level random-effects analysis involving one-sample *t*-tests ($z > 3.00$, $k = 21$, $p < 0.05$, Monte Carlo corrected). The random-effects maps for the left hemisphere for Cohort Two (**Figure 3**, row 2) revealed qualitatively distinct patterns of functional connectivity for the putative dorsal caudate, dorsal caudal putamen, and ventral striatum. (More spatially extensive regions of above threshold correlations in Cohort One than Cohort Two likely results from Cohort One's larger sample size.) Conjunction analyses (conducted by thresholding the one-sample *t*-test images for each group at $z > 3.00$, $k = 21$, $p < 0.05$, Monte Carlo corrected (see Forman et al., 1995), binarizing the thresholded images, and then searching for overlap) across Cohort One and Cohort Two's random-effects analyses revealed largely overlapping patterns of functional connectivity across cohorts for each putative basal ganglia division (**Figure 3**, bottom row). (See **Figure S3** in Supplementary Material for random-effects analyses for the right hemisphere for Cohort Two and conjunction analyses across cohorts.) These data indicate that putative basal ganglia divisions generated for two independent cohorts yield replicable patterns of functional connectivity. Accordingly, this independent replication increases our confidence in using rs-fcMRI to identify putative basal ganglia divisions.

DISCUSSION

The present study demonstrates that a combination of rs-fcMRI and graph theoretic analyses (i.e., modularity optimization) can be used to reliably identify divisions in the basal ganglia of individual subjects. For each subject, multiple divisions were identified and these divisions were similarly located across subjects. Furthermore, the correlation maps generated from modularity optimization groupings were similar across subjects. The putative basal ganglia divisions identified using modularity optimization have strong face validity since the locations of significant cortical-basal ganglia functional connectivity was consistent with the presumed connectivity of basal ganglia divisions.

Our approach to non-invasively parcellating the basal ganglia extends prior methods in ways that facilitate examination of individual subjects. We conducted voxel-wise whole-brain correlations, which allowed us to examine cortical-basal ganglia functional connectivity with a higher resolution than studies that apply large-scale cortical ROIs (Lehericy et al., 2004; Leh et al., 2007; Zhang et al., 2008), which encompassed very large swaths of cortex (e.g., prefrontal cortex) up to multiple lobes (e.g., parietal and occipital cortex). Additionally, by generating divisions for each subject rather than applying ROIs to fixed stereotactic locations (e.g., Di Martino et al., 2008; Harrison et al., 2009) we can better accommodate individual variation in subcortical volume, either total basal ganglia volumes or volumes of particular basal ganglia divisions. Accommodation of individual differences in regional brain volume is particularly important when examining individuals with disorders where basal ganglia volumes are thought to be reduced, such as Tourette's syndrome (see Albin and Mink, 2006) and attention deficit hyperactivity disorder (see Valera et al., 2007). For instance, it is unclear whether volumetric reductions in the caudate in individuals with Tourette's syndrome stem from a volumetric reduction of a particular basal ganglia division or from a more generalized shrinking. Following further validation, future studies could use these methods to identify putative basal ganglia divisions in individual subjects prior to spatial normalization and could help delineate between these alternatives because regional brain volumes and spatial extent characteristics would be retained.

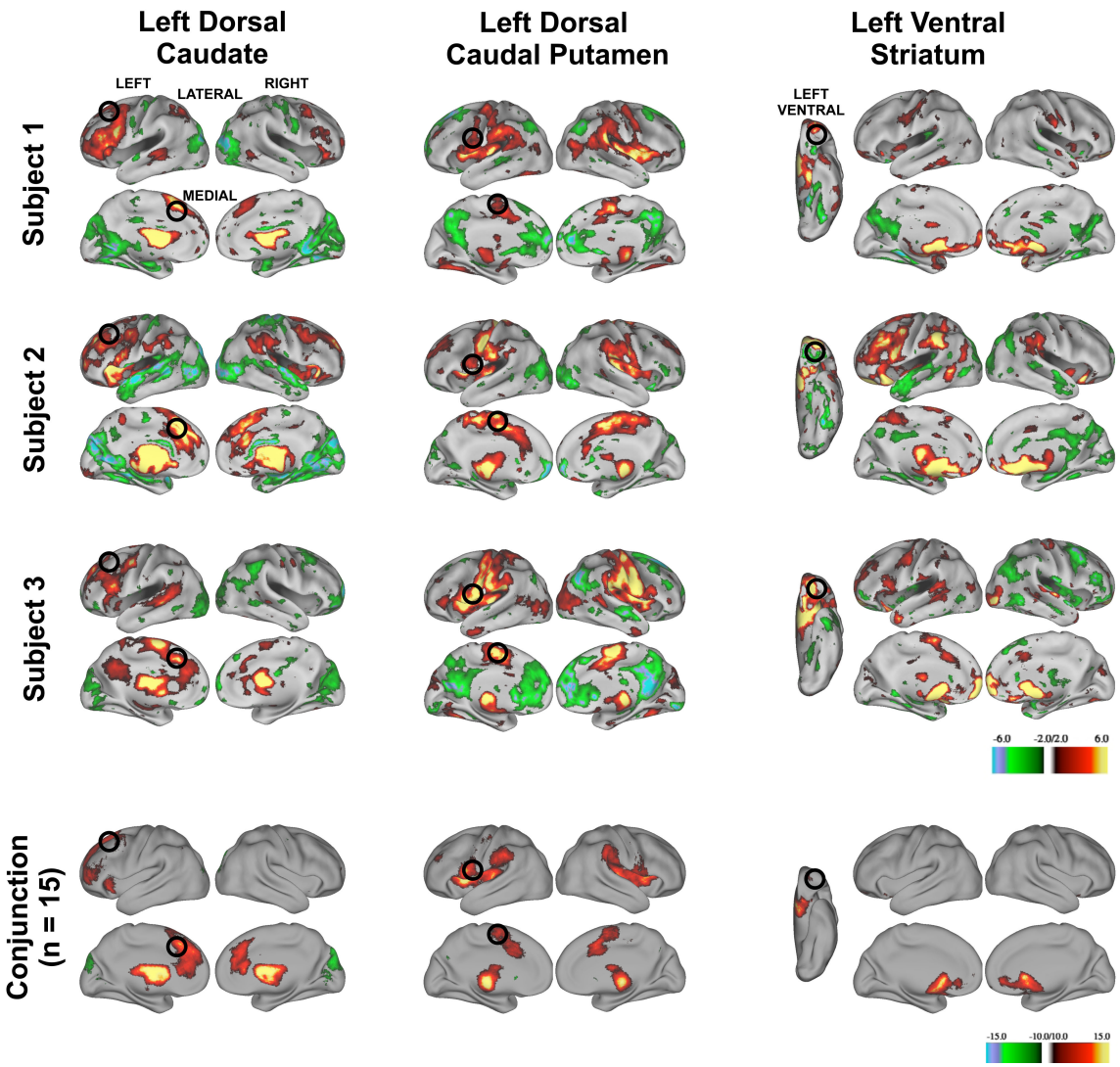

FIGURE 4 | *Z*-transformed rs-fcMRI maps from three representative subject's modularity optimization assignments for the left hemisphere (putative dorsal caudate, left column, putative dorsal caudal putamen, middle column, and putative ventral striatum, right column, $z > 2.00$) are similar. Black circles depict regions identified from the random-effects analysis (superior frontal gyrus: lateral rendering, first column; anterior cingulate cortex, medial rendering, first column; ventral premotor cortex: lateral rendering, second column; pre-supplementary motor cortex: medial rendering second column; orbitofrontal cortex: ventral rendering, third column). Row 4. Conjunction image of all subjects rs-fcMRI maps ($z > 2.00$).

While this method appears to provide a substantial advance in the ability to parcellate the basal ganglia in individual subjects, it is not clear whether this method would successfully parcellate very small subcortical structures, for instance smaller basal ganglia nuclei such as the subthalamic nucleus and substantia nigra. First, it is difficult to distinguish these smaller basal ganglia nuclei from neighboring structures in BOLD scans (e.g., substantia nigra and the nearby ventral tegmental area, Aron et al., 2007). Second, small structures will necessarily yield a smaller number of voxels for analysis than will large structures. Modularity optimization algorithms ought to be more successful with larger networks (*c.* >100 nodes) because groupings in large networks are less influenced by the placement of individual edges. Therefore, the graph theory methods used in the present study may not be appropriate for the smaller networks generated from smaller structures. However, it is likely that the present methods would be appropriate for parcellating other larger, subcortical structures (e.g., the thalamus) on a subject-wise basis.

In this manuscript we have only focused on characterizing three putative basal ganglia divisions. This focused look at putative basal ganglia divisions was predicated on the minimum number of groupings identified across subjects using modularity optimization. However, on average, modularity optimization identified 6–7 groupings. Using rs-fcMRI, Di Martino et al. (2008) reported different patterns of cortical-basal ganglia functional connectivity for six ROIs placed in the caudate and the putamen. Thus, the average number of groupings identified with modularity optimization converges with prior investigations of basal ganglia divisions in humans. Further work is needed to understand the sources of

variability in the number of groupings identified across subjects. For instance, it is possible that tailoring the modularity threshold investigated based on individual rather than group-level network metrics (e.g., edge density, graph connectedness) would reduce the variability in the number of groupings identified with modularity optimization. Additionally, generating objective ways to identify similar modules across subjects on the basis of their anatomical location and functional connectivity patterns (e.g., using assignment algorithms such as the Hungarian algorithm, Kuhn, 1955) is an important direction for future research. The current assignment method (i.e., labeling on the basis of stereotactic coordinates reported in past research) is subjective, as it requires an investigator to make a decision for each module and subject. Nonetheless, it is important to note that qualitatively reliable patterns of cortical-basal ganglia functional connectivity were found for the three putative basal ganglia divisions that were the focus of this manuscript.

Future work is needed to validate the divisions generated with rs-fcMRI and modularity optimization methods. One open question is the extent to which basal ganglia parcellations based on rs-fcMRI data overlap with parcellations based on DTI data. Recent work examining the thalamus suggests that there is partial but not total overlap between rs-fcMRI and DTI-based parcellations (Zhang et al., 2010). It remains to be seen whether this observation is also true for the basal ganglia. It is unlikely that there will be total overlap between functional and anatomical measures of connectivity based on both the findings of Zhang et al. (2008, 2010) and other research that has noted differences between anatomical and functional connectivity, as described in the introduction. Another means for validating putative basal ganglia divisions would involve testing for different task-evoked responses across putative divisions using functional MRI (fMRI). Work from our laboratory has demonstrated that putative cortical areas in left lateral parietal cortex identified using rs-fcMRI had distinct task-evoked fMRI time courses during memory retrieval in a meta-analysis conducted on independent data (Nelson et al., 2010). Again, it remains to be seen whether putative basal ganglia divisions have different task-evoked responses.

There are many interesting questions about cortical-basal ganglia functional connectivity that can be leveraged with a method to parcellate subcortical structures in individual subjects. For example, having a means to identify putative basal ganglia divisions on a subject-wise basis would provide a way to test hypotheses regarding cortical-basal ganglia connectivity in populations known to have reduced basal ganglia volumes. By identifying putative basal ganglia divisions in each subject and using these divisions as shape-preserved ROIs, researchers can ensure that each individual's ROIs are optimally located for each subject, reducing the likelihood that differences in functional connectivity between groups are the result of suboptimal seed placement in one group. For instance, shape-preserved ROIs could be used in lieu of standard spherical ROIs in graph theoretical analyses of functional network organization or between-group comparisons of functional connectivity strength. These methods would improve our understanding of the contributions of cortical-basal ganglia functional connectivity to the development of cognitive control (Liston et al., 2006; Rubia et al., 2006) and would help neuroscientists better understand the neural underpinnings of the many disorders that are characterized by structural and functional basal ganglia dysfunction (e.g., Tourette's Syndrome, attention deficit hyperactivity disorder, Huntington's disease, Parkinson's disease).

ACKNOWLEDGMENTS

The authors thank Kelly McVey and Rebecca Coalson for their help with data collection. This work was supported by the National Institutes of Health NS 007205-28 (Kelly Anne Barnes), NS 061144 (Steven E. Petersen), NS 053425 (Bradley L. Schlaggar) and NS 062489 (Alexander L. Cohen).

SUPPLEMENTARY MATERIAL

The Supplementary Material for this article can be found online at http://www.frontiersin.org/neuroscience/ systemsneuroscience/ paper/10.3389/fnsys.2010.00018/

REFERENCES

Albin, R. L., and Mink, J. W. (2006). Recent advances in Tourette syndrome research. *Trends Neurosci.* 29, 175–182.

Alexander, G. E., Delong, M. R., and Strick, P. L. (1986). Parallel organization of functionally segregated circuits linking basal ganglia and cortex. *Annu. Rev. Neurosci.* 9, 357–381.

Aron, A. R., Behrens, T. E., Smith, S., Frank, M. J., and Poldrack, R. A. (2007). Triangulating a cognitive control network using diffusion-weighted magnetic resonance imaging (MRI) and functional MRI. *J. Neurosci.* 27, 3743–3752.

Butts, C. T. (2009). Revisiting the foundations of network analysis. *Science* 325, 414–416.

Cohen, A. L., Fair, D. A., Dosenbach, N. U., Miezin, F. M., Dierker, D., Van Essen, D. C., Schlaggar, B. L., and Petersen, S. E. (2008). Defining functional areas in individual human brains using resting functional connectivity MRI. *Neuroimage* 41, 45–57.

Di Martino, A., Scheres, A., Margulies, D. S., Kelly, A. M., Uddin, L. Q., Shehzad, Z., Biswal, B., Walters, J. R., Castellanos, F. X., and Milham, M. P. (2008). Functional connectivity of human striatum: a resting state FMRI study. *Cereb. Cortex* 18, 2735–2747.

Dosenbach, N. U., Fair, D. A., Cohen, A. L., Schlaggar, B. L., and Petersen, S. E. (2008). A dual-networks architecture of top-down control. TICS. 12, 99-105.

Draganski, B., Kherif, F., Kloppel, S., Cook, P. A., Alexander, D. C., Parker, G. J., Deichmann, R., Ashburner, J., and Frackowiak, R. S. (2008). Evidence for segregated and integrative connectivity patterns in the human Basal Ganglia. *J. Neurosci.* 28, 7143–7152.

Fair, D. A., Cohen, A. L., Power, J. D., Dosenbach, N. U. F., Church, J. A., Miezin, F. M., Schlaggar, B. L., and Petersen, S. E. (2009). Functional brain networks develop from a "local to distributed" organization. *PLoS Comput. Biol.* 5 doi:10.1371/journal.pcbi.1000381.

Fair, D. A., Dosenbach, N. U. F., Church, J. A., Cohen, A. L., Brahmbhatt, S., Miezin, F. M., Barch, D. M., Raichle, M. E., Petersen, S. E., and Schlaggar, B. L. (2007). Development of distinct control networks through segregation and integration. *Proc. Natl. Acad. Sci. USA* 104, 13507–13512.

Fischl, B., Salat, D. H., Busa, E., Albert, M., Dieterich, M., Haselgrove, C., van der Kouwe, A., Killiany, R., Kennedy, D., Klaveness, S., Montillo, A., Makris, N., Rosen, B., and Dale, A. M. (2002). Whole brain segmentation: automated labeling of neuroanatomical structures in the human brain. *Neuron* 33, 341–355.

Fischl, B., Salat, D. H., van der Kouwe, A. J., Makris, N., Segonne, F., Quinn, B. T., and Dale, A. M. (2004). Sequence-independent segmentation of magnetic resonance images. *Neuroimage* 23(Suppl. 1), S69–S84.

Forman, S. D., Cohen, J. D., Fitzgerald, M., Eddy, W. F., Mintun, M. A., and Noll, D. C. (1995). Improved assessment of significant activation in functional magnetic resonance imaging (fMRI): use of a cluster-size threshold. *Magn. Reson. Med.* 33, 636–647.

Fox, M. D., Snyder, A. Z., Vincent, J. L., Corbetta, M., Van Essen, D. C., and Raichle, M. E. (2005). The human brain is intrinsically organized into dynamic, anticorrelated functional networks. *Proc. Natl. Acad. Sci. USA* 102, 9673–9678.

Fox, M. D., Zhang, D., Snyder, A. Z., and Raichle, M. E. (2009). The global signal

and observed anticorrelated resting state brain networks. *J. Neurophysiol.* 101, 3270–3283.

Gerfen, C. R. (1989). The neostriatal mosaic: striatal patch-matrix organization is related to cortical lamination. *Science* 246, 385–388.

Graybiel, A. M. (1990). Neurotransmitters and neuromodulators in the basal ganglia. *Trends Neurosci.* 13, 244–254.

Haber, S. N. (2003). The primate basal ganglia: parallel and integrative networks. *J. Chem. Neuroanat.* 26, 317–330.

Harrison, B. J., Soriano-Mas, C., Pujol, J., Ortiz, H., Lopez-Sola, M., Hernandez-Ribas, R., Deus, J., Alonso, P., Yucel, M., Pantelis, C., Menchon, J. M., and Cardoner, N. (2009). Altered corticostriatal functional connectivity in obsessive-compulsive disorder. *Arch. Gen. Psychiatry* 66, 1189–1200.

Hedden, T., and Gabrieli, J. D. (2004). Insights into the ageing mind: a view from cognitive neuroscience. *Nat. Rev. Neurosci.* 5, 87–96.

Ihnen, S. K., Church, J. A., Petersen, S. E., and Schlaggar, B. L. (2009). Lack of generalizability of sex differences in the fMRI BOLD activity associated with language processing in adults. *Neuroimage* 45, 1020–1032.

Kuhn, H. W. (1955). The Hungarian method for the assignment problem. *Nav. Res. Logist. Q.* 2, 83–97.

Lancaster, J. L., Glass, T. G., Lankipalli, B. R., Downs, H., Mayberg, H., and Fox, P. T. (1995). A modality-independent approach to spatial normalization of tomographic images of the human brain. *Hum. Brain Mapp.* 3, 209–223.

Leh, S. E., Ptito, A., Chakravarty, M. M., and Strafella, A. P. (2007). Fronto-striatal connections in the human brain: a probabilistic diffusion tractography study. *Neurosci. Lett.* 419, 113–118.

Lehericy, S., Ducros, M., Krainik, A., Francois, C., Van de Moortele, P. F., Ugurbil, K., and Kim, D. S. (2004). 3-D diffusion tensor axonal tracking shows distinct SMA and pre-SMA projections to the human striatum. *Cereb. Cortex* 14, 1302–1309.

Liston, C., Watts, R., Tottenham, N., Davidson, M. C., Niogi, S., Ulug, A. M., and Casey, B. J. (2006). Frontostriatal microstructure modulates efficient recruitment of cognitive control. *Cereb. Cortex* 16, 553–560.

Middleton, F. A., and Strick, P. L. (2000). Basal ganglia output and cognition: evidence from anatomical, behavioral, and clinical studies. *Brain Cogn.* 42, 183–200.

Miezin, F. M., Maccotta, L., Ollinger, J. M., Petersen, S. E., and Buckner, R. L. (2000). Characterizing the hemodynamic response: effects of presentation rate, sampling procedure, and the possibility of ordering brain activity based on relative timing. *Neuroimage* 11, 735–759.

Mink, J. W. (1996). The basal ganglia: focused selection and inhibition of competing motor programs. *Prog. Neurobiol.* 50, 381–425.

Nelson, S. M., Cohen, A. L., Power, J. D., Wig, G. S., Miezin, F. M., Wheeler, M. E., Velanova, K., Donaldson, D. I., Phillips, J. S., Schlaggar, B. L., and Petersen, S. E. (2010). A parcellation scheme for human left lateral parietal cortex. Neuron (in press).

Newman, M. E. (2006). Modularity and community structure in networks. *Proc. Natl. Acad. Sci. USA* 103, 8577–8582.

Postuma, R. B., and Dagher, A. (2006). Basal ganglia functional connectivity based on a meta-analysis of 126 positron emission tomography and functional magnetic resonance imaging publications. *Cereb. Cortex* 16, 1508–1521.

Rubia, K., Smith, A. B., Woolley, J., Nosarti, C., Heyman, I., Taylor, E., and Brammer, M. (2006). Progressive increase of frontostriatal brain activation from childhood to adulthood during event-related tasks of cognitive control. *Hum. Brain Mapp.* 27, 973–993.

Snyder, A. Z. (1996). "Difference image vs. ratio image error function forms in PET-PET realignment," in *Quantification of Brain Function Using PET*, eds R. Myer, V. J. Cunningham, D. L. Bailey, and T. Jones (San Diego, CA: Academic Press), 131–137.

Valera, E. M., Faraone, S. V., Murray, K. E., and Seidman, L. J. (2007). Meta-analysis of structural imaging findings in attention-deficit/hyperactivity disorder. *Biol. Psychiatry* 61, 1361–1369.

Vincent, J. L., Patel, G. H., Fox, M. D., Snyder, A. Z., Baker, J. T., Van Essen, D. C., Zempel, J. M., Snyder, L. H., Corbetta, M., and Raichle, M. E. (2007). Intrinsic functional architecture in the anesthetized monkey brain. *Nature* 447, 46–47.

Zhang, D., Snyder, A. Z., Fox, M. D., Sansbury, M. W., Shimony, J. S., and Raichle, M. E. (2008). Intrinsic functional relations between human cerebral cortex and thalamus. *J. Neurophysiol.* 100, 1740–1748.

Zhang, D., Snyder, A. Z., Shimony, J. S., Fox, M. D., and Raichle, M. E. (2010). Noninvasive functional and structural connectivity mapping of the human thalamocortical system. *Cereb. Cortex* 20, 1187–1194.

Conflict of Interest Statement: The authors declare that the research was conducted in the absence of any commercial or financial relationships that could be construed as a potential conflict of interest.

Received: 19 February 2010; paper pending published: 23 March 2010; accepted: 11 May 2010; published online: 10 June 2010.

Citation: Barnes KA, Cohen AL, Power JD, Nelson SM, Dosenbach YBL, Miezin FM, Petersen SE and Schlaggar BL (2010) Identifying basal ganglia divisions in individuals using resting-state functional connectivity MRI. Front. Syst. Neurosci. ***4****:18. doi: 10.3389/fnsys.2010.00018*

frontiers in
SYSTEMS NEUROSCIENCE

ORIGINAL RESEARCH ARTICLE
published: 17 June 2010
doi: 10.3389/fnsys.2010.00023

Resting-state functional connectivity differences in premature children

Eswar Damaraju[1]*, John R. Phillips[1,2], Jean R. Lowe[2], Robin Ohls[2], Vince D. Calhoun[1,2] and Arvind Caprihan[1]

[1] *The Mind Research Network, Albuquerque, NM, USA*
[2] *Department of Pediatrics, University of New Mexico, Albuquerque, NM, USA*

Edited by:
Lucina Q. Uddin, Stanford University, USA

Reviewed by:
Peter Fransson, Karolinska Institutet, Sweden
Nico Dosenbach, Washington University in St. Louis, USA

***Correspondence:**
Eswar Damaraju, The Mind Research Network, 1101 Yale Blvd NE, Albuquerque, NM 87106, USA.
e-mail: edamaraju@mrn.org

We examine the coherence in the spontaneous brain activity of sleeping children as measured by the blood oxygenation level dependent (BOLD) functional magnetic resonance imaging (fMRI) signals. The results are described in terms of resting-state networks (RSN) and their properties. More specifically, in this study we examine the effect of severe prematurity on the spatial location of the visual, temporal, motor, basal ganglia, and the default mode networks, the temporal response properties of each of these networks, and the functional connectivity between them. Our results suggest that the anatomical locations of the RSNs are well developed by 18 months of age and their spatial locations are not distinguishable between premature and term born infants at 18 months or at 36 months, with the exception of small spatial differences noted in the basal ganglia area and the visual cortex. The two major differences between term and pre-term children were present at 36 but not 18 months and include: (1) increased spectral energy in the low frequency range (0.01–0.06 Hz) for pre-term children in the basal ganglia component, and (2) stronger connectivity between RSNs in term children. We speculate that children born very prematurely are vulnerable to injury resulting in weaker connectivity between resting-state networks by 36 months of age. Further work is required to determine whether this could be a clinically useful tool to identify children at risk of developmental delay related to premature birth.

Keywords: resting-state networks, independent component analysis, functional network connectivity, functional magnetic resonance imaging, premature children

INTRODUCTION

Patterns of low frequency spontaneous correlations in large-scale brain regions in humans have been detected (Biswal et al., 1995) from blood oxygenation level dependent (BOLD) functional magnetic resonance imaging (fMRI) signals collected at rest. These correlations are used to obtain resting-state networks (RSNs), which may represent functional connectivity within the brain, and have been largely studied in adult populations (Buckner et al., 2008). Among these RSNs, a default mode network (DMN) has been identified which is characterized by a decrease in neuronal activation when the subject concentrates on an external task (Binder et al., 1999; Raichle et al., 2001). Differences in the functional connectivity of RSNs have been implicated in neurological disorders such as Schizophrenia (Garrity et al., 2007; Rotarska-Jagiela et al., 2010) and Alzheimer's disease (Greicius et al., 2004; Sorg et al., 2007). In this paper we study the maturation of RSN functional connectivity during early human development in healthy term born children and in former premature children between 18 and 36 months of age.

Extremely low birth weight (ELBW) premature infants have a high risk of developmental delay. Almost half of the ELBW infants go on to develop moderate to severe cognitive intellectual impairment (Hack et al., 2004; Taylor et al., 2004; Vohr et al., 2004; Wilson-Costello et al., 2005) and even premature children with normal IQs are at high risk for school failure due to deficits in executive function (Vicari et al., 2004). The mechanisms underlying these deficits are often not well understood. While many ELBW children exhibit white matter (WM) injury on clinical MRI scans, not all do, and it often isn't until later school age that cognitive deficits become evident (Anderson and Doyle, 2003). Because earlier treatment is generally more effective for neurocognitive problems associated with prematurity, a method of more accurately identifying those children at risk for developmental delay would be of tremendous clinical benefit.

Recent advances in neuroimaging offer an opportunity to better characterize the effects of prematurity on brain *structure*. High resolution imaging identifies regional brain volumes that may be more sensitive to the effects of prematurity than overall structure (Kesler et al., 2004; Thompson et al., 2007; Tzarouchi et al., 2009), and diffusion tensor imaging suggests that fractional anisotropy identifies WM abnormalities not apparent on standard MRI scans (Miller et al., 2002; Anjari et al., 2007). In a recent review of neuroimaging in prematurity, 16 studies using diffusion tensor imaging and 10 high resolution structural studies were identified (Ment et al., 2009). However the effect of prematurity on brain *function* has been less well studied. This report focuses on one aspect of brain function, resting-state networks that are related to functional networks and can be obtained in sleeping children.

Only several studies have examined the RSNs in infants. In two studies Fransson et al. have presented results on the presence of RSNs. In the first study (Fransson et al., 2007) 12 pre-term infants were imaged 41-weeks gestational age and in the second, 19 term unsedated infants (Fransson et al., 2009) were studied. In both

these groups RSNs were found in the sensory cortices, parietal and temporal areas, and the prefrontal cortex. Another study (Gao et al., 2009) compared DMNs and their functional connectivity in neonates, 1-year-old and 2-year-old infants. They found the presence of an incomplete DMN in neonates, which was developed in 1-year olds and was similar to adults in 2-year olds. Recently longitudinal neural network development was studied in pre-term children (Smyser et al.) from postmenstrual age of 26–40 weeks. They were able to find RSNs in various cortical regions and map their spatial growth longitudinally as a function of child's age. Although the presence of RSNs have been demonstrated in infants as early as 42 weeks, no study has examined the effects of prematurity on the spatial and temporal properties of RSNs systematically. Our goal was to compare age and prematurity dependent RSN property differences and their functional network connectivity (FNC) (Jafri et al., 2008). Forty seven children participated in this study, where we compare differences in RSNs in premature (≤1500 g) and full-term children imaged at 18–22 months and 36–48 months of age.

Temporally coherent networks of low frequency spontaneous oscillations were found from BOLD data collected on sleeping children. We call these networks as RSNs to mean networks found when the subjects were not actively doing a specific task. This does not exclude the presence of these networks during a task as well.

Currently there are two main methods for doing rs-fcMRI analysis. The first method consisted of the seed based correlation approach in which few region of interest (ROI) time series are selected a priori and voxelwise cross-correlation is computed across the whole brain (Fox et al., 2005). The ROI approach is more suitable to study adult resting fMRI data as the ROI's are well defined by many researchers and may not be completely evolved in a younger population (Fair et al., 2008). The second approach to identify RSNs uses independent component analysis (ICA). The advantage of ICA is that it is a model free data-driven approach that decomposes the data into linear mixtures of spatially independent and temporally coherent source signals/components. The applicability of the technique to resting fMRI data to extract RSNs has been demonstrated previously (Beckmann and Smith, 2004; Greicius et al., 2004; Calhoun and Adali, 2006; Damoiseaux et al., 2006). In this paper we use a ROI based rs-fcMRI analysis, where the ROIs are defined by the ICA spatial maps. Rather than define ROIs based on some atlas that may not be representative of functional units in infants, we treat ICA as a clustering algorithm to define regions with high within cluster correlations. We define functional ROIs based on the data itself. Although, the goals of both these methods is to identify functional connectivity, the network nodes and the time courses used for functional connectivity are different in the two methods. The ICA method defines a spatial map across the whole brain while the ROI based method uses locally defined clusters. The ICA method uses time courses associated with each ICA spatial map, while the ROI based method uses BOLD time response local to that specific ROI after removing effects of physiological noise. Thus there are significant differences between the two approaches and it is reassuring that the results of the two methods are similar.

Once the functional connectivity network is obtained graph-theoretic metrics can be used to study network properties (Bullmore and Sporns, 2009). These include parameters such as path-length, network clustering, modularity, and small-world topology. At least two recent papers discuss differences in network properties between children and adults (Fair et al., 2009; Supekar et al., 2009). An interesting finding was that development of children to adults was accompanied by a decrease in connectivity of short range connections and an increase in long-range connectivity. In this paper we do not discuss such differences in network metrics.

MATERIALS AND METHODS

PARTICIPANTS

In this study we recruited very low birth weight premature infants (≤1500 g at birth) and full-term children at 18–22 months and 36–48 months of age. All of the subjects sustained normal development and had no abnormalities on neurologic examination or on standard MRI scan. The subjects were categorized into four groups: (a) 16 premature infants at 18 months (P18), (b) 13 premature infants at 36 months (P36), (c) 9 full-term infants at 18 months (F18), and (d) 9 full-term infants at 36 months (F36). All experiments were done on sleeping children. The term children were not sedated while some premature children were lightly sedated with 50 mg/kg chloral hydrate administered orally. Prior to scanning, written informed consent was obtained from the parents and the study was approved by Institutional Review Board of the University of New Mexico. Light chloral hydrate sedation (50 mg/kg orally) was used for 11 of 16 premature infants at 18 months and 9 of 13 premature infants at 36 months. The mean gestational age for pre-term 18-month-old children was 28.7 weeks (±1.38, range 26.3–30.5 weeks) and the mean gestational age for pre-term 36-month-old children was 29.9 weeks (±1.58, range 28–32 weeks).

DATA ACQUISITION

Initially, a high resolution five-echo T1-weighted magnetization prepared rapid gradient-echo (MPRAGE) image was acquired on a 3T Siemens Trio scanner [TE = 1.64, 3.5, 5.36, 7.22, and 9.08 ms, TR = 2530 ms, flip angle = 7°, FOV = 256 mm, matrix size = 256 × 256, 1 mm^3 isotropic voxel]. The resting-state data was collected from a gradient-echo echo-planar sequence [TE = 29 ms, TR = 2 s, FOV = 240 mm, matrix size = 64 × 64, 32 slices, thickness 4.45 mm]. Resting-state data was collected for 5 min 16 s resulting in 158 volumes of BOLD fMRI data per subject.

DATA ANALYSIS

The data was preprocessed using a mixture of free and commercial packages including SPM[1], GIFT[2], AFNI (Cox, 1996) and MATLAB (The Mathworks Inc). The first four volumes of the functional data were discarded to account for T1 equilibrium effects. The remaining 154 volumes of EPI data of each subject was first motion corrected (INRIA align) followed by slice time correction. The data was then de-spiked using AFNI. Each subject's de-spiked EPI data was aligned to an infant's template obtained from the subjects in our study. In order to compare the 18-month and the 36-month infants we pooled our data and obtained one common template. A two step procedure was used to reduce the effect of the adult template (Altaye et al., 2008). We first aligned all the infant T1 images to the adult MNI template. The mean of these infant T1 registered images was our study specific infant template. In the second step, the spatial normalization was repeated by registering each infant's image to

[1]www.fil.ion.ucl.ac.uk/spm

[2]http://icatb.sourceforge.net

the infant template found in the first step. The spatially normalized images were resampled to 3 mm isotropic cubic voxels and then smoothed with a 6-mm Gaussian kernel. Finally each voxel's time series within the brain tissue was normalized to a mean of 100.

All of the preprocessed data from both the age groups was analyzed together in a single group ICA framework as implemented in the GIFT package. A two step data reduction approach using principal component analysis (PCA) was taken prior to performing the ICA analysis. In the first step, 80 principal components were obtained from each individual subject data to retain most of the subject specific variance. Then each of the subject's reduced data was concatenated in time and a second PCA was performed to retain 30 components. Recent extensive experiments on simulated and real fMRI data sets in our lab have shown that accounting for greater subject specific variance by retaining more components at the first PCA reduction step yields more reliable group and subject specific back reconstructed maps using GIFT package (Erhardt et al., 2010). Then Infomax ICA algorithm was used to obtain 30 independent components. The stability of the estimated components was ensured using 10 ICASSO (Himberg and Hyvarinen, 2003) iterations. Individual subject specific maps were subsequently obtained using the improved back reconstruction algorithm implemented in GIFT package.

Out of the 30 independent components, a set of 14 resting-state networks within the cortex were identified (**Figure 1**). These networks are listed in **Table 1**. The remaining components corresponded to subject's motion or were spatially confined to cerebrospinal fluid (CSF), and blood vessels. The independent component spatial maps obtained were first *z*-scored and one-sample random effects maps for the whole group were generated. Each subject's reconstructed ICA time courses were orthogonalized with respect to their estimated motion parameters, and representative WM and CSF signals. CSF and WM regions were identified based on the infant template found earlier. Several small ROI's were manually drawn in the CSF and WM regions of the template and the mean time signal in CSF and WM was calculated for each subject for use in orthogonalization. Spectral analysis was performed on these time courses. Subject specific time courses were variance normalized. Time course spectra were then determined using multi-taper spectral estimation[3]. In our data, the power spectrum had a peak at approximately 0.03 Hz and we compared for the differences in the power spectrum within the low frequency range (0.01–0.06 Hz) by averaging across this range for the four infant groups. The average spectral power was obtained in the low frequency range 0.01–0.06 Hz because it has been suggested in the literature that the cross-correlations between resting-state BOLD data is reflected in frequencies less than 0.1 Hz (Cordes et al., 2001).

An increased power density at a frequency can be caused by higher within network connectivity at that frequency. In addition, higher power density at a frequency makes it easier to detect connectivity between networks associated with that frequency. The ICA time course has contributions from the whole brain weighted by the ICA spatial map. For simplicity we assume that there are only two voxels and two frequencies present. The ICA time course can then be expressed as $x(t) = \sum_{k=1}^{2} A_k \cos(\omega_0 t + \alpha_k) + \sum_{k=1}^{2} B_k \cos(2\omega_0 t + \beta_k)$, where k indexes spatial location, and the signal has energy at two frequencies. The power spectrum has two peaks, one at ω_0, with a height $P_1 = 1/2\left(\sum_{j=1}^{2}\sum_{k=1}^{2} A_j A_k \cos(\alpha_j - \alpha_k)\right)$ and another at $2\omega_0$ with a height $P_2 = 1/2\sum_{j=1}^{2}\sum_{k=1}^{2}\left(B_j B_k \cos(\beta_j - \beta_k)\right)$. If we further assume that amplitudes are all equal to one, then $P_1 = 1 + \cos(\alpha_1 - \alpha_2)$ and $P_2 = 1 + \cos(\beta_1 - \beta_2)$. $\cos(\alpha_1 - \alpha_2)$ and $\cos(\beta_1 - \beta_2)$ are the correlation coefficients between the signals at the two voxels, and at the two frequencies respectively. If $\alpha_1 - \alpha_2 = 0$, then $P_1 = 2$, and if $\beta_1 - \beta_2 = \pi$, then $P_2 = 0$. In other words, with equal contributions from different voxels, the total energy will be higher at a frequency where the contributions are coherent. This shows that a stronger within network connectivity at a frequency can lead to a higher power spectrum peak for that frequency. Unfortunately we cannot conclude the reverse. If the power spectrum has higher energy at some frequency, we cannot conclude that the within network correlations are higher at that frequency.

Another advantage of a signal with higher energy is that in the presence of noise, the accuracy of correlation coefficient calculation increases for higher signal amplitudes. The correlation coefficient between $A_1\cos(\omega_0 t + \alpha_1) + \theta_1(t)$ and $A_2\cos(\omega_0 t + \alpha_2)$ is $\cos(\alpha_1 - \alpha_2)$ if noise $\theta(t)$ is zero. On the other hand, the correlation coefficient tends to zero with increasing noise variance. Thus in the absence of noise, the signal amplitude does not matter for correlation calculations; but with noise, a higher signal-to-noise ratio improves accuracy of correlation coefficient estimates, making it easier to detect connectivity.

Two sample *t*-tests (assuming unequal variance) were performed to investigate the effects of age and prematurity on power spectrum differences. Significant *p*-values are reported after correcting for multiple comparisons using false discovery rate (FDR) (Benjamini and Hochberg, 1995). Significance of the observed effect was also verified by permutation tests. Subject group membership was randomly permuted 10000 times and null distribution of group differences was obtained. The probability of observed difference given the empirical null was obtained. This *p*-value was corrected for multiple comparisons.

FUNCTIONAL CONNECTIVITY

To assess the strength of functional connectivity within an ICA network across groups, two sample *t*-tests (assuming unequal variance) were performed on the spatial maps to test age and term related differences. To restrict the search space, first a one-sample *t*-test for a given spatial map was performed for the corresponding group. For example to test term related effect in the 18-month kid group, for each ICA spatial map a one-sample *t*-test was performed on all of the 18-month kid's data. This map was thresholded at a FDR corrected $p < 0.05$ value and all the positively active voxels in this thresholded map were used to define a mask. The two sample *t*-tests for that independent component were then performed within these voxels. The resulting maps were thresholded at an FDR corrected value of $p < 0.05$.

FUNCTIONAL NETWORK CONNECTIVITY

The 14 (manually selected) resting-state networks were divided into the following five functionally defined major groups with sub-networks. These being: (1) Visual networks, (2) Default mode networks, (3) Temporal network, (4) Motor network, and (5) Basal ganglia. These are discussed in **Table 1**.

[3]http://chronux.org

We computed correlation between each pair of ICA time courses (Jafri et al., 2008). These correlation values were converted to z-scores using Fisher's Z transform $[z = 1/2\ln(1+r)/(1-r)]$, and two sample t-tests were performed on these z-scores to probe age and term related effects. In order to calculate the group mean correlation, we averaged the Z-scores and back calculated the correlation. The results of differences in correlations between different groups are presented similarly. We calculate the Z-score for the group mean difference and for presentation convert it back to a correlation.

There is considerable discussion in the literature in merits of simply averaging the untransformed correlations (Schmidt-Hunter method, Schmidt and Hunter, 1999) or averaging the Z-scores after transformation. We believe that both the methods will give similar results. Monte-Carlo simulation studies have shown that Schmidt-Hunter method results in estimates with an under-bias and the Fisher's transform method leads to a slight over-bias (Law, 1995). Even for the Schmidt-Hunter method the significance is tested by using Fisher's Z transform. The conversion of Z-score back to a correlation is less common but has been used previously in fMRI data analysis (see Gao et al., 2009).

REGION OF INTEREST ANALYSES

Additionally region of interest (ROI) based connectivity analysis was also performed. One-sample t-tests were performed on the 14 group ICA networks. These maps were thresholded at an arbitrary value of $t > 5$ and clusters of at least 80 contiguous voxels were obtained. A total of 44 regions of interest (ROIs) were obtained from all of the 14 independent components. A multiple regression was performed on each subject's preprocessed BOLD fMRI data with their estimated motion parameters and their WM and CSF signals as regressors and residuals were obtained. ROI time courses for the clusters defined above were obtained by weighted average of these residual fMRI time series, free of physiological and motion artifacts, within voxels of each cluster. The weighting factor, a value in the range 0–1, was obtained by scaling the contribution or loading value of the voxel in the cluster with respect to all the voxels in the spatial map that survived a threshold of $t > 5$. Correlation matrices between these ROI time courses were computed for each subject. This resulted in 946 correlations per subject. These values were Fisher Z transformed. PCA was performed on the Fisher Z transformed correlation matrix of all subjects (946×47 matrix). The loading parameters/principal component coefficients of first and second eigenvectors were used to probe for age and term related effects. For visualization, correlation matrix projected into first two eigenvector spaces is plotted. The loading values for each group were plotted in the inset of these figures. Also the mean difference Fisher Z transformed maps between full-term and pre-term infants at 18 months and 36 months were obtained. These maps were inverse Z transformed to obtain a mean difference in correlation strength across groups and plotted.

RESULTS

SPATIAL MAPS

All of the children at 18 and 36 months exhibited well developed resting-state networks. Except for the right and left lateral fronto-parietal networks, we found all other major RSNs found in adults. The children exhibited a sub-cortical RSN (IC12) not seen in the adult population. The hippocampal formation is usually considered as part of the DMN. In our ICA analysis it manifested within the component consisting of primarily visual regions (IC22 and IC23). The spatial maps of RSNs are summarized in **Figure 1**, and **Table 1** summarizes the network properties with their functional grouping. The volumes in **Table 1** were calculated by thresholding the spatial maps at an arbitrary value of $t > 5$ and retaining clusters of at least 80 contiguous voxels.

To compare the functional connectivity differences within each IC, we performed two sample t-tests with subjects as random factor probing the differences in spatial extent of independent component networks with age or term. Our data revealed that spatially IC's were similar between pre-term and full-term children at both ages. However, a main effect of age was observed ($p < 0.05$ whole brain FDR corrected) in IC02, the bilateral visual cortex and IC12, basal ganglia including bilateral amygdala and putamen (**Figure 2**).

TIME COURSES

The power spectrum of the temporal response for each network was compared for group differences across subjects. The signal power had a maximum in the range (0.02–0.05 Hz) for all subjects. This supports the trend in resting-state analysis to filter the data below 0.1 Hz. The signal power in the low frequency range (0.01–0.06 Hz) was higher in pre-term infants at FDR corrected $p < 0.05$ than term born infants at 36 months in IC12, bilateral amygdala, and putamen (**Figure 3**). Although there was a trend

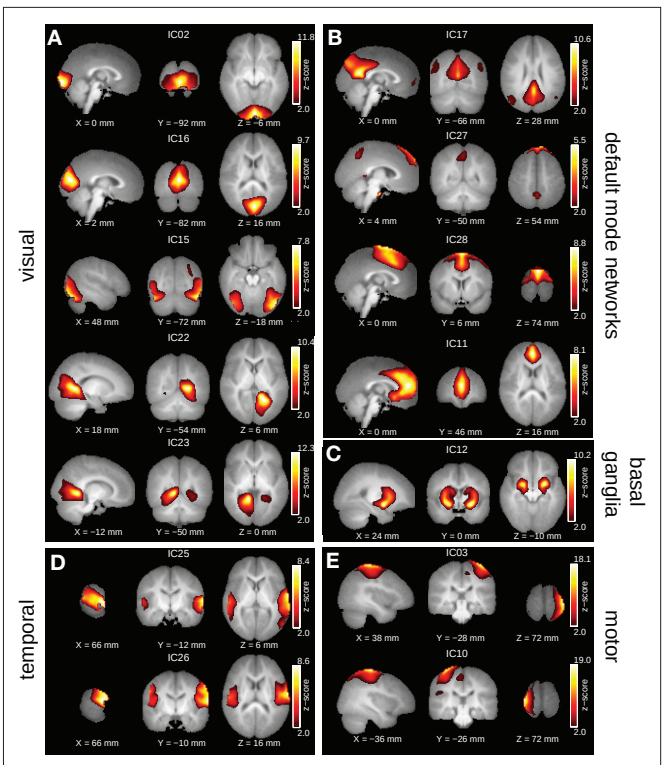

FIGURE 1 | Group ICA estimated resting-state patterns grouped into: (A) Visual resting-state networks, (B) Default mode networks, (C) Basal ganglia, (D) Temporal networks, and (E) Motor networks. Group maps are z-scored and voxels above a z thresholded of 2 are displayed. The left hemisphere of the brain corresponds to the left side of the image.

Table 1 | Resting-state networks obtained from group ICA. Clusters of at least 120 voxels at a threshold $t > 5$ are reported.

Component number, Talairach regions	Broadman areas	Volume (mm^3)	Maximum *T*	MNI coordinates in mm LPI
(1) VISUAL NETWORKS				
IC02 – Bilateral visual				
Bilateral lingual gyrus	17,18	2820	24	(1,–93,–9)
IC16 – Bilateral medial visual				
Bilateral medial primary visual areas	17	3800	34.1	(2,–81,9)
IC15 – Bilateral secondary visual				
Bilateral secondary visual areas	19,39	6500	28	(39,–80,–1)
Right middle cingulate cortex	24	144	9.8	(2,6,34)
IC22 – Right visual/hippocampal formation				
Right lingual and right parahippocampal gyrus	17,30	4820	25.3	(20,–59,3)
Left parahippocampal gyrus	36	585	10	(–24,–51,–8)
IC23 – Right visual/hippocampal formation				
Left lingual and left parahippocampal gyrus	17,30	5120	30.9	(–12,–53,0)
Left paracentral lobule	31	384	7.2	(–7,–33,52)
Right precentral gyrus	4	147	10.2	(46,–26,68)
(2) DEFAULT MODE NETWORKS				
IC17 – Post. cingulated cortex/Inferior parietal lobe				
Bilateral posterior cingulate cortex	31	3000	32.5	(0,54,5)
Left angular gyrus	39	1230	18.1	(–45,–73,32)
Right angular gyrus	39	1110	17.4	(45,–70,32)
Bilateral mid orbital gyrus		466	8.9	(0,54,5)
IC27 – Bilateral angular gyrus/Sup, medial gyrus				
Bilateral superior medial frontal gyrus	8	2170	18.8	(1,34,50)
Bilateral precuneus		887	15.8	(–1,–56,50)
Left angular gyrus		211	15.2	(–48,–68,32)
Left hippocampus	37	161	10.9	(–18,–20,–15)
Right hippocampus	37	121	10.2	(18,–21,–11)
IC28 – Superior frontal gyrus				
Bilateral dorsal medial prefrontal cortex	6	4890	30.7	(2,7,62)
IC11 – Bilateral anterior cingulate				
Bilateral anterior cingulate cortex	32	4000	27.2	(0,34,21)
Bilateral cuneus	19	375	7.6	(4,–93,28)
(3) TEMPORAL NETWORKS				
IC25 – Bilateral posterior temporal cortex				
Right superior temporal gyrus		3600	25.9	(56,–27,3)
Left superior temporal gyrus		1879	17.2	(–51,–37,10)
Bilateral precuneus	7	612	7.7	(0,–54,67)
Bilateral medial frontal gyrus	6	151	6.7	(–2,–16,54)
IC26 – Bilateral middle temporal cortex				
Right rolandic operculum	43	3189	24	(54,–11,25)
Left rolandic operculum	43	2140	16.9	(–47,–18,25)
Bilateral cuneus	19	476	6.5	(0,23,40)
Bilateral medial frontal gyrus	32	233	9	(1,23,40)
(4) MOTOR CORTEX				
IC03 – Right motor cortex				
Right precentral gyrus	4	3390	26.3	(34,–28,65)
Left postcentral gyrus	5	125	8.2	(–37,–46,69)
IC10 – Left motor cortex				
Left precentral gyrus	4	4116	22.2	(–31,–33,61)
Right calcarine gyrus	17	293	7	(13,–76,–3)
Right postcentral gyrus	5	138	8.5	(43,–46,65)
(5) BASAL GANGLIA				
IC12 – Bilateral putamen/amygdala				
Left putamen		1700	26.2	(–24,1,5)
Right putamen		1670	20	(26,1,5)

Table 2 | ROI labels for Figures 5 6 and 7.

R – Right	IFG – Inferior frontal gyrus
Vis – Visual	PreCG – Precentral gyrus
Cun – Cuneus	PoCG – Post central gyrus
PreCu – Precuneus	HF – Hippocampal formation
Put – Putamen	Bi – Bilateral
FFG – Fusiform gyrus	S – Secondary
Ang – Angular gyrus	MOG – Middle occipital gyrus
Amy – Amygdala	MeFG – Medial frontal gyrus
Hip – Hippocampus	dMePFC – Dorsal medial prefrontal cortex
L – Left	SMA – Supplementary motor area
SPL – Superior parietal lobe	STG – Superior temporal gyrus
IPL – Inferior parietal lobe	ITG – Inferior temporal gyrus
SFG – Superior frontal gyrus	ACC – Anterior cingulate cortex
	MCC – Middle cingulate cortex

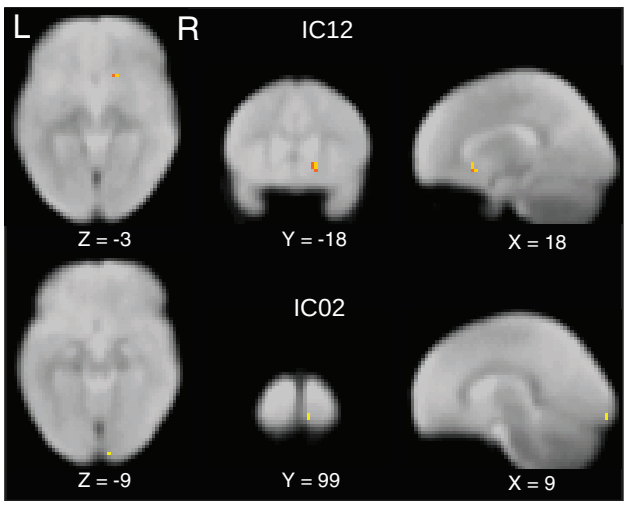

FIGURE 2 | Independent component maps depicting significant age related differences in two sample random effects analysis. Maps are thresholded at a whole brain voxelwise FDR corrected $p < 0.05$.

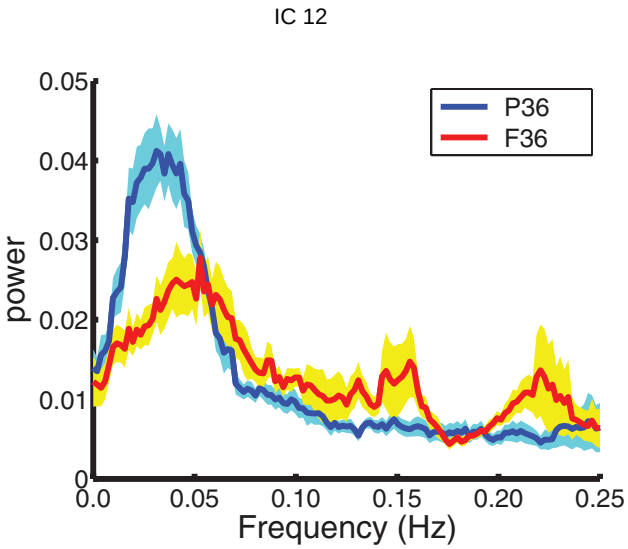

FIGURE 3 | Spectral analysis of ICA time courses of basal ganglia (IC12) component. Plotted here is the mean spectral power for pre-term children (blue) at 36 months along with their standard errors (cyan) and mean spectral power for full term children (red) at 36 months along with their standard errors (yellow).

for signal power in the low frequency range (0.01–0.06 Hz) to be higher in pre-term infants in several RSNs, we did not see significant differences. A similar comparison was done comparing 18-month and 36-month-old infants. No age dependent differences were observed in the spectral power of respective IC time courses. Differences between the time course spectral properties for the sedated and unsedated children were compared for the 18-month and the 36-month group and no significant differences were found. The signal power in the low frequency range (0.01–0.06 Hz) was higher in pre-term infants even after the sedated children were removed.

FUNCTIONAL NETWORK CONNECTIVITY BASED ON ICA COMPONENTS

Functional network connectivity between two independent components was defined as the correlation between their time courses. A correlation matrix between each pair of 14 ICA components was calculated and is shown in **Figure 4A**. Only the lower half of the correlation matrix excluding the diagonal is shown. The ICA components have been ordered according to the groups indicated in **Table 1** (Visual, DMN, Motor, Temporal, and the Basal Ganglia region). We probed for differences in correlation between these sub-networks as a function of prematurity. The results are summarized in **Figure 4B**. In the default mode networks, we did not observe any significant difference in correlation between the pre-term and term born children nor did we observe any age related effects. In the visual network the pre-term children had higher correlation between the Bilateral secondary visual (IC15) and the Bilateral medial visual (IC16) ($p = 0.03$, FDR corrected) at 18 months. For the temporal/motor network there was significantly higher correlation in pre-term infants between left motor cortex (IC10) and the bilateral posterior temporal cortex (IC25) at 18 months and at 36 months of age ($p < 0.05$, FDR corrected). Connectivity differences between the sedated and unsedated pre-term children were studied for the two age groups. The difference in mean correlation values is plotted for 18-month group (**Figure 5A**) and 36-month group (**Figure 5B**). Since the number of unsedated children is low, significance of differences was assessed using a permutation test. The cells which depict significant correlation differences after multiple comparison correction are enclosed in a black square. The effect of sedation seems to be more in the 18-month children. None of the correlation strength differences reached significance for 36-month group.

FUNCTIONAL NETWORK CONNECTIVITY BASED ON ROI ANALYSIS

Spatial clusters obtained from independent component analysis were used to define ROI's. Mean ROI time courses were computed from each subject's preprocessed fMRI time courses that were

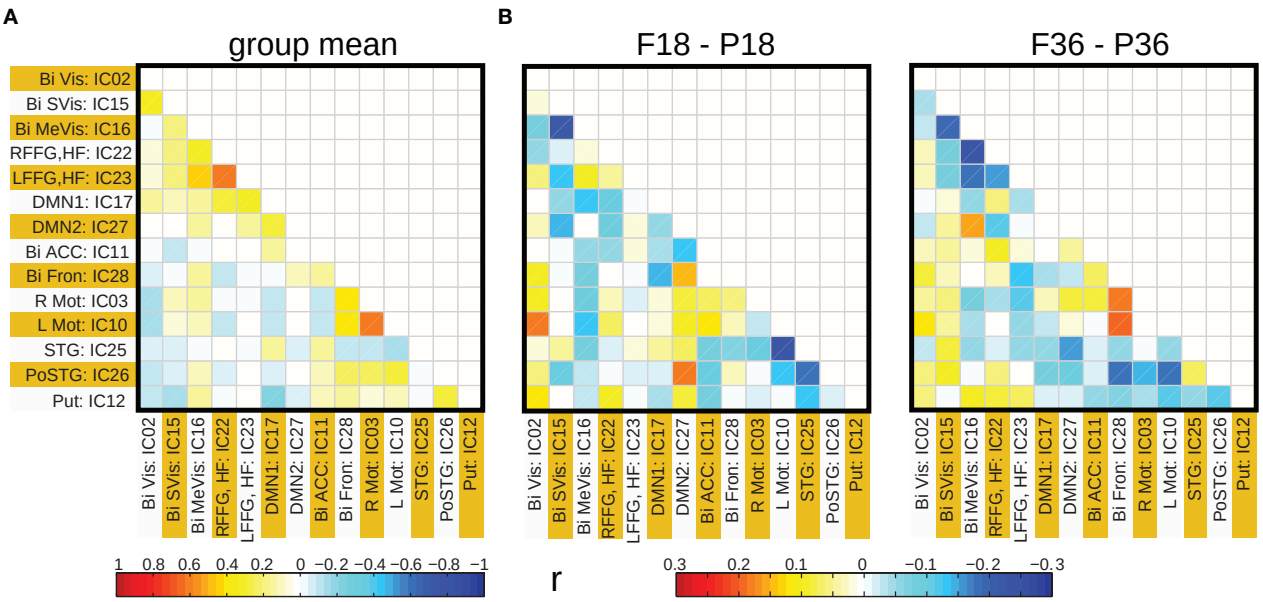

FIGURE 4 | (A) Group functional network connectivity map: Map of correlations between ICA time courses were Fisher *Z* transformed and averaged across all subjects. The resultant values are inverse *Z* transformed to obtain mean group correlation. **(B)** Mean difference in connectivity (correlation) between full term and pre-term children at 18 months (left panel) and at 36 months (right panel).

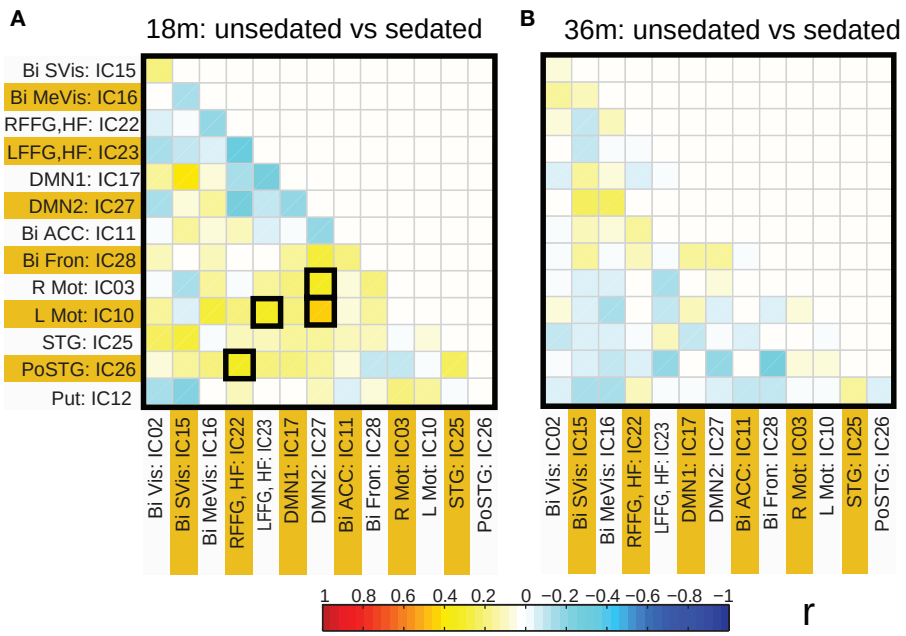

FIGURE 5 | Connectivity differences in ICA based functional connectivity between pre-term unsedated and sedated children for the 18-month (A) and the 36-month (B) groups. The cells with significant connectivity differences ($p < 0.05$ after FDR correction) are enclosed in black squares. No significant differences were observed for the 36-month group.

orthogonalized with respect to their motion parameters, CSF and WM signals. We then investigated the effects of prematurity and age in the correlation between these time courses. **Figure 6A** depicts the overall correlation between these ROI time courses collapsed across all subjects and the corresponding regions are indicated in **Figure 6B**. Time courses were arranged such that neighboring brain areas are placed closer in the matrix. A strong positive correlation can be observed among different visual areas and also among motor

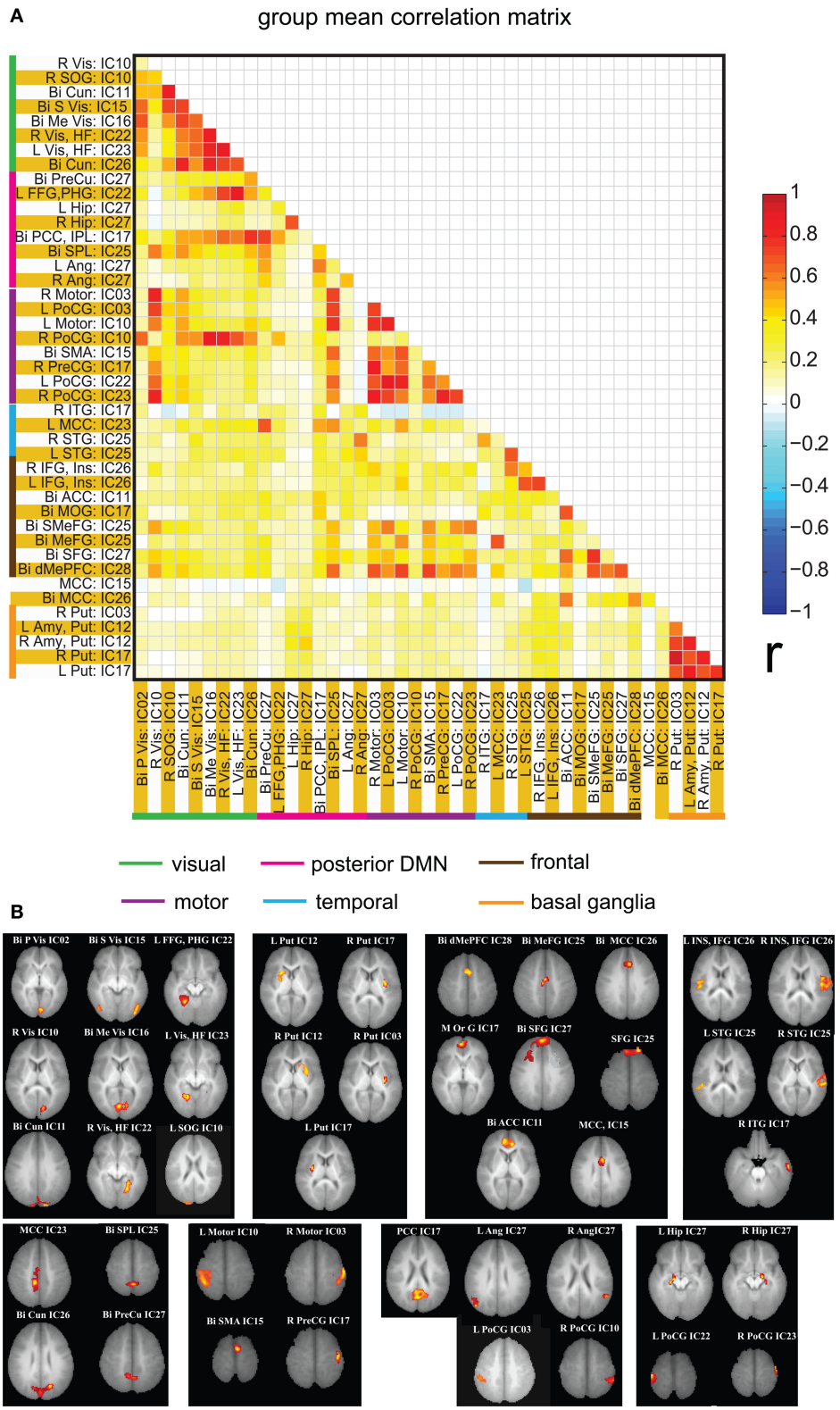

FIGURE 6 | (A) Mean correlation matrix of the all the subjects for all of the ROI pairs. The correlation values obtained for each pair were Fisher *Z* transformed, averaged across all of the subjects and finally inverse Fisher *Z* transformed to obtain a mean correlation value for each pair. The color coding next to ROI labels shows the grouping of regions based on their location in brain. Abbreviations of labels are listed in **Table 2** and the brain regions are displayed in **(B)**. **(B)** Brain maps depicting the weighted ROI masks used in ROI analysis.

networks. Also positive correlation exists between visual and motor networks, and motor and frontal networks. Results from the PCA of subject specific correlation matrices are presented in **Figures 7A,B**. The PCA we did is a variant on the standard PCA. In the standard analysis the subjects would be the number of samples and the mean would be subtracted across subjects. We changed the roles of samples and their attributes, with the mean along the attributes, the column of the correlation matrix (946×47) matrix being subtracted. This has the effect of the first principal component score (**Figure 7A**) reflecting the pattern of a shifted group mean plot (**Figure 6**). The corresponding subject loadings (inset **Figure 6A**) did not show any difference across groups. The second principal component score represents modulation or variances in the connectivity among different regions. Here a main effect of prematurity in the group loadings (inset **Figure 7B**) is evident ($p = 0.009$). The unsedated subjects in the premature group are marked with fill in the dots. The observed difference in loadings is preserved in the 36-month children as most of the unsedated kids fall in the same distribution as the sedated kids do. Insights into the second principal component score map can be obtained from the group differences in the correlation maps between pre-term and full-term kids depicted in **Figures 8A,B** for ages 18 months and 36 months respectively. It should be noted that stronger connectivity among visual areas in pre-term infants compared to full terms at both ages, a stronger connectivity among visual and motor networks and motor and frontal regions in full-term infants compared to pre-term infants is reflected in the second PCA score. The third principal component score mainly corresponded to regions of weak correlations (values of $r < 0.1$) in mean correlation matrix shown in **Figure 6**. So the third and higher PCA components were not considered for further analysis. Connectivity differences between sedated, and unsedated pre-term children was studied for the two age groups (**Figure 9**). A trend of stronger connectivity differences between sedated and unsedated children is apparent in the 18-month group, but not in the 36-month group. None of the differences survived multiple comparison correction.

DISCUSSION

The effects of prematurity and age on the RSNs of children at 18 and 36 months was investigated. Our group independent component analysis yielded RSNs similar to those observed in adults. Visual (**Figure 1A**), default-mode (**Figure 1B**), temporal (**Figure 1D**) and motor networks (**Figure 1E**) consistently observed in adults (for reference see Figure 1 in both Damoiseaux et al., 2006; Calhoun et al., 2008) were present as early as 18 months. The fronto-parietal network (Figures 1C,D Damoiseaux et al., 2006), which is usually lateralized in adults is not present in our data. This network is consistently shown to be involved in active memory tasks and may not be present prior to 3 years of age. We observed an additional network in the basal ganglia that encompasses caudate nucleus,

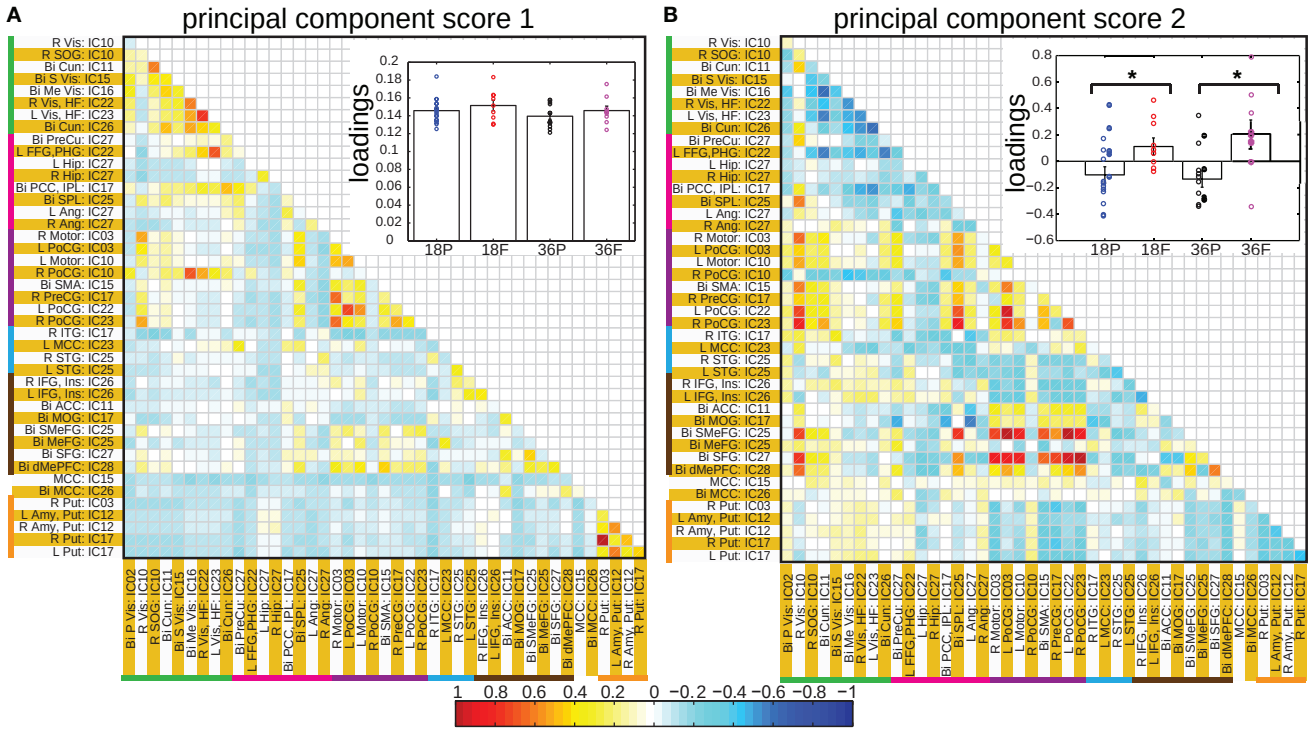

FIGURE 7 | Principal component analysis results: Individual correlation values of all of the subjects projected into first (A) and second (B) principal component space. The insets in each panel show bar graphs of group mean loadings with standard errors for each of the four groups for the corresponding component score. Subject specific loadings are plotted in circles overlaid on top of bar graphs. * represents significant difference between pre-term and full term groups for corresponding age groups. In inset of **(B)**, for the pre-term group, loadings for unsedated children are displayed in filled circles shifted slightly to the right.

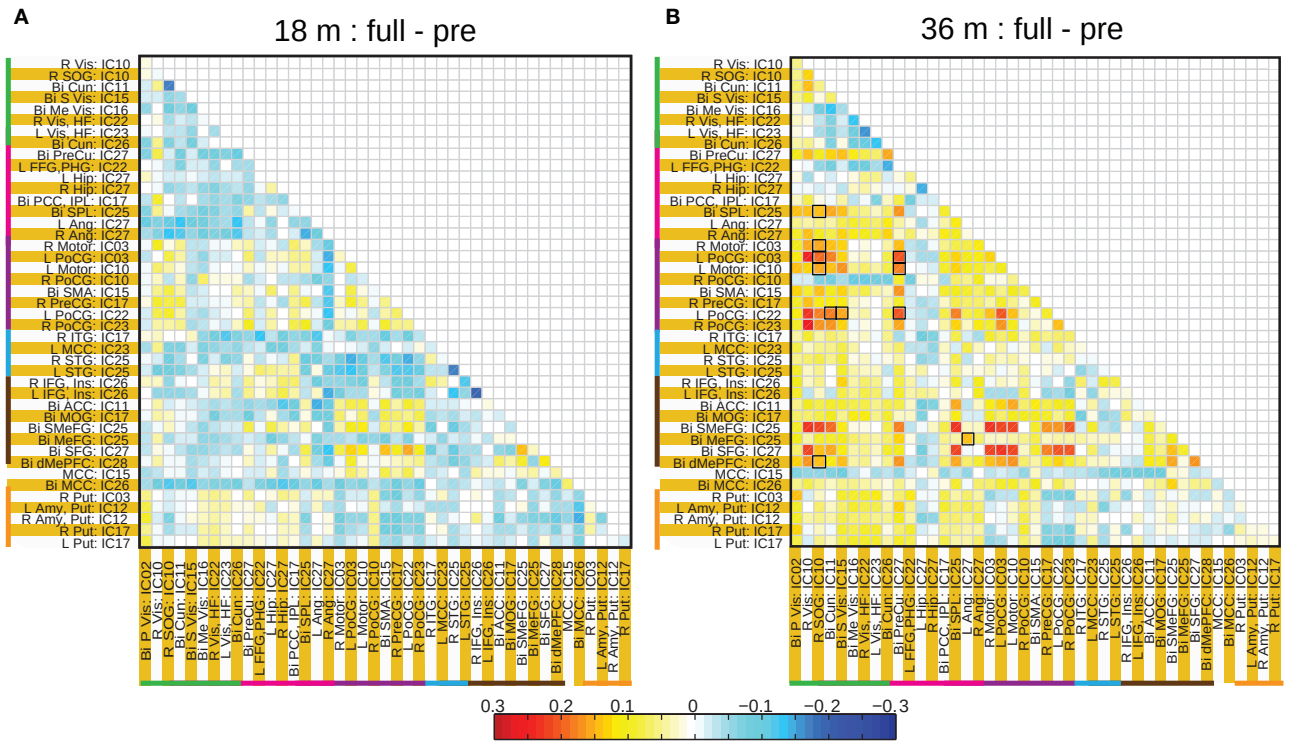

FIGURE 8 | Difference in ROI based group average correlation maps between full-term and pre-term children at age 18 months (A) and at 36 months (B). The cells enclosed in black square represent, significant connectivity difference between groups based on a two sample *t*-test assuming unequal variance and surviving and FDR corrected threshold of $p < 0.05$.

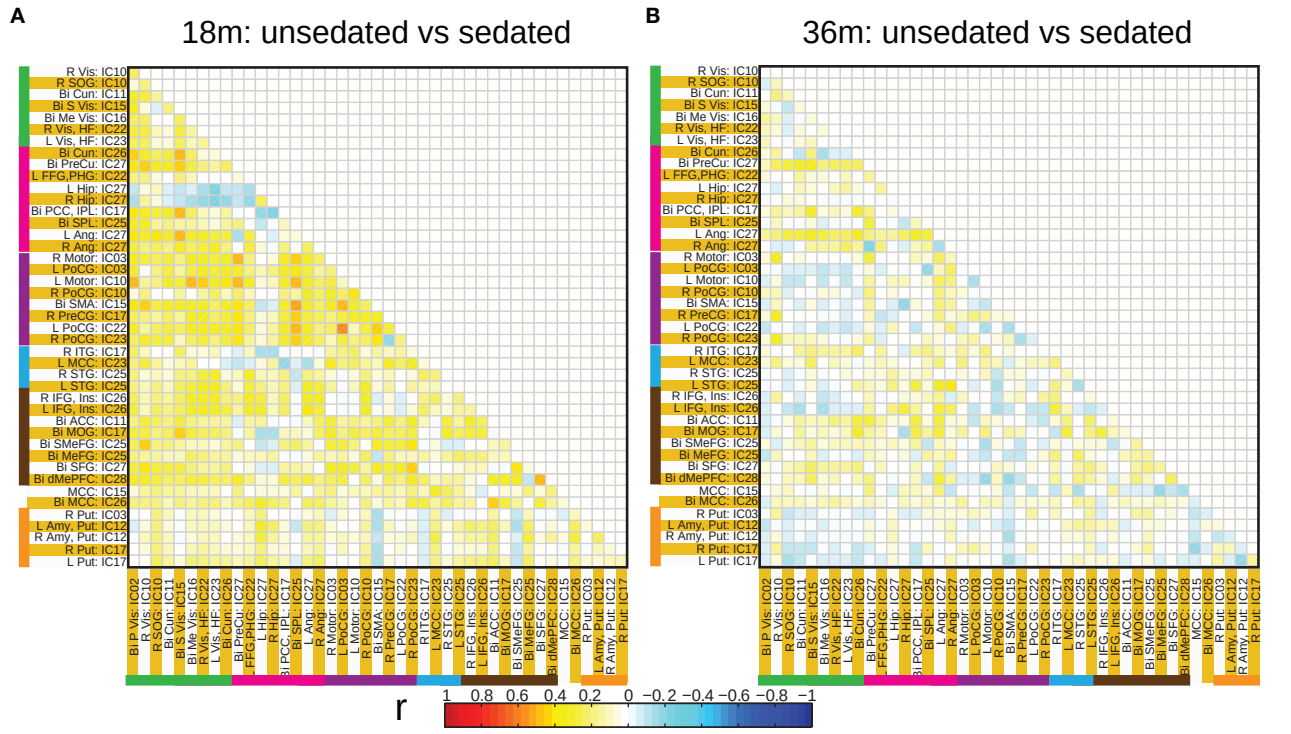

FIGURE 9 | Connectivity differences in the ROI based functional connectivity between pre-term unsedated and sedated children for the 18 month (A) and the 36 month (B) groups. Although no significant differences were observed at an FDR corrected $p < 0.05$ for either groups, a trend towards higher connectivity for unsedated children was observed for 18-month group as compared to sedated children.

putamen and amygdala. This is consistent with the recent finding by Fransson et al. (2009) who observed the network in term born infants scanned when they were sleeping naturally. The sensorimotor component (**Figure 1E**) showed predominant hemispheric lateralization with a small but significant cluster in contralateral hemisphere. This is supported by a recent study by (Liu et al., 2008) in which they observed the same unilateralization of the network in 9 out of 11 infants scanned at 12 months. This effect is speculated to be mediated by the breakdown of effective cortical connectivity in the motor cortex during certain stages of sleep.

The same spatial maps existed in premature as well as term born children at both ages suggesting a similar pattern of network development. This finding should be interpreted with caution, however, as only premature children with normal development and normal brain structures were included. Therefore this may only suggest that prematurity *per se* does not interfere with the normal process of functional brain network development. Development of functional brain networks may indeed be affected by lesions sometimes associated with prematurity (such as periventricular leukomalacia or intraventricular hemorrhage), or with more subtle injury resulting in cognitive deficits that are not clinically apparent until subjects are older.

The role of different frequency bands towards functional connectivity in adults has been previously studied (Wu et al., 2008). They showed that 0.01–0.06 Hz band demonstrated strong cortical connections, while connections between limbic structures was distributed over a wider frequency range (0.01–0.14 Hz). Although we did not compare the role of different frequency bands towards functional connectivity we did see higher power density in the 0.01–0.06 Hz band in pre-terms at 36 months of age in amygdala and putamen regions (**Figure 3**).

The two methods of calculating network connectivity (ICA components and hybrid ROI approach) gave similar group mean connectivity patterns as seen by comparing **Figures 4A and 6**. One difference between them was that there were considerable more negative correlations present with the ICA method. The similarity is remarkable and one reason for the differences can be that the ICA spatial maps extend over the whole brain and can in part be negative. In the ROI method we obtained the regions from only the positive part of the ICA map which had a t-value >5. The patterns for the difference between premature and full-term children were also similar with two methods (compare **Figures 4B and 8**). In the visual area the premature children had higher connectivity at both 18 months and 36 months of age with both methods of analysis. However, regions with statistically significant network connectivity were different between the two methods. In the ICA method we found significant differences in connectivity only in the visual area and between the temporal and the motor cortex, while with the hybrid ROI method we found significant differences in motor – frontal and the motor – visual areas.

A significant difference we found was stronger connectivity in the resting-state networks in term born children at 36 but not 18 months of age compared to former premature children. This was consistently identified in the two strongest networks present: motor – frontal and motor – visual networks (**Figure 7**). Prior work by Chugani (1998) using PET scans in the first year of life showed regional changes in cerebral metabolism that occurred starting in the primary sensory motor cortex and deep gray matter (newborn) to parietal lobes (3 months) to frontal lobes (8 months). A somewhat similar pattern of myelination occurs, with primary sensorimotor and visual pathways myelinating before parietal and finally frontal lobes (for review see Marsh et al. (2008)). It is of interest that networks involving the motor (and possibly premotor) and visual areas were the strongest we identified, raising the possibility that resting-state network development, although occurring later, follows a similar pattern as does early brain metabolism and myelination. In our subjects there was consistently stronger network connectivity in the term born children compared to premature children. Thus, the connectivity, not simply the presence, of resting-state networks may be particularly sensitive to the effects of prematurity.

Only minor effects of age were observed spatially in our group of children between 18-months and 36-months old. The children at 36 months exhibited a stronger contribution to visual cortex and basal ganglia components compared to 18-month sample. Similarly, the only difference in the time course of the premature and the term born infants was in the basal ganglia network. It should be pointed out that our conclusions are dependent on our methods of analysis. Our method of back-projection of group spatial ICA maps and time courses to individual subjects does preserve differences but enhancing differences is not the primary objective in the initial PCA data reduction step and subsequent ICA analysis. Alternate methods which incorporate prior information about the subject's group are being developed and may increase sensitivity to group differences (Sui et al., 2009a,b).

Our ROI based functional connectivity analysis was based on regions-of-interest being defined by ICA spatial maps. We avoid selecting ROIs based purely on anatomical considerations, or some form of atlas. Instead we use the data itself to define functionally connected regions. We treat ICA as a means of cluster analysis, where disjoint brain regions are identified with correlated BOLD response. An advantage of this hybrid ROI approach is that by decomposing an ICA network into smaller contiguous clusters allows us to define connectivity between regions whose function is known from prior work. Our method is not based on pre-defined atlas with sharp boundaries but clusters and the associated weighting function obtained from the data itself. Thus functional associations in the data are preserved and the data defines the location and weighting of the cluster. A disadvantage of this ICA based cluster definition is that we have not taken any advantage of ICA's filtering properties. In ICA the time course of one voxel is factored into multiple time courses which can be shared between different ICA networks and those associated with noise get factored out into separate components. In the proposed hybrid method we do not have this advantage and each voxel's time course had to be further filtered to remove effects of physiological noise. The hybrid method does use ICA to calculate the fractional contribution of each time course to the mean cluster time course.

A problem with our approach is that we have used the same data sets for doing the ICA analysis and selecting the ROIs and then doing a ROI based connectivity analysis on these regions (Kriegeskorte et al., 2009; Vul et al., 2009). If validation of the ICA method was our goal then our results would have been stronger if the groups we had used for identifying clusters were based on one group of subjects and then the ROI analysis for these clusters

done on a separate group of subjects. The present analysis is valid to show that the clusters found by ICA also show high correlations for the same subjects even when the time courses are pulled directly from the input data. This is interesting because the ICA algorithm is based on mutual information cost function and does not directly use correlations as basis of optimization. Thus it is important to understand the differences between the meaning of correlations obtained from the time courses corresponding to ICA maps and correlations obtained directly from the input data based on a cluster. This consistency of the correlations between the two different time courses is intuitively expected but additional work needs to be done to tie down the connection between the two approaches.

In order to address the problem of sedation we have looked at the spectral properties of the time courses and found no difference in the energy distribution. Some differences were found in the functional connectivity of sedated and unsedated pre-term children. We found a trend for stronger connectivity in unsedated pre-term children as compared to sedated children for the 18-month group. No such differences were found for the 36-month group. Although the amount of chloral hydrate administered was the same proportion of the child's weight, the previous observation may indicate that at the younger age of 18 months the children were more sensitive to sedation. Our results presented for the 36-month group for the time course spectral energy and the difference in connectivity between pre-term and term children was not changed by considering sedation.

Our results suggest that the anatomical locations of the RSNs are well developed by 18 months of age and their spatial locations are not distinguishable between premature and term born infants at 18 months or at 36 months, with the exception of small spatial differences noted in the basal ganglia area and the visual cortex. The two major differences between term and pre-term children were present at 36 but not 18 months and include: (1) increased spectral energy in the low frequency range (0.01–0.06 Hz) for pre-term children in the basal ganglia component, and (2) stronger connectivity between RSNs in term children. We speculate that children born very prematurely are vulnerable to injury resulting in weaker connectivity between resting-state networks by 36 months of age. Further work including longitudinal studies of brain-behavioral relationships will be necessary to determine whether the resting-state networks connectivity properties may indeed be early markers of brain injury associated with prematurity.

ACKNOWLEDGMENTS

We thank Susann Duvall, Erica Montague, Lynette Silva, Catherine Smith, and Diana South for their help in scanning the children at night. This work was supported by an internal grant from The Mind Research Network and NIH grant R01 EB000840 to Dr. Calhoun.

REFERENCES

Altaye, M., Holland, S. K., Wilke, M., and Gaser, C. (2008). Infant brain probability templates for MRI segmentation and normalization. *Neuroimage* 43, 721–730.

Anderson, P., and Doyle, L. W. (2003). Neurobehavioral outcomes of school-age children born extremely low birth weight or very preterm in the 1990s. *JAMA* 289, 3264–3272.

Anjari, M., Srinivasan, L., Allsop, J. M., Hajnal, J. V., Rutherford, M. A., Edwards, A. D., and Counsell, S. J. (2007). Diffusion tensor imaging with tract-based spatial statistics reveals local white matter abnormalities in preterm infants. *Neuroimage* 35, 1021–1027.

Beckmann, C. F., and Smith, S. M. (2004). Probabilistic independent component analysis for functional magnetic resonance imaging. *IEEE Trans. Med. Imaging* 23, 137–152.

Benjamini, Y., and Hochberg, Y. (1995). Controlling the false discovery rate: a practical and powerful approach to multiple testing. *J. R. Stat. Soc. Series B Stat. Methodol.* 57, 289–300.

Binder, J. R., Frost, J. A., Hammeke, T. A., Bellgowan, P. S., Rao, S. M., and Cox, R. W. (1999). Conceptual processing during the conscious resting state. A functional MRI study. *J. Cogn. Neurosci.* 11, 80–95.

Biswal, B., Yetkin, F. Z., Haughton, V. M., and Hyde, J. S. (1995). Functional connectivity in the motor cortex of resting human brain using echo-planar MRI. *Magn. Reson. Med.* 34, 537–541.

Buckner, R. L., Andrews-Hanna, J. R., and Schacter, D. L. (2008). The brain's default network: anatomy, function, and relevance to disease. *Ann. N. Y. Acad. Sci.* 1124, 1–38.

Bullmore, E., and Sporns, O. (2009). Complex brain networks: graph theoretical analysis of structural and functional systems. *Nat. Rev. Neurosci.* 10, 186–198.

Calhoun, V. D., and Adali, T. (2006). 'Unmixing' functional magnetic resonance imaging with independent component analysis. *IEEE Eng. Med. Biol.* 25, 79–90.

Calhoun, V. D., Kiehl, K. A., and Pearlson, G. D. (2008). Modulation of temporally coherent brain networks estimated using ICA at rest and during cognitive tasks. *Hum. Brain Mapp.* 29, 828–838.

Chugani, H. T. (1998). A critical period of brain development: studies of cerebral glucose utilization with PET. *Prev. Med.* 27, 184–188.

Cordes, D., Haughton, V. M., Arfanakis, K., Carew, J. D., Turski, P. A., Moritz, C. H., Quigley, M. A., and Meyerand, M. E. (2001). Frequencies contributing to functional connectivity in the cerebral cortex in "resting-state" data. *AJNR Am. J. Neuroradiol.* 22, 1326–1333.

Cox, R. W. (1996). AFNI: Software for analysis and visualization of functional magnetic resonance neuroimages. *Comput. Biomed. Res.* 29, 162–173.

Damoiseaux, J. S., Rombouts, S. A. R. B., Barkhof, F., Scheltens, P., Stam, C. J., Smith, S. M., and Beckmann, C. F. (2006). Consistent resting-state networks across healthy subjects. *Proc. Natl. Acad. Sci. U.S.A.* 103, 13848–13853.

Erhardt, E., Rachakonda, E., Bedrick, E., Adali, T., and Calhoun, V. D. (2010). "Comparison of Multi-Subject ICA Methods for Analysis of fMRI data," in *16th Annual Meeting of the Organization for Human Brain Mapping*, 6–10 June, Barcelona, Spain.

Fair, D. A., Cohen, A. L., Dosenbach, N. U. F., Church, J. A., Miezin, F. M., Barch, D. M., Raichle, M. E., Petersen, S. E., and Schlaggar, B. L. (2008). The maturing architecture of the brain's default network. *Proc. Natl. Acad. Sci. U.S.A.* 105, 4028–4032.

Fair, D. A., Cohen, A. L., Power, J. D., Dosenbach, N. U., Church, J. A., Miezin, F. M., Schlaggar, B. L., and Petersen, S. E. (2009). Functional brain networks develop from a "local to distributed" organization. *PLoS Comput. Biol.* 5, e1000381. doi:10.1371/journal.pcbi.1000381.

Fox, M. D., Snyder, A. Z., Vincent, J. L., Corbetta, M., Van Essen, D. C., and Raichle, M. E. (2005). The human brain is intrinsically organized into dynamic, anticorrelated functional networks. *Proc. Natl. Acad. Sci. U.S.A.* 102, 9673–9678.

Fransson, P., Skiold, B., Engstrom, M., Hallberg, B., Mosskin, M., Aden, U., Lagercrantz, H., and Blennow, M. (2009). Spontaneous brain activity in the newborn brain during natural sleep–an fMRI study in infants born at full term. *Pediatr. Res.* 66, 301–305.

Fransson, P., Skiold, B., Horsch, S., Nordell, A., Blennow, M., Lagercrantz, H., and Aden, U. (2007). Resting-state networks in the infant brain. *Proc. Natl. Acad. Sci. U.S.A.* 104, 15531–15536.

Gao, W., Zhu, H., Giovanello, K. S., Smith, J. K., Shen, D., Gilmore, J. H., and Lin, W. (2009). Evidence on the emergence of the brain's default network from 2-week-old to 2-year-old healthy pediatric subjects. *Proc. Natl. Acad. Sci. U.S.A.* 106, 6790–6795.

Garrity, A. G., Pearlson, G. D., McKiernan, K., Lloyd, D., Kiehl, K. A., and Calhoun, V. D. (2007). Aberrant functional connectivity of the 'default mode' in schizophrenia. *Am. J. Psychiatry* 164, 450–457.

Greicius, M. D., Srivastava, G., Reiss, A. L., and Menon, V. (2004). Default-mode network activity distinguishes

Alzheimer's disease from healthy aging: evidence from functional MRI. *Proc. Natl. Acad. Sci. U.S.A.* 101, 4637–4642.

Hack, M., Youngstrom, E. A., Cartar, L., Schluchter, M., Taylor, H. G., Flannery, D., Klein, N., and Borawski, E. (2004). Behavioral outcomes and evidence of psychopathology among very low birth weight infants at age 20 years. *Pediatrics* 114, 932–940.

Himberg, J., and Hyvarinen, A. (2003). ICASSO: software for investigating the reliability of ICA estimates by clustering and visualization. In *Proceedings of IEEE Workshop on Neural Networks for Signal Process,* (Toulouse, France), 259–268.

Jafri, M., Pearlson, G. D., Stevens, M., and Calhoun, V. D. (2008). A method for functional network connectivity among spatially independent resting-state components in schizophrenia. *Neuroimage* 39, 1666–1681.

Kesler, S. R., Ment, L. R., Vohr, B., Pajot, S. K., Schneider, K. C., Katz, K. H., Ebbitt, T. B., Duncan, C. C., Makuch, R. W., and Reiss, A. L. (2004). Volumetric analysis of regional cerebral development in preterm children. *Pediatr. Neurol.* 31, 318–325.

Kriegeskorte, N., Simmons, W. K., Bellgowan, P. S. F., and Baker, C. I. (2009). Circular analysis in systems neuroscience: the dangers of double dipping. *Nat. Neurosci.* 12, 535–540.

Law, K. S. (1995). The use of Fisher's Z in Scmidt-Hunter-type meta-analyses. *J. Educ. Behav. Stat.* 20, 287–306.

Liu, W.-C., Flax, J. F., Guise, K. G., Sukul, V., and Benasich, A. A. (2008). Functional connectivity of the sensorimotor area in naturally sleeping infants. *Brain Res.* 1223, 42–49.

Marsh, R., Gerber, A. J., and Peterson, B. S. (2008). Neuroimaging studies of normal brain development and their relevance for understanding childhood neuropsychiatric disorders. *J. Am. Acad. Child Adolesc. Psychiatry* 47, 1233–1251.

Ment, L. R., Hirtz, D., and Huppi, P. S. (2009). Imaging biomarkers of outcome in the developing preterm brain. *Lancet Neurol.* 8, 1042–1055.

Miller, S. P., Vigneron, D. B., Henry, R. G., Bohland, M. A., Ceppi-Cozzio, C., Hoffman, C., Newton, N., Partridge, J. C., Ferriero, D. M., and Barkovich, A. J. (2002). Serial quantitative diffusion tensor MRI of the premature brain: development in newborns with and without injury. *J. Magn. Reson. Imaging* 16, 621–632.

Raichle, M. E., MacLeod, A. M., Snyder, A. Z., Powers, W. J., Gusnard, D. A., and Shulman, G. L. (2001). A default mode of brain function. *Proc. Natl. Acad. Sci. U.S.A.* 98, 676–682.

Rotarska-Jagiela, A., van de Ven, V. G., Oertel-Knöchel, V., Uhlhaas, P. J., Vogeley, K., and Linden, D. E. (2010). Resting-state functional network correlates of psychotic symptoms in schizophrenia. *Schizophr. Res.* [Epub ahead of print].

Schmidt, F. L., and Hunter, J. E. (1999). Comparison of three meta-analysis methods revisited: an analysis of Johnson, Mullen, and Salas (1995). *J. Appl. Psychol.* 84, 144–148.

Smyser, C. D., Inder, T. E., Shimony. J. S., Hill, J. E., Degnan, A. J., Snyder, A. Z. and Neil, J. J. (2010). Longitudinal analysis of neural network development in preterm infants. *Cereb. Cortex.* doi: 10-1093/cercor/bhq035 [Epub ahead of print].

Sorg, C., Riedl, V., Muhlau, M., Calhoun, V. D., L., L., Drzezga, A., Forstl, H., Kurz, A., Zimmer, C., and Wohlschlager, A. (2007). Selective changes of resting-state networks in patients at high risk for Alzheimer's disease – an example for profiling functional brain disorders. *Proc. Natl. Acad. Sci. U.S.A.* 104, 18760–18765.

Sui, J., Adali, T., Pearlson, G. D., and Calhoun, V. D. (2009a). An ICA-based method for the identification of optimal FMRI features and components using combined group-discriminative techniques. *Neuroimage* 46, 73–86.

Sui, J., Adali, T., Pearlson, G. D., Clark, V. P., and Calhoun, V. D. (2009b). A method for accurate group difference detection by constraining the mixing coefficients in an ICA framework. *Hum. Brain Mapp.* 30, 2953–2970.

Supekar, K., Musen, M., and Menon, V. (2009). Development of large-scale functional brain networks in children. *PLoS Biol.* 7, e1000157. doi:10.1371/journal.pbio.1000157.

Taylor, H. G., Minich, N. M., Klein, N., and Hack, M. (2004). Longitudinal outcomes of very low birth weight: neuropsychological findings. *J. Int. Neuropsychol. Soc.* 10, 149–163.

Thompson, D. K., Warfield, S. K., Carlin, J. B., Pavlovic, M., Wang, H. X., Bear, M., Kean, M. J., Doyle, L. W., Egan, G. F., and Inder, T. E. (2007). Perinatal risk factors altering regional brain structure in the preterm infant. *Brain* 130, 667–677.

Tzarouchi, L. C., Astrakas, L. G., Xydis, V., Zikou, A., Kosta, P., Drougia, A., Andronikou, S., and Argyropoulou, M. I. (2009). Age-related grey matter changes in preterm infants: an MRI study. *Neuroimage* 47, 1148–1153.

Vicari, S., Caravale, B., Carlesimo, G. A., Casadei, A. M., and Allemand, F. (2004). Spatial working memory deficits in children at ages 3–4 who were low birth weight, preterm infants. *Neuropsychology* 18, 673–678.

Vohr, B. R., Wright, L. L., Dusick, A. M., Perritt, R., Poole, W. K., Tyson, J. E., Steichen, J. J., Bauer, C. R., Wilson-Costello, D. E., and Mayes, L. C. (2004). Center differences and outcomes of extremely low birth weight infants. *Pediatrics* 113, 781–789.

Vul, E., Harris, C., Winkielman, P., and Pashler, H. (2009). Puzzlingly high correlations in fMRI studies of emotion, personalty, and social cognition. *Perspect. Psychol. Sci.* 4, 274–290.

Wilson-Costello, D., Friedman, H., Minich, N., Fanaroff, A. A., and Hack, M. (2005). Improved survival rates with increased neurodevelopmental disability for extremely low birth weight infants in the 1990s. *Pediatrics* 115, 997–1003.

Wu, C. W., Gu, H., Lu, H., Stein, E. A., Chen, J. H., and Yang, Y. (2008). Frequency specificity of functional connectivity in brain networks. *Neuroimage* 42, 1047–1055.

Conflict of Interest Statement: The authors declare that the research was conducted in the absence of any commercial or financial relationships that could be construed as a potential conflict of interest.

Received: 06 February 2010; paper pending published: 25 February 2010; accepted: 19 May 2010; published online: 17 June 2010.

Citation: Damaraju E, Phillips J, Lowe JR, Ohls R, Calhoun VD and Caprihan A (2010) Resting-state functional connectivity differences in premature children. Front. Syst. Neurosci. ***4****:23. doi: 10.3389/fnsys.2010.00023*

frontiers in
SYSTEMS NEUROSCIENCE

ORIGINAL RESEARCH ARTICLE
published: 18 May 2010
doi: 10.3389/fnsys.2010.00010

Maturing thalamocortical functional connectivity across development

Damien A. Fair[1]*, Deepti Bathula[1], Kathryn L. Mills[1], Taciana G. Costa Dias[1], Michael S. Blythe[1], Dongyang Zhang[2], Abraham Z. Snyder[2], Marcus E. Raichle[2], Alexander A. Stevens[1,3], Joel T. Nigg[1,3] and Bonnie J. Nagel[1,3]*

[1] *Department of Psychiatry, Oregon Health and Science University, Portland, OR, USA*
[2] *Department of Radiology, Washington University School of Medicine, St. Louis, MO, USA*
[3] *Department of Behavioral Neuroscience, Oregon Health and Science University, Portland, OR, USA*

Edited by:
Lucina Q. Uddin, Stanford University, USA

Reviewed by:
Beatriz Luna, University of Pittsburgh, USA
Daniel Margulies, Max Planck Institute, Germany

****Correspondence:***
Damien A. Fair, Department of Psychiatry, Oregon Health and Science University, 3181 SW Sam Jackson Park Road UHN80R1, Portland, OR 97239, USA.
e-mail: damien.fair@aya.yale.edu;
Bonnie J. Nagel, Department of Psychiatry, Oregon Health and Science University, 3181 SW Sam Jackson Park Road DC7P, Portland, Oregon 97239, USA.
e-mail: nagelb@ohsu.edu

Recent years have witnessed a surge of investigations examining functional brain organization using resting-state functional connectivity MRI (rs-fcMRI). To date, this method has been used to examine systems organization in typical and atypical developing populations. While the majority of these investigations have focused on cortical–cortical interactions, cortical–subcortical interactions also mature into adulthood. Innovative work by Zhang et al. (2008) in adults have identified methods that utilize rs-fcMRI and known thalamo-cortical topographic segregation to identify functional boundaries in the thalamus that are remarkably similar to known thalamic nuclear grouping. However, despite thalamic nuclei being well formed early in development, the developmental trajectory of functional thalamo-cortical relations remains unexplored. Thalamic maps generated by rs-fcMRI are based on functional relationships, and should modify with the dynamic thalamo-cortical changes that occur throughout maturation. To examine this possibility, we employed a strategy as previously described by Zhang et al. to a sample of healthy children, adolescents, and adults. We found strengthening functional connectivity of the cortex with dorsal/anterior subdivisions of the thalamus, with greater connectivity observed in adults versus children. Temporal lobe connectivity with ventral/midline/posterior subdivisions of the thalamus weakened with age. Changes in sensory and motor thalamo-cortical interactions were also identified but were limited. These findings are consistent with known anatomical and physiological cortical–subcortical changes over development. The methods and developmental context provided here will be important for understanding how cortical–subcortical interactions relate to models of typically developing behavior and developmental neuropsychiatric disorders.

Keywords: development, thalamus, functional connectivity, subcortical, MRI, fcMRI, nuclei

INTRODUCTION

Recent years have witnessed a surge of investigations examining brain function and organization using the relatively new technique of resting-state functional connectivity MRI (rs-fcMRI) (Biswal et al., 1995). rs-fcMRI measures correlate, low frequency (usually <0.1 Hz) blood oxygenation level dependent (BOLD) fluctuations between brain regions while subjects are at rest, not performing goal-directed tasks (Biswal et al., 1995; Fox et al., 2005; Fair et al., 2007a,b, 2008; Fox and Raichle, 2007). By cross correlating the BOLD signal time series between different regions or voxels, one can determine which regions are 'functionally connected' (see Friston et al., 1993; Lee et al., 2003 for specific definition). To date, this method has been used in several domains to examine systems-level brain organization in typical and atypical populations (Biswal et al., 1995; Fox et al., 2006; Hampson et al., 2006; Andrews-Hanna et al., 2007; Dosenbach et al., 2007; Fair et al., 2007a, 2008, 2009; Greicius et al., 2007; Seeley et al., 2007; Uddin et al., 2008; Church et al., 2009).

Recent work has shown that rs-fcMRI is also quite useful for studying the maturation of functional brain networks. This work has led to key insights regarding typical and atypical brain development (Fair et al., 2007a, 2008, 2009; Fransson et al., 2007; Kelly et al., 2009; Supekar et al., 2009). Whereas the majority of these investigations have focused on cortical–cortical interactions, subcortical structures and their cortical interactions also develop during childhood and adolescence (Jones, 2007). Indeed, recent rs-fcMRI studies have suggested distinct developmental changes that occur between cortical and subcortical structures (Fair et al., 2007a, 2009; Kelly et al., 2009; Supekar et al., 2009). Thus, important insights regarding brain development are likely to emerge from additional examination of cortical–subcortical functional relationships.

Knowledge concerning the developmental trajectory of rs-fcMRI is especially lacking with regards to the thalamus, a key structure for nearly all brain operations. Innovative work by Zhang et al. (2008, 2009) in adults has recently used rs-fcMRI to map thalamo-cortical interactions. This methodology utilizes known cortical connectional anatomy (Alexander and Crutcher, 1990; Jones, 2007) to identify functional boundaries in the thalamus and other subcortical structures. In this procedure (Zhang et al., 2008), regions of interest (ROIs) are identified that encompass major subdivisions of the cortex (see **Figure 1**). The average spontaneous signal generated in each cortical ROI is then correlated with all of the voxels in the thalamus. Using a 'winner take all' strategy, where the cortical subdivision that correlates strongest with a given voxel 'wins,' Zhang et al. partitioned the thalamus into distinct subdivisions

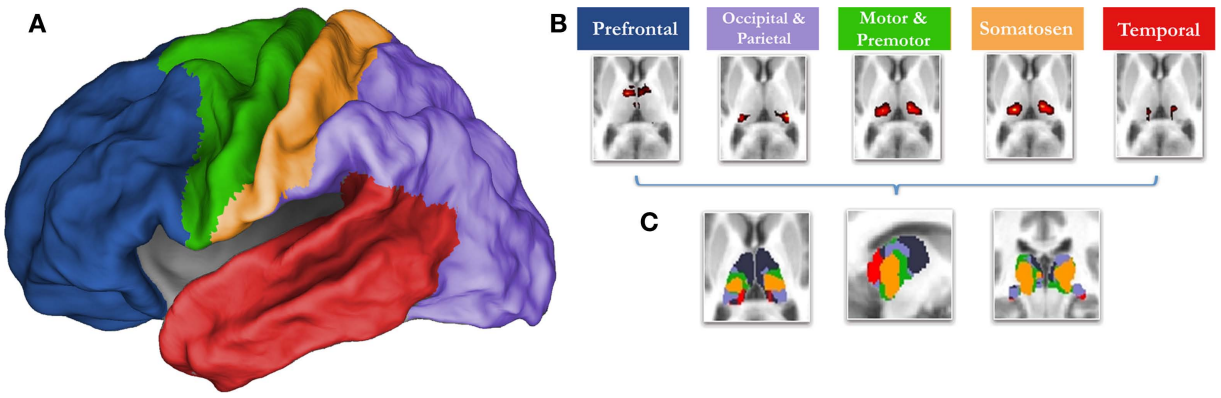

FIGURE 1 | The 'winner take all' strategy for identifying subdivisions of the thalamus (Zhang et al., 2008), utilizes known thalamocortical topographic segregation (Alexander and Crutcher, 1990; Jones, 2007) to identify functional boundaries in the thalamus. (A) Regions of interest (ROIs) used for the current analysis. These regions are composed of five disjoint cortical subdivisions, which include the prefrontal cortex (blue), motor/premotor (green), somatosensory (yellow), parietal/occipical cortex (purple), and temporal corex (red). **(B)** The average spontaneous signal generated from each cortical ROI is then correlated with all of the voxels in the thalamus. This creates five voxelwise statistical maps of the thalamus. **(C)** The strength of connectivity is then compared for each cortical ROI within each voxel. The cortical subdivision that correlates strongest with any given voxel 'wins.' The given voxel is then assigned the color of the winning cortical ROI. The resulting thalamic subdivisions are in substantial agreement with known thalamic nuclear grouping based on postmortem human studies (Morel, 2007; Mai et al., 2008) and anatomical track-tracing data from other mammalian species (Nieuwenhuys, 1988; Webster et al., 1995; Jones, 2007)

(**Figure 1**). The spatial organization of these thalamic subdivisions is in substantial agreement with known thalamic nuclear grouping based on postmortem human studies (Morel, 2007; Mai et al., 2008) and anatomical track-tracing data from other mammalian species (Nieuwenhuys, 1988; Webster et al., 1995; Jones, 2007). The rs-fcMRI results also are remarkably similar to tract-tracing results based on diffusion tensor imaging (DTI) (Behrens et al., 2003; Johansen-Berg et al., 2005; Zhang et al., 2009).

While anatomically distinct nuclear groups are well formed within the thalamus early in development (Jones, 2007), it is unknown whether thalamo-cortical fcMRI is the same in children and adults. Because the thalamic maps generated by fcMRI are based on functional relationships, we hypothesized they should not mimic organization found in adulthood, but should track the dynamic thalamocortical changes that are believed to occur throughout maturation (e.g., the pruning of temporal-thalamic contacts, and increased frontal-subcortical coherence over age) (Giedd et al., 1999; Jones, 2007; Galinanes et al., 2009). This developmental characterization between thalamus and cortex has the potential to lay the groundwork for a better understanding of how cortical–subcortical interactions contribute to the shift from reflexive, stimulus-bound behavior in childhood, to the goal-directed and more flexible functioning found in adulthood. It will also provide the neural context necessary to examine how cortical-thalamic interactions relate to prominent models of several developmental neuropsychiatric disorders. Hence, we employed a strategy previously detailed by Zhang et al. to study correlated spontaneous brain activity between the cortex and the thalamus in healthy children, adolescents, and adults.

MATERIALS AND METHODS

PARTICIPANTS

Participants were recruited through a combination of public advertisements, county mailings, and via the Oregon Health & Sciences University local outreach systems. Participants were screened with a series of interviews and questionnaires for inclusion. Informed consent was obtained from all subjects in accordance with the guidelines and approval of the Oregon Health & Science University Human Investigation Review Board. A total of 52 subjects (17 aged 7–9; 21 aged 11–16; 14 aged 19–32) were included in the study (see **Table 1**; **Table S1** in Supplementary Material). All participants were free of major sensory, medical, neurological, or psychiatric (including substance abuse) illness and had normal-range intelligence.

DATA ACQUISITION AND PROCESSING

Participants were scanned using a 3.0 Tesla Siemens Magnetom Tim Trio scanner with a twelve-channel head-coil at the OHSU Advanced Imaging Research Center (AIRC). One high resolution T1-weighted MPRAGE sequence (orientation = sagittal, TE = 3.58 ms, TR = 2300 ms, 256 × 256 matrix, resolution = $(1\ mm)^3$, 1 average, total scan time = 9 min 14 s) was collected. Blood-oxygen level dependent (BOLD)-weighted functional imaging was collected in an oblique plane (parallel to the ACPC line) using T2*-weighted echo-planar imaging. Resting data from adult participants were originally collected as part of a separate study. As such, acquisition parameters were slightly different for adults and children/adolescents (adults: TR = 2000 ms, TE = 30 ms, flip angle = 90°, FOV = 240 mm, 36 slices, slice thickness = 3.5 mm in-plane resolution = 3.75 mm^2; children: TR = 2000 ms, TE = 30 ms, flip angle = 90°, FOV = 240 mm, 36 slices covering the whole brain, slice thickness = 3.8 mm, in-plane resolution = 3.8 mm^2). Steady state magnetization was assumed after five frames (~10 s). The parameters for this acquisition have been optimized (e.g., oblique acquisition) to reduce susceptibility artifact, which causes signal drop out in orbitofrontal cortex. Three rest runs of 3.5-min duration obtained for all children. Two rest runs of 5-min duration were obtained for all adolescents and adults. During rest periods, subjects were verbally instructed to continue to stay still, view a

Table 1 | Subject characteristics.

	Adults		Adolescents		Children	
	Mean	**Std. Dev.**	**Mean**	**Std. Dev.**	**Mean**	**Std. Dev.**
Age	25.33	3.85	13.02	1.37	8.57	0.67
Mvmt. (rms)	0.36	0.40	0.41	0.21	0.34	0.33
Gender	%	N	%	N	%	N
Male	50	7	61.90	13	29.4	5
Female	50	7	38.10	8	70.6	12

cross in the middle of the screen, and be sure to stay awake. The stimulus display consisted of the standard fixation-cross in the center of the stimulus field.

Functional images were processed to reduce artifacts (Miezin et al., 2000). These steps included: (i) removal of a central spike caused by MR signal offset, (ii) correction of odd vs. even slice intensity differences attributable to interleaved acquisition without gaps, (iii) correction for head movement within and across runs, and (iv) within run intensity normalization to a whole brain mode value of 1000. Atlas transformation of the functional data was computed for each individual via the MP-RAGE scan. The fMRI data then were resampled (3 mm cubic voxels) in Talairach atlas space (Talairach and Tournoux, 1988) as defined by the spatial normalization procedure (Lancaster et al., 1995). This resampling combined movement correction and atlas transformation in one interpolation. All subsequent operations were performed on the atlas-transformed volumetric time series. For presentation purposes, voxel boundaries were interpolated to 1 mm^3 voxels and displayed using CARET software (Van Essen et al., 2001).

Participant head motion was measured and corrected using rigid body translation and rotation. Summary statistics were calculated as root mean square (RMS) values for translation and rotation about the *x*, *y*, and *z*-axes. Total RMS values were calculated on a run-by-run basis for each participant. BOLD runs with excessive movement (>2 mm RMS) were excluded from further analysis. Movement was relatively low in all groups (see **Table 1**).

FUNCTIONAL CONNECTIVITY PRE-PROCESSING

The functional data were additionally pre-processed in two ways for two separate analysis strategies, as outlined below. In the first analysis (total (marginal) correlation – see below) pre-processing was carried out as previously described (Fox et al., 2005; Fair et al., 2007a,b, 2008, 2009) to reduce spurious variance unlikely to reflect neuronal activity (Fox and Raichle, 2007). These steps included: (i) a temporal band-pass filter ($0.009\ Hz < f < 0.08\ Hz$), (ii) regression of six parameters obtained by rigid body head motion correction, (iii) regression of the whole brain signal averaged over the whole brain, (iv) regression of ventricular signal averaged from ventricular region of interest (ROI), and (v) regression of white matter signal averaged from a white matter ROI. Regression of first derivative terms for whole brain, ventricular, and white matter signals were also included in the correlation pre-processing. These pre-processing steps are, in part, intended to remove developmental changes in connectivity driven by changes in respiration and heart rate over age. Pre-processing in preparation for the second analysis (partial correlation – see below) was similar except that the whole brain signal was not included as a nuisance regressor. The correlation procedures associated with these two separate pre-processing strategies are described below (*in* Correlations between cortical subdivisions and thalamus).

CORTICAL ROI DEFINITION

Cortical ROI definition was as in Zhang et al. (2008). In short, the cortex in each hemisphere was partitioned into five subregions (**Figure 1**). The MP-RAGE image from a normal young adult volunteer (not included in this study) was segmented along the gray/white boundary and deformed to the population-average, landmark and surface-based (PALS)-B12 atlas (Van Essen, 2005) using SureFit and CARET software (Van Essen and Drury, 1997; Van Essen et al., 2001). Partition boundaries were manually drawn based on major sulcal landmarks, following work by Behrens et al. (2003). Five cortical ROIs were thus defined: (1) frontopolar and frontal cortex including the orbital surface and anterior cingulate; (2) motor and premotor cortex (Brodmann areas 6 and 4 – excluding adjacent portions of cingulate cortex); (3) somatosensory cortex (Brodmann areas 3, 1, 2, 5, and parts of 40); (4) parietal and occipital cortex including posterior cingulate and lingual gyrus; (5) temporal cortex including the lateral surface, temporal pole, and parahippocampal areas (**Figure 1**). For details see (Zhang et al., 2008, 2009).

CORRELATIONS BETWEEN CORTICAL SUBDIVISIONS AND THALAMUS

Resting state (fixation) data from 52 subjects (17 aged 7–9; 21 aged 11–16; 14 aged 19–32) were included in the analyses. The adolescent age range was chosen for two reasons. First, while there are several ways of defining adolescence, we chose an age-range that best encompasses the peripubertal years – a time of dynamic behavioral and neural maturation (Paus, 2005). By age 11, many children have initiated early pubertal processes (especially among females), and by age 16, most youth have attained pubertal maturation (Kreipe, 1992). The second consideration regarded our prior connectivity results, which have shown significant transitions in connectivity between similar age groups (e.g., see Fair et al., 2007a). All participants contributed between 420–630 s of resting-state data. The data were first analyzed with a total correlation procedure, which included whole brain signal regression in the initial pre-processing steps (see Functional Connectivity Pre-processing). In this case, for the five cortical subdivisions, an average resting state timeseries was extracted and correlated (r) with all voxels of the thalamus separately and for each individual. Shared variance among the five cortical subdivisions is accounted for in this instance with the initial whole brain signal regression. This procedure is similar to the total correlation procedure used in Zhang et al. (2008). In the second analysis, whole brain signal regression was not used in the initial pre-processing. Rather, shared variance was accounted for by partial correlation, wherein the correlation between a cortical ROI and the thalamus was computed after covarying out the other four cortical regions. Total correlation yielded slightly less specificity but more uniformity across subjects in comparison to partial correlation. In both analyses, to calculate statistical significance within each age group, we first applied Fischer's z transformation to the correlation coefficients (r) to improve normality. From here, these values were converted to Z scores by dividing by the square root of the variance within each group, as in Fox et al. (2005). Z-score maps were then

combined across subjects using a fixed effects analysis. Results presented here are restricted to the thalamus, whose boundaries were created by manual tracing of the atlas template. For the 'winner take all' strategy (see **Figure 3**), the cortical subdivision that correlated most strongly for any given voxel was assigned the designated color for the 'winning' cortical subdivision.

To test significant change over development, direct comparisons between the two end point groups, children and adults, were performed. This between-group end point approach, as opposed to using the entire sample, has been shown to be more robust to potential non-linear changes (Fair et al., 2006). For such direct comparisons, we performed two-sample, two-tailed *t*-tests (random effects analysis assuming unequal variance; $p \leq 0.05$) for each cortical subdivision applied to Fischer *z*-transformed *r* values. For the voxelwise, fixed effects maps, thresholding based on Monte Carlo simulation was implemented (Forman et al., 1995). To obtain multiple comparisons corrected, $p < 0.05$ voxel clusters, a threshold of 35 contiguous voxels with a *Z*-value > 2.5 was used. Maps showing statistically significant changes with age were uncorrected (as few voxels passed our stringent correction), and displayed with a threshold of $Z > 2$.

RESULTS

FUNCTIONAL CONNECTIVITY OF CORTICAL SUBDIVISIONS WITHIN THE THALAMUS IN ADULTS SHOW A SPATIAL ORGANIZATION IN AGREEMENT WITH KNOWN THALAMIC NUCLEAR GROUPING

Replicating prior reports, (Zhang et al., 2008, 2009), in our adult sample, correlations between the thalamus and each cortical subdivision were distinct, with substantial correspondence with known axonal connectivity with thalamic nuclei in primates (Jones, 2007; Morel, 2007). Specifically, the parietal-occipital cortical subdivision showed strong correlations with the lateral and posterior portions of the thalamus. This portion of the thalamus and dorsal brain stem are comprised of lateral pulvinar, lateral geniculate, and superior colliculus, which contain combinations of afferent input, and projections, to parietal occipital association areas and primary visual cortex (Lock et al., 2003; Jones, 2007) (see **Figure 2** – row 1, column 2; **Figure S1** in Supplementary Material). The temporal cortical ROI correlated strongly with medial, inferior, and posterior portions of the thalamus. This segment of the thalamus and dorsal brainstem presumptively corresponds to medial pulvinar, inferior/superior colliculi, medial geniculate, and medial dorsal nucleus (Webster et al., 1995; Jones, 2007), which have combinations of inputs from, and projections to, temporal cortex (see **Figure 2** – row 1, column 5; **Figure S2** in Supplementary Material). The prefrontal cortical subdivision showed strong interactions with dorsal, medial, and anterior portions of the thalamus. This thalamic area contains medial dorsal and the anterior nuclear groups, with inputs and outputs to cingulate and prefrontal portions of the cortex (Jones, 2007) (see **Figure 2** – row 1, column 1; **Figure S3** in Supplementary Material). Somatosensory cortical areas strongly correlated with ventral, lateral, and posterior thalamic regions, which presumptively correspond to ventral posteriolateral and posteriomedial nuclei (Jones, 2007); see **Figure 2**, row 1, column 4, and **Figure S4** in Supplementary Material. Finally, the motor cortex subdivision correlated strongly with lateral and ventral thalamic areas that presumptively correspond to ventral lateral and ventral anterior nuclei (see **Figure 2** – row 1, column 3; **Figure S5** in Supplementary Material). As can be seen in **Figure 3**, these findings are perhaps most clearly evident in 'winner take all' displays (Zhang et al., 2008, 2009); also see **Figure S6** in Supplementary Material).

FUNCTIONAL CONNECTIVITY OF CORTICAL SUBDIVISIONS WITH THE THALAMUS CHANGES SUBSTANTIALLY OVER DEVELOPMENT

Although thalamic nuclear groups are defined early in development (Jones, 2007), we saw substantial differences in connectivity patterns between our younger participants and adults. **Figure 2** (rows 1–3) suggests a transitional change from childhood, through adolescence, to adulthood for thalamo-frontal and thalamo-temporal interactions. Specifically, frontal lobe correlations are weak in childhood and appear to strengthen by adulthood. Temporal lobe correlations with the thalamus, however, are much stronger in children, and weaken progressively in adolescence and adulthood. This finding was obtained both by total correlation (**Figure 2**) and partial correlation analyses (**Figure S7** in Supplementary Material). The finding also held true when looking at raw correlation values (*r*), rather than *z* statistics (**Figure S8** in Supplementary Material).

This particular finding (i.e., increased thalamo-frontal interactions and decreased thalamo-temporal interactions over age) is clearly seen in the 'winner take all' displays. In adolescents (**Figure 3**), the picture was slightly modified from what was seen in the adult group. Along the midline bilaterally, the thalamo-temporal correlations encompassed a greater portion of anterior and midline thalamus, while frontal lobe correlations encompassed much less of the anterior portions of the thalamus. This trend, in which frontal (and to a lesser extent, motor) correlations give way to temporal correlations, was observed to an even greater extent in the youngest age group. In children, thalamo-temporal correlations were stronger and more widespread – not only encroaching on areas occupied by thalamo-frontal correlations in adults, but also parts of the thalamus functionally connected with motor/premotor, somatosensory, and occipital/parietal areas. In contrast, the spatial extent of the thalamo-frontal interaction was minimal in children and somewhat stronger in the adolescent group although, still limited relative to the adults. This dynamic can also be observed in **Movie S1–S4** in Supplementary Material. Again, **Figure S9** in Supplementary Material shows these findings were largely unchanged when using partial correlations. (Our child and adolescent groups had a slight excess of females and males, respectively. Accordingly, we repeated our analysis using equal numbers of males and females in each group. These findings, shown in **Figure S10** in Supplementary Material, suggest that gender had minimal effect on the overall patterns observed here.)

Direct statistical comparisons between children and adults confirmed the qualitative observations for the frontal–thalamic and temporal–thalamic interactions. Thalamo-cortical interactions observed with somatosensory cortex were qualitatively similar, but showed statistical differences between groups of both increased (lateral/inferior) and decreased (medial/dorsal) connectivity with specific parts of the thalamus (**Figure 4**). Similar findings were observed for motor-premotor cortex. Correlations with the occipital/parietal ROI appeared qualitatively unchanged across age groups. This observation was also confirmed with the direct statistical comparisons (**Figure 4**). The direct comparisons between children and adults using partial correlations (without whole brain

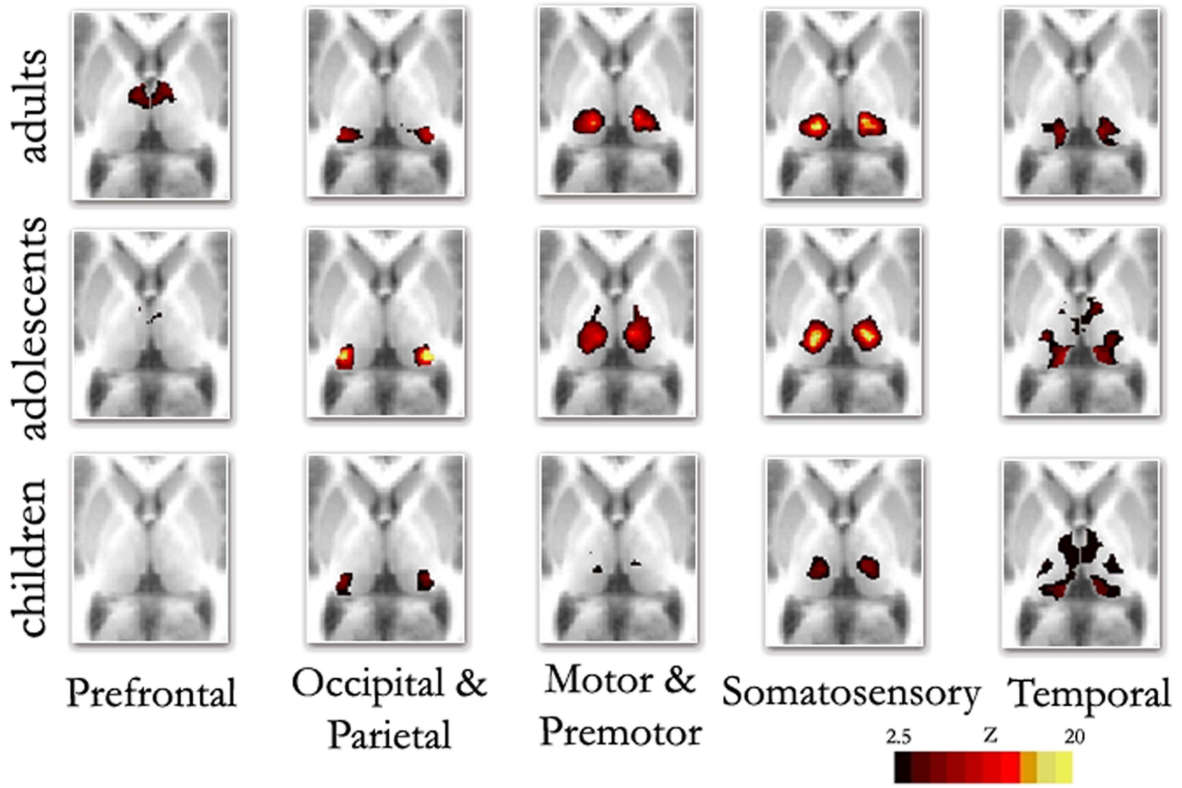

FIGURE 2 | Fixed effects functional mapping of the thalamus for each cortical ROI, in each age group (Children, Adolescents, Adults). This qualitative comparison appears to show substantial change over development regarding the thalamo-cortical functional interactions. The functional neuroanatomy of the adult group is quite similar to previous publications (Zhang et al., 2008, 2009). The most prominent differences between age groups shows frontal lobe interactions that are weaker in children and appear to increase over age. In contrast, temporal lobe interactions are much stronger in children, but weaken progressively in adolescents and adults: Transverse $Z = +8$

signal regression – **Figure S11** in Supplementary Material) were slightly different in that statistical differences observed between somatosensory and motor-premotor ROIs appeared weaker.

DISCUSSION

In this report we replicate prior findings that demonstrate spatially distinct BOLD correlations between the thalamus and specific cortical subdivisions that are in substantial correspondence with known thalamic connectivity in primates (Jones, 2007; Morel, 2007). We also saw significant development in thalamo-cortical correlations over maturation via rs-fcMRI. Specifically, we showed a progressive strengthening of functional connectivity of the frontal cortex with dorsal/anterior subdivisions of the thalamus. We also saw a systematic weakening of temporal lobe connectivity with ventral/midline/posterior subdivisions of the thalamus. Premotor-motor and somatosensory cortical subdivisions also showed increased connectivity in lateral/inferior portions of the thalamus and decreased connectivity in medial/dorsal portions of the thalamus. Occipital–parietal correlations with the thalamus were relatively stable over our samples.

Of note, considering the nature of the BOLD response, it is conceivable that developmental differences in the hemodynamic response could affect our results (D'Esposito et al., 2003). We feel this is unlikely considering reports suggesting that changes observed over development with fMRI are not the product of changes in hemodynamic response mechanisms over age (Kang et al., 2003; Wenger et al., 2004). Similarly, we also note that our observations could be affected by physiologic noise such as respirations and heart rate, but believe this is also unlikely for two reasons. First, most of these nuisance signals are likely removed with our band-pass filter and/or the removal of shared variance via partial correlations or whole brain signal regression. Second, the observations in this report (and elsewhere, Fair et al., 2007a, 2009; Kelly et al., 2009; Supekar et al., 2009) show age-related changes over development that occur in both directions (i.e., strengthen and weaken). It would be difficult to explain how a difference in heart rate or respiration could account for these opposing dynamics. With that said, it would be beneficial for future reports to include these additional physiologic noise parameters as regressors into the processing strategy of rs-fcMRI; however, it will be equally interesting in future reports to determine how brain oscillations might actually drive cardiac and respiratory fluctuations. Assuming that the age-related alterations described here represent true change in functional connections, the question then becomes: What are the neurobiological underpinnings of that change?

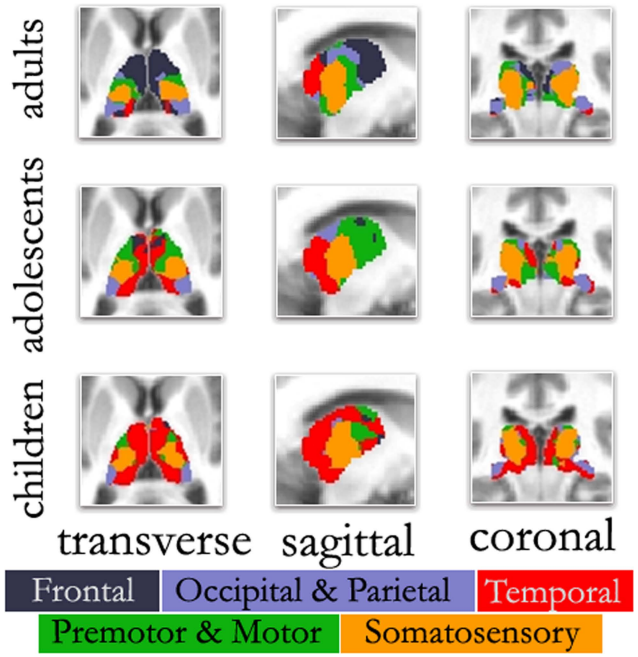

FIGURE 3 | 'Winner take all' displays across age. As previously observed, the color-coded thalamus based on the winner take all strategy in adults shows a functional organization that is remarkably similar to known nuclear groupings in the primate thalamus. However, the picture is different in adolescents and children. In agreement with **Figure 2**, in both adolescents and to a greater extent children, thalamo-temporal interactions encompass a greater portion of anterior and midline thalamus, while the frontal lobe interactions encompass much less of the anterior portions of the thalamus. In children, thalamo-temporal interactions not only encroach on areas that, in adults, are dominated by thalamo-frontal interactions, but also impinge on thalamic zones that later become functionally more connected with motor/premotor, somatosensory, and occipical/parietal cortex (also see Movies in Supplementary Material); Transverse $Z = +8$, Sagittal $X = -12$, Coronal $Y = -27$.

CHANGES IN THE FUNCTIONAL RELATIONSHIPS OF CORTICAL STRUCTURES WITH THE THALAMUS MAY, IN PART, REFLECT CHANGES IN THE UNDERLYING NEURAL SUBSTRATE

There are multiple sources of developmental change that may account for the changes in functional connectivity observed from the child to adult thalamus reported here. Based on comparisons of this method with similar methods using DTI in adults (Zhang et al., 2009), it is clear that some of the functional relationships seen here are related to large fiber-tracts connecting the cortex with specific subdivisions of the thalamus. This is not to say that nuclear groupings are not fully developed early in development (at birth thalamic nuclei are known to be composed of connectional and functionally distinct cell types; Jones, 2007). Nor is this to say that large fiber bundles are growing or being eliminated over the age span studied here; these are in place by ~9 months of age (Conel, 1939–1963). However, there does continue to be significant refinement in connectional anatomy that occurs well into young adulthood.

For example, axonal retraction and the elimination of axon collaterals continues throughout development and aging (O'Leary, 1989; Luo and O'Leary, 2005). Following a proliferation of synapses early in development, there is a protracted period of synaptic pruning that reaches adult levels in the late second decade of life (Huttenlocher, 1979; Huttenlocher et al., 1982; Elman et al., 1996; Huttenlocher and Dabholkar, 1997; Casey et al., 2005; Jones, 2007). Importantly, these regressive processes are not random. They are selective, reduce connectivity between specific regions, and occur in both cortical and subcortical structures (Ebbesson, 1980; Greenough et al., 1987; Luo and O'Leary, 2005; Jones, 2007).

Such phenomena may account for some of the findings shown here. For example, work conducted by Webster et al. (1995) in developing macaques provides a compelling parallel with regard to weakening thalamo-temporal connectivity over age. In this study, the authors compared the subcortical connections of inferior temporal cortex (Areas TE and TEO) in infant vs. adult monkeys. While the connectional anatomy was similar in infant and adult monkeys, there was significant refinement of the subcortical connections. Specifically, while projections from TE (and to a more limited extent TEO) to the nucleus medial dorsalis were present in infants and adults, they were more widespread in infants and significantly reduced in the adult animals. The same was true for connections from area TE projecting to the superior colliculus. Similar changes potentially occur in medial and polar aspects of the temporal lobe (Russchen et al., 1987). Importantly, both frontal and temporal cortical subdivisions share anatomical connections to the nucleus medial dorsalis (Webster et al., 1995; Jones, 2007), which is consistent with the thalamo-temporal and thalamo-frontal connectivity seen here (**Figure 3**). Hence, the refinement of inferior temporal lobe projections directly to nucleus medial dorsalis, may, in part, account for the reduced thalamo-temporal connectivity observed during development.

The reduced connectivity associated with somatosensory and motor-premotor cortical subdivisions is also likely related to similar phenomena as the temporal lobe. For example, in mice, relay neurons of the ventral posterior medial nucleus undergo significant dendritic refinement over age, with more than 300% reduction in the extent of their dendritic fields from age P6 to adulthood (Brown et al., 1995; Zantua et al., 1996; Jones, 2007). Work by Dennis O'Leary and colleagues (Luo and O'Leary, 2005) has shown in rodents, that cortical layer V neurons, after early extensive interstitial branching, acquire functionally appropriate connections through selective elimination, dictated by the cortical area in which the neuron is located. For example, in newborns, motor and visual neurons project to common targets in the brainstem and spinal cord. During maturation, functionally appropriate connections are acquired through selective axon elimination, determined by the cortical area (i.e., motor or visual) in which the neuron is located.

In addition to a reduction in thalamo-temporal correlations, we also demonstrated increased thalamo-frontal correlations across development. One commonly cited contributor to increased connectivity between regions is myelination. Indeed, myelination has been shown to be closely related to rs-fcMRI measures (Hagmann et al., 2008; Greicius et al., 2009) (although this has not yet been examined in children). Myelination increases at least through young adulthood. It proceeds from primary sensory and motor regions to association areas (Flechsig, 1920;

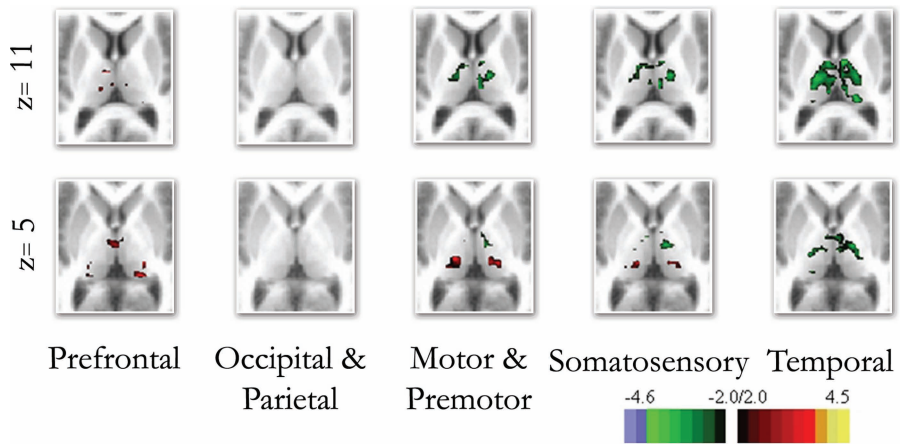

FIGURE 4 | Direct comparison between the end groups (i.e., children and adults). The direct comparison between children and adults confirmed many of the qualitative findings shown in **Figure 3**. Frontal connectivity with the thalamus increases with age, and Temporal connectivity with the thalamus weakens with age. Differences in connectivity between children and adults with premotor/motor and somatosensory cortex were also revealed with the direct comparisons, while the occipical/parietal ROI showed very little difference between the groups.

Brody et al., 1987; Paus et al., 2001; Sowell et al., 2002), roughly following the hierarchical organization introduced by Felleman and Van Essen (1991). As such, increased signal propagation, through the maturation of the myelin sheath, is a likely contributor to the increased interaction between the frontal cortex and subregions of the thalamus, particularly those in the anterior and medial dorsal portion (Luna and Sweeney, 2004; Fair et al., 2007a, 2008; Kelly et al., 2009).

CHANGES IN THE FUNCTIONAL RELATIONSHIPS OF CORTICAL STRUCTURES WITH THE THALAMUS LIKELY REFLECT CHANGES BEYOND THE MATURING NEURAL SUBSTRATE

Changes in cortical-subcortical dynamics, particularly with the frontal cortex, are likely not solely due to changes in the underlying neural substrate (Honey et al., 2007; Fair et al., 2009; Lewis et al., 2009). It is now apparent that the connectivity signal measured via rs-fcMRI is not a pure representation of monosynaptic anatomical connectivity (Vincent et al., 2007; Hagmann et al., 2008; Zhang et al., 2008), and thus, other explanations must be considered. For example, modeling work has shown that complex spatial and temporal patterns of synchronous activity can develop over time in the absence of external input and without changes in the neuroanatomy (Honey et al., 2007). Other work by Galinanes et al. (2009) has shown, in mice, that subcortical neurons in the striatum are more temporally tuned to frontal cortical rhythms in adults than they are in infancy (i.e., they are more strongly functionally connected – albeit in different frequency ranges than examined here). Importantly, Galinanes found that these changes in functional properties are unlikely to be secondary to direct development of anatomical changes per se, but rather the modulation of functional properties through the maturation of the dopaminergic system. While this work targeted the striatum, similar phenomena could be occurring indirectly (or directly) in the thalamus without direct changes in the gross neuroanatomy, and independently of myelination.

These types of functional changes identified by Galinanes and colleagues highlight an important aspect regarding thalamic organization and the developmental changes observed in this report. As put by Sherman and Guillery (2006), 'It is important to distinguish the functional input that carries the messages for transmission to the cortex, the driver, from the many other inputs, the modulators, which can modify the way in which the message is transmitted…' The circuitry of the thalamus is complex. Its function is determined not only by the driver connectional anatomy to the cortex, but also modulators (interneurons, other subcortical inputs, various neurotransmitter systems) (Sherman and Guillery, 2006; Jones, 2007). Indeed, throughout the thalamus, driver synapses to relay cells encompass only a fraction of the total number synapses (~2–10%) (Sherman and Guillery, 2006). To the contrary, modulatory synapses to relay cells account for over 90% of synaptic contacts with relay neurons. Importantly, many properties related to modulatory action continue to develop postnatally (Jones, 2007). Hence, it is likely that increases and decreases in thalamo-cortical connectivity seen here over age are influenced by maturation of modulatory systems (Jones, 2007).

FUTURE DIRECTIONS

In this report, we showed dynamic maturing functional interactions between the thalamus and cortex. The gross partitioning of cortical regions, as used in the present study, is adequate to produce connectivity maps with thalamic nuclei that are consistent with known structural connectivity, and is promising. In addition, there appears to be little difference in results obtained by partial vs. total correlation analysis. However, it is important to note that while the currently applied methods appear well suited for identifying distinct subcortical structures in adults, they do not provide the same specificity in children. This difference likely reflects functional and anatomic maturational mechanisms. Alternative rs-fcMRI techniques may be better suited for identifying nuclear

groupings specific to children and adolescents (e.g., Cohen et al., 2008; Margulies et al., 2009). Other complementary connectivity methods may additionally assist in differentiating changes across development related to extent versus strength or magnitude in connectivity. For example, as noted in the Introduction section, anatomically distinct nuclear groups and large fiber tracts are well formed within the thalamus early in development (Jones, 2007). As such, anatomically based methods that utilize large fiber bundles (see Behrens et al., 2003; Asato et al., 2010, as opposed to functionally based methods, may prove successful in further differentiating nuclear groupings and extent of connectivity in children.

In future work it will also be necessary to observe how changes in thalamo-cortical functional connectivity relate to developmental changes in behavior. It is likely that the cortical-subcortical interactions observed here will correspond to a shift from reflexive, stimulus-bound behavior in childhood, to the goal-directed, self-organized, and more flexible functioning in young adulthood (Stuss, 1992) – a distinct hypothesis that can be tested. For example, recent theories suggest that, during childhood and early adolescence, goal-directed behavior is governed by principles of approach and avoidance, with regulation and balance of this system developing across adolescence and into adulthood (Ernst et al., 2009). While early approach and avoidance is thought to be subserved by subcortical and limbic brain regions (consistent with greater thalamo-temporal interactions in children), emerging control of these affective and appetitive behaviors (among others – see Bunge et al., 2002) occurs in concert with the maturation of subcortical to prefrontal cortex interactions (consistent with emerging increased thalamo-frontal interactions shown across our sample) (Chambers et al., 2003; Casey et al., 2008). Along the same lines, identifying how these cortical–subcortical interactions relate to models of neuropsychiatric disorders will also be of interest in future work.

ACKNOWLEDGMENTS

Research was supported by the Oregon Clinical and Translational Research Institute (Fair), Medical Research Foundation (Fair), UNCF Merck postdoctoral fellowship (Fair), Ford Foundation (Fair), R01 MH59105 (Nigg), NS06833 (Raichle), K08 NS52147 (Nagel), Portland Alcohol Research Center (P60 AA010760 – Nagel), and the OHSU Neuropsychiatric Institute (Nigg).

SUPPLEMENTARY MATERIAL

The Supplementary Material for this article can be found online at http://www.frontiersin.org/systemsneuroscience/paper/10.3389/fnsys.2010.00010/

REFERENCES

Alexander, G. E., and Crutcher, M. D. (1990). Basal ganglia-thalamocortical circuits: parallel substrates for motor,oculomotor,prefrontal and limbic functions. *Prog. Brain Res.* 85, 119–146.

Andrews-Hanna, J. R., Snyder, A. Z., Vincent, J. L., Lustig, C., Head, D., Raichle, M. E., and Buckner, R. L. (2007). Disruption of large-scale brain systems in advanced aging. *Neuron* 56, 924–935.

Asato, M. R., Terwilliger, R., Woo, J., and Luna, B. (2010). White matter development in adolescence: a DTI study. *Cereb. Cortex*. doi:10.1093/cercor/bhp282.

Behrens, T. E., Johansen-Berg, H., Woolrich, M. W., Smith, S. M., Wheeler-Kingshott, C. A., Boulby, P. A., Barker, G. J., Sillery, E. L., Sheehan, K., Ciccarelli, O., Thompson, A. J., Brady, J. M., and Matthews, P. M. (2003). Non-invasive mapping of connections between human thalamus and cortex using diffusion imaging. *Nat. Neurosci.* 6, 750–757.

Biswal, B., Yetkin, F. Z., Haughton, V. M. and Hyde, J. S. (1995). Functional connectivity in the motor cortex of resting human brain using echo-planar MRI. *Magn. Reson. Med.* 34, 537–541.

Brody, B. A., Kinney, H. C., Kloman, A. S., and Gilles, F. H. (1987). Sequence of central nervous system myelination in human infancy. I. An autopsy study of myelination. *J. Neuropathol. Exp. Neurol.* 46, 283–301.

Brown, K. E., Arends, J. J., Wasserstrom, S. P., Zantua, J. B., Jacquin, M. F., and Woolsey, T. A. (1995). Developmental transformation of dendritic arbors in mouse whisker thalamus. *Brain Res. Dev. Brain Res.* 86, 335–339.

Bunge, S. A., Dudukovic, N. M., Thomason, M. E., Vaidya, C. J., and Gabrieli, J. D. (2002). Immature frontal lobe contributions to cognitive control in children: evidence from fMRI. *Neuron* 33, 301–311.

Casey, B. J., Jones, R. M., and Hare, T. A. (2008). The adolescent brain. *Ann. N. Y. Acad. Sci.* 1124, 111–126.

Casey, B. J., Tottenham, N., Liston, C., and Durston, S. (2005). Imaging the developing brain: what have we learned about cognitive development? *Trends Cogn. Sci.* 9, 104–110.

Chambers, R. A., Taylor, J. R., and Potenza, M. N. (2003). Developmental neurocircuitry of motivation in adolescence: a critical period of addiction vulnerability. *Am. J. Psychiatry* 160, 1041–1052.

Church, J. A., Fair, D. A., Dosenbach, N. U., Cohen, A. L., Miezin, F. M., Petersen, S. E., and Schlaggar, B. L. (2009). Control networks in paediatric Tourette syndrome show immature and anomalous patterns of functional connectivity. *Brain* 132(Pt 1), 225–238.

Cohen, A. L., Fair, D. A., Dosenbach, N. U., Miezin, F. M., Dierker, D., Van Essen, D. C., Schlaggar, B. L., and Petersen, S. E. (2008). Defining functional areas in individual human brains using resting functional connectivity MRI. *Neuroimage* 41, 45–57.

Conel, J. L. (1939–1963). *The Postnatal Development of the Human Cerebral Cortex*. Cambridge, MA: Harvard University Press.

D'Esposito, M., Deouell, L. Y., and Gazzaley, A. (2003). Alterations in the BOLD fMRI signal with ageing and disease: a challenge for neuroimaging. *Nat. Rev. Neurosci.* 4, 863–872.

Dosenbach, N. U., Fair, D. A., Miezin, F. M., Cohen, A. L., Wenger, K. K., Dosenbach, R. A. T., Fox, M. D., Snyder, A. Z., Vincent, J. L., Raichle, M. E., Schlaggar, B. L., and Petersen, S. E. (2007). Distinct brain networks for adaptive and stable task control in humans. *PNAS* 104, 11073–11078.

Ebbesson, S. O. (1980). The parcellation theory and its relation to interspecific variability in brain organization, evolutionary and ontogenetic development, and neuronal plasticity. *Cell Tissue Res.* 213, 179–212.

Elman, J. L., Bates, E. A., Johnson, M. H., and Karmiloff-Smith, A. (1996). *Rethinking Innateness: A Connectionist Perspective on Development*. Cambridge, MA: The MIT Press.

Ernst, M., Romeo, R. D., and Andersen, S. L. (2009). Neurobiology of the development of motivated behaviors in adolescence: a window into a neural systems model. *Pharmacol. Biochem. Behav.* 93, 199–211.

Fair, D. A., Brown, T. T., Petersen, S. E., and Schlaggar, B. L. (2006). A comparison of ANOVA and correlation methods for investigating cognitive development with fMRI. *Dev. Neuropsychol.* 30, 531–546.

Fair, D. A., Cohen, A. L., Dosenbach, N. U., Church, J. A., Miezin, F. M., Barch, D. M., Raichle, M. E., Petersen, S. E., and Schlaggar, B. L. (2008). The maturing architecture of the brain's default network. *PNAS* 105, 4028–4032.

Fair, D. A., Cohen, A. L., Power, J. D., Dosenbach, N. U., Church, J. A., Miezin, F. M., Schlaggar, B. L., and Petersen, S. E. (2009). Functional brain networks develop from a "local to distributed" organization. *PLoS Comput. Biol.* 5, e1000381. doi: 10.1371/journal.pcbi.1000381.

Fair, D. A., Dosenbach, N. U. F., Church, J. A., Cohen, A. L., Brahmbhatt, S., Miezin, F. M., Barch, D. M., Raichle, M. E., Petersen, S. E., and Schlaggar, B. L. (2007a). Development of distinct control networks through segregation and integration. *PNAS* 104, 13507–13512.

Fair, D. A., Schlaggar, B. L., Cohen, A. L., Miezin, F. M., Dosenbach, N. U., Wenger, K. K., Fox, M. D., Snyder, A. Z., Raichle, M. E., and Petersen, S. E. (2007b). A method for using blocked and event-related fMRI data to study "resting state" functional connectivity. *Neuroimage* 35, 396–405.

Felleman, D. J., and Van Essen, D. C. (1991). Distributed hierarchical processing in the primate cerebral cortex. *Cereb. Cortex* 1, 1–47.

Flechsig, P. E. (1920). *Anatomie des Menschlichen Gehirn und Ruckenmarks, auf Myelogenetischer Grundlage*. Leipzig: G. Thieme.

Forman, S. D., Cohen, J. D., Fitzgerald, M., Eddy, W. F., Mintun, M. A., and Noll, D. C. (1995). Improved assessment of significant activation in functional magnetic resonance imaging (fMRI): use of a cluster-size threshold. *Magn. Reson. Med.* 33, 636–647.

Fox, M. D., Corbetta, M., Snyder, A. Z., Vincent, J. L., and Raichle, M. E. (2006). Spontaneous neuronal activity distinguishes human dorsal and ventral attention systems. *PNAS* 103, 10046–10051.

Fox, M. D., and Raichle, M. E. (2007). Spontaneous fluctuations in brain activity observed with functional magnetic resonance imaging. *Nat. Rev. Neurosci.* 8, 700–711.

Fox, M. D., Snyder, A. Z., Vincent, J. L., Corbetta, M., Van Essen, D. C., and Raichle, M. E. (2005). The human brain is intrinsically organized into dynamic, anticorrelated functional networks. *PNAS* 102, 9673–9678.

Fransson, P., Skiold, B., Horsch, S., Nordell, A., Blennow, M., Lagercrantz, H., and Aden, U. (2007). Resting-state networks in the infant brain. *PNAS* 104, 15531–15536.

Friston, K. J., Frith, C. D., and Frackowiak, R. S. J. (1993). Time-dependent changes in effective connectivity measured with PET. *Hum. Brain Mapp.* 1, 69–80.

Galinanes, G. L., Taravini, I. R., and Murer, M. G. (2009). Dopamine-dependent periadolescent maturation of corticostriatal functional connectivity in mouse. *J. Neurosci.* 29, 2496–2509.

Giedd, J. N., Blumenthal, J., Jeffries, N. O., Castellanos, F. X., Liu, H., Zijdenbos, A., Paus, T., Evans, A. C., and Rapoport, J. L. (1999). Brain development during childhood and adolescence: a longitudinal MRI study. *Nat. Neurosci.* 2, 861–863.

Greenough, W. T., Black, J. E., and Wallace, C. S. (1987). Experience and brain development. *Child Dev.* 58, 539–559.

Greicius, M. D., Flores, B. H., Menon, V., Glover, G. H., Solvason, H. B., Kenna, H., Reiss, A. L., and Schatzberg, A. F. (2007). Resting-state functional connectivity in major depression: abnormally increased contributions from subgenual cingulate cortex and thalamus. *Biol. Psychiatry* 62, 429–437.

Greicius, M. D., Supekar, K., Menon, V., and Dougherty, R. F. (2009). Resting-state functional connectivity reflects structural connectivity in the default mode network. *Cereb. Cortex* 19, 72–78.

Hagmann, P., Cammoun, L., Gigandet, X., Meuli, R., Honey, C. J., Wedeen, V. J., and Sporns, O. (2008). Mapping the structural core of human cerebral cortex. *PLoS Biol.* 6, e159. doi: 10.1371/journal.pbio.0060159.

Hampson, M., Driesen, N. R., Skudlarski, P., Gore, J. C., and Constable, R. T. (2006). Brain connectivity related to working memory performance. *J. Neurosci.* 26, 13338–13343.

Honey, C., Kotter, R., Breakspear, M., and Sporns, O. (2007). Network structure of cerebral cortex shapes functional connectivity on multiple time scales. *PNAS* 104, 10240–10245.

Huttenlocher, P. R. (1979). Synaptic density in human frontal cortex – developmental changes and effects of aging. *Brain Res.* 163, 195–205.

Huttenlocher, P. R., and Dabholkar, A. S. (1997). Regional differences in synaptogenesis in human cerebral cortex. *J. Comp. Neurol.* 387, 167–178.

Huttenlocher, P. R., de Courten, C., Garey, L. J., and Van der Loos, H. (1982). Synaptogenesis in human visual cortex – evidence for synapse elimination during normal development. *Neurosci. Lett.* 33, 247–252.

Johansen-Berg, H., Behrens, T. E., Sillery, E., Ciccarelli, O., Thompson, A. J., Smith, S. M., and Matthews, P. M. (2005). Functional-anatomical validation and individual variation of diffusion tractography-based segmentation of the human thalamus. *Cereb. Cortex* 15, 31–39.

Jones, E. G. (2007). *The Thalamus*. Cambridge, UK: University Press.

Kang, H.-S. C., Burgund, E. D., Lugar, H. M., Petersen, S. E., and Schlaggar, B. L. (2003). Comparison of functional activation foci in children and adults using a common stereotactic space. *Neuroimage* 19, 16–28.

Kelly, A. M., Di Martino, A., Uddin, L. Q., Shehzad, Z., Gee, D. G., Reiss, P. T., Margulies, D. S., Castellanos, F. X., and Milham, M. P. (2009). Development of anterior cingulate functional connectivity from late childhood to early adulthood. *Cereb. Cortex* 19, 640–657.

Kreipe, R. (1992). "Normal somatic adolescent growth and development," in *Textbook of Adolescent Medicine*, ed. L. Bralow (Philadelphia: W.B. Sounders Company), 44–67.

Lancaster, J. L., Glass, T. G., Lankipalli, B. R., Downs, H., Mayberg, H., and Fox, P. T. (1995). A modality-independent approach to spatial normalization of tomographic images of the human brain. *Hum. Brain Mapp.* 3, 209–223.

Lee, L., Harrison, L. M., and Mechelli, A. (2003). A report of the functional connectivity workshop, Dusseldorf 2002. *Neuroimage* 19(Pt 1), 457–465.

Lewis, C. M., Baldassarre, A., Committeri, G., Romani, G. L., and Corbetta, M. (2009). Learning sculpts the spontaneous activity of the resting human brain. *PNAS* 106, 17558–17563.

Lock, T. M., Baizer, J. S., and Bender, D. B. (2003). Distribution of corticotectal cells in macaque. *Exp. Brain Res.* 151, 455–470.

Luna, B., and Sweeney, J. A. (2004). The emergence of collaborative brain function: FMRI studies of the development of response inhibition. *Ann. N. Y. Acad. Sci.* 1021, 296–309.

Luo, L., and O'Leary, D. D. (2005). Axon retraction and degeneration in development and disease. *Annu. Rev. Neurosci.* 28, 127–156.

Mai, J., Paxinos, G., and Voss, T. (2008). *Atlas of the Human Brain*. Amsterdam: Elsevier/Academic Press.

Margulies, D. S., Vincent, J. L., Kelly, C., Lohmann, G., Uddin, L. Q., Biswal, B. B., Villringer, A., Castellanos, F. X., Milham, M. P., and Petrides, M. (2009). Precuneus shares intrinsic functional architecture in humans and monkeys. *PNAS* 106, 20069–20074.

Miezin, F., Maccotta, L., Ollinger, J., Petersen, S., and Buckner, R. (2000). Characterizing the hemodynamic response: effects of presentation rate, sampling procedure, and the possibility of ordering brain activity based on relative timing. *Neuroimage* 11, 735–759.

Morel, A. (2007). *Stereotactic Atlas of the Human Thalamus and Basal Ganglia*. New York: Informa Healthcare.

Nieuwenhuys, R. (1988). *The Human Central Nervous System: A Synopsis and Atlas*. New York: Springer-Verlag.

O'Leary, D. D. M. (1989). Do cortical areas emerge from a protocortex? *Trends Neurosci.* 12, 400–406.

Paus, T. (2005). Mapping brain maturation and cognitive development during adolescence. *Trends Cogn. Sci. (Regul. Ed.)* 9, 60–68.

Paus, T., Collins, D. L., Evans, A. C., Leonard, G., Pike, B., and Zijdenbos, A. (2001). Maturation of white matter in the human brain: a review of magnetic resonance studies. *Brain Res. Bull.* 54, 255–266.

Russchen, F. T., Amaral, D. G., and Price, J. L. (1987). The afferent input to the magnocellular division of the mediodorsal thalamic nucleus in the monkey, *Macaca fascicularis*. *J. Comp. Neurol.* 256, 175–210.

Seeley, W. W., Menon, V., Schatzberg, A. F., Keller, J., Glover, G. H., Kenna, H., Reiss, A. L., and Greicius, M. D. (2007). Dissociable intrinsic connectivity networks for salience processing and executive control. *J. Neurosci.* 27, 2349–2356.

Sherman, S. M., and Guillery, R. W. (2006). *Exploring the Thalamus and Its Role in Cortical Function*. Cambridge: MIT Press.

Sowell, E. R., Trauner, D. A., Gamst, A., and Jernigan, T. L. (2002). Development of cortical and subcortical brain structures in childhood and adolescence: a structural MRI study. *Dev. Med. Child Neurol.* 44, 4–16.

Stuss, D. T. (1992). Biological and psychological development of executive functions. *Brain Cogn.* 20, 8–23.

Supekar, K., Musen, M., and Menon, V. (2009). Development of large-scale functional brain networks in children. *PLoS Biol.* 7, e1000157. doi: 10.1371/journal.pbio.1000157.

Talairach, J., and Tournoux, P. (1988). *Co-Planar Stereotaxic Atlas of the Human Brain*. New York: Thieme Medical Publishers, Inc.

Uddin, L. Q., Kelly, A. M., Biswal, B. B., Margulies, D. S., Shehzad, Z., Shaw, D., Ghaffari, M., Rotrosen, J., Adler, L. A., Castellanos, F. X., and Milham, M. P. (2008). Network homogeneity reveals decreased integrity of default-mode network in ADHD. *J. Neurosci. Methods* 169, 249–254.

Van Essen, D. C. (2005). A population-average, landmark- and surface-based (PALS) atlas of human cerebral cortex. *Neuroimage* 28, 635–662.

Van Essen, D. C., Dickson, J., Harwell, J., Hanlon, D., Anderson, C. H., and Drury, H. A. (2001). An integrated software suite for surface-based analyses of cerebral cortex. *J. Am. Med. Inform. Assoc.* 41, 1359–1378. Available at: http://brainmap.wustl.edu/caret.

Van Essen, D. C., and Drury, H. A. (1997). Structural and functional analyses of human cerebral cortex using a surface-based atlas. *J. Neurosci.* 17, 7079–7102.

Vincent, J. L., Patel, G. H., Fox, M. D., Snyder, A. Z., Baker, J. T., Van Essen, D. C., Zempel, J. M., Snyder, L. H., Corbetta, M., and Raichle, M. E. (2007). Intrinsic functional architecture in the anesthetized monkey brain. *Nature* 447, 46–47.

Webster, M. J., Bachevalier, J., and Ungerleider, L. G. (1995). Transient subcortical connections of inferior temporal areas TE and TEO in infant macaque monkeys. *J. Comp. Neurol.* 352, 213–226.

Wenger, K. K., Visscher, K. M., Miezin, F. M., Petersen, S. E., and Schlaggar, B. L. (2004). Comparison of sustained and transient activity in children and adults using a mixed blocked/event-

related fMRI design. *Neuroimage* 22, 975–985.

Zantua, J. B., Wasserstrom, S. P., Arends, J. J., Jacquin, M. F., and Woolsey, T. A. (1996). Postnatal development of mouse "whisker" thalamus: ventroposterior medial nucleus (VPM), barreloids, and their thalamocortical relay neurons. *Somatosens. Mot. Res.* 13, 307–322.

Zhang, D., Snyder, A. Z., Fox, M. D., Sansbury, M. W., Shimony, J. S., and Raichle, M. E. (2008). Intrinsic functional relations between human cerebral cortex and thalamus. *J. Neurophysiol.* 100, 1740–1748.

Zhang, D., Snyder, A. Z., Shimony, J. S., Fox, M. D., and Raichle, M. E. (2009). Noninvasive functional and structural connectivity mapping of the human thalamocortical system. *Cereb. Cortex* 20, 1187–1194.

Conflict of Interest Statement: The authors declare that the research was conducted in the absence of any commercial or financial relationships that could be construed as a potential conflict of interest.

Received: 05 February 2010; paper pending published: 01 March 2010; accepted: 06 April 2010; published online: 18 May 2010.

Citation: Fair DA, Bathula D, Mills KL, Dias TGC, Blythe MS, Zhang D, Snyder AZ, Raichle ME, Stevens AA, Nigg JT and Nagel BJ (2010) Maturing thalamocortical functional connectivity across development. Front. Syst. Neurosci. ***4****:10. doi: 10.3389/fnsys.2010.00010*

frontiers in
SYSTEMS NEUROSCIENCE

ORIGINAL RESEARCH ARTICLE
published: 17 June 2010
doi: 10.3389/fnsys.2010.00022

Network scaling effects in graph analytic studies of human resting-state fMRI data

***Alex Fornito*[1,2]*, *Andrew Zalesky*[2] *and Edward T. Bullmore*[1,3]**

[1] *Department of Psychiatry, Brain Mapping Unit, University of Cambridge, UK*
[2] *Melbourne Neuropsychiatry Centre, Department of Psychiatry, University of Melbourne, Melbourne, VIC, Australia*
[3] *GSK Clinical Unit Cambridge, Addenbrooke's Hospital, Cambridge, UK*

Edited by:
Lucina Q. Uddin, Stanford University, USA

Reviewed by:
Mika Rubinov, The University of New South Wales, Australia
Jason Bohland, Boston University, USA
Dante R. Chialvo, Northwestern University, USA

***Correspondence:**
Alex Fornito, Melbourne Neuropsychiatry Centre, Levels 2 & 3, 161 Barry St, Carlton South, Victoria, 3053 Australia.
e-mail: af397@cam.ac.uk

Graph analysis has become an increasingly popular tool for characterizing topological properties of brain connectivity networks. Within this approach, the brain is modeled as a graph comprising *N* nodes connected by *M* edges. In functional magnetic resonance imaging (fMRI) studies, the nodes typically represent brain regions and the edges some measure of interaction between them. These nodes are commonly defined using a variety of regional parcellation templates, which can vary both in the volume sampled by each region, and the number of regions parcellated. Here, we sought to investigate how such variations in parcellation templates affect key graph analytic measures of functional brain organization using resting-state fMRI in 30 healthy volunteers. Seven different parcellation resolutions (84, 91, 230, 438, 890, 1314, and 4320 regions) were investigated. We found that gross inferences regarding network topology, such as whether the brain is small-world or scale-free, were robust to the template used, but that both absolute values of, and individual differences in, specific parameters such as path length, clustering, small-worldness, and degree distribution descriptors varied considerably across the resolutions studied. These findings underscore the need to consider the effect that a specific parcellation approach has on graph analytic findings in human fMRI studies, and indicate that results obtained using different templates may not be directly comparable.

Keywords: spontaneous, BOLD, complex, cortex

INTRODUCTION

Our perceptions, thoughts, emotions and experiences are the product of dynamic interactions occurring between functionally specialized regions of the brain. Thus, a complete understanding of such phenomena will only be possible once we understand how these interactions are organized and coordinated. An important step toward this goal involves developing detailed maps of the brain's connectivity architecture, the so-called neural connectome (Sporns et al., 2005), at either the anatomical or functional level, at varying spatio-temporal resolutions.

Recent work on functional brain networks has focused on characterizing connectivity patterns of spontaneous, low-frequency (<0.1 Hz) fluctuations of the blood-oxygenation-level-dependent (BOLD) signal measured using functional Magnetic Resonance Imaging (fMRI). This followed seminal observations that such fluctuations show a high degree of coherence and spatial organization when participants are not engaged in a specific task; a condition commonly referred to as the resting-state (Biswal et al., 1995; Beckmann et al., 2005; Fox et al., 2005; Salvador et al., 2005a,b). The organization of these resting-state networks recapitulates functional networks observed across a range of cognitive, emotional, motor, and perceptual tasks (Fox et al., 2006; Vincent et al., 2007; Smith et al., 2009). They are robust across individuals and time (Damoiseaux et al., 2006; Buckner et al., 2009; Shehzad et al., 2009), can affect task-evoked activity (Fox and Raichle, 2007; Hesselmann et al., 2008), correlate with behavioral measures (Seeley et al., 2007; Kelly et al., 2008; van den Heuvel et al., 2009), and emerge from underlying neuronal dynamics (Nir et al., 2007; Shmuel and Leopold, 2008). Such observations have led to the postulate that these so-called resting-state networks represent an intrinsic property of functional brain organization (Fox and Raichle, 2007). They therefore provide an attractive means by which to characterize functional connectome properties.

One method for understanding rs-fMRI connectivity at a whole-brain level is graph analysis. Within this framework, the brain is represented as a graph comprising *N* nodes connected by *M* edges. In fMRI analyses, the nodes typically correspond to brain regions and the edges to some measure of inter-regional interaction, such as a supra-threshold temporal correlation between regional time series. Representing the brain in this way enables the application of a rich set of mathematical tools and theoretical concepts to understand brain network topology and dynamics (Strogatz, 2001; Albert and Barabasi, 2002; Newman, 2003; Bullmore and Sporns, 2009; Rubinov and Sporns, 2009). In particular, graph analytic studies of rs-fMRI data have demonstrated that functional brain networks display a small-world topology which provides high communication efficiency for relatively low connection cost, high resilience to random and targeted attack, and a hierarchical modular organization which offers optimal adaptability to varying circumstances (Simon, 1962; Achard et al., 2006; Achard and Bullmore, 2007; Bullmore and Sporns, 2009; Meunier et al., 2009). These properties can be compromised by disease (Liu et al., 2008; He et al., 2009; Wang et al., 2009b), and may therefore provide important connectivity-based markers of neural integrity.

The combination of graph analysis and fMRI offers a powerful means for characterizing brain networks. However, the field is nascent, and several methodological challenges require resolution. One of the most difficult involves the appropriate selection of brain regions to represent the network nodes. The majority of studies have used an *a priori* anatomical template as the basis for regional parcellation. These templates, such as those included in the Automated Anatomical Labeling (AAL) toolbox (Tzourio-Mazoyer et al., 2002), the ANIMAL atlas (Collins et al., 1995), or the automated regional parcellation provided with software packages such as Freesurfer (Fischl et al., 2004), are generated by manual delineation of distinct brain regions in either a single individual (e.g., AAL) or sample of individuals (e.g., Freesurfer), and then mapped on to the brains of new participants using some spatial normalization routine. The mean time series is then extracted for each region, and pair-wise correlations between regional time series are computed to obtain a functional connectivity matrix. While the approach is straightforward and has proven useful, it is limited for several reasons. First, there is no accepted gold standard for regional parcellation, because, particularly in the cortex, there are no clear macroscopic boundaries that can be used to delineate adjacent regions. Thus, the criteria used are inherently arbitrary and vary from one template to the next. Second, the regions can vary in size from tens to thousands of voxels, which can affect resulting connectivity estimates (Salvador et al., 2008). Finally, because the regions are often large, it is likely that they include signals from several different functional sub-regions, which can complicate interpretation of region-specific findings.

More recently, some investigators have used parcellation methods that do not depend on arbitrary regional definitions. For example, Hagmann et al. (2007) used a random-seeding method to parcellate the cortical surface (gray/white matter boundary) into 500–4000 regions of approximately equal size. These regions were then projected out to fill the cortical volume for use with fMRI data in subsequent work (Hagmann et al., 2008; Honey et al., 2009). In addition, voxel-based approaches have been employed (Eguiluz et al., 2005; van den Heuvel et al., 2008; Hayasaka and Laurienti, 2010). With this approach, each image voxel is treated as a distinct network node. While such methods are computationally intensive, typically requiring analysis of networks of many thousands of nodes and many more edges, they demonstrate that a high degree of spatial specificity is achievable in graph analytic studies.

The range of possible parcellation strategies available for defining network nodes in graph analysis of fMRI data highlights the importance of understanding the degree to which the results of any one study may be contingent on the particular parcellation scheme employed. To our knowledge, three studies have attempted to directly compare the results obtained using different parcellation methods. In one, Zalesky et al. (2010) compared the results obtained from diffusion-MRI derived anatomical connectivity networks when using the AAL (82 regions) and random-seed generated templates comprising 100, 500, 1000, 2000, 3000, and 4000 regions. General decisions about network topology, such as whether the brain is small-world or scale-free, were not affected by parcellation scale, but differences did emerge when topology was quantified in terms of specific organizational parameters such as path length and clustering. However, this study did not investigate inter-individual variability of network metrics and it is unclear whether their results apply to measures computed from resting-state functional connectivity networks. Hayasaka and Laurienti (2010) compared rs-fMRI networks generated at the voxel- and region-wise levels, as well as two intermediate resolutions, and found a trend for increasing small-worldness, scale-freeness, and connectedness at higher resolutions. Wang et al. (2009a) compared the results obtained using two different anatomical parcellations applied to rs-fMRI data–the AAL (90 regions) and ANIMAL (70 regions) templates and reached similar conclusions, although they did not examine spatial scaling effects (i.e., the use of a coarse or fine-grained template). The available literature suggests that there may indeed be some effect of spatial scale on rs-fMRI network topology. For example, studies using coarser templates have concluded that resting-state functional brain organization is characterized by an exponentially truncated degree distribution (Achard et al., 2006; Hagmann et al., 2007), whereas voxel-based studies suggest the distribution follows a power law and is therefore scale-free (Eguiluz et al., 2005; van den Heuvel et al., 2008). Such conclusions have important implications for understanding how the brain might respond to disease or damage (Albert et al., 2000; Achard et al., 2006), and should therefore be methodologically validated.

Our goal in the current study was to examine the effects of parcellation scale on graph analytic measures of resting-state functional brain organization. To this end, we calculated a number of commonly used metrics from functional connectivity matrices generated using parcellation schemes spanning a wide range of spatial scales, and quantified the differences and similarities between them. More specifically, we focused on the following network properties, as these are by far the most commonly studied in the literature: functional connectivity, network connectedness, clustering coefficient, characteristic path length, small-worldness, and degree distribution. These measures are fundamental to most graph analytic studies of network topology and are the basis upon which inferences regarding network small-worldness or scale-freeness are made. Our results draw attention to the potential role different parcellation strategies may have in influencing the findings of graph analytic studies, and should inform interpretation of any findings derived using such methods.

MATERIALS AND METHODS

PARTICIPANTS

Thirty (19 male) participants took part in the study. The mean age of the sample was 26.77 years (SD = 10.30 years). Five participants were left-handed. All volunteers were free of personal or family history of serious mental illness or neurological disorder, and had no history of substance abuse or head injury. All participants gave written, informed consent in accordance with local ethics committee guidelines.

IMAGING PARAMETERS

Scans were acquired at the Magnetic Resonance Imaging and Spectroscopy Unit (MRIS), Addenbrooke's Hospital, Cambridge, UK, using a GE Signa HDxt system (General Electric, Milwaukee WI, USA) operating at 3 Tesla (3T). For rs-fMRI analyses, 512 echo-planar imaging (EPI) volumes depicting blood oxygen level

dependent (BOLD) contrast were acquired of the whole-brain using the following parameters: repetition time (TR) = 1600 ms; echo time (TE) = 35 ms; number of excitations (NEX) = 1; number of slices = 23; slice thickness = 7 mm plus 0 mm interslice gap (spacing between slices = 7mm); Flip Angle (FA) = 90°; field of view (FOV) = 240 mm × 240 mm; image matrix size = 64 × 64; voxel dimensions = 3.75 mm × 3.75 mm.

IMAGE PRE-PROCESSING

For each individual, functional volumes were realigned using a rigid-body transformation to correct for geometric displacements associated with head movements and rotations. Temporal motion correction was then performed by regressing the current and lagged first and second order displacements against the time series of the realigned images. The residuals of this regression were then used for further analysis. These steps were implemented using freely available software[1]. Finally, the realigned, temporally corrected images were spatially normalized to the International Consortium for Brain Mapping echo-planar imaging template supplied with SPM5[2] using a 12-parameter affine transformation (Jenkinson and Smith, 2001), as implemented in the FSL toolkit[3]. The accuracy of all normalizations was verified via visual inspection. The images were re-sliced to 2 mm^3 voxels during the spatial normalization.

TEMPLATE GENERATION

To construct parcellation templates of varying spatial resolution, we used an algorithm adapted from that described by Zalesky et al. (2010) for partitioning the AAL template into N contiguous regions while constraining the ROI volumes to be as uniform as possible. To generate a parcellation of finer scale than the native AAL resolution, each node composing the AAL template was subdivided into a set of micro nodes. Each micro node was constrained to lie within the volume encapsulated by its parent AAL node and each micro node was ensured to be contiguous.

The parcellation was performed using the following algorithm: Let N be the total number of desired nodes (i.e., the number of micro nodes). The number of micro nodes into which an AAL node was subdivided was proportional to its volume. Specifically, if an AAL node encapsulated V% of the total gray-matter volume, it was subdivided into $K = VN$ micro nodes. This constraint promoted uniformity in the volumes encapsulated by micro nodes. To subdivide an AAL node into K micro nodes, K voxels encapsulated by the AAL node were chosen at random. Each of these voxels defined the "origin" of a distinct micro node. The remaining voxels encapsulated by the AAL node were then assigned to one and only one of the K origins. In particular, a voxel was assigned to the origin to which it was closest, as dictated by the shortest Euclidean distance. Any ties in distance were broken randomly. This guaranteed contiguity of each micro node. The allocation procedure was repeated independently for each AAL node. An alternative approach would involve arbitrary parcellation of the binarized AAL mask without respecting the existing divisions of the AAL template (i.e., permit a micro-node to lie across multiple AAL nodes), but this method would permit non-sensical nodes that, for example, include both hemispheres.

The above procedure was repeated six times, for N = 100, 250, 500, 1000, 1500, and 5000. We also generated networks using the original AAL, resulting in a total of seven parcellation scales being studied. Each of these templates was applied to the participants' functional data to extract regional mean time series. To minimize noise associated with variable acquisition coverage in different individuals, we only retained ROIs where at least 70% of the voxels contained a non-zero signal. ROIs not meeting this criterion in all subjects were excluded from further analysis. This ensured that all networks within a parcellation scale were constructed from the same number of nodes. The final result was seven templates, comprising 84, 91, 230, 438, 890, 1314, and 4320 regions. From hereon, these will be referred to as aal84, parc91, parc230, parc438, parc890, parc1314, and parc4320, respectively. The aal prefix is intended to denote that the ROI boundaries for that template are based on those of the original AAL. The parc prefix denotes that the ROI boundaries have been determined using the algorithm described above. Details about ROI volumes at each parcellation scale are presented in **Table 1**.

GRAPH ANALYSIS

Network construction

At each parcellation scale, for each subject, the mean time series of each region was extracted and decomposed into four distinct frequency bands using the maximal overlap discrete wavelet transform (Percival and Walden, 2000; Bullmore et al., 2004; Achard et al., 2006). We used the mean time series of each region, as this is the most commonly used method for estimating regional activity fluctuations. We note that other techniques, such as extracting the principal eigenvector, may also provide a representative sample of regional activity. The four frequency bands identified were: scale 1, 0.16–0.31 Hz; scale 2, 0.08–0.16 Hz; scale 3, 0.04–0.08 Hz; and scale 4, 0.02–0.04 Hz. In the present analysis, we focused on scale 3 of the wavelet decomposition (0.04–0.08 Hz), as this is the

[1]http://www-bmu.psychiatry.cam.ac.uk/software

[2]http://www.fil.ion.ucl.ac.uk/spm/software/spm5

[3]http://www.fmrib.ox.ac.uk/fsl

Table 1 | Region-of-interest (ROI) volume (mm^3) statistics as a function of parcellation scale.

	aal84	parc91	parc230	parc438	parc890	parc1314	parc4320
Median	11800	11200	4536	2372	1156	768	236
Inter-quartile range	10788	10040	3688	1968	888	600	176
Ratio	0.91	0.89	0.81	0.83	0.77	0.78	0.75

Median represents the median volume across all ROIs in each template. Variability in ROI size was assessed using the inter-quartile range. The Ratio measure was calculated as the inter-quartile range normalized by the median.

band most commonly studied in rs-fMRI analyses and represents a reasonable trade-off between avoiding the physiological noise associated with higher frequency oscillations (Cordes et al., 2001) and the measurement error associated with estimating very low frequency correlations from limited time series (Achard et al., 2008). To correct for BOLD signal fluctuations of a non-neuronal origin, time series extracted from seed regions placed in the white matter and cerebrospinal fluid were regressed against the wavelet-filtered regional time courses, and the residuals of these regressions were used for further analyses (Fox et al., 2005). We did not correct for global signal fluctuations as this step is known to introduce artifactual correlations (Fox et al., 2009; Murphy et al., 2009), and its effects on whole-brain connectivity networks are as yet unclear.

Correlations between each possible pair of regions were computed using the filtered, corrected regional time courses to generate a $N \times N$ functional connectivity matrix for each individual at each parcellation scale. As these connectivity matrices were populated using a continuous association measure (i.e., wavelet correlations), it was necessary to apply a threshold to remove noisy edges and extract an underlying network topology. As the choice of a specific threshold can be arbitrary, we examined network properties across a range of thresholds to test for consistency of the results. These thresholds were expressed as a network connection cost, defined as the proportion of supra-threshold connections relative to the total possible number of connections in the network (Achard and Bullmore, 2007). Thus, a network thresholded at a cost of 10% comprised only the highest 10% of correlation values in the matrix. The sign of the correlations in the connectivity matrices was ignored, so that thresholding was based only on the absolute correlation values.

In our analyses, for templates ranging in resolution from aal84 to parc1314, we examined the full range of costs from 5 to 40%. We chose a minimum bound of 5% to avoid excess network fragmentation at sparser thresholds. The upper bound of 40% was chosen because it represents a liberal limit on estimates of cerebral connectivity reported in the literature (Latora and Marchiori, 2003; Bassett and Bullmore, 2006), and the networks tended toward randomness at higher costs (i.e., estimates of σ, an index of small-worldness, approached those of a random network; see also **Figure 6**). (Note that this approach implicitly assumes that randomness is a spurious property of brain networks.) For parc4320, we only examined costs of 10, 20, 30, and 40% due to the computational time involved in generating network measures for such large networks. After applying each threshold, the matrices were binarized such that supra-threshold connections were assigned to one and sub-threshold connections to zero. These binarized adjacency matrices were then used as a basis for network construction and graph analysis. In total, this procedure resulted in the construction and analysis of 6420 network graphs. A schematic overview of the processing steps using in graph construction is provided in **Figure 1**. We used binary, globally thresholded graphs for network characterization because this is the most frequently used approach in the literature. Other methods, such as spectral graph partitioning (see Boccaletti et al., 2006 for an overview), may also provide useful information and warrant further investigation.

Graph metrics

A number of graph analytic measures can be used to characterize diverse aspects of network organization (reviewed in Rubinov and Sporns, 2009). Here, we concentrated on those most frequently used in the literature, and which pertain to the most fundamental properties of the networks: network connectedness, small-worldness, and the degree distribution.

Network connectedness refers to how well connected the network nodes are. If a path can be traced from any node in the network to all others, the network is connected. In thresholded data such as those provided by fMRI, this can be assessed by computing the size of the largest connected component of the graph as a function of cost. As the connectedness of a network increases, the size of the largest connected component will approach N.

Small-worldness was assessed in relation to five parameters: clustering coefficient, mean minimum path length, λ, γ, and σ. The clustering coefficient, C_i, is the proportion of connections present between a node's neighbors. High values imply that nodes connected to node i are also connected to each other, suggesting node i is situated in a cliquish neighborhood of connectivity. The mean minimum path length, L_i, was computed for each node as the average number of edges comprising the shortest path between node i and all other nodes. The characteristic path length of the network, L_{net}, was simply the average path length of the entire network. Low values indicate that information can be transferred between nodes with only a few connections, which is indicative of a more efficient topological organization (Latora and Marchiori, 2001). In cases where the largest connected component of the network was $<N$, which typically occurs at low connection costs, we set the path length of disconnected nodes to the maximum observed for the network. This helped avoid computational problems associated with estimating path length for an isolated nodes, which is formally defined as ∞ (see also Zalesky et al., 2010). As such, our path length measure was inversely related to the global network efficiency measure proposed elsewhere (Latora and Marchiori, 2001), where disconnected nodes are assigned an efficiency of zero. Separate analyses showed that path length and efficiency values were indeed highly negatively correlated (<-0.90 for most costs and templates), and the general pattern of results concerning the effects of different parcellation scales was consistent.

To diagnose small-worldness, L_{net} and C_{net} were normalized by their corresponding values in comparable random graphs (L_{ran} and C_{ran}, respectively), resulting in estimates of $\lambda = L_{net}/L_{ran}$ and $\gamma = C_{net}/C_{ran}$, respectively. In small-world networks, $\lambda \sim 1$ and $\gamma > 1$. Thus, small-world properties are evident when the scalar summary $\sigma = \gamma/\lambda > 1$ (Humphries et al., 2006). We calculated L_{ran} and C_{ran} using two different methods. One involved using standard analytic approximations for equivalent Erdos–Rényi random graphs (Albert and Barabasi, 2002), where $L_{ran} = \ln(N)/\ln(d)$ and $C_{ran} = d/N$ and d represents the average nodal degree of the ith node. The second method involved using an algorithm that gradually rewired the edges of the thresholded adjacency matrix for each participant to generate a random topology (Maslov and Sneppen, 2002). In both cases, the normalization was matched for network size and mean degree, but the rewiring algorithm also matched for degree distribution. From hereon, we will refer to the Erdos–Rényi method as

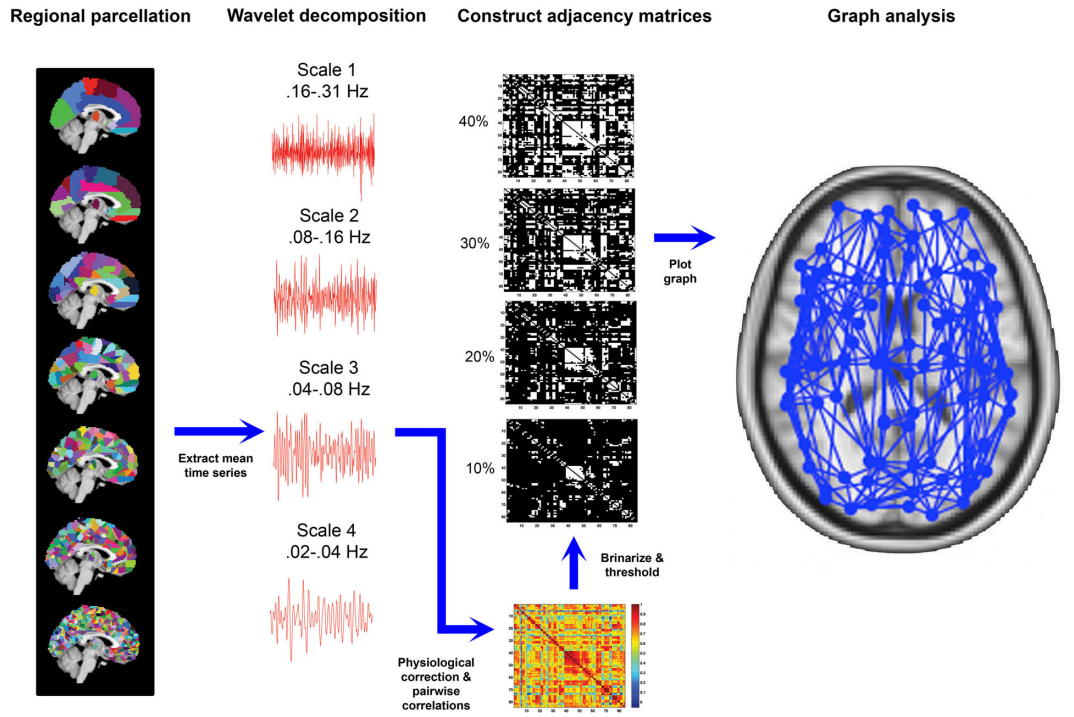

FIGURE 1 | Overview of image processing steps used in generating graph-based representations of whole-brain connectivity network. *Far left:* seven distinct parcellation templates were generated, which divided the brain into (from top to bottom) 84, 91, 230, 438, 890, 1314, or 4230 regions-of-interest. *Middle-left:* the templates were applied to each subject's fMRI volumes and the mean time series of each region were extracted and decomposed into four frequency intervals using a wavelet transform. *Middle-right:* spontaneous oscillations subtended by the wavelet frequency interval 0.04–0.08 Hz were further corrected for physiological noise signals and temporal correlations between each possible pair of regional corrected time series were calculated to generate a functional connectivity matrix for each template for each participant. These matrices were then thresholded and binarized across a range of connection costs (examples shown are for 10, 20, 30, and 40% costs). *Far right:* The thresholded, binarized adjacency matrices were used to generate graph-based representations of network connectivity, such that each region was represented as a node and each supra-threshold correlation as a connecting edge. These graphs were used as a basis for calculating graph metrics.

ER-normalization and the rewiring method as RW-normalization. These abbreviations will be appended as subscripts when referring to the normalized measures γ, λ, and σ to denote the normalization method used in their computation.

By definition, RW-normalization requires generation and measurement of surrogate graphs, increasing computation burden relative to ER-normalization. The time difference between the two can be an important consideration when studying large networks over multiple costs. Accordingly, in the current study, we computed normalized measures for costs of 10, 20, 30, and 40%. In the case of the RW-normalization, 20 random graphs were analyzed per subject per cost at each parcellation scale. Consequently, the normalized parameters γ, λ, and σ were only evaluated at these four costs.

To examine the degree distribution of the networks, we plotted nodal degree against nodal rank in log–log coordinates to diagnose scale-freeness. Typically, an approximately linear rank-degree plot is interpreted as evidence of power-law scaling in the degree distribution, although it does not provide conclusive evidence for such properties (Liu et al., 2005; Clauset et al., 2009). A power-law or scale-free degree distribution suggests that while most nodes possess a low degree, the probability of finding very highly connected nodes (termed network hubs) is higher than expected in a commensurate random network. We used rank-degree plots to avoid the artifacts associated with the binning procedures required for constructing frequency-degree plots (Liu et al., 2005). We formally tested for scale-freeness by fitting models describing power-law (scale-free), exponential and exponentially truncated (broad-scale) distributions to the curves for each subject, and compared their goodness of fit using Akaike's information criterion (AIC). The model with the lowest AIC value was identified as the one providing the best fit to the data. We used simple least squares estimation, consistent with prior work (e.g., Achard et al., 2006). Other methods can provide more accurate results when estimating power-law scaling (Bauke, 2007; Clauset et al., 2009), but may be limited in cases where there is a truncation of the power-law, as in the present data (see below). All graph analyses were performed using Matlab 7.8.0 (MathWorks, Inc) using a combination of freely available tools[4,5,6] and custom code.

STATISTICAL ANALYSES

We performed two types of analyses: one focused on mean differences, and the other on individual differences. To test whether there were any mean differences in network parameters as a function of parcel-

[4]http://sites.google.com/a/brain-connectivity-toolbox.net/bct/

[5]http://www.boost.org/doc/libs/1_41_0/libs/graph/doc/index.html

[6]http://www.atmos.washington.edu/~wmtsa/

lation scale, we ran separate repeated measures analyses of variance at each cost examined, using parcellation scale as the independent variable. This analysis was intended to determine whether mean differences between parcellation scales were of sufficient magnitude to be considered statistically significant. As the analysis was intended to highlight parcellation scales where there may be differences, we adopted an exploratory threshold of $\alpha = 0.05$, uncorrected.

While different parcellation scales may show mean differences in absolute parameter estimates, they may still preserve the pattern of relative differences between individuals. Such relative differences are generally those of primary interest in correlational or case–control experiments. Thus, to quantify whether relative differences were preserved across scales, we computed the correlation between each pair of scales for each measure at costs of 10, 20, 30, and 40%. Spearman rank correlations were used to account for non-normality of the data.

RESULTS

PARCELLATION SCALE AND FUNCTIONAL CONNECTIVITY ESTIMATES

Table 2 presents measures of average connectivity, and variability in connectivity, as a function of parcellation scale. There was a general trend for average functional connectivity, as measured by the median correlation in each individual's connectivity matrix, to decrease with increasing spatial resolution of the template; from the lowest to the highest resolution, there was an approximate decrease of 38% in the mean correlation value. Measures of between-subject variability in mean connectivity, and within-subject variability in connectivity estimates, remained relatively consistent across parcellation scales. **Figure 2** presents the sample averaged correlation histograms at each parcellation scale. The shapes of each distribution are highly similar, but their mean value is shifted toward zero with increasing spatial resolution.

To examine how changes in ROI size associated with each parcellation scale were related to regional functional connectivity estimates, we used the following procedure. At each parcellation scale, for each subject, we calculated the mean correlation value of each brain region. We then correlated these regional mean correlation values with the volume of each region to obtain a correlation value for each participant at each scale reflecting the association between average regional connectivity and ROI size. **Figure 3** presents a boxplot of these subject-specific correlation values at each parcellation scale. On average, across all scales, the correlation between ROI size and mean regional connectivity was low (median <0.3), although for some subjects it exceeded 0.5 when coarser templates (i.e., aal84 and parc91) were used. All correlations for more fine-grained templates (i.e., parc890 and higher) were <0.3. This suggests that using more fine-grained templates can reduce the dependence of functional connectivity estimates on ROI size. In addition, **Figure 3** indicates that inter-individual variance in the association between ROI size and connectivity estimates is reduced at higher spatial resolutions, which may serve to increase power in statistical analyses of graph measures.

PARCELLATION SCALE AND GRAPH METRICS

The effects of parcellation scale on network connectedness

To examine how parcellation scale affected network connectedness we calculated the size of the largest connected component, as a proportion of *N*, for each subject at each parcellation scale across the cost range 5–40%. (This analysis was not possible for parc4320, as only four costs were examined at this scale.) The results are presented in **Figure 4** (left). A value of 1 on the *y*-axis indicates that the largest connected component includes all nodes – the network is connected. As can be seen, increasing spatial resolution was associated with greater connectedness. In particular, the parc890 and parc1314 networks were, on average, connected even when the networks were sparse (i.e., cost <10%). In contrast, lower resolution templates only achieved connectedness at higher costs.

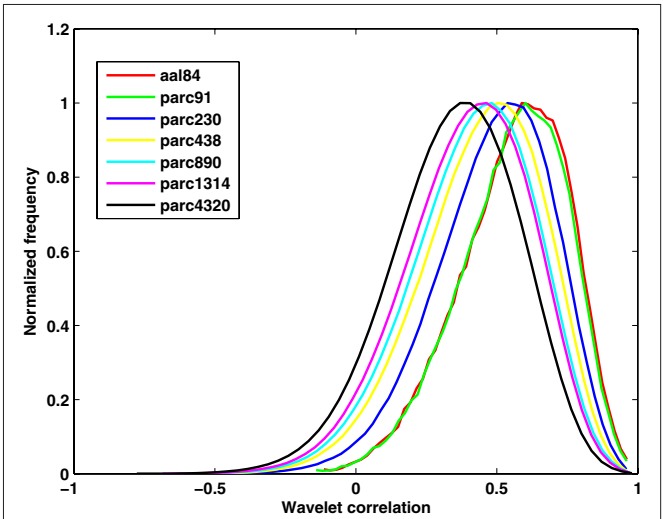

FIGURE 2 | Functional connectivity histograms obtained at each parcellation scale. Each line corresponds to the sample average histogram of correlation values contained in each participant's unthresholded functional connectivity matrix.

Table 2 | Changes in average in functional connectivity, and variability of connectivity estimates, as a function of parcellation scale.

	aal84	parc91	parc230	parc438	parc890	parc1314	parc4320
Mean functional connectivity	0.56	0.56	0.50	0.45	0.43	0.41	0.35
Between-subject variability	0.09	0.09	0.09	0.08	0.08	0.08	0.08
Within-subject variability	0.17	0.17	0.18	0.19	0.19	0.19	0.21

The mean functional connectivity estimates were obtained by computing the average wavelet correlation coefficient for each subject's unthresholded connectivity matrix, and then taking the sample average of these mean values. Between-subject variability was computed by taking the sample standard deviation of the mean correlation value of each subject's matrix. Within-subject variability was computed by calculating the standard deviation of correlation values in each subject's matrix, and then taking the sample mean of these standard deviation values.

To further quantify the degree of similarity between parcellation scales with respect to network connectedness, we calculated the cost at which each subject's network became connected for each parcellation scale. We then computed the correlation between these values for each pair of parcellation scales. This correlation matrix is presented in **Figure 4** (right). Correlations were generally positive, and were highest for scales with similar resolution. For example, the correlation between parc1314 and parc890 was higher than that for parc1314 and aal84.

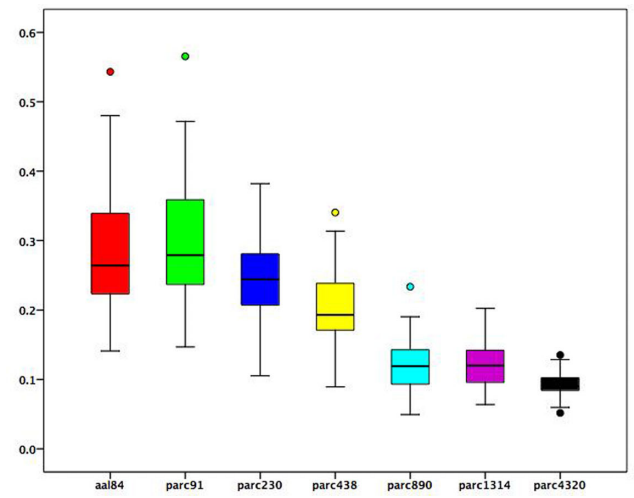

FIGURE 3 | Boxplots of subject-specific correlations between mean regional functional connectivity and regional volumes at each parcellation scale. Boxes represent the inter-quartile range, heavy horizontal lines the median. Whiskers represent the 5th and 95th percentiles. Circles represent values beyond these percentiles.

THE EFFECTS OF PARCELLATION SCALE ON NETWORK SMALL-WORLDNESS

Figure 5 plots the sample mean C_{net} and L_{net} for all parcellations up to parc1314 across costs 5–40%. **Figure 6** plots the sample means for C_{net}, L_{net}, λ, and γ for all parcellations at costs of 10, 20, 30, and 40%. **Figure 7** shows the same for σ. Significant mean differences as a function of parcellation scale were apparent for nearly all costs examined. In general, there was trend for networks defined at higher resolutions to be associated with lower L_{net}. The dependence of C_{net} on parcellation scale varied as a function of cost; higher resolution networks showed increased clustering at costs lower than ~25%, but this trend reversed for higher costs. This effect likely reflects the aforementioned parcellation-dependent effects on network fragmentation: at lower costs, coarse resolution networks were more fragmented, lowering estimates of C_{net}.

The effects of parcellation scale on normalized measures varied depending on which normalization was used. In general, as parcellation resolution increased λ_{ER} estimates increased and λ_{RW} decreased. The only exception to this trend was λ_{ER} at 10% cost, where aal84 and parc91 showed the highest path length. Again, this effect likely reflects increased fragmentation in the observed networks at sparser thresholds. Estimates of γ_{RW} were consistently higher in high-resolution templates, whereas γ_{ER} differences also showed a dependence on cost: at 10%, coarser resolutions showed lower values, whereas this effect reversed at higher costs. Similar trends were observed for σ, such that higher resolutions were associated with lower σ_{RW} values across all costs examined, whereas σ_{ER} differences were contingent on cost in a manner that paralleled the pattern observed for γ_{ER}.

The pair-wise correlations between different parcellation scales for C_{net}, L_{net}, λ_{RW}, γ_{RW}, σ_{ER}, and σ_{RW}, are quantified at costs of 10, 20, 30, and 40% in **Figure 8**. (Matrices for λ_{ER} and γ_{ER} are not shown because they were computed by normalizing λ and γ with a constant value across all individuals, making

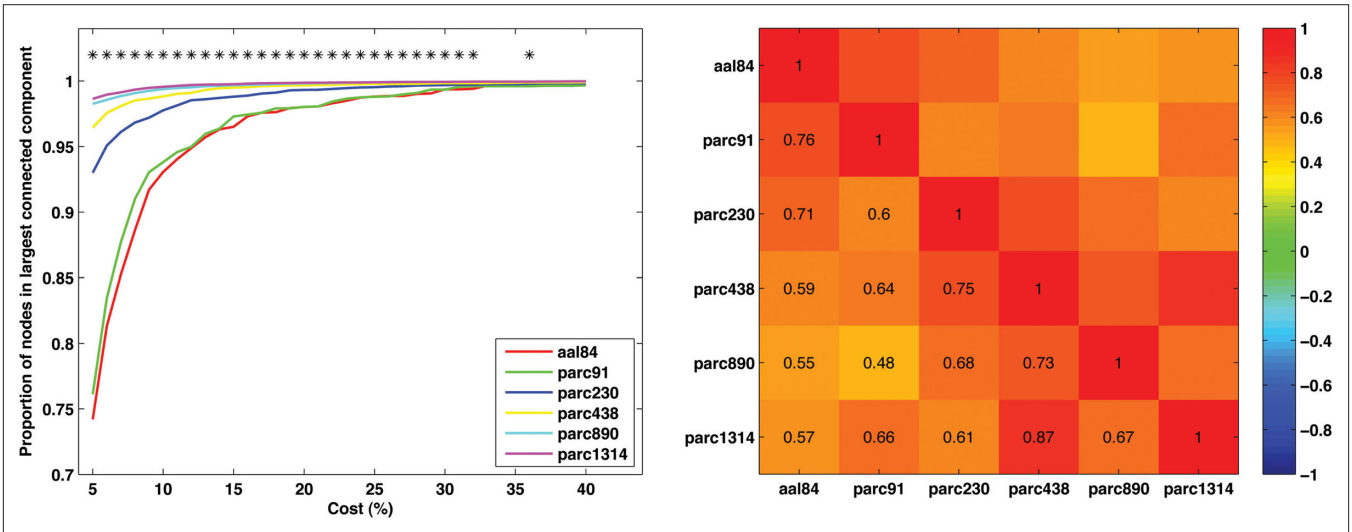

FIGURE 4 | Mean values and individual differences in network connectedness as a function of parcellation scale. *Left:* Sample mean size of largest connected network component for each parcellation scale across all costs examined (*$p < 0.05$). *Right:* correlation matrix of inter-scale associations for the cost at which each individual's network became connected.

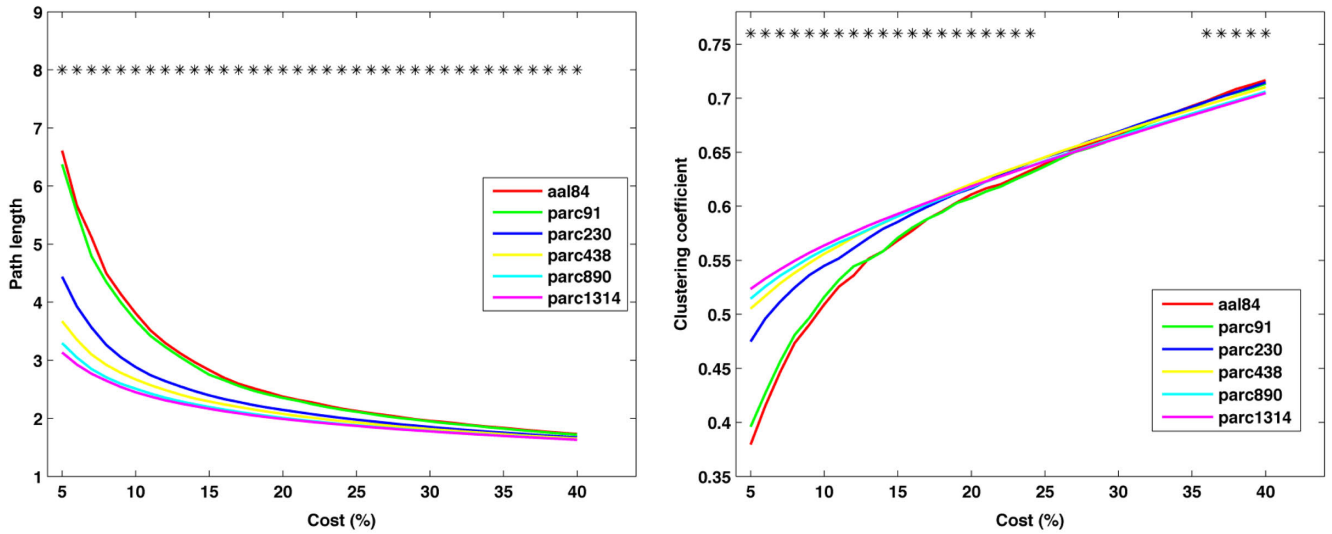

FIGURE 5 | Mean values of global network path length (left) and clustering coefficient (right) at each cost. $^*p < 0.05$.

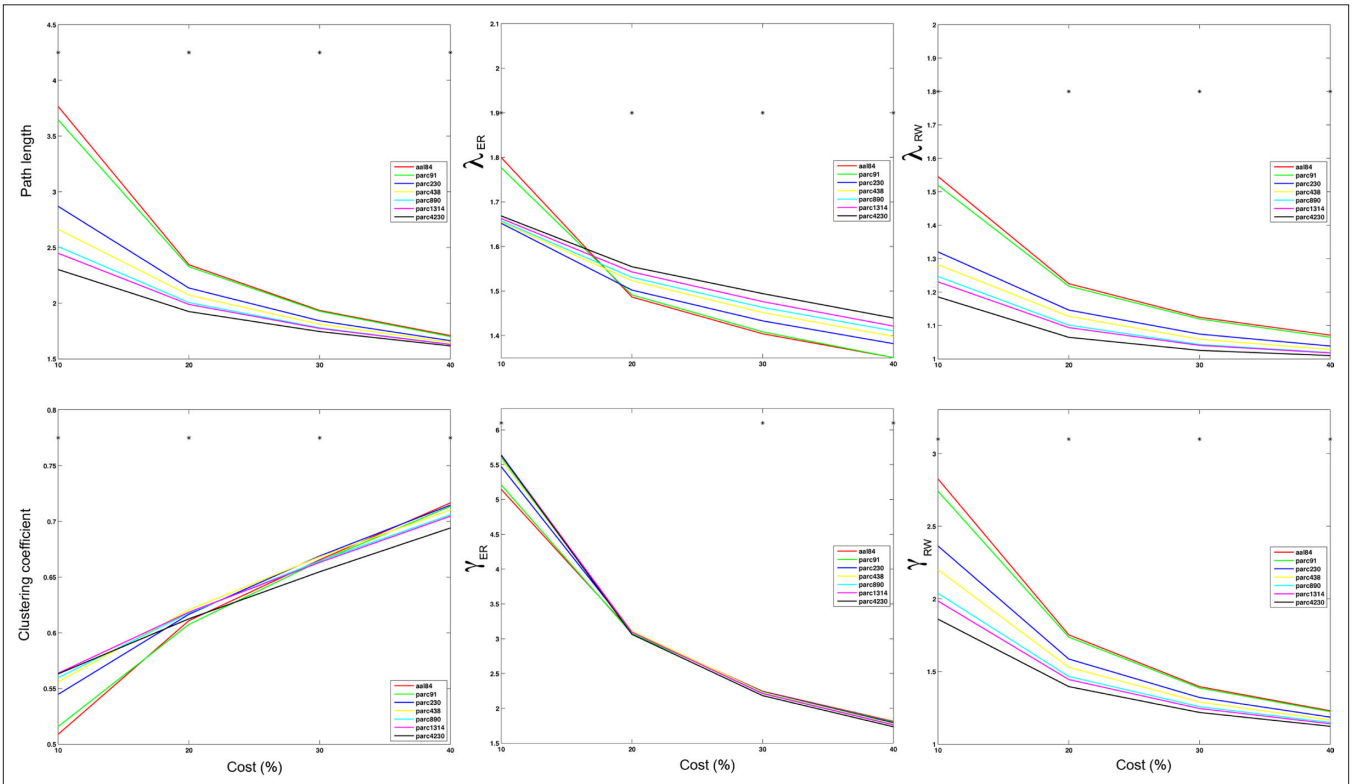

FIGURE 6 | Mean values of global network path length (top left), λ_{ER} (top middle), λ_{RW} (top right), clustering (bottom left), γ_{ER} (bottom middle) and γ_{RW} (bottom right) at costs of 10, 20, 30, and 40% for each parcellation scale. $^*p < 0.05$.

individual differences in these parameters identical to the non-normalized measures.) In general, most measures were highly positively correlated across scales, suggesting preservation of individual differences. Inter-correlations between the two coarsest templates – aal84 and parc91 – and all other scales were lower at sparser costs, particularly for clustering, likely reflecting increased fragmentation of these lower resolution networks. RW-normalization of $C_{net,}$ and L_{net} largely preserved individual differences and led to higher inter-scale correlations. The pattern of inter-scale correlations for σ varied depending on whether it

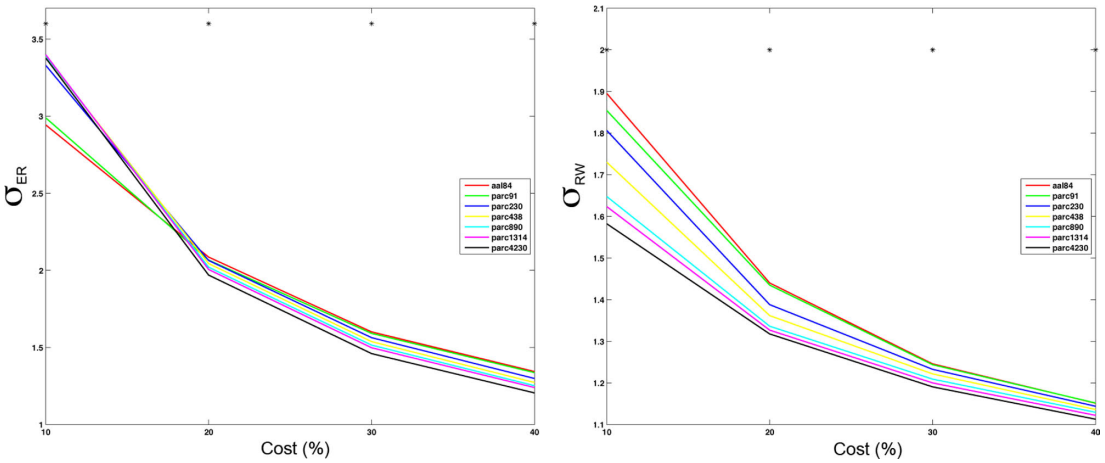

FIGURE 7 | Mean small-worldness (σ) values computing using ER- or RW-normalization (left and right respectively) for each parcellation scale at costs of 10, 20, 30, and 40%. $^*p < 0.05$.

was computed using ER- or RW-normalization: all scales were highly positively correlated (all $r > 0.70$) for RW-normalization, but only pairs of scales similar in size showed high correlations for ER-normalization.

The effects of parcellation scale on network degree distributions

Figure 9 plots the sample mean degree distributions for each parcellation scale at costs of 10, 20, 30, and 40%. The non-linearity of the curves indicates the networks were not scale-free, but rather were characterized by an exponentially truncated power-law function. For all subjects, across all parcellation scales and all costs examined, an exponentially truncated power-law provided a better fit to the data than a power-law or exponential model, as determined using the AIC.

The exponentially truncated power-law model fit to the data was defined as $y_i = cd_i^{\alpha-1}e^{-d_i/k}$ (Achard et al., 2006). The model was linearized by taking the logarithm of both sides and the parameters α, k, and c were fitted using least squares. The three model parameters can be interpreted as follows: $\alpha - 1$ is the scaling exponent, k is the degree of the exponential cutoff (i.e., truncation point) above which the power-law becomes dominated by exponential scaling, and c is a normalization constant. The cutoff degree k models potential biological constraints on network size (e.g., head size) that preclude the formation of very rare, but highly connected hub nodes predicted by a pure power-law model. When plotting the nodal distribution function on doubly logarithmic axes, the scaling exponent, $\alpha - 1$, represents the slope of the distribution over the power-law regime. However, if the cutoff degree is low, the exponential always bears some influence on the power-law, and thus the scaling exponent becomes a poor estimator of slope. This effect was observed in the present study, and so the power-law exponent should be interpreted cautiously.

As shown in **Figure 10**, parcellations with higher spatial resolution were associated with lower values for both $\alpha - 1$ and k. In particular, a marked discrepancy was evident in the fitted cutoff degree between parc4320 and all other scales. This discrepancy indicates the existence of highly connected hub nodes is less probable as the parcellation scale is made finer. This is also consistent with the finding that the network tends toward a more random topology as the scale is made finer, where nodal degrees are binomially distributed (i.e., evenly dispersed about a mean nodal degree). One interpretational caveat is that the networks differed in size, and so the descriptors of the degree distribution may not be directly comparable. The best way of normalizing such values for differences in network size remains an unresolved issue.

Figure 11 plots the inter-scale pair-wise correlations for $\alpha - 1$ and k. The inter-correlations were all positive and generally high, particularly between parcellations with spatial resolution equal to or greater than parc230. This suggests that, despite there being mean differences in these parameters across scales, inter-individual differences are relatively conserved.

The effects of parcellation scale on regional network metrics

Quantitative comparisons of how regional properties vary as a function of parcellation scale are difficult, as there is no one-to-one correspondence between ROI definitions across templates. To get an impression of how parcellation scale affected regional properties, we mapped nodal path length and clustering at each parcellation scale for networks defined at 10% cost (**Figure 12**). The results were broadly consistent across scales. Regions showing the lowest path length were primarily localized to posterior medial parietal and visual cortices, as well as lateral superior parietal, temporal and frontal regions. Regions showing the highest clustering were located in somatomotor cortices, primary visual areas, and lateral temporal and prefrontal regions. Naturally, higher resolutions afforded greater localizing power, and in some cases what seem to be larger regions of homogeneous values split into distinct clusters. For example, the precentral gyrus was one of the regions showing lowest path length at the aal84 scale, but higher resolutions indicated that this effect was mainly driven by a more focal cluster localized to superior

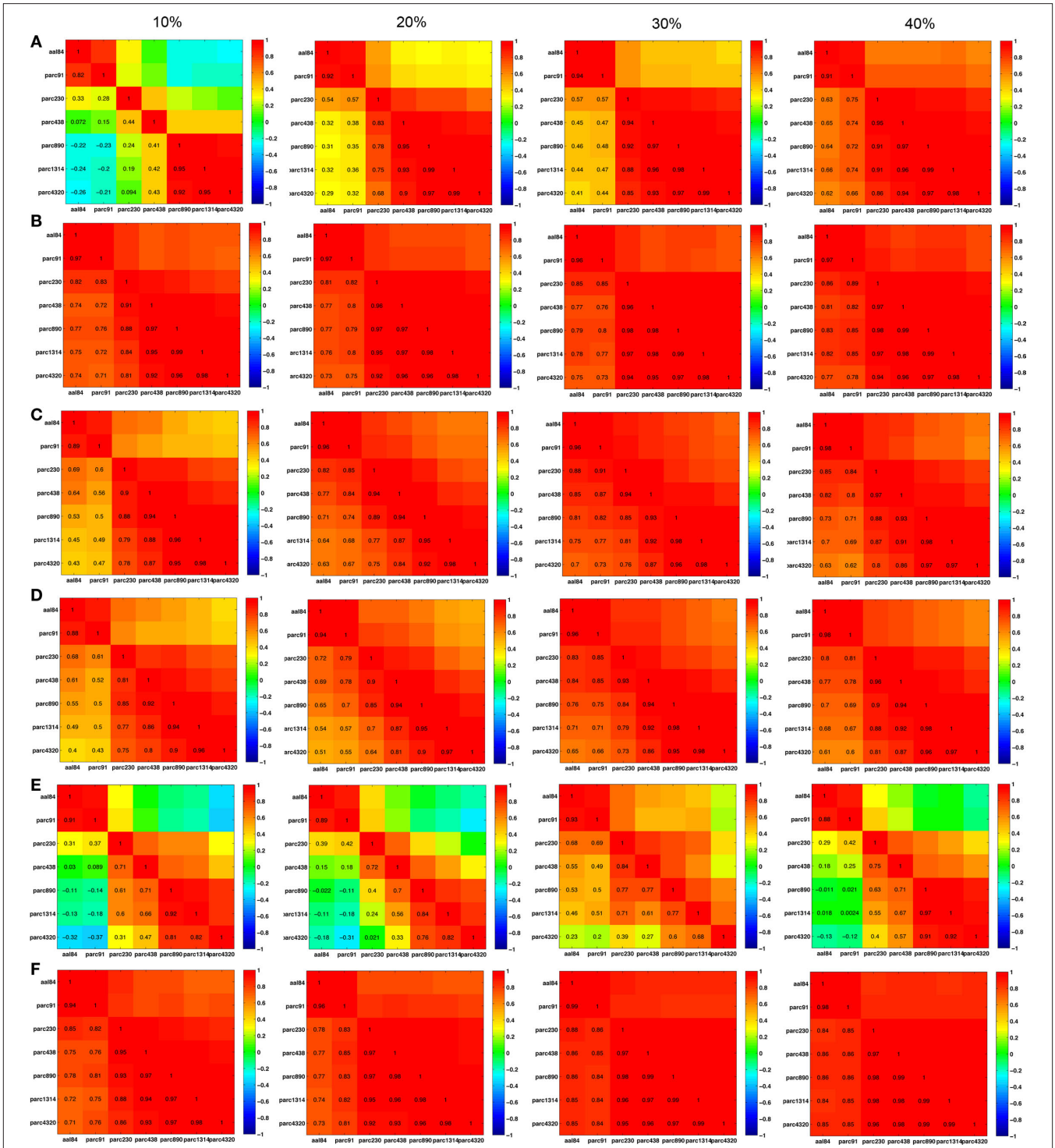

FIGURE 8 | Inter-scale correlations in global network properties at costs of 10, 20, 30, and 40%. (A) Clustering; **(B)** γ_{RW}; **(C)** path length; **(D)** λ_{RW}; **(E)** σ_{ER}; and **(F)** σ_{RW}.

portions of this gyrus. Thus, not surprisingly, higher resolutions afforded greater power for localizing focal effects. The results were very consistent across scales greater than parc890 however, suggesting there may be diminishing returns associated with further increases in resolution.

DISCUSSION

The application of graph analytic techniques to fMRI data has provided researchers with a rich set of tools for characterizing brain network connectivity. An important step when conducting these analyses involves parcellating the brain into distinct regions, which

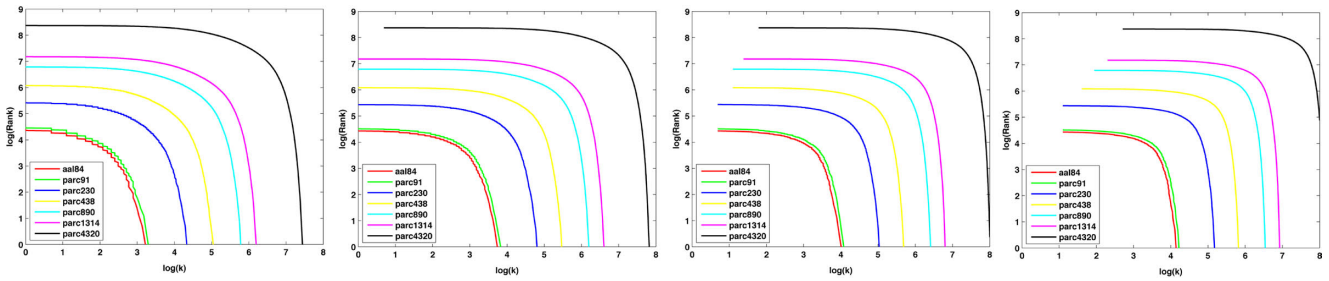

FIGURE 9 | Log–log nodal rank-degree plots for each parcellation scale at costs of 10, 20, 30, and 40%.

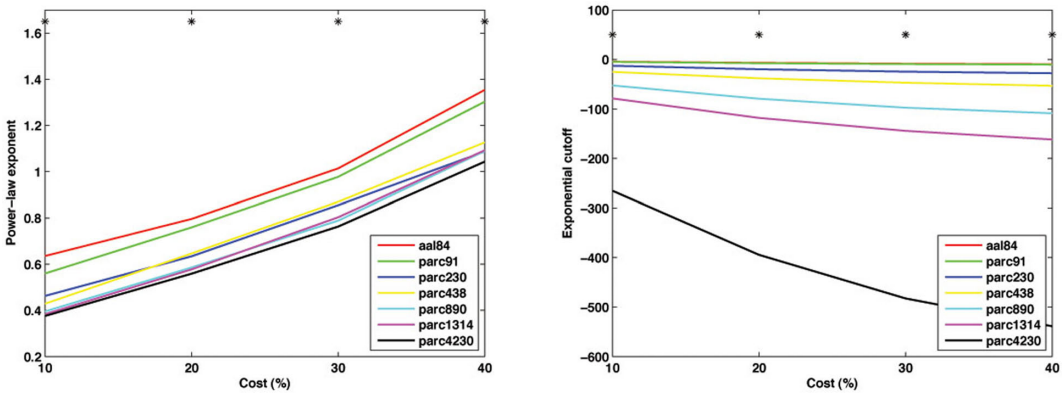

FIGURE 10 | Mean values of the power-law exponent (slope, left) and exponential cutoff (right) of the degree distributions at each parcellation scale for costs of 10, 20, 30 and 40%. $^*p < 0.05$.

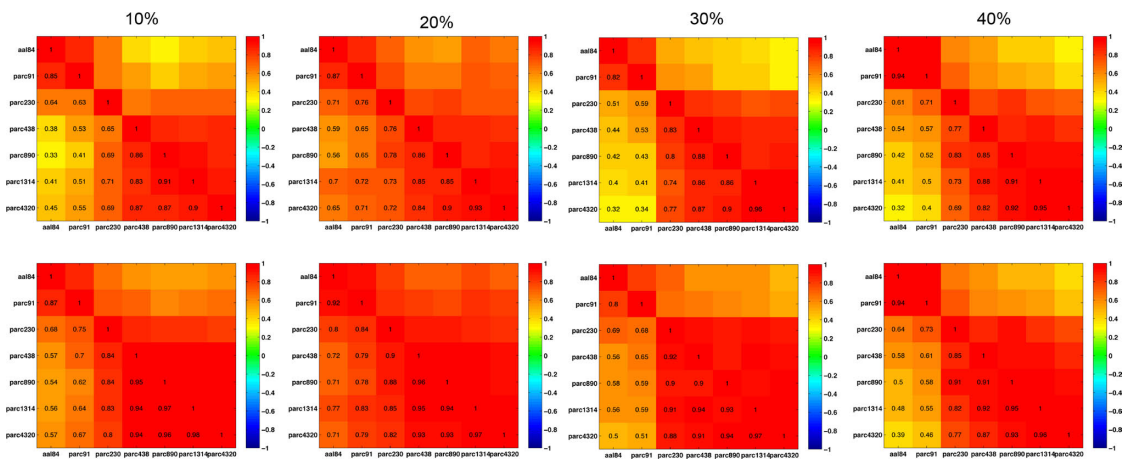

FIGURE 11 | Inter-scale correlations in degree distribution power-law exponents (top row) and exponential cut-off values (bottom row) for costs of 10, 20, 30, and 40% (left to right columns).

serve as network nodes in graph construction. A variety of different parcellation strategies have been employed in the literature, but the effect of differences in such schemes on the findings has been unclear. In this study, we examined the effects of parcellation scale on some of the most commonly used graph analytic measures. We found that while simple inferences regarding network topology, such as whether the network is small-world or scale-free, are robust to the parcellation strategy adopted, there is considerable variation in the exact values defining key parameters of network organization. In addition, while individual differences are generally preserved across parcellation scales, the method used to generate normalized measures such as γ, λ, and σ can have a major effect.

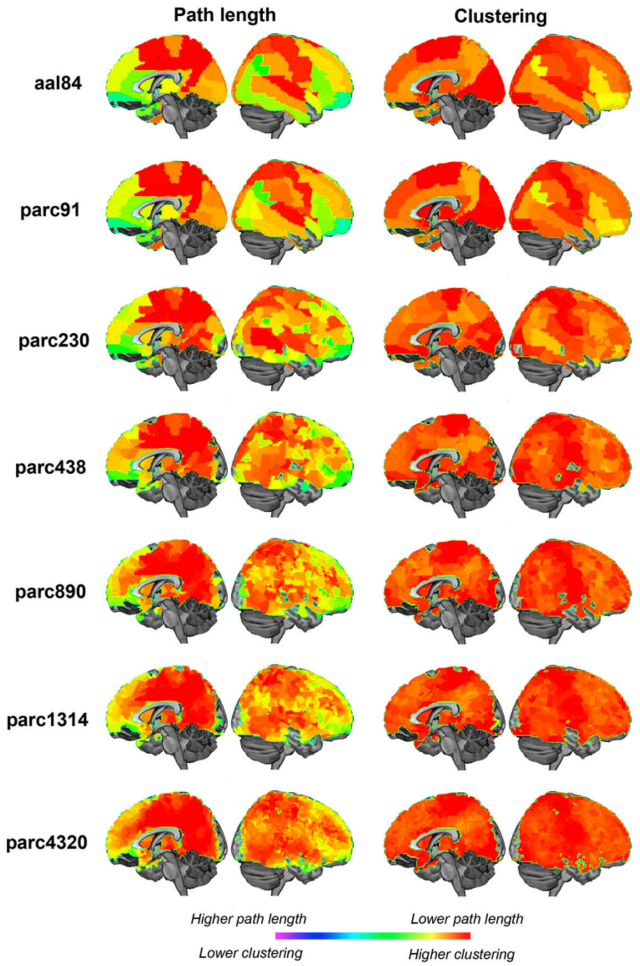

FIGURE 12 | Medial and lateral cortical surface renderings illustrating regional variations in sample mean path length (left) and clustering (right) at each parcellation scale. Path length values have been inverted so that lower values are represented by "hotter" colors.

These findings highlight the need to consider the impact that variations in parcellation strategies may have on the reproducibility of findings in graph analytic studies.

The influence of parcellation scale on functional connectivity

Our findings indicate that higher resolutions were associated with lower mean correlation values. The shape of the correlation distribution was remarkably similar across scales, but each increment in spatial precision shifted the mean of the distribution closer to zero. This may reflect greater noise associated with measurements taken from smaller ROIs, which reduces the likelihood of finding strong correlations with other regions. Indeed, secondary analyses indicated that while there was a ~7% decrease in median covariance between regional time series when moving from the coarsest (aal84) to finest (parc4320) resolution, there was a corresponding ~38% increase in median variance of regional time series. This increased temporal variability reflects noisier measurements at higher resolutions and will reduce any pair-wise time series correlations, which represent a ratio of temporal covariance to variance. However, one attractive property of higher resolution templates was that they showed negligible correlations between regional variations in volume and functional connectivity. For coarser templates, although the median correlation was small-to-moderate ~0.28, there was considerable inter-individual variability in the degree to which nodal size was correlated with regional connectivity; in some cases the correlations approached 0.60. This variability can add noise to analyses of group or individual differences, and reduce power to detect significant effects. In contrast, higher resolution templates were associated with both lower median correlations, and much lower inter-individual variability in correlation values, suggesting that inter-regional variations in size are less of a confound at these scales (particularly parc890 and above). These findings suggest that higher resolution templates may provide a desirable alternative to commonly used low-resolution anatomical parcellations, such as the AAL or ANIMAL templates, but these considerations need to be balanced with the increased error associated with estimation of inter-regional temporal correlations.

Inter-scale differences in global network measures

As with previous investigations (Wang et al., 2009a; Zalesky et al., 2010), we found that gross topological inferences about brain networks, such as whether they are small-world or scale-free, are robust to the specific parcellation scheme employed. However, we observed significant effects of parcellation scale on the absolute values of all graph metrics across most of the costs studied, suggesting that varying network spatial resolutions are associated with sizeable changes in the specific values of key network parameters such as path length, clustering and related measures. This result is consistent with a similar analysis of anatomical networks generated using diffusion-weighted imaging (Zalesky et al., 2010). Together, these findings suggest that comparisons of specific values obtained by different investigators using distinct parcellation schemes should be done cautiously.

In general, coarser networks were associated with higher path length. They were also associated with reduced clustering at sparse costs, but this trend reversed for costs >25%, likely reflecting parcellation-dependent effects on network connectedness. In a fragmented network, disconnected nodes have $C_i = 0$, which lowers the global C_{net} estimate. Coarser templates were associated with greater fragmentation at low costs, suggesting this may have affected C_{net} values.

The effects of parcellation scale on network small-worldness, as indexed by σ, depended on the normalization used to compute the measure. ER-normalization showed a cost-dependent trend paralleling that observed for clustering: coarser resolutions were associated with smaller σ_{ER} at costs <20%, but larger σ_{ER} at higher costs. Again, this likely reflects the effects of increased network fragmentation at sparse costs for coarse scales, which would serve to increase path length and decrease clustering, producing a net reduction in small-worldness. In contrast, there was a consistent trend for higher resolutions to be associated with lower small-worldness when σ was calculated using RW-normalization. This discrepancy may reflect the fact that RW-normalization matches the observed networks for degree distribution whereas ER-normalization is comparable to matching only for size and

mean degree. Thus, the RW approach normalizes the observed parameters by surrogate measures generated from networks better matched for connectivity properties. With the ER model, the probability of a path existing between a pair of nodes is always non-zero. In contrast, with RW-normalization, it is possible for no paths to exist between a pair of nodes for a particular rewiring, thus yielding an infinite path length. To avoid dealing with such infinite values, either the harmonic mean is used, the computation of path lengths is restricted to the largest connected component, or infinite path lengths are replaced with the maximum finite length. Neither of these three alternatives are consistent with the analytic expression for path length derived for the ER model. Therefore, ER- and RW-normalization differ in the way path length is defined, in addition to whether or not the degree distribution is matched to the observed network.

In contrast to our finding, previous studies examining parcellation scale-dependent effects have reported a trend for greater small-worldness at increasing resolutions, using both rs-fMRI (Hayasaka and Laurienti, 2010) and diffusion-imaging (Zalesky et al., 2010). Methodological inconsistencies may account for these findings. In their study of anatomical networks, Zalesky et al. (2010) examined relatively sparse networks unmatched for connection cost or connectedness across parcellation scales, making their results difficult to directly compare with ours. Hayasaka and Laurienti (2010) matched networks based on the lower bound for path length rather than connection cost. This lower bound was computed based on the scaling relationship observed for ER-graphs [$L_{ER} = \ln(N)/\ln(d)$], to avoid assuming a linear relationship between the number of edges and number of nodes in the network. The difficulty with this approach is that there is no guarantee that brain networks will scale similarly to random graphs, which display intrinsically different topological properties. We opted to use cost-based thresholding as it is the most straightforward and widely used method in the literature. However, the best method for thresholding graphs when comparing network parameters is an unresolved issue and requires further investigation.

The trend in our data towards lower values of σ at higher resolutions suggests a tendency towards a more random topology. This trend, combined with the generally lower functional connectivity values and increased temporal variance at these scales suggests higher resolutions may be more susceptible to noise. This contention is also supported by comparing degree distribution parameters across parcellation scales, as the parc4320 template was associated with a lower probability of finding highly connected hubs; that is, connections were distributed more evenly amongst the network nodes, as is characteristic of random graphs.

In traditional, voxel-wise analyses the data are commonly spatially smoothed to increase the signal-to-noise ratio. Smoothing is not a recommended option for graph analytic studies of fMRI data, as it will introduce spuriously high correlations between an index node and its immediate neighbors. Consequently, adopting too high a spatial resolution may be associated with a disproportionate loss in signal-to-noise. Adopting an ROI size that matches the size of the signal one wishes to detect may provide the best trade-off between spatial resolution and signal-to-noise ratio in graph analytic studies of fMRI data, although further work would be necessary to identify the precise relationship between parcellation scale and measurement signal-to-noise. Based on our findings, variations between measures obtained using parc890 and greater were relatively small compared to those obtained using coarser templates and may provide a reasonable spatial scale for exploration of network properties. Another attractive property of higher resolution templates was that they became connected at much lower costs, meaning that analyses of these networks will be less susceptible to the computational problems caused by isolated or disconnected nodes. Greater connectedness with increasing N may be a general property of most complex networks. Random graphs with mean degree $\langle k \rangle > \ln(N)$ are almost surely connected (Albert and Barabasi, 2002), a threshold that is reached at much sparser costs in large networks. While brain networks are not equivalent to random graphs, a similar relationship between N and connectedness likely exists, as suggested by our data (see **Figure 4**).

The effects of parcellation scale on individual differences

Our analysis of mean differences suggested that parcellation scale exerted a considerable effect on the absolute values of key network parameters. However, most investigations are less concerned with estimating the absolute value of a given parameter than with assessing the effects of individual differences in these parameters. For example, researchers may want to test whether a certain network property correlates with some behavioral index (van den Heuvel et al., 2009), or differs between some patient and control group (Liu et al., 2008). Thus, if individual differences across parcellation scales are preserved, then mean differences between them become less important.

To examine how parcellation scale related to individual differences in these measures, we quantified the associations between each pair of scales for each measure at costs of 10, 20, 30, and 40%. Our findings indicated that these inter-scale associations varied depending on the specific network property and cost being studied. Estimates of path length were positively correlated between all scales and across all costs, although the correlations were greater for more densely connected networks. The explanation for this is intuitive: as more connections are added to the network, the topologies begin to resemble each other until cost = 100%, where they yield identical values across individuals. Inter-correlations between scales parc230 and higher were all >0.75, the correlations being >0.90 for scales greater than parc890. The two coarsest scales, aal84 and parc92, were highly correlated with each other, but showed lower correlations with the other scales, suggesting the results obtained at resolutions <200 regions may be less consistent with those obtained at higher resolutions. Raw clustering values were less correlated than path length, although inter-correlations between scales higher than parc890 remained high (i.e., >0.90). This likely reflects the aforementioned differences in network fragmentation. The correlations increased at higher costs suggesting that the topologies converge as more connections are added to the network. Inter-correlations for small-worldness were again dependent on the normalization method, with correlations generally being higher following RW-normalization. A corollary of these findings is that RW-normalization may lead to more reproducible findings.

Together, these data indicate that individual differences are largely preserved for scales greater than ~200 regions, and are particularly reproducible between scales around and exceeding 1000 regions. An

implication of the higher inter-correlations between scales higher than parc890 is that there may be little gain in increasing network resolution much beyond 1000 regions. That is, the values obtained at these higher scales will be highly correlated, but the time taken to compute them will be considerably longer.

Methodological considerations

Many different pre-processing steps are implemented to generate network measures in rs-fMRI analyses, each of which can affect the findings. One under-studied variation regards the choice of temporal filter to isolate the frequency band of interest. We used wavelets because they are well-suited to non-stationary processes such as BOLD signal fluctuations (Bullmore et al., 2004), whereas other authors have used Fourier-based approaches (Salvador et al., 2005a; Liu et al., 2008). We examined the consistency between the approaches by computing intra-subject correlations between frequency-specific functional connectivity values obtained by our approach and those obtained after using a Butterworth filter (cut-offs: 0.04–0.08 Hz). Across subjects and parcellation scales, the median correlation value was 0.95, and all correlations were >0.90, suggesting good agreement between the two approaches. Nonetheless, more detailed comparison of the effects of various temporal filtering approaches may be warranted in the future.

Other methodological variations that may affect the findings include methods for correcting regional time series for physiological fluctuations, particularly as regards the so-called global correction procedure (see Birn et al., 2006; Fox et al., 2009; Murphy et al., 2009; Weissenbacher et al., 2009). An investigation of these methods was beyond the scope of this paper, but may be related to differences between ours and previous findings (Hayasaka and Laurienti, 2010).

We constrained all parcellation scales to fit within the grey matter mask defined by the AAL template as it promoted comparability between the different parcellation schemes used in this study. However, the AAL mask is relatively diffuse and often includes portions of white matter. This may have a more pronounced effect at higher spatial resolutions, as smaller ROIs may be entirely contained within the white matter for some individuals. While we corrected regional time series for white matter signal fluctuations, the problem posed by ROIs contained completely in the white matter is difficult to address without their removal from the network, which would alter the parts of the brain sampled across parcellation scales and result in networks constructed from differing numbers of nodes across individuals. In addition, while the AAL template is widely used in the literature, different templates may differentially sample various parts of gray matter, which may affect the results. While we expect that our findings concerning the effects of varying spatial resolution should be insensitive to the particular initial parcellation template used, this conjecture needs to be verified through further experimentation. Such work would also benefit from comparing the effects of using standard templates (e.g., AAL, ANIMAL) with more recently developed hierarchical parcellation strategies (Thirion et al., 2006; Pohl et al., 2007).

We only generated one template for each spatial scale, as the primary goal of our analysis was to investigate the effects of varying spatial resolution on different network measures. A separate question concerns the robustness of the measures across different parcellations at each scale. We have previously shown that variations in network measures generated using different parcellations at the same scale are very small, being <3% on average (Zalesky et al., 2010), suggesting our findings are generalizable to other parcellations at similar resolutions. In our data, this was also evident in the similar values obtained for all network measures calculated using the aal84 and parc91 templates. Despite the former being defined anatomically and the latter using our random-seeding approach, and slight differences in the number of nodes they comprise, they showed very similar values for all network properties studied. Together, these findings indicate that our results are insensitive to the specific parcellation strategy used at a given parcellation scale.

Across the range of parcellation scales examined, we found consistent evidence that functional brain networks are characterized by an exponentially truncated, so-called broad-scale degree distribution (Amaral et al., 2000), rather than a scale-free topology. While several authors have reported similar findings (Achard et al., 2006; Hagmann et al., 2007), scale-free properties have also been observed, particularly when networks are analyzed at voxel-wise resolution (Eguiluz et al., 2005; van den Heuvel et al., 2008). Hayasaka and Laurienti (2010) found evidence for an exponentially truncated degree distribution in their voxel-based analysis of rs-fMRI networks, suggesting this resolution will not always reveal scale-free properties. However, the degree distribution of their voxel-based network was more scale-free than that of networks studied at lower resolutions. They ascribed this trend to under-representation of low degree nodes at lower resolutions. Whether these low-degree nodes represent a biologically valid characteristic of functional brain networks, or simply reflect a limitation on signal-to-noise at this resolution, remains open to further investigation.

One criticism of using a priori templates for network node definition, as used in the current study, is that they may reduce one's sensitivity to identifying highly connected, yet spatially focal (e.g., voxel-sized) hubs. This is because the topological dominance of such hubs may be obscured when they are grouped as part of a larger region with other voxels (Fraiman et al., 2009; Hayasaka and Laurienti, 2010), reducing sensitivity to identify power-law scaling. The typical ROI volume for the higher resolution templates used in this study was much smaller than the average volume of a typical cytoarchitectonic region, widely regarded as the primary parcellation unit of the cortex, but we still found no evidence for scale-free properties. Highly connected hubs and scale-free topologies may emerge at the resolution of cortical columns, which may be better approximated by voxel-wise approaches (van den Heuvel et al., 2008; Hayasaka and Laurienti, 2010). However, at these resolutions, limitations on the signal-to-noise of current fMRI techniques must be considered, as discussed above. Both broad-scale and scale-free properties have been observed in voxel-based imaging (van den Heuvel et al., 2008; Hayasaka and Laurienti, 2010) and microscopic functional neuronal networks (Yu et al., 2008; Bonifazi et al., 2009), suggesting further work is required to understand the conditions under which scale-free topologies emerge.

A final point worth noting is that rs-fMRI networks, by virtue of being generated from inter-regional correlations in BOLD signal fluctuations, represent a somewhat abstract basis for network definition. While correlated with underlying anatomical connectivity, additional functional connections are often present, likely reflecting the existence of polysynaptic interactions (Vincent et al., 2007; Honey et al.,

2009). As such, the precise meaning of some topological properties of functional networks remains unclear and may require further validation. In addition, while it is often assumed that resting-state dynamics are stable and enduring (Damoiseaux et al., 2006; Shehzad et al., 2009), and that any topological properties measured in this state should therefore inform us about the intrinsic functional organization of the brain (Fox and Raichle, 2007), there is evidence to suggest rs-fMRI measures can be modulated by current or preceding psychological states (Albert et al., 2009; Barnes et al., 2009; Lewis et al., 2009), suggesting these measures may also index a more dynamic component of brain activity (Fornito and Bullmore, 2010). Thus, further investigation into the robustness of these measures is warranted.

CONCLUSIONS

In this study we examined the effects of different parcellation scales on measures of brain network organization derived from the application of graph analytic techniques to human rs-fMRI data. We found that gross topological inferences about the small-worldness or scale-freeness of the networks are robust to parcellation scale, but that the absolute values of relevant network parameters show considerable sensitivity to the spatial resolution employed. Importantly, individual differences in these measures were largely conserved when using more than 250 regions, and particularly for templates employing around 1000 regions, suggesting this scale may provide a reasonable trade-off between increased spatial resolution and attentuated signal-to-noise ratio. In addition, the confounding effects of inter-regional variations in volume were largely reduced at higher resolutions, further supporting their use in future studies. There may be diminishing returns on increasing the resolution beyond a certain point however, as reductions in signal-to-noise ratio may affect some network properties. These findings highlight the need to consider the potential impact of the methods used to generate brain networks on the findings of graph analytic studies of rs-fMRI data.

REFERENCES

Achard, S., Bassett, D. S., Meyer-Lindenberg, A., and Bullmore, E. (2008). Fractal connectivity of long-memory networks. *Phys. Rev. E. Stat. Nonlin. Soft Matter Phys.* 77, 036104.

Achard, S., and Bullmore, E. (2007). Efficiency and cost of economical brain functional networks. *PLoS Comput. Biol.* 3, e17. doi:10.1371/journal.pcbi.0030017.

Achard, S., Salvador, R., Whitcher, B., Suckling, J., and Bullmore, E. (2006). A resilient, low-frequency, small-world human brain functional network with highly connected association cortical hubs. *J. Neurosci.* 26, 63–72.

Albert, N. B., Robertson, E. M., and Miall, R. C. (2009). The resting human brain and motor learning. *Curr. Biol.* 19, 1023–1027.

Albert, R., and Barabasi, A. L. (2002). Statistical mechanics of complex networks. *Rev Modern Phys.* 74, 47–97.

Albert, R., Jeong, H., and Barabasi, A. L. (2000). Error and attack tolerance of complex networks. *Nature* 406, 378–382.

Amaral, L. A., Scala, A., Barthelemy, M., and Stanley, H. E. (2000). Classes of small-world networks. *Proc. Natl. Acad. Sci. U.S.A.* 97, 11149–11152.

Barnes, A., Bullmore, E. T., and Suckling, J. (2009). Endogenous human brain dynamics recover slowly following cognitive effort. *PLoS ONE* 4, e6626. doi:10.1371/journal.pone.0006626.

Bassett, D. S., and Bullmore, E. (2006). Small-world brain networks. *Neuroscientist* 12, 512–523.

Bauke, H. (2007). Parameter estimation for power-law distributions by maximum likelihood methods. *Eur. Phys. J. B* 58, 167–173.

Beckmann, C. F., DeLuca, M., Devlin, J. T., and Smith, S. M. (2005). Investigations into resting-state connectivity using independent component analysis. *Philos. Trans. R. Soc. Lond. B Biol. Sci.* 360, 1001–1013.

Birn, R. M., Diamond, J. B., Smith, M. A., and Bandettini, P. A. (2006). Separating respiratory-variation-related fluctuations from neuronal-activity-related fluctuations in fMRI. *Neuroimage* 31, 1536–1548.

Biswal, B., Yetkin, F. Z., Haughton, V. M., and Hyde, J. S. (1995). Functional connectivity in the motor cortex of resting human brain using echo-planar MRI. *Magn. Reson. Med.* 34, 537–541.

Boccaletti, S., Latora, V., Moreno, Y., Chavez, M., and Hwang, D.-U. (2006). Complex networks: structure and dynamics. *Phys. Rep.* 424, 175–308.

Bonifazi, P., Goldin, M., Picardo, M. A., Jorquera, I., Cattani, A., Bianconi, G., Represa, A., Ben-Ari, Y., and Cossart, R. (2009). GABAergic hub neurons orchestrate synchrony in developing hippocampal networks. *Science (New York, NY)* 326, 1419–1424.

Buckner, R. L., Sepulcre, J., Talukdar, T., Krienen, F. M., Liu, H., Hedden, T., Andrews-Hanna, J. R., Sperling, R. A., and Johnson, K. A. (2009). Cortical hubs revealed by intrinsic functional connectivity: mapping, assessment of stability, and relation to Alzheimer's disease. *J. Neurosci.* 29, 1860–1873.

Bullmore, E., Fadili, J., Maxim, V., Sendur, L., Whitcher, B., Suckling, J., Brammer, M., and Breakspear, M. (2004). Wavelets and functional magnetic resonance imaging of the human brain. *Neuroimage* 23(Suppl. 1), S234–S249.

Bullmore, E., and Sporns, O. (2009). Complex brain networks: graph theoretical analysis of structural and functional systems. *Nat. Rev. Neurosci.* 10, 186–198.

Clauset, A., Shalizi, C. R., and Newman, M. E. J. (2009). Power-law distributions in empirical data. *SIAM Rev.* 51, 661–703.

Collins, D. L., Holmes, C., Peters, T., and Evans, A. (1995). Automatic 3D model-based neuroanatomical segmentation. *Hum. Brain Mapp.* 3, 190–208.

Cordes, D., Haughton, V. M., Arfanakis, K., Carew, J. D., Turski, P. A., Moritz, C. H., Quigley, M. A., and Meyerand, M. E. (2001). Frequencies contributing to functional connectivity in the cerebral cortex in "resting-state" data. *AJNR Am. J. Neuroradiol.* 22, 1326–1333.

Damoiseaux, J. S., Rombouts, S. A., Barkhof, F., Scheltens, P., Stam, C. J., Smith, S. M., and Beckmann, C. F. (2006). Consistent resting-state networks across healthy subjects. *Proc. Natl. Acad. Sci. U.S.A.* 103, 13848–13853.

Eguiluz, V. M., Chialvo, D. R., Cecchi, G. A., Baliki, M., and Apkarian, A. V. (2005). Scale-free brain functional networks. *Phys. Rev. Lett.* 94, 018102.

Fischl, B., van der Kouwe, A., Destrieux, C., Halgren, E., Ségonne, F., Salat, D. H., Busa, E., Seidman, L. J., Goldstein, J. M., Kennedy, D., Caviness, V., Makris, N., Rosen, B., and Dale, A. M. (2004). Anatomically parcellating the human cerebral cortex. *Cereb. Cortex* 14, 11–22.

Fornito, A., and Bullmore, E. T. (2010). What can spontaneous fluctuations of the blood oxygenation-level-dependent signal tell us about psychiatric disorders? *Curr. Opin. Psychiatry* 23, 239–249.

Fox, M. D., and Raichle, M. E. (2007). Spontaneous fluctuations in brain activity observed with functional magnetic resonance imaging. *Nat. Rev. Neurosci.* 8, 700–711.

Fox, M. D., Snyder, A. Z., Vincent, J. L., Corbetta, M., Van Essen, D. C., and Raichle, M. E. (2005). The human brain is intrinsically organized into dynamic, anticorrelated functional networks. *Proc. Natl. Acad. Sci. U.S.A.* 102, 9673–9678.

Fox, M. D., Snyder, A. Z., Zacks, J. M., and Raichle, M. E. (2006). Coherent spontaneous activity accounts for trial-to-trial variability in human evoked brain responses. *Nat. Neurosci.* 9, 23–25.

Fox, M. D., Zhang, D., Snyder, A. Z., and Raichle, M. E. (2009). The global signal and observed anticorrelated resting state brain networks. *J. Neurophysiol.* 101, 3270–3283.

Fraiman, D., Balenzuela, P., Foss, J., and Chialvo, D. R. (2009). Ising-like dynamics in large-scale functional brain networks. *Phys. Rev. E. Stat. Nonlin. Soft Matter Phys.* 79, 061922.

Hagmann, P., Cammoun, L., Gigandet, X., Meuli, R., Honey, C. J., Wedeen, V. J., and Sporns, O. (2008). Mapping the structural core of human cerebral cortex. *PLoS Biol.* 6, e159. doi:10.1371/journal.pcbi.1000748.

Hagmann, P., Kurant, M., Gigandet, X., Thiran, P., Wedeen, V. J., Meuli, R., and Thiran, J. P. (2007). Mapping human whole-brain structural networks with diffusion MRI. *PLoS ONE* 2, e597. doi:10.1371/journal.pone.0000597.

Hayasaka, S., and Laurienti, P. J. (2010). Comparison of characteristics between region-and voxel-based network analyses in resting-state fMRI data. *Neuroimage* 50, 499–508.

He, Y., Dagher, A., Chen, Z., Charil, A., Zijdenbos, A., Worsley, K., and Evans,

A. (2009). Impaired small-world efficiency in structural cortical networks in multiple sclerosis associated with white matter lesion load. *Brain* 132, 3366–3379.

Hesselmann, G., Kell, C. A., Eger, E., and Kleinschmidt, A. (2008). Spontaneous local variations in ongoing neural activity bias perceptual decisions. *Proc. Natl. Acad. Sci. U.S.A.* 105, 10984–10989.

Honey, C. J., Sporns, O., Cammoun, L., Gigandet, X., Thiran, J. P., Meuli, R., and Hagmann, P. (2009). Predicting human resting-state functional connectivity from structural connectivity. *Proc. Natl. Acad. Sci. U.S.A.* 106, 2035–2040.

Humphries, M. D., Gurney, K., and Prescott, T. J. (2006). The brainstem reticular formation is a small-world, not scale-free, network. *Proc. Biol. Sci.* 273, 503–511.

Jenkinson, M., and Smith, S. (2001). A global optimisation method for robust affine registration of brain images. *Med. Image Anal.* 5, 143–156.

Kelly, A. M., Uddin, L. Q., Biswal, B. B., Castellanos, F. X., and Milham, M. P. (2008). Competition between functional brain networks mediates behavioral variability. *Neuroimage* 39, 527–537.

Latora, V., and Marchiori, M. (2001). Efficient behavior of small-world networks. *Phys. Rev. Lett.* 5,198701.

Latora, V., and Marchiori, M. (2003). Economic small-world behavior in weighted networks. *Eur. Phys. J. B* 32, 249–263.

Lewis, C. M., Baldassarre, A., Committeri, G., Romani, G. L., and Corbetta, M. (2009). Learning sculpts the spontaneous activity of the resting human brain. *Proc. Natl. Acad. Sci. U.S.A.* 106, 17558–17563.

Liu, L., Alderson, D., Doyle, J. C., and Willinger, W. (2005). Towards a theory of scale-free graphs: definitions, properties and implications. *Internet Math.* 2, 431–523.

Liu, Y., Liang, M., Zhou, Y., He, Y., Hao, Y., Song, M., Yu, C., Liu, H., Liu, Z., and Jiang, T. (2008). Disrupted small-world networks in schizophrenia. *Brain* 131, 945–961.

Maslov, S., and Sneppen, K. (2002). Specificity and stability in topology of protein networks. *Science (New York, NY)* 296, 910–913.

Meunier, D., Lambiotte, R., Fornito, A., Ersche, K. D., and Bullmore, E. T. (2009). Hierarchical modularity in human brain functional networks. *Front. Neuroinformatics* 3, 37. doi:10.3389/neuro.11.037.2009.

Murphy, K., Birn, R. M., Handwerker, D. A., Jones, T. B., and Bandettini, P. A. (2009). The impact of global signal regression on resting state correlations: are anti-correlated networks introduced? *Neuroimage* 44, 893–905.

Newman, M. J. E. (2003). The structure and function of complex networks. *SIAM Rev.* 45, 167–256.

Nir, Y., Fisch, L., Mukamel, R., Gelbard-Sagiv, H., Arieli, A., Fried, I., and Malach, R. (2007). Coupling between neuronal firing rate, gamma LFP, and BOLD fMRI is related to interneuronal correlations. *Curr. Biol.* 17, 1275–1285.

Percival, D. B., and Walden, A. T. (2000). *Wavelet Methods for Time Series Analysis*. Cambridge: Cambridge University Press.

Pohl, K. M., Bouix, S., Nakamura, M., Rohlfing, T., McCarley, R. W., Kikinis, R., Grimson, W. E. L., Shenton, M. E., and Wells, W. M. (2007). A hierarchical algorithm for MR brain image parcellation. *IEEE Trans. Med. Imaging* 26, 1201–1212.

Rubinov, M., and Sporns, O. (2009). Complex network measures of brain connectivity: uses and interpretations. *Neuroimage*. [Epub ahead of print].

Salvador, R., Martinez, A., Pomarol-Clotet, E., Gomar, J., Vila, F., Sarro, S., Capdevila, A., and Bullmore, E. (2008). A simple view of the brain through a frequency-specific functional connectivity measure. *Neuroimage* 39, 279–289.

Salvador, R., Suckling, J., Coleman, M. R., Pickard, J. D., Menon, D., and Bullmore, E. (2005a). Neurophysiological architecture of functional magnetic resonance images of human brain. *Cereb. Cortex* 15, 1332–1342.

Salvador, R., Suckling, J., Schwarzbauer, C., and Bullmore, E. (2005b). Undirected graphs of frequency-dependent functional connectivity in whole brain networks. *Philos. Trans. R. Soc. Lond. B Biol. Sci.* 360, 937–946.

Seeley, W. W., Menon, V., Schatzberg, A. F., Keller, J., Glover, G. H., Kenna, H., Reiss, A. L., and Greicius, M. D. (2007). Dissociable intrinsic connectivity networks for salience processing and executive control. *J. Neurosci.* 27, 2349–2356.

Shehzad, Z., Kelly, A. M., Reiss, P. T., Gee, D. G., Gotimer, K., Uddin, L. Q., Lee, S. H., Margulies, D. S., Roy, A. K., Biswal, B. B., Petkova, E., Castellanos, F. X., and Milham, M. P. (2009). The resting brain: unconstrained yet reliable. *Cereb. Cortex* 19, 2209–2229.

Shmuel, A., and Leopold, D. A. (2008). Neuronal correlates of spontaneous fluctuations in fMRI signals in monkey visual cortex: Implications for functional connectivity at rest. *Hum. Brain Mapp.* 29, 751–761.

Simon, H. A. (1962). The architecture of complexity. *Proc. Am. Philos. Soc.* 106, 467–482.

Smith, S. M., Fox, P. T., Miller, K. L., Glahn, D. C., Fox, P. M., Mackay, C. E., Filippini, N., Watkins, K. E., Toro, R., Laird, A. R., and Beckmann, C. F. (2009). Correspondence of the brain's functional architecture during activation and rest. *Proc. Natl. Acad. Sci. U.S.A.* 106, 13040–13045.

Sporns, O., Tononi, G., and Kotter, R. (2005). The human connectome: a structural description of the human brain. *PLoS Comput. Biol.* 1, e42. doi:10.1371/journal.pcbi.0010042.

Strogatz, S. H. (2001). Exploring complex networks. *Nature* 410, 268–276.

Thirion, B., Flandin, G., Pinel, P., Roche, A., Ciuciu, P., and Poline, J. B. (2006). Dealing with the shortcomings of spatial normalization: multi-subject parcellation of fMRI datasets. *Hum. Brain Mapp.* 27, 678–693.

Tzourio-Mazoyer, N., Landeau, B., Papathanassiou, D., Crivello, F., Etard, O., Delcroix, N., Mazoyer, B., and Joliot, M. (2002). Automated anatomical labeling of activations in SPM using a macroscopic anatomical parcellation of the MNI MRI single-subject brain. *Neuroimage* 15, 273–289.

van den Heuvel, M. P., Stam, C. J., Boersma, M., and Hulshoff Pol, H. E. (2008). Small-world and scale-free organization of voxel-based resting-state functional connectivity in the human brain. *Neuroimage* 43, 528–539.

van den Heuvel, M. P., Stam, C. J., Kahn, R. S., and Hulshoff Pol, H. E. (2009). Efficiency of functional brain networks and intellectual performance. *J. Neurosci.* 29, 7619–7624.

Vincent, J. L., Patel, G. H., Fox, M. D., Snyder, A. Z., Baker, J. T., Van Essen, D. C., Zempel, J. M., Snyder, L. H., Corbetta, M., and Raichle, M. E. (2007). Intrinsic functional architecture in the anaesthetized monkey brain. *Nature* 447, 83–86.

Wang, J., Wang, L., Zang, Y., Yang, H., Tang, H., Gong, Q., Chen, Z., Zhu, C., and He, Y. (2009a). Parcellation-dependent small-world brain functional networks: a resting-state fMRI study. *Hum. Brain Mapp.* 30, 1511–1523.

Wang, L., Zhu, C., He, Y., Zang, Y., Cao, Q., Zhang, H., Zhong, Q., and Wang, Y. (2009b). Altered small-world brain functional networks in children with attention-deficit/hyperactivity disorder. *Hum. Brain Mapp.* 30, 638–649.

Weissenbacher, A., Kasess, C., Gerstl, F., Lanzenberger, R., Moser, E., and Windischberger, C. (2009). Correlations and anticorrelations in resting-state functional connectivity MRI: a quantitative comparison of preprocessing strategies. *Neuroimage* 47, 1408–1416.

Yu, S., Huang, D., Singer, W., and Nikolic, D. (2008). A small world of neuronal synchrony. *Cereb. Cortex* 18, 2891–2901.

Zalesky, A., Fornito, A., Harding, I. H., Cocchi, L., Yucel, M., Pantelis, C., and Bullmore, E. T. (2010). Whole-brain anatomical networks: does the choice of nodes matter? *Neuroimage* 50, 970–983.

Conflict of Interest Statement: The authors declare that the research was conducted in the absence of any commercial or financial relationships that could be construed as a potential conflict of interest.

Received: 29 January 2010; paper pending published: 27 February 2010; accepted: 19 May 2010; published online: 17 June 2010.

*Citation: Fornito A, Zalesky A and Bullmore ET (2010) Network scaling effects in graph analytic studies of human resting-state fMRI data. Front. Syst. Neurosci. **4**:22. doi: 10.3389/fnsys.2010.00022*

frontiers in
SYSTEMS NEUROSCIENCE

ORIGINAL RESEARCH ARTICLE
published: 15 July 2010
doi: 10.3389/fnsys.2010.00033

Glutamatergic and resting-state functional connectivity correlates of severity in major depression – the role of pregenual anterior cingulate cortex and anterior insula

Dorothea I. Horn[1], Chunshui Yu[2], Johann Steiner[1], Julia Buchmann[1], Joern Kaufmann[3], Annemarie Osoba[1], Ulf Eckert[1], Kathrin C. Zierhut[1], Kolja Schiltz[1], Huiguang He[4], Bharat Biswal[5], Bernhard Bogerts[1] and Martin Walter[1]*

[1] *Department of Psychiatry, Otto-von-Guericke University, Magdeburg, Germany*
[2] *Department of Radiology, Tianjin Medical University General Hospital, Tianjin, China*
[3] *Department of Neurology, Otto-von-Guericke University, Magdeburg, Germany*
[4] *Key Lab of Complex Systems and Intelligent Science, Institute of Automation, Chinese Academy of Science, Beijing, China*
[5] *Department of Radiology, New Jersey Medical School, University of Medicine and Dentistry New Jersey, Newark, NJ, USA*

Edited by:
Lucina Q. Uddin, Stanford University, USA

Reviewed by:
Anke Henning, Institute for Biomedical Engineering, Switzerland
Laura M. Rowland, University of Maryland School of Medicine, USA
Alexander Sartorius, Zentralinstitut für Seelische Gesundheit, Germany

****Correspondence:***
Martin Walter, CANLAB, Department of Psychiatry, Leipziger Str. 44, 39120 Magdeburg, Germany.
e-mail: martin@canlab.de

Glutamatergic mechanisms and resting-state functional connectivity alterations have been recently described as factors contributing to major depressive disorder (MDD). Furthermore, the pregenual anterior cingulate cortex (pgACC) seems to play an important role for major depressive symptoms such as anhedonia and impaired emotion processing. We investigated 22 MDD patients and 22 healthy subjects using a combined magnetic resonance spectroscopy (MRS) and resting-state functional magnetic resonance imaging (fMRI) approach. Severity of depression was rated using the 21-item Hamilton depression scale (HAMD) and patients were divided into severely and mildly depressed subgroups according to HAMD scores. Because of their hypothesized role in depression we investigated the functional connectivity between pgACC and left anterior insular cortex (AI). The sum of Glutamate and Glutamine (Glx) in the pgACC, but not in left AI, predicted the resting-state functional connectivity between the two regions exclusively in depressed patients. Furthermore, functional connectivity between these regions was significantly altered in the subgroup of severely depressed patients (HAMD > 15) compared to healthy subjects and mildly depressed patients. Similarly the Glx ratios, relative to Creatine, in the pgACC were lowest in severely depressed patients. These findings support the involvement of glutamatergic mechanisms in severe MDD which are related to the functional connectivity between pgACC and AI and depression severity.

Keywords: major depressive disorder, pregenual anterior cingulate cortex, anterior insula, functional magnetic resonance imaging, glutamate, magnetic resonance spectroscopy, functional connectivity, resting state

INTRODUCTION

Major depressive disorder (MDD) is characterized by persistent negative feelings of sadness, guilt, and worthlessness and further by ruminating thoughts, cognitive impairments, and somatic complaints. These various symptoms are accompanied by abnormal activity in several brain regions as observed in a number of imaging studies. This supports the notion of a complex network underlying the pathology of depression. It also questions the existence of a few core regions with primarily impaired brain function. Such specific regions, however, would be highly useful to guide regional invasive therapies such as deep brain stimulation (Mayberg et al., 2005; Lozano et al., 2008) or imaging guided treatment prediction or monitoring (MacQueen, 2009).

The medial prefrontal cortex and the anterior cingulate cortex (ACC) have been identified as key structures for MDD, with abnormalities not only in fMRI activation but also in baseline metabolism or perfusion. In accordance with these *in vivo* findings, post mortem investigations in MDD have revealed reductions in neuronal and glial cell densities, size, and arborization (Ongür et al., 1998; Cotter et al., 2001; Manji et al., 2001). On a molecular level, reduced expression of glial enzymes allowing for glutamate (Glu) reuptake from the synaptic cleft and its conversion to non-excitotoxic glutamine have been observed (Choudary et al., 2005). During the past few years, the hypothesis of a complex metabolic abnormality in the ACC has been developed which links psychological abnormalities in MDD to abnormal baseline metabolism in astrocytes and neurons and even to disease related immunological processes in microglia (Dantzer et al., 2008).

Proton NMR spectroscopy (MRS) is a widely used tool to measure brain metabolites *in vivo*. MRS enables the detection of metabolites, among them, the total concentration of Glutamate in the brain tissue. A continuous recycling of glutamate between neurons and glial cells takes place in the brain. As neurotransmission progresses, neuronal glutamate is released into the synaptic cleft. From there it is taken up by glial cells and converted to glutamine. Glutamine is afterwards transported back into the neurons where it is reconverted to glutamate (Rothman et al., 2003). Glutamate levels do not only reflect glutamatergic neurotransmitter activity, but also the synthesis of glutamate through the tricarboxylic acid (TCA) cycle. Total glutamate measurements as observed by MRS therefore are not specific to the constant flux through the glutamate–glutamine

cycle. Glutamatergic alterations in several brain regions have been implicated in neurological or psychiatric diseases using MRS (Auer et al., 2000; Hasler et al., 2007).

In a previous study (Walter et al., 2009), it has been shown that impairments of the neuronal–glial unit can be visualized both on a functional and a molecular level using a combination of fMRI and MRS. In the pregenual portion of the ACC (pgACC) abnormally reduced amplitudes of negative BOLD responses were found in a group of unmedicated MDD patients. Reduced BOLD amplitudes during task were further related to abnormal glutamate concentrations in the same region. This finding is compatible with the hypothesis that the extent of functional responses that appear on top of baseline neuronal activity depends on the metabolic baseline level of the involved neuronal–astroglial unit and the degree of anaerobic glucose consumption (Raichle and Mintun, 2006). In this first combined resting-state fMRI–MRS study in MDD, we extend previous work (Walter et al., 2009) that relates the amplitudes of negative BOLD responses in pgACC to regional GABA (gamma-amino butyric acid) ratios. Interestingly, glutamatergic modulations of BOLD responses were only present in depressed patients, while the GABAergic modulations seen in healthy controls (Northoff et al., 2007) disappeared. A glutamatergic but not GABAergic deficit in pgACC was also reported by Hasler et al. (2007).

A newly arising interrelation of functional responses with a metabolic marker that includes glial functioning would be well in accordance with converging findings in rodents, where pharmacological astroglial disruptions consequently lead to anhedonic behavior such as reduced sucrose preference (Banasr and Duman, 2008). Additionally, agents like riluzole that manipulate the neurotransmission of glutamate, prevented depression-like behavior in a rat model (Banasr et al., 2010). The glial hypothesis, mainly pioneered by researchers such as Sanacora and Raijkowska (Rajkowska et al., 1999; Kugaya and Sanacora, 2005; Rajkowska and Miguel-Hidalgo, 2007), thus serves as a crucial addition to other neuronal concepts of primarily serotonergic dysfunction. As proposed by some authors the complex situation in both neuronal and glial compartments, which forms the basis for task-related responses, can be investigated at rest (Raichle and Mintun, 2006; Raichle and Snyder, 2007; Shulman et al., 2007). The concept of spontaneous resting-state fluctuations first described by Biswal et al. (1995) seems ideal to investigate alterations of this system on the functional level (Fox and Raichle, 2007).

Resting-state functional connectivity (rsFC) is defined as the correlation of spontaneous low frequency BOLD signal time courses of distinct brain regions. In major depression, altered resting-state behavior in the default mode components has been shown (Greicius et al., 2007). Indications for a cortico-limbic dysfunction (Mayberg, 1997) were also found during task and rest (Anand et al., 2005a,b). These findings are related to a large number of altered functional responses in emotional core regions including medial prefrontal cortex and limbic structures (Rigucci et al., 2009), but most of these remain outside the classic task-positive attention regions such as dorsal ACC, anterior insula (AI) or lateral prefrontal cortex. Task-negative regions respond with a decrease in BOLD signal to attentional tasks while task-positive regions are specifically activated at the same time. While the exact nature of functional anticorrelations at rest and the effects of preprocessing strategies remain unclear to date (Fox et al., 2009; Murphy et al., 2009), the functional separation of task-positive and task-negative regions using task and resting-state studies (Fox et al., 2005; Buckner and Vincent, 2007; Uddin et al., 2009; Neumann et al., 2010) is well accepted. Disease severity related alterations of rsFC in this intrinsic organization of the brain were recently described for major depression (Zhou et al., 2010).

Complex impairments of emotional and self awareness underlie the clinical symptoms of anhedonia, rigid affect or ruminations as well as negative self concept and altered social interactions. Taking this into account it is highly important to investigate the relationship of pgACC pathologies to dysfunctions in other domains especially those involved in the processing of emotions. Given the increasing evidence for the involvement of the insular cortex in the conscious processing of affect as well as the generation of percepts of self awareness in a subjective timeframe (Craig, 2009), one has to hypothesize functional abnormalities in the AI. In a recent study, Grimm et al. (2009a,b) showed altered neural responses in the salience network (Seeley et al., 2007) that are related to impaired judgments of self-relatedness of emotional stimuli. This study further provided evidence for left lateralized effects, which are well in accordance with a forebrain asymmetry of emotional valence and parasympathetic processing in left AI, which is also the putative target of vagal nerve stimulation in MDD (Craig, 2005).

The majority of depressive symptoms are present even in the absence of specific tasks when the patients are mainly engaged in exaggerated, negatively colored self-referential processing, continuous negative moods, and ruminative thoughts. Therefore it seems important to investigate the putative neural substrates during such abnormal functioning, i.e. at rest. Such baseline alterations, characterized by impaired rsFC between pgACC and AI, might be directly related to abnormal metabolite or cellular measures.

We thus aimed to investigate the relationship of altered baseline processes displayed in rs fMRI with the metabolic representations of neuronal–glial functioning seen in MRS. Pregenual ACC is a primary region of interest due to the vast literature on functional and metabolite abnormalities. It was thus tested if abnormal glutamatergic levels in pgACC would influence rsFC with AI/frontal operculum. The second region, as part of the task-positive, attention set network, was chosen because of strong direct anatomical connections with ACC in the macaque and human brain (Mesulam and Mufson, 1982; Mufson and Mesulam, 1982; Augustine, 1996) as well as its proposed role for the switching between anticorrelated networks (Sridharan et al., 2008).

Given the hypothesized primary deficit in the pgACC, we intend to further test if the putative abnormal anticorrelative behavior could be traced back to a molecular deficit in pgACC without direct relations to the metabolite profiles in AI. The aim was to test the specificity of glutamatergic deficiencies as symptoms of glial-neuronal pathology in pgACC. This would support the concept of altered functional network behavior outside the pgACC, at least in the salience network, as a consequence of a primary neuronal glial decline in pgACC in the case of MDD and may help to identify disease specific abnormalities in otherwise overlapping findings of abnormal resting-state behavior.

To prove the clinical relevance of such functional and metabolic abnormalities, we further tested their relation to markers of clinical severity of depression. During treatment response or remission, as indicated by decreasing scores of the HAMD, many of the

initially described affective symptoms disappear whereas a number of cognitive–attentional deficits persist. Because of this observation we hypothesized a primary glutamatergic deficit in an affective region, i.e., pgACC, which is directly related to clinical severity and which drives the extent of abnormal rsFC between pgACC and AI. We further hypothesize that Glx concentrations in AI, which has stronger connections to other cognitive regions, are not related to severity or rsFC. The primary focus on pgACC is supported by the fast and strong effects of the glutamate modulating NMDA antagonist ketamine on HAMD scores in treatment resistant MDD patients (Zarate et al., 2006) since ketamine leads to increases of Glu concentrations in exactly this region (Rowland et al., 2005).

Table 1 | Demographic and clinical description of subjects meeting the quality criteria

	Healthy controls	Patients HAMD ≤ 15	Patients HAMD > 15	All patients
Number	22	8	10	18
Male/Female	12/10	5/3	5/5	10/8
Mean age	34.14	37.62	40.5	39.22
[SD]	[6.67]	[12.82]	[13.1]	[12.67]
Mean HAMD	0	12.75	20.7	17.17
[SD]		[1.83]	[2.95]	[4.74]

MATERIALS AND METHODS

SUBJECTS

Twenty-two subjects with an acute MDD episode were recruited from the inpatient and outpatient department of psychiatry at the University of Magdeburg. Primarily, these patients were clinically diagnosed according to the ICD-10 criteria (WHO, 1992). Exclusion criteria were major medical illness, history of seizures, medication with glutamate modulating drugs (ketamine, riluzole, etc.) or benzodiazepines prior electroconvulsive therapy (ECT) treatments and pregnancy, as well as all contraindications against MRI. Specific psychiatric exclusion criteria consisted of atypical forms of depression, any additional psychiatric disorder, and a history of substance abuse or dependence. For a better specification of the depressive symptoms, all patients were rated by clinical questionnaires, among them the Hamilton depression scale. The HAMD was first developed by Hamilton (1960) to rate the acute state of depressive patients. Since then it has been known to accurately describe the disease severity of patients with an acute depressive episode. Moreover, the scores reflect the effects of drug-induced improvement in disease. We used the German version of the 21-item HAMD (CIPS, 1996) for clinical subgroup analysis.

Twenty-two healthy subjects without any psychiatric, neurological, or medical illness were self-referred from study advertisements. All volunteers completed the mini-international neuropsychiatric interview (MINI) to specifically ensure the absence of any ICD-10 psychiatric disorders (Sheehan et al., 1998). The study was approved by the institutional review board of the University of Magdeburg and all subjects gave written informed consent before inclusion. All subjects underwent fMRI and MRS in an identical paradigm. All patients were medicated using SSRI, NRI, and SNRI alone or with new generation antidepressants including agomelatine or lithium. Due to specific MRS quality criteria (see below) 19 patients were finally included to the analysis while for one subject rs fMRI data could not be used. The composition of the sex- and age-matched groups is described in **Table 1**. Neither the controls compared to all patients (*t*-test, $P = 0.137$) nor the subgroups of healthy controls, mildly and severely depressed patients (one-way ANOVA, $F = 1.49$, $P = 0.238$) differed significantly by age.

RESTING-STATE fMRI DATA ACQUISITION AND ANALYSIS

The measurements were performed on a 3 Tesla Siemens MAGNETOM Trio scanner (Siemens, Erlangen, Germany) with an eight-channel phased-array head coil. For acquisition of the resting-state fMRI data, the subjects were told to lie still in the scanner with their eyes closed. Functional time series of 488 time points were acquired with an echo-planar imaging sequence. The following acquisition parameters were used: echo time = 25 ms, field of view = 22 cm, acquisition matrix = 44 × 44, isometric voxel size = 5 × 5 × 5 mm^3. Twenty-six contiguous axial slices covered the entire brain with a repetition time of 1250 ms (flip angle = 70°). The first five acquisitions were discarded to reach steady state and limit T1 effects. High resolution T1-weighted structural MRI scans of the brain were acquired for structural reference using a 3D-MPRAGE sequence (TE = 4.77 ms, TR = 2500 ms, T1 = 1100 ms, flip angle = 7°, bandwidth = 140 Hz/pixel, acquisition matrix = 256 × 256 × 192, isometric voxel size = 1.0 mm^3).

Data was analyzed using the data processing assistant for resting-state fMRI (DPARSF[1], Yan Chao-Gan, State Key Laboratory of Cognitive Neuroscience and Learning, Beijing Normal University, China) which includes resting-state fMRI data analysis toolkit (REST, by Song Xiao-Wei et al.[1]). Both toolboxes work on basis of the spm5 software package (Wellcome Trust Center for Neuroimaging, London, England). Functional data was corrected for differences in slice acquisition time, motion-corrected using a least squares approach and a six-parameter (rigid body) linear transformation, spatially normalized and smoothed by using a 4-mm full-width-at-half-maximum Gaussian kernel. The data was linear detrended and filtered by a band pass filter (0.01–0.08 Hz) to eliminate low frequency fluctuations. The preprocessing steps followed the standard protocol published by Yan and Zang (2010). Accordingly, an additional regression of nuisance covariates was applied during which the functional data was corrected for the six head movement parameters and for global mean signal as well as for white matter and cerebrospinal fluid signal. This correction is discussed to elicit negative correlations between the time courses of normally anticorrelated resting-state network regions (Murphy et al., 2009).

By merging the individually placed spectroscopy voxel positions in normalized space, two regions of interest (ROI) where defined. The pgACC which belongs to the medial prefrontal cortex is localized in the rostral part of Brodmann area 24 and was defined by the Montreal Neurological Institute (MNI) coordinates (x, y, z): 0, 41, 9. The ROI for left AI was placed with the center at 39, 19, 4. Both ROIs had a radius of 10 mm resulting in a volume of approximately 4 ml, which is in line with the size of the MRS voxels.

To compute the rsFC of the ROIs, the time course of every ROI was extracted and a correlation analysis was run to elicit the correlation coefficient of the different time courses. The correlation coefficient

[1]www.restfmri.net

therefore reflects a statistical interrelation of the BOLD time courses in the specific ROIs but no direction or causality. Correlation coefficients close to 1 hereby mean that the time courses have a high synchronicity. Brain morphology was assessed using the fully automated Civet pipeline of the Montreal Neurological Institute (Lerch and Evans, 2005; Ad-Dab'bagh et al., 2006). Following this, the tissue composition and cortical thickness of the whole brain and the specified MRS voxels could be included in the analysis as cofactors.

MRS DATA ACQUISITION AND ANALYSIS

Single voxel proton MRS data was acquired at rest for each subject from a first volume of interest of $10 \times 20 \times 20$ mm^3 = 4.0 ml which was placed in bilateral pgACC and from a second one of $15 \times 10 \times 20$ mm^3 = 3.0 ml which was placed in the frontal operculum of the left AI (**Figure 1**). The location and extent of the pgACC voxel was oriented on our previous findings of altered self awareness, impaired BOLD responses and altered glutamatergic levels in depressed patients (Grimm et al., 2009a,b; Walter et al., 2009).

The measurements were performed on a 3T Siemens MAGNETOM Trio scanner. A PRESS (point-resolved spectroscopy) sequence with the following acquisition parameters was used for both voxels: echo time = 80 ms, repetition time = 2000 ms, 256 averages, bandwidth = 1200 Hz, acquisition time = 853 ms and water suppression. The echo time of 80 ms was used according to the results of Schubert et al. (2004). Manual shimming was performed to improve magnetic field homogeneity set by the automatic shim routine. Additionally, water reference data with radiofrequency pulses for water suppression switched off (TR = 10s, four averages) were acquired for eddy current correction. The acquisition time for every voxel added up to 8 min and 40 s. Spectra were analyzed using LCModel version 6.1.0 (Provencher, 1993). Sixteen different metabolites (Creatine, Glutamate, myo-Inositole, Lactate, NAA, Phosphocholine, Taurine, Aspartate, GABA, Glutamine, Glucose, Alanine, NAAG, Phosphocreatine, Guanine, and Glycerophosphocholine) were fitted using a basis set including all these substances. Since creatine has been described to be an appropriate internal reference for the measured metabolite concentrations in MDD (Yildiz-Yesiloglu and Ankerst, 2006), all metabolite values are given as creatine (Cr) ratios. Cramer-Rao lower bounds (Cavassila et al., 2001), an estimate of the fitting error, was used as a quality criterion to exclude datasets with unreliable quantification results. Hence, analyses of group effects were restricted to subjects meeting the strict quality criteria to indicate reliable spectral identification (Cramer-Rao lower bounds <20%). We did not have to reject spectra due to a poor line width since all used spectra had a full-width-at-half maximum smaller than 12 Hz. The signal to noise ratio was larger than eight for all subjects.

STATISTICAL ANALYSIS

Correlation coefficients of BOLD time courses of pgACC and AI, metabolite levels in both of the regions and HAMD scores were correlated by applying Pearson correlation analysis (SPSS, version 15; SPSS Inc, Chicago, IL, USA). Statistical significance was set at $P < 0.05$. Significant correlations were controlled for confounding effects of age by partial correlation. Extreme values were defined as exceeding the 25th or 27th percentile by more than three interquartile ranges in either direction and were consequently removed. All correlations were calculated separately for healthy controls and MDD patients. To test for intergroup differences, one-way ANOVA was first run followed by two-sample *t*-tests. The significance threshold was also set at $P = 0.05$.

RESULTS

PREDICTION OF RESTING-STATE CONNECTIVITY BETWEEN pgACC AND ANTERIOR INSULA IN DEPRESSION BY MRS

The Glx to creatine ratio in pgACC predicted the functional connectivity between this region and the left AI (**Figure 2**). This relationship between metabolite profiles and functional connectivity was specific for depressed patients ($r = -0.51$, $P = 0.031$) while healthy controls did not show this effect ($r = -0.15$, $P = 0.49$). The same effect could also be observed when only Glu ratios were looked at for the depressed patients ($r = -0.488$, $P = 0.04$) and remained insignificant for the healthy controls ($r = -0.111$, $P = 0.62$).

Lower Glx ratios in pgACC predicted weaker negative correlations, i.e., functional connectivity between pgACC and AI. Patients with the lowest Glx ratios even showed positive correlation coefficients. In contrast, Glx measures in the insula failed to predict the connectivity between the two regions ($P = 0.7$). No correlations were found between gray matter contents of the MRS single voxels and functional connectivities or Glx ratios. Also, patients and controls did not differ in their relative gray and white matter tissue compositions in the two voxels.

Since age has been described to be a factor influencing functional connectivity (Damoiseaux et al., 2008) its effects were explored specifically, but no correlation of age with connectivity values or Glx ratios was found in our samples of either patients or controls.

ALTERED CONNECTIVITIES AND RELATED METABOLITE LEVELS WITH RELEVANCE FOR CLINICAL SEVERITY OF DEPRESSION

Supporting the clinical relevance of the predescribed findings, a significant correlation between HAMD and rsFCs between AI and pgACC could be detected ($r = -0.617$, $P = 0.006$) (**Figure 3A**).

Furthermore symptom severity was predicted by relative Glu and Glx levels only in pgACC (Glu: $r = -0.51$, $P = 0.031$/Glx: $r = -0.44$, $P = 0.068$) (**Figure 3B**) while no such effect was seen for Glx or Glu values in the AI (Glu: $r = 0.092$, $P = 0.72$/Glx: $r = 0.052$, $P = 0.84$). To test the relevance of altered connectivities and related metabolite levels for clinical severity of depression directly, we divided the patients into a severely depressed and a mildly depressed group with a median split according to HAMD scores (median: 16). This resulted in two groups (eight and 10 patients) with no significant differences in age, size, or gender composition (**Table 1**).

As illustrated in **Figures 4 and 5**, one-way ANOVAs revealed group effects for Glx and rsFC with altered Glu and Glx ratios in pgACC (Glu: $F = 8.35$, $P = 0.001$/Glx: $F = 6.993$, $P = 0.003$). Different FCs between both regions ($F = 4.64$, $P = 0.016$) were detected for severely depressed patients compared to both other groups, while no significant effects were found for Glu or Glx ratios in AI (Glu: $F = 0.8$, $P = 0.457$/Glx: $F = 0.91$, $P = 0.41$).

ALTERED FUNCTIONAL CONNECTIVITY BETWEEN pgACC AND AI IN SEVERELY DEPRESSED PATIENTS

A direct comparison of the functional connectivities of pgACC and AI revealed significantly higher correlations of signal time courses for severely depressed patients with HAMD scores 16 or

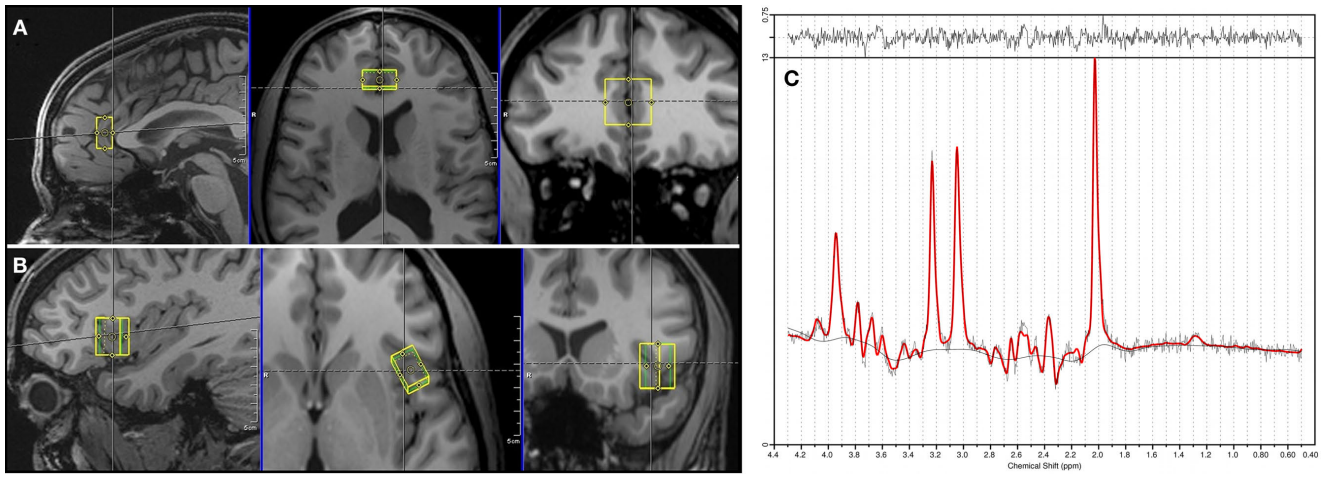

FIGURE 1 | Positioning of the spectroscopy voxels (A: pgACC, B: AI) and a representative spectrum of pgACC **(C).**

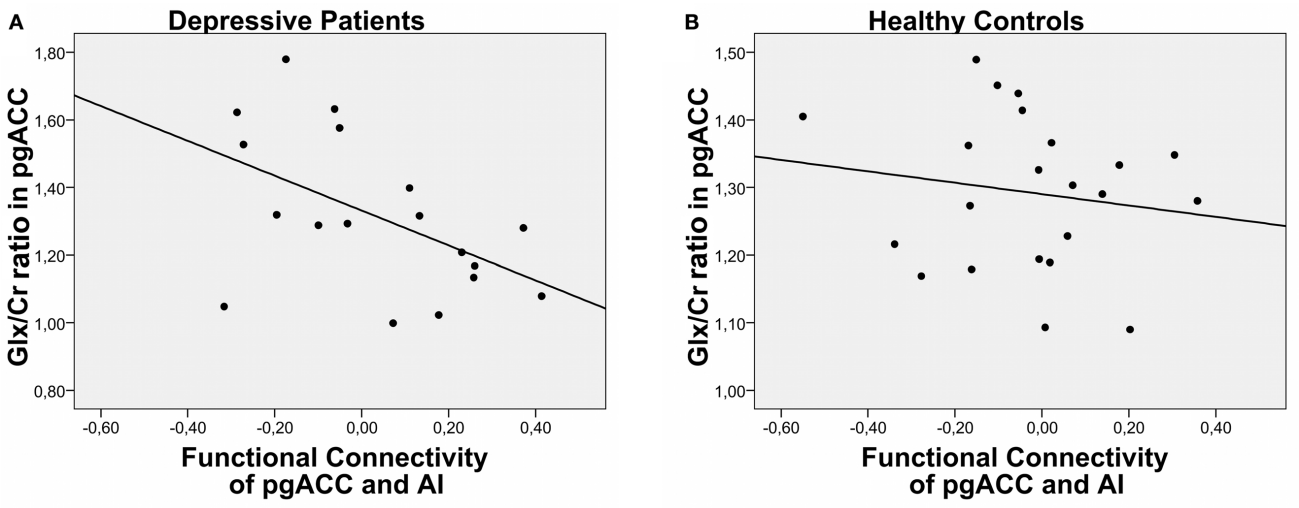

FIGURE 2 | Correlation of functional connectivity between pgACC and AI and Glx/Cr ratios for depressed patients (A) and healthy controls **(B)** ratios was found in our samples of either patients or controls.

higher (mean FC[SD] = 0.15[0.21]) than for healthy controls (mean FC = −0.03[0.21]) (T = −2.26, P = 0.03) and mildly depressed patients (mean FC = −0.12[0.14]) (T = −3.1, P = 0.007) (**Figure 4**). No significant differences in FCs were found between the mildly depressed group and healthy controls.

DEPRESSION SEVERITY IS RELATED TO THE METABOLITE PROFILE IN pgACC

Similar to the functional connectivities, a direct comparison of the Glu and Glx levels in pgACC revealed lower ratios for acutely depressed patients with HAMD scores 16 or higher than for healthy controls (Glu: T = 2.59, P = 0.015/Glx: T = 1.75, P = 0.09) as well when compared to mildly depressed patients (Glu: T = 3.73, P = 0.002/Glx: T = 2.941, P = 0.01). In contrast to the connectivity findings a significant difference of Glu and Glx levels between healthy controls and mildly depressed patients was observed (Glu: T = −2.42, P = 0.022/Glx: T = −2.454, P = 0.037).

Although we did not have *a priori* hypotheses for abnormal values of myo-Inositole, creatine or NAA, we also tested for differences in these metabolites in one-way ANOVA's (P > 0.22). We could however not find any significant alterations for the patients (see also **Table 2**).

DISCUSSION

Our findings provide first evidence for abnormal glutamatergic modulation of resting-state brain activity in depression. In severely depressed patients, functional connectivity between pgACC and AI was linearly correlated with Glx/Cr ratios in the pgACC. Such a correlation was not evident in healthy controls. When exploring the clinical relevance of

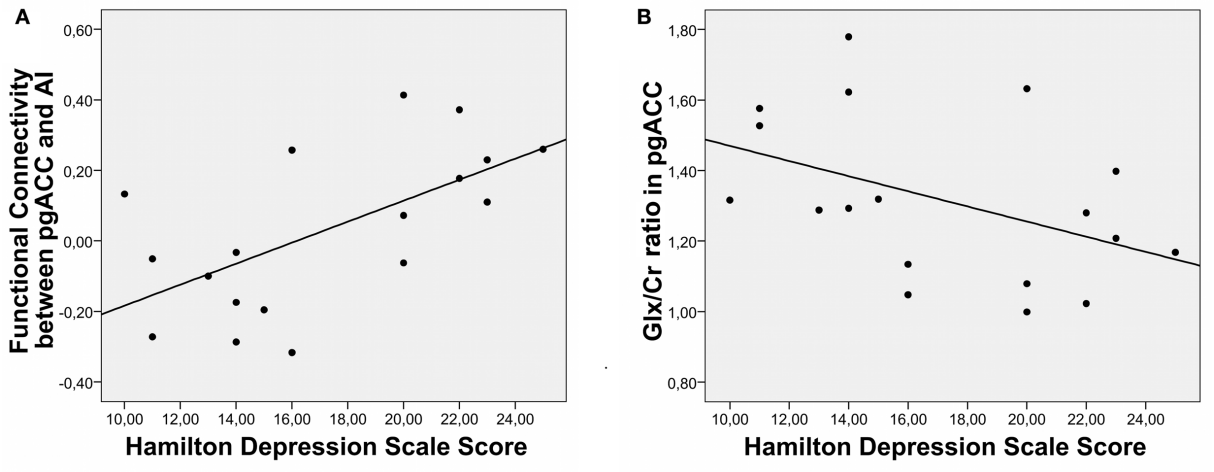

FIGURE 3 | Correlation of clinical severity of depression with RSFC (A) as well as with Glx/Cr ratios in pgACC **(B).**

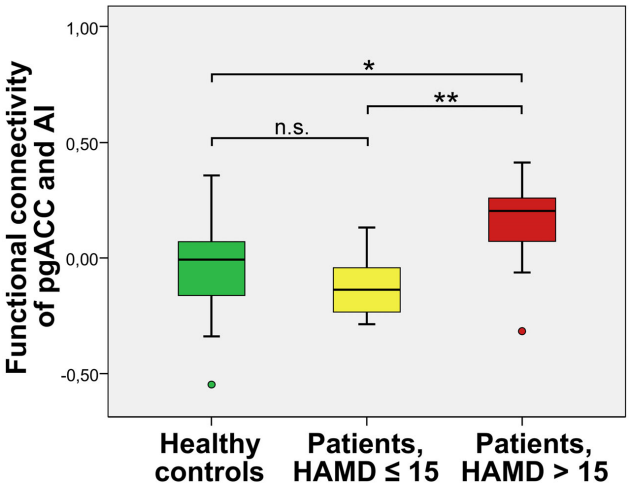

FIGURE 4 | Severely depressed patients with altered functional connectivity between pgACC and AI (box plot showing median, interquartile range, sample minimum and maximum;*$P < 0.05$, **$P < 0.01$, n.s.: not significant.

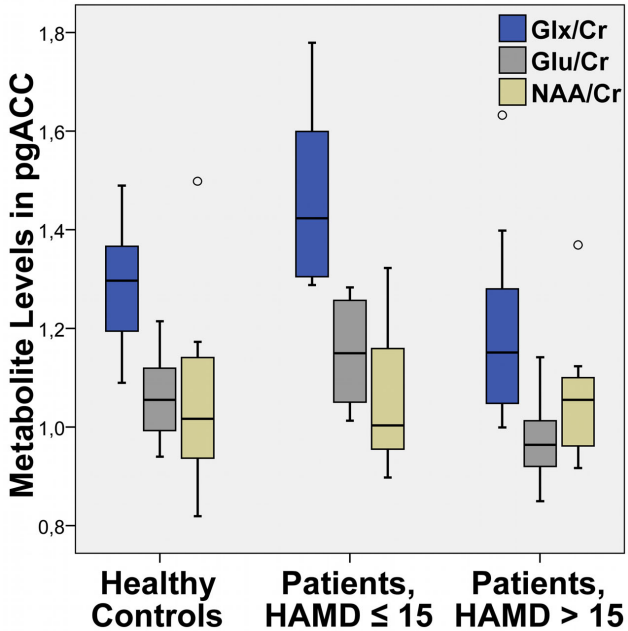

FIGURE 5 | Mean levels of the sum value of Glu and Gln (Glx), glutamate (Glu) and NAA relative to creatine (Cr) in pgACC (box plot showing median, interquartile range, sample minimum and maximum).

this metabolic impact on resting-state connectivity, a trend for linear correlation of HAMD with both factors was found. Consequently, direct comparison of Glx/Cr ratios revealed lower concentrations in severely depressed patients as compared to healthy controls and mildly depressed patients. However, this glutamatergic deficit was only present in pgACC and was accompanied by abnormal functional connectivities at rest. Only severely depressed patients showed weaker negative or even positive correlations of time courses in pgACC and AI.

The evidence of a glutamatergic deficit and its importance for functional alterations in ACC reported here is in line with similar findings from our group in an unmedicated highly depressed patient population (Walter et al., 2009). In this group of patients with HAMD scores of 24 or higher, we found that lower levels of glutamine and glutamate predicted weaker functional responses in the pgACC using a 2D JPRESS MRS sequence. Functional responses were weaker in patients compared to healthy controls. In support of an effect of anhedonia on brain activity, specifically highly anhedonic patients showed impaired negative BOLD responses during a cognitive task. This is mirrored by our findings in this new study that showed that even the more general marker of HAMD scores was able to turn out subgroups differing in their baseline connectivity and metabolite levels. Correlation of rsFC and Glx/Cr ratios was specific to the patient group and pathologically altered rsFC were found to be prominent only in the severely depressed group.

Table 2 | Mean levels of fitted metabolites with valid spectra (CRLB < 20 in at least 75% of the subjects).

	Healthy controls		Patients HAMD ≤ 15		Patients HAMD > 15	
	pgACC	AI	pgACC	AI	pgACC	AI
Creatine (Cr)	5.64 ± 1.6	3.88 ± 2.94	4.9 ± 1.6	3.62 ± 1.92	5.65 ± 1.66	4.79 ± 1.53
Glutamate/Cr	1.06 ± 0.08	0.82 ± 0.61	1.15 ± 0.11	1.01 ± 0.45	0.98 ± 0.09	1.06 ± 0.19
myo-Inositole/Cr	0.71 ± 0.14	0.49 ± 0.34	0.71 ± 0.07	0.58 ± 0.31	0.67 ± 0.09	0.70 ± 0.15
NAA/Cr	1.04 ± 0.15	0.85 ± 0.59	1.06 ± 0.15	1.03 ± 0.44	1.06 ± 0.13	1.11 ± 0.14
Glx/Cr	1.29 ± 0.11	0.92 ± 0.69	1.47 ± 0.19	1.21 ± 0.54	1.2 ± 0.2	1.19 ± 0.2

This leads to at least three main conclusions:

Firstly, we extend the observations of impaired brain function of pgACC in a resting-state condition: In contrast to the abnormalities within DMN or cortico–limbic connectivities which were previously reported (Greicius et al., 2007; Anand et al., 2009), our study shows altered correlations between pgACC and AI. These regions belong to different networks with opposing behavior upon external stimulation. While pgACC has strongest rsFC with the ventromedial prefrontal part of the default mode network (Margulies et al., 2007) the AI is positively correlated to the task-positive attention set network. The AI belongs to this network together with the dorsal ACC (Dosenbach et al., 2008) and both are of specific importance for the processing of a stimulus' salience (Seeley et al., 2007). A newly proposed network model of insula function describes its role in saliency and switching between networks (Menon and Uddin, 2010). This is in line with the observation that depressive patients are less able to down-regulate the DMN activity during tasks (Sheline et al., 2009). Our results may thus help to explain specific MDD symptoms like ruminating thoughts and the clinical impression of depressed patients being "caught" in their depressed mood. Such hyper stable assignment of the AI to the default mode network may impair its flexibility in coordinating the patients' attention being directed either towards the external world or the internal perception of self-related processes.

Secondly, we extend the previously described glutamatergic modulation of abnormal fMRI responses (Walter et al., 2009) to a baseline condition. This supports the hypothesis that altered basic conditions of the network architecture lead to abnormal functional responses, such as, for example, decreased negative BOLD responses during cognitive tasks in a region belonging to the DMN (Mennes et al., 2010). Resting-state alterations and impaired reactivity to external stimulations in the pgACC were thus both shown to depend on glutamatergic metabolite levels. Therefore we assume that rsFC of this region is able to directly predict the degree of excitability in terms of subjective reports and functional responses in patients during stimulation (Hampson et al., 2006). This direct prediction still remains to be shown for MDD and related symptoms in the future.

Thirdly, we substantiate the importance of altered metabolite and functional levels in this key region of the ACC to the severity of depressive symptoms, since in both rsFC and Glx/Cr ratios the severely depressed patients (HAMD scores of 16 or higher) showed the strongest alterations. In an animal model glial changes that where induced by chronic and unpredictable stress could be reversed or blocked by treating the rats with riluzole which influences the glutamatergic neurotransmission (Banasr et al., 2010). In terms of clinical treatment this pregenual glial-neuronal deficit would favor the use of glutamatergic drugs in patients showing such functional and neurotransmitter patterns. A previous study showed that a relative hypometabolism in exactly this region discerns treatment resistant patients from those responsive to selective serotonin reuptake inhibitor (SSRI) treatment (Mayberg, 1997). Our findings can further explain the specific efficacy of glutamatergic drugs such as ketamine in severe, treatment resistant depression (Zarate et al., 2006) which leads to increased glutamate/glutamine levels in pgACC (Rowland et al., 2005).

The depicted molecular deficit in the pgACC is related to functional connectivity between this region and AI. Interestingly, we did not find an interdependence of FCs and AI ratios of Glx or Glu to Cr. This is accompanied by prominent histoarchitectonic findings in the pgACC from a large number of postmortem studies. These suggest reduced glial densities and expression of enzymes allowing for glutamate reuptake and conversion to glutamine (Rajkowska et al., 1999; Cotter et al., 2001; Rajkowska and Miguel-Hidalgo, 2007). In this context, the reversible reductions of Glx would mirror a hypometabolic state with lowered glutamine cycling between glial cells and neurons, which by itself is highly energy demanding (Raichle and Mintun, 2006). Such altered baseline metabolism would thus result in altered functional connectivities, given that these can be regarded elementary for normal adaptive brain functions in healthy human beings. It has recently been reported that inter-individual differences in resting-state functional connectivity predict task-induced BOLD activity (Mennes et al., 2010). While reduced anticorrelations could be regarded as signs of decreased flexibility of the brain to react upon external stimulations, these altered connectivities could additionally be considered as the underlying sources of reduced functional responses upon explicit stimulation and consequently altered affective processing in MDD. Interestingly, we did not observe significant differences in NAA, myo-Inositole or creatine levels suggesting a specific relationship of glutamatergic mechanisms and abnormal rsFCs in depression. Stable concentrations of creatine in all groups also validate the approach of reporting the metabolite concentrations relative to creatine, since, in principle, the altered ratios could be a result of abnormal levels of creatine due to its involvement in brain metabolism.

In schizophrenia, similar mechanisms of altered connectivity between fronto-parietal and default mode cortical networks have been observed. In an independent component analysis, healthy subjects showed less correlation between these two networks than

patients when correlations are generally positive (Jafri et al., 2008). At the same time they showed more negative values of connectivity than schizophrenic patients when global signal removal has caused the correlation values to be negative (Whitfield-Gabrieli et al., 2009). Here, we show such alterations in pgACC and AI and further provide a molecular dimension focusing glutamatergic mechanisms that are in line with existing postmortem and pharmacological evidence.

Notably, the anticorrelation between pgACC and AI is not a robust finding in the literature and also in our current sample, only a subset of healthy controls showed anticorrelations after global mean regression. Some regions belonging to the DMN like medial prefrontal and posterior cingulate cortex show consistently strong anticorrelations with task-positive regions like dorsal ACC and dorsolateral prefrontal cortex (DLPFC). In contrast to such regions, pgACC is variously correlated with the opposed networks. It shows less direct anticorrelations, but nevertheless strong anatomical connections and closer anatomical vicinity to a large set of cortical regions. Similarly, AI is functionally connected to dorsal ACC, and to a weaker extent, to DLPFC. Taking their anatomical interposition between task-positive and task-negative networks into account, this may support pgACC and AI's pivotal role in communicating the anticorrelated behavior (Menon and Uddin, 2010; Sridharan et al., 2008) of their associated networks. Such perspective might be in support of interpreting our results as representation of disturbed network modulation in MDD. The role of global mean regression in increasing observation of so called anticorrelations is a subject of current investigation. While there is evidence that these may not be present without the regression of global means (Murphy et al., 2009), others argue for an existence of these negative correlations in the absences of global mean regression if other means of physiological noise correction are considered (Chang and Glover, 2009; Fox et al., 2009). It is also possible to take a more conservative perspective and to accept that any additional introduction of nuisance covariates may lead to a reduction in correlation values and further towards negative values (Weissenbacher et al., 2009). The observed interdependence of rsFCs and Glx values may then at best be interpreted by the different degrees of assignment of the AI to task positive or default mode networks.

The role of the AI cortex in the pathophysiology of depression is less evident in the previous literature. One study reported relative hypermetabolism of AI in MDD which is correlated with disease severity (Brody et al., 2001). The absence of extensive postmortem findings in the AI might also indicate that the altered rsFC between pgACC and AI is driven by pgACC dysfunction. This may explain why clinical symptoms found in major depression exceed core functions of the pgACC, such as attribution of hedonic valences. Impaired AI–pgACC connectivity during emotional stimulation, internally or externally generated, may thus be responsible for reduced intensities or color of experienced emotions, since the AI may be crucial for the conscious experience of emotions (Uddin and Menon, 2009).

Another proposed role of AI is the switching between DMN and attentional networks (Sridharan et al., 2008). Therefore the postulated impairment of anticorrelated resting-state behavior could also be relevant in a number of cognitive tasks. Specific tasks require adaptive and efficient switching and transient reassignment of different network modules. Such cognitive and attentional deficits are frequently observed in severe depression. Since the AI is part of the cingulo-opercular attention set system (Dosenbach et al., 2008) as well as the salience network (Seeley et al., 2007), changes of its functional connectivity may be responsible for commonly observed negative bias in MDD (Bermpohl et al., 2009).

Salvadore et al. (2009) reported rostral ACC activity in an elaborate magneto encephalography (MEG) study to be predictive of subsequent treatment response to ketamine. Based on our findings, such predictions may in principle be possible using the more direct detection of altered baseline processing, which in the case of resting-state fMRI can be feasible within less than 10 min and without patients' active contribution to a specific task.

It has to be critically acknowledged that all patients in the current study have been on antidepressant pharmacotherapy. Although we have previously reported glutamatergic abnormalities in an unmedicated sample (Walter et al., 2009), potential confounds of medication cannot be fully ruled out. It may be of interest that glutamatergic abnormalities can be found in both medicated and unmedicated patients. But future studies, powered for adequate subgroup analyses, should focus on potential dose or treatment effects of serotonergic agents with potential downstream effects on glutamate levels.

A major limitation concerns the interpretation of MRS glutamate values. Although previous studies employed 1D PRESS MRS sequences at field strengths of 3 Tesla or even lower reporting both Glx and Glu (Auer et al., 2000), the separation of Glu and Gln should be regarded critically given limited line separation. By using an optimal echo time of 80 ms the contributions of Gln or GABA to the Glu signal should be minimal (Schubert et al., 2004; Mullins et al., 2008). Although findings for Glu and Glx strongly converged in our current analysis and Glx levels are strongly dominated by glutamate since it is the most abundant metabolite in comparison to GABA, Gln, or NAAG, one should be aware that Glu and Glx may concern slightly different effects. In a recent study using 2D JPRESS sequences, it could be shown that Gln predicts fMRI amplitudes in pgACC for both patients and controls, while Glu was correlated with fMRI responses only in the patient group (Walter et al., 2009). Another study (Brennan et al., 2010) reports subtle changes in the Gln/Glu ratio, which might be buried in the Glx estimates. This strongly motivates the use of sequences with sufficient separation of Glu and Gln. In our study the covariance of Glu and Gln values in the Fisher information matrix reaches a critical value of 0.3. Therefore a more conservative interpretation should rely only on the sum values of Glu and Gln despite the optimum echo time and high measurement repetitions of 256 samples. The use of a 2D approach that would make use of J coupling information was however not possible given that coverage of multiple regions plus additional resting-state fMRI acquisition would not be possible due to heavily increased acquisition times.

Although the findings of the present study are in line with predictions from previous task fMRI–MRS studies, future investigations should directly link task responses, resting-state behavior and specific clinical symptoms for better inference. Longitudinal treatment studies are also of specific interest because of the observed impact of depression severity on the glutamatergic abnormalities. Although only present on a trend level, we found that rsFCs in the mildly depressed subgroup were lower than the levels observed in healthy controls. While this might be well in line with slightly increased Glx and Glu levels, any interpretation in the direction of overshooting correlates of treatment response should be carefully limited given the setup of our study, which did not allow for balanced longitudinal

observations. The mildly depressed group should not be confused with partially recovered patients. Recent observations by Brennan et al. (2010) however, would suggest increased glutamine–glutamate cycling in the course of recovery which subsequently may lead to increases as observed in the mildly depressed subgroup.

Future studies will also have to integrate as many regions as possible into such a multimodal framework. Given the technical constraints of the MRS measurements, whole brain coverage is not practical. The current approach may benefit from its strong hypothesis driven character but multivoxel acquisitions as provided by chemical shift imaging (CSI) sequences may help to investigate regional specificity of our findings.

Our study provides a first promising step to combine evidence from elaborate activation studies and baseline investigations, which do not only concern the functional architecture at rest but also its molecular and finally its cellular representations. Future studies are necessary not only to replicate these findings in a larger sample but also to relate the observed mechanisms to pharmacological responses and more specific clinical characterizations.

DISCLOSURE

The study was funded by SFB 779.

ACKNOWLEDGMENTS

We are grateful for the important suggestions and discussions with Dr. Helen Mayberg. We thank Dr. Cameron Craddock and Thomas M. Malone for their skillful technical support and help during preparation of the revised manuscript.

REFERENCES

Ad-Dab'bagh, Y., Lyttelton, O., Muehlboeck, J. S., Lepage, C., Einarson, D., Mok, K., Ivanov, O., Vincent, R. D., Lerch, J., Fombonne, E., and Evans, A. C. (2006). "The CIVET image-processing environment: a fully automated comprehensive pipeline for anatomical neuroimaging research," in *Proceedings of the 12th Annual Meeting of the Organization for Human Brain Mapping*, ed. M. Corbetta (Elsevier, Florence).

Anand, A., Li, Y., Wang, Y., Lowe, M. J., and Dzemidzic, M. (2009). Resting state corticolimbic connectivity abnormalities in unmedicated bipolar disorder and unipolar depression. *Psychiatry Res.* 171, 189–198.

Anand, A., Li, Y., Wang, Y., Wu, J., Gao, S., Bukhari, L., Mathews, V. P., Kalnin, A., and Lowe, M. J. (2005a). Activity and connectivity of brain mood regulating circuit in depression: a functional magnetic resonance study. *Biol. Psychiatry* 57, 1079–1088.

Anand, A., Li, Y., Wang, Y., Wu, J., Gao, S., Bukhari, L., Mathews, V. P., Kalnin, A., and Lowe, M. J. (2005b). Antidepressant effect on connectivity of the mood-regulating circuit: an FMRI study. *Neuropsychopharmacology* 30, 1334–1344.

Auer, D. P., Pütz, B., Kraft, E., Lipinski, B., Schill, J., and Holsboer, F. (2000). Reduced glutamate in the anterior cingulate cortex in depression: an in vivo proton magnetic resonance spectroscopy study. *Biol. Psychiatry* 47, 305–313.

Augustine, J. R. (1996). Circuitry and functional aspects of the insular lobe in primates including humans. *Brain Res. Brain Res. Rev.* 22, 229–244.

Banasr, M., Chowdhury, G. M. I., Terwilliger, R., Newton, S. S., Duman, R. S., Behar, K. L., and Sanacora, G. (2010). Glial pathology in an animal model of depression: reversal of stress-induced cellular, metabolic and behavioral deficits by the glutamate-modulating drug riluzole. *Mol. Psychiatry* 15, 501–511.

Banasr, M., and Duman, R. S. (2008). Glial loss in the prefrontal cortex is sufficient to induce depressive-like behaviors. *Biol. Psychiatry* 64, 863–870.

Bermpohl, F., Walter, M., Sajonz, B., Lucke, C., Hagele, C., Sterzer, P., Adli, M., Heinz, A., and Northoff, G. (2009). Attentional modulation of emotional stimulus processing in patients with major depression–alterations in prefrontal cortical regions. *Neurosci. Lett.* 463, 108–113.

Biswal, B., Yetkin, F. Z., Haughton, V. M., and Hyde, J. S. (1995). Functional connectivity in the motor cortex of resting human brain using echo-planar MRI. *Magn. Reson. Med.* 34, 537–541.

Brennan, B. P., Hudson, J. I., Jensen, J. E., McCarthy, J., Roberts, J. L., Prescot, A. P., Cohen, B. M., Pope, H. G., Renshaw, P. F., and Ongür, D. (2010). Rapid enhancement of glutamatergic neurotransmission in bipolar depression following treatment with riluzole. *Neuropsychopharmacology* 35, 834–846.

Brody, A. L., Saxena, S., Mandelkern, M. A., Fairbanks, L. A., Ho, M. L., and Baxter, L. R. (2001). Brain metabolic changes associated with symptom factor improvement in major depressive disorder. *Biol. Psychiatry* 50, 171–178.

Buckner, R. L., and Vincent, J. L. (2007). Unrest at rest: default activity and spontaneous network correlations. *Neuroimage* 37, 1091–1096; discussion 1097–1099.

Cavassila, S., Deval, S., Huegen, C., van Ormondt, D., and Graveron-Demilly, D. (2001). Cramér-Rao bounds: an evaluation tool for quantitation. *NMR Biomed.* 14, 278–283.

Chang, C., and Glover, G. H. (2009). Effects of model-based physiological noise correction on default mode network anti-correlations and correlations. *Neuroimage* 47, 1448–1459.

Choudary, P. V., Molnar, M., Evans, S. J., Tomita, H., Li, J. Z., Vawter, M. P., Myers, R. M., Bunney, W. E., Akil, H., Watson, S. J., and Jones, E. G. (2005). Altered cortical glutamatergic and GABAergic signal transmission with glial involvement in depression. *Proc. Natl. Acad. Sci. U.S.A.* 102, 15653–15658.

CIPS. (1996). *Internationale Skalen für Psychiatrie*. Göttingen: Beltz Test GmbH.

Cotter, D., Mackay, D., Landau, S., Kerwin, R., and Everall, I. (2001). Reduced glial cell density and neuronal size in the anterior cingulate cortex in major depressive disorder. *Arch. Gen. Psychiatry* 58, 545–553.

Craig, A. D. B. (2005). Forebrain emotional asymmetry: a neuroanatomical basis? *Trends Cogn. Sci. (Regul. Ed.)* 9, 566–571.

Craig, A. D. B. (2009). How do you feel–now? The anterior insula and human awareness. *Nat. Rev. Neurosci.* 10, 59–70.

Damoiseaux, J. S., Beckmann, C. F., Arigita, E. J. S., Barkhof, F., Scheltens, P., Stam, C. J., Smith, S. M., and Rombouts, S. A. R. B. (2008). Reduced resting-state brain activity in the "default network" in normal aging. *Cereb. Cortex* 18, 1856–1864.

Dantzer, R., O'Connor, J. C., Freund, G. G., Johnson, R. W., and Kelley, K. W. (2008). From inflammation to sickness and depression: when the immune system subjugates the brain. *Nat. Rev. Neurosci.* 9, 46–56.

Dosenbach, N. U. F., Fair, D. A., Cohen, A. L., Schlaggar, B. L., and Petersen, S. E. (2008). A dual-networks architecture of top-down control. *Trends Cogn. Sci. (Regul. Ed.)* 12, 99–105.

Fox, M. D., and Raichle, M. E. (2007). Spontaneous fluctuations in brain activity observed with functional magnetic resonance imaging. *Nat. Rev. Neurosci.* 8, 700–711.

Fox, M. D., Snyder, A. Z., Vincent, J. L., Corbetta, M., van Essen, D. C., and Raichle, M. E. (2005). The human brain is intrinsically organized into dynamic, anticorrelated functional networks. *Proc. Natl. Acad. Sci. U.S.A.* 102, 9673–9678.

Fox, M. D., Zhang, D., Snyder, A. Z., and Raichle, M. E. (2009). The global signal and observed anticorrelated resting state brain networks. *J. Neurophysiol.* 101, 3270–3283.

Greicius, M. D., Flores, B. H., Menon, V., Glover, G. H., Solvason, H. B., Kenna, H., Reiss, A. L., and Schatzberg, A. F. (2007). Resting-state functional connectivity in major depression: abnormally increased contributions from subgenual cingulate cortex and thalamus. *Biol. Psychiatry* 62, 429–437.

Grimm, S., Boesiger, P., Beck, J., Schuepbach, D., Bermpohl, F., Walter, M., Ernst, J., Hell, D., Boeker, H., and Northoff, G. (2009a). Altered negative BOLD responses in the default-mode network during emotion processing in depressed subjects. *Neuropsychopharmacology* 34, 932–843.

Grimm, S., Ernst, J., Boesiger, P., Schuepbach, D., Hell, D., Boeker, H., and Northoff, G. (2009b). Increased self-focus in major depressive disorder is related to neural abnormalities in subcortical-cortical midline structures. *Hum. Brain Mapp.* 30, 2617–2627.

Hamilton, M. (1960). A rating scale for depression. *J. Neurol. Neurosurg. Psychiatry* 23, 56–62.

Hampson, M., Driesen, N. R., Skudlarski, P., Gore, J. C., and Constable, R. T. (2006). Brain connectivity related to working memory performance. *J. Neurosci.* 26, 13338–13343.

Hasler, G., van der Veen, J. W., Tumonis, T., Meyers, N., Shen, J., and Drevets, W. C. (2007). Reduced prefrontal glutamate/glutamine and gamma-aminobutyric acid levels in major depression determined using proton magnetic resonance spectroscopy. *Arch. Gen. Psychiatry* 64, 193–200.

Jafri, M. J., Pearlson, G. D., Stevens, M., and Calhoun, V. D. (2008). A method for functional network connectivity among spatially independent resting-state components in schizophrenia. *Neuroimage* 39, 1666–1681.

Kugaya, A., and Sanacora, G. (2005). Beyond monoamines: glutamatergic function in mood disorders. *CNS Spectr.* 10, 808–819.

Lerch, J. P., and Evans, A. C. (2005). Cortical thickness analysis examined through power analysis and a population simulation. *Neuroimage* 24, 163–173.

Lozano, A. M., Mayberg, H. S., Giacobbe, P., Hamani, C., Craddock, R. C., and Kennedy, S. H. (2008). Subcallosal cingulate gyrus deep brain stimulation for treatment-resistant depression. *Biol. Psychiatry* 64, 461–467.

MacQueen, G. M. (2009). Magnetic resonance imaging and prediction of outcome in patients with major depressive disorder. *J. Psychiatry Neurosci.* 34, 343–349.

Manji, H. K., Drevets, W. C., and Charney, D. S. (2001). The cellular neurobiology of depression. *Nat. Med.* 7, 541–547.

Margulies, D. S., Kelly, A. M. C., Uddin, L. Q., Biswal, B. B., Castellanos, F. X., and Milham, M. P. (2007). Mapping the functional connectivity of anterior cingulate cortex. *Neuroimage* 37, 579–588.

Mayberg, H. S. (1997). Limbic-cortical dysregulation: a proposed model of depression. *J. Neuropsychiatry Clin. Neurosci.* 9, 471–481.

Mayberg, H. S., Lozano, A. M., Voon, V., McNeely, H. E., Seminowicz, D., Hamani, C., Schwalb, J. M., and Kennedy, S. H. (2005). Deep brain stimulation for treatment-resistant depression. *Neuron* 45, 651–660.

Mennes, M., Kelly, C., Zuo, X.-N., Di Martino, A., Biswal, B., Castellanos, F. X., and Milham, M. P. (2010). Inter-individual differences in resting state functional connectivity predict task-induced BOLD activity. *Neuroimage*. 50, 1690–1701.

Menon, V., and Uddin, L. Q. (2010). Saliency, switching, attention, and control: a network model of insula function. *Brain Struct. Funct*. 214, 655–667.

Mesulam, M. M., and Mufson, E. J. (1982). Insula of the old world monkey. III: efferent cortical output and comments on function. *J. Comp. Neurol.* 212, 38–52.

Mufson, E. J., and Mesulam, M. M. (1982). Insula of the old world monkey. II: afferent cortical input and comments on the claustrum. *J. Comp. Neurol.* 212, 23–37.

Mullins, P. G., Chen, H., Xu, J., Caprihan, A., and Gasparovic, C. (2008). Comparative reliability of proton spectroscopy techniques designed to improve detection of J-coupled metabolites. *Magn. Reson. Med.* 60, 964–969.

Murphy, K., Birn, R. M., Handwerker, D. A., Jones, T. B., and Bandettini, P. A. (2009). The impact of global signal regression on resting state correlations: are anti-correlated networks introduced? *Neuroimage* 44, 893–905.

Neumann, J., Fox, P. T., Turner, R., and Lohmann, G. (2010). Learning partially directed functional networks from meta-analysis imaging data. *Neuroimage* 49, 1372–1384.

Northoff, G., Walter, M., Schulte, R. F., Beck, J., Dydak, U., Henning, A., Boeker, H., Grimm, S., and Boesiger, P. (2007). GABA concentrations in the human anterior cingulate cortex predict negative BOLD responses in fMRI. *Nat. Neurosci.* 10, 1515–1517.

Ongür, D., Drevets, W. C., and Price, J. L. (1998). Glial reduction in the subgenual prefrontal cortex in mood disorders. *Proc. Natl. Acad. Sci. U.S.A.* 95, 13290–13295.

Provencher, S. W. (1993). Estimation of metabolite concentrations from localized in vivo proton NMR spectra. *Magn. Reson. Med.* 30, 672–679.

Raichle, M. E., and Mintun, M. A. (2006). Brain work and brain imaging. *Annu. Rev. Neurosci.* 29, 449–476.

Raichle, M. E., and Snyder, A. Z. (2007). A default mode of brain function: a brief history of an evolving idea. *Neuroimage* 37, 1083–1090; discussion 1097–1099.

Rajkowska, G., and Miguel-Hidalgo, J. J. (2007). Gliogenesis and glial pathology in depression. *CNS Neurol. Disord. Drug Targets* 6, 219–233.

Rajkowska, G., Miguel-Hidalgo, J. J., Wei, J., Dilley, G., Pittman, S. D., Meltzer, H. Y., Overholser, J. C., Roth, B. L., and Stockmeier, C. A. (1999). Morphometric evidence for neuronal and glial prefrontal cell pathology in major depression. *Biol. Psychiatry* 45, 1085–1098.

Rigucci, S., Serafini, G., Pompili, M., Kotzalidis, G. D., and Tatarelli, R. (2009). Anatomical and functional correlates in major depressive disorder: the contribution of neuroimaging studies. *World J. Biol. Psychiatry,* 1–16.

Rothman, D. L., Behar, K. L., Hyder, F., and Shulman, R. G. (2003). In vivo NMR studies of the glutamate neurotransmitter flux and neuroenergetics: implications for brain function. *Annu. Rev. Physiol.* 65, 401–427.

Rowland, L. M., Bustillo, J. R., Mullins, P. G., Jung, R. E., Lenroot, R., Landgraf, E., Barrow, R., Yeo, R., Lauriello, J., and Brooks, W. M. (2005). Effects of ketamine on anterior cingulate glutamate metabolism in healthy humans: a 4-T proton MRS study. *Am. J. Psychiatry* 162, 394–396.

Salvadore, G., Cornwell, B. R., Colon-Rosario, V., Coppola, R., Grillon, C., Zarate, C. A., and Manji, H. K. (2009). Increased anterior cingulate cortical activity in response to fearful faces: a neurophysiological biomarker that predicts rapid antidepressant response to ketamine. *Biol. Psychiatry* 65, 289–295.

Schubert, F., Gallinat, J., Seifert, F., and Rinneberg, H. (2004). Glutamate concentrations in human brain using single voxel proton magnetic resonance spectroscopy at 3 Tesla. *Neuroimage* 21, 1762–1771.

Seeley, W. W., Menon, V., Schatzberg, A. F., Keller, J., Glover, G. H., Kenna, H., Reiss, A. L., and Greicius, M. D. (2007). Dissociable intrinsic connectivity networks for salience processing and executive control. *J. Neurosci.* 27, 2349–2356.

Sheehan, D. V., Lecrubier, Y., Sheehan, K. H., Amorim, P., Janavs, J., Weiller, E., Hergueta, T., Baker, R., and Dunbar, G. C. (1998). The mini-international neuropsychiatric interview (MINI): the development and validation of a structured diagnostic psychiatric interview for DSM-IV and ICD-10. *J. Clin. Psychiatry* 59(Suppl. 20), 22–33; quiz 34–57.

Sheline, Y. I., Barch, D. M., Price, J. L., Rundle, M. M., Vaishnavi, S. N., Snyder, A. Z., Mintun, M. A., Wang, S., Coalson, R. S., and Raichle, M. E. (2009). The default mode network and self-referential processes in depression. *Proc. Natl. Acad. Sci. U.S.A.* 106, 1942–1947.

Shulman, R. G., Rothman, D. L., and Hyder, F. (2007). A BOLD search for baseline. *Neuroimage* 36, 277–281.

Sridharan, D., Levitin, D. J., and Menon, V. (2008). A critical role for the right fronto-insular cortex in switching between central-executive and default-mode networks. *Proc. Natl. Acad. Sci. U.S.A.* 105, 12569–12574.

Uddin, L. Q., Kelly, A. M., Biswal, B. B., Xavier Castellanos, F., and Milham, M. P. (2009). Functional connectivity of default mode network components: correlation, anticorrelation, and causality. *Hum. Brain Mapp.* 30, 625–637.

Uddin, L. Q., and Menon, V. (2009). The anterior insula in autism: under-connected and under-examined. *Neurosci. Biobehav. Rev.* 33, 1198–1203.

Walter, M., Henning, A., Grimm, S., Schulte, R. F., Beck, J., Dydak, U., Schnepf, B., Boeker, H., Boesiger, P., and Northoff, G. (2009). The relationship between aberrant neuronal activation in the pregenual anterior cingulate, altered glutamatergic metabolism, and anhedonia in major depression. *Arch. Gen. Psychiatry* 66, 478–486.

Weissenbacher, A., Kasess, C., Gerstl, F., Lanzenberger, R., Moser, E., and Windischberger, C. (2009). Correlations and anticorrelations in resting-state functional connectivity MRI: a quantitative comparison of preprocessing strategies. *Neuroimage* 47, 1408–1416.

Whitfield-Gabrieli, S., Thermenos, H. W., Milanovic, S., Tsuang, M. T., Faraone, S. V., McCarley, R. W., Shenton, M. E., Green, A. I., Nieto-Castanon, A., LaViolette, P., Wojcik, J., Gabrieli, J. D. E., and Seidman, L. J. (2009). Hyperactivity and hyperconnectivity of the default network in schizophrenia and in first-degree relatives of persons with schizophrenia. *Proc. Natl. Acad. Sci. U.S.A.* 106, 1279–1284.

WHO. (1992). *The ICD-10 Classification of Mental and Behavioral Disorders. Clinical Descriptions and Diagnostic Guidelines*. Geneva: World Health Organization.

Yan, C.-G., and Zang, Y.-F. (2010). DPARSF: a MATLAB toolbox for "pipeline" data analysis of resting-state fMRI. *Front. Syst. Neurosci.* 4, 13. doi:10.3389/fnsys.2010.00013.

Yildiz-Yesiloglu, A., and Ankerst, D. P. (2006). Review of 1H magnetic resonance spectroscopy findings in major depressive disorder: a meta-analysis. *Psychiatry Res.* 147, 1–25.

Zarate, C. A., Singh, J. B., Carlson, P. J., Brutsche, N. E., Ameli, R., Luckenbaugh, D. A., Charney, D. S., and Manji, H. K. (2006). A randomized trial of an N-methyl-D-aspartate antagonist in treatment-resistant major depression. *Arch. Gen. Psychiatry* 63, 856–864.

Zhou, Y., Yu, C., Zheng, H., Liu, Y., Song, M., Qin, W., Li, K., and Jiang, T. (2010). Increased neural resources recruitment in the intrinsic organization in major depression. *J. Affect Disord.* 121, 220–230.

Conflict of Interest Statement: The authors declare that the research was conducted in the absence of any commercial or financial relationships that could be construed as a potential conflict of interest.

*Received: 05 February 2010; paper pending published: 10 March 2010; accepted: 18 June 2010; published online: 15 July 2010. Citation: Horn DI, Yu C, Steiner J, Buchmann J, Kaufmann J, Osoba A, Eckert U, Zierhut KC, Schiltz K, He H, Biswal B, Bogerts B and Walter M (2010) Glutamatergic and resting-state functional connectivity correlates of severity in major depression – the role of pregenual anterior cingulate cortex and anterior insula. Front. Syst. Neurosci. **4**:33. doi: 10.3389/fnsys.2010.00033*

frontiers in
SYSTEMS NEUROSCIENCE

ORIGINAL RESEARCH ARTICLE
published: 05 August 2010
doi: 10.3389/fnsys.2010.00035

Adolescent resting state networks and their associations with schizotypal trait expression

Annalaura Lagioia[1,2,3], Dimitri Van De Ville[2,4]*, Martin Debbané[1,5], François Lazeyras[2,6] and Stephan Eliez[1,7]

[1] *Office Médico-Pédagogique Research Unit, Department of Psychiatry, University of Geneva, Geneva, Switzerland*
[2] *Department of Radiology and Medical Informatics, University of Geneva, Geneva, Switzerland*
[3] *Lemanic Neuroscience Doctoral School, Faculty of Psychology and Educational Sciences, University of Geneva, Geneva, Switzerland*
[4] *Institute of Bioengineering, École Polytechnique Fédérale de Lausanne, Lausanne, Switzerland*
[5] *Adolescence Clinical Psychology Research Unit, Faculty of Psychology and Educational Sciences, University of Geneva, Geneva, Switzerland*
[6] *University Hospital Geneva, Geneva, Switzerland*
[7] *Department of Genetic Medicine and Development, School of Medicine, University of Geneva, Geneva, Switzerland*

Edited by:
Lucina Q. Uddin, Stanford University, USA

Reviewed by:
Matthew Hoptman, Nathan S. Kline Institute, USA
Katie Karlsgodt, University of California, Los Angeles, USA

****Correspondence:***
Dimitri Van De Ville, Department of Radiology and Medical Informatics, University of Geneva Rue Gabrielle-Perret-Gentil, 4, 1211 Geneva 14. e-mail: dimitri.vandeville@epfl.ch

The rising interest in temporally coherent brain networks during baseline adult cerebral activity finds convergent evidence for an identifiable set of resting state networks (RSNs). To date, little is know concerning the earlier developmental stages of functional connectivity in RSNs. This study's main objective is to characterize the RSNs in a sample of adolescents. We further examine our data from a developmental psychopathology perspective of psychosis-proneness, by testing the hypothesis that early schizotypal symptoms are linked to disconnection in RSNs. In this perspective, this study examines the expression of adolescent schizotypal traits and their potential associations to dysfunctional RSNs. Thirty-nine adolescents aged between 12 and 20 years old underwent an 8-min functional magnetic resonance imaging (fMRI) "resting state" session. In order to explore schizotypal trait manifestations, the entire population was assessed by the Schizotypal Personality Questionnaire (SPQ). After conventional processing of the fMRI data, we applied group-level independent component analysis (ICA). Twenty ICA maps and associated time courses were obtained, among which there were RSNs that are consistent with findings in the literature. We applied a regression analysis at group level between the energy of RSN-associated time courses in different temporal frequency bins and the clinical measures (3 in total). Our results highlight the engagement of six relevant RSNs; (1) a default-mode network (DMN); (2) a dorso-lateral attention network; (3) a visual network (VN); (4) an auditory network (AN); (5) a sensory motor network (SMN); (6) a self-referential network (SRN). The regression analysis reveals a statistically significant correlation between the clinical measures and some of the RSNs, specifically the visual and the AN. In particular, a positive correlation is obtained for the VN in the low frequency range (0.05 Hz) with SPQ measures, while the AN correlates negatively in the high frequency range (0.16–0.19 Hz). Trend-like significance for the SRN may hint to its implication in disorganized thoughts and behaviors during adolescence. Unlike DMN activity in schizophrenic patients, adolescent DMN was unrelated to schizotypal trait expression. This suggests that relationships between the DMN and schizotypy may be modified in later developmental stages of both functional connectivity and psychotic expression. These results are discussed in light of RSNs literature involving children, adults, and individuals with schizophrenia.

Keywords: fMRI, default mode network, ICA, adolescence, psychosis, personality, SPQ, schizotypy

INTRODUCTION

Over the past 15 years, functional magnetic resonance imaging (fMRI) studies have devoted sustained interest in the intrinsic baseline activity of the brain, also referred to as the brain's resting state or its default-mode activity. During this resting state, the brain's blood oxygen level-dependent (BOLD) signal displays spontaneous fluctuations in its low or high frequencies showing a high degree of temporal correlation across separated cortical areas. These temporal correlations underline intrinsic functional connectivity between functional networks which are crucial for processes such as vision, auditory processing, language, (Hampson et al., 2002; Beckmann et al., 2005); in particular the default-mode network (DMN) has constituted the main interest of past studies that implemented seed-voxel techniques (Biswal et al., 1995; Raichle et al., 2001) as well as independent component analysis (ICA) (Greicius et al., 2004; van de Ven et al., 2004; Beckmann et al., 2005). Through analyses such as an ICA of the functional connectivity between widespread brain areas, several plausible functional resting state networks (RSN) can be inferred (Gusnard et al., 2001; Greicius et al., 2003; Van den Heuvel et al., 2009). One of the principal networks observable during the brain's resting state is the DMN, generally thought to implicate the posterior cingulate cortex (PCC), the posterior lateral parietal cortices

and the medial prefrontal cortex (MPFC) (Broyd et al., 2009). Other networks have also been identified, including a self-referential system engaging the medial prefrontal regions, a posterior network involved in visual processing, an attention network engaging superior frontal and parietal cortex, a superior temporal system and a network engaging precentral and postcentral cortex (Gusnard et al., 2001; Greicius et al., 2003; Fox and Raichle, 2007; Mantini et al., 2007).

More recently, neuroscientific investigations of RSNs examined the developmental characteristics of baseline cerebral activity by comparing functional connectivity in children and adults (Fair et al., 2008; Supekar et al., 2009, 2010). Although children show relatively immature connectivity in the DMN, cross-sectional data illustrates that specialized functional networks operate as early as age 7 following a local distribution of anatomically proximal clusters of activity (Fair et al., 2008). Brain maturation, most notably cerebral pruning and myelinization during adolescence (Sowell et al., 2004), sustains the development of large-scale networks that cast longer range functional connectivity and greatly enhance cortico-cortical networks (Supekar et al., 2009, 2010). In parallel to these observations, studies on RSNs in children and adolescents have started to address the issue of functional connectivity maturation in relation to the development of high-level cognitive abilities occurring during adolescence. The main dimensions of investigation concern within-network functional connectivity and the degree to which networks interfere/facilitate reciprocal interactions (Stevens et al., 2009). In a developmental study conducted by Kelly et al. (2009) targeting cingulate based intrinsic components networks, the authors report a significant age related shift in functional connectivity patterns by comparing children, adolescents and adults. While children showed a more dispersed pattern of correlation with seed region of interest (ROI), young adults exhibited a better constrained correlation pattern in line with that observed in adult participants. These finding are consistent with age related developmental trajectories of functional connectivity (Fair et al., 2008). In adolescent samples, studies have examined task-related modifications in neural networks (Stevens et al., 2007, 2009). Recently, Stevens et al. (2009) compared a group of 48 adolescents to a group of 52 adults and reported 13 common RSNs using ICA (Stevens et al., 2009). They further suggested that age is associated with greater within-network connectivity and increased efficiency between network influences. Together, these preliminary findings suggest that adolescence constitutes a crucial period for the deployment of functional connectivity networks that enhance information processing efficiency, and thus prompt further characterization of the RSNs during adolescence.

RSN investigations during adolescence can also lead to a deeper understanding in psychopathology research, especially because many serious psychiatric disorders emerge during late adolescence transitioning into early adulthood (Paus et al., 2008). Schizophrenia is one of the psychiatric disorders that typically unfolds with increased manifestations of schizotypal traits during adolescence (such as transient hallucination and delusion-like symptoms), which can potentially progress into clinically meaningful manifestations of psychosis. While a number of RSN investigations have been performed with adults meeting the diagnostic criteria of schizophrenia (Garrity et al., 2007), information is lacking concerning the early expression of schizotypal traits and its underlying RSN correlates. The results already reported in schizophrenia research can guide such examinations designed to assess the relationships between baseline cerebral activity and early schizotypal trait manifestations. To date, the functional connectivity data on RSNs in schizophrenia show some disparity, perhaps due to methodological differences and extensive heterogeneity in the schizophrenic samples. Nevertheless, three observations can be drawn from this quickly evolving literature; (1) studies showing greater DMN connectivity in their schizophrenia samples suggest exaggerated allocation of attention to introspective activity together with increased preoccupation for unexpected or novel external events; (2) in line with the first observations, studies finding increased anti-correlation between RSN networks interpret their results as representing the characteristic rivalry between introspective and extrospective mental activity in schizophrenia; (3) Finally, studies find specific deactivations for central nodes of the DMN such as the middle frontal gyrus and precuneus, suggesting that they are associated with the positive symptom dimension of schizophrenia (Broyd et al., 2009). Indeed, in a recent study (Rotarska-Jagiela et al., 2010) investigating aberrant DMN in schizophrenic patients, a significant correlation was found between positive symptoms and deactivation of the right frontal parietal network. It remains to be determined whether increased schizotypal traits during adolescence are associated with any one or many of the DMN alterations previously observed in adults with schizophrenia.

In this context, the present study carries two principal aims. Firstly, we wish to describe the functional organization of endogenous activation in adolescent baseline cerebral activity by examining functional connectivity of the putative DMN as well as other significant RSNs. Secondly, we wish to investigate the potential relationships between schizotypal trait expression and functional connectivity of the different RSNs in our adolescent sample. In order to conduct this examination, we employ an ICA to identify the functional connectivity of RSNs among widespread brain regions.

MATERIALS AND METHODS

PARTICIPANTS

The study included 39 adolescents, 12–20 years old, who spoke French as their mother tongue (22 females, 17 males), with normal or corrected to normal vision. Participants were recruited through the Child and Adolescent outpatient Public Service (Office Médico Pédagogique) of Geneva member of the University of Geneva's Psychiatry Department and of the Canton of Geneva Education Department. The motive for recruiting adolescents from the community ($n = 16$) in combination with those seeking psychological help ($n = 23$) was to obtain a distribution representing the wide range of schizotypy trait expression in our final sample. The sample mean age was 16.19, SD 2.201. All participants underwent an intellectual assessment, using the Wechsler Intelligence Scale for Children-III block design subtest (mean = 11.32, SD 3.5). In order to investigate psychotic symptoms and their dimensions, subjects completed the Schizotypal Personality Questionnaire (SPQ), translated into French and validated by Dumas et al. (2000). A clinical psychologist observed the questionnaire progression to guarantee that subjects understood all questionnaire items. The questionnaire looks at three main factor scores (Cognitive-Perceptual, Interpersonal, and Disorganization) and nine subscale scores (Ideas of Reference, Social Anxiety, Odd Beliefs/Magical Thinking, Unusual Perceptual Experiences, Eccentric/Odd Behavior and Appearance, No Close Friends, Odd Speech, Constricted Affect, Suspiciousness/Paranoid Ideation). It has been

applied to explore the multiple dimensional analyses of schizotypy (Rossi and Daneluzzo, 2002), and it is valid with adolescents (Axelrod et al., 2001). In order to insure that our adolescent's group distribution was normal, we tested for normality of distribution regarding the SPQ total score and the three subscale scores. The results indicate that full scale and subscale measures had normal distributions (SPQ total score: Kolmogorov–Smirnov $Z = 0.56$, $p = 0.91$; SPQ positive score: Kolmogorov–Smirnov $Z = 0.97$, $p = 0.31$; SPQ negative score: Kolmogorov–Smirnov $Z = 0.55$, $p = 0.80$; SPQ disorganization score: Kolmogorov–Smirnov $Z = 0.66$, $p = 0.78$).

Furthermore, we looked in the clinical files of the patients to find additional psychiatric diagnoses: four participants met CIM-10 diagnosis (European equivalent of DSM-IV) at time of participation (one attention deficit hyperactivity disorder, one generalized anxiety disorder, two schizotypal personality disorder). Only the last two participants had higher than group average schizotypy scores, which would be expected from their clinical diagnosis.

Written informed consent was obtained from participants and their parents under protocols approved by the Institutional Review Board of the Department of Psychiatry of the University of Geneva Medical School.

IMAGING ACQUISITION AND DATA ANALYSIS

fMRI data acquisition

Scanning was performed using a 3 Tesla Trio Tim Siemens at the *Hôpitaux Universitaires* of Geneva. High resolution 3D anatomical images were acquired [repetition time (TR) = 2500 ms, echo time (TE) = 30 ms, 192 coronal slices, slice thickness = 1.1 mm, slice gap = 0.5 mm, flip angle = 8°, field of view (FOV) = 220 mm^2], followed by a resting state functional scan of 8 min, containing 200 BOLD images (TR = 2400 ms, TE = 30 ms, 38 axial slices, slice thickness = 3.20 mm, no gap, flip angle = 85°, FOV = 235 mm^2). Subject's head was stabilized with a vacuum cushion to minimize motion.

fMRI data analysis

Data were processed and analyzed using Statistical Parametric Mapping (SPM) 5, (Welcome Department of Neuroscience, London, UK). Functional images were at first corrected for motion by realigning every image with respect to the first one. Next, slice timing correction was performed using the middle slice as a reference, under descending acquisition. Structural images of each participant were coregistered to the mean of the realigned functional images. Gray matter separation was established by segmentation of the anatomical image. Realigned and slice-timed images were then spatially normalized into the Montreal Neurological Institute (MNI) template using 3 mm × 3 mm × 3 mm isotropic voxels, followed by spatial smoothing with an isotropic Gaussian smoothing Kernel of 10 mm full width half maximum (FWHM). Relevant RSNs were identified by ICA. ICA is a technique able to separate spatio-temporal BOLD signal into spatially statistically independent components (Beckmann and Smith, 2004). Each of the determined components is the expression of temporal waveform associated to specific brain network activity extracted from all regions. ICA allows separating out physiological artifacts and at the same time to identify functional active networks. Recently ICA has been employed for the identification of RSNs (Greicius et al., 2004; van de Ven et al., 2004; Mantini et al., 2007).

Group-level spatial ICA was conducted for all 39 participants, using the GIFT implementation (Calhoun et al., 2001; Calhoun and Adali, 2006; available at http://icatb.sourceforge.net/, version 1.3b) that relies on the infomax algorithm (Bell and Sejnowski, 1995). Spatial ICA decomposes the data into spatial components and associated time courses based on a criterion that favors spatial independence. The group-level analysis is applied on the preprocessed data. The spatial components were converted into *z*-values (Beckmann et al., 2005) while time courses were calibrated as signal percentage change. The number of components was chosen as 20, which is consistent with the minimum description length estimate. Each of the spatial components was manually inspected for the presence of obvious artifacts that get effectively separated out by ICA (e.g., motion, ventricles) (Stevens et al., 2006). We retained six RSNs components that were consistent with the literature (Mantini et al., 2007).

ICA correlation with clinical measures

Regression analysis of the ICA findings against the clinical measures was conducted using custom scripts in Matlab 7.9 (R2009b) that relied upon the functionality of the GIFT implementation. In particular, a linear regression analysis was applied at the group level between the energy of the RSN-associated time courses, separated into 6 frequency bins (range 0.02–0.19 Hz: 0.02, 0.05, 0.09, 0.12, 0.16, and 0.19 Hz), and 3 clinical measures (SPQ positive factor, SPQ negative factor, SPQ disorganized factor). The design matrices of the regression analyses contained the respective clinical measure together with a constant regressor, for which we ran a *t*-test for the clinical measure of interest with 36 degrees of freedom. We dealt with multiple comparisons (3 clinical measures × 6 frequency bins) using Bonferroni correction. Frequency-dependent behavior of correlation between clinical measures and RSN temporal behavior is an important feature since past studies have effectively demonstrated the presence of low frequency oscillations in typical RSNs (0.01–0.1 Hz) (Mantini et al., 2007), while modulation of high frequency components has been found in schizophrenic patients (Keri and Janka, 2000; Garrity et al., 2007).

In what follows, we report both corrected and uncorrected *p*-values. We consider $p < 0.05$ corrected as being strongly significant ($t > 2.95$). For some correlations, we also report less significant values, but that could be of interest for future studies.

RESULTS

DESCRIPTIVE AND CLINICAL MEASURES

Table 1 shows the mean scores obtained during the neuropsychological evaluation.

Table 1 | Descriptive and clinical measures of age, intelligence and results of the self-response questionnaires (total and subscale scores).

Total sample ($n = 39$)	Average	SD	Range
Age (years)	16.19	2.201	12–19
IQ (block design)	11.32	3.465	5–18
SPQ total score	21.74	14.545	1–58
Positive (cognitive-perceptual)	8.18	6.480	8–26
Negative (interpersonal)	7.42	5.898	0–19
Disorganization	6.45	4.440	0–19

CONSISTENT RESTING STATE NETWORKS FOUND ACROSS ADOLESCENTS

Peak activity were obtained by the implement of SPM 5 one sample *t*-test run for each relevant RSN. The spatial maps in **Figures 1A–F** show the six identified RSNs. **Tables 2–7** summarize the active regions and the MNI peak coordinates, as well as Brodmann areas (BA) in which activation occurs. The results are explained on the base of past evidence of RSNs and they

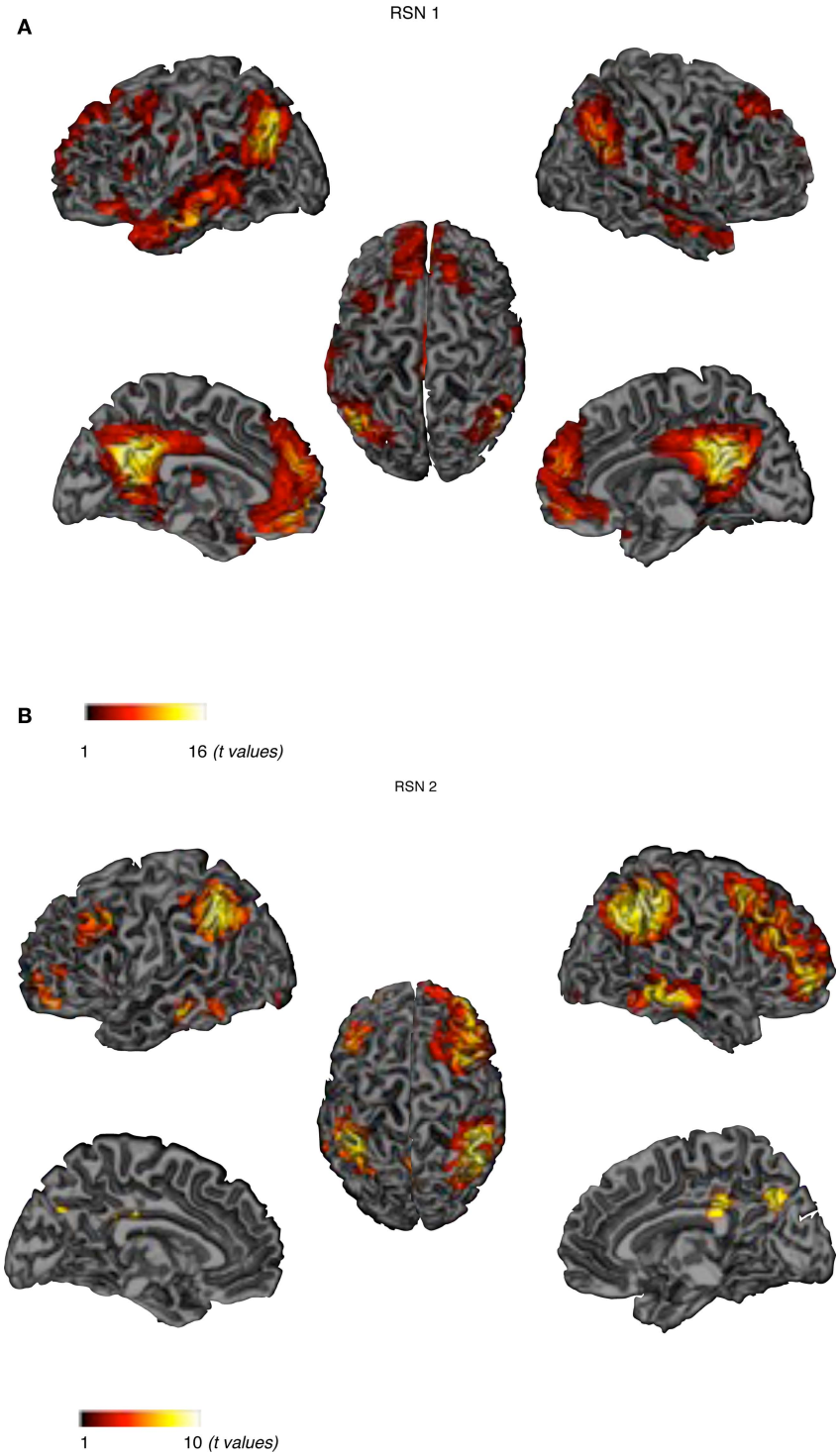

FIGURE 1 | Cortical representation of the activity in the six RSNs. For each RSN (Left) Lateral and medial views of left hemisphere. (Center) Dorsal view. (Right) Lateral and medial views of right hemisphere. **(A)** Default-mode network – DMN, **(B)** dorso-lateral attention network – DAN. *(continued)*

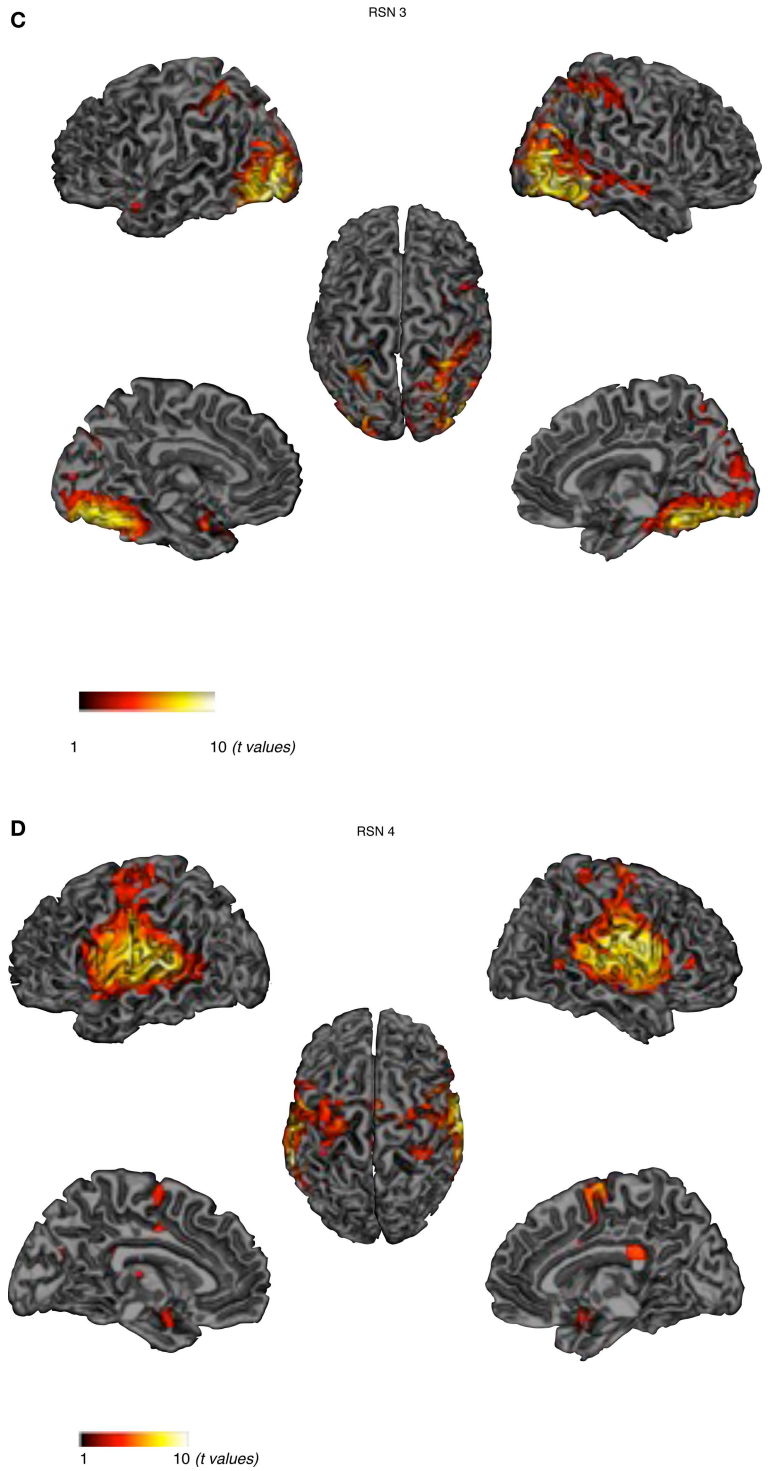

FIGURE 1 | Cortical representation of the activity in the six RSNs. For each RSN (Left) Lateral and medial views of left hemisphere. (Center) Dorsal view. (Right) Lateral and medial views of right hemisphere. **(C)** visual network – VN, **(D)** auditory network – AN. *(continued)*

are described by highlighting the functional system they sustain (Beckmann et al., 2005; De Luca et al., 2006; Mantini et al., 2007; Jafri et al., 2008).

RSN 1

This network is represented by the DMN, which includes the bilateral superior gyrus, anterior cingulate, the MPFC and the parietal

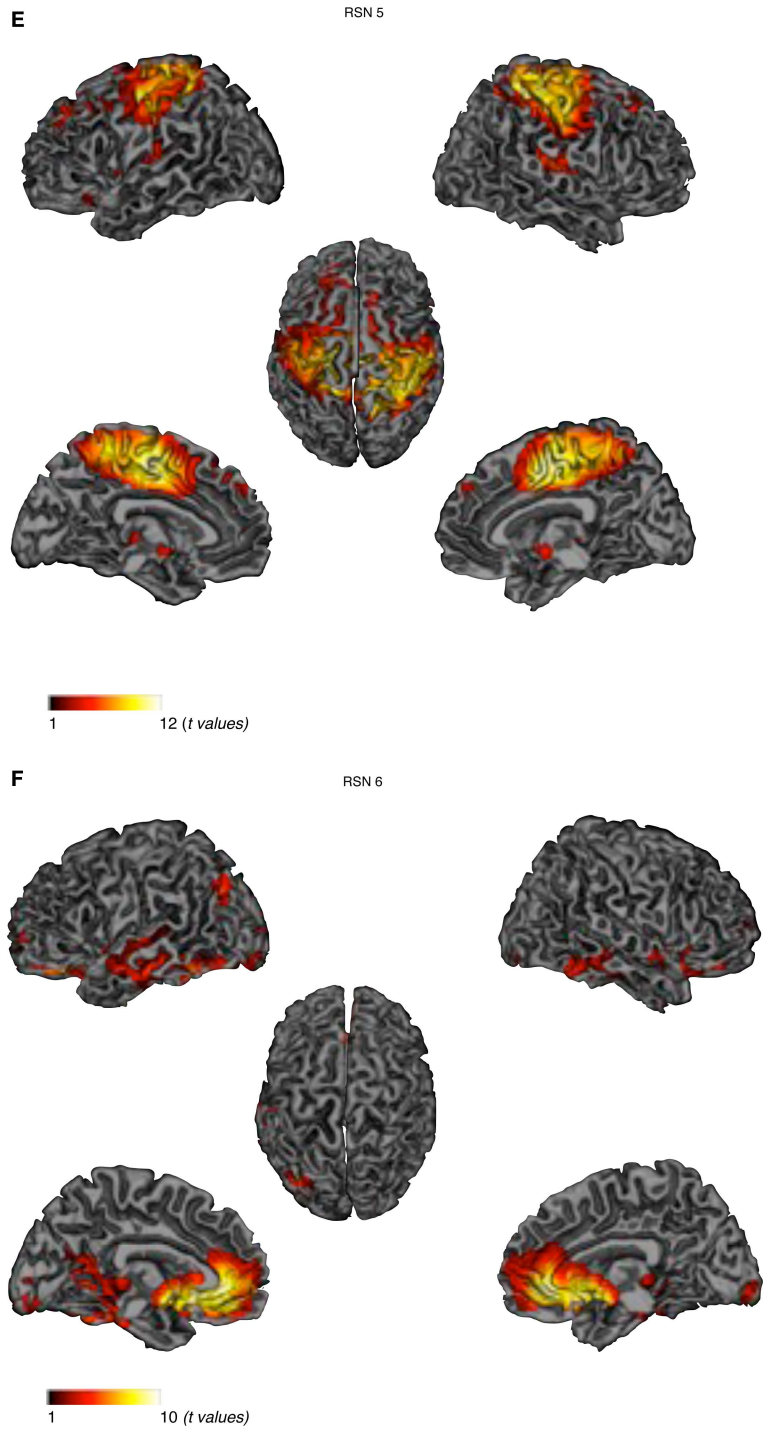

FIGURE 1 | Cortical representation of the activity in the six RSNs. For each RSN (Left) Lateral and medial views of left hemisphere. (Center) Dorsal view. (Right) Lateral and medial views of right hemisphere. **(E)** sensory motor network – SMN, **(F)** self-referential network – SRN.

cortex. Activity was also underlined in the left temporal gyrus. This network as been conceptualized as a "stand-alone" function or system (Raichle et al., 2001; Garrity et al., 2007). Briefly, this system is thought to hold recognition, self-projection and cognitive demands.

RSN 2

The dorso-lateral attention network (DAN) including the bilateral inferior parietal gyrus and the bilateral superior frontal sulcus; this system appears to be related to goal directed responses (Mantini et al., 2007).

Table 2 | fMRI peak values for RSN 1 default-mode.

Anatomical label	Hemi	BA	MNI (*x, y, z*)	*t* Value
Cingulate gyrus	R	31	3, –57, 30	18.92
Inferior parietal lobule	L	39	–45, –69, 39	13.84
Superior temporal gyrus	L	39	–48, –55, 27	13.55
	L	21	–55, –24, –5	9.49
Supramarginal gyrus	R	40	51, –55, 27	17.07
Medial frontal gyrus	R	10	–6, 51, –9	11.88
	R	9	3, 51, 18	11.51
Anterior cingulate	L	10	–3, 57, 0	11.72
Middle temporal gyrus	L	21	–63, –18, –18	11.00
	L	21	–57, –3, –21	10.58
Middle temporal gyrus	R	21	51, 12, –33	6.90
Precentral gyrus	R	4	60, –6, –21	9.55
	R	6	51, –9, 33	4.40
Parahippocampal gyrus	L	27	–24, –33, –12	7.36
Lingual gyrus	R	18	18, –84, –21	7.23
Insula	R	13	45, –9, 18	4.13

Table 3 | fMRI peak values for RSN 2 dorso-lateral attention network.

Anatomical label	Hemi	BA	MNI (*x, y, z*)	*t* Value
Inferior parietal lobule	R	40	42, –51, 48	10.74
	R	40	35, –53, 39	10.05
	L	40	–48, –51, 45	7.73
Cuneus	R	7	9, –69, 33	9.23
Middle temporal gyrus	R	22	57, –45, –6	9.23
	L	20	–57, –36, –15	5.83
	L	21	–53, –30, –12	5.72
Middle frontal gyrus	R	9	48, 27, 36	8.95
	R	10	35, 57, –3	8.39
Middle frontal gyrus	L	8	–48, 18, 45	5.28
	L	8	–42, 24, 45	4.78
	L	9	–45, 30, 33	3.89
	L	10	–33, 46, –7	5.05
Inferior frontal gyrus	R	10	42, 54, 3	8.92
Superior frontal gyrus	R	8	3, 30, 45	5.89
	L	10	–30, 57, 0	4.38

Table 4 | fMRI peak values for RSN 3 visual network.

Anatomical label	Hemi	BA	MNI (*x, y, z*)	*t* Value
Middle temporal gyrus	R	37	48, –60, –6	10.60
	R	39	42, –78, 6	10.35
	L	21	–51, 9, –21	3.69
Middle occipital gyrus	R	19	42, –81, –3	10.37
Parahippocampal gyrus	L		–36, 15, –21	4.00
Superior temporal gyrus	R	38	51, 9, –21	3.74

RSN 3

Visual network (VN) involving the occipital and bilateral temporal regions; this functional system has been linked to the visual processing network and mental imagery (Ganis et al., 2004; Mantini et al., 2007). Brain areas active in RSN 3 are thought to include the retinotopic system. Core regions of this network have been found to be abnormal in schizophrenic patients (Levy et al., 2000).

Table 5 | fMRI peak values for RSN 4 auditory network.

Anatomical label	Hemi	BA	MNI (*x, y, z*)	*t* Value
Superior temporal gyrus	L	22	–60, –42, 15	9.64
Inferior frontal gyrus	R	46	51, 36, 6	3.80
Insula	L	13	–53, –21, 24	8.91
Precentral gyrus	L	4	–45, –18, 42	7.53
	R	4	53, –15, 27	8.42
Postcentral gyrus	R	40	63, –24, 15	8.94
	R	2	39, –39, 66	3.80
Medial frontal gyrus	R	6	3, –3, 60	5.39
	R	6	5, –5, 69	5.28
	R	6	0, –5, 69	5.28
Parahippocampal gyrus	L	2	–21, –3, –15	4.27
Precuneus	L	31	–15, –72, 24	3.40

Table 6 | fMRI peak values for RSN 5 sensory motor network.

Anatomical label	Hemi	BA	MNI (*x, y, z*)	*t* Value
Paracentral gyrus	L	31	–6, –12, 51	12.41
Cingulate gyrus	L	24	6, –3, 48	11.89
Precentral gyrus	L	6	–21, –21, 57	11.75
Insula	R		39, –15, 3	8.01
	L	40	–51, –27, 18	4.76
Postcentral gyrus	R	40	54, –24, 15	7.01
Posterior cingulate	L	29	–9, –45, –18	5.23
Inferior frontal gyrus	L	47	–36, 21, –18	4.37
Superior frontal gyrus	L	9	0, 51, 36	4.03
Superior temporal gyrus	L	22	–54, 3, 0	4.00

Table 7 | fMRI peak values for RSN 6 self-referential network.

Anatomical label	Hemi	BA	MNI (*x, y, z*)	*t* Value
Medial frontal gyrus	R	10	3, 51, –9	11.64
Anterior cingulate	R	24	6, 36, –3	13.53
Inferior temporal gyrus	L	37	–57, –54, –12	6.15
Superior temporal gyrus	R	38	51, 9, –21	3.74
Insula	R	15	48, 9, –9	5.78
Parahippocampal gyrus	L	36	–3, –33, –21	5.75
	L	36	–3, –33, –21	5.75
Fusiform gyrus	R	20	45, –33, –21	5.05

RSN 4

Auditory network (AN) including the superior temporal and inferior frontal gyrus: these regions are known for being responsible in auditory processing and language comprehension. Studies on positive psychotic symptoms have found the temporal gyrus to be implied in auditory hallucinations (Gaser et al., 2004).

RSN 5

Sensory motor network (SMN), involving the precentral, postcentral gyrus and portion of the frontal gyrus corresponding to the primary sensory motor cortex (Biswal et al., 1995; Fox et al., 2006) and the supplementary motor areas.

RSN 6

Self-referential network (SRN) including the medial prefrontal, the anterior cingulate cortex and the hypothalamus: this network it is thought to involve the self-referential system (Mantini et al., 2007). It has been established that these areas are engaged in executive functions and they have been described as being abnormal in schizophrenic patients (Chan et al., 2006).

CORRELATIONS BETWEEN SPQ MEASURES AND RSNs

In **Figures 2A–C** we show the results of the regression analyses between the IC time courses and the clinical measures. In particular, strong significant positive correlations were found between the low frequency bin (0.05 Hz) of the VN and the positive SPQ factor, $p = 0.0000$ corrected. Significant positive correlations were also revealed for the VN low frequency range (0.05 Hz) and the SPQ negative factor $p < 0.0324$ corrected. Significant positive correlation was also underlined with the disorganized factor, $p < 0.0018$ corrected, in the same frequency (0.05 Hz). In the high frequency bins (0.16 and 0.19 Hz) a strong negative correlation was uncovered between the AN and disorganized factor, $p < 0.0054$ corrected, and $p < 0.0072$ corrected respectively. A weaker correlation was also uncovered between the disorganized subscale and SRN, $p = 0.0041$ uncorrected in the high frequency bin (0.16 Hz). **Table 8** shows corrected, uncorrected *p*-values and *t*-values for each correlation.

DISCUSSION

The first objective of this study was to characterize the putative DMN as well as other potential RSNs in a sample of adolescents. The ICA analyses performed upon the resting state data acquisition obtained through fMRI revealed a DMN network together with five reliable RSNs in our adolescent sample. These first results will be discussed in light of previous literature regarding RSNs in adult populations. Our second objective was to assess the relationship between schizotypal trait expression and the functional connectivity of reliable RSNs in our sample. Our results suggest that discrete dimensions of schizotypal trait expression may be selectively associated with three different RSNs, namely the SRN, the AN, and the VN. These results will be discussed in relation to the literature on RSN studies involving individuals with schizophrenia.

RESTING STATE NETWORKS IN ADOLESCENCE

The identification of six reliable RSNs in our adolescent sample further characterizes functional connectivity during this important developmental period. A recent study by Stevens and collaborators described three networks composed of traditional DMN components in their sample of adolescents aged between 12 and 20 years old (Stevens et al., 2009). One of these networks, Component 11 described by these authors, is perhaps the closest match to the DMN network found in our sample. The fact that we only found one main DMN network may be due to methodological issues such as the length of the fMRI acquisition sequence and the sample composition that differ from the previous study. When visually comparing our findings to analogous results reported in an adult sample (Mantini et al., 2007), we may observe a more definite engagement of the left superior and middle temporal gyri during baseline cerebral activity in our sample, although any interpretation would deserve caution and further empirical evidence. We may consider that this temporal region covers BA 21, which plays an important part in auditory processing and also underlies language processing. Interestingly, parts of BA 21 appear to be robustly implicated with expression of psychotic symptoms such as hallucinations and delusions in schizophrenic patients as well as in subjects at risk of developing psychosis (McGuire et al., 1995; Allen et al., 2004). However our data do not indicate a clear linear correlation between activity in adolescent DMN and their expression of perceptual aberrations as measured by the SPQ. It may be that during adolescent brain maturation, functional connectivity in the DMN is not fully constituted as to show definite links to symptomatic makers as in adults with schizophrenia. Another explanation may be that important dysfunctions in DMN functional connectivity sustain more serious manifestations of psychosis, which themselves commonly unfold during adulthood. Our finding requires further research in children with childhood-onset schizophrenia and adolescents with a very high-risk for developing schizophrenia to further elucidate the relationship between DMN activity and clinical levels of schizophrenia.

ADOLESCENT RSNs AND SCHIZOTYPAL TRAIT EXPRESSION

Conversely, the expression of adolescent schizotypal traits correlates with the VN's functional connectivity in our sample of adolescents. We note that low frequency oscillations deficits for visual stimuli are well documented in schizophrenia (Spencer, 2008). The possible interpretations linking VN to early schizotypal trait expression merit caution, as mixed reports have implicated a variety of psychotic symptoms in schizophrenia (Broyd et al., 2009; Uhlhaas and Singer, 2010). We suggest that the positive correlation between VN low frequency bins and adolescent schizotypy scores could involve processes such as mental imagery, and more generally, social cognitive information processing. In the current study, both the positive, negative, and disorganization factors were positively correlated with the VN. This network included the visual cortex areas together with occipito-temporal areas, which comprise neuronal links shared by perceptual processing and mental imagery (Ganis et al., 2004). Indeed, the inferior temporal cortices can be activated by both mental imagery and visual perception (Ganis et al., 2004). Convergent evidence from schizophrenia research suggests that schizophrenic patients display increased vividness when engaged in mental imagery (Sack et al., 2005; Oertel et al., 2009). More generally, the occipito-temporal regions involved in this network also play an active role in social perception, in particular the interpretation of social intentions and actions using biological motion, facial expression and gaze information (Pelphrey et al., 2003). Therefore, the significant correlation of schizotypal trait dimensions in adolescence with the posterior RSN network involving in mental imagery and social perception may lead us to consider how social cognitive processes contribute to the disruption of social functioning in schizotypic youths. It is noteworthy to mention that social isolation is one of the best predictive factors for psychosis onset in

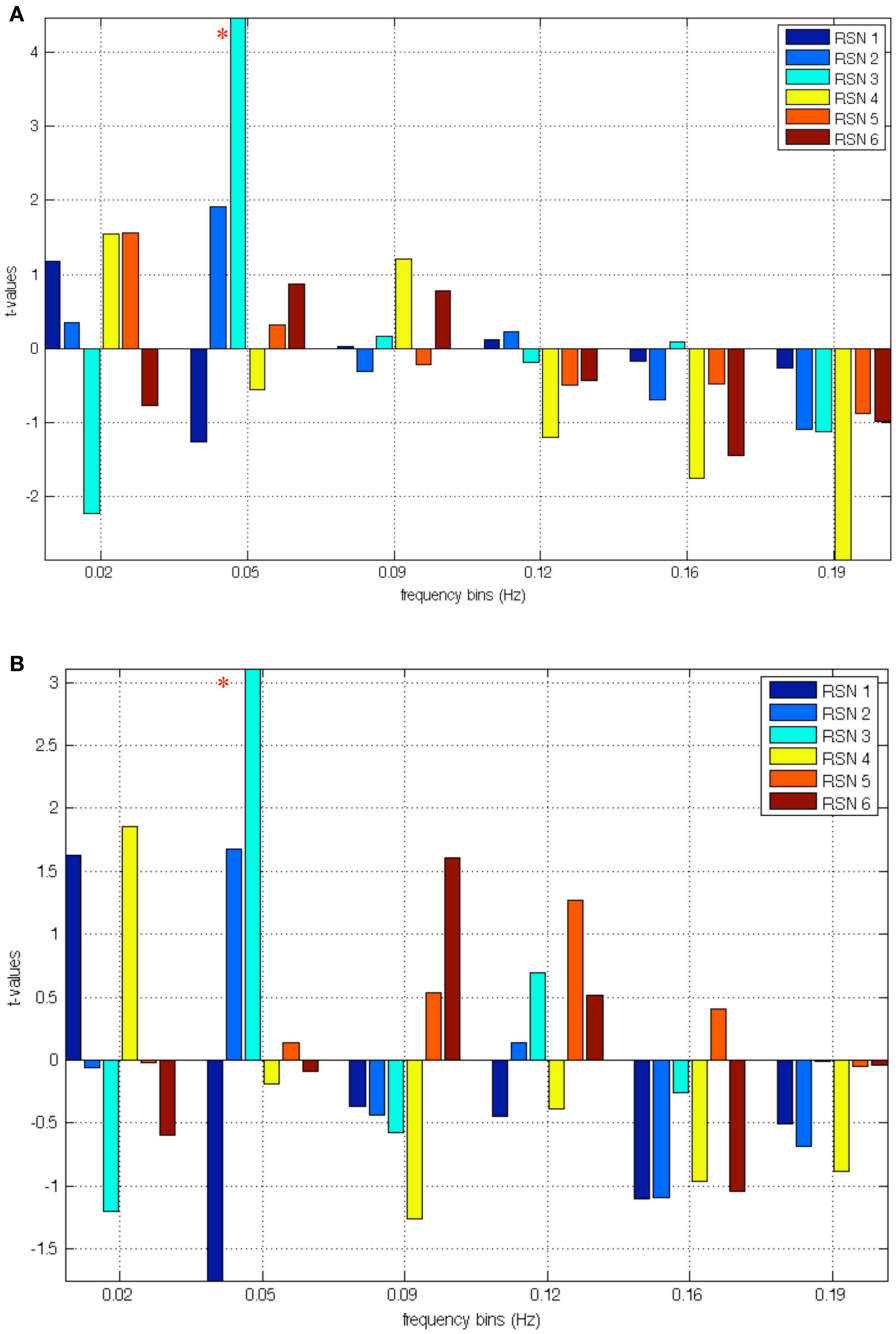

FIGURE 2 | (A) Correlation between relevant RSNs frequency bins and scores at the positive factor; the red asterisk indicates significant correlations with RSN 3 (VN). **(B)** Correlation between relevant RSNs frequency bins and scores at the negative factor; the red asterisk indicates correlations with RSN 3 (VN). (*Continued*)

youths expressing high levels of schizotypy. Our results suggest that increased activity in the VN may underlie mental representation processes that promote schizotypal trait expression.

We may also consider that the VN and the AN identified in this study, both correlating with the schizotypy measure, are composed of anatomically proximal regions. As mentioned in the introduction, the development of functional connectivity from childhood to adolescence proceeds from local to more widely distributed networks (Supekar et al., 2009). It is thought that the segregated local networks in childhood tend, with maturational change promoting long range functional connectivity, to distend and reorganize themselves within an integrated arrangement of interconnected cerebral networks (Fair et al., 2008; Supekar et al., 2010). The adolescent period represents a key transitional epoch where functional connectivity maturation takes place. In light of these developmental processes, we may hypothesize that our results reflect disturbed

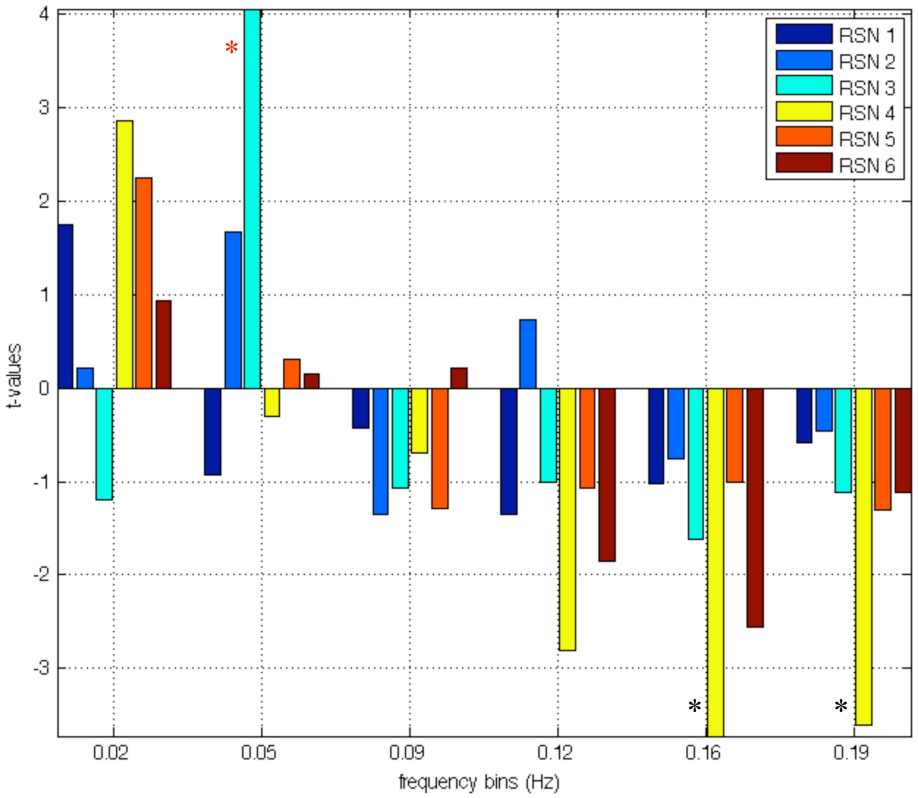

FIGURE 2 | (C) Correlation between relevant RSNs frequency bins and scores at the disorganized factor; the red asterisk indicates significant correlations with RSN 3 (VN); the black asterisks indicate negative correlations with disorganized factor and hypo-connectivity of RSN 4 (AN).

Table 8 | Statistical results for correlation between SPQ measures and RSN frequency bins.

Clinical correlation	*p* uncorrected	*p* corrected	*t* Values
0.05 HZ			
SPQ positive × VN	0.0000	0.0000	4.4713
SPQ negative × VN	0.0018	0.0324	3.1102
SPQ disorg × VN	0.0001	0.0018	4.0605
0.12 HZ			
SPQ disorg × AN	0.0040		–2.8044
0.16 HZ			
SPQ disorg × AN	0.0003	0.0054	–3.7250
SPQ disorg × SRN	0.0041		–2.7901
0.19 HZ			
SPQ disorg × AN	0.0004	0.0072	–3.6030

maturational processes of local networks (visual, auditory) that still operate in segregated fashion. If complex information such as that involved in social exchange requires sophisticated social cognitive processes involving multi-network integrated functional connectivity, then poorly integrated local networks may set the stage for faulty information processing in adolescents. In this view, faulty local network connectivity or altered functional connectivity maturation could hypothetically constitute the developmental antecedents of schizotypal trait expression.

POSSIBLE IMPLICATIONS OF SELF-REFERENTIAL PROCESSING

It is possible to gain further insight into schizotypal trait expression during adolescence by looking at the SRN observed in our sample. The SRN involves the coordination of cerebral structures responsible for *reality monitoring*, which is the capacity to accurately discriminate mental events originating from oneself from mental events originating from an external agent (Johnson et al., 1993). Reality monitoring deficits have been observed in several studies involving schizophrenic patients (Vinogradov et al., 1997, 2008) as well as in adolescents showing schizotypal traits (Debbané et al., 2009). Reality monitoring deficits observed along the continuum of schizotypal expression, from benign to clinically meaningful manifestations, lead several theorists to argue that such reality monitoring deficits contribute to the formation of psychotic symptoms (Frith and Frith, 2003). In our study, we observe a significant correlation (uncorrected) between dysfunctional connectivity of SRN and schizotypy trait expression. More precisely, the SRN functional connectivity negatively correlates with the disorganization dimension, which is comprised of both odd speech and odd behaviors. The RSN activation in this study includes both parts of BA 21 discussed above as well as the involvement of the MPFC, which we know sustains a variety of self-referential processes (D'Argembeau et al., 2005; Simons et al., 2008; Vinogradov et al., 2008). We may hypothesize that a disorganization in speech may involve inefficient connectivity between areas sustaining self-referential processes and areas

sustaining language functions, which can already be observed in the expression of the disorganization trait in adolescence. This may sustain the hypothesis suggesting that impaired language and thought functions in schizophrenia are a result of disruptions in the processes of higher order construction of self-relevant meaning (Kuperberg et al., 2009). The finding that the AN correlates with the disorganization dimension in our adolescent sample further contributes to the hypothesis that cerebral areas sustaining language processing can contribute to odd/disorganized speech manifestations and altered language processing. Furthermore, high frequency (0.20 Hz) oscillations have been found in schizophrenic patients when compared to normal controls (Garrity et al., 2007). Relevant RSNs have shown typical frequency oscillations below 0.1 Hz (Cordes et al., 2001). However, significantly stronger power in higher frequencies has been seen in the DMN of a sample schizophrenic patients, specifically between the 0.1 and 0.24 Hz (Garrity et al., 2007). This finding suggested less temporal synchronicity between the brain regions involved. In addition, Cordes and colleagues have highlighted that harmonic respiratory cycles do not arise under 0.25 Hz (to 0.5 Hz), and cardiac rate arises around 0.9 Hz, therefore none of the physiological noise should arise into the low frequency bins (0.1 Hz). These oscillations may be representative of less effective connections between brain regions which enable information processing (Garrity et al., 2007).

To conclude, in agreement with previous studies on adult RSNs (Gusnard and Raichle, 2001; Gusnard et al., 2001; Raichle et al., 2001; Mantini et al., 2007), we report on six reliable RSNs identified in baseline cerebral activity in an adolescent population. Significant correlation with schizotypal trait expression could be observed with the auditory and VNs. This study provides an illustration of the influences of baseline cerebral activity on personality characteristics during adolescence. More specifically, altered connectivity in the self-referential and ANs may intensify the expression of disorganized speech and behavior, while increased functional connectivity in the VN may constitute a putative mechanism which perpetuates increased vividness in mental imagery and undermine social evaluation. Further research on adolescent samples are required to better understand the influence of resting state activity on personality trait expression.

ACKNOWLEDGMENTS

The authors would like to thank the volunteer participants. Additional thanks go to the LAVIM neuroimaging plateform, as well as the Adolescent Outpatient Psychiatry Services, Drs Dario Balanzin, Serges Djapo-Yogwa and Danny Dukes for their collaboration. This work has been supported in part by the centre for bio medical imaging of the University of Geneva, Lausanne and EPFL. Our gratitude also goes to Pascal Challande and Frank Henry for the help with data acquisition. This work was funded by the Gertrude Von Meissner Foundation (ME 7871) grant to S. Eliez and M. Debbané, and by the Swiss National Science Foundation (PP00B-102864) grants to S. Eliez and by the grant PP00P2-123438 to Dimitri Van De Ville.

SUPPLEMENTARY MATERIAL

The Supplementary Material for this article can be found online at http://www.frontiersin.org/neuroscience/systemsneuroscience/paper/10.3389/fnsys.2010.00035/

REFERENCES

Allen, P. P., Johns, L. C., Fu, C. H., Broome, M. R., Vythelingum, G. N., and McGuire, P. K. (2004). Misattribution of external speech in patients with hallucinations and delusions. *Schizophr. Res.* 69, 277–287.

Axelrod, S. R., Grilo, C. M., Sanislow, C., and McGlashan, T. H. (2001). Schizotypal personality questionnaire brief: factor structure and convergent validity in inpatient adolescents. *J. Pers. Disord.* 15, 168–179.

Beckmann, C. F., De Luca, M., Devlin, J. T., and Smith, S. M. (2005). Investigations into resting-state connectivity using independent component analysis. *Philos. Trans. R. Soc. Lond., B, Biol. Sci.* 360, 1001–1013.

Beckmann, C. F., and Smith, S. M. (2004). Probabilistic independent component analysis for functional magnetic resonance imaging. *IEEE Trans. Med. Imaging* 23, 137–152.

Bell, A. J., and Sejnowski, T. J. (1995). An information maximisation approach to blind separation and blind deconvolution. *Neural Comput.* 7, 1129–1159.

Biswal, B., Yetkin, F. Z., Haughton, V. M., and Hyde, J. S. (1995). Functional connectivity in the motor cortex of resting human brain using echo-planar MRI. *Magn. Reson. Med.* 34, 537–541.

Broyd, S. J., Charmaine, D., Debener, S., Helps, S. K., James, C. J., and Sonuga-Barke, E. J. S. (2009). Default-mode brain dysfunction in mental disorders: a systematic review. *Neurosci. Biobehav. Rev.* 33, 279–296.

Calhoun, V., and Adali, T. (2006). Unmixing fMRI with independent component analysis. *IEEE Eng. Med. Biol. Mag.* 25, 79–90.

Calhoun, V., Adali, T., Pearlson, G., and Pekar, J. (2001). A method for making group inferences from functional MRI data using independent component analysis. *Hum. Brain Mapp.* 14, 140–151.

Chan, R. C. K., Chen, E. Y. H., and Law, C. W. (2006). Specific executive dysfunction in patients with first-episode medication-naïve schizophrenia. *Schizophr. Res.* 82, 51–64.

Cordes, D., Haughton, V. M., Arfanakis, K., Carew, J. D., Turski, P. A., Moritz, C. H., Quigley, M. A., and Meyerand, M. E. (2001). Frequencies contributing to functional connectivity in the cerebral cortex in "Resting-state" Data. *AJNR Am. J. Neuroradiol.* 22, 1326–1333.

D'Argembeau, A., Collette, F., Van der Linden, M., Laureys, S., Del Fiore, G., Degueldre, C., Luxen, A., and Salmon, E. (2005). Self-referential reflective activity and its relationship with rest: a PET study. *Neuroimage* 25, 616–624.

Debbané, M., Van der Linden, M., Gex-Fabry, M., and Eliez, S. (2009). Cognitive and emotional associations to positive schizotypy during adolescence. *J. Child. Psychol. Psychiatry* 50, 326–334.

De Luca, M., Beckmann, C. F., De Stefano, N., Matthews, P. M., and Smith, S. M. (2006). fMRI resting state networks define distinct modes of long-distance interactions in the human brain. *Neuroimage* 29, 1359–1367.

Dumas, P., Bouafia, S., Gutknecht, C., Saoud, M., Dalery, J., and d'Amato, T. (2000). Validation of the French version of the Raine Schizotypal Personality Disorder Questionnaire – categorical and dimensional approach to schizotypal personality traits in a normal student population. *Encephale* 26, 23–29.

Fair, D., Cohen, A. L., Dosenbach, N. U. F., Church, J. A., Miezin, F. M., Barch, D. M., Raichle, M. E., Petersen, S. E., and Schlaggar, B. L. (2008). The maturing architecture of the brain's default network. *Proc. Natl. Acad. Sci. U.S.A.* 105, 1028–1032.

Fox, M. D., and Raichle, M. E. (2007). Spontaneous fluctuations in brain activity observed with functional magnetic resonance imaging. *Nat. Rev. Neurosci.* 8, 700–711.

Fox, M. D., Snyder, A. Z., Zacks, J. M., and Raichle, M. E. (2006). Coherent spontaneous activity accounts for trial-to-trial variability in human evoked brain responses. *Nat. Neurosci.* 9, 23–25.

Frith U., and Frith, C. D. (2003). Development and neurophysiology of mentalizing. *Philos. Trans. R. Soc. Lond., B, Biol. Sci.* 358, 459–473.

Ganis, G., Thompson, W. L., and Kosslyn, M. S. (2004). Brain areas underlying visual mental imagery and visual perception: an fMRI study. *Brain Res. Cogn. Brain Res.* 20, 226–241.

Garrity, A. G., Pearlson, G. D., McKiernan, K., Lloyd, D., Kiehl, K. A., and Calhoun, V. D. (2007). Aberrant "default mode" functional connectivity in schizophrenia. *Am. J. Psychiatry* 164, 450–457.

Gaser, C., Nenadic, I., Volz, H. P., Büchel, C., and Sauer, H. (2004). Neuroanatomy of "hearing voices": a frontotemporal brain structural abnormality associated with auditory hallucinations in schizophrenia. *Cereb. Cortex* 14, 91–96.

Greicius, M. D., Krasnow, B., Reiss, A. L., and Menon, V. (2003). Functional connectivity in the resting brain: a network analysis of the default mode hypothesis. *Proc. Natl. Acad. Sci. U.S.A.* 100, 253–258.

Greicius, M. D., Srivastava, G., Reiss, A. L., and Menon, V. (2004). Default-mode network activity distinguishes Alzheimer's disease from healthy aging: evidence from functional MRI. *Proc. Natl. Acad. Sci. U.S.A.* 101, 4637–4642.

Gusnard, D. A., Akbudak, E., Shulman, G. L., and Raichle, M. E. (2001). Medial prefrontal cortex and self-referential mental activity: relation to a default mode of brain function. *Proc. Natl. Acad. Sci. U.S.A.* 98, 4259–4264.

Gusnard, D. A., and Raichle, M. E. (2001). Searching for a baseline: functional imaging and the resting human brain. *Nat. Rev. Neurosci.* 2, 685–694.

Hampson, M., Peterson, B. S., Skudlarski, P., Gatenby, J. C., and Gore, J. C. (2002). Detection of functional connectivity using temporal correlations in MR images. *Hum. Brain Mapp.* 15, 247–262.

Jafri, M. J., Pearlson, G. D., Stevens, M., and Calhoun, V. D. (2008). A method for functional network connectivity among spatially independent resting-state components in schizophrenia. *Neuroimage* 39, 1666–1681.

Johnson, M. K., Hashtroudi, S., and Lindsay, D. S. (1993). Source monitoring. *Psychol. Bull.* 114, 28.

Kelly, C. A. M., Di Martino, A., Uddin, L. Q., Shehzad, Z., Gee, D. G., Reiss, P. T., Margulies, S., Castellanos, F. X., and Milham, M. P. (2009). Development of anterior cingulate functional connectivity from late childhood to early adulthood. *Cereb. Cortex* 19, 640–657.

Keri, S., and Janka, Z. (2000). Cognitive dysmetria in schizophrenia. *Am. J. Psychiatry* 157, 662–663.

Kuperberg, G. R., Kreher, D. A., and Ditman, T. (2009). What can event-related potentials tell us about language, and perhaps even thought, in schizophrenia? *Int. J. Psychophysiol.* 75, 66–76.

Levy, D. L., Lajonchere, C. M., Dorogusker, B., Min, D., Lee, S., Tartaglini, A., Lieberman, J. A., and Mendell, N. R. (2000). Quantitative characterization of eye tracking dysfunction in schizophrenia. *Schizophr. Res.* 42, 171–185.

Mantini, D., Perrucci, M. G., Del Gratta, D., Romani, G. L., and Corbetta, M. (2007). Electrophysiological signatures of resting state networks in the human brain. *Proc. Natl. Acad. Sci. U.S.A.* 104, 13170–13175.

McGuire, P. K., Silbersweig, D. A., Wright, I., Murray, R. M., David, A. S., Frackowiak, R. S., and Frith, C. D. (1995). Abnormal monitoring of inner speech: a physiological basis for auditory hallucinations. *Lancet* 346, 596–600.

Oertel, V., Rotarska-Jagiela, A., van de Ven, V., Haenschel, C., Grube, M., Stangier, U., Maurer, k., and Linden, D. E. J. (2009). Mental imagery vividness as a trait marker across the schizophrenia spectrum. *Psychiatry Res.* 167, 1–11.

Paus, T., Keshavan, M., and Giedd, J. N. (2008). Why do many psychiatric disorders emerge during adolescence? *Nat. Rev. Neurosci.* 9, 947–957.

Pelphrey, K. A., Mitchell, T. V., McKeown, M. J., Goldstein, J., Allison, T., and McCarthy, G. (2003). Brain activity evoked by the perception of human walking: controlling for meaningful coherent motion. *J. Neurosci.* 23, 6819–6825.

Raichle, M. E., MacLeod, A. M., Snyder, A. Z., Powers, W. J., Gusnard, D. A., and Shulman, G. L. (2001). A default mode of brain function. *Proc. Natl. Acad. Sci. U.S.A.* 98, 676–682.

Rossi, A., and Daneluzzo, E. (2002). Schizotypal dimensions in normals and schizophrenic patients: a comparison with other clinical samples. *Schizophr. Res.* 54, 67–75.

Rotarska-Jagiela, A., van de Ven, V., Oertel Knöchel, V., Uhlhaas, P., Vogeley, K., and Linden, D. E. J. (2010). Resting-state functional network correlates of psychotic symptoms in schizophrenia. *Schizophr. Res.* 17, 21–31.

Sack, A. T., Camprodon, J. A., Pascual-Leone, A., and Goebel, R. (2005). The dynamics of interhemispheric compensatory processes in mental imagery. *Science* 308, 702–704.

Simons, J. S., Henson, R. N. A., Gilbert, S. J., and Fletcher, P. C. (2008). Separable forms of reality monitoring supported by the anterior prefrontal cortex. *J. Cogn. Neurosci.* 20, 447–457.

Sowell, E. R., Thompson, P. M., and Toga, A. W. (2004). Mapping changes in the human cortex throughout the span of life. *Neuroscientist* 10, 372–392.

Spencer, K. M. (2008). Visual gamma oscillations in schizophrenia: implications for understanding neural circuitry abnormalities. *Clin. EEG Neurosci.* 39, 65–68.

Stevens, M. C., Kiehl, K. A., Pearlson, G. D., and Calhoun, V. D. (2007). Functional neural networks underlying response inhibition in adolescents and adults. *Behav. Brain Res.* 181, 12–22.

Stevens, M. C., Pearlson, G. D., and Calhoun, V. D. (2006). Functional neural circuits for mental time keeping. *Hum. Brain Mapp.* 28, 394–408.

Stevens, M. C., Pearlson, G. D., and Calhoun, V. D. (2009). Changes in the interaction of resting-state neural networks from adolescence to adulthood. *Hum. Brain Mapp.* 30, 2356–2366.

Supekar, K., Musen, M., and Menon, V. (2009). Development of large-scale functional brain networks in children. *PLoS Biol.* 7, e1000157. doi: 10.1371/journal.pbio.1000157.

Supekar, K., Uddin, L. Q., Prater, K., Amin, H., Greicius, M. D., and Menon, V. (2010). Development of functional and structural connectivity within the default mode network in young children. *Neuroimage* 52, 290–301.

Uhlhaas, P. J., and Singer, W. (2010). Abnormal neural oscillation and synchrony in schizophrenia. *Nat. Rev. Neurosci.* 11, 100–113.

van de Ven, V. G., Formisano, E., Prvulovic, D., Roeder, C. H., and Linden, D. E. J. (2004). Functional connectivity as revealed by spatial independent component analysis of fMRI measurements during rest. *Hum. Brain Mapp.* 22, 165–178.

Van den Heuvel, M. P., Mandl, R. C. W., Kahn, R. S., and Hulshoff Pol, E. H. (2009). Functionally linked resting-state networks reflect the underlying structural connectivity architecture of the human brain. *Hum. Brain Mapp.* 3, 3127–3141.

Vinogradov, S., Luks, T. L., Schulman, B. J., and Simpson, G. V. (2008). Deficit in a neural correlate of reality monitoring in schizophrenia patients. *Cereb. Cortex* 18, 2532–2539.

Vinogradov, S., Willis-Shore, J., Poole, J. H., Marten, E., Ober, B. A., and Shenaut, G. K. (1997). Clinical and neurocognitive aspects of source monitoring errors in schizophrenia. *Am. J. Psychiatry* 154, 1530–1537.

Conflict of Interest Statement: The authors declare that the research was conducted in the absence of any commercial or financial relationships that could be construed as a potential conflict of interest.

Received: 05 February 2010; paper pending published: 25 March 2010; accepted: 02 July 2010; published online: 05 August 2010.
Citation: Lagioia A, Van De Ville D, Debbané M, Lazeyras F and Eliez S (2010) Adolescent resting state networks and their associations with schizotypal trait expression. Front. Syst. Neurosci. ***4****:35. doi: 10.3389/fnsys.2010.00035*

frontiers in
SYSTEMS NEUROSCIENCE

ORIGINAL RESEARCH ARTICLE
published: 07 June 2010
doi: 10.3389/fnsys.2010.00017

Functional implications of age differences in motor system connectivity

Jeanne Langan[1,2], Scott J. Peltier[3], Jin Bo[1], Brett W. Fling[1,2], Robert C. Welsh[4,5] and Rachael D. Seidler[1,2,6]*

[1] School of Kinesiology, University of Michigan, Ann Arbor, MI, USA
[2] Department of Biomedical Engineering, University of Michigan, Ann Arbor, MI, USA
[3] Department of Psychology, University of Michigan, Ann Arbor, MI, USA
[4] Institute of Gerontology, University of Michigan, Ann Arbor, MI, USA
[5] Department of Radiology, University of Michigan, Ann Arbor, MI, USA
[6] Department of Psychiatry, University of Michigan, Ann Arbor, MI, USA

Edited by:
Lucina Q. Uddin,
Stanford University, USA

Reviewed by:
Martijn van den Heuvel,
Universitair Medisch Centrum Utrecht, Netherlands
Christophe Habas,
Université Pierre et Marie Curie, France

Correspondence:
Rachael D. Seidler,
Department of Psychology and School of Kinesiology, University of Michigan, 401 Washtenaw Avenue, Ann Arbor, MI 48109-2214, USA.
e-mail: rseidler@umich.edu

Older adults show less lateralized task-related brain activity than young adults. One potential mechanism of this increased activation is that age-related degeneration of the corpus callosum (CC) may alter the balance of inhibition between the two hemispheres. To determine whether age differences in interhemispheric connectivity affect functional brain activity in older adults, we used magnetic resonance imaging (MRI) to assess resting functional connectivity and functional activation during a simple motor task. We found that older adults had smaller CC area compared to young adults. Older adults exhibited greater recruitment of ipsilateral primary motor cortex (M1), which was associated with longer reaction times. Additionally, recruitment of ipsilateral M1 in older adults was correlated with reduced resting interhemispheric connectivity and a larger CC. We suggest that reduced interhemispheric connectivity reflects a loss of the ability to inhibit the non-dominant hemisphere during motor task performance for older adults, which has a negative impact on performance.

Keywords: aging, corpus callosum, fMRI, functional connectivity, motor cortex

INTRODUCTION

Older adults have been shown to recruit more of the brain than young adults to perform a given task. The hemispheric asymmetry reduction in older adults (HAROLD) model characterizes this phenomenon in cognitive tasks (Cabeza, 2001). It describes the finding that older adults typically have less lateralized prefrontal cortex recruitment than younger adults during the performance of cognitive tasks (cf. Reuter-Lorenz and Lustig, 2005). Similarly, older adults performing motor tasks tend to recruit more brain regions compared to young adults, particularly the primary motor cortex (M1) ipsilateral to the moving limb (Mattay et al., 2002; Ward and Frackowiak, 2003; Heuninckx et al., 2005, 2008; Riecker et al., 2006).

The recruitment of additional brain regions by older adults has been associated with enhanced performance of both cognitive (Reuter-Lorenz et al., 2000; Cabeza et al., 2002) and motor tasks (Mattay et al., 2002; Heuninckx et al., 2008), suggesting that increased activation in older adults serves a compensatory purpose. In contrast, there are examples of older adults demonstrating greater activation yet exhibiting diminished (Madden et al., 1999) or similar performance to young adults (Hutchinson et al., 2002). Thus, over-activation may also reflect nonspecific activity or dedifferentiation (Li et al., 2001; Li and Sikstrom, 2002; for a review see Seidler et al., 2010).

Ipsilateral motor activation in older adults may be the result of structural decline of the corpus callosum (CC), possibly leading to recruitment of the ipsilateral cortex via interhemispheric motor overflow. The CC is the primary means of communication between hemispheres. Unimanual movement of the dominant hand has a net inhibitory effect on the ipsilateral M1 (Sohn et al., 2003; Vercauteren et al., 2008). The reduced CC integrity that accompanies aging (Sullivan et al., 2002; Head et al., 2004) may disrupt interhemispheric balance; indeed, older adults demonstrate reduced inhibition between hemispheres compared to young adults (Talelli et al., 2008a,b). As callosal connections between the two motor cortices appear to have a net inhibitory effect (Ferbert et al., 1992; Netz, 1999; De Gennaro et al., 2004; Duque et al., 2007), callosal degeneration with age may lead to greater activation of the ipsilateral M1 (due to reduced inhibition from the contralateral M1) during motor task performance. However, a complete section of the CC leads to an absence of ipsilateral activation during tactile stimulation (Fabri et al., 1999), suggesting that the relationship between CC integrity and ipsilateral activation in sensorimotor tasks may be nonlinear. Therefore, while some degeneration of the CC may lead to less lateralized task processing (Muller-Oehring et al., 2007), extensive damage or complete section of the CC would likely abolish ipsilateral activation.

Motor task difficulty has also been shown to have an impact on recruitment of ipsilateral M1. More complex motor tasks result in greater recruitment of brain regions, particularly the ipsilateral M1 (Seidler et al., 2004; Verstynen et al., 2005). This raises the question of whether ipsilateral M1 activity in older adults is due to age differences in task difficulty. Advances in imaging analyses, such as resting state functional connectivity (fcMRI), provide a way to assess communication between cortical regions without incorporating a task.

Regions with similar functions and known anatomical connections have shown strong correlations in the low-frequency blood oxygen level dependent (BOLD) signal, commonly referred to as

fcMRI (Fox and Raichle, 2007; Rogers et al., 2007; Vincent et al., 2007). Examples of functional connectivity of anatomical regions with structural connections between hemispheres include motor networks (Biswal et al., 1995; Xiong et al., 1999; De Luca et al., 2005), visual networks (Lowe et al., 1998; Cordes et al., 2000) and auditory networks (Cordes et al., 2000). Moreover, resting state connectivity networks exhibit stability across data sets collected from different participants using differing acquisition parameters, locations, and scanners (Biswal et al., 2010). Recently, Lowe et al. (2008) found that measures of callosal integrity correlate with M1 interhemispheric resting state connectivity in patients with multiple sclerosis. Similarly, correlations between M1 in each hemisphere are greatly diminished with CC agenesis (Quigley et al., 2003) or callosal sectioning (Johnston et al., 2008). Taken together these data support that fcMRI is a noninvasive and reliable method for assessing resting state interhemsipheric connectivity.

The goal of the current study was to examine the influence of age differences in interhemispheric connectivity upon brain activation patterns and task performance in older adults. We used a region of interest (ROI) approach (cf. Peltier et al., 2005; Di Martino et al., 2008) to compare resting state connectivity between the two M1s. We hypothesized that: 1. M1 task-related fMRI activation in older adults would be less lateralized, with increased activation serving a compensatory role; 2. Older adults would have smaller CCs and greater M1 resting interhemispheric connectivity; and 3. Older adults demonstrating stronger M1 resting interhemispheric connectivity would demonstrate less laterality in M1 task-related fMRI activation.

MATERIALS AND METHODS

PARTICIPANTS AND PROCEDURE

Young (n = 18, 21.4 ± 2.1 years, nine males) and older (n = 18, 71.7 ± 5.8 years, nine males) adults were recruited from the University of Michigan community and through the University of Michigan National Institutes of Health Claude D. Pepper Older American's Independence Center human subjects and assessment core. All participants signed an internal review board approved consent form prior to entrance into the study. Participants were free of contraindications for an fMRI study as determined by a health questionnaire and were right handed, as verified by the Edinburgh Handedness Inventory (Oldfield, 1971, young adult's mean = 77 ± 14, older adult's mean = 89 ± 10, t = 2.81, df = 32, p = 0.01). Cognitive status was assessed using the Mini Mental Status Examination (minimum inclusion score 27/30, Folstein et al., 1975) and the Mattis Dementia Rating Scale (minimum inclusion score 124/144, Mattis, 1976). Screening occurred on the first of two testing days.

On day one of testing, participants were accepted into the study if they met the above inclusion criteria. They then practiced a motor task using their right (dominant) hand in a mock MRI scanner. Participants were comfortably positioned in the mock scanner with a mirror adjusted to allow visualization of a video screen. A dual potentiometer joystick was used to control the movement of a cursor on the screen. The starting position of the cursor was centered on the screen. Targets would appear randomly above, below, right, or left of the original cursor position. Participants were instructed to move the cursor as quickly and accurately as possible to the target, hold the cursor in the target until the target disappeared and then release the spring-loaded joystick allowing the cursor to return to the original centered position. Real-time feedback of the joystick location was presented as a cursor moving on the display screen. A trial was defined as the time between the appearance and disappearance of the target (2.5 s). The inter-trial interval was 2.5 s. In a single run participants performed two blocks of 12 trials (20 s visual fixation, block of 12 trials, 20 s visual fixation, block of 12 trials, 22 s visual fixation). Participants practiced three runs of the task in the mock scanner to become familiar with the operation of the joystick device and visual feedback display.

The second day of testing was conducted at the University of Michigan Functional MRI Laboratory. A series of scans were performed using a 3.0 T MRI scanner (General Electric, Waukesha, WI, USA). Participants' heads were comfortably restrained to reduce head movement. They wore fMRI compatible mirrored glasses to view a screen for the visual stimuli. During the first scan, which was collected for resting state functional connectivity analyses (fcMRI), participants gazed at a fixation cross. In total, 400 images were acquired in a time span of 5 min using a single-shot gradient-echo reverse-spiral pulse sequence. The repetition time (TR) was 750 ms, echo time (TE) was 30 ms, flip angle (FA) was 50 and field of view (FOV) was 220 mm. Sixteen contiguous, 3.2-mm axial slices were acquired in each TR. Voxel size was 3.4-mm × 3.4 mm × 3.2 mm. These acquisition parameters result in lower signal to noise ratio than the task acquisition parameters (see below), but they allow us to (a) sample at a faster rate (as opposed to TR of 2), so that we have both increased degrees of freedom after the low-pass filter, and less chance of high frequency physiological noise aliasing into our frequency band of interest; and (b) acquire 400 samples in 5 min, as opposed to only 150 samples with a 2 s TR. It would have taken over 13 min to acquire 400 samples with a 2 s TR, which was considered prohibitive given the older population being studied. Cardiac (measured with pulse oximeter) and respiratory (measured with chest plethysmography) signals were acquired for use in the data analyses.

During the motor task fMRI scans, participants performed two runs of the joystick task as previously described using their right hand. A single-shot gradient-echo reverse-spiral pulse sequence was also used to acquire the fMRI data. Pulse sequence parameters were TR/TE/FA/FOV of 2000 ms/30 ms/80/220 mm respectively. Forty, 3.2-mm-thick slightly oblique axial slices (no gap) were acquired. A total of 91 images were acquired, with each run lasting 182 s. High-resolution anatomical images were also acquired using a T1-weighted gradient-echo pulse sequence with the following parameters: TR/TE/FA/FOV 200 ms/3.7 ms/90/220 mm and a voxel size of 1 mm × 1 mm × 1.2 mm.

BEHAVIORAL DATA ANALYSIS

Custom Labview 6.1 software (National Instruments) was used to analyze the joystick data offline. A dual pass Butterworth digital filter (Winter 1990) using a cutoff frequency of 10 Hz was used to filter the raw data. The resultant joystick path was calculated by computing the square root of the sum of the squared X and Y coordinate data at each time point. The tangential velocity profile was then calculated through differentiation. The optimal algorithm of Teasdale (Teasdale et al., 1993) was used to determine move-

ment onset and offset. Performance on the task was measured by reaction time (RT), initial endpoint error (IEE), and final endpoint error (FEE). RT was calculated by subtracting the time of the target presentation from the time of the movement onset. IEE represents the distance from the joystick controlled cursor and the target at the end of the first ballistic movement. The algorithm used to calculate IEE identifies a period of acceleration following a period of deceleration or a change in the sign of the velocity. FEE is the distance from the target at movement offset.

MRI DATA ANALYSIS

fMRI data

The first three volumes per run were discarded to allow for signal equilibration. High-pass filtering was used to remove low-frequency drift. Motion correction was performed using MCFLIRT and the brain extraction tool (BET) was used to strip the skull from images (using FSL toolboxes, http://www.fmrib.ox.ac.uk/fsl). Statistical Parametric Mapping version 5 (SPM5: www.fil.ion.ucl.ac.uk/spm/software/spm5/) was used for subsequent analyses. A mean functional image was created for each participant. All functional and structural images were aligned to this mean functional image. The Montreal Neurological Institute (MNI) template was used for spatial normalization (Mazziotta et al., 1995). The structural image was normalized to MNI space first and the resulting parameters were applied to the functional images. Functional images were spatially smoothed using a full width at half-maximum 8-mm Gaussian smoothing kernel. Boxcar models synchronized to the effect of interest and convolved with an estimate of the hemodynamic response function were used for statistical analyses. A general linear model analysis was first conducted at an individual level across runs contrasting periods of movement with rest. The first level statistics were used to identify the MNI coordinates with the most significant activations in the hand knob region of the left primary M1 in each individual for the fcMRI analysis (see description below). Also at the first level, percent signal change for the motor task relative to the rest periods was calculated and averaged across runs. Second level random effects analyses were run for single group whole brain (uncorrected $p = 0.0001$), and ROI analyses in the right primary somatosensory cortex and M1 (sensorimotor cortex, uncorrected $p = 0.005$). Between group analyses were also run for whole brain (uncorrected $p = 0.001$) and ROI analyses in the right sensorimotor cortex (uncorrected $p = 0.005$).

fcMRI data

The first 10 volumes were discarded to allow the signal to reach a steady state. Motion correction and the use of BET were the same as described for fMRI. Second-order harmonics of the simultaneously recorded cardiac and respiratory signals were regressed out in image space using RETROICOR (Glover et al., 2000). Linear trends were removed from the data to eliminate the effect of gross signal drifts. Low-pass filtering was performed with a cut-off frequency of 0.08 Hz. No other temporal or spatial smoothing was performed on the fcMRI data. The hand knob region of the left M1 was identified visually for each subject. The hand knob has a distinct omega shape making it a good anatomical landmark (Yousry et al., 1997). In each individual the most active region in their hand knob during the fMRI task served as their seed for the fcMRI ROI analysis. The seed consisted of four neighboring voxels. The time courses from each of the four voxels in the seed region were averaged together to create one representative time course characterizing signal changes in the seed region over the length of the scan. Then, a correlation analysis between this representative time course of the seed region and all other voxels in the brain was performed. The degree of connectivity was quantified for each individual by calculating the average *z* score of all suprathreshold voxels in the resting state correlation map ($p < 0.05$, cluster threshold >9 contiguous voxels). In performing significance calculations, the degrees of freedom were decreased to reflect the reduced number of degrees of freedom in the low-pass filtered data.

The SPM toolbox WFU_Pickatlas (Maldjian et al., 2003) was used to define M1 and the primary somatosensory cortex. We combined these two regions of interest to create a sensorimotor cortex mask. The sensorimotor cortex mask was refined to reflect the cortex in common with all participants. Two older adults were removed from the analyses as their head position in the 16 slice fcMRI acquisition remarkably reduced the size of the sensorimotor cortex mask. The sensorimotor cortex mask was used as a ROI to calculate the percent signal change in suprathreshold voxels ($p > 0.001$ uncorrected, cluster threshold >9 contiguous voxels) in the task related fMRI data for each participant. In the fcMRI data the mask delineated the *z* scores used to calculate a metric reflecting interhemispheric balance between the seed region in the left M1 and the right sensorimotor cortex for each participant. **Figure 1** illustrates the time course of the seed region in the left hemisphere and the time course of a suprathreshold voxel in the right sensorimotor cortex for one representative participant. The correlation between these two time courses denotes functional interhemispheric connectivity. Correlations between the seed region and the right sensorimotor cortex will be referred to as sensorimotor cortex interhemispheric connectivity. In the group analyses using the right sensorimotor cortex mask the cluster threshold was >4 contiguous voxels for both fMRI and fcMRI data. To determine the degree of laterality in fMRI activation, a laterality index using the percent signal change in the sensorimotor cortex was calculated with the following formula: laterality index = (left sensorimotor cortex − right sensorimotor

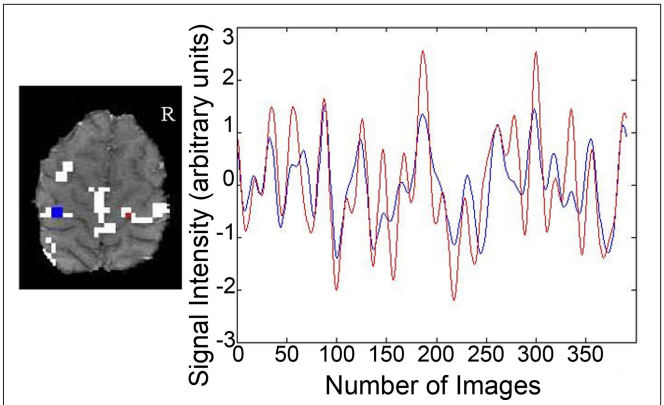

FIGURE 1 | Connectivity data from a representative participant. The seed region and corresponding time course for a single participant are depicted in blue. Voxels having correlation strength above threshold are shown in white. The time course for a suprathreshold voxel and the corresponding voxel are shown in red.

cortex)/(left sensorimotor cortex + right sensorimotor cortex)*100. A score of 100 would reflect complete lateralization to the left side. Conversely, a score of −100 would indicate complete lateralization to the right side.

Anatomical data-CC morphology

A custom Matlab program (MATLAB, MathWorks Inc. R2007b) was used to manually outline the CC from a mid-sagittal slice taken of a high-resolution T1 image. Another custom MATLAB program was then used to divide the CC into seven sub-regions as previously described by Witelson (1989). Individual variation in the size of these sections has been shown to relate to brain functional activity during sensory and motor processing (Stancak et al., 2002, 2003a,b) as well as correlations with the laterality of task processing in older adults (Muller-Oehring et al., 2007). In the Witelson scheme, the CC is separated into seven regions to roughly correspond to distinct anatomical connections of the caudal/orbital prefrontal, inferior premotor cortices (region 1), prefrontal cortices (2), premotor and supplementary motor areas (3), primary motor cortices (4), primary sensory cortices (5), superior temporal and posterior parietal cortices (6) and occipital, inferior temporal cortices (7) (**Figure 2**). However, it should be noted that these subdivisions were originally based upon anatomical work conducted in monkeys. More recent DTI tractography data from humans indicates that these regions, particularly 3–6, may be shifted posteriorly in the CC (Hofer and Frahm, 2006; Wahl et al., 2007; Bartels et al., 2008). Wahl et al. (2007) suggest that this posterior shift, particularly noted in callosal motor fibers, may be due to the significantly larger prefrontal cortex volume in humans as compared to monkeys (Eccles, 1989). Therefore, when considering our results, it is appropriate to consider fibers passing through CC regions 3–6 as connecting primary motor (5/6), premotor (3/4), and supplementary motor (3/4) regions of the two hemispheres. Boundaries indicating the anteriormost (ACC) and posteriormost (PCC) border define the length of the CC (ACC–PCC line, **Figure 2**). The genu line, perpendicular to the ACC–PCC line, was placed at the anteriormost point of the inner convexity of the anterior CC defining regions 1 (rostrum) and 2 (genu). All other regions are defined as a proportion of the CC (see **Figure 2**). Cross-sectional area was calculated for each of the seven sub-regions. Three independent raters performed all steps to ensure CC measurements were reliable. The mean value of the raters was used in the analyses.

Intracranial area was also calculated for each subject utilizing the same custom MATLAB programs. The same mid-sagittal slice was used to measure the CC area and intracranial area for each subject. An outline was drawn along the interior border of the skull with a straight line connecting the nasion and the inion. The cross-sectional area of each CC sub-region was normalized to intracranial area to control for any atrophy and/or degeneration that may have occurred in the brains of our older adult participants. Two independent raters performed intracranial area measurements to establish reliability. The mean value of the raters was used in the analyses.

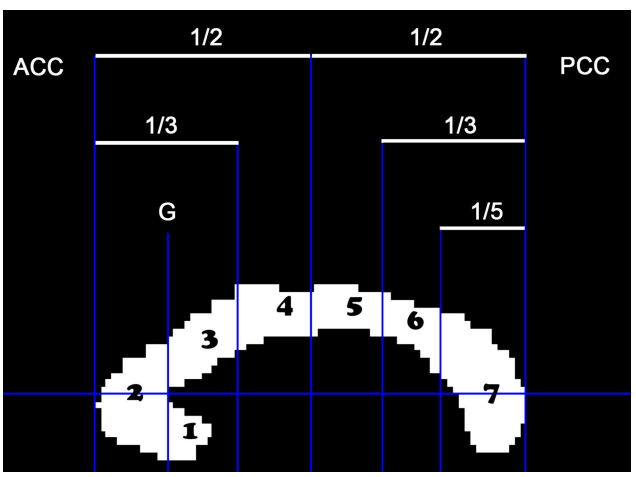

FIGURE 2 | The cross-sectional area of the mid-sagittal CC was parsed into seven regions: (1) rostrum, (2) genu, (3) rostral truncus, (4) anterior intermediate truncus, (5) posterior intermediate truncus, (6) isthmus, (7) splenium.

STATISTICAL ANALYSES

Statistical analyses were conducted in SPSS. Between group differences were analyzed using independent *t* tests. Correlations were assessed between the sensorimotor cortex interhemispheric connectivity, percent signal change in the right sensorimotor cortex, fMRI laterality index, the motor performance variables, and fMRI activation peaks resulting from the contrast of older adults > young adults. Scores that were outside 2.5 standard deviations from the mean for the group were excluded from the analyses. Inter-rater reliability for CC and intracranial area measurements was assessed with Krippendorff's alpha (Hayes and Krippendorff, 2007).

RESULTS

BEHAVIORAL RESULTS

Older adults did not perform at the same level as young adults on the motor task (**Table 1**); they took longer to initiate movements, moved more slowly during the initial ballistic movement towards the target, and ended the movement further from the target.

MOTOR TASK-RELATED fMRI RESULTS

The young adults and older adults recruited overlapping brain regions while performing the motor task, primarily in motor regions such as the bilateral precentral gyrus, left postcentral gyrus, right inferior and superior parietal lobe, and cerebellum. There were no regions where young adults showed greater activation

Table 1 | Older adults did not perform at the same level as young adults (all variables significantly different between the two age groups at $p < 0.01$).

Variable	YA	OA
RT (ms)	481 ± 100	622 ± 154
IEE (mm)	10.78 ± 1.06	19.43 ± 1.43
PSMT (ms)	484 ± 67	599 ± 98
FEE (mm)	6.79 ± 1.08	12.81 ± 4.69

RT, reaction time; IEE, initial endpoint error; PSMT, primary submovement time; FEE, final endpoint error.

than older adults. Similar to previous studies, older adults showed greater activation compared to young adults in many brain regions (**Table 2**); of particular interest to the current study is the right (ipsilateral) sensorimotor cortex. **Figure 3** illustrates regions where older adults had greater activation within the right sensorimotor cortex ROI than the young adults (see also **Table 3**). There were no regions in the right sensorimotor cortex ROI analysis where young adults demonstrated greater activation compared to older adults.

Only older adults demonstrated a statistically significant correlation between percent signal change in the right sensorimotor cortex and motor behavior. Older adults that had longer RTs demonstrated more activation in the right sensorimotor cortex (df = 14, $r = 0.57$, $p = 0.02$, **Figure 4**). We did not find statistically significant correlations between fMRI measurements and IEE or FEE. Although not significant, the correlation between percent signal change in the right sensorimotor cortex and FEE (df = 13 $r = 0.41$, $p = 0.13$) in older adults suggests that kinematic performance may also be negatively impacted by increased activation in the right sensorimotor cortex.

RESTING STATE fcMRI RESULTS

Young and older adults demonstrated resting state connectivity between the left M1 seed region and some similar brain regions such as the left sensorimotor cortex, supplementary motor area, and bilateral parietal regions. There are few regions in which the young adults demonstrated statistically greater connectivity than the older adults (**Figure 5A**). In contrast, the older adults showed greater connectivity than the young adults in several right hemisphere regions (**Figure 5B**). **Figure 6** presents the results of the right sensorimotor cortex ROI analysis. Older adults show stronger regions

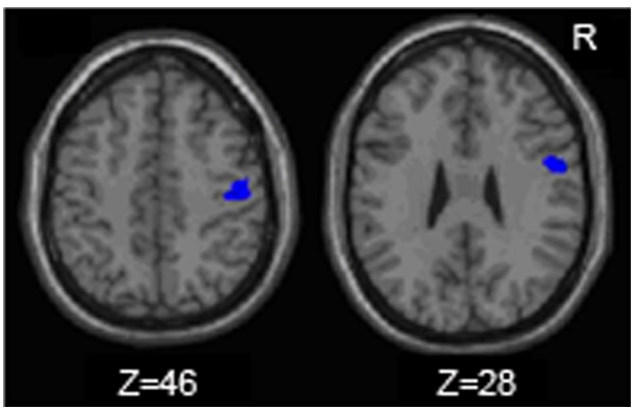

FIGURE 3 | Regions within the sensorimtor cortex ROI in which the older adults exhibited more motor task related activation (fMRI) than the young adults.

Table 2 | Regions in which older adults exhibit more fMRI task-related activation than young adults (uncorrected $p = 0.001$, whole brain analysis).

Anatomical location	BA	Cluster size	Coordinates of peaks	*z* score
FRONTAL AREAS				
L Superior frontal gyrus	9	79	–38 42 30	3.9
L Middle frontal gyrus	8		–36 34 40	3.38
L Precentral gyrus	6	23	–40 –12 42	3.62
R Medial frontal gyrus	9	25	16 38 30	3.58
R Middle frontal gyrus	10	27	38 50 22	3.36
R Middle frontal gyrus	46	39	46 26 26	3.34
L Inferior frontal gyrus	44	36	–36 10 28	3.31
L Middle frontal gyrus	9		–30 10 34	3.15
TEMPORAL AREAS				
R Middle temporal gyrus	21	136	42 0 –22	3.85
PARIETAL AREAS				
R Precuneus	7	805	12 –56 46	4.54
L Precuneus	7		–2 –50 52	3.99
R Precuneus	7		12 –48 44	3.97
R Cuneus	19		20 –84 34	3.37
R Postcentral gyrus	1	34	40 –20 46	3.31
R Postcentral gyrus	3		50 –12 44	3.22
R Fusiform gyrus	37	10	34 –44 –14	3.45
SUBCORTICAL AREAS				
L Cerebellum (HIII)		70	–12 –34 –22	4.59
L Cerebellum (Crus I)		59	30 –70 –30	3.97
L Cerebellum (Crus I)		15	–22 –72 –36	3.4

BA, Brodmann's area; L, left; R, right.

Table 3 | Regions in which older adults exhibit more fMRI task-related activation than young adults within the right sensorimotor cortex ROI (uncorrected $p = 0.005$).

Anatomical location	BA	Cluster size	Coordinate of peaks	*z* score
FRONTAL AREAS				
R precentral gyrus	6	115	52 0 28	3.16
PARIETAL AREAS				
R postcentral gyrus	3	132	50 –12 44	3.05
R postcentral gyrus	3		42 –18 46	2.82

BA, Brodmann's area; R, right.

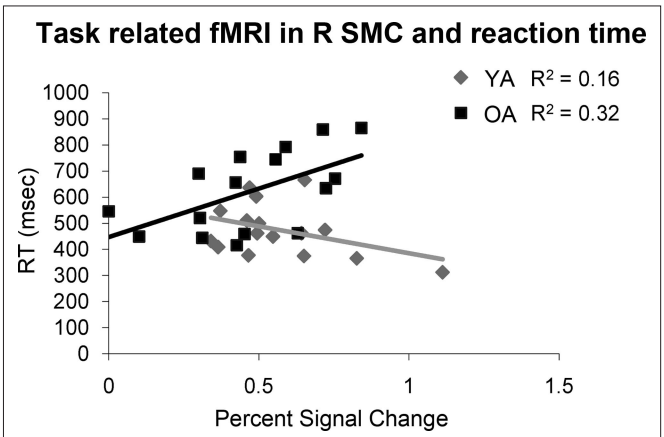

FIGURE 4 | Older adults (OA) demonstrate a significant positive correlation between reaction time and fMRI activation in the right sensorimotor cortex (R SMC) while young adults (YA) do not.

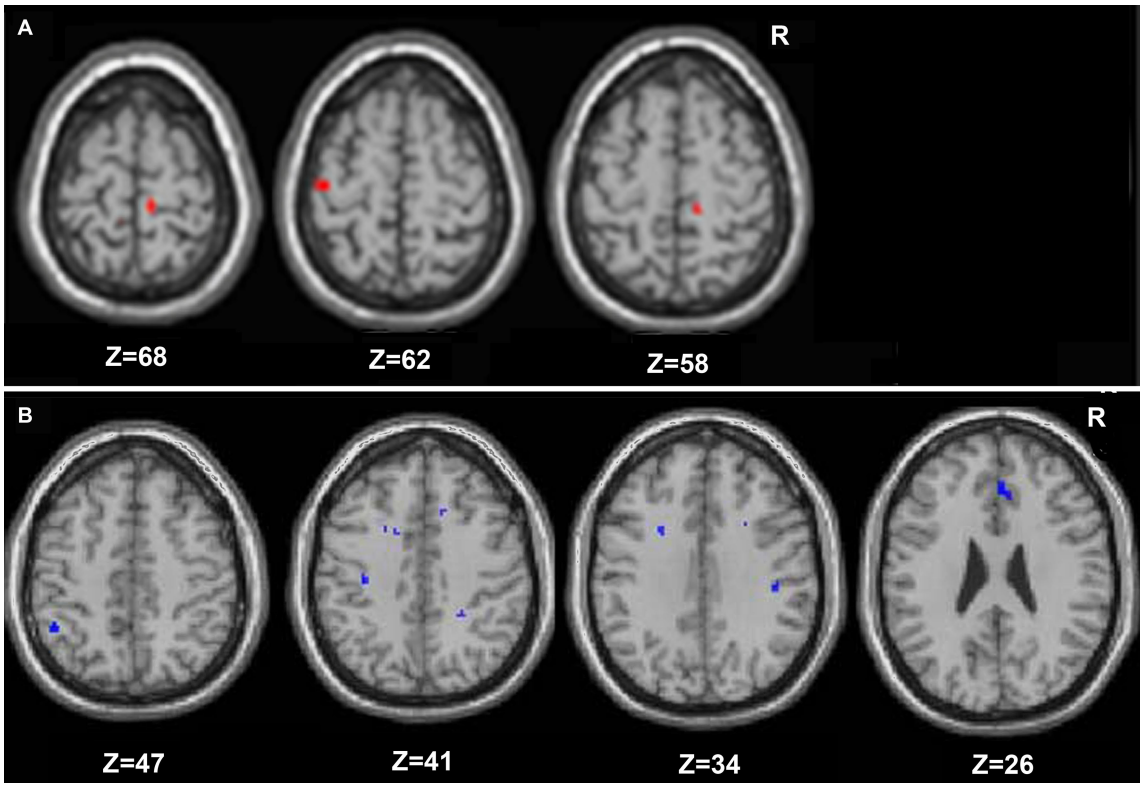

FIGURE 5 | Regions in which young adults exhibited greater resting functional connectivity than older adults are presented in (A), and areas in which the older adults had greater connectivity than the young are in (B) (whole brain analyses).

of sensorimotor cortex interhemispheric connectivity compared to young adults (**Figures 6A,B**, **Table 4**). Interestingly, older adults that display stronger sensorimotor cortex interhemispheric connectivity also demonstrate reduced percent signal change in the right sensorimotor cortex during the fMRI task (df = 14, $r = -0.52$, $p = 0.04$, **Figure 7**).

CORPUS CALLOSUM RESULTS

Inter-rater reliability scores for both CC measurements and intracranial measurements were good (Krippendorff's alpha = 0.91 and 0.89 respectively). The overall mid-sagittal cross-sectional area of the CC (normalized to intracranial area) was diminished in older adults compared to young adults ($t_{(32)} = 2.28$, $p = 0.03$). In particular, regions thought to link the premotor and supplementary motor cortices such as the genu ($t_{(32)} = 3.61$, $p < 0.01$), and primary motor cortices such as the intermediate truncus ($t_{(32)} = 2.78$, $p = 0.01$), posterior intermediate truncus ($t_{(32)} = 2.23$, $p = 0.03$), and isthmus ($t_{(32)} = 2.17$, $p = 0.04$) were smaller in older adults than young adults (**Figures 8A,B**). We hypothesized that older adults with reductions in these regions would demonstrate stronger interhemispheric communication between motor cortices, greater task-related fMRI activation in the right (ipsilateral) sensorimotor cortex and better performance. We found that older adults with smaller genu size had greater sensorimotor cortex interhemispheric connectivity (**Figure 9**, df = 14, $r = -0.49$, $p = 0.05$). In addition, older adults demonstrated a negative relationship between size of the anterior and posterior intermediate truncus and fMRI laterality index (df = 12, $r = -0.55$, $p = 0.04$ and df = 12, $r = -0.57$, $p = 0.03$ respectively). That is, older adults that had greater mid-sagittal area in the anterior and posterior intermediate truncus recruited the right sensorimotor cortex more during the motor task. While the young adults demonstrated similarities to the older adults in the relationship between CC genu area and interhemipheric connectivity, it did not reach statistical significance (df = 16, $r = -0.42$, $p = 0.10$). No other CC region was correlated with the fMRI laterality index in young adults ($p > 0.18$).

DISCUSSION

The data supported our hypothesis that older adults would show decreased lateralization of M1 activity during motor task performance. These findings replicate the results of previous fMRI studies of the aging motor system (Mattay et al., 2002; Ward and Frackowiak, 2003; Riecker et al., 2006). We further hypothesized that greater activation during the fMRI task would be associated with better performance. Unlike previous research (Mattay et al., 2002), we found that OA with greater ipsilateral M1 activation had longer RTs.

These results demonstrate that additional activation in older adults is not universally compensatory. Similarly, Riecker et al. (2006) found that over-activation in older adults did not scale with increasing task difficulty, and interpreted this as a non-compensatory effect. The bulk of the work supporting the idea of compensatory over-recruitment relates to prefrontal activation and cognitive tasks (Reuter-Lorenz et al., 2000; Cabeza et al., 2002;

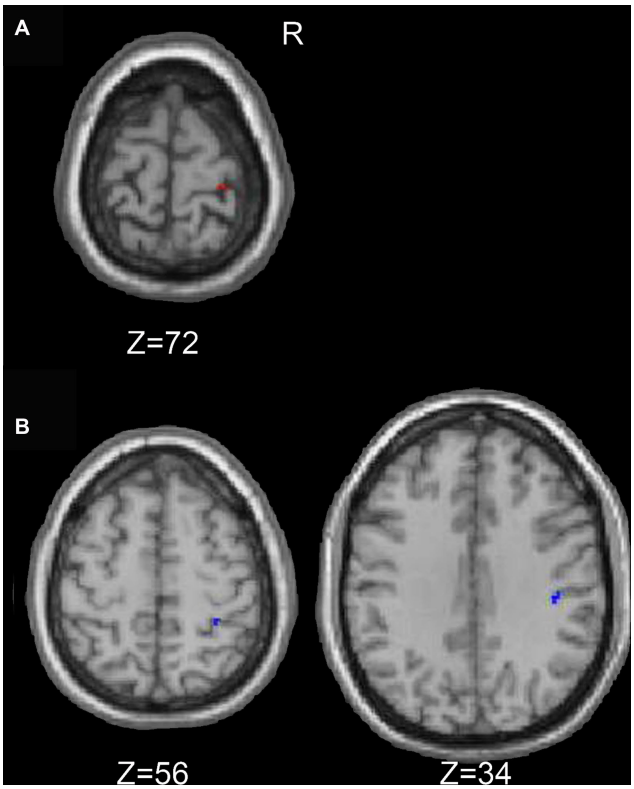

FIGURE 6 | Regions in which the young exhibited greater resting functional connectivity than the older adults are presented in (A), and areas in which the older adults had greater connectivity than the young adults are in (B) (right sensorimotor cortex ROI analyses).

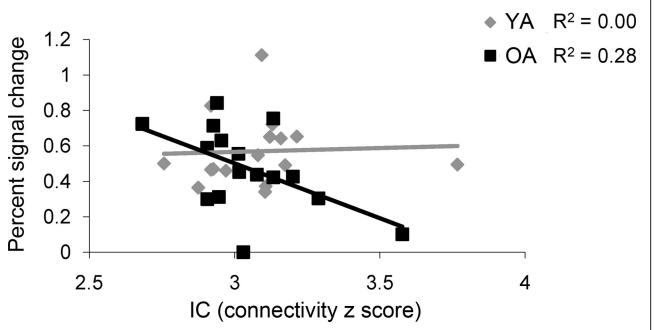

FIGURE 7 | The older adults (OA) had a negative correlation between resting functional connectivity strength in the right sensorimotor cortex (R SMC) ROI and fMRI activation in the same region, while the young adults (YA) did not.

Table 4 | Young adults (YA) versus older adults (OA) R sensorimotor cortex fcMRI (uncorrected $p = 0.01$, right sensorimotor cortex ROI analyses).

Anatomical location	BA	Cluster size	Coordinates of peaks	*z* score
YA > OA				
Parietal areas				
R Postcentral gyrus	1	9	28 –28 72	3.24
OA > YA				
Frontal areas				
R Precentral gyrus	6	7	58 2 30	2.92
Parietal areas				
R Postcentral gyrus	2	7	42 –24 34	3.2
R Postcentral gyrus	2	5	32 –38 56	2.66

BA, Brodmann's area; R, right.

Paxton et al., 2008). While over-activation of prefrontal regions may enhance cognitive task performance in older adults, increased activation in the ipsilateral M1 may be counterproductive to the performance of unimanual motor tasks. In young adults, movement of the dominant hand has an overall inhibitory effect on the ipsilateral M1 (Sohn et al., 2003). Indeed, such inhibitory processes factor strongly into the execution of precise unimanual movements. Motor evoked potentials induced through transcranial magnetic stimulation (TMS) are greater in hand muscles used during a movement thus showing decreased inhibition. Meanwhile muscles that are not engaged to produce a movement show higher levels of inhibition (Liepert et al., 1998; Stinear and Byblow, 2002), a characteristic that would reduce unintended movements. Ipsilateral muscles assessed by motor evoked potentials also showed increased inhibition following simple movements (Leocani et al., 2000). This pattern of interhemispheric inhibition, coupled with our findings, suggests that older adults that maintain the ability to inhibit the ipsilateral M1 during movement are able to perform unimanual motor tasks more efficiently. Therefore, increased activation in older adults may have positive or negative consequences for task performance, depending on the role that the brain region plays in the task. This view is supported by previous research (Colcombe et al., 2005; Wierenga et al., 2008).

As predicted, older adults demonstrated greater resting connectivity compared to young adults in both the whole brain and right sensorimotor cortex ROI analyses. Taniwaki et al. (2007) used structural equation modeling to measure effective connectivity associated with motor task performance and also found increased interhemispheric connectivity between ventral premotor cortices, supplementary motor areas and sensorimotor cortex in older adults. In contrast, others have reported age-related decreases in functional connectivity (Wu et al., 2007; Taniwaki et al., 2007), particularly in the basal ganglia thalamocortical motor loop during a self initiated motor task in older adults. Combined, these data suggest that aging may have differential effects on subcortical–cortical and cortico–cortical connectivity. Increased connectivity in cortical regions throughout the brain may influence performance for older adults. In a study examining speech perception under conditions of decreased clarity of speech, stronger functional connectivity between cortical regions remote to the auditory cortex was associated with greater comprehension (Obleser et al., 2007). Age differences in connectivity throughout the brain are intriguing and deserve further research. However, here we focus our discussion on interhemispheric connectivity between sensorimotor cortices and the relationship to motor task-related activation and cross-sectional area of the CC.

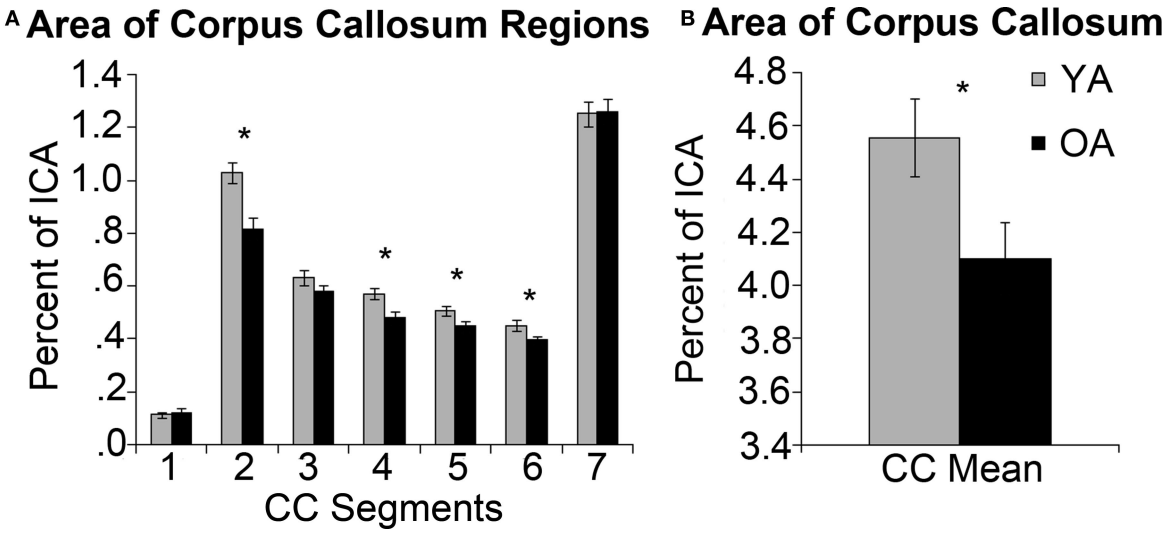

FIGURE 8 | (A) Normalized area of CC regions and standard error (SE) in young adults (YA) and older adults (OA). The CC is divided into seven regions: (1) rostrum, (2) genu, (3) rostral truncus, (4) anterior intermediate truncus, (5) posterior intermediate truncus, (6) isthmus, (7) splenium. (**B**) Mean cross-sectional area of the entire CC and SE. Asterisk indicates significant group differences at $p < 0.05$.

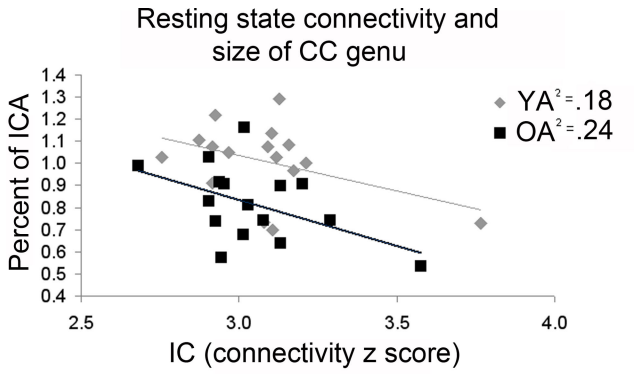

FIGURE 9 | Older adults (OA) with smaller area in the corpus callosum genu demonstrated greater interhemispheric connectivity (IC). While young adults (YA) mimicked this pattern, the correlation did not reach statistical significance.

We hypothesized that older adults who demonstrate stronger resting state interhemispheric connectivity would exhibit less lateralized task-related motor cortical activity. Previous work suggests that age-related changes in the CC disrupt interhemispheric balance, resulting in disinhibition of the ipsilateral hemisphere (Talelli et al., 2008a,b). In the current study we found that older adults demonstrated both increased connectivity and decreased laterality of task-related motor cortical activation compared to the young adults. Interestingly, we found a *negative* correlation between sensorimotor cortex interhemispheric connectivity and task-related fMRI activation in the right sensorimotor cortex. This pattern suggests that older adults with greater interhemishperic connectivity more effectively inhibited the ipsilateral sensorimotor cortex. A study with young adults demonstrated similar findings using an encoding task (Putnam et al., 2008). During a verbal encoding task that is typically lateralized to the left prefrontal cortex, young adults with greater anterior callosal fractional anisotropy, a measurement of white matter integrity, activated the right prefrontal cortex less than young adults with lower fractional anisotropy. Young adults also demonstrated a negative correlation between encoding accuracy and right inferior prefrontal cortex activation (Putnam et al., 2008). Interhemispheric inhibition is believed to be mediated through excitatory neurons in the motor cortices that synapse onto local inhibitory networks (Chen, 2004). It may be that older adults with stronger connectivity better engage the local inhibitory networks, resulting in less ipsilateral activation during a task and better performance.

Integrity of the CC impacts movement efficacy. Prior to complete myelination of the CC, children display bilateral movements or muscle activation during tasks intended to be unilateral. This is known as motor overflow or in cases where there is overt movement, mirror movements (Addamo et al., 2007). On the other end of the age spectrum, older adults show a reduction in number and integrity of CC fibers (Sullivan et al., 2002; Head et al., 2004) potentially impacting connectivity and unimanual motor control. We found the size of the CC was diminished in older adults, specifically in the following regions: the genu, anterior and posterior intermediate truncus, and isthmus. Older adults with smaller genu regions showed greater sensorimotor cortex interhemispheric connectivity. Based on previous studies (Ota et al., 2006) demonstrating age-related degeneration of the CC and disruption of interhemispheric inhibition (Talelli et al., 2008a), we had predicted the CC would be diminished in older adults and sensorimotor cortex interhemispheric connectivity would be greater. However, we anticipated that these traits would lead to disinhibition in the ipsilateral hemisphere. Surprisingly, in our results there was a negative correlation between fMRI laterality index and the size of both the anterior and posterior intermediate truncus. These findings all point toward a reduction in right sensorimotor cortex activation with diminished size of these CC regions.

This pattern of more lateralized activation in combination with diminished CC size has been noted in other studies. For example, behavioral measures of laterality for dichotic word listening, line bisection and turning bias are negatively correlated with callosal size (Yazgan et al., 1995). Movement-related potentials recorded through electroencephalography (EEG) are stronger on the ipsilateral side when the genu and intermediate truncus are larger (Stancak et al., 2000). Additionally, older adults demonstrating strong memory performance also display stronger fractional anisotropy in the CC genu and reduced activation in the right frontal gyrus (Persson et al., 2006). This relationship between CC size or integrity and interhemispheric interactions is likely to be nonlinear, though. While some degeneration of the CC may result in reduced interhemispheric inhibition and greater motor overflow, extensive damage or complete section of the CC would likely abolish or greatly diminish interhemispheric interactions.

Our findings support that age-related resting state physiological changes contribute to functional brain activation patterns and performance. This is important to note as task difficulty has been offered as an explanation for differences in brain activation patterns between older adults and young adults (Smith et al., 2001; Logan et al., 2002; Tisserand and Jolles, 2003). Our data disputes task difficulty as the sole explanation for alterations in brain activation patterns in older adults, because we note changes in motor network connectivity at rest. We found greater resting state interhemispheric connectivity in older adults compared to young adults, and a negative relationship between sensorimotor cortex interhemispheric connectivity and activation in the right sensorimotor cortex in older adults. Thus task difficulty may account for some but not all aspects of age differences in brain recruitment patterns.

It is possible that a stronger degree of right handedness in older adults (Porac, 1993; Dittmar, 2002), a phenomenon also noted in our study, may account for some of the differences we found between older adults and young adults. Environmental theories suggest that the world around us promotes use of the right hand and increased practice leads to more exclusive use of the right hand with aging (Harris, 1990). Since there is a connection between physical activity and brain function (Nudo et al., 1996), greater reliance on the right hand in older adults may influence connectivity and functional brain activation. With that stated, both the young and older adults in our study demonstrated right handedness with mean scores above 75 and only 12 points separating groups on a scale ranging from −100 (extreme left handedness) to +100 (extreme right handedness). While statistically significantly different there may be little practical difference between groups.

Understanding the relationships between neuroanatomy, neurophysiology, and behavioral function in typically aging adults is important as it may lead to better recommendations for healthy aging in this rapidly growing subpopulation. Also, by strengthening our knowledge of typical progression in aging there is the potential to better understand what goes awry in pathological conditions. This research may help to provide insight into pathologies that share characteristics with aging adults, such as multiple sclerosis, a pathology in which the integrity of white matter tracts is reduced due to demyelination. In a study investigating middle aged adults with multiple sclerosis, microstructural damage in the CC [measured through diffusion tensor imaging (DTI) using mean diffusivity value] was positively correlated with activation in ipsilateral M1 during a simple motor task (Lenzi et al., 2007). Interestingly, the same study found a negative correlation between M1 ipsilateral activation and duration of transcollosal inhibition. Moreover, longer inhibition durations in individuals with multiple sclerosis have been shown to be indicative of greater demyelination (Hoppner et al., 1999) and greater disability (Schmierer et al., 2002). This would suggest that deterioration of the CC is associated with greater inhibition of ipsilateral M1. It is clear that brain function, particularly in cases of pathology, are not straight forward (Pantano et al., 2006) and future studies are needed.

This research may also help to provide insight into pathologies that typically impact older adults. Gaining a greater understanding of interhemispheric interactions in healthy older adults is important in light of the role interhemispheric communication may play following stroke. For example, it has been shown that interhemispheric inhibition exerted by the intact hemisphere over the lesioned hemisphere may hinder recovery (Murase et al., 2004; Duque et al., 2005). During movements of the paretic hand there is increased interhemispheric inhibition targeting M1 in the lesioned hemisphere. Learning what role sensorimotor cortex interhemispheric connectivity plays in normal movement and understanding how exercise may alter function in the ipsilateral and contralateral M1 (Duque et al., 2007) may serve an important function in stroke rehabilitation.

One potential limitation of the current study is that we did not incorporate DTI metrics of callosal integrity. However, we felt that this was beyond the scope of the current investigation, particularly given the desire to limit magnet time to a reasonable duration for our older adult participants. Instead, we evaluated and integrated fMRI, structural MRI, and fcMRI metrics. Future research should further investigate the relationships between neuroanatomy and function using a tool such as DTI to better reflect white matter connections and microstructure of axons in the CC (Hagmann et al., 2003; Vernooij et al., 2008).

In conclusion, we found that older adults recruited the ipsilateral sensorimotor cortex to a greater extent during motor task performance than young adults. The cross-sectional area of the CC in older adults was diminished compared to young adults. Older adults with a smaller CC genu demonstrated stronger sensorimotor cortex interhemispheric connectivity. Interestingly, older adults with stronger sensorimotor cortex interhemispheric connectivity retained the ability to inhibit the ipsilateral sensorimotor cortex during a motor task. Furthermore we found that older adults that successfully inhibited the right sensorimotor cortex performed the motor task more proficiently, demonstrating that increased activation is not uniformly beneficial for older adults. The function of the region and the role it plays in the task may determine the relationship between over-activation and performance.

ACKNOWLEDGMENTS

Thanks to C. Amer, B. Downs, S. Durussel-Weston, S. Kaviany, A. Miller, A. Sandusky, D. Scott, and A. Stubbs for their assistance in this study. This work was supported by National Institutes of Health [grant numbers AG024106 (RS), T32-AG000114], and the UM National Institutes of Health Claude D. Pepper Center Human Subjects and Assessment Core (grant number AG024824). The authors declare that there are no actual or potential conflicts of interest.

REFERENCES

Addamo, P. K., Farrow, M., Hoy, K. E., Bradshaw, J. L., and Georgiou-Karistianis, N. (2007). The effects of age and attention on motor overflow production – a review. *Brain Res. Rev.* 54, 189–204.

Bartels, C., Mertens, N., Hofer, S., Merboldt, K. D., Dietrich, J., Frahm, J., and Ehreneich, H. (2008). Callosal dysfunction in amyotrophic lateral sclerosis correlates with diffusion tensor imaging of the central motor system. *Neuromuscul. Disord.* 18, 398–407.

Biswal, B. B., Mennes, M., Zuo, X., Gohel, S., Kelly, C., Smith, S. M., Beckmann, C. F., Adelstein, J. S., Buckner, R. L., Colcombe, S., Dogonowski, A., Ernst, M., Fair, D., Hampson, M., Hoptman, M. J., Hyde, J. S., Kiviniemi, V. J., Kötter, R., Li, S., Lin, C., Lowe, M. J., Mackay, C., Madden, D. J., Madsen, K. H., Margulies, D. S., Mayberg, H. S., McMahon, K., Monk, C. S., Mostofsky, S. H., Nagel, B. J., Pekar, J. J., Peltier, S. J., Petersen, S. E., Riedl, V., Rombouts, S. A., Rypma, B., Schlaggar, B. L., Seidler, R. D., Siegle, G. J., Sorg, C., Teng, G., Veijola, J., Villringer, A., Walter, M., Wang, L., Weng, X., Whitfield-Gabrieli, S., Williamson, P., Windischberger, C., Zang, Y., Zhang, H., Castellanos, F. X., and Milham, M. P. (2010). Towards discovery science of human brain function. *PNAS* 107, 4734–4739.

Biswal, B., Yetkin, F. Z., Haughton, V. M., and Hyde, J. S. (1995). Functional connectivity in the motor cortex of resting human brain using echo-planar MRI. *Magn. Reson. Med.* 34, 537–541.

Cabeza, R. (2001). Cognitive neuroscience of aging: contributions of functional neuroimaging. *Scand. J. Psychol.* 42, 277–286.

Cabeza, R., Anderson, N. D., Locantore, J. K., and McIntosh, A. R. (2002). Aging gracefully: compensatory brain activity in high-performing older adults. *Neuroimage* 17, 1394–1402.

Chen, R. (2004). Interactions between inhibitory and excitatory circuits in the human motor cortex. *Exp. Brain Res.* 154, 1–10.

Colcombe, S. J., Kramer, A. F., Erickson, K. I., and Scalf, P. (2005). The implications of cortical recruitment and brain morphology for individual differences in inhibitory function in aging humans. *Psychol. Aging* 20, 363–375.

Cordes, D., Haughton, V. M., Arfanakis, K., Wendt, G. J., Turski, P. A., Moritz, C. H., Quigley, M. A., and Meyerand, M. E. (2000). Mapping functionally related regions of brain with functional connectivity MR imaging. *Am. J. Neuroradiol.* 21, 1636–1644.

De Gennaro, L., Cristiani, R., Bertini, M., Curcio, G., Ferrara, M., Fratello, F., Romei, V., and Rossini, P. M. (2004). Handedness is mainly associated with an asymmetry of corticospinal excitability and not of transcallosal inhibition. *Clin. Neurophysiol.* 115, 1305–1312.

De Luca, M., Smith, S., De Stefano, N., Federico, A., and Matthews, P. M. (2005). Blood oxygenation level dependent contrast resting state networks are relevant to functional activity in the neocortical sensorimotor system. *Exp. Brain Res.* 167, 587–594.

Di Martino, A., Scheres, A., Margulies, D. S., Kelly, A. M., Uddin, L. Q., Shehzad, Z., Biswal, B., Walters, J. R., Castellanos, F. X., and Milham, M. P. (2008). Functional connectivity of human striatum: a resting state FMRI study. *Cereb. Cortex* 18, 2735–2747.

Dittmar, M. (2002). Functional and postural lateral preferences in humans: interrelations and life-span age differences. *Human Biol.* 74, 569–585.

Duque, J., Murase, N., Celnik, P., Hummel, F., Harris-Love, M., Mazzocchio, R., Olivier, E., and Cohen, L. G. (2007). Intermanual differences in movement-related interhemispheric inhibition. *J. Cogn. Neurosci.* 19, 204–213.

Duque, J., Hummel, F., Celnik, P., Murase, N., Mazzocchio, R., and Cohen, L. G. (2005). Transcallosal inhibition in chronic subcortical stroke. *Neuroimage* 28, 940–946.

Eccles, J. C. (1989). *Evolution of the Brain: Creation of the Self*. London: Routledge.

Fabri, M., Polonara, G., Quattrini, A., Salvolini, U., Del Pesce, M., and Manzoni, T. (1999). Role of the corpus callosum in the somatosensory activation of the ipsilateral cerebral cortex: an fMRI study of callosotomized patients. *Eur. J. Neurosci.* 11, 3983–3994.

Ferbert, A., Priori, A., Rothwell, J. C., Day, B. L., Colebatch, J. G., and Marsden, C. D. (1992). Interhemispheric inhibition of the human motor cortex. *J. Phys.* 453, 525–546.

Folstein, M. F., Folstein, S. E., and McHugh, P. R. (1975). "Mini-mental state" A practical method for grading the cognitive state of patients for the clinician. *J. Psychiatr. Res.* 12, 189–198.

Fox, M. D., and Raichle, M. E. (2007). Spontaneous fluctuations in brain activity observed with functional magnetic resonance imaging. *Nat. Rev. Neurosci.* 8, 700–711.

Glover, G. H., Li, T. Q., and Ress, D. (2000). Image-based method for retrospective correction of physiological motion effects in fMRI: RETROICOR. *Magn. Reson. Med.* 44, 162–167.

Hagmann, P., Thiran, J. P., Jonasson, L., Vandergheynst, P., Clarke. S., Maeder, P., and Meuli, R. (2003). DTI mapping of human brain connectivity: statistical fibre tracking and virtual dissection. *Neuroimage* 19, 545–554.

Harris, L. J. (1990). "Cultural influences on handedness: historical and contemporary theory and evidence," in *Left-Handedness: Behavioral Implications and Anomalies*, ed. S. Coren (Amsterdam, North-Holland: Elsevier) 195–258.

Hayes, A., and Krippendorff, K. (2007). Answering the call for a standard reliability measure for coding data. *Commun. Methods Meas.* 1, 77–89.

Head, D., Buckner, R. L., Shimony, J. S., Williams, L. E., Akbudak, E., Conturo, T. E., McAvoy, M., Morris, J. C., and Snyder, A. Z. (2004). Differential vulnerability of anterior white matter in nondemented aging with minimal acceleration in dementia of the Alzheimer type: evidence from diffusion tensor imaging. *Cereb. Cortex* 14, 410–423.

Heuninckx, S., Wenderoth, N., Debaere, F., Peeters, R., and Swinnen, S. P. (2005). Neural basis of aging: the penetration of cognition into action control. *J. Neurosci.* 25, 6787–6796.

Heuninckx, S., Wenderoth, N., and Swinnen, S. P. (2008). Systems neuroplasticity in the aging brain: recruiting additional neural resources for successful motor performance in elderly persons. *J. Neurosci.* 28, 91–99.

Hofer, S., and Frahm, J. (2006). Topography of the human corpus callosum revisited-comprehensive fiber tractography using diffusion tensor magnetic resonance imaging. *Neuroimage* 32, 989–994.

Hoppner, J., Kunesch, E., Buchmann, J., Hess, A., Grossmann, A., and Benecke, R. (1999). Demyelination and axonal degeneration in corpus callosum assessed by analysis of transcallosally mediated inhibition in multiple sclerosis. *Clin. Neurophysiol.* 110, 748–756.

Hutchinson, S., Kobayashi, M., Horkan, C. M., Pascual-Leone, A., Alexander, M. P., and Schlaug, G. (2002). Age-related differences in movement representation. *Neuroimage* 17, 1720–1728.

Johnston, J. M., Vaishnavi, S. N., Smyth, M. D., Zhang, D. Y., He, B. J., Zempel, J. M., Shimony, J. S., Snyder, A. Z., and Raichle, M. E. (2008). Loss of resting interhemispheric functional connectivity after complete section of the corpus callosum. *J. Neurosci.* 28, 6453–6458.

Lenzi, D., Conte, A., Mainero, C., Frasca, V., Fubelli, F., Totaro, P., Cararnia, F., Inghilleri, M., Pozzilli, C., and Pantano, P. (2007). Effect of corpus callosum damage on ipsilateral motor activation in patients with multiple sclerosis: a functional and anatomical study. *Hum. Brain Mapp.* 28, 636–644.

Leocani, L., Cohen, L. G., Wassermann, E. M., Ikoma, K., and Hallett, M. (2000). Human corticospinal excitability evaluated with transcranial magnetic stimulation during different reaction time paradigms. *Brain* 123, 1161–1173.

Li, S. C., Lindenberger, U., and Sikstrom, S. (2001). Aging cognition: from neuromodulation to representation. *Trends Cogn. Sci. (Regul. Ed.)* 5, 479–486.

Li, S. C., and Sikstrom, S. (2002). Integrative neurocomputational perspectives on cognitive aging, neuromodulation, and representation. *Neurosci. Biobehav. Rev.* 26, 795–808.

Liepert, J., Classen, J., Cohen, L. G., and Hallett, M. (1998). Task-dependent changes of intracortical inhibition. *Exp. Brain Res.* 118, 421–426.

Logan, J. M., Sanders, A. L., Snyder, A. Z., Morris, J. C., and Buckner, R. L. (2002). Under-recruitment and nonselective recruitment: dissociable neural mechanisms associated with aging. *Neuron* 33, 827–840.

Lowe, M. J., Beall, E. B., Sakaie, K. E., Koenig, K. A., Stone, L., Marrie, R. A., and Phillips, M. D. (2008). Resting state sensorimotor functional connectivity in multiple sclerosis inversely correlates with transcallosal motor pathway transverse diffusivity. *Hum. Brain Mapp.* 29, 818–827.

Lowe, M. J., Mock, B. J., and Sorenson, J. A. (1998). Functional connectivity in single and multislice echoplanar imaging using resting-state fluctuations. *NeuroImage* 7, 119–132.

Madden, D. J., Turkington, T. G., Provenzale, J. M., Denny, L. L., Hawk, T. C., Gottlob, L. R., and Coleman, R. E. (1999). Adult age differences in the functional neuroanatomy of verbal recognition memory. *Hum. Brain Mapp.* 7, 115–135.

Maldjian, J. A., Laurienti, P. J., Kraft, R. A., and Burdette, J. H. (2003). An automated method for neuroanatomic and cytoarchitectonic atlas-based interrogation of fMRI data sets. *Neuroimage* 19, 1233–1239.

Mattay, V. S., Fera, F., Tessitore, A., Hariri, A. R., Das, S., Callicott, J. H., and Weinberger, D. R. (2002). Neurophysiological correlates of age-related changes in human motor function. *Neurology* 58, 630–635.

Mattis, S. (1976). "Mental status examination for organic mental syndrome in the elderly patient," in *Geriatric Psychiatry*, eds L. Bellak and T. B. Karasu (New York: Grune & Stratton), 77–121.

Mazziotta, J. C., Toga, A. W., Evans, A., Fox, P., and Lancaster, J. (1995). A probabilistic atlas of the human brain – theory and rationale for its development. *Neuroimage* 2, 89–101.

Murase, N., Duque, J., Mazzocchio, R., and Cohen, L. G. (2004). Influence of interhemispheric interactions on motor function in chronic stroke. *Ann. Neurol.* 55, 400–409.

Muller-Oehring, E. M., Schulte, T., Raassi, C., Pfefferbaum, A., and Sullivan, E. V. (2007). Local-global interference is modulated by age, sex and anterior corpus callosum size. *Brain Res.* 1142, 189–205.

Netz, J. (1999). Asymmetry in transcallosal inhibition. *Electroencephalogr. Clin. Neurophysiol. Suppl.* 51, 137–144.

Nudo, R. J., Milliken, G. W., Jenkins, W. M., and Merzenich, M. M. (1996). Use-dependent alterations of movement representations in primary motor cortex of adult squirrel monkeys. *J. Neurosci.* 16, 2, 785–807.

Obleser, J., Wise, R. J. S., Dresner, M. A., and Scott, S. K. (2007). Functional integration across brain regions improves speech perception under adverse listening conditions. *J. Neurosci.* 27, 2283–2289.

Oldfield, R. C. (1971). Assessment and analysis of handedness – Edinburgh inventory. *Neuropsychologia* 9, 97–113.

Ota, M., Obata, T., Akine, Y., Ito, H., Ikehira, H., Asada, T., and Suhara, T. (2006). Age-related degeneration of corpus callosum measured with diffusion tensor imaging. *Neuroimage* 31, 1445–1452.

Pantano, P., Mainero, C., and Caramia, F. (2006). Functional brain reorganization in multiple sclerosis: evidence from fMRI studies. *J. Neuroimaging* 16, 104–114.

Paxton, J. L., Barch, D. M., Racine, C. A., and Braver, T. S. (2008). Cognitive control, goal maintenance, and prefrontal function in healthy aging. *Cereb. Cortex* 18, 1010–1028.

Peltier, S. J., LaConte, S. M., Niyazov, D. M., Liu, J. Z., Sahgal, V., Yue, G. H., and Hu, X. P. (2005). Reductions in interhemispheric motor cortex functional connectivity after muscle fatigue. *Brain Res.* 1057, 10–16.

Persson, J., Nyberg, L., Lind, J., Larsson, A., Nilsson, L. G., Ingvar, M., and Buckner, R. L. (2006). Structure-function correlates of cognitive decline in aging. *Cereb. Cortex* 16, 907–915.

Porac, C. (1993). Are age trends in adult hand preference best explained by developmental shifts or generational-differences. *Can. J. Exp. Psychol. Revue Canadienne De Psychologie Experimentale* 47, 697–713.

Putnam, M. C., Wig, G. S., Grafton, S. T., Kelley, W. M., and Gazzaniga, M. S. (2008). Structural organization of the corpus callosum predicts the extent and impact of cortical activity in the nondominant hemisphere. *J. Neurosci.* 28, 2912–2918.

Quigley, M., Cordes, D., Turski, P., Moritz, C., Haughton, V., Seth, R., and Meyerand, M. E. (2003). Role of the corpus callosum in functional connectivity. *Am. J. Neuroradiol.* 24, 208–212.

Reuter-Lorenz, P. A., Jonides, J., Smith, E. E., Hartley, A., Miller, A., Marshuetz, C., and Koeppe, R. A. (2000). Age differences in the frontal lateralization of verbal and spatial working memory revealed by PET. *J. Cogn. Neurosci.* 12, 174–187.

Reuter-Lorenz, P. A., and Lustig, C. (2005). Brain aging: reorganizing discoveries about the aging mind. *Curr. Opin. Neurobiol.* 15, 245–251.

Riecker, A., Groschel, K., Ackermann, H., Steinbrink, C., Witte, O., and Kastrup A. (2006). Functional significance of age-related differences in motor activation patterns. *Neuroimage* 32, 1345–1354.

Rogers, B. P., Morgan, V. L., Newton, A. T., and Gore, J. C. (2007). Assessing functional connectivity in the human brain by fMRI. *Magn. Reson. Imaging* 25, 1347–1357.

Schmierer, K., Irlbacher, K., Grosse, P., Roricht, S., and Meyer, B. U. (2002). Correlates of disability in multiple sclerosis detected by transcranial magnetic stimulation. *Neurology* 59, 1218–1224.

Seidler, R. D., Bernard, J. A., Burutolu, T. B., Fling, B. W., Gordon, M. T., Gwin, J. T., Kwak, Y., and Lipps, D. B. (2010). Motor control and aging: links to age-related brain structural, functional, and biochemical effects. *Neurosci. Biobehav. Rev.* 34, 721–733.

Seidler, R. D., Noll, D. C., and Thiers, G. (2004). Feedforward and feedback processes in motor control. *Neuroimage* 22, 1775–1783.

Smith, E. E., Geva, A., Jonides, J., Miller, A., Reuter-Lorenz, P., and Koeppe, R. A. (2001). The neural basis of task-switching in working memory: effects of performance and aging. *Proc. Natl. Acad. Sci. USA* 98, 2095–2100.

Sohn, Y. H., Jung, H. Y., Kaelin-Lang, A., and Hallett, M. (2003). Excitability of the ipsilateral motor cortex during phasic voluntary hand movement. *Exp. Brain Res.* 148, 176–185.

Stancak, A., Lucking, C. H., and Kristeva-Feige, R. (2000). Lateralization of movement-related potentials and the size of corpus callosum. *Neuroreport* 11, 329–332.

Stancak, A., and C. H. Lucking, et al. (2002). The size of corpus callosum and functional connectivities of cortical regions in finger and shoulder movements. *Brain Res. Cogn. Brain Res.* 13, 61–74.

Stancak, A., Cohen, E., Seidler, R. D., Duong, T. Q., and Kim, S. (2003). The size of corpus callosum and the functional activation of motor cortical areas in bimanual and unimanual movements. *Cereb. Cortex* 13, 475–485.

Stancak, A., and J. Svoboda, et al. (2003b). Desynchronization of cortical rhythms following cutaneous stimulation: effects of stimulus repetition and intensity, and of the size of corpus callosurn. *Clin. Neurophysiol.* 114, 1936–1947.

Stinear, J. W., and Byblow, W. D. (2002). Disinhibition in the human motor cortex is enhanced by synchronous upper limb movements. *J. Physiol.* 543, 307–316.

Sullivan, E. V., Pfefferbaum, A., Adalsteinsson, E., Swan, G. E., and Carmelli, D. (2002). Differential rates of regional brain change in callosal and ventricular size: a 4-year longitudinal MRI study of elderly men. *Cereb. Cortex* 12, 438–445.

Talelli, P., Waddingham, W., Ewas, A., Rothwell, J. C., and Ward, N. S. (2008a). The effect of age on task-related modulation of interhemispheric balance. *Exp. Brain Res.* 186, 59–66.

Talelli, P., Ewas, A., Waddingham, W., Rothwell, J. C., and Ward, N. S. (2008b). Neural correlates of age-related changes in cortical neurophysiology. *Neuroimage* 40, 1772–1781.

Taniwaki, T., Okayama, A., Yoshiura, T., Togao, O., Nakamura, Y., Yamasaki, T., Ogata, K., Shigeto, H., Ohyagi, Y., Kira, J., and Tobimatsu, S. (2007). Age-related alterations of the functional interactions within the basal ganglia and cerebellar motor loops in vivo. *Neuroimage* 36, 1263–1276.

Teasdale, N., Bard, C., Fleury, M., Young, D. E., and Proteau, L. (1993). Determining movement onsets from temporal series. *J. Mot. Behav.* 25, 97–106.

Tisserand, D. J., and Jolles, J. (2003). On the involvement of prefrontal networks in cognitive ageing. *Cortex* 39, 1107–1128.

Vercauteren, K., Pleysier, T., Van Belle, L., Swinnen, S. P., and Wenderoth, N. (2008). Unimanual muscle activation increases interhemispheric inhibition from the active to the resting hemisphere. *Neurosci. Letters* 445, 209–213.

Vernooij, M. W., de Groot, M., van der Lugt, A., Ikram, M. A., Krestin, G. P., Hofman, A., Niessen, W. J., and Breteler, M. M. B. (2008). White matter atrophy and lesion formation explain the loss of structural integrity of white matter in aging. *Neuroimage* 43, 470–477.

Verstynen, T., Diedrichsen, J., Albert, N., Aparicio, P., and Ivry, R. B. (2005). Ipsilateral motor cortex activity during unimanual hand movements relates to task complexity. *J. Neurophysiol.* 93, 1209–1222.

Vincent, J. L., Patel, G. H., Fox, M. D., Snyder, A. Z., Baker, J. T., Van Essen, D. C., Zempel, J. M., Snyder, L. H., Corbetta, M., and Raichle, M. E. (2007). Intrinsic functional architecture in the anaesthetized monkey brain. *Nature* 447, 83–86.

Wahl, M., Lauterbach-Soon, B., Hattingen, E., Jung, P., Singer, O., Volz, S., Klein, J. C., Steinmetz, H., and Ziemann, U. (2007). Human motor corpus callosum: topography, somatotopy, and link between microstructure and function. *J. Neurosci.* 27, 12132–12138.

Ward, N. S., and Frackowiak, R. S. J. (2003). Age-related changes in the neural correlates of motor performance. *Brain* 126, 873–888.

Wierenga, C. E., Benjamin, M., Gopinath, K., Perlstein, W. M., Leonard, C. M., Rothi, L. J. G., Conway, T., Cato, M. A., Briggs, R., and Crosson, B. (2008). Age-related changes in word retrieval: role of bilateral frontal and subcortical networks. *Neurobiol. Aging* 29, 436–451.

Winter, D. A. (1990). *Biomechanics and Motor Control of Human Movements*. New York: John Wiley & Sons.

Witelson, S. F. (1989). Hand and sex differences in the isthmus and genu of the human corpus callosum. *Brain* 112, 799–835.

Wu, T., Zang, Y. F., Wang, L., Long, X. Y., Hallett, M., Chen, Y., Li, K. C., and Chan, P. (2007). Aging influence on functional connectivity of the motor network in the resting state. *Neurosci. Lett.* 422, 164–168.

Xiong, J. H., Parsons, L. M., Gao, J. H., and Fox, P. T. (1999). Interregional connectivity to primary motor cortex revealed using MRI resting state images. *Hum. Brain Mapp.* 8, 151–156.

Yazgan, M. Y., Wexler, B. E., Kinsbourne, M., Peterson, B., and Leckman, J. F. (1995). Functional-significance of individual variations in callosal area. *Neuropsychologia* 33, 769–779.

Yousry, T. A., Schmid, U. D., Alkadhi, H., Schmidt, D., Peraud, A., Buettner, A., and Winkler, P. (1997). Localization of the motor hand area to a knob on the precentral gyrus – a new landmark. *Brain* 120, 141–157.

Conflict of Interest Statement: The authors declare that the research was conducted in the absence of any commercial or financial relationships that could be construed as a potential conflict of interest.

*Received: 14 December 2009; paper pending published: 09 February 2010; accepted: 11 May 2010; published online: 07 June 2010. Citation: Langan J, Peltier SJ, Bo J, Fling BW, Welsh RC and Seidler RD (2010) Functional implications of age differences in motor system connectivity. Front. Syst. Neurosci. **4**:17. doi: 10.3389/fnsys.2010.00017*

frontiers in
SYSTEMS NEUROSCIENCE

ORIGINAL RESEARCH ARTICLE
published: 26 August 2010
doi: 10.3389/fnsys.2010.00032

Age-related differences in functional nodes of the brain cortex – a high model order group ICA study

Harri Littow[1], Ahmed Abou Elseoud[1], Marianne Haapea[1,2], Matti Isohanni[2], Irma Moilanen[3], Katariina Mankinen[4], Juha Nikkinen[1], Jukka Rahko[3], Heikki Rantala[4], Jukka Remes[1], Tuomo Starck[1], Osmo Tervonen[1], Juha Veijola[2], Christian Beckmann[5,6] and Vesa J. Kiviniemi[1]*

[1] *Department of Diagnostic Radiology, Oulu University Hospital, Oulu, Finland*
[2] *Department of Psychiatry, Oulu University Hospital, Oulu, Finland*
[3] *Department of Child Psychiatry, Oulu University Hospital, Oulu, Finland*
[4] *Department of Pediatrics, Oulu University Hospital, Oulu, Finland*
[5] *FMRIB Centre, Oxford University, London, UK*
[6] *Centre for Neuroscience, Imperial College London, London, UK*

Edited by:
Lucina Q. Uddin, Stanford University, USA

Reviewed by:
Habib Benali, Laboratoire d'Imagerie Fonctionnelle, France
Lucina Q. Uddin, Stanford University, USA

****Correspondence:***
Vesa J. Kiviniemi, Department of Diagnostic Radiology, Oulu University Hospital, P.O. Box 50, 90029 OYS, Oulu, Finland.
e-mail: vesa.kiviniemi@oulu.fi

Functional MRI measured with blood oxygen dependent (BOLD) contrast in the absence of intermittent tasks reflects spontaneous activity of so-called resting state networks (RSN) of the brain. Group level independent component analysis (ICA) of BOLD data can separate the human brain cortex into 42 independent RSNs. In this study we evaluated age-related effects from primary motor and sensory, and, higher level control RSNs. One hundred sixty-eight healthy subjects were scanned and divided into three groups: 55 adolescents (ADO, 13.2 ± 2.4 years), 59 young adults (YA, 22.2 ± 0.6 years), and 54 older adults (OA, 42.7 ± 0.5 years), all with normal IQ. High model order group probabilistic ICA components (70) were calculated and dual-regression analysis was used to compare 21 RSN's spatial differences between groups. The power spectra were derived from individual ICA mixing matrix time series of the group analyses for frequency domain analysis. We show that primary sensory and motor networks tend to alter more in younger age groups, whereas associative and higher level cognitive networks consolidate and re-arrange until older adulthood. The change has a common trend: both spatial extent and the low frequency power of the RSN's reduce with increasing age. We interpret these result as a sign of normal pruning via focusing of activity to less distributed local hubs.

Keywords: functional magnetic resonance imaging, blood oxygen dependent, independent component analysis, resting state, age, networks, hub

INTRODUCTION

In the mid 1990s, Biswal and Hyde were the first to notice that functionally connected regions of the brain are more synchronized in their activity than what could be expected from the noise in general. It was seen as there were modulated waves carrying information between different regions (Biswal et al., 1995). Since this discovery functional MRI measured with blood oxygen dependent (BOLD) contrast in the absence of intermittent tasks has become a major area of interest in the understanding of brain activity (Kiviniemi et al., 2000, 2003; Fox et al., 2007; Vincent et al., 2007). Spatially independent resting state networks (RSN) have been shown to be differentiable from noise during normal, awake resting conditions, during sleep, and, during anesthesia (Kiviniemi et al., 2000; Fransson et al., 2009; Gao et al., 2009).

The background activity fluctuations of the brain cannot be modeled a priori as in task activation studies, therefore more data driven approaches are needed. Furthermore some of the noise sources in the BOLD data may be difficult to account for and their separation from the neuronal signal is demanding (Birn et al., 2006; Starck et al., 2010). Independent component analysis (ICA) offers an effective tool for both the separation of functional sources and noise in a data driven manner without strong assumptions. ICA separates mixtures of independent source signals by maximizing the non-Gaussianity of the source signals. Spatial domain ICA (sICA) can separate BOLD signal sources that represent reactions to externally cued task-activations, background activity within functional brain (i.e., resting state) networks (RSN), and various physiological noise and artifact sources (McKeown et al., 1998; Calhoun et al., 2001; Kiviniemi et al., 2003; Beckmann and Smith, 2004; van de Ven et al., 2004; Beckmann et al., 2005) ICA methodology yields results that are consistent with the results of other contemporary methods of detecting large scale temporally coherent networks from the BOLD signal data (Long et al., 2008).

Recently it has been shown that at least some 42 robust RSNs can be separated from group ICA runs when the algorithm is given the task to search for high model order (Kiviniemi et al., 2009; Smith et al., 2009). When the model order of the ICA estimation is increased, the separated BOLD signal sources have been shown to split into several functional nodes (Li et al., 2007; Ma et al., 2007; Malinen et al., 2007; Eichele et al., 2008). Higher ICA model order (≈70) enables the detection of sub-networks and other independent sources not detected in lower model orders without overfitting the data (Ma et al., 2007; Malinen et al., 2007; Abou-Elseoud et al., 2010)

Recently a large data collection of over 1000 subjects was able to show age-related differences in the brain networks (Biswal et al., 2010). There are few studies about the functional connectivity development

from childhood to adulthood and they are predominantly focused on the DMN. In the gestationally preterm and term infants, a primitive resting state networks have been found (Fransson, 2005; Fransson et al., 2007; Gao et al., 2009). The DMN connectivity might develop in a non-linear manner from childhood to adulthood (Gao et al., 2009). DMN regions are sparsely functionally connected in children at early school age compared to adults (Fair et al., 2008). Posterior cingulate cortex (PCC) and medial prefrontal cortex (mPFC) are suggested to be major hubs of the DMN and connections between them have been found to be weaker in children than in young adults (Fair et al., 2008; Supekar et al., 2010). There is little knowledge of the maturing of the non-DMN, for instance primary sensory or higher level cognitive resting state networks. The comparison between young and older adults has not previously been done to our knowledge.

In the present study, we evaluated age-related effects ranging from 25 independent resting state networks primary motor and sensory cortices to higher level control networks in 168 subjects divided into three age cohorts. Both spatial and frequency domain effects of high model order ICA components were analyzed. We show that the activity within the primary cortices and higher level cognitive areas alters in different ages and yet has a common trend. Some of the networks undergo splitting into several sources at later age.

MATERIALS AND METHODS

The ethical committee of Oulu University Hospital has approved the studies for which the subjects have been recruited, and informed consent has been obtained from each adult subject and from the parents of adolescent subjects according to the Helsinki declaration. The following data of Northern Finland Birth Cohorts 1986 (NFBC 1986) and 1966 (NFBC 1966, c.f. www.kelo.oulu.fi/NFBC/ for further information) were used: At risk mental stage (ARMS) of NFBC 1986 focusing on ADHD and schizophrenia and a NFBC 1966 study on schizophrenia. From pediatric psychiatry a Childhood Autism Spectrum-study with 30 healthy control children and a pediatric temporal lobe epilepsia study with 26 healthy control children were used. Both NFBC data and the childhood studies have been imaged with an identical resting state fMRI protocol. The healthy controls of all these studies represent the normal Finnish population and therefore they were chosen for the analysis. Fifty-five adolescent subjects (ADO, mean 13.2 ± 2.4 years, 20 ♀), 59 young adults (YA mean 22.2 ± 0.6 years 35 ♀), and 54 older adults (OA, mean 42.7 ± 0.5, 25 ♀ OA), all with normal IQ, and verifiably free of psychiatric and neurological disease, were included.

Subjects were imaged on a GE 1.5 T HDX scanner equipped with an eight-channel head coil using parallel imaging with an acceleration factor of 2. The scanning was performed during January 2007–June 2009. All subjects received identical instructions: to simply rest without motion and focus on a cross on an fMRI dedicated screen which they saw through the mirror system of the head coil. Hearing was protected using ear plugs, and motion was minimized using soft pads fitted over the ears.

The functional scanning was performed using an EPI GRE sequence. The TR used was 1800 ms and the TE was 40 ms. The whole brain was covered, using 28 oblique axial slices 4-mm thick with a 0.4 mm space between the slices. FOV was 25.6 cm × 25.6 cm with a 64 × 64 matrix, and a flip angle of 90°. The resting state scan consisted of 253 functional volumes. The first three images were excluded due to T1 equilibrium effects. In all three studies, the resting state scanning started the protocols, and lasted 7 min and 36 s. In addition to resting state fMRI, T1-weighted scans were taken with 3D FSPGR BRAVO sequence (FOV 24.0 cm, matrix 256 × 256, slice thickness 1.0 mm, TR 12.1 ms, TE 5.2 ms, and flip angle 20°) in order to obtain anatomical images for co-registration of the fMRI data to standard space coordinates.

PRE-PROCESSING OF IMAGING DATA

The pre-processing was identical to our previous study of 55 subjects group PICA (Kiviniemi et al., 2009). The data collection consists of some 580 subjects and healthy subjects with excess motion (>2 mm translational or 1° of rotation) were discarded in order to reduce motion artifacts. Also FSL and ICA were both used to reduce motion artifacts. In short, the head motion in the fMRI data was corrected with FSL 3.3 mcflirt-software (Jenkinson et al., 2002) with default settings. Brain extraction was carried out for motion corrected BOLD volumes with BET software (Smith, 2002) using threshold parameters $f = 0.5$ and $g = 0$; and for 3D FSPGR volumes, using parameters $f = 0.25$ and $g = 0$. The BOLD volumes were spatially smoothed with a 7 mm FWHM Gaussian kernel and the voxel time series were de-trended using a Gaussian linear low-pass filter with a 125-s cutoff. Co-registration into MNI space was carried out using the non-linear FSL 4.14 FNIRT software. Corresponding fMRI volumes were co-registered with corresponding 3D FSPGR volumes that had been co-registered to a MNI152 brain template with a 2-mm voxel size included in FSL. The functional volumes were transferred into the MNI space but down-sampled to 4-mm isotropic resolution in order to reduce computational complexity.

SPATIAL DOMAIN ANALYSIS

The image analysis and IC identification protocols were identical to our previous study (Kiviniemi et al., 2009). Probabilistic independent component analysis (PICA) (Beckmann and Smith, 2004) was used to analyze the data into 70 independent components. The analysis was carried out in two separate ICA runs, one containing the ADO and YA groups and the other containing the YA and OA groups. This was done in order to avoid the blurring of the age-related differences by averaging of the source ICs in a large dataset. The YA group was used as a common marker in both analyses. Also, a joint three group run was performed and there the components indeed were averaged ICs that did not clearly show the age-related intricacies. It is more sensitive to perform group ICA runs to detect source RSN's for dual regression from age groups closer to each other than from the whole age span.

In this study, the model order was chosen to be 70, in correspondence with the high order sICA modeling of the resting state BOLD data, based on previous experience on the matter (Abou-Elseoud et al., 2010). Two neuroradiologists (H.L and V.K) using the same criteria as before, depicted the thresholded IC maps corresponding to the previously depicted RSNs sources (Kiviniemi et al., 2009). Some 30 artifactual (residual motion, mal-alignment, and other noise sources) were discarded initially. From the passing 42 ± 3 IC sources, 21 RSN sources representing primary sensory and motor and control networks were chosen for more detailed spatial and frequency domain analysis. The selection of the RSN sources was based on previous literature, presence of low frequency fluctuations

and personal experience on ICA source selection (Kiviniemi et al., 2003, 2009; Abou-Elseoud et al., 2010). After PICA, dual regression was performed between ADO vs. YA and YA vs. OA groups according to a procedure described previously (Filippini et al., 2009). Mean group *t*-score maps for each age group were obtained from the individual level analysis of the dual-regression program (FSL 4.0.4). The unthresholded mean group *t*-score maps produced by dual-regression script were presented with $6 < t < 12$ arbitrary thresholding. The effect of age was analyzed between the groups with the dual_regression software script of FSL using threshold free cluster enhancement (TFCE)-correction for multiple comparison at a $p < 0.01$ threshold. In the group-comparison analysis one does not want to rely on a fixed assumed null-hypothesis, e.g., the fact that in dual regression the data is used twice can easily induce a bias towards average non-zero regression. The non-parametric TFCE-test avoids any of these issues so as the threshold adapts to the distribution, whatever it is. Secondly we use unthresholded ICA maps on unthresholded data to then derive a new estimate for which we perform a single test. What's more is that the test itself looks at differential effects, i.e., at the relation with age, which has not entered into any analyses before.

FREQUENCY DOMAIN ANALYSIS

Power spectral analysis of the RSN sources is based on a large group PICA analysis with all the 168 subjects analyzed together (group$_{168}$-PICA). This was done in order to obtain matched individual IC signal source time courses for further power spectral analysis. The time courses were extracted from the group$_{168}$PICA mixing matrix as before (Kiviniemi et al., 2009). An FFT power spectrum analysis was performed on the IC time courses individually. Mean power spectra per each group for each of the analyzed IC sources was analyzed. The difference between frequency power of the analyzed RSN sources between the groups (ADO, YA, OA) was analyzed with Student's *t*-test and the results were Bonferroni corrected for multiple comparisons for each spectrum (threshold $p < 0.0025$).

RESULTS

There is a common trend in the age-related effects on resting state networks. Increasing age reduces the spatial extent of the sources and the network hubs consolidate. This is illustrated in **Figures 1, 2, 4, 5 and 8**, and in **Table 1**, where the key-hubs related to functional networks present marked changes with age (for age-group mean maps, c.f. **Figures S1 and S2** in Supplementary material).

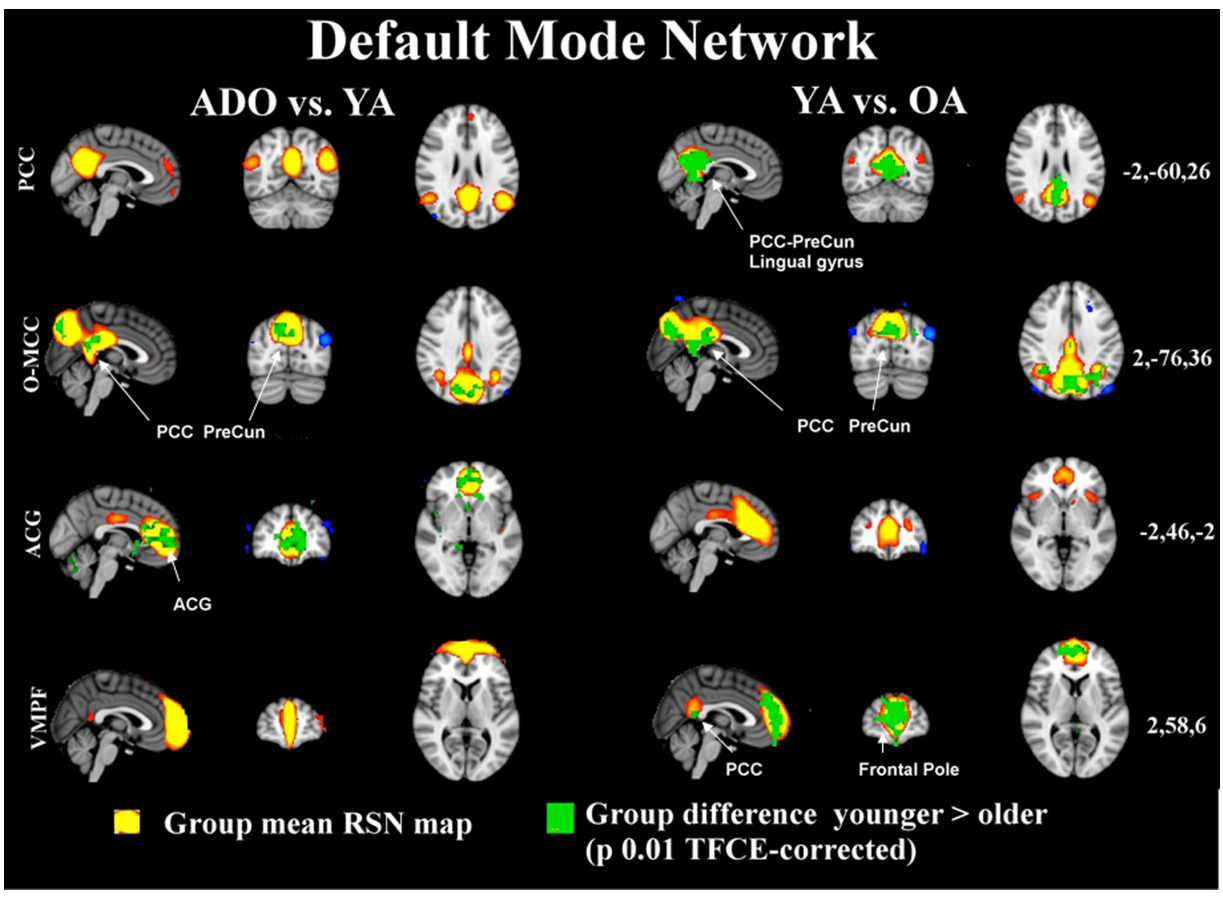

FIGURE 1 | The maps in 3D with MNI (coordinates on the right) background present the group mean RSN sources of ADO and YA and YA and OA of combined groupICA analyses with 5 < z < 10 thresholding in red-yellow colour. The overlaid green colour indicates statistically significant differences between the groups (left ADO vs. YA, on right YA vs. OA) after dual regression. Significant difference areas are named and pointed with white arrows. PCC = posterior cingulate gyrus, PreCun = precuneous, ACG = anterior cingulate gyrus.

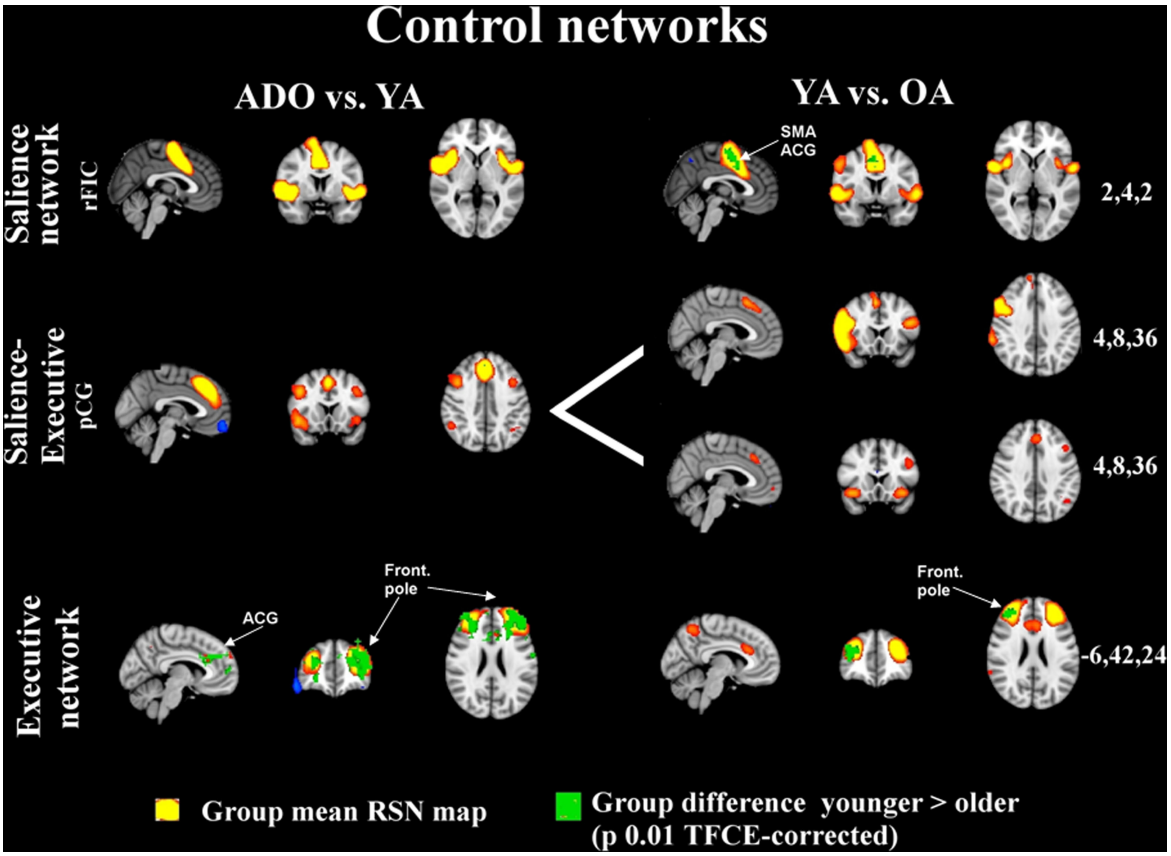

FIGURE 2 | The salience and executive control networks are show with identical thresholding as in Figure 1. It is notable that adolescents and younger adults have a salience-executive signal source which is separated into two components in the older adults. SMA, supplementary motor area; ACG, anterior cingulate gyrus.

DEFAULT MODE AND CONTROL SOURCES

In this study our high model order approach suggested that the posterior cingulate dominant (DMN_{pcc}) default mode network node loses its connection to frontal areas, and, its angular gyri parts become more condensed from adolescence to adulthood. The occipito-medial cingulate ($DMN_{o\text{-}mcc}$) node fuses in the upper posterior cingulate areas in the older adult group and demonstrates bilateral increase in connectivity to neighboring areas in the occipital cortex. Similar fusion can be depicted in the anterior-cingulate node of DMN_{acg} where the activity nodes move toward the front and fuse near the anterior node in the OA group. This component is also shifting backwards and upwards in the most powerful node. Interestingly, the most ventro-medial node at the prefrontal areas (DMN_{vmpf}) strengthens its connection to the posterior cingulated, condenses and shifts somewhat backwards in the most anterior parts. These changes can be best viewed from the **Figure S1** in Supplementary material.

Importantly these age-related changes tend to be more marked in the default mode network sources between the two older cohorts and there are less differences between the younger cohorts. This shows that there are changes occurring between the second and fourth decades in life in these control networks. **Figure 1** shows how the alterations in the DMN occur between the younger and the older cohorts and only frontal areas of the ACG undergo changes in the comparison of the younger cohorts. Similarly, executive and salience related networks also tend to be altering in later years, c.f. **Figure 2**, although the executive network also undergoes marked changes already in early adulthood.

PRIMARY SENSORY AND MOTOR NETWORKS

The primary sensory and motor networks shown in **Figures 4 and 5** tend to be dominated by changes occurring in early rather than late adulthood. The primary motor sources of hands and feet ($M1_{dx,}$ $M1_{sin}$, $M1_{feet}$, respectively) and secondary somatosensory sources (S2) present changes in early adulthood and these networks do not seem to alter much later on. There were no significant alterations in the somatosensory area of the feet ($S_{sen\ Feet}$) and primary auditory network (A1) between any age group, suggesting earlier functional maturation of the sources. The only one of the peri-rolandic sources that alters strongly between all groups is the primary somatosensory source, S1, from the postcentral gyrus.

OCCIPITAL VISUAL SOURCES

The sources at or near the visual cortex seem to be dominated by alterations occurring between all groups. Midline visual ($V1_{dors}$ and $V1_{med}$) sources and dorso-lateral (Vcran) RSN's show differences between all the age groups. $V1_{lat}$ show changes dominantly only in the younger age groups, c.f. **Figure 5**.

Table 1 | RSN differences between the younger and the older ICA group runs.

Name	IC#	Max *t*-score	MaxT score				Center of change			
			MNI-coordinates			# voxels	MNI-coordinates			Anatomical area
			X	Y	Z		X	Y	Z	
ADO AND YA										
Exec	6	6.19	30	38	24	1111	30	42	-8	ACG, F.pole
DMNpcc	11	4.5	–62	–70	28					
S1	13	5.56	–58	2	20	1820	–54	–74	–16	PostCG
A1	14	3.98	–70	–18	16					
DMNo-mcc	16	6.18	2	–86	48	246	6	–46	12	PCC, Precun.
V1lat	19	6.88	–42	–70	4	831	–34	–78	–40	V3–4
PM–PS	20	5.85	42	–86	24	1707	50	–86	0	
SALpCG	23	4.5	–46	34	24	40	–46	30	–16	Brocas area
M1sin	26	6.67	–30	–14	80	348	–38	–26	48	PreCG sin
V1med	29	6.08	–10	–90	36	635	–14	–66	–24	Ling.Gyrus V1
M1dx	31	4.67	50	–26	64	132	54	–26	64	PreCG dx
S2	47	5.27	–2	–34	24	173	–66	–58	32	SMG
M1feet	48	4.9	–50	–18	48	212	–54	–14	4	PreCG
DMNvmpf	49	5.41	14	2	32	1029	2	–18	16	ACG
DMNpcc-V1	51	4.36	26	–58	12					
M1 hands	56	5.36	10	–22	64	143	10	–22	60	PreCG
S1feet	57	3.37	–2	62	12					
V1 dors	58	5.56	2	–94	36	97	10	–86	–8	V1
DMNacg	62	5.26	–10	18	36	872	6	42	–16	ACG
SALrFIC	65	4.13	–50	–70	44					
YA AND OA										
Exec	16	4.57	38	42	24	92	42	42	8	ACG, F. pole
DMNpcc	42	7.4	14	–50	–4	593	10	–54	–8	PCC- Precun.
S2	8	5.58	58	–18	32	333	58	–26	16	
A1	62	4.43	–50	–22	–4					
DMNo-mcc	18	6.07	6	–30	20	554	2	–42	0	PCC, Precun.
V1lat	53	5.58	–30	–78	12	114	38	–62	–32	
PM–PS	47	4.73	22	–62	–32					
SALpCG1	30	5.59	74	–46	–8	1	50	–42	–4	Brocas area
SALpCG2	35	4.47	38	–66	–4					
M1 sin	11	4.12	–38	–42	56					
V1med	66	5.94	14	–62	–20	337	26	–74	–24	Ling.Gyrus V1
M1dx	70	4.52	–62	10	24					
S2	64	4.19	50	–10	72					
M1feet	47	4.73	22	–62	–32					
DMNvmpf	61	4.29	–42	–18	–12					
DMNpcc-vis										
M1 feet	69	3.93	74	–22	32					
S2 feet	20	3.71	–42	–70	–52					
V1dors	29	5.46	–10	–90	20	182	–14	–90	–4	V1
DMN acg	54	4.4	54	–46	20	10	6	6	52	ACG
SALrFIC	40	4.97	58	6	–8	104	2	6	36	SMA, ACG

 # voxels, number of voxels; Exec, executive; DMN, default mode network; pcc, peri-cingulate cortex; mcc, medial cingl.; rFIC, right Fronto-Insular cortex; S1, primary somatosensory cortex; A1, primary auditory center; V1lat; V1med; V1dors; primary lateral/medial/dorsal visual cortex, PM–PS; premotor–postsensory area; SALpCG, Salience + posterior cingulated gyrus; M1, primary motor cortex; S2, secondary somatosensory cortex; vmpf, ventro-medial prefrontal cortex; acg, ACG anterior cingulate gyrus; Supramarg. gyrus, supramarginal gyrus; F. pole, Frontal pole; Ling. G., Lingual Gyrus; Precun., Precuneus; PreCG, Precentral Gyrus; PostCG, Postcentral gyrus; pcc, PCC, posterior cingulated cortex; SMA, supplementary motor area (i.e., juxtapositional lobule).

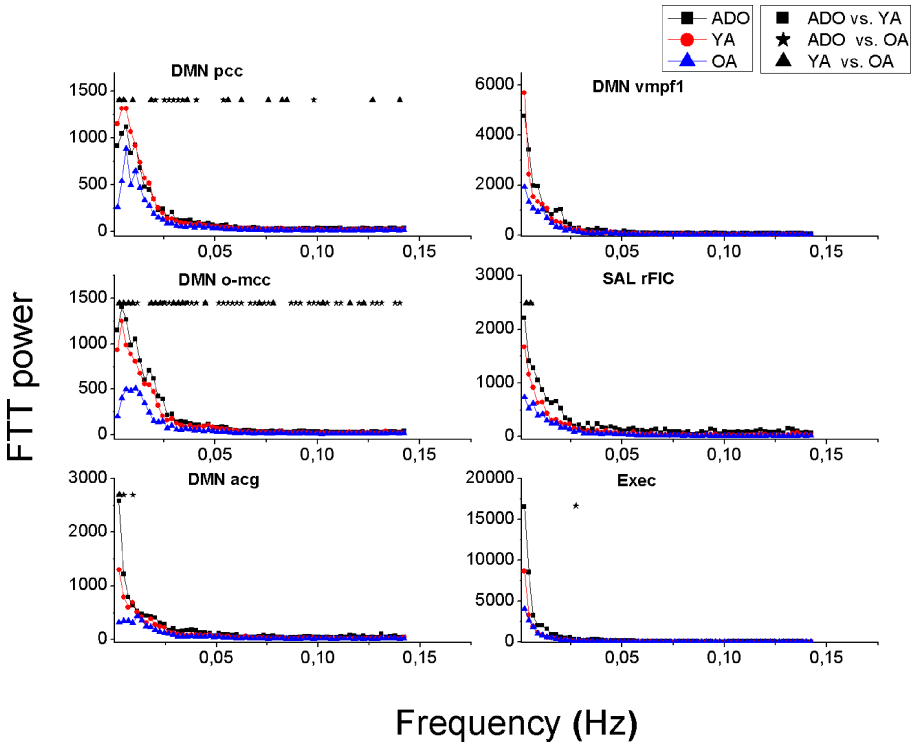

FIGURE 3 | Mean power spectra of the DMN, salience and executive signal sources in each group. Older adults (OA, blue triangles) have less power in all their signal sources compared to younger adults (YA, red circle) and to adolescents (ADO, black box). Significant differences between the groups are marked with symbols ■★▲ above the spectra.

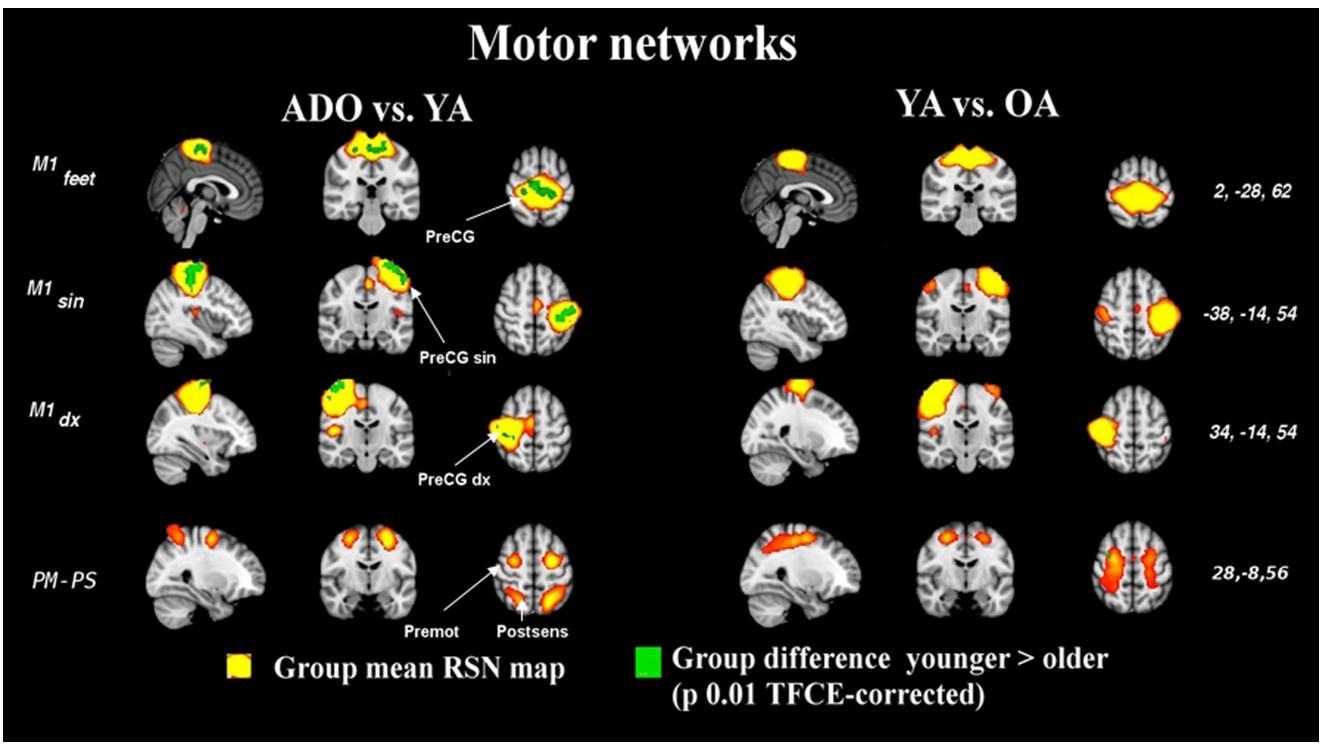

FIGURE 4 | The image parameters and thresholding are the same as in Figure 1. Notably, the changes occur at a young age. The quadrate PM–PS RSN looses integrity in older adulthood altogether, c.f. **Figure S2** in supplementary material. CG, central gyrus, premot, pre-motor cortex, post sens, dorsal to somatosensory cortex.

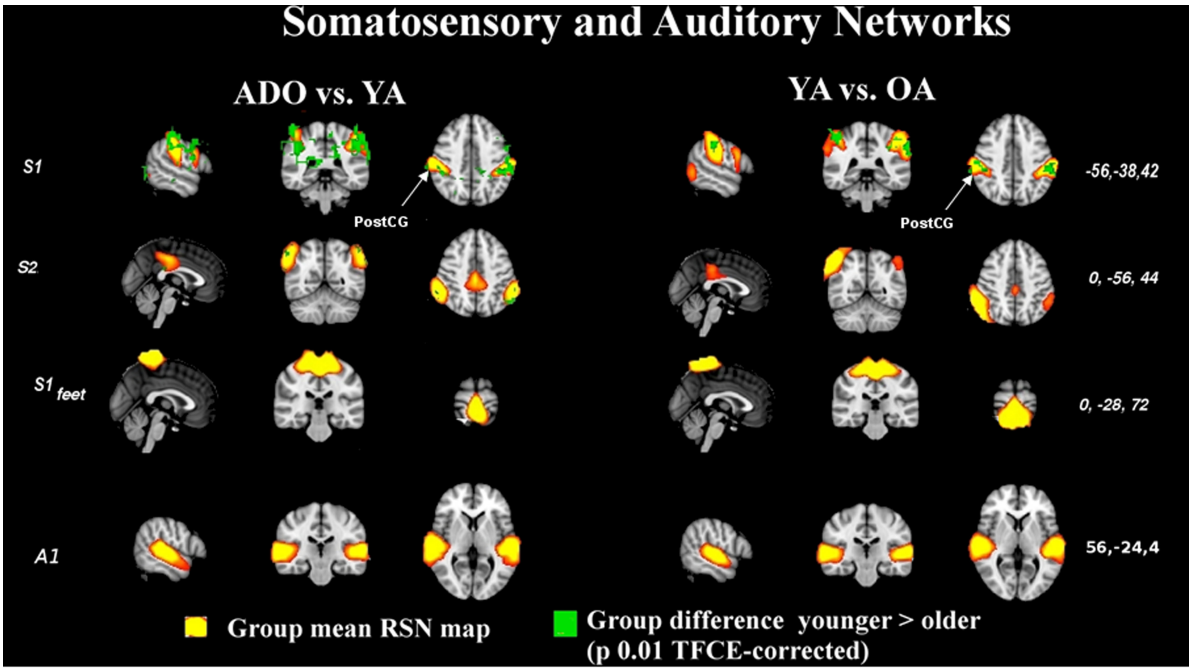

FIGURE 5 | Auditory and somatosensory results shown in the manner as Figure 1. S1 alters through life but the rest of the sources do not alter significantly through time. CG, central gyrus.

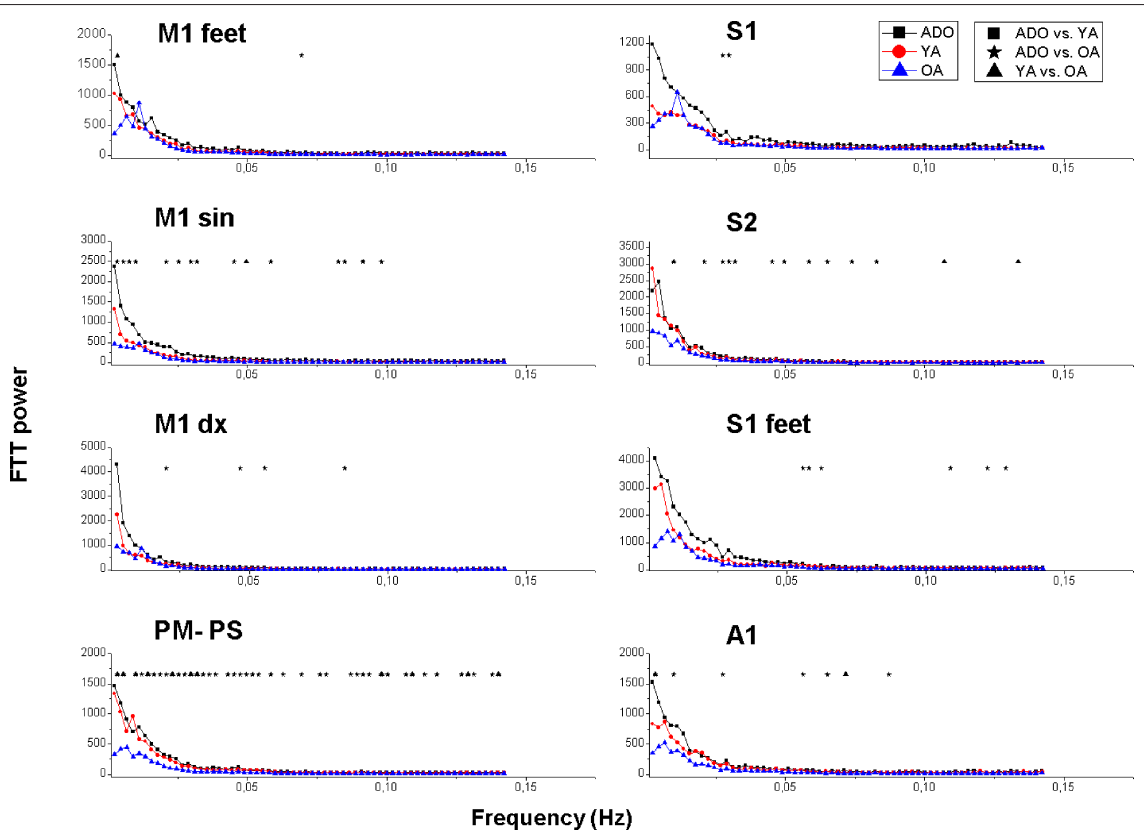

FIGURE 6 | Mean power spectra of in peri-rolandic signal sources presented in a similar way as the power spectral results in Figure 3. The signal sources are visualized in **Figures 4 and 5**.

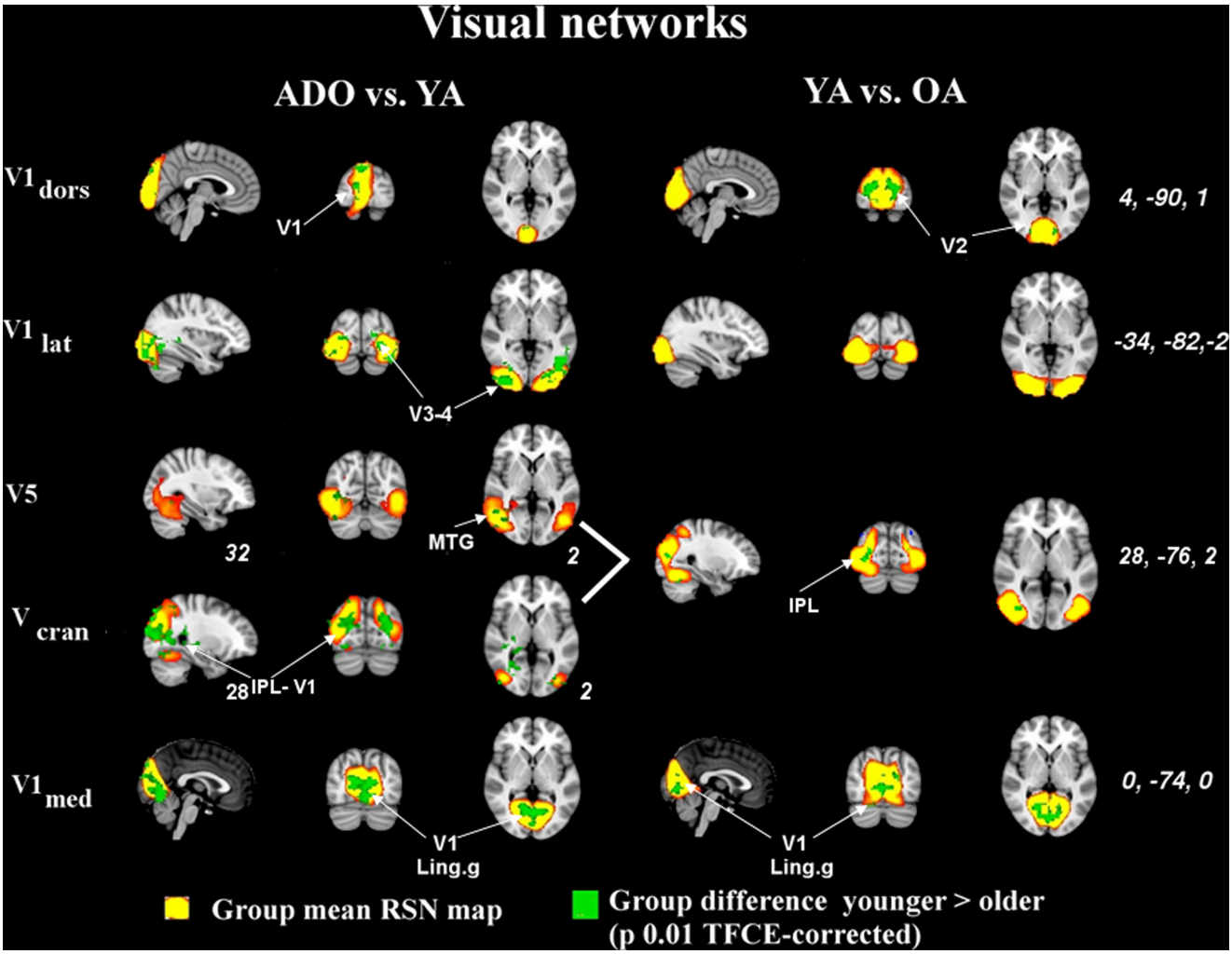

FIGURE 7 | Age-related alterations in visual networks shown with identical thresholding as in the previous images. The younger age groups have more power in their signal sources in general. The difference is smaller between the two older age groups. V5 and Vcran fuse in the older age group into a single large source. IPL, inferior parietal lobule; MTG, medial temporal gyrus; Ling g, lingual gyrus; V1, primary; V2, secondary; V3, tertiary, and, V4, quadrature visual cortex, respectively.

VANISHING AND FUSING RSN's

Not all changes related to age are related to condensing and reduction in the component strength. DMN_{pcc} has two separate sources in the younger cohorts that are not present in the OA cohort; one more caudal is related to visual areas and one more cranial is connected more to posterior cingulate areas, c.f. **Figure S1** in Supplementary material. Both of these DMN sources have bilateral connections but in the visual cortex these are more medial and in the other more lateral and cranial. Similarly V5 and Vcran seen as separate in ADO and YA groups fuse into unified Vcran in OA groups as shown in **Figure 7**.

There is also a mixed salience-executive type frontal network that has a dominant source in the paracingulate areas (S-E pCG in **Figure 1**) in a unified component in the earlier age ranges (ADO and YA). Later in adulthood (OA group) there were no components with similar pCG area dominance. Instead the paracingulate areas were connected more to (at least) two separate sources as is depicted in **Figure 2**. A unique alteration is the almost complete vanishing of a pre-motor and post somatosensory (PM–PS) quadrate network from the adult group. The PM–PS was present in both ADO and YA groups as identical source (**Figure S2** in Supplementary material).

FREQUENCY DOMAIN

The frequency power of the RSN sources reduces invariably as a function of age. This can be seen in **Figures 3, 6 and 8**, where the mean power spectra of the analyzed IC sources representing RSNs are plotted. The ADO group power spectrum is above the YA and OA groups' mean power spectra almost in each source. In DMN sources, Sal_{rFIC} and Exec sources the power spectra of the younger groups (ADO and YA) is markedly similar with decrease in the lowest frequencies in the OA group, see also **Figure 3**.

The power of the primary motor cortex of the right hand (M1 sin) shows the most clear alterations in power with significant changes over a wide range of frequencies. The left hand motor source M1dx has a similar pattern but the differences are less

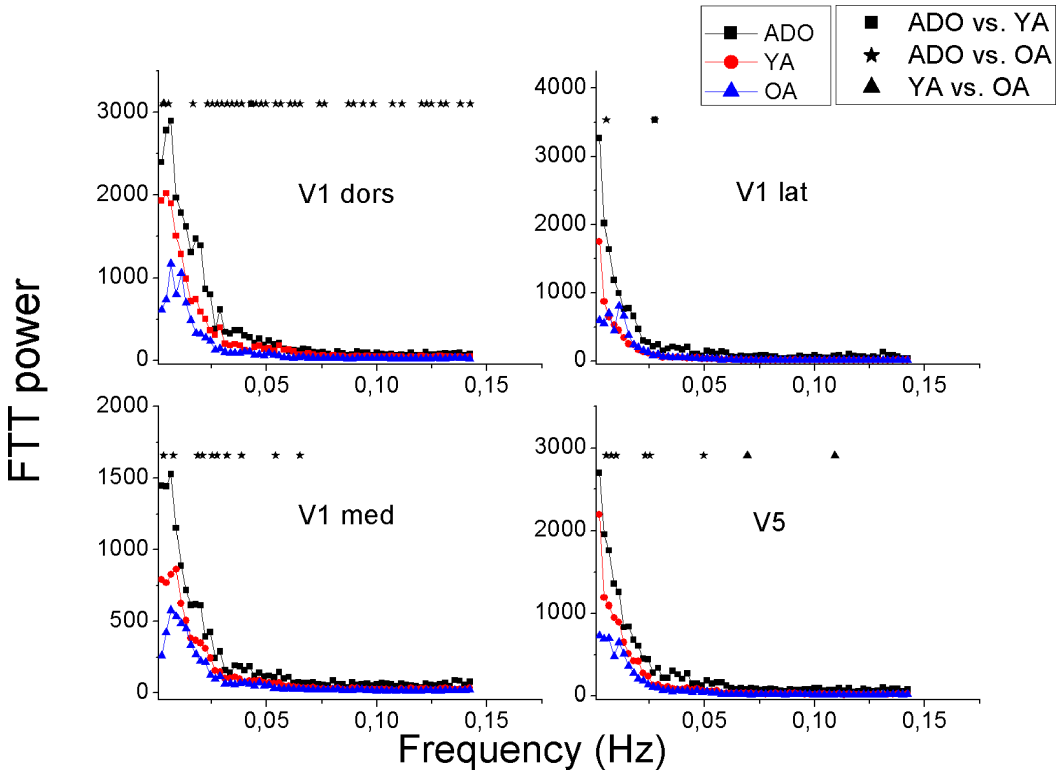

FIGURE 8 | Mean power spectra of Visual signal sources with identical illustration of groups and significant changes as in Figures 3 and 6. The signal sources are shown in **Figure 7**.

marked between the sources. There are some interesting exceptions in the Peri-Rolandic sources that can be depicted. The PM–PS and secondary somatosensory cortex source S2 have in common a nearly identical power spectra in both the ADO and YA groups high above the AO group spectrum with a very significant difference, c.f. **Figure 6**. The feet motor source M1 on the other hand has almost no difference in the power spectra between any of the groups. The primary somatosensory cortex source S1's power in the ADO group seems to be higher but the adult groups have a relatively high power around 0.01 Hz, with a peak in the OA group. In the occipital visual sources a pattern of group differences prevail; the OA group power is below the ADO and the YA group power in each of the selected sources.

Notably the power decrease in the lowest frequencies also alters the shape of the spectrum as a function of the age; increasing age reduces the steepness of the power spectrum. A third aspect related to age is peaks in the power spectra; the OA group has more peaks in the spectrum in 16 spectra, YA in 9 and 7 peaks are in the ADO group. In other words the reducing power seems to reveal peaks from underneath the 1/f curve. In the control networks ($DMN_{pcc,o\text{-}mcc,acg}$) there are spectral peaks with dominating frequencies in occipital sources and the more frontal sources (Sal, Exec, DMN_{vmpf}) there are no clear peaks but rather the spectra have more of a 1/f outline. Also the more medial visual ($V1_{med,dors}$), auditory and somatosensory sources are more dominated by peaked sources with characteristic frequencies. Motor ($M1_{dx,sin}$) and lateral visual ($V1_{lat}$, V5) have more of a 1/f power spectral outline.

DISCUSSION

Our study shows two general changes in resting state sources related to age with dual-regression analysis of high model order group PICA sources. First of all, spatially the sources consolidate and reduce in size with increasing age. This is perfectly in line with the observation by a previous finding by Fair et al. (2007), who detected reduced localized connectivity patterns as a sign of local segregation of brain processes. Developmental changes in whole brain functional connectivity have also been studied by Supekar et al. (2009). Children (ages 7–9 years) and young adults (ages 19–22 years) were scanned and rsfMRI-data was analyzed by using a graphic theoretical approach. Children and young adults' brain had similar organization at the global level, but there were several differences in connectivity. It was shown that the dynamic process of over-connectivity followed by pruning, which rewires connectivity at the neuronal level, also operates at the systems level.

Secondly, the power of the low frequency fluctuations in the independent source time courses also reduces with increasing age. The findings are in line with some of the age-related findings of fractional amplitude of low frequency fluctuations (fALFF) over a group of 1000 subjects, where low model order PICA, seed voxel connectivity and the amplitude of BOLD signal power were analyzed (Biswal et al., 2010). However, the higher model order analysis used in this study offers a more in depth analysis of some of the sources due to increased sensitivity to detect subtle sub-network sources undetected in lower model orders (Kiviniemi et al., 2009;

Abou-Elseoud et al., 2010). In addition, the subject data pool in this study is ethnically more homogenous and the same 1.5 T GE HDx scanner has been used to image the data.

Although these changes are quite general, also some specific alterations exist. Notably the control networks such as default mode, salience, and executive RSN undergo changes still between 22 to 44 years of age, which is not so clearly the case in sensori-motor and visual sources, where the differences between the groups are predominantly between the younger age groups ADO vs. YA. Also previously unpresented shifting can be depicted in DMN-variant ($DMN_{o\text{-}mcc}$ and DMN_{aCG}) sources that are connected to medial parts of the cingulate gyrus. There are interesting vanishing sources that seem to disappear from the OA group (PM–PS, $DMN_{pcc\text{-}caudal}$). A salience-executive network type source Sal_{pCG} is split into several sources, none of which can be identified with a strong source in the paracingulate area. In the ADO and YA groups this map is clearly evident, c.f. **Figure S1** in Supplementary material. Although the cause of the vanishing sources is unclear it may be related to reduced motion of the adult subjects compared to younger ones or simply to age-related degeneration.

Age also alters the spontaneous fluctuation of the networks. The reduced frequency seems to reveal characteristic low frequency power peaks that are not so evident in the younger age groups. Children have higher cerebral blood flow and metabolism than adults (Chugani and Phelps, 1991). The high flow is accompanied by a vasodilatation and relatively large blood vessels. It is a known fact that when blood pressure and volume are decreased the fluctuation amplitude increases and frequency reduces (Jones et al., 1995; Hudetz et al., 1998; Kannurpatti et al., 2008). Since the flow reduces as a function of age then the BOLD fluctuation amplitude should increase and not vice versa as they do. Therefore it is probable that the origin of the decrease of BOLD fluctuations with increasing age is related to non-vascular factors, such as neuronal firing or metabolism (Yang et al., 2007; Kiviniemi, 2008; Wu et al., 2009; Zou et al., 2009).

A study of age-related effects on causality between ICA sources revealed a reduction in causal density by ages between 12 and 30 years (Stevens et al., 2009). Our results agree with these results since the power of the low frequency fluctuation also reduces as a function of age. Previously we have shown that low power on BOLD fluctuations was related to low connectivity, and increasing of the BOLD fluctuation also led to increased connectivity (Kiviniemi et al., 2005). Although speculative, but still causality reductions may also reflect reduction in amplitude of BOLD signal fluctuation (Stevens et al., 2009; Biswal et al., 2010).

We found alterations in DMN from childhood to older adulthood. There are more differences between young adults and older adults than between adolescents and young adults. Adult type DMN has not been detected in sleeping preterm and term infants (Fransson et al., 2007, 2009). It has been observed that neonates have a rather primitive, incomplete default network consisting of six brain regions (Gao et al., 2009). But it has to be mentioned that sleep, in which the young children have to be imaged, there is also reduced DMN activity (Horowitz et al., 2009). It is also found that the default network at 1 year old became more complex and then its changes from 1 to 2 years were more subtle (Gao et al., 2009). In 7–9 year-old children the DMN has been found to be sparsely connected compared to adults (Fair et al., 2008). In our results this connection between occipital and frontal parts of the DMN_{pcc} does still reduce as a function of age. However, the frontal variant DMN_{vmpf} actually does the reverse as a function of age; the connectivity node in the posterior cingulate cortex becomes more strongly connected to the source with increasing age.

Gender differences play a role in the activity of the networks (Biswal et al., 2010). We have not regressed the data with gender or handedness and this remains to be investigated in another study. We chose not to use physiological correction or global mean signal regression methods to improve BOLD data quality. We have done analyses showing that physiological corrections do not improve the ICA results significantly at least at 1.5 T (Starck et al., 2010). Also some of the regression corrections may alter the data and shift the data distributions, which is the domain that ICA uses to define independence.

In conclusion, age-related alterations in human brain cortex networks are mostly reductions in the spatial extent and consolidation of network hubs. Some of the networks alter so much that they cannot be identified in the oldest 44 years age group. Primary sensory and motor networks change more in adolescence while higher control networks like default mode, salience and executive networks show alterations between 20 and 40 s. The spectral power of the low frequency fluctuations of the networks also reduces as a function of age in all networks, with each having a unique change through the years. These changes can be interpreted as a sign of normal pruning via focusing of activity to less distributed local hubs. However, it remains to be seen how much these changes are in fact age-related decline in brain functionality.

ACKNOWLEDGMENTS

Nick Hayward MA, MSc is cordially acknowledged for excellent editorial assistance with language. Academy of Finland grants # 117111,123772,124257,212181,214273; Finnish Medical Foundation, and Finnish Neurological Association grants were used in the production of this research in Department of Radiology. Arvo and Lea Ylppö Foundation, the Alma and K.A. Snellman Foundation, the Foundation for Paediatric Research, the Maire Taponen Foundation, and Special State Grants for Health Research in the Department of Paediatrics and Adolescence, Oulu University Hospital, Finland were supporting pediatric neurology department with grants. Emil Aaltonen Foundation, Sigrid Juselius Foundation, Thule Institute at the University of Oulu, Northern Ostrobothnia Hospital District, Alma, and KA Snellmann Foundation, Oulu, Finland grants were also supporting the study for pediatric psychiatry. Academy of Finland, Sigrid Juselius Foundation, Stanley Medical Research Institute, NARSAD was supporting Department of Psychiatry.

SUPPLEMENTARY MATERIAL

The Supplementary Material for this article can be found online at http://www.frontiersin.org/neuroscience/systemsneuroscience/paper/10.3389/fnsys.2010.00032/

REFERENCES

Abou-Elseoud, A., Starck, T., Remes, J., Nikkinen, J., Tervonen, O., and Kiviniemi, V. (2010). The effect of model order selection in group PICA. *Hum. Brain Mapp.* doi: 10.1002/hbm.20929

Beckmann, C. F., DeLuca, M., Devlin, J. T., and Smith, S. M. (2005). Investigations into resting-state connectivity using independent component analysis. *Philos. Trans. R. Soc. Lond. B. Biol. Sci.* 360, 1001–1013.

Beckmann, C. F., and Smith, S. M. (2004). Probabilistic independent component analysis for functional magnetic resonance imaging.

IEEE Trans. Med. Imaging 23, 137–152.

Biswal, B. B., Mennes, M., Zuo, X. N., Gohel, S., Kelly, C., Smith, S. M., Beckmann, C. F., Adelstein, J. S., Buckner, R. L., Colcombe, S., Dogonowski, A. M., Ernst, M., Fair, D., Hampson, M., Hoptman, M. J., Hyde, J. S., Kiviniemi, V. J., Kötter, R., Li, S. J., Lin, C. P., Lowe, M. J., Mackay, C., Madden, D. J., Madsen, K. H., Margulies, D. S., Mayberg, H. S., McMahon, K., Monk, C. S., Mostofsky, S. H., Nagel, B. J., Pekar, J. J., Peltier, S. J., Petersen, S. E., Riedl, V., Rombouts, S. A., Rypma, B., Schlaggar, B. L., Schmidt, S., Seidler, R. D., Siegle, G. J., Sorg, C., Teng, G. J., Veijola, J., Villringer, A., Walter, M., Wang, L., Weng, X. C., Whitfield-Gabrieli, S., Williamson, P., Windischberger, C., Zang, Y. F., Zhang, H. Y., Castellanos, F. X., and Milham, M. P. (2010). Toward discovery science of human brain function. *Proc. Natl. Acad. Sci. USA* 107, 4734–4739.

Birn, R. M., Diamond, J. B., Smith, M. A., and Bandettini, P. A. (2006). Separating respiratory-variation-related fluctuations from neuronal-activity-related fluctuations in fMRI. *Neuroimage* 31, 1536–1548.

Biswal, B., Yetkin, F. Z., Haughton, V. M., and Hyde, J. S. (1995). Functional connectivity in the motor cortex of resting human brain using echo-planar MRI. *Magn. Reson. Med.* 34, 537–541.

Calhoun, V. D., Adali, T., McGinty, V. B., Pekar, J. J., Watson, T. D., and Pearlson, G. D. (2001). fMRI activation in a visual-perception task: network of areas detected using the general linear model and independent components analysis. *Neuroimage* 14, 1080–1088.

Chugani, H. T., and Phelps, M. E. (1991). Imaging human brain development with positron emission tomography. *J. Nucl. Med.* 32, 23–26.

Eichele, T., Debener, S., Calhoun, V. D., Specht, K., Engel, A. K., Hugdahl, K., von Cramon, D. Y., and Ullsperger, M. (2008). Prediction of human errors by maladaptive changes in event-related brain networks. *Proc. Natl. Acad. Sci. U.S.A.* 105, 6173–6178.

Fair, D. A., Cohen, A. L., Dosenbach, N. U., Church, J. A., Miezin, F. M., Barch, D. M., Raichle, M. E., Petersen, S. E., and Schlaggar, B. L. (2008). The maturing architecture of the brain's default network. *Proc. Natl. Acad. Sci. U.S.A.* 105, 4028–4032.

Fair, D. A., Dosenbach, N. U., Church, J. A., Cohen, A. L., Brahmbhatt, S., Miezin, F. M., Barch, D. M., Raichle, M. E., Petersen, S. E., and Schlaggar, B. L. (2007). Development of distinct control networks through segregation and integration. *Proc. Natl. Acad. Sci. U.S.A.* 104, 13507–13512.

Filippini, N., MacIntosh, B. J., Hough, M. G., Goodwin, G. M., Frisoni, G. B., Smith, S. M., Matthews, P. M., Beckmann, C. F., and Mackay, C. E. (2009). Distinct patterns of brain activity in young carriers of the APOE-epsilon4 allele. *Proc. Natl. Acad. Sci. U.S.A.* 106, 7209–7214.

Fox, M. D., Snyder, A. Z., Vincent, J. L., and Raichle, M. E. (2007). Intrinsic fluctuations within cortical systems account for intertrial variability in human behavior. *Neuron* 56, 171–184.

Fransson, P. (2005). Spontaneous low-frequency BOLD signal fluctuations: an fMRI investigation of the resting-state default mode of brain function hypothesis. *Hum. Brain Mapp.* 26, 15–29.

Fransson, P., Skiold, B., Engstrom, M., Hallberg, B., Mosskin, M., Aden, U., Lagercrantz, H., and Blennow, M. (2009). Spontaneous brain activity in the newborn brain during natural sleep--an fMRI study in infants born at full term. *Pediatr. Res.* 66, 301–305.

Fransson, P., Skiold, B., Horsch, S., Nordell, A., Blennow, M., Lagercrantz, H., and Aden, U. (2007). Resting-state networks in the infant brain. *Proc. Natl. Acad. Sci. U.S.A.* 104, 15531–15536.

Gao, W., Zhu, H., Giovanello, K. S., Smith, J. K., Shen, D., Gilmore, J. H., and Lin, W. (2009). Evidence on the emergence of the brain's default network from 2-week-old to 2-year-old healthy pediatric subjects. *Proc. Natl. Acad. Sci. U.S.A* 106, 6790–6795.

Horovitz, S. G., Braun, A. R., Carr, W. S., Picchioni, D., Balkin, T. J., Fukunaga, M., and Duyn, J. H. (2009). Decoupling of the brain's default mode network during deep sleep. *Proc. Natl. Acad. Sci. U.S.A.* 106, 11376–11381.

Hudetz, A. G., Biswal, B. B., Shen, H., Lauer, K. K., and Kampine, J. P. (1998). Spontaneous fluctuations in cerebral oxygen supply. An introduction. *Adv. Exp. Med. Biol.* 454, 551–559.

Jenkinson, M., Bannister, P., Brady, M., and Smith, S. (2002). Improved optimization for the robust and accurate linear registration and motion correction of brain images. *Neuroimage* 17, 825–841.

Jones, S. C., Williams, J. L., Shea, M., Easley, K. A., and Wie, D. (1995). Cortical cerebral blood flow cycling: anesthesia and arterial blood pressure. *Am. J. Physiol.* 37, H569–H575.

Kannurpatti, S. S., Biswal, B. B., Kim, Y. R., and Rosen, B. R. (2008). Spatio-temporal characteristics of low-frequency BOLD signal fluctuations in isoflurane-anesthetized rat brain. *Neuroimage* 40, 1738–1747.

Kiviniemi, V. (2008). Endogenous brain fluctuations and diagnostic imaging. *Hum. Brain Mapp.* 29, 810–817.

Kiviniemi, V., Jauhiainen, J., Tervonen, O., Paakko, E., Oikarinen, J., Vainionpaa, V., Rantala, H., and Biswal, B. (2000). Slow vasomotor fluctuation in fMRI of anesthetized child brain. *Magn. Reson. Med.* 44, 373–378.

Kiviniemi, V., Kantola, J. H., Jauhiainen, J., Hyvarinen, A., and Tervonen, O. (2003). Independent component analysis of nondeterministic fMRI signal sources. *Neuroimage* 19, 253–260.

Kiviniemi, V., Remes, J., Starck, T., Nikkinen, J., Haapea, M., Silven, O., and Tervonen, O. (2009). Mapping transient hyperventilation induced alterations with estimates of the multi-scale dynamics of BOLD signal. *Front. Neuroinformatics* 3, 18. doi:10.3389/neuro.11.018.2009.

Kiviniemi, V., Ruohonen, J., and Tervonen, O. (2005). Separation of physiological very low frequency fluctuation from aliasing by switched sampling interval fMRI scans. *Magn. Reson. Imaging* 23, 41–46.

Li, Y. O., Adali, T., and Calhoun, V. D. (2007). Estimating the number of independent components for functional magnetic resonance imaging data. *Hum. Brain Mapp.* 28, 1251–1266.

Long, X. Y., Zuo, X. N., Kiviniemi, V., Yang, Y., Zou, Q. H., Zhu, C. Z., Jiang, T. Z., Yang, H., Gong, Q. Y., Wang, L., Li, K. C., Xie, S., and Zang, Y. F. (2008). Default mode network as revealed with multiple methods for resting-state functional MRI analysis. *J. Neurosci. Methods* 171, 349–355.

Ma, L., Wang, B., Chen, X., and Xiong, J. (2007). Detecting functional connectivity in the resting brain: a comparison between ICA and CCA. *Magn. Reson. Imaging* 25, 47–56.

Malinen, S., Hlushchuk, Y., and Hari, R. (2007). Towards natural stimulation in fMRI–issues of data analysis. *Neuroimage* 35, 131–139.

McKeown, M. J., Jung, T. P., Makeig, S., Brown, G., Kindermann, S. S., Lee, T. W., and Sejnowski, T. J. (1998). Spatially independent activity patterns in functional MRI data during the stroop color-naming task. *Proc. Natl. Acad. Sci. U.S.A.* 95, 803–810.

Smith, S. M. (2002). Fast robust automated brain extraction. *Hum. Brain Mapp.* 17, 143–155.

Smith, S. M., Fox, P. T., Miller, K. L., Glahn, D. C., Fox, P. M., Mackay, C. E., Filippini, N., Watkins, K. E., Toro, R., Laird, A. R., and Beckmann, C. F. (2009). Correspondence of the brain's functional architecture during activation and rest. *Proc. Natl. Acad. Sci. U.S.A* 106, 13040–13045.

Starck, T., Remes, J., Nikkinen, J., Tervonen, O., and Kiviniemi, V. (2010). Correction of low-frequency physiological noise from the resting state BOLD fMRI – effect on ICA default mode analysis at 1.5 T. *J. Neurosci. Methods* 186, 179–185.

Stevens, M. C., Pearlson, G. D., and Calhoun, V. D. (2009). Changes in the interaction of resting-state neural networks from adolescence to adulthood. *Hum. Brain Mapp.* 30, 2356–2366.

Supekar, K., Musen, M., and Menon, V. (2009). Development of large-scale functional brain networks in children. *PLoS Biol.* 7, e1000157. doi:10.1371/journal.pbio.1000157.

Supekar, K., Uddin, L. Q., Prater, K., Amin, H., Greicius, M. D., and Menon, V. (2010). Development of functional and structural connectivity within the default mode network in young children 1. *Neuroimage* 52, 290–301.

van de Ven, V. G., Formisano, E., Prvulovic, D., Roeder, C. H., and Linden, D. E. (2004). Functional connectivity as revealed by spatial independent component analysis of fMRI measurements during rest. *Hum. Brain Mapp.* 22, 165–178.

Vincent, J. L., Patel, G. H., Fox, M. D., Snyder, A. Z., Baker, J. T., Van, E., Zempel, J. M., Snyder, L. H., Corbetta, M., and Raichle, M. E. (2007). Intrinsic functional architecture in the anaesthetized monkey brain. *Nature* 447, 83–86.

Wu, C. W., Gu, H., Lu, H., Stein, E. A., Chen, J. H., and Yang, Y. (2009). Mapping functional connectivity based on synchronized CMRO2 fluctuations during the resting state. *Neuroimage* 45, 694–701.

Yang, H., Long, X. Y., Yang, Y., Yan, H., Zhu, C. Z., Zhou, X. P., Zang, Y. F., and Gong, Q. Y. (2007). Amplitude of low frequency fluctuation within visual areas revealed by resting-state functional MRI. *Neuroimage* 36, 144–152.

Zou, Q., Wu, C. W., Stein, E. A., Zang, Y., and Yang, Y. (2009). Static and dynamic characteristics of cerebral blood flow during the resting state. *Neuroimage* 48, 515–524.

Conflict of Interest Statement: The authors declare that the research was conducted in the absence of any commercial or financial relationships that could be construed as a potential conflict of interest.

*Received: 05 February 2010; paper pending published: 16 April 2010; accepted: 18 June 2010; published online: 26 August 2010. Citation: Littow H, Abou Elseoud A, Haapea M, Isohanni M, Moilanen I ,Mankinen K, Nikkinen J, Rahko J, Rantala H, Remes J, Starck T, Tervonen O, Veijola J, Beckmann C and Kiviniemi VJ (2010) Age-related differences in functional nodes of the brain cortex - a high model order group ICA study. Front. Syst. Neurosci. **4**:32. doi: 10.3389/fnsys.2010.00032*

frontiers in
SYSTEMS NEUROSCIENCE

ORIGINAL RESEARCH ARTICLE
published: 10 August 2010
doi: 10.3389/fnsys.2010.00031

Distinct superficial and deep laminar domains of activity in the visual cortex during rest and stimulation

Alexander Maier[1]*, Geoffrey K. Adams[1†], Christopher Aura[1†] and David A. Leopold[1,2]

[1] *Unit on Cognitive Neurophysiology and Imaging, Laboratory of Neuropsychology, National Institute of Mental Health, National Institutes of Health, Bethesda, MD, USA*
[2] *Neurophysiology Imaging Facility, National Institute of Mental Health, National Institute of Neurological Disorder and Stroke, National Eye Institute, National Institutes of Health, Bethesda, MD, USA*

Edited by:
Lucina Q. Uddin, Stanford University, USA

Reviewed by:
Thomas Radman, Nathan Kline Institute for Psychiatric Research, USA
Mark Roberts, Donders Institute for Brain, Cognition and Behaviour, Netherlands
Alex Thiele, Newcastle University, UK

****Correspondence:***
Alexander Maier, Unit on Cognitive Neurophysiology and Imaging, Laboratory of Neuropsychology, National Institute of Mental Health, MSC-4400, Bethesda, MD 20892, USA.
e-mail: maiera@mail.nih.gov

†Present Address:
Geoffrey K. Adams, Department of Neurobiology, Duke University, NC, USA;
Christopher Aura, Comprehensive Neuroscience Center, University of Alabama, Birmingham, AL, USA

Spatial patterns of spontaneous neural activity at rest have previously been associated with specific networks in the brain, including those pertaining to the functional architecture of the primary visual cortex (V1). However, despite the prominent anatomical differences between cortical layers, little is known about the laminar pattern of spontaneous activity in V1. We address this topic by investigating the amplitude and coherence of ongoing local field potential (LFP) signals measured from different layers in V1 of macaque monkeys during rest and upon presentation of a visual stimulus. We used a linear microelectrode array to measure LFP signals at multiple, evenly spaced positions throughout the cortical thickness. Analyzing both the mean LFP amplitudes and between-contact LFP coherences, we identified two distinct zones of activity, roughly corresponding to superficial and deep layers, divided by a sharp transition near the bottom of layer 4. The LFP signals within each laminar zone were highly coherent, whereas those between zones were not. This functional compartmentalization was found not only during rest, but also when the receptive field was stimulated during a visual task. These results demonstrate the existence of distinct superficial and deep functional domains of coherent LFP activity in V1 that may reflect the intrinsic interplay of V1 microcircuitry with cortical and subcortical targets, respectively.

Keywords: resting state, V1, laminae, gamma, LFP, coherence, layers, visual perception

INTRODUCTION

There is abundant activity in the brain in the absence of explicit sensory input or behavioral output, a phenomenon that is commonly observed in both electrophysiological and brain imaging experiments. In fact, most of the brain's enormous energy expenditure appears to arise from spontaneously driven, intrinsic processes, rather than from the interaction with the sensory environment. Sensory stimulation increases local energy consumption above this background of high metabolic activity by only a few percent (Clarke and Sokoloff, 1999; Shulman et al., 2004; Raichle and Mintun, 2006). Yet despite its prominence, the neural processes associated with this spontaneous ongoing activity (SOA) have not been examined in detail until recently, and their significance for normal brain function is poorly understood. Moment-by-moment fluctuations in neural activity that cannot be ascribed to a stimulus or task event are typically treated as random "noise," and are thus averaged out over multiple experimental trials.

Analyzing spontaneous neural activity poses certain experimental challenges, as there are no clearly defined task events to serve as points about which to average. A common approach has therefore been to investigate the temporal covariation between pairs of signals simultaneously measured at different positions in the brain. Approximately 15 years ago, this approach was applied in two different branches of experimental neuroscience – functional magnetic resonance imaging (fMRI) in humans, and electrophysiology in anesthetized cats – with results in each case demonstrating that SOA exhibits reproducible spatiotemporal patterns than can be linked to underlying neural circuits. Using fMRI, Biswal et al. (1995) demonstrated that spontaneous activity within a functional sensorimotor network showed strong covariation even when that network was completely at rest, a phenomenon they dubbed "functional connectivity" based largely on previous electrophysiological work (Gerstein and Perkel, 1969; Gochin et al., 1991; Friston, 1994). In the same year, Arieli et al. (1995) used electrophysiological and optical techniques to show that patterns of intrinsic electrical activity in the visual cortex of anesthetized cats is coordinated at spatial scales up to several millimeters.

Over the next decade, fMRI studies in humans and electrophysiological studies in animals elaborated the degree of organization of SOA signals. Functional connectivity computed from fMRI collected during rest revealed multiple distinct "networks" of covarying (i.e., functionally connected) areas (for a review, see Fox and Raichle, 2007). Early studies focused on cortical networks (Lowe et al., 1998; Greicius et al., 2003; Fox et al., 2005), with more recent ones also demonstrating subcortical networks (Di Martino et al., 2008; Zhang et al., 2008; O'Reilly et al., 2010). Relatively few imaging studies have been conducted in animal models to date, but the basic pattern of resting state networks appears similar in monkeys

and humans (Vincent et al., 2007; Moeller et al., 2009). While there remain questions as to the neural basis and functional significance of these covarying networks, they have been consistently observed under a variety of conditions, drawing considerable attention to the neural underpinnings of SOA (He et al., 2008; Nir et al., 2008; Shmuel and Leopold, 2008; Hayden et al., 2009; Schölvinck et al., 2010). In parallel with fMRI studies, some electrophysiological studies applied the covariation approach to characterize spontaneous signals in animals. For example, Arieli and colleagues extended their original work to show that the spatial map of covariation between the firing rate of neurons and the membrane potentials measured optically over several millimeters closely resembled the functional architecture of orientation columns measured in separate experiments from the same patch of cortex (Tsodyks et al., 1999; Kenet et al., 2003). These findings demonstrated that SOA in V1 is functionally organized across the cortical surface, possibly due to the pattern of horizontal connections known to exist between orientation columns.

One of the most prominent anatomical features of the cerebral cortex is its laminar organization, with individual cortical layers differing substantially in cell types and projection patterns. This dimension is perpendicular to the cortical surface, and therefore currently inaccessible with optical imaging techniques. As a consequence, spatial patterns of SOA across layers are still largely unexplored. One early study, coincidentally published in the same year as the seminal fMRI and optical imaging studies mentioned above, examined differences in spontaneous neural firing rate in area V1 of the awake monkey as a function of layer (Snodderly and Gur, 1995). Mean firing rates differed substantially across the cortical thickness, with cells in layers that receive thalamic input having higher intrinsic firing rates compared to those in other layers. In that study, single electrodes were used to measure activity from one position at a time, so the temporal covariation between layers could not be evaluated.

Using linear multicontact electrode arrays, it has become possible to simultaneously record neural activity at equally spaced intervals across all cortical layers, from the *pia mater* to the white matter. This approach is often used to study the laminar profile of local field potential (LFP) responses in V1 to visual stimulation (Mitzdorf, 1985; Schroeder et al., 1991), whose depth and timing can then be related to the underlying anatomy. However, to date few if any studies have examined how the SOA of field potentials covaries between different layers. Here we investigate the laminar structure of spontaneous neural signals in the primary visual cortex of macaque monkeys by evaluating their temporal correlation as a function of laminar position. Specifically, we ask three fundamental questions. First, how does the amplitude of the LFP signal vary spatially as a function of cortical depth? Second, between which layers do LFP signals display high degrees of temporal coherence? And third, to what extent are the specific patterns of SOA influenced by the presentation of a visual stimulus to a neuron's receptive field?

We report that spontaneous LFP activity in V1 varies significantly as a function of cortical layer, with prominent differences between a superficial compartment (layers 1–4) and a deep compartment (layers 5 and 6). The magnitude of SOA fluctuations in the gamma-range (30–100 Hz) was roughly twice as large in the superficial compartment compared to a deep one. Moreover, the temporal coherence of signals within each zone was substantially stronger than that between zones, with an abrupt discontinuity near the bottom of layer 4. Finally, these laminar patterns were observed during both quiet rest and active stimulation during a visual task. We speculate that this functional compartmentalization of SOA into superficial and deep laminar zones reflects the interplay of V1 with cortical and subcortical targets, respectively.

MATERIALS AND METHODS

SUBJECTS

Two healthy adult male monkeys (*Macaca mulatta*), 98X009 and CB35, were used in the study. All procedures followed US National Institutes of Health guidelines, were approved by the Animal Care and Use Committee of the US National Institute of Mental Health and were conducted with great care for the comfort and well being of the animals.

SURGERY

Monkeys were implanted under sterile conditions and isoflurane anesthesia (1.5–2%) with custom-designed and fabricated fiberglass headposts, fixed to the skull using transcranial ceramic screws (Thomas Recording, Giessen, Germany), Copalite Varnish (Colley and Colley, Ltd., Houston, TX, USA), and self-curing denture acrylic (Lang Inc., Wheeling, IL, USA). In a subsequent surgery, a recording chamber was implanted over V1 using frameless stereotaxy guided by high-resolution anatomical magnetic resonance images (Brainsight, Rogue Research), and a craniotomy was performed inside the chamber. Animals received antibiotics and analgesics post-operatively.

EXPERIMENTAL PARADIGM

There were two conditions evaluated in the main portion of the study: rest and visual stimulation, as well as a third condition (flashing screen) used to generate the current source density (CSD) profile of each session (**Figure S1** in Supplementary Material). Ambient light in the testing room was minimized, though not completely absent. In all cases, the three conditions were collected during the same session, with the electrode in the same place. During the *rest* condition, activity was recorded over a 20-min period during which animals sat alone in a darkened quiet room, with the monitors turned off. The animals were free to move their eyes about, and frequently closed their eyes for brief periods. The *visual stimulation* condition was intended mainly as a behavioral contrast to the resting condition. The monkey was required to maintain its gaze upon a very small dot (0.1 dva) appearing in the middle of a dark screen for periods lasting 5.3 s, during which time visual stimuli were presented away from the fixation spot. The stimuli consisted of a static disk in the receptive field region followed by a surrounding field of moving random dots, with the precise stimulus sequence described elsewhere (Maier et al., 2008). Note that during visual stimulation the monkeys were required to fixate within a window of up to 2 dva radius and receiving a juice reward upon completion of each trial. If a monkey broke fixation, the trial was aborted and re-initiated after a short delay of 100–800 ms. The animal's eye movements were monitored and recorded using an infrared light sensitive camera and commercially

available eye tracking software (Eye Link II, RS Research, Osgoode, Canada). Finally, each session contained a 5–10 min testing period in which the monkey was repeatedly stimulated with a full screen, flashing stimulus. This stimulation was used *post hoc* to compute a conventional pattern of CSD responses to visual stimulation (see below). Once each second the screen was turned from black (~0.2 cd/m^2) to white (~130 cd/m^2) for 100 ms as the monkey fixated near its center.

All visual stimuli were generated using OpenGL-based custom written software (ESS/STIM, courtesy Dr. D. Sheinberg) running on industrial PCs (Kontron, Poway, CA, USA) with NVIDIA Quadro FX 3000 graphics boards. Stimuli were presented on either a single 18″ TFT monitor placed in front of the animals (NEC MultiSync LCD 1860NX with a 1024 × 768 resolution) or two 27″ TFT monitors (X2Gen MV2701, 1024 × 768 resolution) with a diagonal of 32″ (X2Gen MV2701, 1024 × 768 resolution) mounted on opposite walls of the test box at a viewing distance of 80 cm and a custom made mirror stereoscope mounted in front of the head restrained animal.

NEUROPHYSIOLOGICAL RECORDINGS

Laminar LFP was collected during 13 recording sessions (6 in monkey 98X009). During each session, data were recorded under three different conditions (1) viewing a flashing visual screen, used to compute the CSD used to identify layer 4, (2) executing a simple fixation task while being presented visual stimuli, and (3) sitting quietly in a dimly lit room with no explicit task or stimulus (see below). Recordings were performed inside an RF-shielded booth. LFP (defined as extracellular voltage fluctuations in the frequency range between 1 and 100 Hz) were recorded from primary visual cortex in all animals. All recording sites were from dorsal V1, several millimeters posterior to the lunate sulcus, in the parafoveal region of the visual field (see **Figure S2A** in Supplementary Material).

Recordings were performed using a 24-contact microelectrode with an inter-contact spacing of 100 μm (Neurotrack Ltd, Békéscsaba, Hungary), with contact impedances varying between 0.3 and 0.5 MΩ. The multicontact electrode was manually lowered into cortex using a custom designed microdrive and signals were amplified and recorded using the Plexon MAP system (Plexon Inc., Dallas, TX, USA), with the shank of the electrode serving as both the grounding point and the electrical reference. Coarse positioning of the electrode was achieved by monitoring the visually evoked potential during the flashing screen paradigm. Specifically, the electrode position was adjusted according to the position of the polarity reversal of response to the flash (see **Figure S3** in Supplementary Material for intersession accuracy of the electrode placement). Additional alignment, based on the CSD computed offline, was done prior to averaging across sessions (see below).

DATA ANALYSIS

All neurophysiological data were processed and analyzed using custom written code in MATLAB. The LFP was filtered between 1 and 200 Hz, amplified by a factor of 1000 and digitized at 1 kHz for data collection, and subsequently down-sampled to 250 Hz after low-pass filtering with an eighth-order, bi-directional, zero-phase Chebyshev type-1 filter with a cutoff frequency of 100 Hz. This provided a time-varying voltage signal for each channel that served as the basis of further analysis. Frequency analysis was performed using a fast Fourier transform algorithm. Magnitude spectra were computed using a modified Welch's method, with multitaper analysis revealing similar results. The signal was split into Hamming windows of 512 ms length (and 50% overlap). The magnitude of each windowed segment (doubled in signal content to account for negative frequencies as well as normalized using a window-dependent scale factor) was computed, and the results were time-averaged. Power spectral density (PSD) was computed in a similar manner using 256 ms windows, with an additional step of squaring the signal magnitude to obtain the power spectrum.

Coherence estimates were computed as magnitude-squared coherence $C_{xy}(f)$ using Welch's averaged, modified periodogram method and the following formula:

$$C_{xy}(f) = \frac{|P_{xy}(f)|^2}{P_{xx}(f)P_{yy}(f)}$$

where $P_{xx}(f)$ and $P_{yy}(f)$ are the power spectral densities of each individual signal $x(t)$ and $y(t)$, and $P_{xy}(f)$ is their cross PSD. The resulting functions denote the degree of signal correspondence, or coupling, as a function of frequency, with 1 indicating perfect correspondence. All coherence measures were performed by averaging the results computed for overlapping 256 ms epochs and averaged consecutively (Welch's method).

Band-limited power (BLP) was computed by band-pass filtering the signal using a second-order, bi-directional, zero-phase Chebyshev type-1 band-pass filter (frequency ranges are indicated in the text). Power was computed by full-wave rectifying the band-limited signals. This results in a measure of time-varying amplitude, or signal power (in actuality, the square root of the power), in each frequency band and is roughly equivalent to averaging several adjacent rows of a spectrogram (Leopold et al., 2003).

For approximating the layers corresponding to each session prior to alignment and averaging, we relied on data from the flashing screen condition. For each session, data from at least 100 stimulus presentations was averaged for each electrode contact. We applied CSD analysis to this data *post hoc* using a standard algorithm (based on the second spatial derivative estimate of the laminar LFP time series), as well as the spline-based algorithms of the iCSD toolbox for MATLAB (Pettersen et al., 2006). This analysis revealed a robust short-latency current sink in the middle layers for each session (**Figure 3A**). Previous studies have shown that this sink in V1 corresponds most closely to layer 4Cα (Mitzdorf and Singer, 1979; Schroeder et al., 1991). We treated the center of this sink as a point of alignment (the "zero point") for each session, and considered the zone ±200 μm superficial and deep to this reference to be the approximate extent of layer 4, though the results do not critically depend on this approximation. Note that due to this procedure fewer sessions contribute to the shallowest and deepest "adjusted relative depths," although we limited the overall extent of our analysis to ±1000 μm from zero, thus restricting the analysis to depths where the majority of sessions contributed.

RESULTS

The laminar properties of the LFP were evaluated during 13 sessions in two monkeys while they were either at rest in a dark room or while they were actively performing a visual task (see Materials

and Methods). At the beginning of each session a linear multicontact electrode array (**Figure 1**) was inserted perpendicular to the cortical surface of V1 and advanced 2 mm with the monkey at rest. The LFP signal was recorded in parallel from 24 electrode contacts at equally spaced intervals (100 μm) spanning from the *pia mater* to the white matter. The pattern of CSD responses to a flashing stimulus (see Materials and Methods) collected at the beginning of each session was used *post hoc* to establish the spatial positions of individual electrode contacts relative to specific cortical laminae (see **Figures S1A and S2** in Supplementary Material). To verify the stability of the electrode positioning, we also sometimes collected the CSD profile a second time, at the end of the session (see **Figure S5C** in Supplementary Material). This method of anatomical registration is based on previous work in the primary visual cortex of monkeys employing a combination of CSD analysis, microlesions, and *post mortem* histology, which demonstrated that the initial current sink originates in layer 4C, possibly with its peak in layer 4Cα (Mitzdorf and Singer, 1979; Schroeder et al., 1991). We thus took the initial sink as the primary point of alignment, and used this alignment as the basis for averaging data over many sessions. Specifically, we aligned each day's data by centering the LFP traces of the 24 electrode contacts around the initial current sink (see **Figure S2** in Supplementary Material). This created a new reference frame with its zero point located in the middle of layer 4. Then starting from the zero point we coarsely divided the cortex into supragranular (SG, layers 1–3), granular (G, layer 4), and infragranular (IG, layers 5 and 6) zones. The boundaries of these zones, defined as ±250 μm (corresponding to an inclusion criterion of two channels above and below the one upon which we centered the data) are intended only as an approximate reference for the upper and lower bounds of layer 4 (although it did match the extent of the initial sink notably well; see **Figure 2A**).

PREDOMINANCE OF GAMMA ACTIVITY IN UPPER LAYERS

Visual inspection of the raw LFP traces during each session (e.g., **Figure 1**) revealed that certain temporal features in the SOA were shared by only a subset of channels. Notably, there was a stripe of low amplitude, high-frequency activity superimposed on the signals in the more superficial channels. This can be seen clearly in **Figure 2B**, which shows the spectral analysis of a single session as a function of cortical depth. For reference, **Figure 2A** shows the CSD profile obtained from the flashing screen condition used for laminar alignment during the same session. In this example, there is an elevation of high-frequency LFP activity (roughly 30–100 Hz) in the G and deep SG layers, as established from the CSD profile.

This general pattern was observed across all sessions and V1 sites in two monkeys (see **Figure S3** in Supplementary Material for individual sessions). We quantified these spectral differences by calculating the PSD of the LFP for each of the three main laminar compartments. **Figure 3A** plots the PSD averaged across 20 min with the monkeys at rest, on a session-by-session basis (see Materials and Methods). Each line represents the power spectrum of one session, color-coded for signal origin (red = SG; black = G; green = IG). For frequencies above ~30 Hz, the infragranular LFP showed considerably lower power than the supragranular LFP (note the log scale). This pattern proved highly consistent across recording sessions in both animals.

Based on the alignment of electrode contacts described above (see **Figure S4** in Supplementary Material), data from individual sessions could thus be brought into correspondence, estimated to be within 200 μm (see **Figure S5** in Supplementary Material). This allowed us to compute the averaged laminar magnitude spectrum (**Figure 3B**) over all sessions. **Figure 3C** shows the resulting laminar profile of ongoing LFP power in the gamma (30–100 Hz) and sub-gamma (5–20 Hz) frequency ranges. In line with the pattern revealed by the

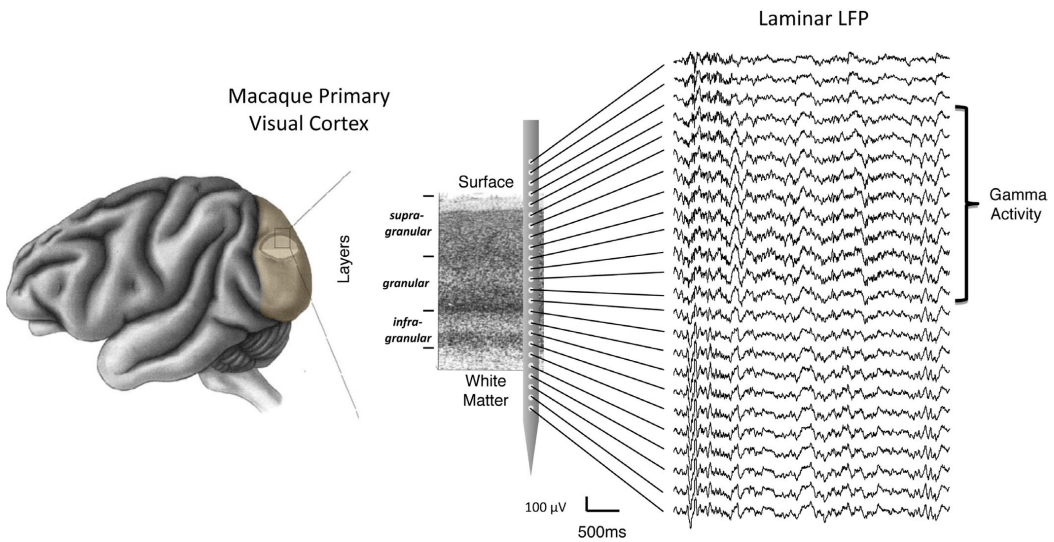

FIGURE 1 | Schematic representation of laminar LFP recordings from a linear multicontact electrode array in the primary visual cortex. For illustrative purposes, the array is depicted overlying a Nissl-stained histological slice, with labels showing individual layers and the corresponding compartments (i.e., supragranular, granular, and infragranular) used in the study. On the right is a sample of extracellular LFP data collected in one experiment. Each trace corresponds to the voltage measured simultaneously as a function of time (see scale bar). In this example, the top contacts span an area reaching from outside the brain (top) to the white matter (bottom). Note the spatial non-uniformity of gamma frequency signals, superimposed on the signals, and restricted to the upper cortical layers.

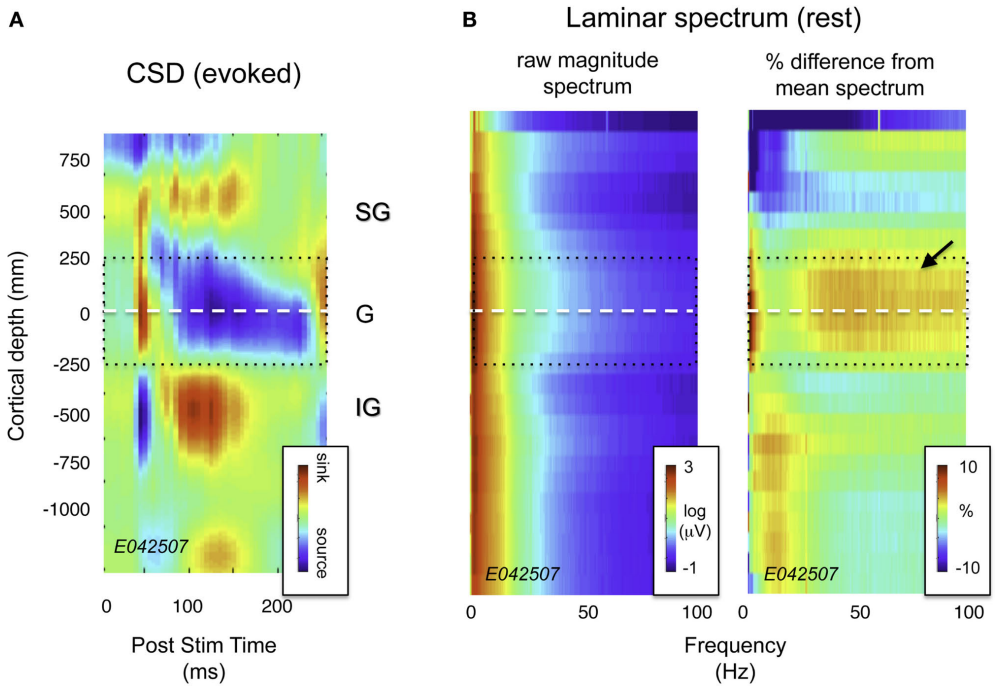

FIGURE 2 | Current source density (CSD) and spectral profile of LFP magnitude as a function of laminar position for one session. (A) CSD profile in response to a flickering screen collected during an example session (monkey CB35). The center of the initial current sink, thought to correspond primarily to thalamic input in layer 4Cα, was used as a point of alignment throughout the study. Dotted lines ±250 μm correspond roughly to the extent of layer 4. **(B)** Spectral laminar profile during rest. On the left is a plot depicting mean LFP magnitude for a representative 20-min period following the CSD experiment with the monkey at rest. Signal magnitude is color-coded on a log scale, and plotted as a function of frequency and cortical depth. On the right is the same data, normalized by the mean spectrum across all layers, and expressed as percent deviation from this mean. Note the elevated LFP magnitude in the granular and deep supragranular layers (arrow). This feature proved highly consistent across sessions (see **Figure 3A**).

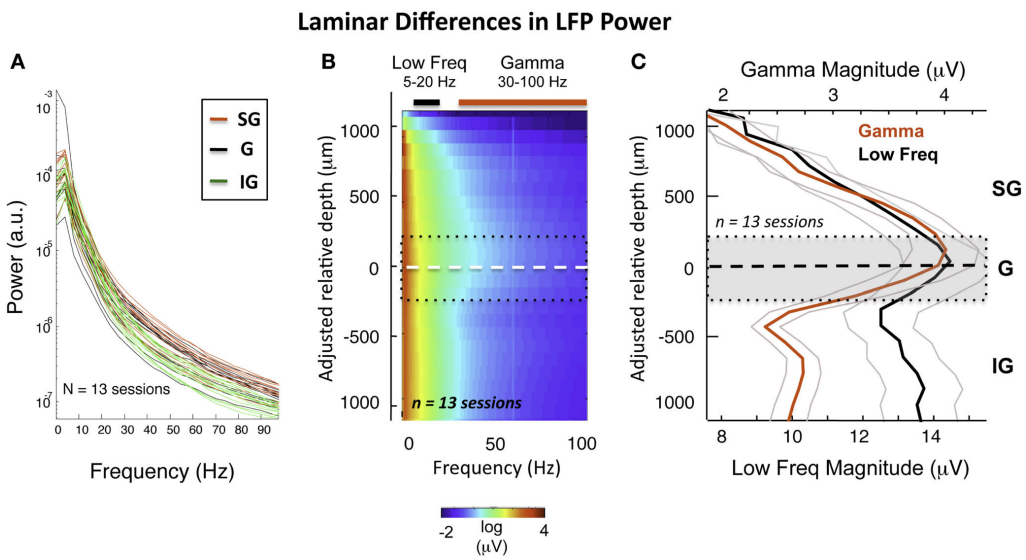

FIGURE 3 | Intersession average following CSD-based realignment. (A) Laminar differences as a function of frequency over all sessions. **(B)** The mean LFP magnitude during resting state over all sessions following alignment, expressed as a function of frequency. The dashed white line represents the "zero point," with the dotted black lines showing rough boundaries of layer 4. The elevated high-frequency activity in the middle and upper layers is clearly visible. The colored bars indicate the frequency range used to compute mean LFP magnitude in **(C)**. **(C)** Laminar distribution of LFP amplitude in gamma and sub-gamma-ranges during rest. Note that the mean gamma-range amplitude is highest in the middle and upper layers.

session-by-session comparison discussed above, we found that, on average, gamma power was roughly 50% higher in the G and SG zone than in the IG zone across the population (red curve). This difference was not present in the sub-gamma-range (black curve).

What might be the basis of the laminar differences in gamma-range power? One possibility is that superficial and deep layers participate in different aspects of the brain's intrinsic activity during the resting state. This conjecture is consistent with the known anatomical segregation of neural afferents, differences in cell types, projection targets, and other aspects of the laminar anatomy (see Discussion). To address whether superficial and deep layers differ in their pattern of functional interactions, we next investigated the laminar covariation of SOA by computing the temporal coherence between all pairs of electrodes.

SUPERFICIAL AND DEEP ZONES OF LFP COHERENCE

To assess the interdependence of the LFP time course in different cortical layers, we computed the magnitude-squared coherence between signals measured from different electrode contacts. Coherence is a measure of similarity in the temporal structure of two signals that quantifies the extent to which two signals are linearly related. A coherence value equal to zero indicates that there is no consistent relationship between the two signals, whereas a value of 1 indicates there is a perfectly linear relationship. For each electrode contact, a spatial profile of coherence can be determined by computing the magnitude-squared coherence between its time course and the time course of the contacts at the other spatial positions. An example of this approach from one session in the resting condition is shown in **Figure 4A**, with coherence pertaining to LFP frequencies in the gamma-range (30–100 Hz). In this figure, two spatial profiles were computed, one for a contact in the G layer, and one for a contact in the IG layers. Note that the contact in the G layer (E_0, red) showed strong coherence with the other G positions and most of the SG positions, but the coherence level fell abruptly in the IG layers. In contrast, the IG contact (E_0, green), situated a mere 200 µm deeper, showed the opposite pattern. Its highest coherence was with the deeper electrodes, whereas it showed minimal coherence with the superficial electrodes. This analysis is expanded in the same session in **Figure 4B**, which shows the laminar coherence profile for 10 different contacts. Pairs of electrodes in the G and SG layers show high coherence in the gamma-range, as do pairs of IG electrodes. However coherence between compartments is much lower, suggesting distinct processes in the upper and lower layers in the gamma-range.

This pattern of laminar coherence was consistent across recording sessions and animals. The population pair-wise coherence in the (30–100 Hz) gamma-range is depicted in **Figure 5B**, adjacent to the mean aligned CSD response for all sessions (**Figure 5A**). Each

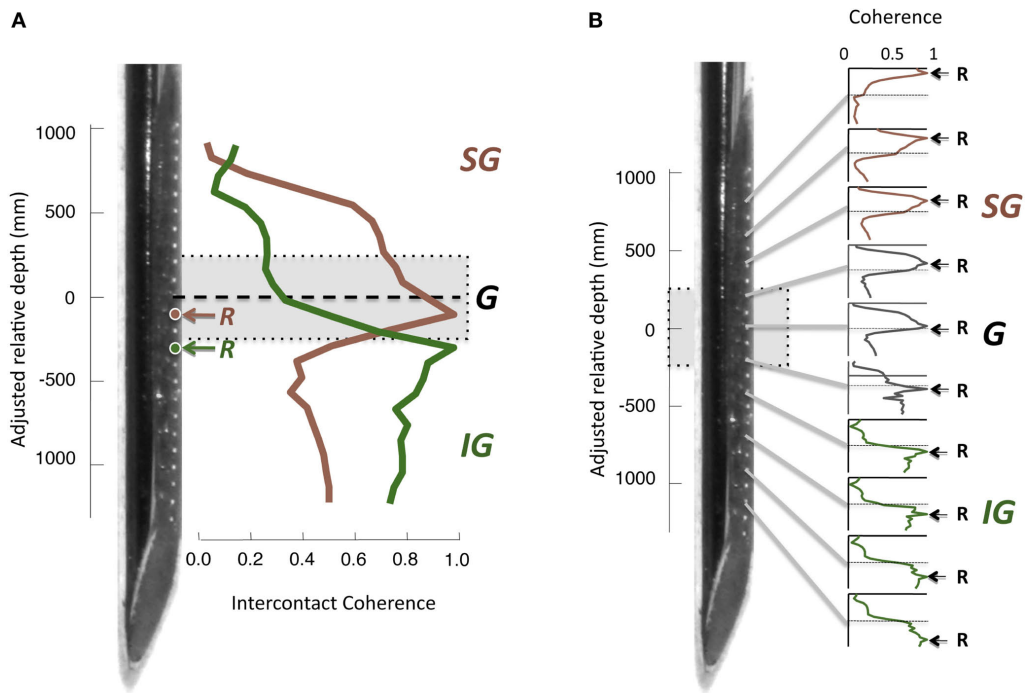

FIGURE 4 | (A) Inter-contact coherence for reference contacts taken from two different laminar compartments. Magnitude-squared coherence in the gamma-range (30–100 Hz) is plotted between each reference electrode and all other electrodes in the array (including contacts located in the white matter at the bottom of the array and outside the brain at the top, respectively). The electrode from the granular zone (green) showed strong correlation with granular and supragranular sites, but weaker coherence with infragranular sites. In contrast, the infragranular contact (red) showed strong coherence with the infragranular contacts, but very low coherence with other sites. Note that the two electrodes chosen for this example (E_0, red and green) are separated by only 200 µm. **(B)** Laminar pattern of inter-contact coherence for 10 different E_0 contact positions, shown in the same format as in **(A)**. The E_0 positions in the infragranular layers elicit a pattern of high coherence only in those layers, suggesting that the gamma-range activity in those layers is highly synchronous, but asynchronous to that in other layers. Conversely, E_0 positions in the supragranular layers are coherent only with signals measured in supragranular contacts. A single contact lying just below the zero point appears to be a transition between supra- and infragranular coherence.

square in the matrix corresponds to the mean gamma-range coherence value over all sessions, relative to the zero-point alignment contact. The large, red squares reflect the strong similarity of signals measured within the same laminar compartment, whereas the blue background reflects the fact that the between-compartment coherence is weak. Note that due to the alignment, the transition between the two compartments is abrupt, even when averaged over all sessions, indicating a sharp discontinuity between zones of coherent activity. The data from each session, shown separately in **Figure S3** in Supplementary Material, demonstrates the day-to-day consistency of these main findings. **Figure 6** shows the same analysis for other frequency ranges. In contrast to LFP amplitude, which showed significant laminar differences in the gamma-range only, LFP coherence of almost all frequencies segregated significantly between laminar compartments.

EFFECTS OF VISUAL STIMULATION

In the experiments described above, the monkeys were at rest, sitting drowsily in a dark room. We next asked whether a similar pattern of laminar coherence would be observed in the presence

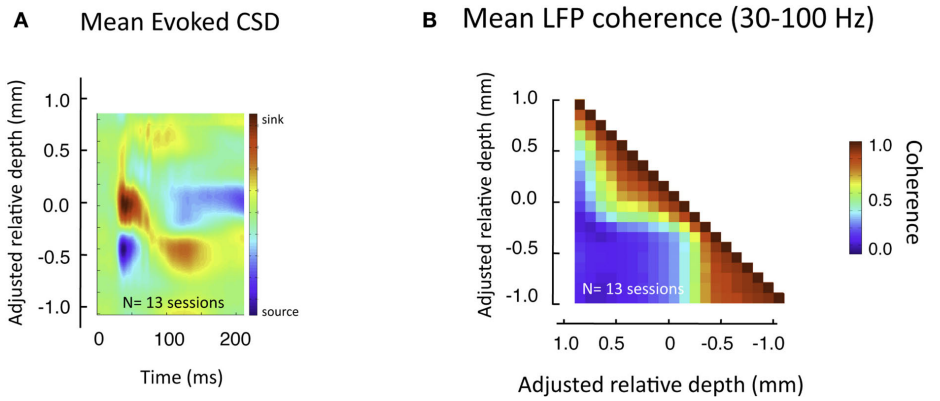

FIGURE 5 | Pair-wise coherence of all sessions in the gamma-range. (A) Average CSD to flashing screen following alignment to initial sink. **(B)** Mean gamma-range coherence, computed between all pairs of laminar positions over all sessions, during rest (see **Figure 7** for effects of visual stimulation). The square regions reveal the high inter-compartmental coherence, with the adjacent blue regions revealing the lack of coherence between compartments.

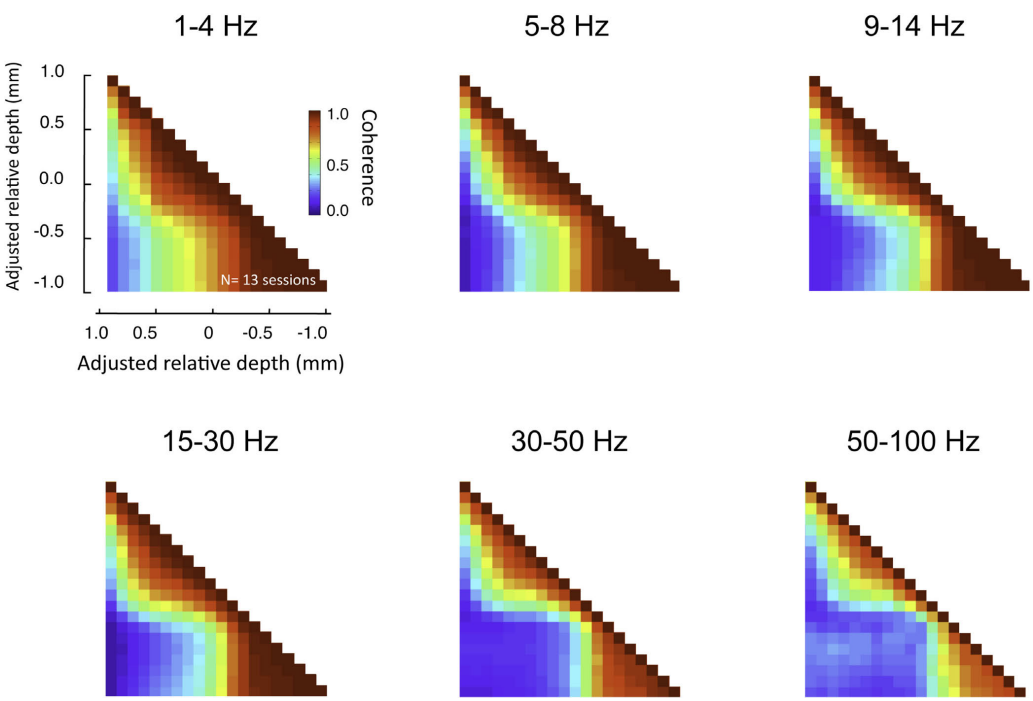

FIGURE 6 | Laminar coherence as a function of frequency (*n* = 13, session; both monkeys). Inter-compartmental coherence for the classic EEG frequency bands (delta = 1–4 Hz, theta = 5–8 Hz, alpha = 9–14 Hz, beta = 15–30 Hz, low gamma = 30–50 HZ, high gamma = 50–100 Hz) is plotted individually using the same format as **Figure 7**. Note that despite differences in the overall coherence, the basic pattern between upper and lower layers remained.

of a visual stimulus. To this end, we compared coherence before, during, and after the presentation of a luminance patch onto the receptive field of the recorded site. In contrast to the resting data, in this case the monkey was actively engaged in the task, and was required to fixate a small point in the middle of a display screen throughout each trial (see Materials and Methods and **Figure S1B** in Supplementary Material). The population pair-wise coherence in the gamma-range for each of these epochs is depicted in **Figure 7** (all conventions are the same as in **Figure 5B**). We chose time windows for this analysis that minimized stimulus-related transients (i.e., >900 ms following stimulus onset and >600 ms following stimulus offset). Note that neither the task nor the stimulus significantly altered the spatial pattern of interlaminar correlation, although the overall level of LFP coherence was lower for all three conditions than during rest. The functional division into two main laminar compartments thus seems to be a fundamental principle of organization in the visual cortex, which is not disrupted by sensory activation and processing.

SLOW POWER FLUCTUATIONS

The above analysis focuses on LFP fluctuations that vary on the time scale of milliseconds (in our case, filtered between 1 and 100 Hz). Another relevant signal that can be computed from the same LFP data pertains to changes that are much slower (<0.1 Hz). This signal, which we term the BLP, corresponds to magnitude of the envelope of the LFP signal filtered in a particular frequency band (Leopold et al., 2003; see Materials and Methods). The BLP signal exhibits properties that are very different from the LFP. For instance, whereas coherence in the LFP in the gamma-range falls to near zero between cortical sites separated by 2.5 mm the slow BLP shows robust coherence between recording sites separated by up to 10.6 mm (Leopold and Logothetis, 2003; Leopold et al., 2003). Based on those findings, it might be expected that the very low frequency fluctuations in the gamma BLP would be highly synchronous between all electrode contacts in the present study since they are spaced within few hundreds of microns of each other. Surprisingly, we found that, like raw LFP described above, the BLP coherence was confined to superficial and deep compartments, with much lower coherence between compartments (**Figure 8**). The slow BLP changes have been shown to correlate strongly with resting state fMRI fluctuations (Shmuel and Leopold, 2008; Schölvinck et al., 2010). Thus the present findings raise the question whether slow fluctuations in the upper and lower laminar zones bear a different relationship to the fMRI signal, which is a topic for future investigation.

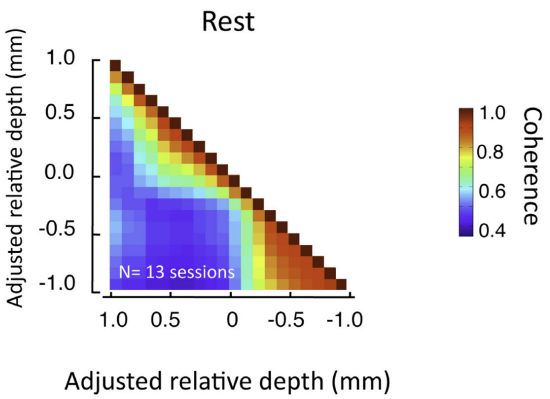

FIGURE 8 | Pair-wise coherence of the slow fluctuations in gamma power computed for all sessions (lasting 20 min each). Data presented in same format as **Figure 7**, but now pertaining to 0.01–0.1 Hz fluctuations in the magnitude of the gamma-range LFP activity. Note these fluctuations show moderate background coherence (i.e., the blue in the plot is roughly 0.5). However, as with the voltage coherence shown above, the power coherence is highest within the same laminar compartment.

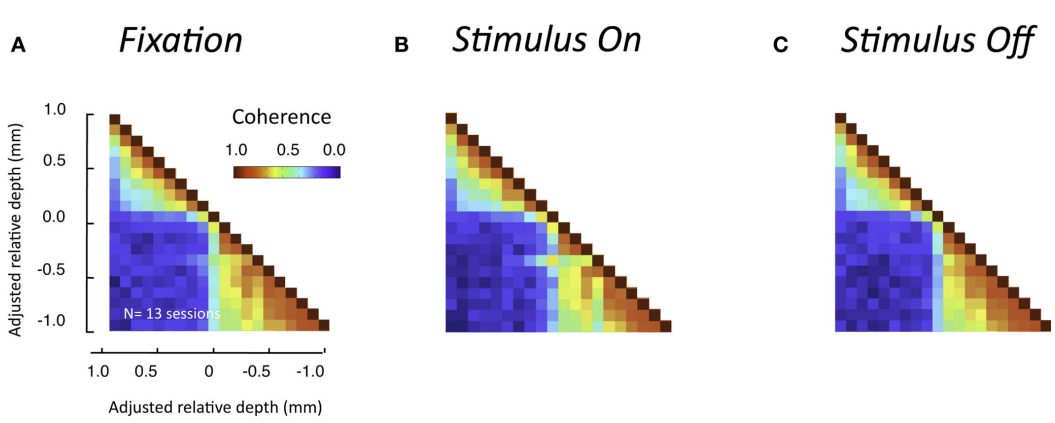

FIGURE 7 | Interlaminar coherence during visual stimulation (*n* = 13 sessions, both monkeys). All conventions are the same as in **Figure 5B**. **(A)** Coherence pattern during fixation before stimulus onset (–300 to 0 ms before stimulus onset). **(B)** Coherence pattern during sustained presentation of a luminance stimulus onto the receptive field (900–1200 ms after stimulus onset). **(C)** Coherence pattern following the removal of the stimulus (600–900 after stimulus offset). Note that despite differences in the overall coherence level compared to the resting condition (**Figure 5**), the spatial pattern between upper and lower layers was similar.

DISCUSSION

Here we report a pronounced segregation in the time course of spontaneous LFP signals in the primary visual cortex of awake macaque monkeys at rest. The compartmentalization into superficial and deep layers, with the transition at or near the bottom of layer 4, may reflect known functional differences between laminae. Specifically, it is possible that the LFP activity in the superficial compartment, from which efferent projections are mainly directed to extrastriate visual areas (Felleman and Van, 1991), is primarily related to corticocortical processing. In contrast, LFP activity in the deep compartment, where efferent projections are largely directed to the lateral geniculate nucleus, pulvinar, and superior colliculus, may then be primarily related to interactions with subcortical structures. This simplified interpretation, is unlikely to be perfectly accurate, however, since the apical dendrites of infragranular neurons have abundant synapses in the supragranular layers and would therefore likely contribute to the supragranular LFP. Nonetheless, the cortical–subcortical hypothesis is a candidate that warrants further investigation.

The within- and between-compartment coherence levels differed substantially for a wide range of frequencies, from an average coherence close to 1 within compartments to close to 0 between compartments (see **Figure 6**). This segregation has not been previously reported, probably because the laminar distribution of SOA coherence has not been investigated in this way. A few experiments have characterized the laminar distribution of spontaneous LFP activity using other approaches. For example, a previous study focused on spontaneous alpha-rhythm oscillations in several visual areas of the monkey, and found a pronounced alpha-range peak in the coherence between the CSD and multiunit signal in the infragranular and granular, but not supragranular layers (Bollimunta et al., 2008). A different study focused on "neuronal avalanches," which are spatiotemporal patterns of spontaneous LFP activity thought to reflect a critical state of network excitability, and found them to exist only in the superficial layers of the macaque somatosensory and motor cortex (Plenz and Thiagarajan, 2007; Petermann et al., 2009; Thiagarajan et al., 2010). Like this previous work, our findings demonstrate clear differences between LFP activity in the superficial and deep cortical layers.

FOCUS ON THE GAMMA-RANGE

We analyzed the gamma-range separately primarily because this range showed pronounced amplitude differences between superficial and deep layers. This frequency range is also of interest because of its relevance for cognitive function (Engel and Singer, 2001; Fries et al., 2007; Fries, 2009; Schroeder and Lakatos, 2009), and because it is thought to reflect distinct and local neural processes (Bartos et al., 2007). Note, however, that the term "gamma" denotes only a range of frequencies rather than any particular mechanism. Importantly, there was no evidence in our study that activity in the gamma-range was oscillatory or even restricted to a narrow range of frequencies.

We observed higher gamma power in the superficial layers than in the deep layers. Several anatomical correlates offer potential explanations this difference. For example, the density of synapses in macaque V1 is highest SG and G layers (O'Kusky and Colonnier, 1982). Also, the relative density of certain receptor subtypes (e.g., AMPA and GABA) in humans (Eickhoff et al., 2007) and the density of interneurons in macaques (Fitzpatrick et al., 1987) are skewed toward the SG and G layers. Since synapses, interneurons and GABA receptors are all believed to be important for the local generation of gamma (Fries et al., 2007), this anatomy may well explain the power distributions we observed. Furthermore, *in vivo* measurements have shown that the laminar density of so-called fast rhythmic bursting neurons, which have been identified as generators of persistent gamma activity *in vitro* (Cunningham et al., 2004), drop sharply in layer 5 compared to the more superficial layers (although there is also an increase in layer 6) (Cardin et al., 2005).

LOCAL FIELD POTENTIAL COHERENCE

The coherence measurement in the present study is sensitive to the LFP synchrony between channels. Although coherence is typically expressed as a function of frequency, it does not isolate signals that are oscillatory in nature, but is instead influenced by any type of synchrony including shared, discrete events. In fact, a wide range of neural processes could account for the distinct superficial and deep zones of coherence we measured. For one, it is interesting to speculate that neuronal avalanches mentioned above, which have been observed in the superficial, but not deep, layers of cortex (Petermann et al., 2009; Thiagarajan et al., 2010), could be a source the within-compartment coherence we measured.

It is important to note that the LFP is a differential measure, and its voltage fluctuations depend to some degree on the position of the electrical reference relative to the active electrodes. The proximity of the electrical reference affects the degree of shared temporal structure between different active electrodes, which, in turn, affects any measure of coherence. In the present study the electrode shank served as the reference, and this shank also served to electrically ground the monkey. This shank surrounded each of the active contacts and was therefore distributed throughout the cortical thickness, minimizing far-field contributions to the measured LFP, and thereby enhancing local differences. Ultimately, it would be desirable to avoid referencing issues altogether by computing either the local electric field (approximated as the first spatial derivative of the voltage along the linear array) or the CSD (approximated as the second spatial derivative of the voltage multiplied by the tissue conductivity). The CSD is thought to reflect synchronous synaptic currents transferred between extracellular and intracellular compartments, and is thereby a step closer than the LFP to the generative neural processes. However, the low SNR of the CSD signal poses a challenge for the type of analysis used in this study, in which signals cannot averaged over many trials.

RELATIONSHIP TO ANATOMICAL ARCHITECTURE

The results described in this study may ultimately shed light on structure-function relationships in the visual cortex. The primary visual cortex differs from other visual and non-visual areas in several key aspects of its cytoarchitecture, including its laminar makeup, including prominent extent of layer 4 compared to other visual areas (Lund, 1988), along with its idiosyncratic microvasculature (Weber et al., 2008). Recent reports find LFP differences between V1 and higher visual areas including laminar differences in the gamma frequency range during cognitive tasks (Buffalo et al., 2004; Chalk et al., 2010). V1 has a laminar distribution of neurotransmitter receptors that distinguish it from other areas (Eickhoff et al., 2007), including cholinergic receptors (Disney and Aoki, 2008), which are thought to

play a role in shaping activity in the gamma frequency band of the LFP (Munk et al., 1996; Fisahn et al., 1998). In the future, a wider sampling of cortical areas using the techniques described here may be useful to gain a deeper understanding of the link between cortical laminar structure and neurophysiological function.

ACKNOWLEDGMENTS

Authors would like to thank Drs. D. Plenz, M. Schmid, and D. McMahon for comments on the manuscript, K. Smith, N. Phipps, and J. Yu for technical assistance, G. Dold, D. Ide, N. Nichols, and T. Talbot design and machining, Dr. D. Sheinberg for help with stimulus software, Dr. W. Vinje for initial acquisition of multicontact electrodes and Drs. M. Wilke, and K.-M. Mueller for discussion. Work was supported by the Intramural Research Programs of the NIMH, NINDS and NEI.

SUPPLEMENTARY MATERIAL

The Supplementary Material for this article can be found online at http://www.frontiersin.org/neuroscience/systemsneuroscience/paper/10.3389/fnsys.2010.00031/

REFERENCES

Arieli, A., Shoham, D., Hildesheim, R., and Grinvald, A. (1995). Coherent spatiotemporal patterns of ongoing activity revealed by real-time optical imaging coupled with single-unit recording in the cat visual cortex. *J. Neurophysiol.* 73, 2072–2093.

Bartos, M., Vida, I., and Jonas, P. (2007). Synaptic mechanisms of synchronized gamma oscillations in inhibitory interneuron networks. *Nat. Rev. Neurosci.* 8, 45–56.

Biswal, B., Yetkin, F. Z., Haughton, V. M., and Hyde, J. S. (1995). Functional connectivity in the motor cortex of resting human brain using echo-planar MRI. *Magn. Reson. Med.* 34, 537–541.

Bollimunta, A., Chen, Y., Schroeder, C. E., and Ding, M. (2008). Neuronal mechanisms of cortical alpha oscillations in awake-behaving macaques. *J. Neurosci.* 28, 9976–9988.

Buffalo, E. A., Fries, P., and Desimone, R. (2004). Layer-specific attentional modulation in early visual areas. *Soc. Neurosci. Abstr. Program No.* 717.6.

Cardin, J. A., Palmer, L. A., and Contreras, D. (2005). Stimulus-dependent gamma (30–50 Hz) oscillations in simple and complex fast rhythmic bursting cells in primary visual cortex. *J. Neurosci.* 25, 5339–5350.

Chalk, M., Herrero, J. L., Gieselmann, M. A., Delicato, L. S., Gotthardt, S., and Thiele, A. (2010). Attention reduces stimulus-driven gamma frequency oscillations and spike field coherence in V1. *Neuron* 66, 114–125.

Clarke, D. D., and Sokoloff, L. (1999). "Circulation and energy metabolism of the brain," in *Basic Neurochemistry: Molecular, Cellular and Medical Aspects*, eds G. J. Siegel, B. W. Agranoff, R. W. Albers, S. K. Fisher, and M. D. Uhler (Philadelphia: Lippencott-Raven), 637–670.

Cunningham, M. O., Whittington, M. A., Bibbig, A., Roopun, A., LeBeau, F. E., Vogt, A., Monyer, H., Buhl, E. H., and Traub, R. D. (2004). A role for fast rhythmic bursting neurons in cortical gamma oscillations in vitro. *Proc. Natl. Acad. Sci. U.S.A.* 101, 7152–7157.

Di Martino, A., Scheres, A., Margulies, D. S., Kelly, A. M., Uddin, L. Q., Shehzad, Z., Biswal, B., Walters, J. R., Castellanos, F. X., and Milham, M. P. (2008). Functional connectivity of human striatum: a resting state FMRI study. *Cereb. Cortex* 18, 2735–2747.

Disney, A. A., and Aoki, C. (2008). Muscarinic acetylcholine receptors in macaque V1 are most frequently expressed by parvalbumin-immunoreactive neurons. *J. Comp. Neurol.* 507, 1748–1762.

Eickhoff, S. B., Rottschy, C., and Zilles, K. (2007). Laminar distribution and co-distribution of neurotransmitter receptors in early human visual cortex. *Brain Struct. Funct.* 212, 255–267.

Engel, A. K., and Singer, W. (2001). Temporal binding and the neural correlates of sensory awareness. *Trends Cogn. Sci. (Regul. Ed.)* 5, 16–25.

Felleman, D. J., and Van, E. D. C. (1991). Distributed hierarchical processing in the primate cerebral cortex. *Cereb. Cortex* 1, 1–47.

Fisahn, A., Pike, F. G., Buhl, E. H., and Paulsen, O. (1998). Cholinergic induction of network oscillations at 40 Hz in the hippocampus in vitro. *Nature* 394, 186–189.

Fitzpatrick, D., Lund, J. S., Schmechel, D. E., and Towles, A. C. (1987). Distribution of GABAergic neurons and axon terminals in the macaque striate cortex. *J. Comp. Neurol.* 264, 73–91.

Fox, M. D., and Raichle, M. E. (2007). Spontaneous fluctuations in brain activity observed with functional magnetic resonance imaging. *Nat. Rev. Neurosci.* 8, 700–711.

Fox, M. D., Snyder, A. Z., Vincent, J. L., Corbetta, M., Van Essen, D. C., and Raichle, M. E. (2005). The human brain is intrinsically organized into dynamic, anticorrelated functional networks. *Proc. Natl. Acad. Sci. U.S.A.* 102, 9673–9678.

Fries, P. (2009). Neuronal gamma-band synchronization as a fundamental process in cortical computation. *Annu. Rev. Neurosci.* 32, 209–224.

Fries, P., Nikolic, D., and Singer, W. (2007). The gamma cycle. *Trends Neurosci.* 30, 309–316.

Friston, K. J. (1994). Functional and effective connectivity in neuroimaging: a synthesis. *Hum. Brain Mapp.* 2, 56–78.

Gerstein, G. L., and Perkel, D. H. (1969). Simultaneously recorded trains of action potentials: analysis and functional interpretation. *Science* 164, 828–830.

Gochin, P. M., Miller, E. K., Gross, C. G., and Gerstein, G. L. (1991). Functional interactions among neurons in inferior temporal cortex of the awake macaque. *Exp. Brain Res.* 84, 505–516.

Greicius, M. D., Krasnow, B., Reiss, A. L., and Menon, V. (2003). Functional connectivity in the resting brain: a network analysis of the default mode hypothesis. *Proc. Natl. Acad. Sci. U.S.A.* 100, 253–258.

Hayden, B. Y., Smith, D. V., and Platt, M. L. (2009). Electrophysiological correlates of default-mode processing in macaque posterior cingulate cortex. *Proc. Natl. Acad. Sci. U.S.A.* 106, 5948–5953.

He, B. J., Snyder, A. Z., Zempel, J. M., Smyth, M. D., and Raichle, M. E. (2008). Electrophysiological correlates of the brain's intrinsic large-scale functional architecture. *Proc. Natl. Acad. Sci. U.S.A.* 105, 16039–16044.

Kenet, T., Bibitchkov, D., Tsodyks, M., Grinvald, A., and Arieli, A. (2003). Spontaneously emerging cortical representations of visual attributes. *Nature* 425, 954–956.

Leopold, D. A., and Logothetis, N. K. (2003). Spatial patterns of spontaneous local field activity in the monkey visual cortex. *Rev. Neurosci.* 14, 195–205.

Leopold, D. A., Murayama, Y., and Logothetis, N. K. (2003). Very slow activity fluctuations in monkey visual cortex: implications for functional brain imaging. *Cereb. Cortex* 13, 422–433.

Lowe, M. J., Mock, B. J., and Sorenson, J. A. (1998). Functional connectivity in single and multislice echoplanar imaging using resting-state fluctuations. *Neuroimage* 7, 119–132.

Lund, J. (1988). Anatomical organization of macaque monkey striate visual cortex. *Annu. Rev. Neurosci.* 11, 253–288.

Maier, A., Wilke, M., Aura, C., Zhu, C., Ye, F. Q., and Leopold, D. A. (2008). Divergence of fMRI and neural signals in V1 during perceptual suppression in the awake monkey. *Nat. Neurosci.* 11, 1193–1200.

Mitzdorf, U. (1985). Current source-density method and application in cat cerebral cortex: investigation of evoked potentials and EEG phenomena 7. *Physiol. Rev.* 65, 37–100.

Mitzdorf, U., and Singer, W. (1979). Excitatory synaptic ensemble properties in the visual cortex of the macaque monkey: a current source density analysis of electrically evoked potentials. *J. Comp. Neurol.* 187, 71–83.

Moeller, S., Nallasamy, N., Tsao, D. Y., and Freiwald, W. A. (2009). Functional connectivity of the macaque brain across stimulus and arousal states. *J. Neurosci.* 29, 5897–5909.

Munk, M. H., Roelfsema, P. R., Konig, P., Engel, A. K., and Singer, W. (1996). Role of reticular activation in the modulation of intracortical synchronization. *Science* 272, 271–274.

Nir, Y., Mukamel, R., Dinstein, I., Privman, E., Harel, M., Fisch, L., Gelbard-Sagiv, H., Kipervasser, S., Andelman, F., Neufeld, M. Y., Kramer, U., Arieli, A., Fried, I., and Malach, R. (2008). Interhemispheric correlations of slow spontaneous neuronal fluctuations revealed in human sensory cortex. *Nat. Neurosci.* 11, 1100–1108.

O'Kusky, J., and Colonnier, M. (1982). A laminar analysis of the number of neurons, glia, and synapses in the adult cortex (area 17) of adult macaque monkeys. *J. Comp. Neurol.* 210, 278–290.

O'Reilly, J. X., Beckmann, C. F., Tomassini, V., Ramnani, N., and Johansen-Berg, H. (2010). Distinct and overlapping functional zones in the cerebellum defined by resting state functional connectivity. *Cereb. Cortex* 20, 953–965.

Petermann, T., Thiagarajan, T. C., Lebedev, M. A., Nicolelis, M. A., Chialvo, D. R.,

and Plenz, D. (2009). Spontaneous cortical activity in awake monkeys composed of neuronal avalanches. *Proc. Natl. Acad. Sci. U.S.A.* 106, 15921–15926.

Pettersen, K. H., Devor, A., Ulbert, I., Dale, A. M., and Einevoll, G. T. (2006). Current-source density estimation based on inversion of electrostatic forward solution: effects of finite extent of neuronal activity and conductivity discontinuities. *J. Neurosci. Methods* 154, 116–133.

Plenz, D., and Thiagarajan, T. C. (2007). The organizing principles of neuronal avalanches: cell assemblies in the cortex? *Trends Neurosci.* 30, 101–110.

Raichle, M. E., and Mintun, M. A. (2006). Brain work and brain imaging. *Annu. Rev. Neurosci.* 29, 449–476.

Schölvinck, M. L., Maier, A., Ye, F. Q., Duyn, J. H., and Leopold, D. A. (2010). Neural basis of global resting-state fMRI activity. *Proc. Natl. Acad. Sci. U.S.A.* 107, 10238–10243.

Schroeder, C. E., and Lakatos, P. (2009). Low-frequency neuronal oscillations as instruments of sensory selection. *Trends Neurosci.* 32, 9–18.

Schroeder, C. E., Tenke, C. E., Givre, S. J., Arezzo, J. C., and Vaughan, H. G. Jr. (1991). Striate cortical contribution to the surface-recorded pattern-reversal VEP in the alert monkey. *Vision Res.* 31, 1143–1157.

Shmuel, A., and Leopold, D. A. (2008). Neuronal correlates of spontaneous fluctuations in fMRI signals in monkey visual cortex: implications for functional connectivity at rest. *Hum. Brain Mapp.* 29, 751–761.

Shulman, R. G., Rothman, D. L., Behar, K. L., and Hyder, F. (2004). Energetic basis of brain activity: implications for neuroimaging. *Trends Neurosci.* 27, 489–495.

Snodderly, D. M., and Gur, M. (1995). Organization of striate cortex of alert, trained monkeys (*Macaca fascicularis*): ongoing activity, stimulus selectivity, and widths of receptive field activating regions. *J. Neurophysiol.* 74, 2100–2125.

Thiagarajan, T. C., Lebedev, M. A., Nicolelis, M. A., and Plenz, D. (2010). Coherence potentials: loss-less, all-or-none network events in the cortex. *PLoS Biol.* 8, e1000278. doi: 10.1371/journal.pbio.1000278.

Tsodyks, M., Kenet, T., Grinvald, A., and Arieli, A. (1999). Linking spontaneous activity of single cortical neurons and the underlying functional architecture. *Science* 286, 1943–1946.

Vincent, J. L., Patel, G. H., Fox, M. D., Snyder, A. Z., Baker, J. T., Van, E. D. C., Zempel, J. M., Snyder, L. H., Corbetta, M., and Raichle, M. E. (2007). Intrinsic functional architecture in the anaesthetized monkey brain. *Nature* 447, 83–86.

Weber, B., Keller, A. L., Reichold, J., and Logothetis, N. K. (2008). The microvascular system of the striate and extrastriate visual cortex of the macaque. *Cereb. Cortex* 18, 2318–2330.

Zhang, D., Snyder, A. Z., Fox, M. D., Sansbury, M. W., Shimony, J. S., and Raichle, M. E. (2008). Intrinsic functional relations between human cerebral cortex and thalamus. *J. Neurophysiol.* 100, 1740–1748.

Conflict of Interest Statement: The authors declare that the research was conducted in the absence of any commercial or financial relationships that could be construed as a potential conflict of interest.

Received: 19 February 2010; paper pending published: 26 March 2010; accepted: 18 June 2010; published online: 10 August 2010.
*Citation: Maier A, Adams GK, Aura C and Leopold DA (2010) Distinct Superficial and deep laminar domains of activity in the visual cortex during rest and stimulation. Front. Syst. Neurosci. **4**:31. doi: 10.3389/fnsys.2010.00031*

frontiers in
SYSTEMS NEUROSCIENCE

REVIEW ARTICLE
published: 06 April 2010
doi: 10.3389/fnsys.2010.00008

Advances and pitfalls in the analysis and interpretation of resting-state FMRI data

David M. Cole[1], Stephen M. Smith[2] and Christian F. Beckmann[1,2]*

[1] *Department of Clinical Neuroscience, Imperial College London, London, UK*
[2] *Department of Clinical Neurology, Centre for Functional Magnetic Resonance Imaging of the Brain, University of Oxford, Oxford, UK*

Edited by:
Lucina Q. Uddin, Stanford University, USA

Reviewed by:
Thomas Meindl, University of Munich, Germany
Catie Chang, Stanford University, USA

Correspondence:
Christian F. Beckmann, Department of Clinical Neuroscience, Imperial College London, Hammersmith Hospital, Du Cane Road, London W12 0NN, UK.
e-mail: c.beckmann@imperial.ac.uk

The last 15 years have witnessed a steady increase in the number of resting-state functional neuroimaging studies. The connectivity patterns of multiple functional, distributed, large-scale networks of brain dynamics have been recognised for their potential as useful tools in the domain of systems and other neurosciences. The application of functional connectivity methods to areas such as cognitive psychology, clinical diagnosis and treatment progression has yielded promising preliminary results, but is yet to be fully realised. This is due, in part, to an array of methodological and interpretative issues that remain to be resolved. We here present a review of the methods most commonly applied in this rapidly advancing field, such as seed-based correlation analysis and independent component analysis, along with examples of their use at the individual subject and group analysis levels and a discussion of practical and theoretical issues arising from this data 'explosion'. We describe the similarities and differences across these varied statistical approaches to processing resting-state functional magnetic resonance imaging signals, and conclude that further technical optimisation and experimental refinement is required in order to fully delineate and characterise the gross complexity of the human neural functional architecture.

Keywords: FMRI, functional connectivity, resting-state, networks, seed-based correlations, independent component analysis

INTRODUCTION

Spontaneous, or 'resting-state', fluctuations in the blood oxygenation level-dependent (BOLD) signal, as measured by functional magnetic resonance imaging (FMRI), may present a valuable data resource for delineating the human neural functional architecture. Consistent, large-scale spatial patterns of coherent signal have been identified in the human brain using both FMRI (Biswal et al., 1995; Lowe et al., 1998) and positron emission tomography (PET; Shulman et al., 1997; Raichle et al., 2001). Techniques assessing functional connectivity, originally applied to BOLD FMRI data alongside studies of model-driven, task-evoked activation, have also proven useful for resting-state research and have greatly supported and contributed to increasing scientific interest in the spontaneous, or 'default' neural activity of the brain at baseline (Gusnard and Raichle, 2001; Raichle et al., 2001; Fox and Raichle, 2007). As outlined in this article, these methods provide useful conceptual complements to the inferences made from task-FMRI data, and hence are increasingly being applied across multiple fields of neuroscience, to further inform our understanding of the fundamental organisation of processing systems in the human brain.

The majority of approaches to analysing resting-state FMRI data have thus far been spatially model-driven, with strong *a priori* hypotheses regarding the functional connectivity of a small number of brain regions of interest (ROIs) or individual voxel locations of interest. Recently, however, a great deal of attention has been focused on the patterns of connectivity between multiple ROIs within spatially distributed, large-scale networks, characterised via both model-driven (e.g., seed-based correlation analysis; Biswal et al., 1995; Greicius et al., 2003; Fox et al., 2005) and data-driven analyses (e.g., independent component analysis; McKeown et al., 1998; Kiviniemi et al., 2003; Beckmann et al., 2005). These patterns have been variously termed 'intrinsic connectivity networks' (Seeley et al., 2007), or 'resting-state networks' (RSNs; Greicius et al., 2003; Beckmann et al., 2005; De Luca et al., 2006). They are purported to reflect the intrinsic energy demands of neuron populations that, via firing together with a common functional purpose, have subsequently wired together through synaptic plasticity (e.g., Saini et al., 2004; Lewis et al., 2009). RSNs can be reliably and reproducibly detected at individual subject and group levels across a range of analysis techniques (Greicius et al., 2004; Damoiseaux et al., 2006; Shehzad et al., 2009; Zuo et al., 2010b).

A characteristic set of co-activating functional systems is found consistently across subjects (Beckmann et al., 2005; Damoiseaux et al., 2006; De Luca et al., 2006; Fox and Raichle, 2007; Smith et al., 2009), stages of cognitive development (Fair et al., 2007; Fransson et al., 2007), degrees of consciousness (Boly et al., 2008; Greicius et al., 2008) and even (to some extent) across species (Vincent et al., 2007). Moreover, individual networks have been shown to be heritable (Glahn et al., 2010) and altered resting (and stimulus-guided) functioning of large-scale networks has been found in correlation with individual differences in behavioural performance (Fox et al., 2007; Kelly et al., 2008), as well as in disease (Greicius et al., 2004; Castellanos et al., 2008; Di Martino et al., 2009; Seeley et al., 2009) and under pharmacological manipulation (Anand et al., 2005; Hong et al., 2009; Kelly et al., 2009). Therefore there is compelling evidence for RSNs as core functional networks in the mammalian brain.

Accordingly, the increase in resting-state research has resulted in the development of a rich array of signal processing techniques. The following is a summary and review of the most widely applied methods, focussing primarily, but not exclusively, on seed-based correlation analysis (SCA) and independent component analysis (ICA). We discuss the commonalities, differences and potential interpretative pitfalls of these and other techniques, but begin by recapitulating the key characteristics and pre-processing requirements of the data.

RESTING-STATE NETWORK ACTIVITY

SPATIOTEMPORAL CHARACTERISTICS

RSNs are localised to grey matter regions (Beckmann et al., 2005; De Luca et al., 2006), and it is now accepted by many that they reflect functional systems supporting core perceptual and cognitive processes. **Figure 1** (reproduced from Beckmann et al., 2005) displays eight RSN maps commonly identified using ICA. These patterns of intrinsic functional connectivity are consistent with stimulus-evoked co-activation patterns in e.g., sensory and motor cortices, language and memory systems and higher cognitive control networks (Biswal et al., 1995; Lowe et al., 1998; Cordes et al., 2000; Hampson et al., 2002; Beckmann et al., 2005; Seeley et al., 2007; Smith et al., 2009). Indeed, in some instances, subsets of RSNs appear to be either up-regulated or down-regulated during specific cognitive tasks. Thus they may be described as either 'task-positive' or (in the case of the DMN) 'task-negative,' in terms of the direction of correlation between the mean network activity and the event timings during the task (Shulman et al., 1997; Gusnard and Raichle, 2001; Greicius et al., 2003; Fox et al., 2005; Kelly et al., 2008).

RSNs display reliable and consistent functional connectivity patterns with specific thalamic (Zhang et al., 2008) and cerebellar nuclei (Habas et al., 2009; Krienen and Buckner, 2009; O'Reilly et al., 2009). Studies of RSNs may therefore enable investigations of both cortico-cerebellar and cortico-subcortical connectivity associations, potentially in greater detail than previously achieved with structural connectivity measures. In particular, due to anatomical constraints (resolution limitations), the relationship of the cerebellum with the rest of the brain is currently more measurable with functional connectivity parcellation approaches than, for example, diffusion tensor

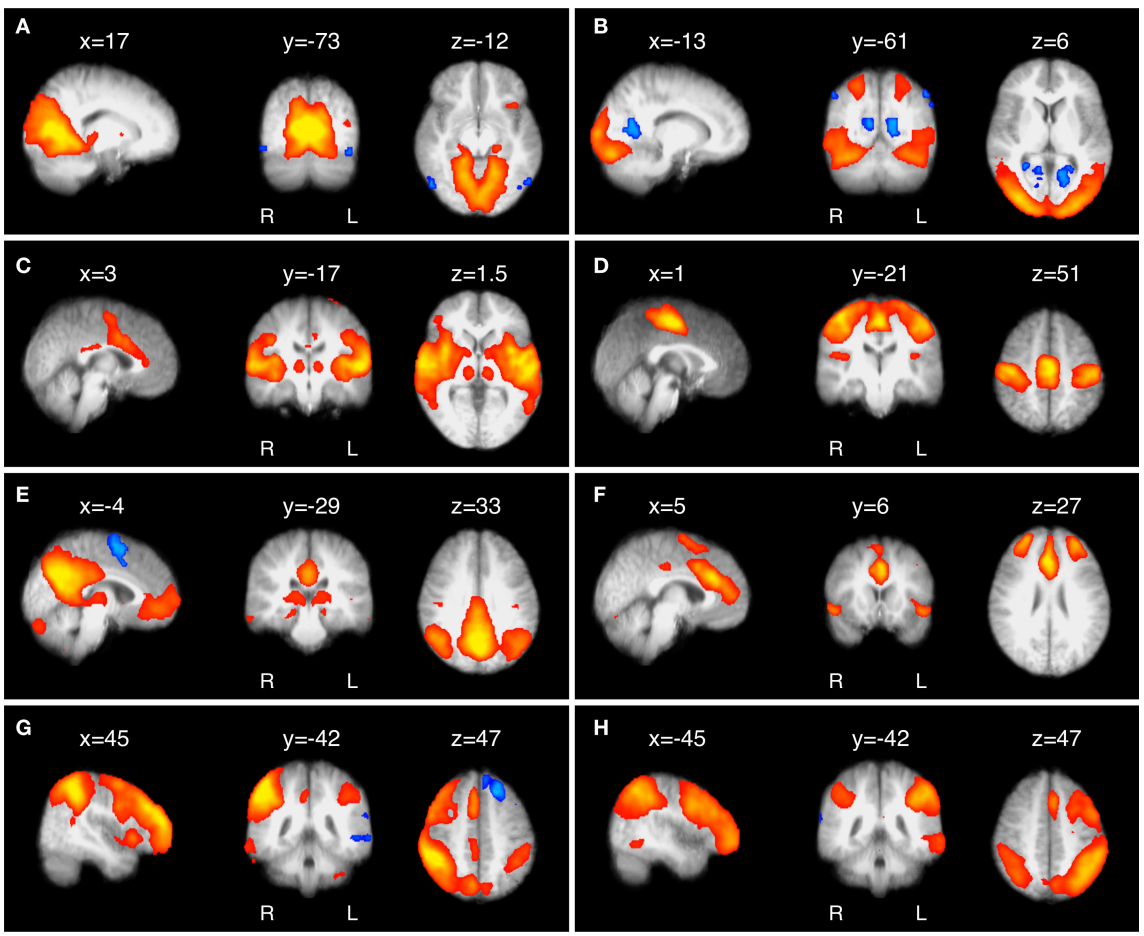

FIGURE 1 | Eight of the most common and consistent RSNs identified by ICA. (A) RSN located in primary visual cortex; **(B)** extrastriate visual cortex; **(C)** auditory and other sensory association cortices; **(D)** the somatomotor cortex; **(E)** the 'default mode' network (DMN), deactivated during demanding cognitive tasks and involved in episodic memory processes and self-referential mental representations; **(F)** a network implicated in executive control and salience processing; and **(G,H)** two right- and left-lateralised fronto-parietal RSNs spatially similar to the bilateral dorsal attention network and implicated in working memory and cognitive attentional processes (for further details, see Beckmann et al., 2005).

imaging. Functional connectivity FMRI measures also provide complementary information to that gained from other imaging modalities and structural connectivity metrics, helping to further map and quantify the neural substrates of systems-level function and dysfunction (e.g., Buckner et al., 2005; Greicius et al., 2009; Seeley et al., 2009).

Importantly, the occurrence of these various observations and the networks involved depend on the nature of neural processes being evoked or induced by the paradigm in question, or even the surrounding context of the resting-state scan. Furthermore, subtle changes in analytic approach to resting data, for example using slightly different spatial seeds in SCA (see **Figure 2** and also Buckner et al., 2008; Hayasaka and Laurienti, 2009), or altering the model order dimensionality estimation in ICA (Kiviniemi et al., 2009; Smith et al., 2009), can have a significant impact on the spatial characteristics of the RSNs identified. For both biological and statistical reasons, sub-regions or 'nodes' of a given RSN may share 'non-stationary' (i.e., time-varying) connectivity relationships within that network or with other identified RSNs (Chang and Glover, 2010; Cole et al., under review). Inferred characteristic RSN patterns can thereby be affected by multiple factors, in terms of the resultant connectivity relationships within and between networks.

SPECTRAL CHARACTERISTICS

RSNs are consistently referred to in the literature as 'low-frequency,' in terms of their spectral power distributions. Early frequency characterisation (Cordes et al., 2000, 2001) localised functionally relevant, spontaneous BOLD oscillations in the lower frequency ranges (0.01–0.08 Hz), separable from respiratory (0.1–0.5 Hz) and cardiovascular (0.6–1.2 Hz) signal frequencies. Additionally, more recent FMRI evidence suggests that, while it is true that the predominant spectral power of RSNs appears in practice at low frequencies, the signal contributions that extend into higher frequencies do so with equal consistency (Niazy et al., 2008). Specifically, it has been shown that filtering RSN signals to account for the frequency content of their haemodynamic response function 'flattens' their power distribution from 0.01 Hz up to 0.15 Hz, instead of being biased towards the lower-frequency end of the spectrum (Smith et al., 2008). This suggests that the low peak power characteristics of BOLD FMRI-derived RSNs are largely induced by the haemodynamics and that underlying RSN 'neural' dynamics may be more 'broadband' than previously thought. Note that many artefactual signals have spectral peaks that are either truly within similar low frequency ranges seen with RSNs, or are aliased by the FMRI temporal sampling into these ranges (e.g., Birn et al., 2008); however it has also been shown that some methods such as ICA and RETROICOR can be used to significantly reduce or even remove these confounds (see below).

RSNs AND ELECTROPHYSIOLOGICAL RECORDINGS

Some groups have acquired simultaneous FMRI and electroencephalography (EEG) resting data, and report evidence of associations between RSN network activity and specific power profiles

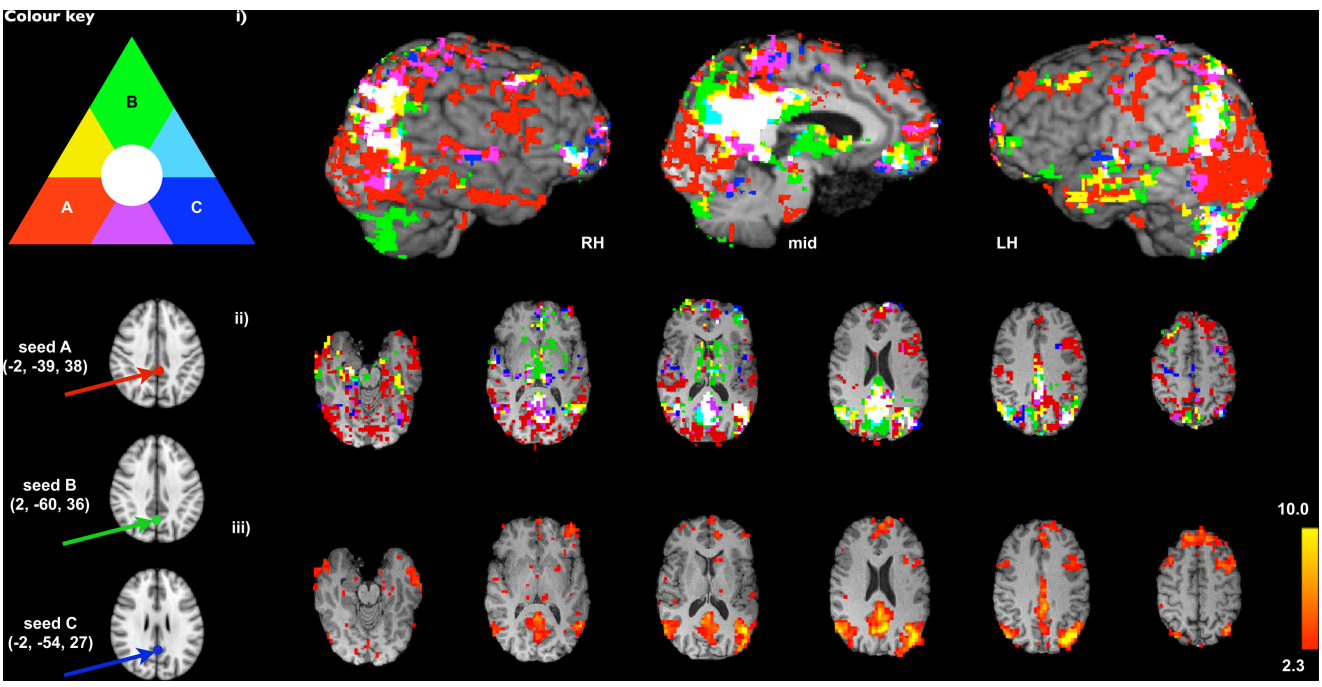

FIGURE 2 | Comparison of SCA-derived versions of the DMN using three different seed voxel locations proposed in the literature (**A**: Fox et al., 2005 in red; **B**: Singh and Fawcett, 2008 in green; **C**: Greicius et al., 2003, in dark blue). The results of SCA analysis using these seeds are displayed (i) as maximum intensity projections (searching up to 12 voxels below the surface or slice on 3-D renderings of a single subject's high-resolution MRI; RH = right hemisphere, mid = midline, LH = left hemisphere), and (ii) as binarised thresholded Z-statistic images on selected slices in the space of the subject's high resolution MRI (cluster-corrected $z = 2.3$, $p < 0.05$). It is clear from the extent of primary (non-overlapping) colours visible (largely red and green), particularly in prefrontal, occipital lobes and subcortical regions, that variations inherent in the seed-selection process can result in a large amount of variability into SCA analysis and subsequent interpretations. (iii) ICA-derived DMN map (Colour bar shows *Z*-statistic values).

within broader EEG frequency spectra (e.g., Laufs et al., 2003; Mantini et al., 2007). With respect to questions regarding the frequency-specificity of resting FMRI data, and their somewhat indirect relationship with broadband EEG spectra, it remains unclear if low-frequency BOLD oscillations can be interpreted as relating directly to the oscillatory activity of neuronal assemblies. Valuable multimodal research with BOLD FMRI and direct electrophysiological recordings, for example in the primary sensory cortices of non-human primates (Logothetis et al., 2001; Goense and Logothetis, 2008), encourages inferred associations between activity in these two data types, despite their characteristic differences in terms of temporal resolution and underlying neurophysiological causes. Indeed, it may be the case that straightforward comparisons can be made across imaging modalities, providing representations of basic sensory or perceptual processes that can validly be interpreted as being analogous. However, given that neural activity across a broad range of oscillatory frequencies is believed to contribute to multi-faceted cognitive functioning (Varela et al., 2001; Buzsaki and Draguhn, 2004), drawing similar conclusions about possible interactions between low-frequency oscillations measured by FMRI and higher frequency neuronal oscillatory activity, for example measurable via EEG, is considerably more complex (e.g., Laufs, 2008).

ACQUISITION AND PRE-PROCESSING OF RESTING-STATE BOLD FMRI DATA

It has been shown that a wide range of sampling rates and a relatively small number of datapoints, compared to the rate and number of samples acquired during the majority of task-FMRI studies, can be used to measure sufficient BOLD activity for identifying RSNs. Typical resting experiments therefore are of the order of 5–10 min, though the identification of an optimal duration of a resting FMRI session (and the possible need for multiple sessions) is an open issue. Van Dijk et al. (2010) suggest that 5 min of recording time is near-asymptotic with regard to correlation map stability. It is unlikely, however, that this generalises to cases where a more detailed parcellation of functional connectivity patterns is sought, e.g., by means of a higher-dimensional ICA decomposition (Kiviniemi et al., 2009; Smith et al., 2009), as in these cases the degree of partial temporal correlation between sub-systems increases, reducing the ability to easily delineate them. Additionally, no consensus exists as to whether there is a significant impact of the precise experimental setting, e.g., whether data is taken while subjects are asleep or awake (Horovitz et al., 2008), and with eyes open or closed (Marx et al., 2004; Bianciardi et al., 2009a). Several recent studies of the stability of RSN patterns through various sleep states (Fukunaga et al., 2006; Horovitz et al., 2009) indicate that the correlation patterns are relatively stable, except for weakening in deep sleep.

Resting BOLD data benefit from the majority of pre-processing steps routinely applied to 'traditional' task-related BOLD FMRI data (Beckmann et al., 2005; Birn et al., 2006). However, there are a number of subtle differences worth noting. For example, high pass temporal filtering applied to *task*-FMRI data may be overly aggressive with respect to removing some of the relevant RSN frequency information (though see *Spectral characteristics*), and a more conservative approach is required in order to preserve powers at low frequency.

Importantly, a substantial portion of the FMRI signal obtainable during rest can be attributed to spontaneous BOLD activity, compared to that attributable to scanner and phsyiological artefacts, even at high field strengths (Bianciardi et al., 2009b); a finding which is presumably replicable in tasks with low cognitive load. However, it has been shown that non-neuronal physiological signals may interfere with end interpretations of resting BOLD data (Birn et al., 2006). Removal of confounding signals, such as respiratory, pulsatile or cardiovascular noise is shown to improve the quality of data attributed to neural activity (Birn et al., 2006, 2008; Van Dijk et al., 2010). It has therefore become common practice in FMRI research (particularly resting-state) to monitor such signals, with specific software packages accordingly developed, to retrospectively correct for their confounding effects post-acquisition (e.g., RETROICOR; Glover et al., 2000) and it can be argued that such noise removal is of particular importance for functional connectivity studies, given the data-driven nature of the analysis, where spurious correlations induced by the presence of structured noise may severely increase the number of false-positive detections. Similarly, other sources of regionally-specific noise such as white-matter and cerebrospinal fluid signals should be accounted for in the analysis (e.g., Fox et al., 2005), as optimal BOLD signal to noise ratio in these regions is far more susceptible to artefact than in cortical grey matter (Tohka et al., 2008). A range of approaches can be employed here, either by (i) restricting the functional data analysis with binary grey matter masks thresholded at an arbitrary level (ii) by including time series from these tissues as nuisance covariates (as in **Figure 2**), or (iii) by employing probabilistic grey matter covariates in inferential analysis stages; i.e., by using additional confound regressors at the between-subject analysis stage which, for any given voxel, encode the relative proportion of grey matter for each subject.

Although concerns about the confounding influence of physiological noise and other structured artefacts in FMRI datasets are clearly warranted, in most cases it has been shown that session-level ICA methods can reliably identify and account for the artefactual influence of non-grey matter, respiratory and cardiovascular signal fluctuation on RSNs (Kiviniemi et al., 2003, 2009; Beckmann et al., 2005; De Luca et al., 2006; Birn et al., 2008). Note, however, that potential difficulties arise when attempting to separate physiological noise components from 'true' neural components using ICA [see Independent component analysis (ICA)]. Attempts to create automated artefact classification algorithms for components identified by ICA have generated mixed results, often with relatively high levels of misclassification (e.g., rates of between 0.2 and 0.3; Tohka et al., 2008). At the group level (see Group-ICA), ICA methods can potentially lose some of the power of single-session data cleanup, so group-ICA approaches may benefit from further (ICA-based or other) cleanup at the pre-processing stage (Biswal et al., 2010). Additionally, it is apparent that some artefactual components share a large degree of spatial and spectral overlap with RSNs, and at low dimensionalities even 'mix' and form parts of the same component in the end decomposition (Birn et al., 2008). However, in most cases the spatial overlap of, for example, the 'default mode network' (DMN; **Figures 1E and 2**) and artefactual respiratory components is relatively minimal, both in the majority of single-subject cases and at the group-ICA level, with peak DMN parietal nodes

being markedly distant from occipital regions strongly affected by respiratory fluctuation (Birn et al., 2008). Additionally, it has recently been demonstrated that separating these signals post-acquisition by manually increasing the dimensionality of the ICA model order, rather than having to collect and utilise physiological data, may more easily account for these confounding effects (Starck et al., 2010). Finally, of topical importance and discussed in detail below, recent evidence suggests that one specific pre-processing procedure commonly applied in connectivity analyses, that of subtracting the global mean signal, may induce spurious negative correlations between RSNs and thereby may do more harm than good (Murphy et al., 2009).

METHODS OF RSN IDENTIFICATION

SEED-BASED CORRELATION ANALYSIS (SCA)

Biswal and colleagues first identified low-frequency coherent, spontaneous BOLD fluctuations bilaterally in the somatomotor cortical regions using a seed-based approach to derive time course models of functional connectivity (Biswal et al., 1995). This method requires the *a priori* selection of a voxel, cluster or atlas region – perhaps based on previous literature or functional activation maps from a localiser experiment – from which to extract time series data. These data are then used as a regressor in a linear correlation analysis or – when augmenting the model with confound regressors of no interest – in a general linear model (GLM) analysis, in order to calculate whole-brain, voxel-wise functional connectivity maps of covariance with the seed region. This is termed *univariate* because the data in each voxel is regressed against the 'model' separately from every other voxel. The SCA technique has proven useful in revealing the connectivity properties of many seed areas, and has been applied in the literature by many groups (e.g., Greicius et al., 2003; Fox et al., 2005; Margulies et al., 2007). The primary advantage of SCA over other methods is that the approach provides a direct answer to a direct question – it shows the network of regions most strongly functionally connected with the seed voxel or ROI). This straightforward interpretability, relative to other methods, makes SCA an attractive approach for many researchers. Recent assessment of the test-retest reliability of these methods has indicated that RSN connectivity relationships can be identified by SCA with moderate to high reliability (Shehzad et al., 2009).

One potential weakness of SCA methods concerns the influence of structured spatial confounds, such as *other* RSNs (than the one under consideration) or structured noise, e.g., residual head motion effects or scanner-induced artefacts. Some of these effects may be partially removed by incorporating specific pre-processing such as temporal filtering, but the presence of residual confounds in the SCA reference time course can negatively influence SCA correlation maps in that estimated 'networks' also include voxels which describe the spatial extent of the artefact. More generally, the univariate approach of correlating the time series of a single voxel with those of each other voxel in a brain image disregards the richness of information available within the statistical relationships between multiple data points. Prior selection of the time series of one sub-region to correlate with and inform the activity of the network as a whole imposes anatomical restrictions on the measurement of network connectivity, and consequently on interpretations of systems-level hypotheses. Fundamentally there are as many possible 'networks' to be derived as there are possible seeds, so discussing and interpreting one resulting spatial map as a distinct and meaningful neurobiological system is an under-representation of the data, as all but one possible 'network' in the data are being ignored. Biologically, the choice of seed may bias connectivity findings towards specific, smaller or overlapping sub-systems, rather than larger, distinct networks (e.g., Buckner et al., 2008). Finally, these issues are all contingent on investigator-specific (seed size or location) and subject-specific (spatial normalisation or functional localisation) choices potentially resulting from the method of *a priori* seed-selection employed (see **Figure 2**). As a caveat, however, we must not underplay the importance to the current field of subjective expertise in carefully selecting seed regions, as well as in identifying and classifying RSNs, both of which have played a major role in shaping our current understanding of these effects.

To illustrate the issue of potential biases attached to seed-selection in SCA, **Figure 2** presents a number of SCA-derived versions of the DMN, alongside the same RSN estimated by ICA (also see Buckner et al., 2008). The DMN seed locations in MNI standard space were selected from three papers in the resting-state FMRI literature: A: Fox et al. (2005, red); B: Singh and Fawcett (2008, green) and C: Greicius et al. (2003, dark blue). Results of SCA using these seeds were calculated using white-matter, CSF and motion confounds, and are displayed as maximum intensity projections (**Figure 2i**), and as binarised statistical maps on selected slices in the space of the subject's high resolution structural MRI (**Figure 2ii**, cluster-corrected $z = 2.3, p < 0.05$). Though there is significant overlap in the extent of the inferred networks independent of the seed voxel location (white), it is clear from the extent of primary (non-overlapping) colours visible (largely red and green), particularly in prefrontal, occipital lobes and subcortical regions, that biases inherent in the seed-selection process can result in a large amount of variability into the results and subsequent interpretations. In order to validly discuss SCA results in terms of networks, some form of consensus mapping is required, where the different versions of a network are combined in order to generate a single consistent representation (e.g., using information theoretic principles such as clustering or principal component analysis (PCA) across the different maps). **Figure 2iii**, for comparison, shows the ICA-derived DMN map from the same data (where the model order, i.e., the number of components, was estimated from the data; see Beckmann and Smith, 2004, for details). Amongst the set of four spatial maps this component map has highest mean spatial correlation with the other three estimates of the DMN. The ICA approach, more fully discussed in the next section, therefore can be viewed as one possible way of generating such consensus maps, eliminating the need to specify explicit seed locations, though at the expense of losing specificity in relation to a single well-defined seed of interest. Note, however, that other aspects of the analysis (such as the choice of the model order in ICA, see below, or the number and nature of confound regressors in a SCA) are likely to introduce other types of variability in the final outputs.

It is important to note here that 'validating' network connectivity maps by simply highlighting visual similarities with a network identified by ICA, a practice adopted increasingly frequently in SCA studies, is not necessarily optimal for comparator selection or useful in terms of inference, without detailed quantification of

this similarity. Importantly, for the above-demonstrated reasons, a large number of researchers are beginning to additionally adopt multivariate methods such as ICA in their standard approaches to analysing spontaneous BOLD fluctuations. Such approaches avoid many of these problems and thereby have complementary advantages to those of SCA methods. Finally, we should re-emphasise the main advantage, with SCA, of being able to ask a straightforward question about connectivity, and receiving a direct answer (within the limit of being able to formulate the original question by means of a well-defined seed).

INDEPENDENT COMPONENT ANALYSIS (ICA)

Initially recognised within neuroscience as a valuable method of separating multiple, uncorrelated signal waveforms in EEG data, ICA was first applied to FMRI data collected during an experimental task (McKeown et al., 1998). Later the same techniques were applied to resting-state FMRI data (Kiviniemi et al., 2003). ICA works by decomposing a two-dimensional data matrix into the time courses and associated spatial maps of the underlying 'hidden' signal sources. Although a number of differing approaches to ICA are used in neuroimaging (implemented as separate software packages), common concepts and core methods underlie their application. One common approach is to estimate maximally statistically independent, non-Gaussian components from FMRI data, by optimising a measure of non-Gaussianity in the estimated maps. Although ICA estimates component maps of maximal spatial independence (from each other), this does not preclude spatial overlap between components (see Beckmann et al., 2005 for details) The ICA method of exploratory FMRI analysis is regarded as preferable to that of PCA, as the spatial independence enforced upon components by (spatial) ICA dictates only that their time courses not be highly co-linear, resulting in a more biologically plausible systems model than that obtained from a PCA decomposition where the analysis enforces orthogonality between time courses, precluding the detection of signals which partially correlate in the temporal domain. Note that while temporal ICA can be carried out as an alternative to spatial ICA (component time courses are orthogonalised but spatial maps are not), it suffers from the same orthogonality issue as PCA and is more susceptible to noise due to the typically smaller number of observations available to drive the estimation.

Importantly, as with SCA, use of the ICA approach has identified networks of spontaneous coherence comparable to known sensory and cognitive processing systems (e.g., **Figure 1**). Persuasively, these include the somatomotor cortical connectivity network found in the first resting connectivity experiments (Biswal et al., 1995), sensory systems in visual and auditory cortices, and, of particular interest to those applying imaging to neuropsychiatric populations, networks apparently reflecting higher-level cognitive processes (e.g., the DMN). In this comparatively unrestricted way, ICA has been used to generate a 'complete' (if simple) picture of the functional hierarchy of integrative and dissociative relationships making up the spontaneous and evoked activity of the human brain (Kiviniemi et al., 2009; Smith et al., 2009). RSNs identified by ICA can be less prone to artefactual effects from noise (including fluctuations in the mean global signal) than those from SCA (see Acquisition and pre-processing of resting-state BOLD FMRI data; also Birn et al., 2008; Murphy et al., 2009), due to the ability of the method to account for the existence of such structured noise effects within additional (non-RSN) ICA components.

Despite some advantages over SCA approaches in terms of avoiding prior spatial assumptions and noise attached to the seed, and the ability to simultaneously compare the coherence of activity in multiple distributed voxels, ICA is not without its challenges. First, unlike PCA, an ICA decomposition is obtained by means of iterative optimisation. This stochastic nature induces a degree of run-to-run variability, so results obtained from such an analysis can differ between analysis runs on even the same data. This type of variability can be reduced when selecting more stringent convergence criteria and software now exists that enables ICA repeatability testing (e.g., ICASSO; Himberg et al., 2004), which can be used to investigate the degree of variability, and estimate 'average' decompositions from across multiple ICA repeats.

Secondly, the processes of dimensionality reduction and model order selection are somewhat arbitrary (i.e., one has to tell ICA how many components to estimate). While approaches exist to optimally select the number of independent components for a given dataset according to *statistical* criteria (for recent reliability testing of multiple models see Zuo et al., 2010b), it must be recognised that there can be no single, 'best' dimensionality or model order for the underlying neurophysiology of multiple distributed systems. There will always be multiple valid solutions for characterising the hierarchical complexity of RSN functional neurobiology. This level of ambiguity simply mirrors the general ambiguity in characterising the brain's functional organisation: while we may validly conceptualise the existence of a visual, auditory, sensory-motor or language system, a more fine-grained characterisation might separate this into specific areas such as the hand knob, visual word form area, fusiform face area etc. Each one of these different types of characterisation is valid at a particular level of complexity. In the case of ICA decompositions, higher dimensionalities of the model have recently been advocated (Kiviniemi et al., 2009; Smith et al., 2009), although the robustness of a given level of decomposition relies on being supported by data quality (e.g. one cannot expect a *robust* 100-dimensional ICA decomposition from a typical 5-min single FMRI session).

Finally, whereas SCA guarantees a result in terms of identifying the brain regions most associated, or functionally connected, with the selected seed (presumed to closely correspond to *the* associated RSN), ICA results may be 'split' into a number of sub-networks, depending on the parameters of the analysis (e.g., at high model order dimensionalities). This can result in the estimation of a large number of components, which may be difficult to identify and classify (Tohka et al., 2008). Further, one ICA decomposition of a given dataset may hide the fact that any given brain region may, over time, share varying connectivity patterns with multiple networks. This variability, or ambiguity, of regional co-activations between network nodes can be referred to as the 'nonstationarity' of a given area in terms of its connectivity with one or more RSNs, and equally affects multiple analysis approaches (for specific investigation of this, see Chang and Glover, 2010, and, with respect to nonstationarity at the neural level, see Popa et al., 2009).

FREQUENCY-DOMAIN ANALYSES

Since Cordes and colleagues originally characterised a number of functional networks of interest as low-frequency BOLD fluctuations, interest in understanding the frequency-specific characteristics of RSNs has developed in parallel to correlation-based methods (Cordes et al., 2000). Specific techniques that have emerged to investigate these aspects of RSN phenomena include 'amplitude of low frequency fluctuations' (ALFF) indices (Zang et al., 2007). The ALFF index is calculated by averaging the square root of the power spectrum of a given low-frequency BOLD time course across the frequencies filtered, then standardising the value relative to the global mean ALFF value. The assumption that all relevant neuronal information contributing to resting-state BOLD fluctuations can be represented by a single figure, calculated only from information inherent in the frequency domain, runs into problems when considering the argument for a greater level of broadband content in neural RSN oscillations than previously thought. This raises the possibility that potentially interesting information is being removed from the analysis by these mathematical procedures. Additionally, some work has suggested that low-frequency measures of resting data may be rather susceptible to cerebral vascular and respiratory artefacts (Zuo et al., 2010a). Indeed, some aspects of the spatial maps derived from these techniques can appear, at least under qualitative examination, to resemble patterns queried as artefactual by experimenters using other techniques, particularly in midline brain regions (e.g., Birn et al., 2006, 2008).

With these issues in mind the ALFF approach has been more recently refined to account for 'fractional' inclusion of information in frequencies outside of the normal range (fALFF; Zou et al., 2008). This is accomplished by calculating 'the ratio of the power at each frequency to the integrated power of the entire frequency range' (i.e., summing the oscillatory amplitudes across the 'typical' 0.01–0.08 Hz range, then dividing by the amplitude sum across a more inclusive range of 0–0.25 Hz). Additionally and optimally, this amended approach involves no bandpass filtering. Although questions may remain over the susceptibility of these techniques to physiological noise, recent independent testing reveals both ALFF and fALFF to have moderate to high levels of reliability and consistency in terms of the (primarily midline) spatial patterns generated (Zuo et al., 2010a). Furthermore, useful diagnostic information about neural processes may be present in the oscillatory amplitude envelopes (e.g., Zang et al., 2007; Zuo et al., 2010a). Such techniques may thereby provide a useful complement to approaches such as SCA and ICA investigating, for example, inter-regional coherencies between multiple BOLD signals (e.g., as applied by Anand et al., 2005).

A number of other frequency-dependent and time-series statistical approaches exist that can be applied to the analysis of spontaneous oscillatory activity in BOLD data. These include linear or nonlinear comparison of fractal dynamics (Wink et al., 2008), measures of frequency-specific mutual information (Salvador et al., 2007), and graph theoretic investigation of such networks in the context of their 'small-world' characteristics by multivariate partial correlation of spectral information from predefined ROIs (Salvador et al., 2005; Achard et al., 2006; Stam and Reijneveld, 2007).

REGIONAL HOMOGENEITY

The regional homogeneity (ReHo) method (Zang et al., 2004) is based on 'Kendall's coefficient of concordance'. This technique is sensitive to the 'purity' of clusters identified as expressing high functional connectivity with a model time series within a given cluster. By virtue of the assumption that neighbouring voxels are temporally similar, clusters identified as strongly connected during task or rest can be tested for their inner homogeneity and the degree to which this is modulated by a given paradigm or differs between groups (e.g., Liu et al., 2006; Paakki et al., 2010). The temporal variability within a cluster is reflected in the assigned homogeneity score. Advantages of the ReHo technique over, e.g., SCA, include its relative insensitivity to possible region-to-region and/or trial-to-trial variability of the haemodynamic response function. Also, unlike with ICA, no assumptions are made regarding the spatial independence of identified maps, and extensions to group analysis are relatively straightforward (Zang et al., 2004). However, this approach is fundamentally local in nature and therefore exhibits a high degree of sensitivity to different levels of spatial smoothing. Also, the insensitivity to shape differences between clusters does preclude drawing inferences on the degree of correspondence between spatially remote regions, making it difficult to characterise the distributed nature of RSNs (Zang et al., 2004).

GROUP ANALYSIS OF RSNs

The majority of techniques for multi-subject analysis of resting-state functional connectivity are not yet as well developed as at the single-subject level. Hence we here discuss only the fundamental principles, and recent advances relating to the two methodologies applied most widely: SCA and ICA. Most of the above-outlined pros and cons of both of these approaches still apply at the group level, along with additional caveats common to all attempts to combine functional neuroimaging datasets in this way, e.g., issues related to co-registration of data into a common space. The gross variability in cortical thickness, folding and, often, functional localisation between separate individuals or subject populations may cause problems for group level inferences. Such variability may instil a registration bias in the location of group analysis inputs (seed-ROIs) or outputs (one or more functionally connected nodes) towards one group or other, or towards a specific subjective characteristic. Similarly, the potential for mis-registration of individual session FMRI data following spatial normalisation may result in functionally segregated, but proximal, regions being assigned the same neuroanatomical label across subjects, marring valid inference. These sources of variability are local in nature and therefore their impact on inferred connectivity patterns is more prominent in voxel-based SCA. In cases of a region-based SCA or ICA such variability typically results in blurring of the estimated spatial patterns (see e.g., **Figure 1**).

One recent study suggests that the network properties of systems, in terms of 'small-world' characteristics inherent in connectivity relationships between nodes, are better approximated by using single voxel seeds rather than larger ROI seeds (Hayasaka and Laurienti, 2009). However, it seems possible that this may be true of a-priori ROIs (such as derived from a standard space template), but that data-derived ROIs (in analogy to ICA spatial maps) would result in seed regions with better performance.

The caveats listed above must inform any assumptions made when extending these findings to robust, efficient and unambiguous group-level interpretations of alterations in biologically plausible networks and their relevance to behaviour.

GROUP-LEVEL SCA

Approaches to SCA, while widely applied and sharing common basic principles, are not universally standardised in terms of group analysis methods. Specifically, methodologies can vary in terms of the precise information brought forward from single-subject analyses to the higher level. In practice, most SCA group studies carry forward voxel-wise regression coefficients (e.g., Greicius et al., 2003) or correlation coefficients (e.g., Fox et al., 2005). These values are identified from an initial, whole-brain analysis of the functional connectivity with the time series extracted from a given seed region. At the higher level, these values are then converted to Z-statistics and averaged across subjects in a standard GLM, followed by standard hypothesis testing. The latter may or may not take into account between-subject variability, i.e., be a mixed-effects or fixed-effects cross-subject analysis).

GROUP-ICA

Although interest in RSN analysis has grown heavily over the past few years, it is only fairly recently that coherent methods have been proposed and validated for comparing such broad, systems-level activity patterns across subjects and/or sessions within an ICA-based framework. One immediate problem when running separate ICA decompositions in separate subjects is that of having to identify the correspondence between estimated spatial components, i.e., selecting which components to carry up to a between-subject analysis. Considering the possible existence of multiple different solutions even within the same subject's data, there might not be any consistent one-to-one mapping between estimated sets of component maps when compared across different subjects. Early efforts advocated running single-session ICA, separately for each subject, then attempting to find the 'best-fit' component to an *a priori* RSN template at the individual level, to carry forward to group comparison stages (e.g., Greicius et al., 2003; Esposito et al., 2005; De Luca et al., 2006). The self-organising, hierarchical clustering of independent components method (Esposito et al., 2005), for example, involves carrying out single-session ICA prior to group analysis with multiple runs (for repeatability testing). However, these approaches are susceptible to the effects of multiple sources of gross variability inherent to unconstrained resting-state FMRI data. Although we know RSNs to be *largely* consistent across healthy individuals (Damoiseaux et al., 2006), there are no guarantees of *exact* correspondence of identified component maps, including RSNs, across subjects. As mentioned above, at a given ICA dimensionality, one RSN could be potentially split into two sub-networks in some subjects, and appear as a single component in others. Such problems may even be driven purely by a difference in the amount of structured noise in certain subjects. This can lead to misinterpretation of apparent subject differences. Similarly, some researchers have advocated the use of separate 'group-ICA' runs per group or experimental condition to be compared prior to further GLM comparison (e.g., Harrison et al., 2008a,b). However, this approach may also be sub-optimal, as it biases towards false-positive findings of group or between-session differences (Calhoun et al., 2001; Beckmann and Smith, 2005).

Further, single-subject ICA followed by group-level matching of components across subjects fails to take advantage of the additional effective signal-to-noise present when all subjects are analysed simultaneously (for example, by the group-ICA methods described below). It is for this reason that group-level ICA can generally support a much higher-dimensional (and therefore more finely-detailed) decomposition than single-session ICA. On the other hand, single-subject ICA has much greater power to model/ignore session-level structured noise than group-level ICA approaches.

Working from the 'top down' by starting with a group-level ICA, and generating subject-specific versions of the resulting group maps solves the problem of between-subject RSN correspondence inherent in the process of combining single-session ICA data.

The first group-ICA model to emerge for FMRI was applied to task data (Calhoun et al., 2001). In the first step of this procedure, data from all subjects are spatially normalised and dimensionality-reduced via PCA (separately for each subject). These reduced datasets are then assumed to contain the most important source signals that have been 'mixed' into the measurements. All reduced datasets are temporally concatenated prior to the application of group-ICA. This identifies voxels that share common temporal patterns of response within and between subjects. By means of temporal concatenation of multiple datasets (**Figure 3**; also see Calhoun et al., 2001), group-ICA can thereby estimate group-level independent components, including RSNs (Beckmann et al., 2005). Due to the unconstrained nature of original BOLD signals in resting data across sessions and subjects such a concatenation approach is more suitable than an alternative tensor ICA method (Beckmann and Smith, 2005).

In order to enable voxel-wise between-subject comparisons Calhoun and colleagues propose to create individual subject components from the group-decomposition via PCA back-projection/reconstruction (Calhoun et al., 2001). Further extensions of this approach enable the testing of within-network (Calhoun et al., 2004a) and between-network (Jafri et al., 2008) connectivity relationships across different task conditions or subject groups. The back-projection method estimates, at the subject level, temporal and spatial information associated with each group component, by projecting the original single-subject data onto projection matrices which combine the group-level unmixing matrix and the subject-level PCA-derived matrices used for dimensionality reduction. Because these PCA matrices are calculated separately for each subject there is no guarantee that, in the reduced data space, consistent (across subjects) information is retained. Hence this approach can suffer from similar issues to those described above as problematic for combining single-session ICA datasets prior to group analysis. The dependence on subject-specific PCA reduction raises the probability of session-specific noise contributions sub-optimally influencing further analyses, thereby confounding any final cross-subject RSN comparisons.

A more recent approach (Beckmann et al., 2009; Filippini et al., 2009) estimates subject-specific RSNs from information contained within the original functional data via a 'dual regression' technique. This approach differs from back-reconstruction by using regression of the group-ICA spatial maps against the original, individual session, functional datasets. The spatial maps from a group-ICA decomposition are first used as a set of GLM (spatial) regressors in a multiple regression analysis. This process generates individualised, session-specific time courses for each independent component in

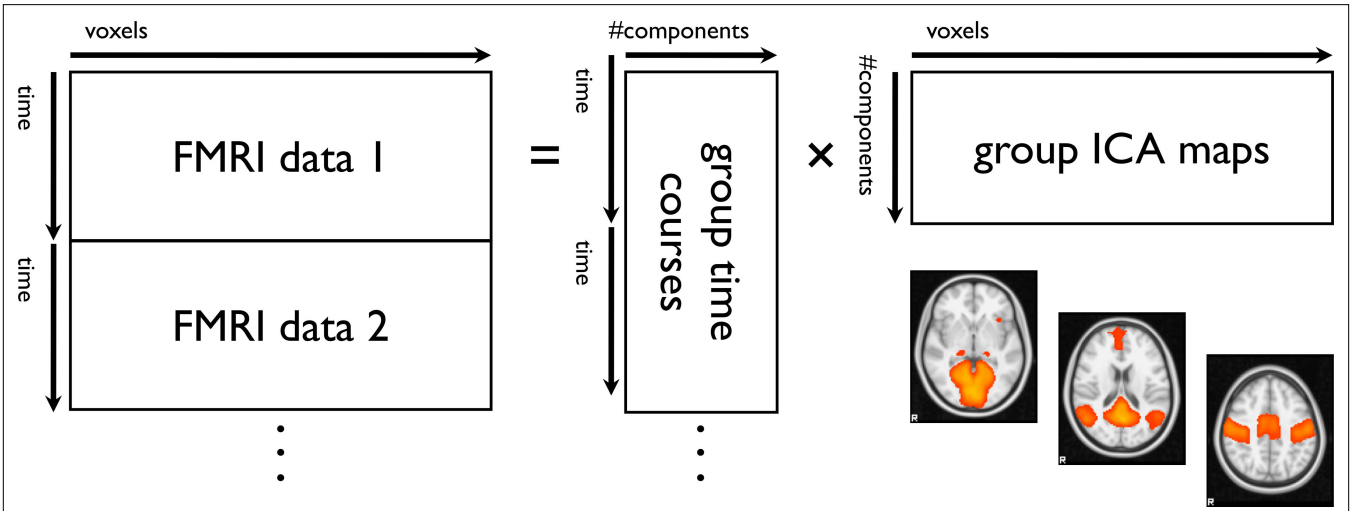

FIGURE 3 | Schematic for temporal concatenation group-ICA.

each subject's functional dataset (also see Calhoun et al., 2004b). These time courses, rather than matrices calculated as part of back-projection, are then normalised and used as GLM (temporal) regressors in a second multiple linear regression against the functional datasets. This generates individualised spatial maps for each original group-level component. The analysis is carried out in a standard coordinate space, so that cross-subject voxel-wise non-parametric statistical testing of RSNs can be carried out. Estimated time series and spatial maps form unbiased least-squares approximations to the original ICA maps at the individual subject level. Note, however, that because the original ICA maps (as well as the subject-specific dual regression estimates) are derived in a data-driven fashion we can not use simple parametric tests in the between-subject analysis and therefore need to resort to non-parametric statistical assessments. This approach has been validated in terms of its ability to estimate session-level RSNs from group-level ICA spatial maps, consistently and more reliably than single-session template-matching approaches (Zuo et al., 2010b).

CONTROVERSIES

It is of course interesting to discuss the most cutting-edge methodological and conceptual advances in current and future resting-state FMRI research. However, it is equally important to note some methodological and conceptual limitations, which it is necessary to be mindful of when conducting and interpreting such research.

ANTI-CORRELATED NETWORKS

A number of studies identifying inverse temporal relationships between systems referred to, for example, as task-positive and task-negative networks, in both the presence and absence of overt cognitive stimulation, have proposed that this coupling may be functionally relevant (Fox et al., 2005; Fransson, 2005; Castellanos et al., 2008; Kelly et al., 2008; Zuo et al., 2010b). Specifically, this phenomenon is thought to hold functional significance in domains of attention, higher cognitive control and even consciousness, by reflecting the efficiency of neural resource allocation between competing and interacting systems, and ultimately the efficiency of global cognitive processing (Fox et al., 2005; Kelly et al., 2008). Similarly this issue may be central to disorders associated with cognitive impairment (Wang et al., 2007; Castellanos et al., 2008). However, there has been vigorous debate about the true 'negativity' of such between-network relationships. Principally, it is apparent that global mean signal regression, a pre-processing procedure routinely carried out in many SCA studies in order to correct for the influence of global, non-neuronal physiological noise, will bias towards finding such an effect of negative coupling, or 'anti-correlation,' between RSN time series (Murphy et al., 2009). This finding may have important implications regarding the validity of a large portion of prior interpretations, primarily between the so-called task-negative DMN and task-positive attentional/cognitive control RSNs. However, whether these procedures actually *create* such an effect, or rather artificially enhance 'true' negative relationships existing between cognitive control RSNs, remains contentious, as multiple studies have not reached identical conclusions on this issue (Chang and Glover, 2009; Fox et al., 2009; Weissenbacher et al., 2009; Van Dijk et al., 2010).

An illustration of the simple mathematical steps underlying the removal of the global mean signal from any given data pool is given in **Figure 4**. The removal of the global mean signal inevitably maps existing correlations into the full correlation range -1 to 1. This does indeed maximise the ability to delineate RSNs from each other, but at the expense of rendering the numerical value (and sign) of the correlation uninterpretable. Note that pair-wise correlations are altered systematically and dramatically without changes to the existence, structure or consistency of individual networks.

Despite outstanding questions regarding the methodological implications of artificially induced negative correlations between time series, their potential relevance to function should not be categorically disregarded (see e.g., Popa et al., 2009). Indeed, the one critical finding on this issue may be precisely that of the great

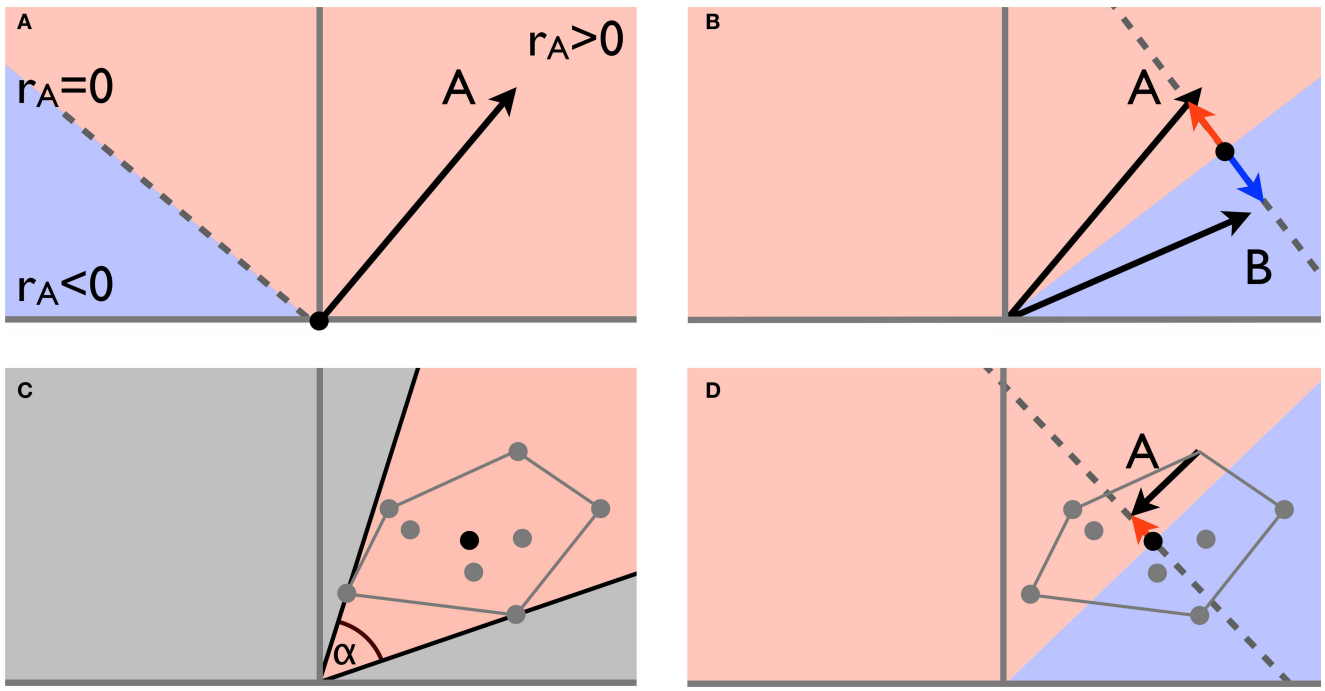

FIGURE 4 | The vector-space illustration of global mean regression. (A) The characteristic time series for network A can be described as a single point in a high-dimensional vector space. Relative to 0 (the zero time series, black dot) the orthogonal plane (dotted line in this example) separates the vector space into an area of positive correlation ($r_A > 0$) and a subspace of time series negatively correlated with A. The correlation between A and any other point is defined by the (cosine of) the inner angle: all points within ± 90° are positively correlated with A, whereas all other points are negatively correlated with A; **(B)** when regressing out the mean of two network-specific time series A and B, the 0 reference point is moved half-way between the two points and the original time series get projected onto the subspace perpendicular to this mean, thereby inducing perfect anti-correlation between A and B as the new characteristic vectors are now aligned at 180°; **(C)** in the more general case of multiple networks (grey dots) the range of possible differences in pair-wise correlations is again determined by the maximum range of the inner angles α: if α is small, pair-wise correlations differ by only a small amount and delineation of different networks becomes difficult, in this example all pair-wise correlations are positive; **(D)** the global mean necessarily lies within the convex hull spanned by all the individual characteristic time series. Global time-series regression moves the 0 reference point somewhere into the convex hull, thereby inevitably inducing spurious negative correlations between the characteristic time series associated with different RSNs. Global mean regression does increase the maximum inner angle between pairs of time courses and therefore facilitates delineation of networks from each other; the resulting correlation scores (and signs thereof), however, are no longer interpretable and reference to these should be avoided.

variability in the degree (and direction) of observed correlations between the DMN and multiple, inconsistently identified task-positive networks at rest. This seems to hold true in comparisons across individuals, and even over time within the same subject; whether between different scanning sessions or within a single session (Chang and Glover, 2010). Based on this, it is important to investigate which factors (e.g., see Applications and extensions) contribute to changing the nature or strength of this relationship, as measured by correlations, with external expressions of behaviour or experimental manipulations. For example, in a recent study testing subjects across different conditions of pharmacotherapy, we overcame these methodological issues in two ways (Cole et al., under review). First, we employed multivariate, probabilistic ICA methods that do not involve global mean signal regression as a pre-processing step, and can account for non-neuronal physiological noise, thereby allowing the independent assessment of correlative relationships between RSNs previously identified as anti-correlated in the literature. Second, we characterise network relationships by means of examining the dynamic changes in the correlation between networks, identified by repeat measures between conditions *within-subjects* (see **Figure 5**). As a method of assessing changes in the correlation between RSNs, such an approach may be complementary, even preferable, to between-group comparisons of RSN spatial maps generated by ICA or *a priori* seed region correlation. By focussing not just on differences between assumed 'static' RSN spatial maps, but also the time-varying, condition-specific characteristics of dynamically fluctuating systems, we avoid making restrictive anatomical assumptions that could limit the interpretability of between-network functional connectivity findings.

NETWORKS WITHIN-NETWORKS

Further to inconsistencies in connectivity relationships identified between networks, it is evident that such relationships can also vary *within* RSNs. For example, prior studies have proposed that distinct patterns of functional connectivity exist, which share some spatial overlap in their foci, but underlie different aspects of cognitive control (Dosenbach et al., 2007; Seeley et al., 2007). With an ICA-based approach one relevant point to consider here is the potential for 'splitting' of networks identified by increasing the number of components. Seeley et al. (2007) identified such a split in

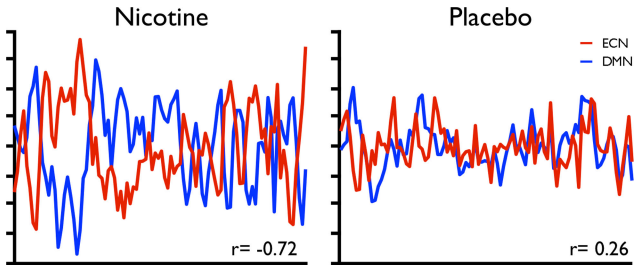

FIGURE 5 | Variability in the strength of inverse coupling between two RSNs (the DMN and a putative executive control network sharing spatial similarity with a combination of regions overlapping with RSN maps from Figures 1F,G,H) associated with individual differences in therapeutic behavioural changes following nicotine pharmacotherapy, compared to placebo. These data are taken from a single subject within a group of smokers tested using resting-state FMRI with repeat measures in a double-blind, placebo-controlled, crossover design (reproduced from Cole et al., under review).

a network suggested to be involved in executive function, revealing separate purported 'control' and 'salience' networks, an effect which has since been replicated (Sridharan et al., 2008; Kiviniemi et al., 2009) and further bolstered by functional and structural evidence from multiple neurological disorders (Seeley et al., 2009). In studies attempting to fully parcellate the complex functional hierarchy of neural sub-systems, the use of high-dimensionality ICA is an important and useful tool (Abou-Elseoud et al., 2010). However, it is important to distinguish between the value of varying the model order to prove a technical methodological point (i.e., demonstrate that systems *can* be made to split into sub-systems, potentially unrelated to the ability to assign biologically meaningful interpretations to such splits), and the value of concentrating on interpreting the results of a testable systems-level hypothesis in larger networks identified at lower model orders.

RECIPROCAL TASK-REST INTERACTIONS

Many authors, including those of the current article, are guilty of referring to the signals identified by various methods as RSNs (or similar terminology), when measurements have not *per se* been collected in the 'resting-state'. Studies incorporating passive visual stimulation, instructed or self-initiated changes in mental state or focus, or occurring immediately following some other experimental manipulation, cannot be described as occurring during true, stimulus-unguided rest. However, a mass of novel data is rapidly rendering such dichotomous distinctions between experimental and resting-states as conceptually unhelpful (Fox and Raichle, 2007; Poldrack et al., 2009; Van Dijk et al., 2010). Firstly, it has been established that the same functional networks are cohesively active during a multitude of tasks as well as at rest (Smith et al., 2009). Secondly, several recent studies have demonstrated direct evidence of the influence exerted by task-related activity and performance over network activity in resting periods, and *vice versa*. The existence and strength of two-way interactions between task and 'RSN' activity has been linked to adaptive learning (Albert et al., 2009; Lewis et al., 2009), response to or recovery from high cognitive load (Pyka et al., 2009; Van Dijk et al., 2010), and individual differences in (Fox et al., 2007; Hesselmann et al., 2008; Hasson et al., 2009; Sadaghiani et al., 2009), or fine-tuning of, cognitive performance (Singh and Fawcett, 2008). Further study is required to establish fully the range and nature of such relationships over varying periods of time.

CORRELATION AND CAUSALITY

As is typically the case in task-FMRI studies, the majority of applied resting-state research also presents the results of statistical analyses (of spatiotemporal, neurophysiological information assumed to reflect neuronal processes), in conjunction with interpretations suggestive of cognitive and behavioural meaning. While strong correlations (e.g., between strength of a network such as the DMN at rest, and a behaviour measure such as reaction time or accuracy in a task) encourage conclusions of said RSNs being relevant to cognitive function, clinical presentation or treatment responsiveness, we can only speculate about the precise order of events and causal relationships between the nodes in this dynamic processing stream.

Dynamical Causal Modelling (DCM, Friston et al., 2003), a popular approach for estimating effective connectivity between brain regions, relies on bilinear neural state equations where system dynamics are induced by external driving inputs, representing experimental manipulations or changes in experimental conditions. As such, DCM is currently ill-suited for the investigation of effective connectivity in resting FMRI data. In other work, attempts to estimate causal relationships between brain regions using lag-based methods such as Granger Causality Analysis (GCA, Goebel et al., 2003) are also problematic. Haemodynamic "blurring" of the neural processes underlying the FMRI signal swamps any causal lag in the neural dynamics (typically of the order of a few milliseconds), and, further, variations in haemodynamic delay across brain regions (potentially of the order of seconds) will cause overwhelming bias in any attempt to estimate causality, thus rendering any causal inference unsafe (David, 2008). Even the original proponents of GCA for FMRI state that "...one should rule out the possibility that influence found from one area to another based on temporal difference in signal variation is due to a systematic difference in the hemodynamic lag at the two areas." (Roebroeck et al., 2005). Unfortunately, in FMRI, we have in general no control over haemodynamic variabilities, and so cannot expect to use such analysis methodologies to estimate causality. Finally, however, there is the potential for more sophisticated network analysis methodology (such as Bayesian Network modelling) to infer causal connections, at least for networks with a limited numbers of nodes, but much work remains to be done to develop and validate these approaches for resting FMRI data; see Ramsey et al. (2010) for pioneering work in this direction.

When analysing the relationship between different networks, questions that remain include whether or not specific RSNs of interest have an optimal degree of coupling with others. It could, for example, be that the activity in the DMN is suppressing activity and/or synchronicity in one or more task-positive networks during rest, and vice versa during task performance. Is this due to incidental network-specific over- or under-activity, or due to 'true' between-network dependencies? Are non-stationary shifts in between-network dynamics interpretable in terms of causal factors? Further study is required in order to address such questions, and that of which specific RSN nodes are involved in maintaining optimal relationships of within- and between-network

connectivity (e.g., Sridharan et al., 2008). Indeed, FMRI alone may be unsuitable for attributing causality in this way (Ramsey et al., 2010), so multimodal approaches are required to provide further insight into such questions, for example via combining resting-state and task-FMRI with EEG or transcranial magnetic stimulation methods.

APPLICATIONS AND EXTENSIONS

The methods presented here are now being widely applied by many imaging researchers worldwide, to probe specific questions relevant to brain function. Notable applications include those investigating individual differences, disease, development, neuroplasticity and treatment efficacy.

In the field of genetics, for example, specific allele variants implicated in neurodegeneration (Filippini et al., 2009), neurodevelopment (Thomason et al., 2009) and cognitive function (Liu et al., 2010) have been associated with RSN functional connectivity phenotypes. Further, identification of these neural connectivity patterns extends into domains of actual clinical presentation, for example in Alzheimer's disease (Greicius et al., 2004; Wang et al., 2007) and other neurodegenerative diseases (Seeley et al., 2009), normal aging (Andrews-Hanna et al., 2007; Damoiseaux et al., 2008), as well as multiple neuropsychiatric (Liu et al., 2006; Greicius et al., 2007; Salvador et al., 2007; Jafri et al., 2008) and neurodevelopmental disorders (Zang et al., 2007; Castellanos et al., 2008; Di Martino et al., 2009; Paakki et al., 2010). Of particular importance is the fact that, relative to task-FMRI, such resting-state investigations require minimal task compliance and therefore allow for the study of differences in brain dynamics in non-normal populations, such as infants, sedated subjects or subjects with severe cognitive or physical impairments. Functional connectivity within and between distinct RSNs can be implicated in a very diverse range of behaviours and neuropsychiatric disorders. In particular, studies have identified a plethora of such relationships involving the DMN (for reviews see Buckner et al., 2008; Greicius, 2008; Broyd et al., 2009). Existing results are promising, suggesting RSNs may be used to characterise patterns of neural activity and coherence approximating functional variability across multiple application domains. However, large 'proof-of-concept' studies with high statistical power (see e.g., Biswal et al., 2010), as well as ongoing meta-analytic research, will make a valuable contribution to the field in years to come.

As noted before (Greicius, 2008), applications of these correlative relationships (typically derived and significance-tested for proof of concept at the group level) to providing clinical diagnostics at the single-subject level are currently far from fully realised. Despite such concerns, pseudo-diagnostic information associating RSN function with within-subject dynamic, intervention-related changes in neurophysiology or behaviour are already apparent, for example in fields of learning (Albert et al., 2009; Lewis et al., 2009) and pharmacological intervention (**Figure 5**; Anand et al., 2005). Additionally, preliminary evidence exists for RSN-related metrics as potential screening devices, for example in Alzheimer's disease (Rombouts et al., 2005; Fleisher et al., 2009).

The study of RSNs has revealed, and will continue to reveal, many interesting observations of the way in which spontaneous connectivity patterns alter under different conditions, though the concrete meaning of these inherent processes, seemingly fundamental to the human neural functional architecture, remains elusive. Task-based FMRI studies have provided the opportunity to test strict hypotheses regarding the discrete activity of a small number of regions in a given derived task model, albeit without necessarily explaining the true distributed nature and complexity of human brain function. One is led to expect that RSN activity measured with the exclusion of artificial, experimentally guided regional BOLD changes may provide a better approximation to the 'baseline' of brain function. However, the unrestricted nature of this data obviously engenders something of an interpretative minefield.

In order to use RSNs to generate a comprehensive neurocognitive functional ontology, it may therefore be beneficial to adopt an approach combining both task- and resting-FMRI. Whereas the majority of resting-state FMRI research has progressed with a view to the potential for results to 'complement' the findings of task-FMRI, one way of addressing questions of functional specialisations and interactions with RSNs may be to turn the system on its head, and adapt task-based approaches in order to *complement* and bolster the interpretations garnered from studies of spontaneous activity patterns, or RSNs. Due to the historic tendency for prior FMRI studies to avoid reporting or discussing task-related *de*activations, this approach may particularly complement existing meta-analytic research comparing resting-state and task-activation studies. Hints at how such a groundbreaking approach might progress are starting to emerge in the literature, either via meta-analytic approaches (Smith et al., 2009) or augmentation of the experimental method (Poldrack et al., 2009). Future extensions should enable a more direct comparison of 'mental state' and resting-state network activity, enabling more definitive classification and diagnostic application of the latter, and thereby ultimately contributing to the thorough characterisation of the human neural functional architecture.

ACKNOWLEDGMENTS

This work was supported by funding from the UK BBSRC and GSK. We thank all involved in the collection of data presented in **Figure 2**, which are provided courtesy of the GSK Clinical Imaging Centre.

REFERENCES

Abou-Elseoud, A., Starck, T., Remes, J., Nikkinen, J., Tervonen, O., and Kiviniemi, V. (2010). The effect of model order selection in group PICA. *Hum. Brain Mapp.* [Epub ahead of print] doi:10.1002/hbm.20929.

Achard, S., Salvador, R., Whitcher, B., Suckling, J., and Bullmore, E. (2006). A resilient, low-frequency, small-world human brain functional network with highly connected association cortical hubs. *J. Neurosci.* 26, 63–72.

Albert, N. B., Robertson, E. M., and Miall, R. C. (2009). The resting human brain and motor learning. *Curr. Biol.* 19, 1023–1027.

Anand, A., Li, Y., Wang, Y., Wu, J., Gao, S., Bukhari, L., Mathews, V. P., Kalnin, A., and Lowe, M. J. (2005). Antidepressant effect on connectivity of the mood-regulating circuit: an FMRI study. *Neuropsychopharmacology* 30, 1334–1344.

Andrews-Hanna, J. R., Snyder, A. Z., Vincent, J. L., Lustig, C., Head, D., Raichle, M. E., and Buckner, R. L. (2007). Disruption of large-scale brain systems in advanced aging. *Neuron* 56, 924–935.

Beckmann, C. F., DeLuca, M., Devlin, J. T., and Smith, S. M. (2005). Investigations into resting-state connectivity using independent component analysis. *Philos. Trans. R. Soc. Lond., B, Biol. Sci.* 360, 1001–1013.

Beckmann, C. F., Mackay, C. E., Filippini, N., and Smith, S. M. (2009). Group comparison of resting-state FMRI data using multi-subject ICA and dual

regression. *Neuroimage* 47(Suppl. 1), S148.

Beckmann, C. F., and Smith, S. M. (2004). Probabilistic independent component analysis for functional magnetic resonance imaging. *IEEE Trans. Med. Imaging* 23, 137–152.

Beckmann, C. F., and Smith, S. M. (2005). Tensorial extensions of independent component analysis for multisubject FMRI analysis. *Neuroimage* 25, 294–311.

Bianciardi, M., Fukunaga, M., van Gelderen, P., Horovitz, S. G., de Zwart, J. A., and Duyn, J. H. (2009a). Modulation of spontaneous fMRI activity in human visual cortex by behavioral state. *Neuroimage* 45, 160–168.

Bianciardi, M., Fukunaga, M., van Gelderen, P., Horovitz, S. G., de Zwart, J. A., Shmueli, K., and Duyn, J. H. (2009b). Sources of functional magnetic resonance imaging signal fluctuations in the human brain at rest: a 7 T study. *Magn. Reson. Imaging* 27, 1019–1029.

Birn, R. M., Diamond, J. B., Smith, M. A., and Bandettini, P. A. (2006). Separating respiratory-variation-related fluctuations from neuronal-activity-related fluctuations in fMRI. *Neuroimage* 31, 1536–1548.

Birn, R. M., Murphy, K., and Bandettini, P. A. (2008). The effect of respiration variations on independent component analysis results of resting state functional connectivity. *Hum. Brain Mapp.* 29, 740–750.

Biswal, B., Yetkin, F. Z., Haughton, V. M., and Hyde, J. S. (1995). Functional connectivity in the motor cortex of resting human brain using echo-planar MRI. *Magn. Reson. Med.* 34, 537–541.

Biswal, B. B., Mennes, M., Zuo, X. N., Gohel, S., Kelly, C., Smith, S. M., Beckmann, C. F., Adelstein, J. S., Buckner, R. L., Colcombe, S., Dogonowski, A. M., Ernst, M., Fair, D., Hampson, M., Hoptman, M. J., Hyde, J. S., Kiviniemi, V. J., Kötter, R., Li, S. J., Lin, C. P., Lowe, M. J., Mackay, C., Madden, D. J., Madsen, K. H., Margulies, D. S., Mayberg, H. S., McMahon, K., Monk, C. S., Mostofsky, S. H., Nagel, B. J., Pekar, J. J., Peltier, S. J., Petersen, S. E., Riedl, V., Rombouts, S. A., Rypma, B., Schlaggar, B. L., Schmidt, S., Seidler, R. D., Siegle, G. J., Sorg, C., Teng, G. J., Veijola, J., Villringer, A., Walter, M., Wang, L., Weng, X. C., Whitfield-Gabrieli, S., Williamson, P., Windischberger, C., Zang, Y. F., Zhang, H. Y., Castellanos, F. X., and Milham, M. P. (2010). Towards discovery science of human brain function. *Proc. Natl. Acad. Sci. U.S.A.* 102, 4734–4739.

Boly, M., Phillips, C., Tshibanda, L., Vanhaudenhuyse, A., Schabus, M., Dang-Vu, T. T., Moonen, G., Hustinx, R., Maquet, P., and Laureys, S. (2008). Intrinsic brain activity in altered states of consciousness: how conscious is the default mode of brain function? *Ann. N. Y. Acad. Sci.* 1129, 119–129.

Broyd, S. J., Demanuele, C., Debener, S., Helps, S. K., James, C. J., and Sonuga-Barke, E. J. (2009). Default-mode brain dysfunction in mental disorders: a systematic review. *Neurosci. Biobehav. Rev.* 33, 279–296.

Buckner, R. L., Andrews-Hanna, J. R., and Schacter, D. L. (2008). The brain's default network: anatomy, function, and relevance to disease. *Ann. N. Y. Acad. Sci.* 1124, 1–38.

Buckner, R. L., Snyder, A. Z., Shannon, B. J., LaRossa, G., Sachs, R., Fotenos, A. F., Sheline, Y. I., Klunk, W. E., Mathis, C. A., Morris, J. C., and Mintun, M. A. (2005). Molecular, structural, and functional characterization of Alzheimer's disease: evidence for a relationship between default activity, amyloid, and memory. *J. Neurosci.* 25, 7709–7717.

Buzsaki, G., and Draguhn, A. (2004). Neuronal oscillations in cortical networks. *Science* 304, 1926–1929.

Calhoun, V. D., Adali, T., Pearlson, G. D., and Pekar, J. J. (2001). A method for making group inferences from functional MRI data using independent component analysis. *Hum. Brain Mapp.* 14, 140–151.

Calhoun, V. D., Adali, T., and Pekar, J. J. (2004a). A method for comparing group fMRI data using independent component analysis: application to visual, motor and visuomotor tasks. *Magn. Reson. Imaging* 22, 1181–1191.

Calhoun, V. D., Pekar, J. J, and Pearlson, G. D. (2004b). Alcohol intoxication effects on simulated driving: exploring alcohol-dose effects on brain activation using functional MRI. *Neuropsychopharmacology* 29, 2097–2107.

Castellanos, F. X., Margulies, D. S., Kelly, C., Uddin, L. Q., Ghaffari, M., Kirsch, A., Shaw, D., Shehzad, Z., Di Martino, A., Biswal, B., Sonuga-Barke, E. J., Rotrosen, J., Adler, L. A., and Milham, M. P. (2008). Cingulate-precuneus interactions: a new locus of dysfunction in adult attention-deficit/hyperactivity disorder. *Biol. Psychiatry* 63, 332–337.

Chang, C., and Glover, G. H. (2009). Effects of model-based physiological noise correction on default mode network anti-correlations and correlations. *Neuroimage* 47, 1448–1459.

Chang, C., and Glover, G. H. (2010). Time-frequency dynamics of resting-state brain connectivity measured with fMRI. *Neuroimage* 50, 81-98.

Cordes, D., Haughton, V. M., Arfanakis, K., Carew, J. D., Turski, P. A., Moritz, C. H., Quigley, M. A., and Meyerand, M. E. (2001). Frequencies contributing to functional connectivity in the cerebral cortex in 'resting-state' data. *AJNR Am. J. Neuroradiol.* 22, 1326–1333.

Cordes, D., Haughton, V. M., Arfanakis, K., Wendt, G. J., Turski, P. A., Moritz, C. H., Quigley, M. A., and Meyerand, M. E. (2000). Mapping functionally related regions of brain with functional connectivity MR imaging. *AJNR Am. J. Neuroradiol.* 21, 1636–1644.

Damoiseaux, J. S., Beckmann, C. F., Arigita, E. J., Barkhof, F., Scheltens, P., Stam, C. J., Smith, S. M., and Rombouts, S. A. (2008). Reduced resting-state brain activity in the 'default network' in normal aging. *Cereb. Cortex* 18, 1856–1864.

Damoiseaux, J. S., Rombouts, S. A., Barkhof, F., Scheltens, P., Stam, C. J., Smith, S. M., and Beckmann, C. F. (2006). Consistent resting-state networks across healthy subjects. *Proc. Natl. Acad. Sci. U.S.A.* 103, 13848–13853.

David, O., Guillemain, I., Saillet, S., Reyt, S., Deransart, C., Segebarth, C., and Depaulis, A. (2008). Identifying neural drivers with functional MRI: an electrophysiological validation. *PLoS Biol.* 6, e315. doi: 10.1371/journal.pbio.0060315.

De Luca, M., Beckmann, C. F., De Stefano, N., Matthews, P. M., and Smith, S. M. (2006). fMRI resting state networks define distinct modes of long-distance interactions in the human brain. *Neuroimage* 29, 1359–1367.

Di Martino, A., Shehzad, Z., Kelly, C., Roy, A. K., Gee, D. G., Uddin, L. Q., Gotimer, K., Klein, D. F., Castellanos, F. X., and Milham, M. P. (2009). Relationship between cingulo-insular functional connectivity and autistic traits in neurotypical adults. *Am. J. Psychiatry* 166, 891–899.

Dosenbach, N. U., Fair, D. A., Miezin, F. M., Cohen, A. L., Wenger, K. K., Dosenbach, R. A., Fox, M. D., Snyder, A. Z., Vincent, J. L., Raichle, M. E., Schlaggar, B. L., and Petersen, S. E. (2007). Distinct brain networks for adaptive and stable task control in humans. *Proc. Natl. Acad. Sci. U.S.A.* 104, 11073–11078.

Esposito, F., Scarabino, T., Hyvarinen, A., Himberg, J., Formisano, E., Comani, S., Tedeschi, G., Goebel, R., Seifritz, E., and Di Salle, F. (2005). Independent component analysis of fMRI group studies by self-organizing clustering. *Neuroimage* 25, 193–205.

Fair, D. A., Dosenbach, N. U., Church, J. A., Cohen, A. L., Brahmbhatt, S., Miezin, F. M., Barch, D. M., Raichle, M. E., Petersen, S. E., and Schlaggar, B. L. (2007). Development of distinct control networks through segregation and integration. *Proc. Natl. Acad. Sci. U.S.A.* 104, 13507–13512.

Filippini, N., MacIntosh, B. J., Hough, M. G., Goodwin, G. M., Frisoni, G. B., Smith, S. M., Matthews, P. M., Beckmann, C. F., and Mackay, C. E. (2009). Distinct patterns of brain activity in young carriers of the APOE-epsilon4 allele. *Proc. Natl. Acad. Sci. U.S.A.* 106, 7209–7214.

Fleisher, A. S., Sherzai, A., Taylor, C., Langbaum, J. B., Chen, K., and Buxton, R. B. (2009). Resting-state BOLD networks versus task-associated functional MRI for distinguishing Alzheimer's disease risk groups. *Neuroimage* 47, 1678–1690.

Fox, M. D., and Raichle, M. E. (2007). Spontaneous fluctuations in brain activity observed with functional magnetic resonance imaging. *Nat. Rev. Neurosci.* 8, 700–711.

Fox, M. D., Snyder, A. Z., Vincent, J. L., Corbetta, M., Van Essen, D. C., and Raichle, M. E. (2005). The human brain is intrinsically organized into dynamic, anticorrelated functional networks. *Proc. Natl. Acad. Sci. U.S.A.* 102, 9673–9678.

Fox, M. D., Snyder, A. Z., Vincent, J. L., and Raichle, M. E. (2007). Intrinsic fluctuations within cortical systems account for intertrial variability in human behavior. *Neuron* 56, 171–184.

Fox, M. D., Zhang, D., Snyder, A. Z., and Raichle, M. E. (2009). The global signal and observed anticorrelated resting state brain networks. *J. Neurophysiol.* 101, 3270–3283.

Fransson, P. (2005). Spontaneous low-frequency BOLD signal fluctuations: an fMRI investigation of the resting-state default mode of brain function hypothesis. *Hum. Brain Mapp.* 26, 15–29.

Fransson, P., Skiold, B., Horsch, S., Nordell, A., Blennow, M., Lagercrantz, H., and Aden, U. (2007). Resting-state networks in the infant brain. *Proc. Natl. Acad. Sci. U.S.A.* 104, 15531–15536.

Friston, K.J., Harrison, L., and Penny, W. (2003). Dynamic causal modelling. *Neuroimage* 19, 1273–1302.

Fukunaga, M., Horovitz, S. G., van Gelderen, P. de Zwart, J. A., Jansma, J. M., Ikonomidou, V. N., Chu, R. Deckers, R. H., Leopold, D. A., and Duyn, J. H. (2006). Large-amplitude, spatially correlated fluctuations in BOLD fMRI signals during extended rest and early sleep stages. *Magn. Reson. Imaging* 24, 979–992.

Glahn, D. C., Winkler, A. M., Kochunov, P., Almasy, L., Duggirala, R., Carless, M. A., Curran, J. C., Olvera, R. L., Laird, A. R., Smith, S. M, Beckmann,

C. F, Fox, P. T., and Blangero, J. (2010). Genetic control over the resting brain. *Proc. Natl. Acad. Sci. U.S.A.* 107, 1223–1228.

Glover, G. H., Li, T. Q., and Ress, D. (2000). Image-based method for retrospective correction of physiological motion effects in fMRI: RETROICOR. *Magn. Reson. Med.* 44, 162–167.

Goense, J. B., and Logothetis, N. K. (2008). Neurophysiology of the BOLD fMRI signal in awake monkeys. *Curr. Biol.* 18, 631–640.

Goebel, R., Roebroeck, A., Kim, D. S., and Formisano, E. (2003). Investigating directed cortical interactions in time-resolved fMRI data using vector autoregressive modeling and Granger causality mapping. *Magn. Reson. Imaging* 21, 1251–1261.

Greicius, M. (2008). Resting-state functional connectivity in neuropsychiatric disorders. *Curr. Opin. Neurol.* 21, 424–430.

Greicius, M. D., Flores, B. H., Menon, V., Glover, G. H., Solvason, H. B., Kenna, H., Reiss, A. L., and Schatzberg, A. F. (2007). Resting-state functional connectivity in major depression: abnormally increased contributions from subgenual cingulate cortex and thalamus. *Biol. Psychiatry* 62, 429–437.

Greicius, M. D., Kiviniemi, V., Tervonen, O., Vainionpaa, V., Alahuhta, S., Reiss, A. L., and Menon, V. (2008). Persistent default-mode network connectivity during light sedation. *Hum. Brain Mapp.* 29, 839–847.

Greicius, M. D., Krasnow, B., Reiss, A. L., and Menon, V. (2003). Functional connectivity in the resting brain: a network analysis of the default mode hypothesis. *Proc. Natl. Acad. Sci. U.S.A.* 100, 253–258.

Greicius, M. D., Srivastava, G., Reiss, A. L., and Menon, V. (2004). Default-mode network activity distinguishes Alzheimer's disease from healthy aging: evidence from functional MRI. *Proc. Natl. Acad. Sci. U.S.A.* 101, 4637–4642.

Greicius, M. D., Supekar, K., Menon, V., and Dougherty, R. F. (2009). Resting-state functional connectivity reflects structural connectivity in the default mode network. *Cereb. Cortex* 19, 72–78.

Gusnard, D. A., and Raichle, M. E. (2001). Searching for a baseline: functional imaging and the resting human brain. *Nat. Rev. Neurosci.* 2, 685–694.

Habas, C., Kamdar, N., Nguyen, D., Prater, K., Beckmann, C. F., Menon, V., and Greicius, M. D. (2009). Distinct cerebellar contributions to intrinsic connectivity networks. *J. Neurosci.* 29, 8586–8594.

Hampson, M., Peterson, B. S., Skudlarski, P., Gatenby, J. C., and Gore, J. C. (2002). Detection of functional connectivity using temporal correlations in MR images. *Hum. Brain Mapp.* 15, 247–262.

Harrison, B. J., Pujol, J., Lopez-Sola, M., Hernandez-Ribas, R., Deus, J., Ortiz, H., Soriano-Mas, C., Yucel, M., Pantelis, C., and Cardoner, N. (2008a). Consistency and functional specialization in the default mode brain network. *Proc. Natl. Acad. Sci. U.S.A.* 105, 9781–9786.

Harrison, B. J., Pujol, J., Ortiz, H., Fornito, A., Pantelis, C., and Yucel, M. (2008b). Modulation of brain resting-state networks by sad mood induction. *PLoS ONE* 3, e1794. doi:10.1371/journal.pone.0001794.

Hasson, U., Nusbaum, H. C., and Small, S. L. (2009). Task-dependent organization of brain regions active during rest. *Proc. Natl. Acad. Sci. U.S.A.* 106, 10841–10846.

Hayasaka, S., and Laurienti, P. J. (2009). Comparison of characteristics between region-and voxel-based network analyses in resting-state fMRI data. *Neuroimage* [Epub ahead of print] doi:10.1016/j.neuroimage.2009.12.051.

Hesselmann, G., Kell, C. A., Eger, E., and Kleinschmidt, A. (2008). Spontaneous local variations in ongoing neural activity bias perceptual decisions. *Proc. Natl. Acad. Sci. U.S.A.* 105, 10984–10989.

Himberg, J., Hyvarinen, A., and Esposito, F. (2004). Validating the independent components of neuroimaging time series via clustering and visualization. *Neuroimage* 22, 1214–1222.

Hong, L. E., Gu, H., Yang, Y., Ross, T. J., Salmeron, B. J., Buchholz, B., Thaker, G. K., and Stein, E. A. (2009). Association of nicotine addiction and nicotine's actions with separate cingulate cortex functional circuits. *Arch. Gen. Psychiatry* 66, 431–441.

Horovitz, S. G., Braun, A. R., Carr, W. S., Picchioni, D., Balkin, T. J., Fukunaga, M., and Duyn, J. H. (2009). Decoupling of the brain's default mode network during deep sleep. *Proc. Natl. Acad. Sci. U.S.A.* 106, 11376–11381.

Horovitz, S. G., Fukunaga, M., de Zwart, J. A., van Gelderen, P., Fulton, S. C., Balkin, T. J., and Duyn, J. H. (2008). Low frequency BOLD fluctuations during resting wakefulness and light sleep: a simultaneous EEG-fMRI study. *Hum. Brain Mapp.* 29, 671–682.

Jafri, M. J., Pearlson, G. D., Stevens, M., and Calhoun, V. D. (2008). A method for functional network connectivity among spatially independent resting-state components in schizophrenia. *Neuroimage* 39, 1666–1681.

Kelly, A. M., Uddin, L. Q., Biswal, B. B., Castellanos, F. X., and Milham, M. P. (2008). Competition between functional brain networks mediates behavioral variability. *Neuroimage* 39, 527–537.

Kelly, C., de Zubicaray, G., Di Martino, A., Copland, D. A., Reiss, P. T., Klein, D. F., Castellanos, F. X., Milham, M. P., and McMahon, K. (2009). L-dopa modulates functional connectivity in striatal cognitive and motor networks: a double-blind placebo-controlled study. *J. Neurosci.* 29, 7364–7378.

Kiviniemi, V., Kantola, J. H., Jauhiainen, J., Hyvarinen, A., and Tervonen, O. (2003). Independent component analysis of nondeterministic fMRI signal sources. *Neuroimage* 19, 253–260.

Kiviniemi, V., Starck, T., Remes, J., Long, X., Nikkinen, J., Haapea, M., Veijola, J., Moilanen, I., Isohanni, M., Zang, Y. F., and Tervonen, O. (2009). Functional segmentation of the brain cortex using high model order group PICA. *Hum. Brain Mapp.* 30, 3865–3886.

Krienen, F. M., and Buckner, R. L. (2009). Segregated fronto-cerebellar circuits revealed by intrinsic functional connectivity. *Cereb. Cortex* 19, 2485–2497.

Laufs, H. (2008). Endogenous brain oscillations and related networks detected by surface EEG-combined fMRI. *Hum. Brain Mapp.* 29, 762–769.

Laufs, H., Krakow, K., Sterzer, P., Eger, E., Beyerle, A., Salek-Haddadi, A., and Kleinschmidt, A. (2003). Electroencephalographic signatures of attentional and cognitive default modes in spontaneous brain activity fluctuations at rest. *Proc. Natl. Acad. Sci. U.S.A.* 100, 11053–11058.

Lewis, C. M., Baldassarre, A., Committeri, G., Romani, G. L., and Corbetta, M. (2009). Learning sculpts the spontaneous activity of the resting human brain. *Proc. Natl. Acad. Sci. U.S.A.* 106, 17558–17563.

Liu, B., Song, M., Li, J., Liu, Y., Li, K., Yu, C., and Jiang, T. (2010). Prefrontal-related functional connectivities within the default network are modulated by COMT val158met in healthy young adults. *J. Neurosci.* 30, 64–69.

Liu, H., Liu, Z., Liang, M., Hao, Y., Tan, L., Kuang, F., Yi, Y., Xu, L., and Jiang, T. (2006). Decreased regional homogeneity in schizophrenia: a resting state functional magnetic resonance imaging study. *Neuroreport* 17, 19–22.

Logothetis, N. K., Pauls, J., Augath, M., Trinath, T., and Oeltermann, A. (2001). Neurophysiological investigation of the basis of the fMRI signal. *Nature* 412, 150–157.

Lowe, M. J., Mock, B. J., and Sorenson, J. A. (1998). Functional connectivity in single and multislice echoplanar imaging using resting-state fluctuations. *Neuroimage* 7, 119–132.

Mantini, D., Perrucci, M. G., Del Gratta, C., Romani, G. L., and Corbetta, M. (2007). Electrophysiological signatures of resting state networks in the human brain. *Proc. Natl. Acad. Sci. U.S.A.* 104, 13170–13175.

Margulies, D. S., Kelly, A. M., Uddin, L. Q., Biswal, B. B., Castellanos, F. X., and Milham, M. P. (2007). Mapping the functional connectivity of anterior cingulate cortex. *Neuroimage* 37, 579–588.

Marx, E., Deutschländer, A., Stephan, T., Dieterich, M., Wiesmann, M., and Brandt, T. (2004). Eyes open and eyes closed as rest conditions: impact on brain activation patterns. *Neuroimage* 21, 1818–1824.

McKeown, M. J., Makeig, S., Brown, G. G., Jung, T. P., Kindermann, S. S., Bell, A. J., and Sejnowski, T. J. (1998). Analysis of fMRI data by blind separation into independent spatial components. *Hum. Brain Mapp.* 6, 160–188.

Murphy, K., Birn, R. M., Handwerker, D. A., Jones, T. B., and Bandettini, P. A. (2009). The impact of global signal regression on resting state correlations: are anti-correlated networks introduced? *Neuroimage* 44, 893–905.

Niazy, R. K., Smith, S. M., and Beckmann, C. F. (2008). "Principal frequency of resting state networks," in *14th Annual Meeting of the Organization for Human Brain Mapping*, 15–19 June, Melbourne, Australia.

O'Reilly, J. X., Beckmann, C. F., Tomassini, V., Ramnani, N., and Johansen-Berg, H. (2009). Distinct and overlapping functional zones in the cerebellum defined by resting state functional connectivity. *Cereb. Cortex* [Epub ahead of print] doi:10.1093/cercor/bhp157.

Paakki, J. J., Rahko, J., Long, X. Y., Moilanen, I., Tervonen, O., Nikkinen, J., Starck, T., Remes, J., Tuula, H., Haapsamo, H., Jussila, K., Kuusikko-Gauffin, S., Mattila, M. L., Zang, Y. F., and Kiviniemi, V. (2010). Alterations in regional homogeneity of resting-state brain activity in autism spectrum disorders. *Brain Res.* [Epub ahead of print] doi:10.1016/j.brainres.2009.12.081.

Poldrack, R. A., Halchenko, Y. O., and Hanson, S. J. (2009). Decoding the large-scale structure of brain function by classifying mental states across individuals. *Psychol. Sci.* [Epub ahead of print] doi:10.1111/j.1467-9280.2009.02460.x.

Popa, D., Popescu, A. T., and Pare, D. (2009). Contrasting activity profile of two distributed cortical networks as a function of attentional demands. *J. Neurosci.* 29, 1191–1201.

Pyka, M., Beckmann, C. F., Schoning, S., Hauke, S., Heider, D., Kugel, H., Arolt, V., and Konrad, C. (2009). Impact of working memory load on FMRI

resting state pattern in subsequent resting phases. *PLoS ONE* 4, e7198. doi:10.1371/journal.pone.0007198.

Raichle, M. E., MacLeod, A. M., Snyder, A. Z., Powers, W. J., Gusnard, D. A., and Shulman, G. L. (2001). A default mode of brain function. *Proc. Natl. Acad. Sci. U.S.A.* 98, 676–682.

Ramsey, J. D., Hanson, S. J., Hanson, C., Halchenko, Y. O., Poldrack, R. A., and Glymour, C. (2010). Six problems for causal inference from fMRI. *Neuroimage* 49, 1545–1558.

Roebroeck, A., Formisano, E., and Goebel, R. (2005). Mapping directed influence over the brain using Granger causality and fMRI. *Neuroimage* 25, 230–242.

Rombouts, S. A., Barkhof, F., Goekoop, R., Stam, C. J., and Scheltens, P. (2005). Altered resting state networks in mild cognitive impairment and mild Alzheimer's disease: an fMRI study. *Hum. Brain Mapp.* 26, 231–239.

Sadaghiani, S., Hesselmann, G., and Kleinschmidt, A. (2009). Distributed and antagonistic contributions of ongoing activity fluctuations to auditory stimulus detection. *J. Neurosci.* 29, 13410–13417.

Saini, S., DeStefano, N., Smith, S., Guidi, L., Amato, M. P., Federico, A., and Matthews, P. M. (2004). Altered cerebellar functional connectivity mediates potential adaptive plasticity in patients with multiple sclerosis. *J. Neurol. Neurosurg. Psychiatr.* 75, 840–846.

Salvador, R., Martinez, A., Pomarol-Clotet, E., Sarro, S., Suckling, J., and Bullmore, E. (2007). Frequency based mutual information measures between clusters of brain regions in functional magnetic resonance imaging. *Neuroimage* 35, 83–88.

Salvador, R., Suckling, J., Schwarzbauer, C., and Bullmore, E. (2005). Undirected graphs of frequency-dependent functional connectivity in whole brain networks. *Philos. Trans. R. Soc. Lond., B, Biol. Sci.* 360, 937–946.

Seeley, W. W., Crawford, R. K., Zhou, J., Miller, B. L., and Greicius, M. D. (2009). Neurodegenerative diseases target large-scale human brain networks. *Neuron* 62, 42–52.

Seeley, W. W., Menon, V., Schatzberg, A. F., Keller, J., Glover, G. H., Kenna, H., Reiss, A. L., and Greicius, M. D. (2007). Dissociable intrinsic connectivity networks for salience processing and executive control. *J. Neurosci.* 27, 2349–2356.

Shehzad, Z., Kelly, A. M., Reiss, P. T., Gee, D. G., Gotimer, K., Uddin, L. Q., Lee, S. H., Margulies, D. S., Roy, A. K., Biswal, B. B., Petkova, E., Castellanos, F. X., and Milham, M. P. (2009). The resting brain: unconstrained yet reliable. *Cereb. Cortex* 19, 2209–2229.

Shulman, G. L., Fiez, J. A., Corbetta, M., Buckner, R. L., Miezin, F. M., Raichle, M. E., and Petersen, S. E. (1997). Common blood flow changes across visual tasks: II. Decreases in cerebral cortex. *J. Cogn. Neurosci.* 9, 648–663.

Singh, K. D., and Fawcett, I. P. (2008). Transient and linearly graded deactivation of the human default-mode network by a visual detection task. *Neuroimage* 41, 100–112.

Smith, S., Niazy, R., Beckmann, C., and Miller, K. (2008). "Resting state networks: neither low frequency nor anti-correlated?" in *14th Annual Meeting of the Organization for Human Brain Mapping*, 15–19 June, Melbourne, Australia.

Smith, S. M., Fox, P. T., Miller, K. L., Glahn, D. C., Fox, P. M., Mackay, C. E., Filippini, N., Watkins, K. E., Toro, R., Laird, A. R., and Beckmann, C. F. (2009). Correspondence of the brain's functional architecture during activation and rest. *Proc. Natl. Acad. Sci. U.S.A.* 106, 13040–13045.

Sridharan, D., Levitin, D. J., and Menon, V. (2008). A critical role for the right fronto-insular cortex in switching between central-executive and default-mode networks. *Proc. Natl. Acad. Sci. U.S.A.* 105, 12569–12574.

Stam, C. J., and Reijneveld, J. C. (2007). Graph theoretical analysis of complex networks in the brain. *Nonlinear Biomed. Phys.* 1, 3.

Starck, T., Remes, J., Nikkinen, J., Tervonen, O., and Kiviniemi, V. (2010). Correction of low-frequency physiological noise from the resting state BOLD fMRI–Effect on ICA default mode analysis at 1.5 T. *J. Neurosci. Methods* 186, 179–185.

Thomason, M. E., Yoo, D. J., Glover, G. H., and Gotlib, I. H. (2009). BDNF genotype modulates resting functional connectivity in children. *Front. Hum. Neurosci.* 3:55. doi: 10.3389/neuro.09.055.2009.

Tohka, J., Foerde, K., Aron, A. R., Tom, S. M., Toga, A. W., and Poldrack, R. A. (2008). Automatic independent component labeling for artifact removal in fMRI. *Neuroimage* 39, 1227–1245.

Van Dijk, K. R., Hedden, T., Venkataraman, A., Evans, K. C., Lazar, S. W., and Buckner, R. L. (2010). Intrinsic functional connectivity as a tool for human connectomics: theory, properties, and optimization. *J. Neurophysiol.* 103, 297–321.

Varela, F., Lachaux, J. P., Rodriguez, E., and Martinerie, J. (2001). The brainweb: phase synchronization and large-scale integration. *Nat. Rev. Neurosci.* 2, 229–239.

Vincent, J. L., Patel, G. H., Fox, M. D., Snyder, A. Z., Baker, J. T., Van Essen, D. C., Zempel, J. M., Snyder, L. H., Corbetta, M., and Raichle, M. E. (2007). Intrinsic functional architecture in the anaesthetized monkey brain. *Nature* 447, 83–86.

Wang, K., Liang, M., Wang, L., Tian, L., Zhang, X., Li, K., and Jiang, T. (2007). Altered functional connectivity in early Alzheimer's disease: a resting-state fMRI study. *Hum. Brain Mapp.* 28, 967–978.

Weissenbacher, A., Kasess, C., Gerstl, F., Lanzenberger, R., Moser, E., and Windischberger, C. (2009). Correlations and anticorrelations in resting-state functional connectivity MRI: a quantitative comparison of preprocessing strategies. *Neuroimage* 47, 1408–1416.

Wink, A. M., Bullmore, E., Barnes, A., Bernard, F., and Suckling, J. (2008). Monofractal and multifractal dynamics of low frequency endogenous brain oscillations in functional MRI. *Hum. Brain Mapp.* 29, 791–801.

Zang, Y., Jiang, T., Lu, Y., He, Y., and Tian, L. (2004). Regional homogeneity approach to fMRI data analysis. *Neuroimage* 22, 394–400.

Zang, Y. F., He, Y., Zhu, C. Z., Cao, Q. J., Sui, M. Q., Liang, M., Tian, L. X., Jiang, T. Z., and Wang, Y. F. (2007). Altered baseline brain activity in children with ADHD revealed by resting-state functional MRI. *Brain Dev.* 29, 83–91.

Zhang, D., Snyder, A. Z., Fox, M. D., Sansbury, M. W., Shimony, J. S., and Raichle, M. E. (2008). Intrinsic functional relations between human cerebral cortex and thalamus. *J. Neurophysiol.* 100, 1740–1748.

Zou, Q. H., Zhu, C. Z., Yang, Y., Zuo, X. N., Long, X. Y., Cao, Q. J., Wang, Y. F., and Zang, Y. F. (2008). An improved approach to detection of amplitude of low-frequency fluctuation (ALFF) for resting-state MRI: fractional ALFF. *J. Neurosci. Methods* 172, 137–141.

Zuo, X. N., Di Martino, A., Kelly, C., Shehzad, Z. E., Gee, D. G., Klein, D. F., Castellanos, F. X., Biswal, B. B., and Milham, M. P. (2010a). The oscillating brain: complex and reliable. *Neuroimage* 49, 1432–1445.

Zuo, X. N., Kelly, C., Adelstein, J. S., Klein, D. F., Castellanos, F. X., and Milham, M. P. (2010b). Reliable intrinsic connectivity networks: Test-retest evaluation using ICA and dual regression approach. *Neuroimage* 49, 2163–2177.

Conflict of Interest Statement: The authors declare that the research was conducted in the absence of any commercial or financial relationships that could be construed as a potential conflict of interest.

Received: 12 February 2010; paper pending published: 28 February 2010; accepted: 17 March 2010; published online: 06 April 2010.

*Citation: Cole DM, Smith SM and Beckmann CF (2010) Advances and pitfalls in the analysis and interpretation of resting-state FMRI data. Front. Syst. Neurosci. **4**:8. doi: 10.3389/fnsys.2010.00008*

frontiers in
SYSTEMS NEUROSCIENCE

REVIEW ARTICLE
published: 17 June 2010
doi: 10.3389/fnsys.2010.00019

Clinical applications of resting state functional connectivity

Michael D. Fox[1]* and Michael Greicius[2]

[1] *Partners Neurology Residency, Massachusetts General Hospital, Brigham and Women's Hospital, Harvard Medical School, Boston, MA, USA*
[2] *Department of Neurology and Neurological Sciences, Stanford University School of Medicine, Stanford, CA, USA*

Edited by:
Lucina Q. Uddin,
Stanford University, USA

Reviewed by:
F. Castellanos,
Nathan Kline Institute, USA; New York University School of Medicine, USA
Yufeng Zang,
Beijing Normal University, China

****Correspondence:***
Michael D. Fox,
Partners Neurology Residency,
Massachusetts General Hospital,
Brigham and Women's Hospital,
Harvard Medical School, 55 Fruit St.,
Boston, MA 02114, USA.
e-mail: foxmdphd@gmail.com

During resting conditions the brain remains functionally and metabolically active. One manifestation of this activity that has become an important research tool is spontaneous fluctuations in the blood oxygen level-dependent (BOLD) signal of functional magnetic resonance imaging (fMRI). The identification of correlation patterns in these spontaneous fluctuations has been termed resting state functional connectivity (fcMRI) and has the potential to greatly increase the translation of fMRI into clinical care. In this article we review the advantages of the resting state signal for clinical applications including detailed discussion of signal to noise considerations. We include guidelines for performing resting state research on clinical populations, outline the different areas for clinical application, and identify important barriers to be addressed to facilitate the translation of resting state fcMRI into the clinical realm.

Keywords: fMRI, fcMRI, neurological disease, psychiatric disease, brain, spontaneous activity, intrinsic activity

INTRODUCTION

Functional magnetic resonance imaging (fMRI) is a non-invasive technique for examining brain function that utilizes changes in blood oxygen level-dependent (BOLD) signal to identify areas of increased or decreased neuronal activity (Logothetis, 2003; Raichle and Mintun, 2006). This technique has proven extremely valuable in the laboratory environment, allowing researchers to identify brain areas associated with the processing of different stimuli or the performance of various cognitive tasks (Raichle, 2000). Further, fMRI has been used extensively to identify abnormalities in these activation patterns in populations of patients with neurological or psychiatric disease.

Despite its success and popularity as a research tool, fMRI has seen relatively little translation into the clinical realm. In general, the fMRI abnormalities seen in clinical research populations have not translated into the ability to obtain useful diagnostic or prognostic information in individual patients (Matthews et al., 2006). While pre-operative fMRI is being used in individual patients to guide neurosurgical intervention, its use has not yet been shown to improve patient outcomes. Although progress is certainly being made, the clinical utility of fMRI has yet to be firmly established.

A recent advance that offers tremendous promise for improving the clinical applicability of fMRI involves focusing on spontaneous modulations in the BOLD signal that occur during resting conditions (for recent review see Fox and Raichle, 2007). In contrast to the traditional task-based approach, resting state studies observe the brain in the absence of overt task performance or stimulation. In these studies, subjects are generally asked to lie quietly under "resting" conditions such as eyes closed or while fixating on a crosshair. Spontaneous modulations in the BOLD signal in the absence of any explicit input or output are then recorded and analyzed. Although alternative approaches exist (Zhu et al., 2005, 2008; Cao et al., 2006; Fox and Raichle, 2007; Zang et al., 2007; Biswal et al., 2010), analysis of these spontaneous fluctuations usually involves the identification of correlations between remote brain areas, commonly referred to as functional connectivity. The term "functional connectivity" has been used in both resting-state and task-state studies and can refer to correlations across subjects, runs, blocks, trials, or individual BOLD time points, an ambiguity which can become confusing (Friston et al., 1993; Horwitz, 2003; Fox and Raichle, 2007; Rogers et al., 2007). We will therefore use the term resting state functional connectivity MRI (fcMRI) for added specificity, and this will be the focus of the present article. The two most popular techniques for performing resting state fcMRI are seed-based correlations and independent components analysis (ICA). In the seed-based technique signal is extracted from a specific region of interest, and a map is created by computing the correlation between this extracted signal and all other brain voxels (Biswal et al., 1995; Fox and Raichle, 2007). In contrast, ICA considers all voxels at once and uses a mathematical algorithm to separate a dataset into distinct systems or networks that are correlated in their spontaneous fluctuations but also maximally independent, usually in the spatial domain (Kiviniemi et al., 2003; Bartels and Zeki, 2004; Beckmann et al., 2005).

Regardless of the technique, a consistent observation is that regions with similar functional properties, such as the left and right somatomotor cortices, exhibit coherent BOLD fluctuations even in the absence of movement under resting conditions (Biswal et al., 1995; Lowe et al., 1998; Cordes et al., 2000; De Luca et al., 2005; Fox et al., 2006b). Similar results have been found in multiple other networks including visual (Lowe et al., 1998; Cordes et al., 2000), auditory (Cordes et al., 2000), language (Cordes et al., 2000; Hampson et al., 2002), dorsal and ventral attention systems (Fox et al., 2006a), corticothalamic circuits (Zhang et al., 2008), and a frontal opercular network that has been related to stimulus salience

(Seeley et al., 2007b). One of the most robustly identified and extensively investigated resting state networks involves a set of regions that routinely decrease their activity during attention demanding tasks, often referred to as the default mode network (Raichle et al., 2001; Greicius et al., 2003; Fox et al., 2005; Fransson, 2005) (**Figure 1**). Interestingly, this network has also been found to be negatively or anti-correlated with regions that tend to increase their activity during attention demanding tasks (Greicius et al., 2003; Fox et al., 2005, 2009; Fransson, 2005; Chang and Glover, 2010). Resting state correlation patterns across various networks have been shown to predict the task-response properties of brain regions (De Luca et al., 2005; Vincent et al., 2006), identify subjects' aptitude for different cognitive tasks (Hampson et al., 2006; Seeley et al., 2007b), and help constrain and refine neuro-anatomical models developed on the basis of task-activation studies (Fox et al., 2006a; Dosenbach et al., 2007).

Given the success of resting state functional connectivity for probing the brain's functional architecture in normal subjects, it is only natural to apply the technique towards understanding brain disease. Two recent reviews detail the large number of studies that have utilized resting state fcMRI to study various neurological and psychiatric conditions (Greicius, 2008; Zhang and Raichle, 2010). Although this list continues to grow on a daily basis, the goal of the present article is not to review the findings from each individual study and the insight each provides towards understanding specific diseases. The field has expanded to the point that resting state reviews focused on each specific disease are rapidly becoming appropriate. Instead, we take a more global perspective on the application of resting state fcMRI in the clinical realm. We detail the theoretical and practical motivations for using resting state fcMRI for clinical applications, describe the different types of clinical applications to which resting state may be applied, provide guidelines for using resting state fcMRI as a clinical tool, and identify barriers to full translation of resting state fcMRI into the clinical realm.

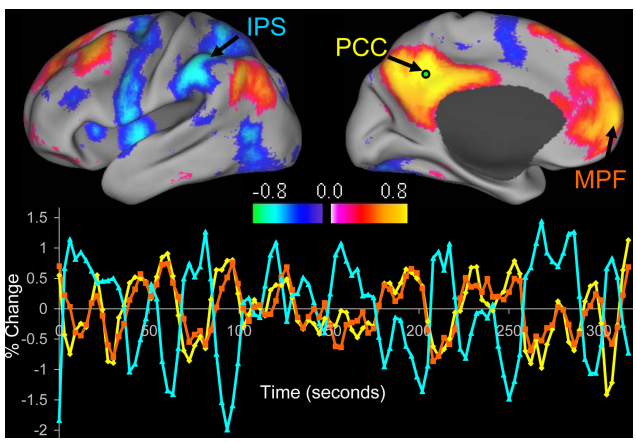

FIGURE 1 | Resting state functional connectivity reveals correlations and anticorrelations with the default mode network. Correlations between a seed region in the posterior cingulate/precuneus (PCC) and all other voxels in the brain for a single subject during resting fixation. Both correlations (positive values) and anticorrelations (negative values) are shown, thresholded at $R = 0.3$. The time course for a single run is shown for the seed region (PCC, yellow), a region positively correlated with this seed region in the medial prefrontal cortex (MPF, orange), and a region negatively correlated with the seed region in the intraparietal sulcus (IPS, blue). Reproduced with permission from (Fox et al., 2005).

WHY USE RESTING STATE fcMRI FOR CLINICAL APPLICATIONS?

CEREBRAL ENERGETICS

There are several motivations, both theoretical and practical for using resting state fcMRI for clinical applications. The first of these motivations comes from an understanding of brain energy metabolism. The resting human brain represents only 2% of total body mass but consumes 20% of the body's energy, most of which is used to support of ongoing neuronal signaling (Ames, 2000; Attwell and Laughlin, 2001; Lennie, 2003; Shulman et al., 2004; Raichle and Mintun, 2006). Task-related increases in neuronal metabolism are usually small (<5%) when compared to this large resting energy consumption (Raichle and Mintun, 2006). Differences in these task-related changes between normal and pathological populations are smaller still, often less than 1%. When attempting to study disease or diagnose patients based on task-related changes, one is therefore focusing on only a very small fraction of the brain's overall activity. Ongoing spontaneous activity may provide a window onto the neural processing that appears to consume the vast majority of the brain's resources and so may prove a richer source of disease-related signal changes.

SIGNAL TO NOISE

Resting state studies may offer a better signal to noise ratio than conventional task-based approaches. To demonstrate this principle, BOLD modulations recorded from the somatomotor cortex are shown during a simple task in which subjects were asked to press a button with their right hand (**Figure 2**) (Fox et al., 2006b). In this case, the subject pressed the button only once during the scanning session. Examining the tracing from the left somatomotor cortex alone (**Figure 2A**), it is impossible to identify when during the session that button press occurred. The signal, or task-related modulation, is very small relative to the tremendous amount of ongoing noise. Even if one focuses only on the time of the button press itself, when task-related BOLD modulation is maximal, the task-related modulation accounts for only 20% of the total BOLD variance (Fox et al., 2006b, 2007b). This means that during a standard fMRI task session over 80% of the BOLD modulation may be discarded as noise. This is why task-related BOLD studies require a large number of trials and extensive averaging to obtain a signal or activation map, and this may be part of the reason why task-based fMRI has found only limited application in the clinical realm.

A critical observation that forms the basis of resting state fcMRI was the finding that much of this "noise" that is so problematic for task-based studies is actually ongoing spontaneous fluctuations that are correlated within distinct cortical networks. This becomes apparent in our button press example when one adds the tracing from the right somatomotor cortex, which is only minimally involved in the right-handed task, to the tracing already shown for the left somatomotor cortex (**Figure 2B**). Much of the "noise" in the left somatomotor cortex is also present on the right. It is important to note that this shared variance is specific

to the somatomotor system and can be directly tied to variability in motor function (Fox et al., 2006b, 2007b). Even if one focuses only on the button press epoch, spontaneous ongoing activity can account for around 60% of the BOLD "noise" (Fox et al., 2006b, 2007b). In fact, one can subtract the ongoing spontaneous activity from the left somatomotor cortex and the single button press response becomes evident (**Figure 2C**).

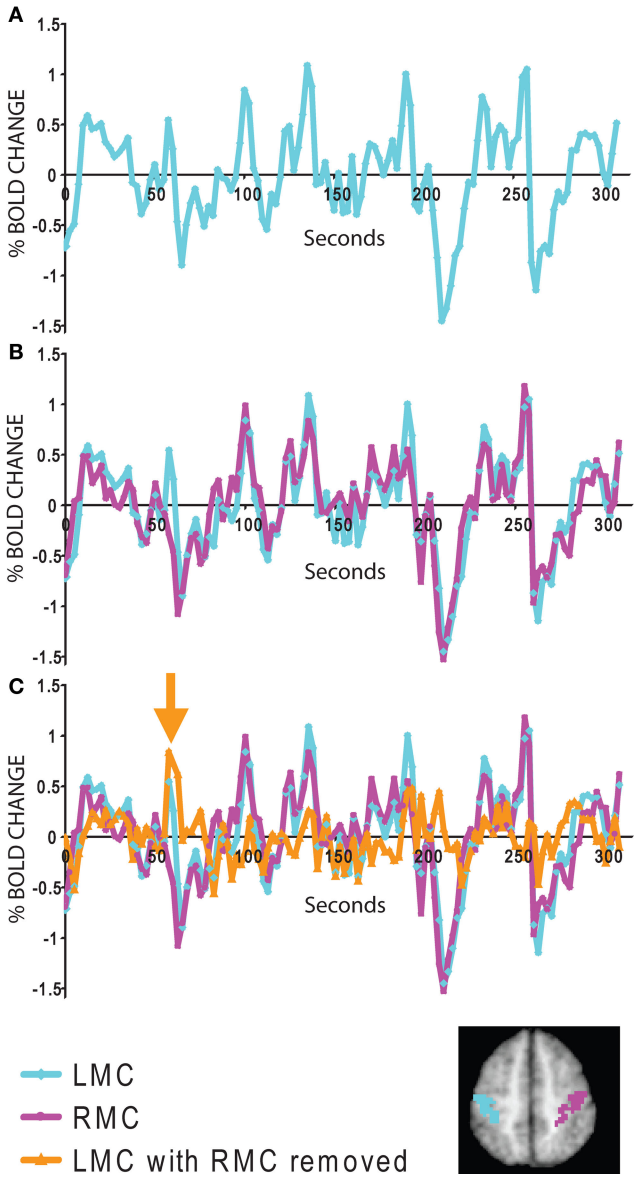

FIGURE 2 | Signal to noise features of spontaneous and task evoked activity. (A) fMRI time course from the left somatomotor cortex (LMC) during a single run when the subject pressed the button once with his right hand. Due to poor signal to noise, it is impossible to identify the task-related activity. **(B)** Comparison of the LMC with the right somatomotor cortex (RMC) shows that much of the noise is ongoing spontaneous activity correlated within the somatomotor system. **(C)** After subtracting the RMC from the LMC, the task-related modulation from the individual button press is evident (orange arrow). The LMC and RMC regions of interest are displayed for convenience on the inset map. Data taken from (Fox et al., 2006b).

Task-activation studies have a poor signal to noise ratio because the signal (task-related modulation) is often small relative to the sea of ongoing noise (including spontaneous activity). In contrast, resting state fcMRI focuses on this ongoing spontaneous activity and uses it as the signal rather than discarding it as noise. System-specific correlation values can be as high as 0.7–0.9 (accounting for 50–80% of the variance) (Fox et al., 2006b, 2007b) (see **Figure 1**). Compared to the 20% signal to noise ratio seen in task-based activation studies, resting state fcMRI studies may enjoy approximately three times the signal to noise ratio. Although additional signal to noise considerations exist (see final section), a 3 to 1 improvement in signal to noise has obvious advantages when attempting to identify imaging abnormalities in individual patients.

MULTI-PURPOSE DATA SETS

In addition to the above signal to noise considerations, resting state fcMRI data sets can be used to study multiple cortical systems. This is in contrast to task-activation analyses which require dedicated data acquisitions for each function one is attempting to localize. For example, if one wants to identify both motor and language systems for pre-operative mapping one would need to perform one acquisition of a motor task and another acquisition of a language task. In fcMRI the same data can be used to examine both systems, effectively doubling the amount of data (or alternatively reducing the acquisition time by half).

EXPANDED PATIENT POPULATIONS

One of the most frequently cited motivations for using resting state fcMRI in clinical studies is that it allows for a broader sampling of patient populations. Due to cognitive dysfunction or physical impairment many patients are simply not capable of performing tasks accurately in the fMRI scanner. When studying disease, this often means that we are sampling the least impaired subjects in a patient group as opposed to the most impaired subjects likely to show the largest signal abnormalities. In addition to limiting our sensitivity for detecting disease related changes, this introduces the problem of whether observed abnormalities can be generalized to the average (and often sicker) disease population. Resting state fcMRI requires no task and places only minimal demands on the patient. Further, spontaneous activity continues when subjects are asleep (Fukunaga et al., 2006; Horovitz et al., 2006) and sedated (Kiviniemi et al., 2003; Peltier et al., 2005; Vincent et al., 2007; Greicius et al., 2008b) opening up the possibility of obtaining resting state activity in any patient population. Of note, it remains unclear if individual differences observed during the awake state persist during sleep or sedation and is an important area for future research.

CIRCUMVENTING TASK-RELATED CONFOUNDS

One important advantage of resting state fcMRI is that it may circumvent confounds that can complicate interpretation of task-based studies. For example, working memory tasks have been used extensively to study patients with schizophrenia. However, a difference in activation between patients and control subjects observed during the task could represent differences in task performance, effort, task strategy, or an underlying disease-specific brain abnormality. A second example involves longitudinal studies

which utilize repeated task-based scanning sessions to examine drug effects or disease progression. These repeated task sessions can be confounded by practice effects or adaptation to the task. By eliminating the task, resting state fcMRI can circumvent some of these interpretative ambiguities and may allow for identification of more fundamental abnormalities underlying disease.

TYPES OF CLINICAL APPLICATIONS

IDENTIFYING GROUP DIFFERENCES IN BRAIN DISEASE

Although there are several ways in which resting state fcMRI may be applied to clinical populations, by far the largest application has been comparing resting state correlation patterns between groups of normal subjects and those with neurological or psychiatric disease (for recent reviews see Fox and Raichle, 2007; Greicius, 2008; Zhang and Raichle, 2010). The goal is that through identification of group differences one may begin to better understand the functional abnormalities underlying different disease states leading ultimately to a reliable resting state fcMRI marker that can be interpreted at the single subject level. This knowledge could in turn lead to identification of new treatments or drug targets. Disturbances in the correlation structure of spontaneous activity have now been reported for a significant number of disease states (see **Table 1**).

The goal of the current review is not to detail the individual findings of over 60 publications across 20 disease states. As mentioned in the introduction, we are rapidly approaching the point where reviews of resting state abnormalities for each particular disease state are becoming appropriate. However, tabulating the studies in this manner does lead to a few important observations. First, resting state fcMRI studies have been published on almost all major neurological and psychiatric diseases as well as a number of related conditions. While replication plays a role, the novelty of simply comparing correlation patterns between two groups is subsiding, and the route is paved for more advanced analyses (see next section). Second, the consistency of resting state abnormalities various greatly by disease state, from excellent consistency across Alzheimer's, MCI, and PIB-positive patients to inconsistent and occasionally opposing findings in schizophrenia. There may be several reasons for this heterogeneity, and some mechanism to reconcile disparate findings is needed. Third, a seemingly disproportionate number of studies seem to focus on the default mode network as opposed to other resting state networks. While this may be appropriate in diseases like Alzheimer's with known or theoretical pathology in these regions, some of this focus may stem from a misconception that the default mode network is somehow special in showing large-amplitude coherent BOLD fluctuations at rest (for additional discussion see Fox and Raichle, 2007; Zhang and Raichle, 2010).

OBTAINING DIAGNOSTIC AND PROGNOSTIC INFORMATION

Given the substantial group comparison literature now available (**Table 1**), the route is paved for more advanced analyses of resting state abnormalities. One important advance is to relate the resting state differences seen between two groups to a relevant clinical variable. For example, pathological disturbances in intrinsic activity have been correlated with the severity of disease in depression (Greicius et al., 2007), schizophrenia (Bluhm et al., 2007), and neglect (He et al., 2007). Relating resting state abnormalities to a relevant clinical variable speaks directly to the potential clinical relevance of a given finding and greatly increases confidence that the reported resting state abnormality will be reproducible.

Another important advance towards identifying prognostic or diagnostic markers on individual patients is to calculate the ability of observed resting state abnormalities to segregate healthy from disease states. Not surprisingly, the vast majority of this work has focused on the disease state with the most reproducible resting state abnormalities, Alzheimers, (Li et al., 2002; Greicius et al., 2004; Wang et al., 2006a; Supekar et al., 2008) (**Figure 3**) and the potentially associated condition of PIB positivity (Hedden et al., 2009; Sheline et al., 2010). By looking at different resting state fcMRI measures and setting a threshold, one can calculate the sensitivity and specificity of that marker for segregating healthy and disease states (**Figure 3A**). In Alzheimers, sensitivity ranges from 72–85% and specificity from 77–80% (Li et al., 2002; Greicius et al., 2004; Wang et al., 2006a; Supekar et al., 2008). Instead of picking just one threshold, receiver operating characteristic (ROC) curves can show the sensitivity and specificity at several different thresholds and have been usefully applied in Alzheimers (Li et al., 2002; Supekar et al., 2008) (**Figures 3B,C**). Although not yet applied to Alzheimers, techniques such as machine vector learning and advanced pattern recognition may further improve the utility of resting state fcMRI abnormalities as brain disease biomarkers (Haynes and Rees, 2006; Norman et al., 2006). Thus far, these segregation studies have been retrospective and the criteria for identifying a disease has been optimized for a specific data set. Future work applying these criteria prospectively towards new datasets will serve as an important test of their potential clinical relevance as a diagnostic or prognostic marker.

LONGITUDINAL STUDIES AND TREATMENT EFFECTS

One area for which resting state fcMRI is extremely well suited is longitudinal studies and monitoring treatment effects. For example, much may be learned by following disease progression in neuro-degenerative disorders such as Alzheimer's or amyotrophic lateral sclerosis (ALS). Similarly, one can examine the effect of clinical intervention by studying subjects before and after treatment. Normalization of resting state brain abnormalities with drug therapy may prove to be a useful surrogate outcome in clinical trials or help pharmaceutical companies decide which drugs to bring to large-scale clinical trials in the first place. Along these lines, resting state fcMRI abnormalities in depression have been shown to dissipate with drug treatment (Anand et al., 2005b), and improvement in regional correlations has been shown to match functional recovery in spatial neglect following stroke (He et al., 2007).

CLUSTERING IN HETEROGENEOUS DISEASE STATES

To date segregation has focused largely on differentiating healthy from disease states. However one important role for resting state connectivity analyses may be segregating patients within a disease category. For example, schizophrenia is widely regarded as a very heterogeneous disorder, and this heterogeneity can greatly hinder the sensitivity of clinical trials. One could imagine placing the resting state patterns of hundreds of patients with schizophrenia into an algorithm that would cluster the patients into groups

Table 1 | Group differences in resting state fcMRI patterns observed in various brain diseases or conditions.

Disease/condition	References	Findings
Alzheimer's	(Li et al., 2002; Greicius et al., 2004; Wang et al., 2006a,b, 2007; Allen et al., 2007; Supekar et al., 2008)	Decreased correlations within the DMN including hippocampi, decreased anticorrelations with the DMN, and reduced local connectivity as reflected in clustering coefficients
PIB positive	(Hedden et al., 2009; Sheline et al., 2010)	Decreased correlations within the DMN
Mild cognitive impairment	(Li et al., 2002; Sorg et al., 2007)	Decreased correlations within the DMN and decreased anticorrelations with the DMN.
Fronto-temporal dementia	(Seeley et al., 2007a, 2008)	Decreased correlations within the salience network
Healthy aging	(Andrews-Hanna et al., 2007; Damoiseaux et al., 2008)	Decreased correlations within the DMN
Multiple sclerosis	(Lowe et al., 2002; De Luca et al., 2005)	Decreased correlations within the somatomotor network
ALS	(Mohammadi et al., 2009)	Decreased connectivity within the DMN and within the somatomotor network (esp. premotor cortex)
Depression	(Anand et al., 2005a,b, 2009; Greicius et al., 2007; Bluhm et al., 2009a)	Variable: Decreased corticolimbic connectivity (esp. with dorsal anterior cingulate), increased connectivity within the DMN (esp. subgenual prefrontal cortex), decreased connectivity between DMN and caudate
Bipolar	(Anand et al., 2009)	Decreased corticolimbic connectivity
PTSD	(Bluhm et al., 2009c)	Decreased connectivity within the DMN
Schizophrenia	(Liang et al., 2006; Liu et al., 2006, 2008; Bluhm et al., 2007, 2009b; Salvador et al., 2007; Zhou et al., 2007; Jafri et al., 2008; Whitfield-Gabrieli et al., 2009)	Variable: Decreased or increased correlations within the DMN. Decreased, increased or unchanged correlations and anticorrelations between the DMN and other systems.
Schizophrenia 1° relatives	(Whitfield-Gabrieli et al., 2009)	Increased connectivity within the DMN
ADHD	(Zhu et al., 2005, 2008; Cao et al., 2006; Tian et al., 2006; Zang et al., 2007; Castellanos et al., 2008; Wang et al., 2009)	Variable: reduced connectivity within the DMN, reduced anticorrelations with the DMN, increased connectivity in the salience network
Autism	(Cherkassky et al., 2006; Kennedy and Courchesne, 2008; Monk et al., 2009; Weng et al., 2010)	Decreased connectivity within the DMN (although hippocampus is variable and connectivity may be increased in younger patients)
Tourette syndrome	(Church et al., 2009)	Delayed maturation of task-control and cingulo-opercular networks
Epilepsy	(Waites et al., 2006; Lui et al., 2008; Bettus et al., 2009; Zhang et al., 2009b,c)	Variable: decreased connectivity in multiple networks including the medial temporal lobe, decreased connectivity within the DMN (esp. in patients with generalized seizures)
Blindness	(Liu et al., 2007; Yu et al., 2008)	Decreased connectivity within the visual cortices and between visual cortices and other sensory and multimodal regions
Chronic pain	(Greicius et al., 2008a; Cauda et al., 2009a,c,d)	Variable: Increased/decreased connectivity within the salience network, decreased connectivity in attention networks
Neglect	(He et al., 2007)	Decreased connectivity within the dorsal and ventral attention networks
Coma/vegetative state	(Boly et al., 2009; Cauda et al., 2009b; Vanhaudenhuyse et al., 2010)	Progressively decreased DMN connectivity with progressive states of impaired consciousness
Generalized anxiety disorder	(Etkin et al., 2009)	increased connectivity between amygdala and frontoparietal control network and decreased connectivity between amygdala and salience network

*DMN = default mode network including regions in the posterior cingulate/precuneus, lateral parietal cortex, medial temporal lobes, and medial prefrontal cortex (**see Figure 1**). Salience network: includes regions in the dorsal anterior cingulate and bilateral fronto/insular cortices; dACC = dorsal anterior cingulated cortex; PIB = Pittsburg compound B, a marker of amyloid plaque accumulation in the brain. PTSD = post-traumatic stress disorder; ALS = amyotrophic lateral sclerosis; ADHD = attention deficit hyperactivity disorder. Note: some references (Greicius et al., 2004; He et al., 2007) reflect "near-rest" conditions in which task-related variance has been minimized and other references (Zhu et al., 2005, 2008; Cao et al., 2006; Zang et al., 2007) reflect local changes in spontaneous BOLD fluctuations as opposed to correlations in these fluctuations between separate regions.*

with similar resting state abnormalities. Similarly, retrospective analysis of drug effects could identify subgroups that benefited from a particular therapy.

PRE-OPERATIVE MAPPING AND TARGETING INTERVENTION

The area in which traditional task-based fMRI has shown the greatest promise for clinical translation is in pre-operative functional

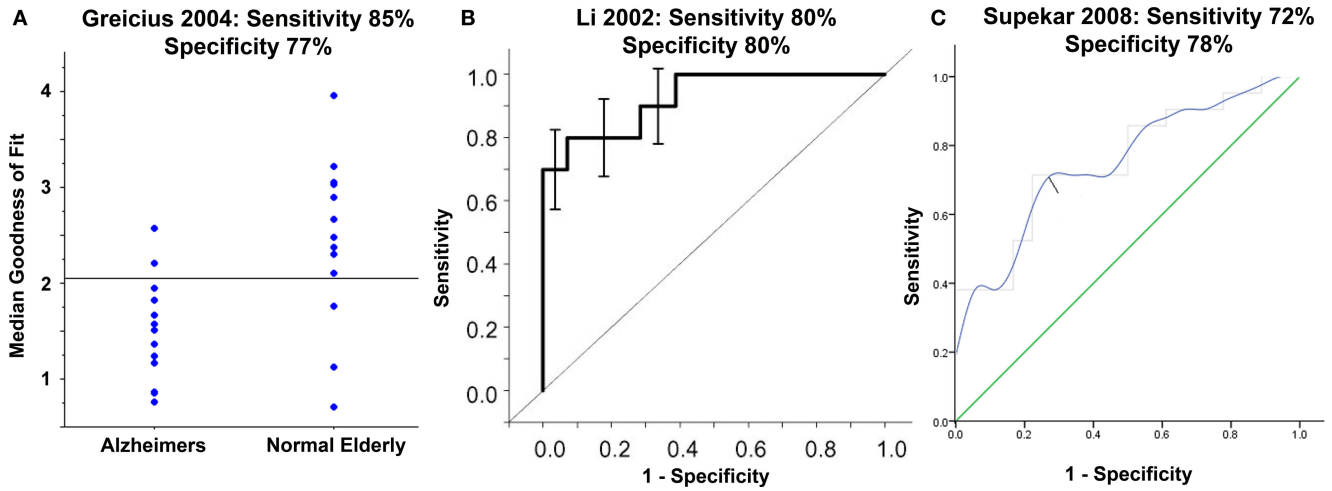

FIGURE 3 | Moving towards resting state abnormalities as a diagnostic marker in Alzheimers: Using parameters derived from resting state functional connectivity and choosing an appropriate threshold one can show good segregation between patients with Alzheimers disease (AD) and healthy elderly (A). Instead of picking just one threshold, receiver operating characteristic (ROC) curves can show the sensitivity and specificity at several different thresholds **(B,C)**. Below each figure are the sensitivity and specificity values obtained by choosing the ideal threshold to segregate the populations in each study. Adapted with permission from (Li et al., 2002; Greicius et al., 2004; Supekar et al., 2008).

brain mapping to help guide neurosurgical planning (Haberg et al., 2004; Vlieger et al., 2004; Matthews et al., 2006). This is used most often to identify brain areas used in movement and language so that these areas can be avoided during surgical resection, but it has also been combined with EEG to identify foci of epileptic activity (Lemieux, 2004). fMRI defined brain regions correlate with intra-operative electrophysiology (Vlieger et al., 2004), Wada testing (Binder et al., 1996; Adcock et al., 2003), loss-of-function post-operatively (Haberg et al., 2004), and are frequently mentioned in neurosurgery notes (Haberg et al., 2004). However, patients frequently lack the ability to perform tasks well (Pujol et al., 1998) and patient movement during tasks can be a significant problem (Lee et al., 1999).

As mentioned earlier, the advantages of resting state fMRI may circumvent many of the current limitations hindering task-based pre-operative mapping. Indeed several articles have recently been published showing strong proof of concept for resting state fcMRI as a pre-operative mapping tool in patients with neurosurgical conditions (Kokkonen et al., 2009; Liu et al., 2009; Shimony et al., 2009; Zhang et al., 2009a). These articles have shown good correlation between resting state fcMRI results, task-based mapping, and intra-operative cortical stimulation in these patients (**Figure 4**).

Just as resting state fcMRI may guide surgeons in their operative approach, it may also be used to guide several other clinical interventions where localization of a functional region is critical. Examples include placement of EEG recording grids, deep brain stimulators, and transcranial magnetic stimulation (TMS).

BARRIERS TO CLINICAL APPLICABILITY/FUTURE WORK

GUIDELINES FOR STUDYING CLINICAL POPULATIONS WITH fcMRI

Despite the promise of resting state fcMRI for improving the translation of functional imaging into the clinical realm, several challenges remain. One of the largest barriers is inconsistent results across studies. When studies are relatively consistent, as in Alzheimers, it is easy to build on these results and move towards using resting state fcMRI for diagnostic and prognostic purposes. However, when studies are inconsistent as in schizophrenia, one is left wondering which result, if any, is most likely to be reproducible and therefore clinically relevant. Different study designs, processing techniques, analysis approaches, and regions or systems of interest make comparing studies very difficult.

One of the first steps towards improving translation is to begin to improve our ability to replicate and compare results from different resting state studies. While individual labs will always differ in their analytical approach (and this is a good thing) there are certain standards or guidelines that may help improve reproducibility and strengthen the conclusions that can be made (**Table 2**). Some of these guidelines may appear generic and obvious, however resting state fcMRI presents a unique set of challenges in study design and analysis that may benefit from explicit delineation.

Table 2 | Guidelines for studies of clinical populations with resting state fcMRI.

(1)	*A priori* hypotheses regarding a region or network with abnormal fcMRI and clear criteria for selecting this region or network
(2)	*A priori* hypothesis and demonstration of a region or network with normal fcMRI to serve as a control
(3)	Correlation with clinical variables whenever possible
(4)	Stringent correction for multiple comparisons
(5)	An analysis of movement in patients and control subjects
(6)	An analysis of the differential impact of pre-processing in patients and control subjects
(7)	A discussion of how current findings relate to prior fcMRI findings

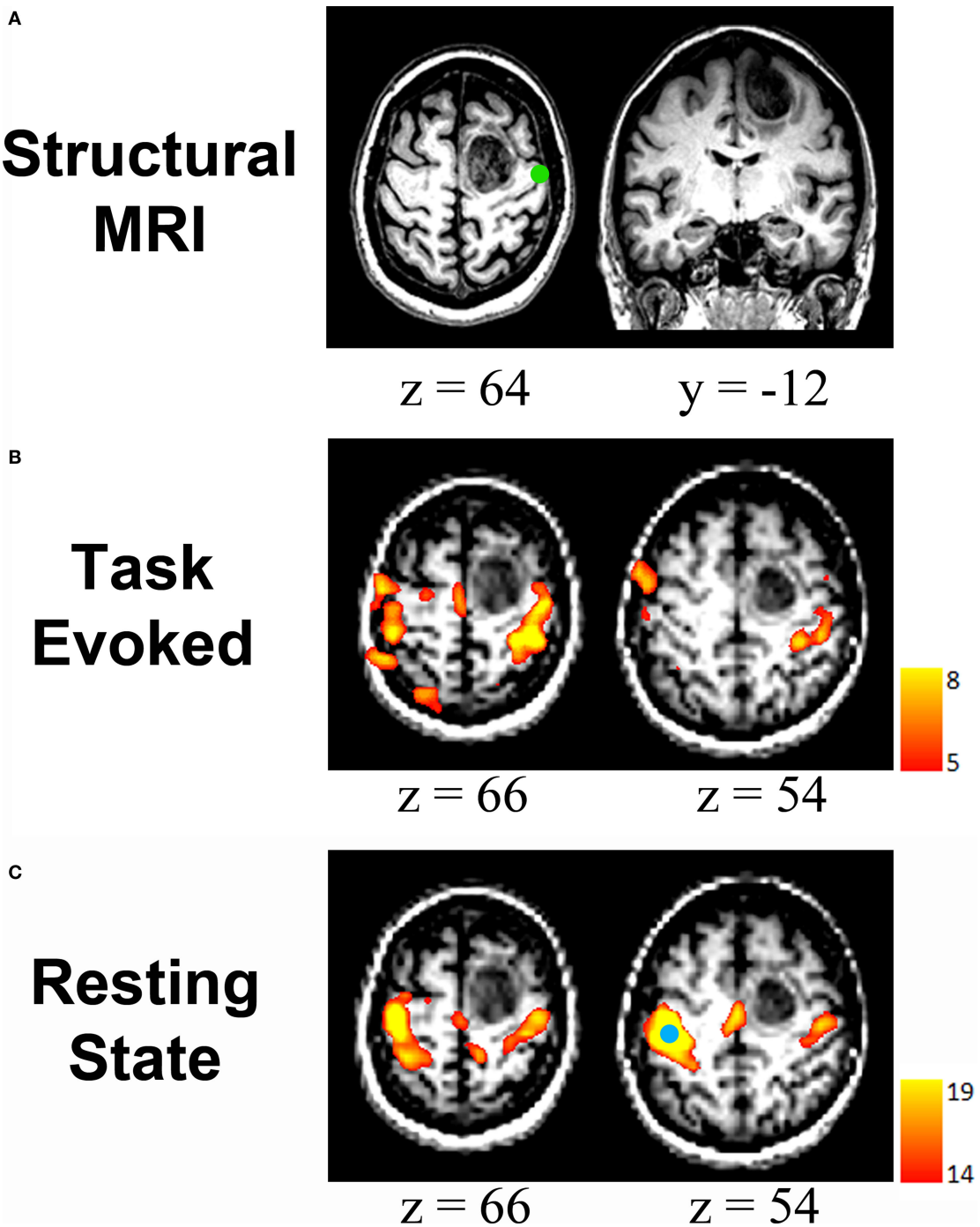

FIGURE 4 | Resting state fcMRI in pre-operative brain mapping: **(A)** Structural MRI scan showing a mass in the right frontal cortex. Green circle represents the location of ipsilateral hand response to intra-operative cortical stimulation. **(B)** Task-related mapping showing activity within the sensorimotor network but also small responses in parietal cortex that are seemingly unrelated to motor function or sensation. **(C)** Resting-state correlation mapping showing that the sensorimotor network is largely unaffected by the tumor anterior to the central sulcus. Seed region is shown (blue circle). All images are displayed left-on-left. Adapted with permission from (Zhang et al., 2009a).

(1) The first guideline concerns a priori identification of either a region (seed-based analysis) or network (ICA) that one expects may be abnormal. This hypothesis can be based on prior imaging data (either task-based or resting state), pathology, or simply the clinical features of the disease combined with theory suggesting localization of the relevant impaired functions. If the a priori motivation for the study is clearly presented in the introduction, then even a well-powered, negative finding can represent an advance. Analyses of a large number of seed regions or components can be an effective

means of generating hypotheses, but such exploratory work must be followed by targeted analyses that are powered to disconfirm spurious findings. Similar to choosing which region or network one is interested in, one must also clearly identify a priori how that network will be identified. If one is using a seed region, the coordinates for that seed region should be justified, for example as a focus of activation from a previously published study. Similarly, if one is studying a network in the form of an ICA component, one needs to specify an objective approach for identifying that system such as spatial correlation to an a priori template (Greicius et al., 2004, 2007), however see also (Zuo et al., 2009) for possible limitations of this approach.

(2) Perhaps as important as the first guideline, the second guideline involves a priori identification of regions or networks that one expects NOT to vary between the disease and healthy state. A good choice for many diseases may be primary sensory systems such as visual, somatomotor, or auditory. Of course, it is theoretically possible that a disease state exists which impacts every brain system and region such that a normal control is not possible. However in these cases alternative control strategies should be pursued to show that the findings are not artifactual.

(3) As mentioned in an earlier section, any study which can show a relationship between identified resting state fcMRI abnormalities and clinical variables such as disease severity increases the confidence that a finding will be clinically relevant and reproducible.

(4) The fourth guideline concerns correction for multiple comparisons. This becomes especially pertinent if one is looking for differences across a large number of seed regions or components or if one is attempting to correlate resting state abnormalities with several different clinical variables. The probability of finding a significant relationship increases as the number of variables one is trying to relate increases. Several methods to correct for these multiple comparisons exist, the simplest and most stringent being Bonferroni correction (Abdi, 2007). Clearly there are cases where one doesn't know a priori which clinical variable or component may be of interest, and an effect that does not pass Bonferroni does not mean the effect is not interesting, it simply means that the relationship would benefit from repeat and targeted testing.

(5) The fifth guideline concerns movement correction and comes from the recognition that patient populations are often going to be less cooperative lying in the scanner than control populations, especially when they are required to do nothing but stare at a fixation cross for 10 min. While task-based studies can partially compensate for movement by averaging across a large number of trials, the nature of the signal used in resting state makes it particularly susceptible to movement confounds. Movement parameters are often used as co-regressors in resting state fMRI to try to minimize artificial correlations, however if large group differences in movement are present this remains a confounding variable. In such instances, one could look to see if movement correlated on a subject to subject basis with the finding of interest. If the patients that moved the most also showed the largest difference in resting state correlation values then there should be an elevated index of suspicion. Note that identification of control networks that are not different between the two groups will also help in this regard (see point #2).

(6) Similar to the above movement analysis, one should examine the impact of pre-processing on the two groups of subjects to insure that they do not differ. For example, much has been written on the pronounced effect of global signal regression on resting state correlations and anticorrelations (Chang and Glover, 2009, 2010; Fox et al., 2009; Murphy et al., 2009; Weissenbacher et al., 2009). Although there is benefit to this pre-processing maneuver including improved correspondence with anatomical connectivity (Fox et al., 2009), one must ensure that the effect of the pre-processing was not different in the two groups. In this example, one could examine the variance removed by global regression and show that it is not significantly different between patients and controls. If there is a group difference then one may want to repeat the analysis without removing the global signal and determine if the effect of interest remains. Similarly in ICA, there is a large impact on results based on the number of components one chooses. Due to a difference in variance in a patient population from movement or any other confounding factor, a certain component could be split at a different point in patients and controls. Repeating a finding with a slightly higher or lower number of components (such as plus and minus 25% of the initial number of components) could increase confidence in the result.

(7) The final guideline concerns reconciling findings with previously published work. Although this point may seem obvious and is certainly not specific to resting state fcMRI, its importance makes it worth mentioning. If the current resting state fcMRI findings conflict with prior fcMRI work, it is crucial to explore possible etiologies of the conflict. It should not be sufficient to simply mention that other work has been done with differing conclusions. Resolving the discrepancy may involve additional analyses to directly explore differences in processing methodology, but such analyses are critical for accelerating consensus in the field and clinical applicability.

THE CASE FOR COLLABORATION

Despite the increasing number of papers being published on a daily basis by individual labs, clinical applicability of fcMRI is not likely to move forward without enhanced collaboration and data sharing between labs. Different processing techniques for analyzing resting state data make comparison across studies difficult. The majority of resting state articles focus on a few seed regions or a single network, leaving unexplored the vast majority of the brain's functional architecture. Finally, almost all studies focus on normal subjects or a single disease population making it difficult to assess reproducibility or determine the sensitivity or specificity of an identified abnormality for a specific disease.

In this review we explored several factors that make resting state fcMRI well-suited for translation into the clinical realm. However there are also several features that make it well-suited for databasing, data sharing, and collaboration. Due to the nature of spontaneous BOLD data, a single dataset can be used for multiple analyses and can address a wide variety of neuroscience questions. Furthermore, the paradigms used to study spontaneous BOLD

activity are relatively simple compared to task-based imaging studies with multiple stimuli presented at varying intervals. These factors make spontaneous BOLD data ideally suited for reanalysis and inclusion in a database.

The above factors have motivated the creation of two online databases focused on resting state fcMRI data. The first is both an analysis package and database termed BrainSCAPE (Spontaneous Correlation Analysis Processing Engine)[1] (Fox et al., 2007a). This tool allows users to upload, analyze, and share their spontaneous BOLD data as well as analyze freely shared data from other labs. More recently a second database has been launched termed the NITRIC 1000 connectome project[2] and includes a large number of functional connectivity datasets freely available for download (Biswal et al., 2010). By providing access to multiple datasets, effects in one study can easily be confirmed and compared with results from multiple other datasets. We anticipate that collaborative projects such as these will accelerate advances in the field and may prove valuable in assessing the sensitivity and specificity of intrinsic abnormalities underlying human disease.

TECHNIQUE DEVELOPMENT

Finally, an improvement in clinical utility is likely to come from further technique development. One area that is likely to be essential as we move from studies of groups of patients to obtaining prognostic and diagnostic information on a single patient is improving signal to noise. As mentioned at the beginning of this article, studies of resting state fluctuations do enjoy a potential signal to noise advantage over task-based studies. However, in task-based studies one can improve the signal to noise by simply increasing the number of trials and the amount of averaging. The technique for improving signal to noise in resting state studies is less straight forward. It is important to recognize that not all spontaneous BOLD fluctuations are due to underlying neuronal fluctuations in distinct cortical systems but may also come from non-neuronal sources. Although the quantitative impact of these noise sources is likely small relative to neuronal fluctuations, spontaneous BOLD modulation can be measured in a water phantom (Zarahn et al., 1997), and physiological fluctuations such as cardiac or respiratory activity can account for a significant fraction of spontaneous BOLD variance in human data (Glover et al., 2000; Wise et al., 2004; Birn et al., 2006; Lund et al., 2006; Chang and Glover, 2009). Improvements in signal to noise could therefore come from reducing the contribution of these non-neuronal fluctuations.

One strategy to account for non-neuronal noise is to employ a high sampling rate which prevents aliasing of higher frequency cardiac or respiratory activity (Biswal et al., 1995; Lowe et al., 1998; Cordes et al., 2001; De Luca et al., 2006); however this comes with the limitation of reduced spatial coverage. Alternatively, physiological parameters can be measured during BOLD acquisition and removed from the data through linear regression (Glover et al., 2000; Rombouts et al., 2003; Birn et al., 2006; Deshpande et al., 2006; Lund et al., 2006; Chang et al., 2009; Chang and Glover, 2009). Finally, noise sources can be isolated from the BOLD data itself through techniques such as ICA (Kiviniemi et al., 2003; Bartels and Zeki, 2004; Beckmann et al., 2005), regressing out signals common to all voxels (the global signal) (Zarahn et al., 1997; Macey et al., 2004; Fox et al., 2005, 2009), or regressing out signals from regions likely to have a relatively high degree of physiological artifact relative to the amount of neuronal activity such as the ventricles or white matter (Rombouts et al., 2003; Fox et al., 2005). By improving signal to noise, one can begin to reduce scan time and improve clinical applicability.

Other technique advances that may be helpful are increasing the fMRI data that can be used for resting state analyses. For example, research may be expanded by using resting epochs from block design task data (Fair et al., 2007) or removing task-related variance and performing fcMRI analyses on the residual (Arfanakis et al., 2000; Fair et al., 2007; He et al., 2007).

Finally, improved clinical applicability will likely come from moving beyond the fMRI scanner to multimodal investigations of spontaneous activity. Spontaneous fluctuations in the BOLD signal have been shown to correlate with EEG (Laufs et al., 2003), local field potentials (Shmuel and Leopold, 2008), and slow cortical potentials recorded with subdural electrode grids (He et al., 2008). Also resting state functional connectivity analyses are now being done with spontaneous fluctuations observed with near infrared spectroscopy (White et al., 2009). Such techniques raise the potential for studying continuous resting state correlations in situations where an MRI scanner is not practical such as real-time monitoring in intensive care units or operating rooms.

CONCLUSIONS

Resting state fluctuations in the BOLD signal of fMRI provide good signal to noise, require minimal patient compliance, can be obtained under anesthesia, and are well suited for translation into the clinical realm. Clinical applications include research studies focused on group differences, biomarkers for obtaining diagnostic and prognostic information in a single subject, and guidance of invasive and non-invasive treatments. Several guidelines for resting state studies of brain disease have been proposed here and may improve the reproducibility of findings and facilitate clinical translation. Finally, improvement in processing techniques of the fMRI signal as well moving beyond the fMRI signal to other modalities that can also assess low-frequency fluctuations are likely to be important as we begin to realize the potential of resting state fluctuations in the clinical realm.

[1]www.brainscape.org

[2]www.nitrc.org/projects/fcon_1000

REFERENCES

Abdi, H. (2007). "Bonferroni and Šidák corrections for multiple comparisons," in *Encyclopedia of Measurement and Statistics*, ed. N. J. Salkind (Thousand Oaks, CA: Sage).

Adcock, J. E., Wise, R. G., Oxbury, J. M., Oxbury, S. M., and Matthews, P. M. (2003). Quantitative fMRI assessment of the differences in lateralization of language-related brain activation in patients with temporal lobe epilepsy. *Neuroimage* 18, 423–438.

Allen, G., Barnard, H., McColl, R., Hester, A. L., Fields, J. A., Weiner, M. F., Ringe, W. K., Lipton, A. M., Brooker, M., McDonald, E., Rubin, C. D., and Cullum, C. M. (2007). Reduced hippocampal functional connectivity in Alzheimer disease. *Arch. Neurol.* 64, 1482–1487.

Ames, A. I. (2000). CNS energy metabolism as related to function. *Brain Res. Rev.* 34, 42–68.

Anand, A., Li, Y., Wang, Y., Lowe, M. J., and Dzemidzic, M. (2009). Resting state corticolimbic connectivity abnormalities in unmedicated bipolar disorder and unipolar depression. *Psychiatry Res.* 171, 189–198.

Anand, A., Li, Y., Wang, Y., Wu, J., Gao, S., Bukhari, L., Mathews, V. P., Kalnin, A., and Lowe, M. J. (2005a). Activity and connectivity of brain mood regulating circuit in depression: a functional magnetic

resonance study. *Biol. Psychiatry* 57, 1079–1088.

Anand, A., Li, Y., Wang, Y., Wu, J., Gao, S., Bukhari, L., Mathews, V. P., Kalnin, A., and Lowe, M. J. (2005b). Antidepressant effect on connectivity of the mood-regulating circuit: an fMRI study. *Neuropsychopharmacology* 30, 1334–1344.

Andrews-Hanna, J. R., Snyder, A. Z., Vincent, J. L., Lustig, C., Head, D., Raichle, M. E., and Buckner, R. L. (2007). Disruption of large-scale brain systems in advanced aging. *Neuron* 56, 924–935.

Arfanakis, K., Cordes, D., Haughton, V. M., Moritz, C. H., Quigley, M. A., and Meyerand, M. E. (2000). Combining independent component analysis and correlation analysis to probe interregional connectivity in fMRI task activation datasets. *Magn. Reson. Imaging* 18, 921–930.

Attwell, D., and Laughlin, S. B. (2001). An energy budget for signaling in the grey matter of the brain. *J. Cereb. Blood Flow Metab.* 21, 1133–1145.

Bartels, A., and Zeki, S. (2004). The chronoarchitecture of the human brain – natural viewing conditions reveal a time-based anatomy of the brain. *Neuroimage* 22, 419–433.

Beckmann, C. F., DeLuca, M., Devlin, J. T., and Smith, S. M. (2005). Investigations into resting-state connectivity using independent component analysis. *Philos. Trans. R. Soc. Lond., B, Biol. Sci.* 360, 1001–1013.

Bettus, G., Guedj, E., Joyeux, F., Confort-Gouny, S., Soulier, E., Laguitton, V., Cozzone, P. J., Chauvel, P., Ranjeva, J. P., Bartolomei, F., and Guye, M. (2009). Decreased basal fMRI functional connectivity in epileptogenic networks and contralateral compensatory mechanisms. *Hum. Brain Mapp.* 30, 1580–1591.

Binder, J. R., Swanson, S. J., Hammeke, T. A., Morris, G. L., Mueller, W. M., Fischer, M., Benbadis, S., Frost, J. A., Rao, S. M., and Haughton, V. M. (1996). Determination of language dominance using functional MRI: a comparison with the Wada test. *Neurology* 46, 978–984.

Birn, R. M., Diamond, J. B., Smith, M. A., and Bandettini, P. A. (2006). Separating respiratory-variation-related fluctuations from neuronal-activity-related fluctuations in fMRI. *Neuroimage* 31, 1536–1548.

Biswal, B., Yetkin, F., Haughton, V., and Hyde, J. (1995). Functional connectivity in the motor cortex of resting human brain using echo-planar MRI. *Magn. Reson. Med.* 34, 537–541.

Biswal, B. B., Mennes, M., Zuo, X. N., Gohel, S., Kelly, C., Smith, S. M., Beckmann, C. F., Adelstein, J. S., Buckner, R. L., Colcombe, S., Dogonowski, A. M., Ernst, M., Fair, D., Hampson, M., Hoptman, M. J., Hyde, J. S., Kiviniemi, V. J., Kotter, R., Li, S. J., Lin, C. P., Lowe, M. J., Mackay, C., Madden, D. J., Madsen, K. H., Margulies, D. S., Mayberg, H. S., McMahon, K., Monk, C. S., Mostofsky, S. H., Nagel, B. J., Pekar, J. J., Peltier, S. J., Petersen, S. E., Riedl, V., Rombouts, S. A., Rypma, B., Schlaggar, B. L., Schmidt, S., Seidler, R. D., Siegle, G. J., Sorg, C., Teng, G. J., Veijola, J., Villringer, A., Walter, M., Wang, L., Weng, X. C., Whitfield-Gabrieli, S., Williamson, P., Windischberger, C., Zang, Y. F., Zhang, H. Y., Castellanos, F. X., and Milham, M. P. (2010). Toward discovery science of human brain function. *Proc. Natl. Acad. Sci. U.S.A.* 107, 4734–4739.

Bluhm, R., Williamson, P., Lanius, R., Theberge, J., Densmore, M., Bartha, R., Neufeld, R., and Osuch, E. (2009a). Resting state default-mode network connectivity in early depression using a seed region-of-interest analysis: decreased connectivity with caudate nucleus. *Psychiatry Clin. Neurosci.* 63, 754–761.

Bluhm, R. L., Miller, J., Lanius, R. A., Osuch, E. A., Boksman, K., Neufeld, R. W., Theberge, J., Schaefer, B., and Williamson, P. C. (2009b). Retrosplenial cortex connectivity in schizophrenia. *Psychiatry Res.* 174, 17–23.

Bluhm, R. L., Williamson, P. C., Osuch, E. A., Frewen, P. A., Stevens, T. K., Boksman, K., Neufeld, R. W., Theberge, J., and Lanius, R. A. (2009c). Alterations in default network connectivity in posttraumatic stress disorder related to early-life trauma. *J. Psychiatry Neurosci.* 34, 187–194.

Bluhm, R. L., Miller, J., Lanius, R. A., Osuch, E. A., Boksman, K., Neufeld, R., Theberge, J., Schaefer, B., and Williamson, P. (2007). Spontaneous low-frequency fluctuations in the BOLD signal in schizophrenic patients: anomalies in the default network. *Schizophr. Bull.* 33, 1004–1012.

Boly, M., Tshibanda, L., Vanhaudenhuyse, A., Noirhomme, Q., Schnakers, C., Ledoux, D., Boveroux, P., Garweg, C., Lambermont, B., Phillips, C., Luxen, A., Moonen, G., Bassetti, C., Maquet, P., and Laureys, S. (2009). Functional connectivity in the default network during resting state is preserved in a vegetative but not in a brain dead patient. *Hum. Brain Mapp.* 30, 2393–2400.

Cao, Q., Zang, Y., Sun, L., Sui, M., Long, X., Zou, Q., and Wang, Y. (2006). Abnormal neural activity in children with attention deficit hyperactivity disorder: a resting-state functional magnetic resonance imaging study. *Neuroreport* 17, 1033–1036.

Castellanos, F. X., Margulies, D. S., Kelly, C., Uddin, L. Q., Ghaffari, M., Kirsch, A., Shaw, D., Shehzad, Z., Di Martino, A., Biswal, B., Sonuga-Barke, E. J., Rotrosen, J., Adler, L. A., and Milham, M. P. (2008). Cingulate-precuneus interactions: a new locus of dysfunction in adult attention-deficit/hyperactivity disorder. *Biol. Psychiatry* 63, 332–337.

Cauda, F., D'Agata, F., Sacco, K., Duca, S., Cocito, D., Paolasso, I., Isoardo, G., and Geminiani, G. (2009a). Altered resting state attentional networks in diabetic neuropathic pain. *J. Neurol. Neurosurg. Psychiatry*. [Epub ahead of print].

Cauda, F., Micon, B. M., Sacco, K., Duca, S., D'Agata, F., Geminiani, G., and Canavero, S. (2009b). Disrupted intrinsic functional connectivity in the vegetative state. *J. Neurol. Neurosurg. Psychiatr.* 80, 429–431.

Cauda, F., Sacco, K., D'Agata, F., Duca, S., Cocito, D., Geminiani, G., Migliorati, F., and Isoardo, G. (2009c). Low-frequency BOLD fluctuations demonstrate altered thalamocortical connectivity in diabetic neuropathic pain. *BMC Neurosci.* 10, 138.

Cauda, F., Sacco, K., Duca, S., Cocito, D., D'Agata, F., Geminiani, G. C., and Canavero, S. (2009d). Altered resting state in diabetic neuropathic pain. *PLoS ONE* 4, e4542. doi: 10.1371/journal.pone.0004542.

Chang, C., Cunningham, J. P., and Glover, G. H. (2009). Influence of heart rate on the BOLD signal: the cardiac response function. *Neuroimage* 44, 857–869.

Chang, C., and Glover, G. H. (2009). Effects of model-based physiological noise correction on default mode network anti-correlations and correlations. *Neuroimage* 47, 1448–1459.

Chang, C., and Glover, G. H. (2010). Time-frequency dynamics of resting-state brain connectivity measured with fMRI. *Neuroimage* 50, 81–98.

Cherkassky, V. L., Kana, R. K., Keller, T. A., and Just, M. A. (2006). Functional connectivity in a baseline resting-state network in autism. *Neuroreport* 17, 1687–1690.

Church, J. A., Fair, D. A., Dosenbach, N. U., Cohen, A. L., Miezin, F. M., Petersen, S. E., and Schlaggar, B. L. (2009). Control networks in paediatric Tourette syndrome show immature and anomalous patterns of functional connectivity. *Brain* 132, 225–238.

Cordes, D., Haughton, V. M., Arfanakis, K., Wendt, G. J., Turski, P. A., Moritz, C. H., Quigley, M. A., and Meyerand, M. E. (2000). Mapping functionally related regions of brain with functional connectivity MR imaging. *Am. J. Neuroradiol.* 21, 1636–1644.

Cordes, D., Haughton, V. M., Arfanakis, K., Wendt, G. J., Turski, P. A., Moritz, C. H., Quigley, M. A., and Meyerand, M. E. (2001). Frequencies contributing to functional connectivity in the cerebral cortex in 'resting-state' data. *Am. J. Neuroradiol.* 22, 1326–1333.

Damoiseaux, J. S., Beckmann, C. F., Arigita, E. J., Barkhof, F., Scheltens, P., Stam, C. J., Smith, S. M., and Rombouts, S. A. (2008). Reduced resting-state brain activity in the "default network" in normal aging. *Cereb. Cortex.* 18, 1856–1864.

De Luca, M., Beckmann, C. F., De Stefano, N., Matthews, P. M., and Smith, S. M. (2006). fMRI resting state networks define distinct modes of long-distance interactions in the human brain. *Neuroimage* 29, 1359–1367.

De Luca, M., Smith, S. M., De Stefano, N., Federico, A., and Matthews, P. M. (2005). Blood oxygenation level dependent contrast resting state networks are relevant to functional activity in the neocortical sensorimotor system. *Exp. Brain Res.* 167, 587–594.

Deshpande, G., LaConte, S., Peltier, S., and Hu, X. (2006). Tissue specificity of nonlinear dynamics in baseline fMRI. *Magn. Reson. Med.* 55, 626–632.

Dosenbach, N. U., Fair, D. A., Miezin, F. M., Cohen, A. L., Wenger, K. K., Dosenbach, R. A. T., Fox, M. D., Snyder, A. Z., Vincent, J. L., Raichle, M. E., Schlagger, B. L., and Petersen, S. E. (2007). Distinct brain networks for adaptive and stable task control in humans. *Proc. Natl. Acad. Sci. U.S.A.* 104, 11073–11078.

Etkin, A., Prater, K. E., Schatzberg, A. F., Menon, V., and Greicius, M. D. (2009). Disrupted amygdalar subregion functional connectivity and evidence of a compensatory network in generalized anxiety disorder. *Arch. Gen. Psychiatry* 66, 1361–1372.

Fair, D. A., Schlaggar, B. L., Cohen, A. L., Miezin, F. M., Dosenbach, N. U., Wenger, K. K., Fox, M. D., Snyder, A. Z., Raichle, M. E., and Petersen, S. E. (2007). A method for using blocked and event-related fMRI data to study "resting state" functional connectivity. *Neuroimage* 35, 396–405.

Fox, M. D., Corbetta, M., Snyder, A. Z., Vincent, J. L., and Raichle, M. E. (2006a). Spontaneous neuronal activity distinguishes human dorsal and ventral attention systems. *Proc. Natl. Acad. Sci. U.S.A.* 103, 10046–10051.

Fox, M. D., Snyder, A. Z., Zacks, J. M., and Raichle, M. E. (2006b). Coherent spontaneous activity accounts for trial-to-trial variability in human evoked brain responses. *Nat. Neurosci.* 9, 23–25.

Fox, M. D., Marcus, D. M., Snyder, A. Z., and Raichle, M. E. (2007a). "BrainSCAPE: an online spontnaeous correlation analysis processing environment for

fMRI BOLD data," in *Organization for Human Brain Mapping Annual Meeting*, Chicago, IL.

Fox, M. D., Snyder, A. Z., Vincent, J. L., and Raichle, M. E. (2007b). Intrinsic fluctuations within cortical systems account for intertrial variability in human behavior. *Neuron* 56, 171–184.

Fox, M. D., and Raichle, M. E. (2007). Spontaneous fluctuations in brain activity observed with functional magnetic resonance imaging. *Nat. Rev. Neurosci.* 8, 700–711.

Fox, M. D., Snyder, A. Z., Vincent, J. L., Corbetta, M., Van Essen, D. C., and Raichle, M. E. (2005). The human brain is intrinsically organized into dynamic, anticorrelated functional networks. *Proc. Natl. Acad. Sci. U.S.A.* 102, 9673–9678.

Fox, M. D., Zhang, D., Snyder, A. Z., and Raichle, M. E. (2009). The global signal and observed anticorrelated resting state brain networks. *J. Neurophysiol.* 101, 3270–3283.

Fransson, P. (2005). Spontaneous low-frequency BOLD signal fluctuations: an fMRI investigation of the resting-state default mode of brain function hypothesis. *Hum. Brain Mapp.* 26, 15–29.

Friston, K. J., Frith, C. D., Liddle, P. F., and Frackowiak, R. S. J. (1993). Functional connectivity: the principal component analysis of large (PET) data sets. *J. Cereb. Blood Flow Metab.* 13, 5–14.

Fukunaga, M., Horovitz, S. G., Van Gelderen, P., de Zwart, J. A., Jansma, J. M., Ikonomidou, V. N., Chu, R., Deckers, R. H. R., Leopold, D. A., and Duyn, J. H. (2006). Large-amplitude, spatially correlated fluctuations in BOLD fMRI signals during extended rest and light sleep. *Magn. Reson. Imaging* 24, 979–992.

Glover, G. H., Li, T. Q., and Ress, D. (2000). Image-based method for retrospective correction of physiological motion artifacts in fMRI: RETROICOR. *Magn. Reson. Med.* 44, 162–167.

Greicius, M. (2008). Resting-state functional connectivity in neuropsychiatric disorders. *Curr. Opin. Neurol.* 21, 424–430.

Greicius, M. D., Barad, M., Ueno, T., and Mackey, S. C. (2008a). "Chronic pain remodels the brain's salience network: a resting-state fMRI study," in *14th International Meeting of the Organization for Human Brain Mapping Melbourne*, Australia.

Greicius, M. D., Kiviniemi, V., Tervonen, O., Vainionpaa, V., Alahuhta, S., Reiss, A. L., and Menon, V. (2008b). Persistent default-mode network connectivity during light sedation. *Hum. Brain Mapp.* 29, 839–847.

Greicius, M. D., Flores, B. H., Menon, V., Glover, G. H., Solvason, H. B., Kenna, H., Reiss, A. L., and Schatzberg, A. F. (2007). Resting-state functional connectivity in major depression: abnormally increased contributions from subgenual cingulate cortex and thalamus. *Biol. Psychiatry* 62, 429–437.

Greicius, M. D., Krasnow, B., Reiss, A. L., and Menon, V. (2003). Functional connectivity in the resting brain: a network analysis of the default mode hypothesis. *Proc. Natl. Acad. Sci. U.S.A.* 100, 253–258.

Greicius, M. D., Srivastava, G., Reiss, A. L., and Menon, V. (2004). Default-mode network activity distinguishes Alzheimer's disease from healthy aging: evidence from functional MRI. *Proc. Natl. Acad. Sci. U.S.A.* 101, 4637–4642.

Haberg, A., Kvistad, K. A., Unsgard, G., and Haraldseth, O. (2004). Preoperative blood oxygen level-dependent functional magnetic resonance imaging in patients with primary brain tumors: clinical application and outcome. *Neurosurgery* 54, 902–914; discussion 914–905.

Hampson, M., Driesen, N. R., Skudlarski, P., Gore, J. C., and Constable, R. T. (2006). Brain connectivity related to working memory performance. *J. Neurosci.* 26, 13338–13343.

Hampson, M., Peterson, B. S., Skudlarski, P., Gatenby, J. C., and Gore, J. C. (2002). Detection of functional connectivity using temporal correlations in MR images. *Hum. Brain Mapp.* 15, 247–262.

Haynes, J. D., and Rees, G. (2006). Decoding mental states from brain activity in humans. *Nat. Rev. Neurosci.* 7, 523–534.

He, B. J., Snyder, A. Z., Vincent, J. L., Epstein, A., Shulman, G. L., and Corbetta, M. (2007). Breakdown of functional connectivity in frontoparietal networks underlies behavioral deficits in spatial neglect. *Neuron* 53, 905–918.

He, B. J., Snyder, A. Z., Zempel, J. M., Smyth, M. D., and Raichle, M. E. (2008). Electrophysiological correlates of the brain's intrinsic large-scale functional architecture. *Proc. Natl. Acad. Sci. U.S.A.* 105, 16039–16044.

Hedden, T., Van Dijk, K. R., Becker, J. A., Mehta, A., Sperling, R. A., Johnson, K. A., and Buckner, R. L. (2009). Disruption of functional connectivity in clinically normal older adults harboring amyloid burden. *J. Neurosci.* 29, 12686–12694.

Horovitz, S. G., Fukunaga, M., de Zwart, J. A., Van Gelderen, P., Fulton, S. C., Balkin, T. J., and Duyn, J. H. (2006). "The default-mode network connectivity during awake and early sleep: a simultaneous EEG-BOLD-fMRI study," in *Organization for Human Brain Mapping Annual Meeting*, Florence, Italy 686 M-PM.

Horwitz, B. (2003). The elusive concept of brain connectivity. *Neuroimage* 19, 466–470.

Jafri, M. J., Pearlson, G. D., Stevens, M., and Calhoun, V. D. (2008). A method for functional network connectivity among spatially independent resting-state components in schizophrenia. *Neuroimage* 39, 1666–1681.

Kennedy, D. P., and Courchesne, E. (2008). The intrinsic functional organization of the brain is altered in autism. *Neuroimage* 39, 1877–1885.

Kiviniemi, V., Kantola, J. H., Jauhiainen, J., Hyvarinen, A., and Tervonen, O. (2003). Independent component analysis of nondeterministic fMRI signal sources. *Neuroimage* 19, 253–260.

Kokkonen, S. M., Nikkinen, J., Remes, J., Kantola, J., Starck, T., Haapea, M., Tuominen, J., Tervonen, O., and Kiviniemi, V. (2009). Preoperative localization of the sensorimotor area using independent component analysis of resting-state fMRI. *Magn. Reson. Imaging* 27, 733–740.

Laufs, H., Krakow, K., Sterzer, P., Eger, E., Beyerle, A., Salek-Haddadi, A., and Kleinschmidt, A. (2003). Electroencephalographic signatures of attentional and cognitive default modes in spontaneous brain activity fluctuations at rest. *Proc. Natl. Acad. Sci. U.S.A.* 100, 11053–11058.

Lee, C. C., Ward, H. A., Sharbrough, F. W., Meyer, F. B., Marsh, W. R., Raffel, C., So, E. L., Cascino, G. D., Shin, C., Xu, Y., Riederer, S. J., and Jack, C. R., Jr. (1999). Assessment of functional MR imaging in neurosurgical planning. *AJNR Am. J. Neuroradiol.* 20, 1511–1519.

Lemieux, L. (2004). Electroencephalography-correlated functional MR imaging studies of epileptic activity. *Neuroimaging Clin. N. Am.* 14, 487–506.

Lennie, P. (2003). The cost of cortical computation. *Curr. Biol.* 13, 493–497.

Li, S. J., Li, Z., Wu, G., Zhang, M. J., Franczak, M., and Antuono, P. G. (2002). Alzheimer disease: evaluation of a functional MR imaging index as a marker. *Radiology* 225, 253–259.

Liang, M., Zhou, Y., Jiang, T., Liu, Z., Tian, L., Liu, H., and Hao, Y. (2006). Widespread functional disconnectivity in schizophrenia with resting-state functional magnetic resonance imaging. *Neuroreport* 17, 209–213.

Liu, H., Buckner, R. L., Talukdar, T., Tanaka, N., Madsen, J. R., and Stufflebeam, S. M. (2009). Task-free presurgical mapping using functional magnetic resonance imaging intrinsic activity. *J. Neurosurg.* 111, 746–754.

Liu, H., Liu, Z., Liang, M., Hao, Y., Tan, L., Kuang, F., Yanhong, Y., Xu, L., and Jiang, T. (2006). Decreased regional homogeneity in schizophrenia: a resting state functional magnetic resonance imaging study. *Neuroreport* 17, 19–22.

Liu, Y., Liang, M., Zhou, Y., He, Y., Hao, Y., Song, M., Yu, C., Liu, H., Liu, Z., and Jiang, T. (2008). Disrupted small-world networks in schizophrenia. *Brain*. 131(Pt 4), 945–961.

Liu, Y., Yu, C., Liang, M., Li, J., Tian, L., Zhou, Y., Qin, W., Li, K., and Jiang, T. (2007). Whole brain functional connectivity in the early blind. *Brain*. 130(Pt 8), 2085–2096.

Logothetis, N. K. (2003). The underpinnings of the BOLD functional magnetic resonance imaging signal. *J. Neurosci.* 23, 3963–3971.

Lowe, M. J., Mock, B. J., and Sorenson, J. A. (1998). Functional connectivity in single and multislice echoplanar imaging using resting-state fluctuations. *Neuroimage* 7, 119–132.

Lowe, M. J., Phillips, M. D., Lurito, J. T., Mattson, D. L., Dzemidzic, M., and Mathews, V. P. (2002). Multiple sclerosis: low-frequency temporal blood oxygen level-dependent fluctuations indicate reduced functional connectivity – initial results. *Radiology* 224, 184–192.

Lui, S., Ouyang, L., Chen, Q., Huang, X., Tang, H., Chen, H., Zhou, D., Kemp, G. J., and Gong, Q. (2008). Differential interictal activity of the precuneus/posterior cingulate cortex revealed by resting state functional MRI at 3T in generalized vs. partial seizure. *J. Magn. Reson. Imaging* 27, 1214–1220.

Lund, T. E., Madsen, K. H., Sidaros, K., Luo, W., and Nichols, T. E. (2006). Non-white noise in fMRI: does modeling have an impact? *Neuroimage* 29, 54–66.

Macey, P. M., Macey, K. E., Kumar, R., and Harper, R. M. (2004). A method for the removal of global effects from fMRI time series. *Neuroimage* 22, 360–366.

Matthews, P. M., Honey, G. D., and Bullmore, E. T. (2006). Applications of fMRI in translational medicine and clinical practice. *Nat. Rev. Neurosci.* 7, 732–744.

Mohammadi, B., Kollewe, K., Samii, A., Krampfl, K., Dengler, R., and Munte, T. F. (2009). Changes of resting state brain networks in amyotrophic lateral sclerosis. *Exp. Neurol.* 217, 147–153.

Monk, C. S., Peltier, S. J., Wiggins, J. L., Weng, S. J., Carrasco, M., Risi, S., and Lord, C. (2009). Abnormalities of intrinsic functional connectivity in autism spectrum disorders. *Neuroimage* 47, 764–772.

Murphy, K., Birn, R. M., Handwerker, D. A., Jones, T. B., and Bandettini, P. A.

(2009). The impact of global signal regression on resting state correlations: are anti-correlated networks introduced? *Neuroimage* 44, 893–905.

Norman, K. A., Polyn, S. M., Detre, G. J., and Haxby, J. V. (2006). Beyond mind-reading: multi-voxel pattern analysis of fMRI data. *Trends Cogn. Sci. (Regul. Ed.)* 10, 424–430.

Peltier, S. J., Kerssens, C., Hamann, S. B., Sebel, P. S., Byas-Smith, M., and Hu, X. (2005). Functional connectivity changes with concentration of sevoflurane anaesthesia. *Neuroreport* 16, 285–288.

Pujol, J., Conesa, G., Deus, J., Lopez-Obarrio, L., Isamat, F., and Capdevila, A. (1998). Clinical application of functional magnetic resonance imaging in presurgical identification of the central sulcus. *J. Neurosurg.* 88, 863–869.

Raichle, M. E. (2000). "A brief history of human functional brain mapping," in *Brain Mapping The Systems*, eds A. W. Toga and J. C. Mazziotta (San Diego: Academic Press), 33–75.

Raichle, M. E., MacLeod, A. M., Snyder, A. Z., Powers, W. J., Gusnard, D. A., and Shulman, G. L. (2001). A default mode of brain function. *Proc. Natl. Acad. Sci. U.S.A.* 98, 676–682.

Raichle, M. E., and Mintun, M. A. (2006). Brain work and brain imaging. *Annu. Rev. Neurosci.* 29, 449–476.

Rogers, B. P., Morgan, V. L., Newton, A. T., and Gore, J. C. (2007). Assessing functional connectivity in the human brain by fMRI. *Magn. Reson. Imaging* 25, 1347–1357.

Rombouts, S. A. R. B., Stam, C. J., Kuijer, J. P. A., Scheltens, P., and Barkhof, F. (2003). Identifying confounds to increase specificity during a "no task condition". Evidence for hippocampal connectivity using fMRI. *Neuroimage* 20, 1236–1245.

Salvador, R., Martinez, A., Pomarol-Clotet, E., Sarro, S., Suckling, J., and Bullmore, E. (2007). Frequency based mutual information measures between clusters of brain regions in functional magnetic resonance imaging. *Neuroimage* 35, 83–88.

Seeley, W. W., Allman, J. M., Carlin, D. A., Crawford, R. K., Macedo, M. N., Greicius, M. D., Dearmond, S. J., and Miller, B. L. (2007a). Divergent social functioning in behavioral variant frontotemporal dementia and Alzheimer disease: reciprocal networks and neuronal evolution. *Alzheimer Dis. Assoc. Disord.* 21, S50–57.

Seeley, W. W., Menon, V., Schatzberg, A. F., Keller, J., Glover, G. H., Kenna, H., Reiss, A. L., and Greicius, M. D. (2007b). Dissociable intrinsic connectivity networks for salience processing and executive control. *J. Neurosci.* 27, 2349–2356.

Seeley, W. W., Crawford, R. K., Miller, B. L., and Greicius, M. D. (2008). "Cortical neurodegeneration syndromes target human structural-functional covariance networks," in *14th International Meeting of the Organization for Human Brain Mapping Melbourne*, Australia.

Sheline, Y. I., Raichle, M. E., Snyder, A. Z., Morris, J. C., Head, D., Wang, S., and Mintun, M. A. (2010). Amyloid plaques disrupt resting state default mode network connectivity in cognitively normal elderly. *Biol. Psychiatry* 67, 584–587.

Shimony, J. S., Zhang, D., Johnston, J. M., Fox, M. D., Roy, A., and Leuthardt, E. C. (2009). Resting-state spontaneous fluctuations in brain activity: a new paradigm for presurgical planning using fMRI. *Acad. Radiol.* 16, 578–583.

Shmuel, A., and Leopold, D. A. (2008). Neuronal correlates of spontaneous fluctuations in fMRI signals in monkey visual cortex: implications for functional connectivity at rest. *Hum. Brain Mapp.* 29, 751–761.

Shulman, R. G., Rothman, D. L., Behar, K. L., and Hyder, F. (2004). Energetic basis of brain activity: implications for neuroimaging. *Trends Neurosci.* 27, 489–495.

Sorg, C., Riedl, V., Muhlau, M., Calhoun, V. D., Eichele, T., Laer, L., Drzezga, A., Forstl, H., Kurz, A., Zimmer, C., and Wohlschlager, A. M. (2007). Selective changes of resting-state networks in individuals at risk for Alzheimer's disease. *Proc. Natl. Acad. Sci. U.S.A.* 104, 18760–18765.

Supekar, K., Menon, V., Rubin, D., Musen, M., and Greicius, M. D. (2008). Network analysis of intrinsic functional brain connectivity in Alzheimer's disease. *PLoS Comput. Biol.* 4, e1000100. doi: 10.1371/journal.pcbi.1000100.

Tian, L., Jiang, T., Wang, Y., Zang, Y., He, Y., Liang, M., Sui, M., Cao, Q., Hu, S., Peng, M., and Zhuo, Y. (2006). Altered resting-state functional connectivity patterns of anterior cingulate cortex in adolescents with attention deficit hyperactivity disorder. *Neurosci. Lett.* 400, 39–43.

Vanhaudenhuyse, A., Noirhomme, Q., Tshibanda, L. J., Bruno, M. A., Boveroux, P., Schnakers, C., Soddu, A., Perlbarg, V., Ledoux, D., Brichant, J. F., Moonen, G., Maquet, P., Greicius, M. D., Laureys, S., and Boly, M. (2010). Default network connectivity reflects the level of consciousness in non-communicative brain-damaged patients. *Brain* 133(Pt 1), 161–171.

Vincent, J. L., Patel, G. H., Fox, M. D., Snyder, A. Z., Baker, J. T., Van Essen, D. C., Zempel, J. M., Snyder, L. H., Corbetta, M., and Raichle, M. E. (2007). Intrinsic functional architecture in the anesthetized monkey brain. *Nature* 447, 83–86.

Vincent, J. L., Snyder, A. Z., Fox, M. D., Shannon, B. J., Andrews, J. R., Raichle, M. E., and Buckner, R. L. (2006). Coherent spontaneous activity identifies a hippocampal-parietal mnemonic network. *J. Neurophysiol.* 96, 3517–3531.

Vlieger, E. J., Majoie, C. B., Leenstra, S., and Den Heeten, G. J. (2004). Functional magnetic resonance imaging for neurosurgical planning in neurooncology. *Eur. Radiol.* 14, 1143–1153.

Waites, A. B., Briellman, R. S., Saling, M. M., Abbott, D. F., and Jackson, G. D. (2006). Functional connectivity networks are disrupted in left temporal lobe epilepsy. *Ann. Neurol.* 59, 335–343.

Wang, K., Jiang, T., Liang, M., Wang, L., Tian, L., Zhang, X., Li, K., and Liu, Z. (2006a). Discriminative analysis of early Alzheimer's disease based on two intrinsically anti-correlated networks with resting-state fMRI. *Med. Image Comput. Comput. Assist. Interv. Int. Conf. Med. Image Comput. Comput. Assist. Interv.* 9, 340–347.

Wang, L., Zang, Y., He, Y., Liang, M., Zhang, X., Tian, L., Wu, T., Jiang, T., and Li, K. (2006b). Changes in hippocampal connectivity in the early stages of Alzheimer's disease: evidence from resting state fMRI. *Neuroimage* 31, 496–504.

Wang, K., Liang, M., Wang, L., Tian, L., Zhang, X., Li, K., and Jiang, T. (2007). Altered functional connectivity in early Alzheimer's disease: a resting-state fMRI study. *Hum. Brain Mapp.* 28, 967–978.

Wang, L., Zhu, C., He, Y., Zang, Y., Cao, Q., Zhang, H., Zhong, Q., and Wang, Y. (2009). Altered small-world brain functional networks in children with attention-deficit/hyperactivity disorder. *Hum. Brain Mapp.* 30, 638–649.

Weissenbacher, A., Kasess, C., Gerstl, F., Lanzenberger, R., Moser, E., and Windischberger, C. (2009). Correlations and anticorrelations in resting-state functional connectivity MRI: a quantitative comparison of preprocessing strategies. *Neuroimage* 47, 1408–1416.

Weng, S. J., Wiggins, J. L., Peltier, S. J., Carrasco, M., Risi, S., Lord, C., and Monk, C. S. (2010). Alterations of resting state functional connectivity in the default network in adolescents with autism spectrum disorders. *Brain Res.* 1313, 202–214.

White, B. R., Snyder, A. Z., Cohen, A. L., Petersen, S. E., Raichle, M. E., Schlaggar, B. L., and Culver, J. P. (2009). Resting-state functional connectivity in the human brain revealed with diffuse optical tomography. *Neuroimage* 47, 148–156.

Whitfield-Gabrieli, S., Thermenos, H. W., Milanovic, S., Tsuang, M. T., Faraone, S. V., McCarley, R. W., Shenton, M. E., Green, A. I., Nieto-Castanon, A., LaViolette, P., Wojcik, J., Gabrieli, J. D., and Seidman, L. J. (2009). Hyperactivity and hyperconnectivity of the default network in schizophrenia and in first-degree relatives of persons with schizophrenia. *Proc. Natl. Acad. Sci. U.S.A.* 106, 1279–1284.

Wise, R. J. S., Ide, K., Poulin, M. J., and Tracey, I. (2004). Resting state fluctuations in arterial carbon dioxide induce significant low frequency variations in BOLD signal. *Neuroimage* 21, 1652–1664.

Yu, C., Liu, Y., Li, J., Zhou, Y., Wang, K., Tian, L., Qin, W., Jiang, T., and Li, K. (2008). Altered functional connectivity of primary visual cortex in early blindness. *Hum. Brain Mapp.* 29, 533–543.

Zang, Y. F., He, Y., Zhu, C. Z., Cao, Q. J., Sui, M. Q., Liang, M., Tian, L. X., Jiang, T. Z., and Wang, Y. F. (2007). Altered baseline brain activity in children with ADHD revealed by resting-state functional MRI. *Brain Dev.* 29, 83–91.

Zarahn, E., Aguirre, G. K., and D'Esposito, M. (1997). Empirical analyses of BOLD fMRI statistics. I. Spatially unsmoothed data collected under null-hypothesis conditions. *Neuroimage* 5, 179–197.

Zhang, D., Johnston, J. M., Fox, M. D., Leuthardt, E. C., Grubb, R. L., Chicoine, M. R., Smyth, M. D., Snyder, A. Z., Raichle, M. E., and Shimony, J. S. (2009a). Preoperative sensorimotor mapping in brain tumor patients using spontaneous fluctuations in neuronal activity imaged with functional magnetic resonance imaging: initial experience. *Neurosurgery* 65, 226–236.

Zhang, Z., Lu, G., Zhong, Y., Tan, Q., Liao, W., Chen, Z., Shi, J., and Liu, Y. (2009b). Impaired perceptual networks in temporal lobe epilepsy revealed by resting fMRI. *J. Neurol.* 256, 1705–1713.

Zhang, Z., Lu, G., Zhong, Y., Tan, Q., Yang, Z., Liao, W., Chen, Z., Shi, J., and Liu, Y. (2009c). Impaired attention network in temporal lobe epilepsy: a resting FMRI study. *Neurosci. Lett.* 458, 97–101.

Zhang, D., and Raichle, M. E. (2010). Disease and the brain's dark energy. *Nat. Rev. Neurol.* 6, 15–28.

Zhang, D., Snyder, A. Z., Fox, M. D., Sansbury, M. W., Shimony, J. S., and Raichle, M. E. (2008). Intrinsic functional relations between human cerebral cortex and thalamus. *J. Neurophysiol.* 100, 1740–1748.

Zhou, Y., Liang, M., Jiang, T., Tian, L., Liu, Y., Liu, Z., Liu, H., and Kuang, F. (2007). Functional dysconnectivity of the dorsolateral prefrontal cortex in first-episode schizophrenia using resting-state fMRI. *Neurosci. Lett.* 417, 297–302.

Zhu, C. Z., Zang, Y. F., Cao, Q. J., Yan, C. G., He, Y., Jiang, T. Z., Sui, M. Q., and Wang, Y. F. (2008). Fisher discriminative analysis of resting-state brain function for attention-deficit/hyperactivity disorder. *Neuroimage* 40, 110–120.

Zhu, C. Z., Zang, Y. F., Liang, M., Tian, L. X., He, Y., Li, X. B., Sui, M. Q., Wang, Y. F., and Jiang, T. Z. (2005). Discriminative analysis of brain function at resting-state for attention-deficit/hyperactivity disorder. *Med. Image Comput. Comput. Assist. Interv. Int. Conf. Med. Image Comput. Comput. Assist. Interv.* 8, 468–475.

Zuo, X. N., Kelly, C., Adelstein, J. S., Klein, D. F., Castellanos, F. X., and Milham, M. P. (2009). Reliable intrinsic connectivity networks: test-retest evaluation using ICA and dual regression approach. *Neuroimage* 49, 2163–2177.

Conflict of Interest Statement: The authors declare that the research was conducted in the absence of any commercial or financial relationships that could be construed as a potential conflict of interest.

Received: 09 February 2010; paper pending published: 11 March 2010; accepted: 11 May 2010; published online: 17 June 2010.

*Citation: Fox MD and Greicius M (2010) Clinical applications of resting state functional connectivity. Front. Syst. Neurosci. **4**:19. doi: 10.3389/fnsys.2010.00019*

frontiers in
SYSTEMS NEUROSCIENCE

REVIEW ARTICLE
published: 23 June 2010
doi: 10.3389/fnsys.2010.00020

The relation of ongoing brain activity, evoked neural responses, and cognition

Sepideh Sadaghiani[1,2,3]*, Guido Hesselmann[4], Karl J. Friston[5] and Andreas Kleinschmidt[1,2]

[1] *Institut National de la Santé et de la Recherche Médicale Unité 992 Cognitive Neuroimaging Unit, Gif-sur-Yvette, France*
[2] *NeuroSpin, I2BM, DSV, CEA, Gif-sur-Yvette, France*
[3] *International Max Planck Research School of Neural and Behavioural Sciences, University of Tübingen, Tübingen, Germany*
[4] *Department of Neurobiology, Weizmann Institute of Science, Rehovot, Israel*
[5] *Wellcome Trust Centre for Neuroimaging, University College London, London, UK*

Edited by:
Lucina Q. Uddin,
Stanford University, USA

Reviewed by:
Mike Fox, Partners Healthcare, USA
Gordon Shulman, Washington University School of Medicine, USA

****Correspondence:***
Sepideh Sadaghiani, Institut National de la Santé et de la Recherche Médicale Unité 992, NeuroSpin, CEA/SAC/DSV/I2BM, Bât 145, Point Courrier 156, F-91191 Gif-sur-Yvette, France.
e-mail: sepideh.sadaghiani@gmail.com

Ongoing brain activity has been observed since the earliest neurophysiological recordings and is found over a wide range of temporal and spatial scales. It is characterized by remarkably large spontaneous modulations. Here, we review evidence for the functional role of these ongoing activity fluctuations and argue that they constitute an essential property of the neural architecture underlying cognition. The role of spontaneous activity fluctuations is probably best understood when considering both their spatiotemporal structure and their functional impact on cognition. We first briefly argue against a "segregationist" view on ongoing activity, both in time and space, which would selectively associate certain frequency bands or levels of spatial organization with specific functional roles. Instead, we emphasize the functional importance of the full range, from differentiation to integration, of intrinsic activity within a hierarchical spatiotemporal structure. We then highlight the flexibility and context-sensitivity of intrinsic functional connectivity that suggest its involvement in functionally relevant information processing. This role in information processing is pursued by reviewing how ongoing brain activity interacts with afferent and efferent information exchange of the brain with its environment. We focus on the relationship between the variability of ongoing and evoked brain activity, and review recent reports that tie ongoing brain activity fluctuations to variability in human perception and behavior. Finally, these observations are discussed within the framework of the free-energy principle which – applied to human brain function – provides a theoretical account for a non-random, coordinated interaction of ongoing and evoked activity in perception and behavior.

Keywords: ongoing activity, spontaneous activity, resting state functional connectivity, intrinsic functional connectivity, fMRI, prestimulus activity, variability, fluctuations

INTRODUCTION

Our review is based on the premise that – just as man-made architectures (and probably even more so) – the nature of biological systems is best understood by jointly considering their form and function. We will attempt to apply this view to ongoing brain activity. Our review of the form of ongoing or "spontaneous" brain activity will cover its temporal and spatial structure. Instead of attempting to be exhaustive in this respect, we will selectively emphasize some aspects mainly for two reasons; first, because we feel they may be under-represented in a field that is currently dominated by the notion of "resting state networks"; second, because we feel that these aspects are helpful when pondering the function of ongoing activity. In the second part of our review, function will then be the theme developed in more detail. We will focus on cognitive consequences of ongoing activity *fluctuations*, for the simple reason that they permit the most direct probes of functional significance for a phenomenon that is no longer fully "spontaneous" when bound into a context so as to measure function. Across this analysis of form and function we will then discuss how one theoretical framework, that of "free energy" introduced by one of us (Friston, 2005), may provide important clues for understanding the nature of ongoing brain activity. Our review will mainly concentrate on the human brain and functional MRI. The latter has been informative due to its superb localizing power and its exquisite capability to record the dynamics of neuronal population activity across the entire brain and to hence capture large-scale functional connectivity patterns. Yet, for instance when addressing temporal properties as below, limitations of hemodynamic signals will lead us to also discuss electrophysiological findings as well as observations relying on invasive procedures that cannot usually be applied in human subjects.

THE TEMPORAL STRUCTURE OF ONGOING BRAIN ACTIVITY

One of the most prominent features of ongoing activity is the fact that it fluctuates over time. This in itself can give rise to interesting speculations regarding function. If one thinks of a car engine, where such behavior would be functionally deleterious, one might wonder whether, and if so how, such fluctuations can be associated with a functional benefit (McDonnell and Abbott, 2009). Let us first consider the formal properties of these temporal fluctuations.

Ongoing human brain activity recorded by local electrocorticography (Freeman et al., 2000) shows a power law scaling but also an embedding of discrete peaks reflecting band-limited oscillatory activity. Interestingly, power in these distinct frequency bands is in turn also modulated over time with a predominance of very slow

frequencies (Leopold et al., 2003; Nir et al., 2008). Descriptively, it has been shown that there is a coupling or nesting of the higher-frequency electrical activity into the infra-slow (usually defined as <0.1 Hz) fluctuations (Vanhatalo et al., 2004; He et al., 2010) but the mechanisms and directionality of this relation are not yet fully understood. Studies comparing invasive electrophysiological recordings with functional neuroimaging results have obtained evidence of coupling between hemodynamic signals and both slow cortical potentials (He et al., 2008) as well as power of high-frequency band-limited activity, both evoked and spontaneous (Nir et al., 2007; Shmuel and Leopold, 2008).

We conclude from these observations that the temporal properties of ongoing activity can serve to warn us against a preoccupation with the "millisecond range" when studying brain function. Yet, assuming a conservative stance, we also conclude that there is currently no reason for a rebound into a view where infra-slow fluctuations in a specific frequency range could be considered a distinct entity of neural processes, other than those active in the processing of, for instance, sensory events. Studies using fMRI have established an apparent predominance of slow fluctuations in ongoing brain activity but there are several caveats to be borne in mind. First, the issue of whether the actual neural activity reflected in the hemodynamic signals shows power law scaling as in electrical recordings is still being debated (Cole et al., 2010). It is certain that the low pass filter characteristics of hemodynamic signals only permit tracking of slow neural activity modulations, cutting off little above the range of the infra-slow frequencies. And there are additional concerns related to the fact that – in spite of quantitative differences – even "BOLD signal" variations from a water phantom can readily manifest power law scaling due to properties of the MRI scanner (Zarahn et al., 1997; but see also Fox et al., 2007). It has also not been established that the spatial pattern of functional connectivity depends on the temporal scale under consideration, other than obvious effects related to signal power.

Together, we suggest thinking of the presently available evidence as an indication that brain activity over time may display at least partially scale-invariant characteristics. Such pink noise or power law scaling is not a privilege of the brain or even of biological systems but a feature of many if not all complex systems (Mandelbrot, 1998). Its ubiquitous presence does not denigrate its importance though. Regarding the brain, several researchers have emphasized the importance of this temporal structure for endowing neural processes with an inherent long-term memory (Linkenkaer-Hansen et al., 2001; Buzsáki, 2006). The memory function in this view does not reside in a specific frequency range but merely has a holistic pattern. However, for an alternative opinion and a more differentiated discussion of these issues we refer readers to a recent review by Raichle (2010).

THE SPATIAL STRUCTURE OF ONGOING BRAIN ACTIVITY

Our main point in the previous section was to review the literature that safeguards us against a temporal "segregationist" view. We believe that there is a similar danger in the spatial domain. The reason why many laboratories have focused on infra-slow fluctuations is that due to their power and their at least partial distinctness from other, namely "noise" signal sources in functional neuroimaging, these fluctuations have proven useful for studying the spatial structure of ongoing brain activity. Such functional connectivity studies have also focused on the only paradigm which permits an apparently unambiguous assignment of signal variations to ongoing brain activity; namely, the "resting state". Despite concerns about contributions from technical and physiological noise, the rationale of these so-called resting-state functional connectivity studies has been validated by concurrent electrophysiological recordings. In particular, it has been established that slow fluctuations in power of band-limited oscillations can be directly linked to the ongoing activity fluctuations observed with fMRI (Shmuel and Leopold, 2008) and involve similar distributed spatial structures (Laufs et al., 2003).

With this functional imaging approach, it is now well established that spontaneous brain activity fluctuations are spatially organized into a largely reproducible structure. The emphasis in a (large) literature, whose review is beyond the scope of this article, has been to define anatomically such resting-state or intrinsic functional connectivity networks (ICNs). We will adopt the latter terminology because there is reason to believe that similar correlational structures persist even when subjects are exposed to vivid sensory stimulation (Golland et al., 2007). The definition of ICNs revolves essentially around two issues, that of constituent regions and that of boundaries. And this definition has relied on two approaches, one hypothesis-driven as exemplified in analysis of functional connectivity with a so-called seed region (e.g., Biswal et al., 1997; Greicius et al., 2003), the other data-driven as exemplified by independent component analyses (e.g., Beckmann et al., 2005). The ultimate goal of these analyses is to derive an anatomical segregation from the recordings of ongoing brain activity fluctuations. Notwithstanding a great degree of convergence and robustness across many different laboratories, both of these approaches have proven to be heavily influenced by user-dependent settings. What such settings usually express is the user's expectation regarding the degree of modularity in ongoing brain activity. While some laboratories emphasize big dichotomies (e.g., Fox et al., 2006b; Golland et al., 2008), others seek to establish a fine-grained differentiation (e.g., Margulies et al., 2007).

In this context, we would like to emphasize that the actual data structure does not suggest clear-cut modularity but only a gradual differentiation. The reason for such graded modularity is that the correlational structure of ongoing activity is bound together in a hierarchy. This structure is probably best thought of as a tree with the underlying activity correlations displaying a hierarchy from global to local levels (Ferrarini et al., 2009). These levels of organization range from the entirety of gray matter as the trunk, over systems of regions as the branches to within-region correlations as the foliage (Marrelec et al., 2008; Meunier et al., 2009). In fact, the strong presence of variance shared across all local levels and reflected in global gray matter (Schölvinck et al., 2010) correlation has led to considerable confusion regarding the degree of diversification or antagonism that can be observed across different ICNs (Fox et al., 2009; Murphy et al., 2009). ICNs can be considered a mid-level cross-section of this hierarchical tree where regions within an ICN share a lot of variance and where this variance is sufficiently distinct from that expressed in other ICNs to draw a separating line. As a function of whether one emphasizes similarity or distinctness of local variations in ongoing activity, data-driven analyses will produce quite different numbers of ICNs (e.g., Varoquaux et al., 2010). In our metaphor, this corresponds to the distance of the cross-section from the ground.

As a consequence of the hierarchical organization of ongoing activity, raising the level of cross-section higher from the ground will yield more fine-grained subdivisions of networks both at anatomical and functional connectivity levels. As an example, the postero-medial part of the most extensively studied ICN, the default-mode network, has recently been subdivided into three precuneus parts and a posterior cingulate part on the basis of distinct large-scale intrinsic connectivity patterns, each of which suggest different functional roles (Margulies et al., 2009). Another example involves the difficulty in anatomical and functional definition of the so-called "task-positive" system. An initially useful step was to distinguish the "task-negative" default-mode ICN from "task-positive" regions, the latter referring to a large set of regions showing activation in most types of cognitive paradigms (Fox et al., 2005). Using seed regions in the dorsal attention network, the resulting intrinsic connectivity system was not confined to the dorsal attention system as defined in paradigm-based studies (Corbetta and Shulman, 2002) but due to shared variance also included anterior insula/frontal operculum, anterior prefrontal cortex, and inferolateral parietal and frontal areas. These additional areas partially overlap with an added ICN, termed the fronto-parietal control system conceptualized to serve cognitive control (Vincent et al., 2008). Conversely, other studies dissected cognitive control functions into two distinct ICNs, a cingulo-insular-thalamic and a lateral parieto-frontal network for sustained vs. adaptive/executive cognitive control, respectively (Dosenbach et al., 2006, 2007; Seeley et al., 2007). These findings clarify that the hierarchically embedded levels of spatial structure in intrinsic connectivity range down to sub-network and ultimately sub-region correlations. In fact, albeit on a different temporal scale, such patterns can even be recovered within single areas, and align with their mesoscopic functional architecture (Kenet et al., 2003).

Over and above the issue of modularity, defining ICNs in terms of anatomical boundaries has also proven difficult. This difficulty is largely due to the fact that "networks" are not clear-cut and rigid sets of constituent regions. Rather, the term "network" should be thought of as a gradual clustering according to a similar activity profile. As such, this term can of course help to interpret, communicate and compare experimental results but should not mislead to consider networks as strictly segregated. The spatial patterns are susceptible to precise positioning of seed regions and it has for instance been demonstrated that there are fairly smooth transitional zones between ICNs (Cohen et al., 2008). Even though some of these difficulties may be due to the intrinsic spatial smoothness of hemodynamic signals rather than underlying neural architecture, such observations may account for observed discrepancies. With respect to the task-positive regions however, these difficulties also stem from the existence of an ensemble of several interconnected task-positive ICNs. Accordingly, the labeling issue becomes most critical for connection hubs such as the anterior insula (Sterzer and Kleinschmidt, 2010) which has been suggested to orchestrate activity across different ICNs (Sridharan et al., 2008). In addition to the ICNs discussed above, the anterior insula has also been characterized as a major node in a right-lateralized ventral attention system (Eckert et al., 2008). This latter system (Fox et al., 2006b) in turn widely overlaps with the aforementioned control systems, especially the lateral fronto-parietal subsystem. Together, we conclude that similar to what we emphasized in the temporal domain, ongoing activity variations also show a nested structure in the spatial domain that expresses an embedding of modularity into a hierarchy.

THE FUNCTION OF ONGOING BRAIN ACTIVITY

FUNCTIONAL CONNECTIVITY, STRUCTURAL CONNECTIVITY AND COGNITIVE CONTEXT

The difficulties in adequately capturing the spatiotemporal form of intrinsic brain activity that we have discussed in the previous section should not be thought of as mere empty battles of nomenclature. This form is important when pondering the function of intrinsic activity, and any proposal with respect to this function will be benchmarked against its potential for accounting for this spatiotemporal structure. The perspective that we have proposed in the previous section for functional connectivity is reminiscent of descriptions of structural brain connectivity and we have already appealed to these similarities in the tree metaphor (Bullmore and Sporns, 2009). A hypothesis about what determines the form of ongoing brain activity that ensues is that intrinsic functional connectivity simply reflects some neural "noise" that plays out on a non-random structural connectivity; and therefore takes on the shape of a limited set of spatial patterns (i.e., dynamics on structure). Indeed, computational simulations of functional connectivity using noisy input generate functional covariance patterns that reflect underlying structural circuitry (Sporns et al., 2000). And empirical evidence has been reported showing strong correspondence of intrinsic functional and anatomical connectivity (Skudlarski et al., 2008; Greicius et al., 2009). In more comprehensive investigations, at the level of the entire brain, this match has been confirmed but systematic quantitative analysis also revealed that it is not perfect. In other words, structural connectivity permitted only a partial prediction of the empirically observed functional connectivity (Honey et al., 2009). Of course, the imperfection in predicting functional from structural connectivity could simply reflect limitations in the methods applied for data acquisition and analysis. Yet, an important alternative hypothesis is that with underlying structural connectivity as a backbone functional connectivity is shaped by additional context-dependent modulation.

At first glance, this hypothesis seems to be at odds with the persistence of spatial ICN patterns across different levels of context and consciousness, from task- and stimulus-induced active states (Fair et al., 2007; Golland et al., 2007; Eckert et al., 2008), over resting wakefulness (Greicius et al., 2003; Fox et al., 2005; Fransson, 2005), light and deep sleep (Horovitz et al., 2007, 2009; Nir et al., 2008), light sedation (Greicius et al., 2008), to deep anesthesia in monkeys (Vincent et al., 2007) and severe disorders of consciousness as in vegetative state patients (Boly et al., 2009). Furthermore, the finding of robust intrinsic activity patterns in the absence of consciousness also suggests that intrinsic activity fluctuations cannot be considered merely or entirely the neural correlates of conscious, mentation or mind-wandering that in the absence of an explicit task paradigm simply remains experimentally uncontrolled (Buckner and Vincent, 2007).

However, evidence in favor of the hypothesis that ongoing brain activity is in fact context-sensitive has now been accumulated by a range of studies. Although functional connectivity patterns persist qualitatively across wide ranges of different functional contexts, as mentioned above, they do nonetheless express quantitative

changes. They differ for instance quantitatively between the healthy awake brain and the brain in a state of pathological unconsciousness, where functional connectivity within the so-called default-mode network decreases with the degree of consciousness; across minimally conscious state, vegetative state and ultimately coma (Vanhaudenhuyse et al., 2010). They also differ quantitatively in the healthy brain between wakefulness and deep (slow-wave) sleep, a state of physiological unconsciousness (Horovitz et al., 2009). It is noteworthy that the reduction in connectivity between posterior and frontal areas of the default-mode network during sleep is anatomically selective, and that fluctuation amplitudes within regions remain unchanged. This result makes it unlikely that modulations in intrinsic connectivity simply reflect a change of noise levels propagating through an anatomically connected system.

And even during the state of wakefulness (and on a shorter time scale) intrinsic connectivity patterns express differences that can be related to recent cognitive experience. Over the course of one scanning session, i.e., a time span that in all likelihood does not involve gross structural connectivity changes, adaptive modulation of intrinsic functional connectivity has been reported after visuomotor learning (Albert et al., 2009), episodic memory (Tambini et al., 2010) and language tasks (Waites et al., 2005; Hasson et al., 2009). These findings show that functional context interacts with the expression of intrinsic activity and thus motivates further experimental investigation of the functional significance of intrinsic activity.

A common critique of these latter studies is that they might collapse "true intrinsic" activity with reverberating traces of previous cognitive experience. Of course, the same critique holds for "pure" resting-state studies during wakefulness, because they at least include task-unrelated mind-wandering that constitutes an ongoing cognitive content (Mason et al., 2007; Christoff et al., 2009) and by its very nature cannot be considered to lack context. The only way to dissociate "true intrinsic" activity from more specifically context-related neural processes would be if there were spatiotemporal hallmarks selectively tagging intrinsic activity. Our review of its temporal and spatial form, however, suggests, at least to us, that no such properties can currently be identified with confidence. Alternatively, one may question whether such dissociation is inevitably justified and necessary and this leads one to consider the actual function of ongoing activity. We propose that its function is intimately related to cognition, and this relation is inherent to the brain, be it in a "resting" or active state. This proposal could seem at odds with the studies that we have discussed above and that show qualitative spatial correspondence between ICNs across very different functional brain states. But it is as true that ICNs strongly resemble spatial patterns with sets of regions that typically co-activate (or deactivate) in cognitive activation studies as a function of the paradigm (Smith et al., 2009). We therefore argue that function cannot be assigned purely on the basis of spatial patterns.

COGNITIVE CONSEQUENCES OF SPONTANEOUS ACTIVITY FLUCTUATIONS

In this section, we review a different way of addressing the function of ongoing activity. In this approach, the functional consequences of ongoing activity are assessed by studying whether fluctuations in ongoing activity can account for behavioral variability. From the previous sections we can derive the following predictions for such an account: (1) ongoing activity should affect behavior with a time constant that is sufficiently slow to be captured by hemodynamic signals. (2) The spatial pattern within which ongoing activity affects behavior should be context-dependent and should be detectable precisely at that position within a hierarchical structure that best matches the functional demands of a given context. In the following, we review evidence for both predictions from recent neuroimaging studies.

Two lines of earlier research suggested that there might indeed be a link between ongoing activity fluctuations and behavioral variability. One is that behavioral performance when repeating the same task over and over again shows fluctuations with a qualitatively similar temporal profile as ongoing activity, i.e., high power at low frequencies (Gilden, 2001). The other is that neural responses evoked by identical stimuli fluctuate over time. The latter effect has been very explicitly tied to ongoing activity fluctuations by examining the dependence of evoked response variations on trial-by-trial fluctuations of pre-stimulus activity levels. In an influential study, Arieli et al. (1996) investigated ongoing and stimulus-evoked activity with concurrent optical and electrophysiological methods in anesthetized cats. They found that variability of evoked responses could be largely accounted for by the initial level of ongoing activity just prior to stimulus onset. Their data show a linear relationship between ongoing activity immediately before stimulation and evoked activity levels. Simply adding the averaged stimulus-related activity increment to the pattern of ongoing activity in an individual trial provided an excellent prediction of the actually measured activity level during the evoked response in that trial. Recently, several functional neuroimaging studies have not only revisited this issue but also established links between neural and behavioral variability.

Functional imaging findings

At a very different spatial and temporal resolution than Arieli et al., Fox et al. (2006a) made a similar observation using fMRI. They found that trial-to-trial variability of finger movement-related activity in motor cortex could be largely accounted for by ongoing activity fluctuations measured in the contralateral motor cortex, the one ipsilateral to the finger that was moved (**Figure 1**). Their clever approach tackled the problem that the relative contribution of ongoing and task-related activity cannot be separated by analyzing activity in the task-relevant region during the evoked response. By removing trial by trial the simultaneously recorded activity level in a region that belongs to the same ICN but was not engaged by the task from the signal in the task-relevant region they "cleaned away" the ongoing and retained the evoked component.

From the perspective of data analysis in functional imaging, this procedure is very attractive. It suggests that averaging across trials provides a good way for estimating a veridical evoked activity change, the response, and that the latter shows little if any variability. And removing the variability related to ongoing activity and hence tightening the residual variability of the evoked response estimate yields a clear-cut gain in statistical sensitivity. Yet, the same group established in a subsequent study that the trial-by-trial variability

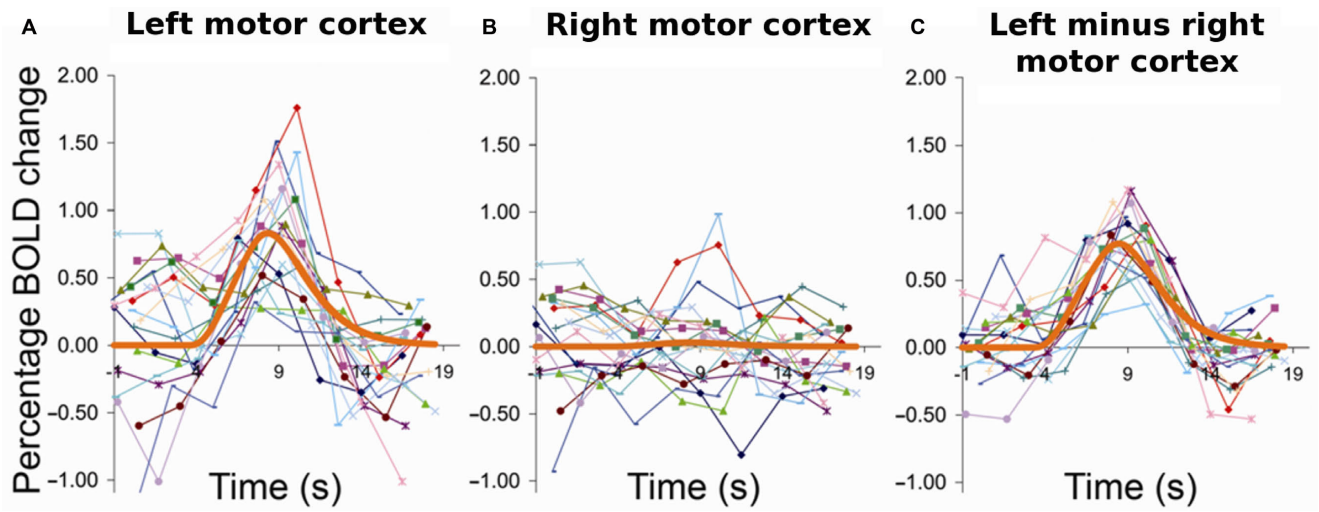

FIGURE 1 | Ongoing activity fluctuations account for variability in trial-to-trial evoked responses. Subjects pressed a response button with their right hand at long intervals (>14 s) in response to visual indication. **(A)** Left, i.e., task-invoked motor cortex; **(B)** right motor cortex; **(C)** left motor cortex after removal of activity from right motor cortex. Each curve corresponds to the raw time course of one trial for the same individual subject. The thick orange line represents the respective best-fit gamma function. The event-related activity in left motor cortex showed high trial-to-trial variability. Strong variability was likewise observed in the spontaneous activity in the other, i.e., right hemisphere and could account for a major portion of variance of the left hemispheric evoked responses on a trial-by-trial basis. Reprinted from Fox et al. (2006a) with permission from Nature Publishing Group.

in task-related motor cortex activation was functionally meaningful and translated into behavioral variability as measured by the force that subjects applied in different trials when pressing a response button (Fox et al., 2007). In other words, the aforementioned procedure of removing inter-trial variability, albeit attractive from a signal processing perspective, is far less tempting for that line of research which seeks to establish neural correlates of behavior.

From a methodological point of view, a limitation of the aforementioned approach is that it is grounded in the assumption that motor cortex ipsilateral to the moving finger is silent in this paradigm. Indeed, distal upper limb movements are represented almost exclusively contralaterally but with greater force they involve co-innervation of more proximal musculature, which in turn is represented more bilaterally in motor cortex (reviewed in Kleinschmidt and Toni, 2004). Other groups have therefore explored alternative approaches to the issue of whether ongoing activity fluctuations are functionally relevant. Instead of using simultaneously recorded signal in a region that belongs to the same ICN but is silent in a task context, several groups have taken pre-stimulus signal in the same region that will subsequently respond to a given stimulus as a measure of ongoing activity. This approach is hence similar to the one adopted by Arieli et al. (1996) but on a different time scale.

Boly et al. (2007) investigated the perceptual impact of pre-stimulus activity fluctuations in a somatosensory detection task. For somatosensory stimuli close to perceptual threshold pre-stimulus activity levels in large distributed systems resembling ICNs indicated whether or not a stimulus was perceived on a given trial. The system biasing towards perceiving the stimulus comprised the thalamus, dorsal anterior cingulate cortex (dACC) and anterior insula/inferior frontal gyrus, as well as parieto-frontal areas including intraparietal sulcus and dorso-lateral prefrontal cortex. As discussed in the previous section, these areas commonly show activation or "task-positive" behavior in a wide range of cognitive task settings (Corbetta et al., 2002; Smith et al., 2009). Conversely, on trials where subjects missed the threshold stimulus, pre-stimulus activity levels were higher in posterior cingulate (PCC), parahippocampal and lateral parietal components of the default-mode network. This latter network is known to show deactivation or "task-negative" behavior in most task settings (Gusnard and Raichle, 2001).

Taken together, these observations could further support a simple dichotomy in which higher ongoing activity in "task-positive" brain networks would facilitate perceptual performance whereas higher activity levels in the default-mode network would degrade performance. A recent study speaks against the generality of this scenario by showing that functional context determines in which brain regions ongoing activity will affect perceptual performance and whether this will be a facilitating or detrimental effect (Sadaghiani et al., 2009). In a free-response, auditory detection task, we presented broad-band noise stimuli in unpredictable intervals of 20–40 s and at individual detection threshold. Subjects pressed a button whenever they perceived the target sound. Successful detection as compared to misses was preceded by significantly higher pre-stimulus activity in early auditory cortex (**Figure 3A**) as well as in two ICNs. Perceptual performance was better with higher pre-stimulus activity in a network comprising thalamus, anterior insula and dACC, which suggests a role for this ICN in maintaining alertness and task-set (**Figure 2A**). Conversely, and counter to common intuition, higher baseline activity in the dorsal attention system of parietal and frontal areas biased towards misses (**Figure 2B**) presumably expressing the lack of spatial connotation in our stimulus and task. The observation of opposite effects in these two task-positive ICNs shows that in spite of shared variance, the networks are sufficiently segregated to exert independent influences on perceptual outcome. And finally, higher baseline activity in

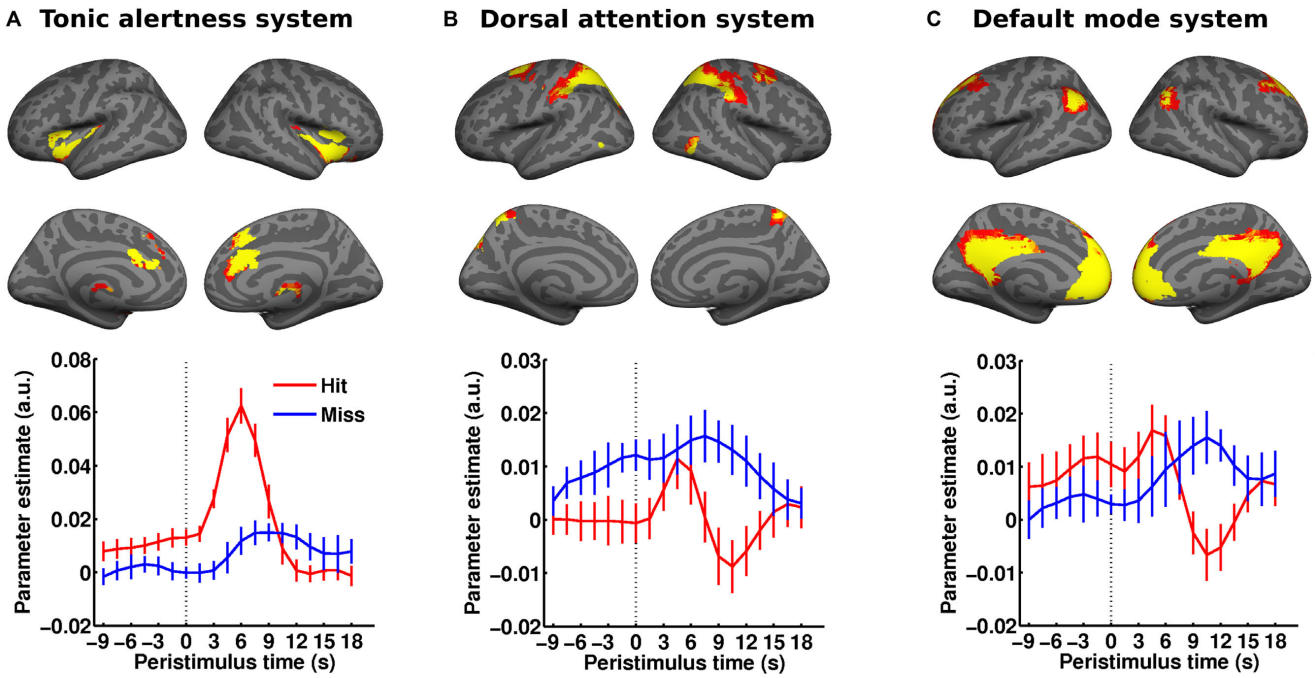

FIGURE 2 | Distributed ongoing activity fluctuations in large-scale ICNs impact perceptual performance. (A–C) Subjects performed a free-response auditory detection task (cf. **Figure 3A**). The pre-stimulus BOLD signal (dotted vertical line marking stimulus onset) from three ICNs (rendered on a canonical inflated cortical surface) was examined as a function of perceptual outcome. Hits were preceded by significantly higher pre-stimulus activity in the tonic alertness ICN **(A)** as well as the default-mode ICN **(C)** while higher pre-stimulus activity in the dorsal attention ICN **(B)** foreshadowed misses. Error bars represent standard error across subjects. Adapted with permission from Sadaghiani et al. (2009). For comparison with a somatosensory threshold detection task please cf. Figure 2 in Boly et al. (2008). This figure was not reprinted here due to fees requested by the publisher John Wiley and Sons for reprint permission.

the precuneus/PCC region of the default-mode network preceded hits, which in turn yielded a biphasic response with a "task-positive" activation component preceding the typical but delayed deactivation (**Figure 2C**). At first glance, this finding might appear at odds with the existing literature but it probably reflects the importance of retrieving a memory template of the target for successful performance on the continuous sensory input (Shannon and Buckner, 2004; Daselaar et al., 2009).

Thus, in the context of a non-localized and non-semantic auditory stimulus and a task that depends on recognition memory but not spatial attention, the usual effects from activity in default-mode and dorsal spatial attention systems were reversed. Of note, the time courses of pre-stimulus effects in these two networks were very distinct, making it unlikely that signal change in one was simply (epiphenomenally) mirrored by that in the other. In other words, these opposite effects were presumably independent of one another rather than reflecting a hard-wired antagonism between these two ICNs that others have claimed based on the observation of intrinsic anticorrelation (Fox et al., 2005). These findings highlight that context determines the influence ongoing fluctuations exert on stimulus processing and ultimately perception.

It seems fair to posit that where and how ongoing activity fluctuations impact on perceptual decisions depends on which sensory features and cognitive faculties are relevant in a given context. Accordingly, one might expect that in perceptual decisions, which do not involve an all-or-none success of detection but a choice between two closely matched alternatives, generic contributions from ICNs become less important and that a pre-stimulus effect might only be detectable in a single task-relevant region (rather than throughout the entire network to which this region belongs). In this case, it would be purely local variations in activity and not those throughout a distributed system that would exert an influence (cf. previous section on hierarchical structure of ongoing activity). Such a mechanism would make it mandatory to estimate ongoing activity from pre-stimulus signal in the task-relevant region instead of from simultaneous signal in a reference region of the same ICN. Evidence for such a scenario has been provided by two separate but closely related experiments.

In a perceptual decision task on Rubin's ambiguous vase-faces figure, subjects had to report on each trial whether they perceived the vase or the two faces in profile. The presentation of the stimuli was sparse at long and variable intervals (range 20–50 s), and the stimuli were presented only briefly (Hesselmann et al., 2008b). Subjects reported face percepts on approximately half of the trials and vase percepts on the other trials. Higher pre-stimulus activity levels in the right fusiform face area (FFA), a region specialized for face processing, were found to bias towards the percept of faces rather than a vase (**Figure 3B**). This finding was later replicated in the domain of visual motion perception (Hesselmann et al., 2008a). In this study, short events of random dot motion with near-threshold coherence levels were presented, and subjects indicated on each trial whether they perceived coherent or random motion. Here, subjects' perceptual decisions were biased by

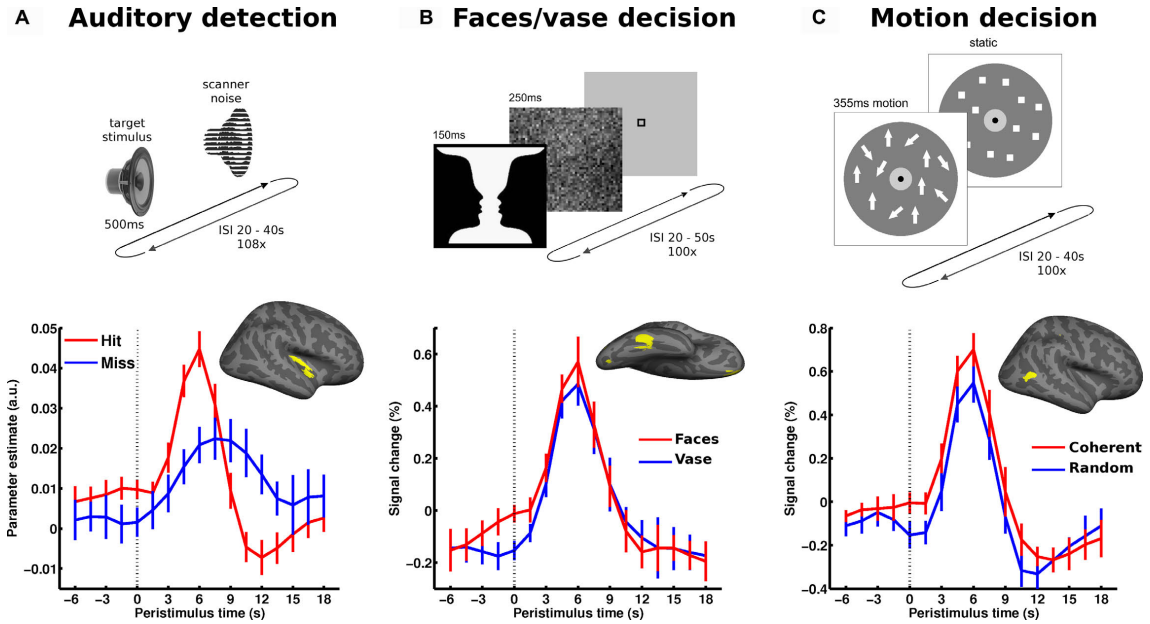

FIGURE 3 | Local spontaneous variations in ongoing activity of specialized sensory regions impact perception. The upper part illustrates the paradigm: **(A)** auditory detection experiment: in a free-response setting subjects detected an auditory target stimulus presented at perceptual threshold. **(B)** Perceptual decision on an ambiguous figure: subjects reported either faces or vase perception in response to flashes of the faces-vase ambiguous figure. **(C)** Motion decision experiment: random dot motion was presented at motion coherence threshold and subjects decided trial by trial whether motion was coherent or random. In all experiments, trials followed at long and unpredictable intervals. In each experiment, the pre-stimulus BOLD signal (dotted vertical line marking stimulus onset) was examined as a function of perceptual outcome and sampled from accordingly specialized sensory areas. The corresponding regions of interest (early auditory cortex, FFA and hMT+, respectively) are presented on a canonical inflated cortical surface of the right hemisphere. In all experiments, higher pre-stimulus time course in the respective sensory region biased towards perceiving stimulus properties for which these regions are particularly sensitive. Error bars represent standard error across subjects. For more details see Hesselmann et al. (2008a,b); Sadaghiani et al. (2009).

pre-stimulus activity levels in right middle temporal cortex (V5/hMT+), a region crucially involved in the analysis and perception of wide-field coherent motion. Specifically, perception of coherent motion was preceded by significantly higher ongoing activity in V5/hMT+ (**Figure 3C**). In both experiments, no other task-related cortical regions showed a significant link between pre-stimulus activity and perceptual outcome.

Electro- and magnetoencephalographic findings

Electro- (EEG) and magnetoencephalography (MEG) studies have also established links between ongoing activity and behavior. While less informative in terms of spatial localization, these studies have identified distinct oscillation bands that carry signals, which predict perceptual performance. Using MEG, Jensen and colleagues observed that visual discriminability of a threshold stimulus decreased with an increase in pre-stimulus occipito-parietal α band power (van Dijk et al., 2008). Likewise, they reported that in a go no-go task false alarms were preceded by higher levels of α band power in the occipital cortex and bilateral somatosensory cortices (μ rhythm) as compared to correct withholds on no-go trials (Mazaheri et al., 2009). Not only responses to natural stimuli but also to artificial direct cortical stimulation are influenced by the power of ongoing oscillations: Using transcranial magnetic stimulation, phosphene-perception was only induced following lower pre-stimulation α amplitudes (Romei et al., 2008), suggesting that occipital alpha power indexes cortical excitability. Evidence linking such observations in EEG frequency bands to the infra-slow frequency range covered by imaging studies comes from work by Palva and colleagues. They investigated pre-stimulus power fluctuations using full-band EEG sensitive to infra-slow fluctuations (<0.1 Hz) in a somatosensory threshold detection task within a free-response setting. They found highest detection rates and shortest reaction times to be associated with intermediate power levels (inverse u-shaped relation) of α, β and γ band oscillations over sensorimotor cortices, and with highest power of these bands over parietal electrodes (Linkenkaer-Hansen et al., 2004). Interestingly, in this task setting the phase of infra-slow fluctuations was found to be strongly correlated to the power of higher frequencies (1–40 Hz) and to be highly predictive of hits and misses on a trial-by-trial basis (Monto et al., 2008). Recently, electrophysiological studies have not only shown power but also phase of band-limited oscillatory activity to affect perceptual performance. For example, trial-to-trial variability in perceptual outcome has been related to the phase of EEG α and θ band oscillations in visual threshold detection tasks (Busch et al., 2009; Mathewson et al., 2009).

THE RELATION OF ONGOING AND EVOKED NEURAL ACTIVITY

The above findings are important because they show that across many temporal scales variability in ongoing activity – which is commonly obscured by normalization to pre-stimulus baseline – contributes to the way in which the brain (and ultimately, the observer) responds to sensory stimuli. The imaging studies show that the topography of

these effects is compatible with a hierarchical view on intrinsic brain activity and depends on context. In the two experiments discussed above, which involve fairly subtle perceptual decisions, we targeted areas that we considered likely to respond more strongly during one of the two possible perceptual interpretations of the ambiguous stimuli used. Despite identical sensory input in each experiment, we indeed confirmed that face-percept trials using the Rubin stimulus yielded higher evoked FFA responses and coherent-percept trials using the dot motion stimulus higher evoked hMT+ responses (**Figures 3B,C**). Together with the aforementioned effects observed in pre-stimulus signal these findings could be believed to confirm a behavior equivalent to the one in the study by Arieli et al. (1996) that we discussed above. In other words, a single stimulus would, on each trial, evoke a fixed activity increment which would add to the level of ongoing activity encountered on that trial. Variations in ongoing activity would then determine perceptual outcome by yielding variations in peak activity that would, or not, pass a threshold required for a perceptual decision. By such a mechanism, even a simple additive relationship between ongoing and evoked activity could become functionally significant (note that we have to call on a threshold mechanism – which is by definition non-linear – to make a linear effect of ongoing activity functionally interesting).

The important consequence from such a mechanism – that also provides an easily testable hypothesis – would be that the relation between ongoing and evoked activity should not depend on perceptual outcome because the latter would be determined solely by the peak activity of the response. We could reject this hypothesis in both experiments by showing a significant interaction between evoked and ongoing activity when predicting perceptual outcome. Specifically, peak and pre-stimulus activity levels in hMT+ correlated less when dot motion was perceived as coherent rather than random (**Figures 4A,B**). Likewise, peak activity levels in FFA were significantly less correlated with pre-stimulus signal when subjects perceived faces than when they reported a vase (**Figures 4C,D**). These observations show that the mechanism by which ongoing activity affects subsequent perception is independent from the one that can be observed during stimulus processing. In other words, the latter does not result from a mere passive propagation of effects preceding stimulus presentation. The theoretical implications of these findings for models of perceptual decision-making have been discussed in the respective publications (Hesselmann et al., 2008a,b). Yet, there is reason to believe that both linear (e.g., under anesthesia, Arieli et al., 1996, or in passive viewing, Bianciardi et al., 2009) and non-linear interactions can be observed and future work will need to clarify which parameters determine the regime under which ongoing and evoked activity interact (see Kisley and Gerstein, 1999, for a study on changes in linearity as a function of depth of anesthesia).

THE NATURE OF ONGOING BRAIN ACTIVITY

Comparing spontaneous fluctuations and variability after cueing

We have argued above that ongoing activity is modulated by cognitive context and that spontaneous activity fluctuations can be thought of as fluctuations of an internal and predictive contextual representation. It therefore appears sensible to compare results from such studies with those where context has been explicitly modulated by introducing cues that prepare for an upcoming cognitive challenge. Several studies have employed such cues to study the variability of evoked neural and perceptual responses to a single stimulus (or a group of equivalent stimuli) (Super et al., 2003; Sapir et al., 2005; Thut et al., 2006; Wyart and Tallon-Baudry, 2009). Typically, in these paradigms, a cue will appear that can indicate a task-relevant location or feature for a stimulus that will be presented after a brief but often variable delay. These studies in general try to understand which neural mechanisms underpin selective attention. As behavior and evoked responses are modulated by attention, variability in a cue-induced anticipatory signal that correlates with perceptual performance on the subsequent stimulus can be considered a neural signature of preparatory attention. Of course, this interpretation does not speak to the mechanism that generates this variability in the first place but only suggests that attentional preparation is subject to a variability of an unknown origin that is behaviorally relevant. The similarity of this conclusion with that from the aforementioned studies on spontaneous fluctuations suggests a need for closer examination and comparison.

From our perspective, variability in cortical activity following an orientating cue presents a special case and currently remains ambiguous. One interpretation could be that this variability is the same as that seen in ongoing activity and that the cue will hence be more or less efficient, both neurally and perceptually, as a function of the state of the system prior to cueing. Another view could be that the neural response elicited by the cue could in itself be variable and that this variability translates into perceptual performance. As we have discussed previously, simply removing the effects of pre-cue baseline would not permit arbitrating between these two scenarios, since the amplitude of the cue response may be subject to interactions with pre-cue activity levels. However, analyses as those reviewed above that preserve pre-cue "baseline" signal fluctuations could be used to disambiguate the functional nature of cued settings.

Another line of comparison regards the interpretation of the cortical signal. If the pre-stimulus signal expresses a level of preparatory attention in studies using cues, does this permit the conclusion that in studies without cues fluctuations of ongoing activity can be thought of as fluctuations in attention? If one were to make this claim it would have to survive a couple of benchmark checks. The most important one is that evoked responses to target stimuli should be enhanced by attention. This enhancement could reflect anything between a true response gain as implied in earlier studies (Chawla et al., 1999) and a simple additive effect of fixed stimulus-driven increment in the presence of an increased background activity (Sylvester et al., 2009). In both our studies addressing signal variations in the absence of cues, however, the opposite behavior was found. The higher pre-stimulus signal was, the smaller the actual incremental evoked response amplitude in regions that were critical to the percept on those trials, i.e., V5/hMT+ for motion coherence detection (**Figures 4A,B**) and the FFA for face perception (**Figures 4C,D**).

Predictive coding and free-energy formulations

So how can these observations about intrinsic fluctuations be understood functionally? We will address this under a predictive coding account of neuronal activity, given that cues furnish exogenous and explicit predictions. In what follows, it is important to realize that optimal predictions or expectations rest on two distinct processes. The first is predicting the content of a percept (e.g., what caused

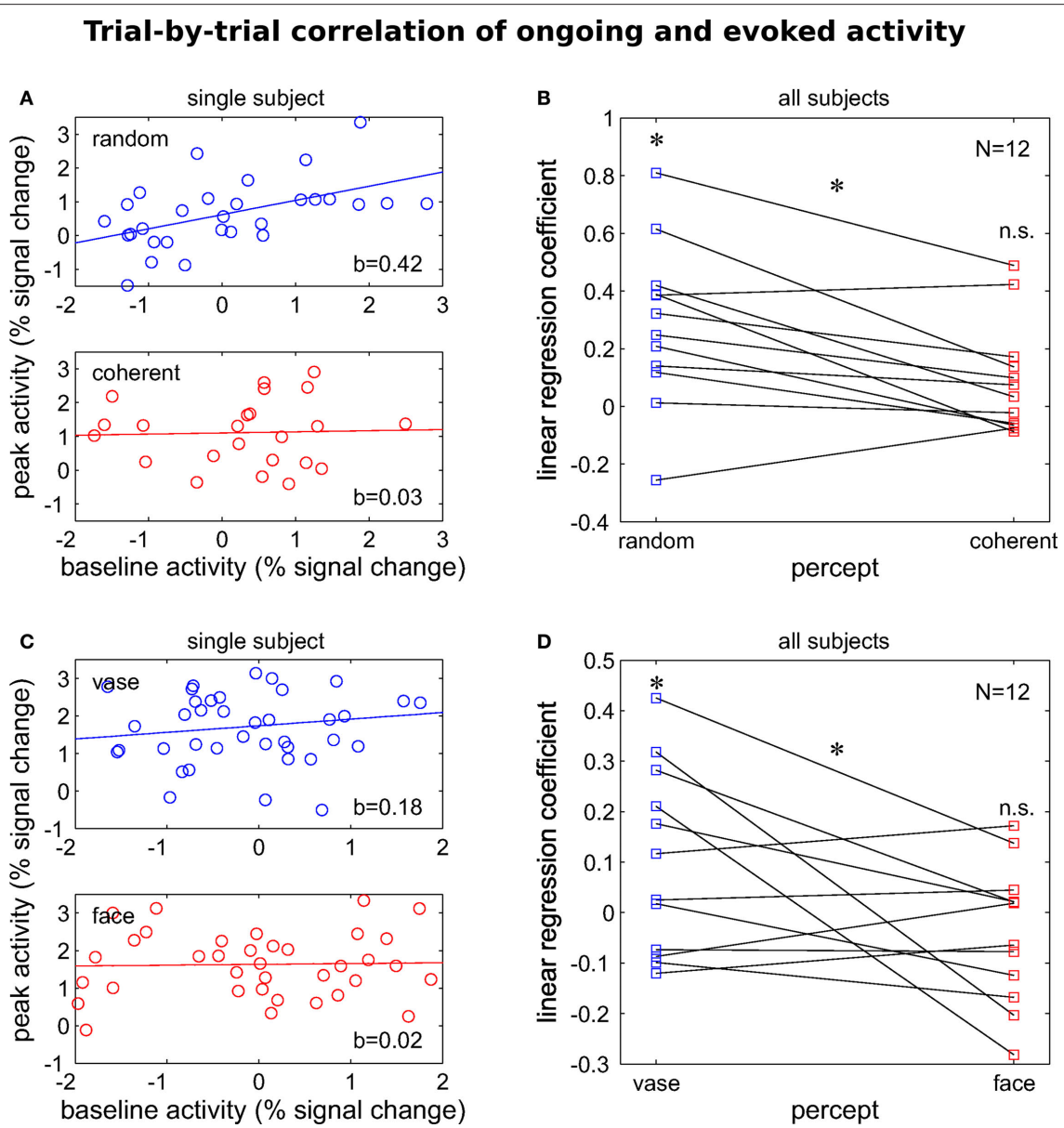

FIGURE 4 | Percept-dependent and non-linear interaction of evoked responses with pre-stimulus baseline activity. Percept-dependent linear regression was performed between trial-by-trial pre-stimulus activity at –1.5 s and peak activity at 6 s relative to stimulus onset. For two independent experiments, the regression is illustrated for one representative single subject and the regression coefficient is given for the group. **(A,B)** The motion decision experiment (for stimuli cf. **Figure 3C**): coefficients were significantly larger than 0 when motion was perceived as coherent ($t_{11} = 3.55$, $p < 0.01$) but not when it was perceived as random ($t_{11} = 1.7$, n.s.) and significantly different between the two perceptual outcomes ($t_{11} = 3.24$, $p < 0.01$, paired). Adapted with permission from Hesselmann et al. (2008a). **(C,D)** The face-vase decision experiment (cf. **Figure 3B**): likewise, coefficients showed a trend >0 when faces were perceived ($t_{11} = 1.88$, $p = 0.087$) but not when the vase was perceived ($t_{11} = –1.06$, n.s.). Importantly, they were significantly different between the two perceptual outcomes ($t_{11} = 2.31$, $p < 0.05$, paired). Dataset from Hesselmann et al. (2008b). All tests are two-sided t statistics.

the stimulus) and the second is properly inferring the uncertainty or precision of that prediction (e.g., the probabilistic context in which a stimulus appears). This difference is illustrated nicely by the difference between the effects of cueing and priming.

Cues are usually employed in attentional paradigms to guide predictions about task-relevant locations or features (context) but not about the actual target (content). In other words, knowing that a target will appear at a given location within the next couple of seconds does not provide any information about the content of the target's features; e.g., whether a grating will be slanted to the left or right. Cues call for allocation of attentional resources to the appropriate sensory channels, without biasing to one outcome in these channels, or another. In what follows, we consider this in terms of optimizing the synaptic gain of selected channels. This may also help understand the electrophysiological correlates of non-spatial attentional or perceptual processes; e.g., related to the feature

class, in contrast to spatial attention (Wyart and Tallon-Baudry, 2009). Conversely, sensory priming induces expectations about the content of sensory input, which we will assume is mediated by priming–dependent changes in synaptic activity and efficacy. In accord with this view, priming effects are associated with reduced evoked response amplitudes and are, of course, readily embraced by predictive coding accounts (Henson, 2003).

Recently, it has been proposed that a single fundamental principle might govern brain activity underlying action, perception, attention and learning (Friston, 2005, 2009, 2010). In its most simple form, the free-energy principle states that the brain seeks to minimize surprise (more formally, the negative log-probability of a sensory outcome). This is achieved by continuously updating an internal model that generates top-down predictions of sensory input. Unexpected sensory inputs that cannot be "explained away" by an internal model of the current states of the world emerge as bottom-up prediction errors (hence predictive coding). These prediction errors are accumulated or assimilated by higher cortical areas to update the model and optimize its predictions. Perception rests on the optimization of top-down predictions (or, model) to best explain away the bottom-up prediction error caused by incoming sensory information, a notion embraced by Bayesian formulations (Kersten et al., 2004; Hohwy et al., 2008). In the present context, the free-energy formulation is of interest because it covers many observations about evoked responses but it is not confined to them. When applied to the specific issue of ongoing cortical activity and its relation to evoked responses (and subsequent perception), the free-energy principle can account for many reported empirical findings and yields further testable predictions.

The free-energy formulation (Friston, 2009) requires the brain to represent the causes of sensory input (by optimizing synaptic activity; i.e., perceptual inference), and its internal model of contextual and causal regularities (by optimizing short and long-term changes in synaptic gain and efficacy; i.e, attention and peceptual learning). Crucially, all changes in synaptic activity, gain and efficacy minimize the same thing; namely free energy, which under some simplifying assumptions is just the amount of prediction error. In line with this view, Lewis et al. (2009) observed that intensive training shapes intrinsic connectivity between visual areas and higher order frontal and parietal regions that presumably generate visuospatial top-down predictions. In terms of the distinction above, synaptic (neuronal) activity encodes the content percepts, while synaptic gain encodes contextual precision (cf. attentional gain). In what follows, we will consider ongoing activity as reflecting neuronal activity that predicts the causes of sensory inputs and then turn to interpretations that cover fluctuations in synaptic gain or precision.

Ongoing activity and predictions

Perceptual inference and learning speaks to a general principle, according to which past experiences inform predictions of the future to optimize behavior. The idea that ongoing activity patterns reflect a historically informed internal model of causal dynamics in the world (that serves to generate predictions of future sensory input) fits nicely with the role of neural "replay" in memory formation (Jeffery, 2004; Foster and Wilson, 2006). Indeed, the itinerant (wandering or searching) dynamics that characterize intrinsic fluctuations have been proposed as mathematical models of short-term memory (Bick and Rabinovich, 2009) and have been discussed explicitly in terms of free-energy minimization (Kiebel et al., 2009b).

It is important to realize that this interpretation does not restrict the role of ongoing activity to brain states that are accessible to introspection. The most basic version of this mechanism might be seen during the perception of music and speech, where, mathematically, the itinerant dynamics conform to stable heteroclinic channels that show winner-less competition (Seliger et al., 2003; Kiebel et al., 2009a). However, these dynamics also manifest in the absence of sensory information – just because sensory inputs are not currently available does not mean that the brain models the world as having stopped. Important examples here include optimization (consolidation) of synaptic strengths during sleep (Vyazovskiy et al., 2008; Diekelmann and Born, 2010). Another example is optimization or selection of competing internal models, using itinerant searches over different hypotheses (models) about the world. This view links itinerant (*wandering*) dynamics to "mind *wandering*" often invoked to explain resting-state fluctuations. This link provides a formal and precise role for ongoing itinerant activity that has been exploited in perception (e.g., Kiebel et al., 2009a) and planning (e.g., Namikawa and Tani, 2010). In machine learning and robotics, the itinerancy mandated by sensitivity to initial conditions and some forms of chaotic dynamics is now one of the main candidates for explaining how trajectories into the future are explored and selected. This fits comfortably with the notion that brain activity can be formulated in terms of itinerant dynamics (e.g., Tsuda, 2001). One important feature of itinerancy is that it enables ongoing activity to express fluctuations that ensure transitions between different (meta)stable neuronal states (Deco et al., 2009). Itinerant fluctuations of this activity reflect the dynamic nature of the underlying internal model that does not remain locked in a stationary mode but remains malleable by continuously exploring hypotheses regarding future experience and action. It is for this reason that functional connectivity measures, which describe the extent of wandering activity (and not stationary activity levels), provide such an informative description. Similar neural population behavior has also been observed on shorter temporal and smaller spatial scales (Wackermann et al., 1993; Kenet et al., 2003).

Ongoing activity and precision

In free-energy formulations of predictive coding, a major contributor to measured neuronal activity is precision-weighted prediction error. This precision weighting is implemented by increases in synaptic gain (cf. attentional modulation) so that prediction errors are boosted selectively according to the context established by predictions or cues). This means that fluctuating activity levels may reflect not just itinerant optimization of predictions but fluctuations in their precision. Evidence for this interpretation of ongoing activity fluctuations (as a modulation in precision or gain afforded to afferent information) comes from investigations of false vs. correct perceptual inference. Intrinsic brain activity (as indexed by fMRI signal) could be interpreted as a correlate of sensory evidence in random walk or race models (in essence an extension of signal detection theory over time Smith and Ratcliff, 2004; Gold and Shadlen, 2007) or as a proxy for precision in free-energy formulations of predictive coding (Friston,

2008). Crucially, these two accounts can be tested against findings in threshold detection paradigms discussed above (Hesselmann et al., 2008a; Sadaghiani et al., 2009). The former (evidence accumulation) framework suggests high pre-stimulus activity (i.e., a high starting level for the random walk) will bias towards subsequent stimulus detection (true hits or false alarms). Conversely, the latter (predictive coding) framework suggests that high ongoing activity (i.e., precise prediction errors) will bias towards subsequently correct inference (hits or correct rejections). In two independent datasets, we recently found that pre-stimulus activity levels were associated with the latter perceptual outcome and hence support the interpretation of ongoing activity as reflecting the precision of perceptual inference (Hesselmann et al., 2010) (**Figure 5**).

The implementation of precision in the predictive coding framework is necessitated by the presence of noise in environmental states or sensory input and plays a key role in regulating the reliability or relative weighting of bottom-up prediction errors against top-down predictions. Thus, this gain could represent a mechanism that is very suitable for mediating selective attention (Friston, 2009). Of note however, a shared final common neural pathway does not imply that fluctuations in ongoing activity necessarily reflect fluctuations in attention (cf. the discussion of cueing paradigms in the previous section and itinerant optimization of neuronal activity above). In conclusion, the free-energy formulation presents an attractive theoretical framework for a unified approach to a diversity of neurophysiological observations, including those related to ongoing activity fluctuations.

SUMMARY

In the recent years, intrinsic brain activity has become a new and enticing focus of interest and research into brain function (Fox and Raichle, 2007). In spite of conceptual concerns about studying unconstrained brain activity (Morcom and Fletcher, 2007a,b) studies of intrinsic brain activity during rest as well as in paradigm settings have proven very fruitful in understanding the functional role of ongoing activity and its relation to cognitive processes (Buckner et al., 2008; Greicius, 2008; Hesselmann et al., 2008b; Sadaghiani et al., 2009).

Ongoing activity is organized in a functional architecture at various temporal and spatial scales (Kenet et al., 2003; Bassett et al., 2006; Meunier et al., 2009). It has been established that evoked neural responses are embedded into this underlying functional architecture (Tsodyks et al., 1999) and cannot be fully understood in isolation from the context established by ongoing activity. Therefore, trial-to-trial variability in evoked responses is not just noise but a non-random function of network fluctuations (Fontanini and Katz, 2008). For this reason the current review of ongoing activity considered its spatiotemporal structure in relation to moment-to-moment variability in cognition.

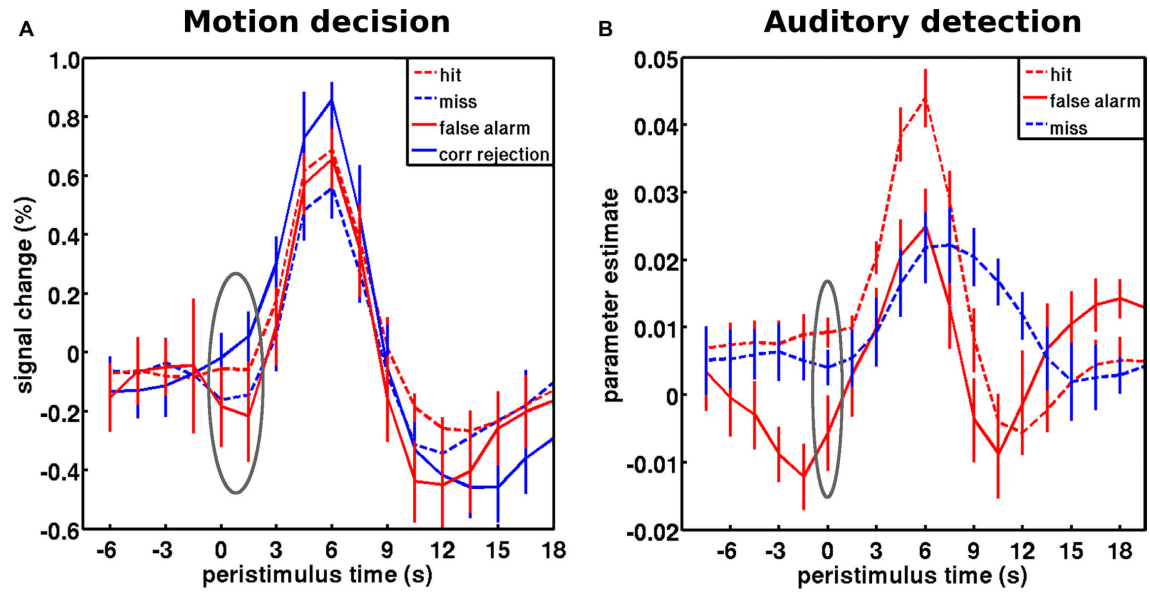

FIGURE 5 | Baseline activity levels in false vs. correct inferences are captured by the predictive coding framework. (A) Peristimulus fMRI signal time courses from the motion decision experiment: for stimuli and region of interest cf. **Figure 3C**. Hits and misses correspond to trials at threshold motion coherence level (on average 13%), while correct rejections and false alarms correspond to occasional trails with a quasi-random coherence level (1%). Pre-stimulus activity showed a main effect of accuracy, correct vs. incorrect (consistent with predictive coding), but no main effect of percept, coherent vs. incoherent (predicted by evidence accumulation). Pre-stimulus activity prior to hits was significantly greater than misses; and pre-stimulus activity in false alarms were significantly less than in correct rejects. **(B)** Peristimulus time courses from the auditory detection experiment: for stimuli and region of interest cf. **Figure 3A**. False alarms occurred occasionally when subjects reported to hear the target stimulus in the absence of stimulation. As assumed by predictive coding, false inference (false alarms and misses) were each preceded by significantly lower levels of activity in auditory cortex than veridical hits. Note that this free-response paradigm does not furnish correct rejection trials (i.e., subjects are not required to indicate the stimulus is absent). The gray ellipse covers the pre-stimulus period submitted to statistical testing. The time courses for hits and misses correspond to the respective time courses in **Figure 3**. However, note that only a subset of subjects that had a sufficient number of wrong inferences was included in this analysis. Error bars represent standard error across subjects. Adapted with permission from Hesselmann et al. (2010).

With respect to structure, we emphasized that behaviorally relevant ongoing activity is hierarchically organized and does not seem restricted to clear-cut temporal or spatial scales. The spatial patterns of ICNs and the membership of constituent regions are gradual and display a global-to-local connectivity, reminiscent of small-world topologies (Bullmore and Sporns, 2009). We further discussed that the strength of these correlations is constrained by structural connectivity but is modulated by mental states and current context, strongly suggesting a functional component to intrinsic activity fluctuations (i.e., dynamics on structure).

We have tried to substantiate the role of intrinsic fluctuations in terms of the necessarily itinerant dynamics entailed by internal (generative) models of the world the brain might use to make predictions about its sensorium. In doing this, we hoped to establish a formal link between the notion of mind wandering and itinerancy (wandering dynamics) in computational accounts of perceptual learning and inference. Furthermore, we extended this account to include the modulation of prediction error signals by their precision and suggested that measured fluctuations in neuronal activity may reflect modulations in synaptic gain; of the sort seen in fast synchronized neuronal exchanges and attentional modulation.

It has been argued that evoked response variability is coordinated rather than arbitrary and substantiates the very essence of cognition as it translates into behavioral variability (Buzsáki, 2006). From this point of view, we reviewed evidence that ongoing brain activity fluctuations influence trial-by-trial behavior and perception of identical stimuli. Site and sign of this impact depend on cognitive context and the functional role of a given region or neuroanatomical system. This cognitive variability over time is the visible manifestation of a continuous trajectory of ongoing activity, an itinerant trajectory that can be thought of as a memory trace building up within a complex and adaptive system. Intrinsic activity hence constitutes the brain's internal context for processing external information and generating behavior (Kenet et al., 2003; Fontanini and Katz, 2008). Future progress on these issues can only be made by treating ongoing activity as a signal instead of noise and by shifting from a behaviorist stance that records evoked responses to a constructivist approach that interrogates neural history records as the substrate of a process of active perceptual synthesis.

ACKNOWLEDGMENTS

S. Sadaghiani is supported by the Friedrich-Ebert Foundation (Germany). G. Hesselmann is supported by a Minerva fellowship (Max Planck Society). Our research is funded by the Agence Nationale de la Recherche (SPONTACT grant), France.

REFERENCES

Albert, N. B., Robertson, E. M., and Miall, R. C. (2009). The resting human brain and motor learning. *Curr. Biol.* 19, 1023–1027.

Arieli, A., Sterkin, A., Grinvald, A., and Aertsen, A. (1996). Dynamics of ongoing activity: explanation of the large variability in evoked cortical responses. *Science* 273, 1868–1871.

Bassett, D. S., Meyer-Lindenberg, A., Achard, S., Duke, T., and Bullmore, E. (2006). Adaptive reconfiguration of fractal small-world human brain functional networks. *Proc. Natl. Acad. Sci. U.S.A.* 103, 19518–19523.

Beckmann, C. F., DeLuca, M., Devlin, J. T., and Smith, S. M. (2005). Investigations into resting-state connectivity using independent component analysis. *Philos. Trans. R. Soc. Lond., B, Biol. Sci.* 360, 1001–1013.

Bianciardi, M., Fukunaga, M., van Gelderen, P., Horovitz, S. G., de Zwart, J. A., and Duyn, J. H. (2009). Modulation of spontaneous fMRI activity in human visual cortex by behavioral state. *Neuroimage* 45, 160–168.

Bick, C., and Rabinovich, M. I. (2009). Dynamical origin of the effective storage capacity in the brain's working memory. *Phys. Rev. Lett.* 103, 218101.

Biswal, B. B., Kylen, J. V., and Hyde, J. S. (1997). Simultaneous assessment of flow and BOLD signals in resting-state functional connectivity maps. *NMR. Biomed.* 10, 165–170.

Boly, M., Balteau, E., Schnakers, C., Degueldre, C., Moonen, G., Luxen, A., Phillips, C., Peigneux, P., Maquet, P., and Laureys, S. (2007). Baseline brain activity fluctuations predict somatosensory perception in humans. *Proc. Natl. Acad. Sci. U.S.A.* 104, 12187–12192.

Boly, M., Phillips, C., Balteau, E., Schnakers, C., Degueldre, C., Moonen, G., Luxen, A., Peigneux, P., Faymonville, M.-E., Maquet, P., and Laureys, S. (2008). Consciousness and cerebral baseline activity fluctuations. *Hum. Brain Mapp.* 29, 868–874.

Boly, M., Tshibanda, L., Vanhaudenhuyse, A., Noirhomme, Q., Schnakers, C., Ledoux, D., Boveroux, P., Garweg, C., Lambermont, B., Phillips, C., Luxen, A., Moonen, G., Bassetti, C., Maquet, P., and Laureys, S. (2009). Functional connectivity in the default network during resting state is preserved in a vegetative but not in a brain dead patient. *Hum. Brain Mapp.* 30, 2393–2400.

Buckner, R. L., Andrews-Hanna, J. R., and Schacter, D. L. (2008). The brain's default network: anatomy, function, and relevance to disease. *Ann. N. Y. Acad. Sci.* 1124, 1–38.

Buckner, R. L., and Vincent, J. L. (2007). Unrest at rest: default activity and spontaneous network correlations. *Neuroimage* 37, 1091–1096.

Bullmore, E., and Sporns, O. (2009). Complex brain networks: graph theoretical analysis of structural and functional systems. *Nat. Rev. Neurosci.* 10, 186–198.

Busch, N. A., Dubois, J., and VanRullen, R. (2009). The phase of ongoing EEG oscillations predicts visual perception. *J. Neurosci.* 29, 7869–7876.

Buzsáki, G. (2006). *Rhythms of the Brain*. New York: Oxford UP.

Chawla, D., Rees, G., and Friston, K. J. (1999). The physiological basis of attentional modulation in extrastriate visual areas. *Nat. Neurosci.* 2, 671–676.

Christoff, K., Gordon, A. M., Smallwood, J., Smith, R., and Schooler, J. W. (2009). Experience sampling during fMRI reveals default network and executive system contributions to mind wandering. *Proc. Natl. Acad. Sci. U.S.A.* 106, 8719–8724.

Cohen, A. L., Fair, D. A., Dosenbach, N. U. F., Miezin, F. M., Dierker, D., Van Essen, D. C., Schlaggar, B. L., and Petersen, S. E. (2008). Defining functional areas in individual human brains using resting functional connectivity MRI. *Neuroimage* 41, 45–57.

Cole, D., Smith, S., and Beckamnn, C. (2010). Advances and pitfalls in the analysis and interpretation of resting-state FMRI data. *Front. Syst. Neurosci.* 4:8. doi: 10.3389/fnsys.2010.00008.

Corbetta, M., Kincade, J. M., and Shulman, G. L. (2002). Neural systems for visual orienting and their relationships to spatial working memory. *J. Cogn. Neurosci.* 14, 508–523.

Corbetta, M., and Shulman, G. L. (2002). Control of goal-directed and stimulus-driven attention in the brain. *Nat. Rev. Neurosci.* 3, 201–215.

Daselaar, S. M., Prince, S. E., Dennis, N. A., Hayes, S. M., Kim, H., and Cabeza, R. (2009). Posterior midline and ventral parietal activity is associated with retrieval success and encoding failure. *Front. Hum. Neurosci.* 3:13. doi: 10.3389/neuro.09.013.2009.

Deco, G., Rolls, E. T., and Romo, R. (2009). Stochastic dynamics as a principle of brain function. *Prog. Neurobiol.* 88, 1–16.

Diekelmann, S., and Born, J. (2010). The memory function of sleep. *Nat. Rev. Neurosci.* 11, 114–126.

Dosenbach, N. U. F., Fair, D. A., Miezin, F. M., Cohen, A. L., Wenger, K. K., Dosenbach, R. A. T., Fox, M. D., Snyder, A. Z., Vincent, J. L., Raichle, M. E., Schlaggar, B. L., and Petersen, S. E. (2007). Distinct brain networks for adaptive and stable task control in humans. *Proc. Natl. Acad. Sci. U.S.A.* 104, 11073–11078.

Dosenbach, N. U. F., Visscher, K. M., Palmer, E. D., Miezin, F. M., Wenger, K. K., Kang, H. C., Burgund, E. D., Grimes, A. L., Schlaggar, B. L., and Petersen, S. E. (2006). A core system for the implementation of task sets. *Neuron* 50, 799–812.

Eckert, M. A., Menon, V., Walczak, A., Ahlstrom, J., Denslow, S., Horwitz, A., and Dubno, J. R. (2008). At the heart of the ventral attention system: the right anterior insula. *Hum. Brain Mapp.* 30, 2530–2541.

Fair, D. A., Schlaggar, B. L., Cohen, A. L., Miezin, F. M., Dosenbach, N. U. F., Wenger, K. K., Fox, M. D., Snyder, A.

Z., Raichle, M. E., and Petersen, S. E. (2007). A method for using blocked and event-related fMRI data to study "resting state" functional connectivity. *Neuroimage* 35, 396–405.

Ferrarini, L., Veer, I. M., Baerends, E., van Tol, M. J., Renken, R. J., van der Wee, N. J., Veltman, D. J., Aleman, A., Zitman, F. G., Penninx, B. W., van Buchem, M. A., Reiber, J. H., Rombouts, S. A., and Milles, J. (2009). Hierarchical functional modularity in the resting-state human brain. *Hum. Brain Mapp.* 30, 2220–2231.

Fontanini, A., and Katz, D. B. (2008). Behavioral states, network states, and sensory response variability. *J. Neurophysiol.* 100, 1160–1168.

Foster, D. J., and Wilson, M. A. (2006). Reverse replay of behavioural sequences in hippocampal place cells during the awake state. *Nature* 440, 680–683.

Fox, M. D., and Raichle, M. E. (2007). Spontaneous fluctuations in brain activity observed with functional magnetic resonance imaging. *Nat. Rev. Neurosci.* 8, 700–711.

Fox, M. D., Snyder, A. Z., Vincent, J. L., Corbetta, M., Van Essen, D. C., and Raichle, M. E. (2005). The human brain is intrinsically organized into dynamic, anticorrelated functional networks. *Proc. Natl. Acad. Sci. U.S.A.* 102, 9673–9678.

Fox, M. D., Snyder, A. Z., Vincent, J. L., and Raichle, M. E. (2007). Intrinsic fluctuations within cortical systems account for intertrial variability in human behavior. *Neuron* 56, 171–184.

Fox, M. D., Snyder, A. Z., Zacks, J. M., and Raichle, M. E. (2006a). Coherent spontaneous activity accounts for trial-to-trial variability in human evoked brain responses. *Nat. Neurosci.* 9, 23–25.

Fox, M. D., Corbetta, M., Snyder, A. Z., Vincent, J. L., and Raichle, M. E. (2006b). Spontaneous neuronal activity distinguishes human dorsal and ventral attention systems. *Proc. Natl. Acad. Sci. U.S.A.* 103, 10046–10051.

Fox, M. D., Zhang, D., Snyder, A. Z., and Raichle, M. E. (2009). The global signal and observed anticorrelated resting state brain networks. *J. Neurophysiol.* 101, 3270–3283.

Fransson, P. (2005). Spontaneous low-frequency BOLD signal fluctuations: an fMRI investigation of the resting-state default mode of brain function hypothesis. *Hum. Brain Mapp.* 26, 15–29.

Freeman, W. J., Rogers, L. J., Holmes, M. D., and Silbergeld, D. L. (2000). Spatial spectral analysis of human electrocorticograms including the alpha and gamma bands. *J. Neurosci. Methods* 95, 111–121.

Friston, K. (2005). A theory of cortical responses. *Philos. Trans. R. Soc. Lond., B, Biol. Sci.* 360, 815–836.

Friston, K. (2008). Hierarchical models in the brain. *PLoS Comput. Biol.* 4, e1000211. doi: 10.1371/journal.pcbi.1000211.

Friston, K. (2009). The free-energy principle: a rough guide to the brain? *Trends Cogn. Sci.* 13, 293–301.

Friston, K. (2010). The free-energy principle: a unified brain theory? *Nat. Rev. Neurosci.* 11, 127–138.

Gilden, D. L. (2001). Cognitive emissions of 1/f noise. *Psychol. Rev.* 108, 33–56.

Gold, J. I., and Shadlen, M. N. (2007). The neural basis of decision making. *Annu. Rev. Neurosci.* 30, 535–574.

Golland, Y., Bentin, S., Gelbard, H., Benjamini, Y., Heller, R., Nir, Y., Hasson, U., and Malach, R. (2007). Extrinsic and intrinsic systems in the posterior cortex of the human brain revealed during natural Sensory Stimulation. *Cereb. Cortex* 17, 766–777.

Golland, Y., Golland, P., Bentin, S., and Malach, R. (2008). Data-driven clustering reveals a fundamental subdivision of the human cortex into two global systems. *Neuropsychologia* 46, 540–553.

Greicius, M. (2008). Resting-state functional connectivity in neuropsychiatric disorders. *Curr. Opin. Neurol.* 21, 424–430.

Greicius, M. D., Kiviniemi, V., Tervonen, O., Vainionpää, V., Alahuhta, S., Reiss, A. L., and Menon, V. (2008). Persistent default-mode network connectivity during light sedation. *Hum. Brain Mapp.* 29, 839–847.

Greicius, M. D., Krasnow, B., Reiss, A. L., and Menon, V. (2003). Functional connectivity in the resting brain: a network analysis of the default mode hypothesis. *Proc. Natl. Acad. Sci. U.S.A.* 100, 253–258.

Greicius, M. D., Supekar, K., Menon, V., and Dougherty, R. F. (2009). Resting-state functional connectivity reflects structural connectivity in the default mode network. *Cereb. Cortex (New York, NY:* 1991) 19, 72–78.

Gusnard, D. A., and Raichle, M. E. (2001). Searching for a baseline: functional imaging and the resting human brain. *Nat. Rev. Neurosci.* 2, 685–694.

Hasson, U., Nusbaum, H. C., and Small, S. L. (2009). Task-dependent organization of brain regions active during rest. *Proc. Natl. Acad. Sci. U.S.A.* 106, 10841–10846.

He, B. J., Snyder, A. Z., Zempel, J. M., Smyth, M. D., and Raichle, M. E. (2008). Electrophysiological correlates of the brain's intrinsic large-scale functional architecture. *Proc. Natl. Acad. Sci. U.S.A.* 105, 16039–16044.

He, B. J., Zempel, J. M., Snyder, A. Z., and Raichle, M. E. (2010). The temporal structures and functional significance of scale-free brain activity. *Neuron* 66, 353–369.

Henson, R. N. (2003). Neuroimaging studies of priming. *Prog. Neurobiol.* 70, 53–81.

Hesselmann, G., Kell, C. A., and Kleinschmidt, A. (2008a). Ongoing activity fluctuations in hMT+ bias the perception of coherent visual motion. *J. Neurosci.* 28, 14481–14485.

Hesselmann, G., Kell, C. A., Eger, E., and Kleinschmidt, A. (2008b). Spontaneous local variations in ongoing neural activity bias perceptual decisions. *Proc. Natl. Acad. Sci. U.S.A.* 105, 10984–10989.

Hesselmann, G., Sadaghiani, S., Friston, K. J., and Kleinschmidt, A. (2010). Predictive coding or evidence accumulation? False inference and neuronal fluctuations. *PLoS ONE* 5, e9926. doi: 10.1371/journal.pone.0009926.

Hohwy, J., Roepstorff, A., and Friston, K. (2008). Predictive coding explains binocular rivalry: an epistemological review. *Cognition* 108, 687–701.

Honey, C. J., Sporns, O., Cammoun, L., Gigandet, X., Thiran, J. P., Meuli, R., and Hagmann, P. (2009). Predicting human resting-state functional connectivity from structural connectivity. *Proc. Natl. Acad. Sci. U.S.A.* 106, 2035–2040.

Horovitz, S. G., Braun, A. R., Carr, W. S., Picchioni, D., Balkin, T. J., Fukunaga, M., and Duyn, J. H. (2009). Decoupling of the brain's default mode network during deep sleep. *Proc. Natl. Acad. Sci. U.S.A.* 106, 11376–11381.

Horovitz, S. G., Fukunaga, M., de Zwart, J. A., van Gelderen, P., Fulton, S. C., Balkin, T. J., and Duyn, J. H. (2007). Low frequency BOLD fluctuations during resting wakefulness and light sleep: a simultaneous EEG-fMRI study. *Hum. Brain Mapp.* 29, 671–682.

Jeffery, K. J. (2004). Remembrance of futures past. *Trends Cogn. Sci. (Regul. Ed.)* 8, 197–199.

Kenet, T., Bibitchkov, D., Tsodyks, M., Grinvald, A., and Arieli, A. (2003). Spontaneously emerging cortical representations of visual attributes. *Nature* 425, 954–956.

Kersten, D., Mamassian, P., and Yuille, A. (2004). Object perception as Bayesian inference. *Annu. Rev. Psychol.* 55, 271–304.

Kiebel, S. J., Daunizeau, J., and Friston, K. J. (2009a). Perception and hierarchical dynamics. *Front. Neuroinformatics* 3:20. doi: 10.3389/neuro.11.020.2009.

Kiebel, S. J., von Kriegstein, K., Daunizeau, J., and Friston, K. J. (2009b). Recognizing sequences of sequences. *PLoS Comput. Biol.* 5, e1000464. doi: 10.1371/journal.pcbi.1000464.

Kisley, M. A., and Gerstein, G. L. (1999). Trial-to-trial variability and state-dependent modulation of auditory-evoked responses in cortex. *J. Neurosci.* 19, 10451–10460.

Kleinschmidt, A., and Toni, I. (2004) "Functional magnetic resonance imaging of the human motor cortex," in *Motor Cortex in Voluntary Movements: A Distributed System for Distributed Functions*, eds A. Riehle and E. Vaadia, Boca-Raton, FL: CRC Press, pp. 49–84.

Laufs, H., Krakow, K., Sterzer, P., Eger, E., Beyerle, A., Salek-Haddadi, A., and Kleinschmidt, A. (2003). Electroencephalographic signatures of attentional and cognitive default modes in spontaneous brain activity fluctuations at rest. *Proc. Natl. Acad. Sci. U.S.A.* 100, 11053–11058.

Leopold, D. A., Murayama, Y., and Logothetis, N. K. (2003). Very slow activity fluctuations in monkey visual cortex: implications for functional brain imaging. *Cereb. Cortex* 13, 422–433.

Lewis, C. M., Baldassarre, A., Committeri, G., Romani, G. L., and Corbetta, M. (2009). Learning sculpts the spontaneous activity of the resting human brain. *Proc. Natl. Acad. Sci. U.S.A.* 106, 17558–17563.

Linkenkaer-Hansen, K., Nikouline, V. V., Palva, J. M., and Ilmoniemi, R. J. (2001). Long-range temporal correlations and scaling behavior in human brain oscillations. *J. Neurosci.* 21, 1370–1377.

Linkenkaer-Hansen, K., Nikulin, V. V., Palva, S., Ilmoniemi, R. J., and Palva, J. M. (2004). Prestimulus oscillations enhance psychophysical performance in humans. *J. Neurosci.* 24, 10186–10190.

Mandelbrot, B. (1998). *Multifractals and 1/f Noise: Wild Self-Affinity in Physics*. New York: Springer.

Margulies, D. S., Kelly, A. M. C., Uddin, L. Q., Biswal, B. B., Castellanos, F. X., and Milham, M. P. (2007). Mapping the functional connectivity of anterior cingulate cortex. *Neuroimage* 37, 579–588.

Margulies, D. S., Vincent, J. L., Kelly, C., Lohmann, G., Uddin, L. Q., Biswal, B. B., Villringer, A., Castellanos, F. X., Milham, M. P., and Petrides, M. (2009). Precuneus shares intrinsic functional architecture in humans and monkeys. *Proc. Natl. Acad. Sci. U.S.A.* 106, 20069–20074.

Marrelec, G., Bellec, P., Krainik, A., Duffau, H., Pelegrini-Issac, M., Lehericy, S., Benali, H., and Doyon, J. (2008). Regions, systems, and the brain: hierarchical measures of functional integration in fMRI. *Med. Image Anal.* 12, 484–496.

Mason, M. F., Norton, M. I., Van Horn, J. D., Wegner, D. M., Grafton, S. T., and Macrae, C. N. (2007). Wandering

minds: the default network and stimulus-independent thought. *Science* 315, 393–395.

Mathewson, K. E., Gratton, G., Fabiani, M., Beck, D. M., and Ro, T. (2009). To see or not to see: prestimulus {alpha} phase predicts visual awareness. *J. Neurosci.* 29, 2725–2732.

Mazaheri, A., Nieuwenhuis, I. L., van Dijk, H., and Jensen, O. (2009). Prestimulus alpha and mu activity predicts failure to inhibit motor responses. *Hum. Brain Mapp.* 30, 1791–1800.

McDonnell, M. D., and Abbott, D. (2009). What is stochastic resonance? Definitions, misconceptions, debates, and its relevance to biology. *PLoS Comput. Biol.* 5, e1000348. doi: 10.1371/journal.pcbi.1000348.

Meunier, D., Lambiotte, R., Fornito, A., Ersche, K. D., and Bullmore, E. T. (2009). Hierarchical modularity in human brain functional networks. *Front. Neuroinformatics* 3:37. doi: 10.3389/neuro.11.037.2009.

Monto, S., Palva, S., Voipio, J., and Palva, J. M. (2008). Very slow EEG fluctuations predict the dynamics of stimulus detection and oscillation amplitudes in humans. *J. Neurosci.* 28, 8268–8272.

Morcom, A. M., and Fletcher, P. C. (2007a). Does the brain have a baseline? Why we should be resisting a rest. *Neuroimage* 37, 1073–1082.

Morcom, A. M., and Fletcher, P. C. (2007b). Cognitive neuroscience: the case for design rather than default. *Neuroimage* 37, 1097–1099.

Murphy, K., Birn, R. M., Handwerker, D. A., Jones, T. B., and Bandettini, P. A. (2009). The impact of global signal regression on resting state correlations: are anti-correlated networks introduced? *Neuroimage* 44, 893–905.

Namikawa, J., and Tani, J. (2010). Learning to imitate stochastic time series in a compositional way by chaos. *Neural Netw.* 23, 625–638.

Nir, Y., Fisch, L., Mukamel, R., Gelbard-Sagiv, H., Arieli, A., Fried, I., and Malach, R. (2007). Coupling between neuronal firing rate, gamma LFP, and BOLD fMRI is related to interneuronal correlations. *Curr. Biol.* 17, 1275–1285.

Nir, Y., Mukamel, R., Dinstein, I., Privman, E., Harel, M., Fisch, L., Gelbard-Sagiv, H., Kipervasser, S., Andelman, F., Neufeld, M. Y., Kramer, U., Arieli, A., Fried, I., and Malach, R. (2008). Interhemispheric correlations of slow spontaneous neuronal fluctuations revealed in human sensory cortex. *Nat. Neurosci.* 11, 1100–1108.

Raichle, M. E. (2010). Two views of brain function. *Trends Cogn. Sci. (Regul. Ed.)* 14, 180–190.

Romei, V., Brodbeck, V., Michel, C., Amedi, A., Pascual-Leone, A., and Thut, G. (2008). Spontaneous fluctuations in posterior alpha-band EEG activity reflect variability in excitability of human visual areas. *Cereb. Cortex* 18, 2010–2018.

Sadaghiani, S., Hesselmann, G., and Kleinschmidt, A. (2009). Distributed and antagonistic contributions of ongoing activity fluctuations to auditory stimulus detection. *J. Neurosci.* 29, 13410–13417.

Sapir, A., d'Avossa, G., McAvoy, M., Shulman, G. L., and Corbetta, M. (2005). Brain signals for spatial attention predict performance in a motion discrimination task. *Proc. Natl. Acad. Sci. U.S.A.* 102, 17810–17815.

Schölvinck, M. L., Maiera, A., Yec, F. Q., Duynd, J. H., and Leopold, D. A. (2010). Neural basis of global resting-state fMRI activity. *Proc. Natl. Acad. Sci. U.S.A.* 107, 10238–10243.

Seeley, W. W., Menon, V., Schatzberg, A. F., Keller, J., Glover, G. H., Kenna, H., Reiss, A. L., and Greicius, M. D. (2007). Dissociable intrinsic connectivity networks for salience processing and executive control. *J. Neurosci.* 27, 2349–2356.

Seliger, P., Tsimring, L. S., and Rabinovich, M. I. (2003). Dynamics-based sequential memory: winnerless competition of patterns. *Phys. Rev. E. Stat. Nonlin. Soft Matter Phys.* 67, 011905.

Shannon, B. J., and Buckner, R. L. (2004). Functional-anatomic correlates of memory retrieval that suggest nontraditional processing roles for multiple distinct regions within posterior parietal cortex. *J. Neurosci.* 24, 10084–10092.

Shmuel, A., and Leopold, D. A. (2008). Neuronal correlates of spontaneous fluctuations in fMRI signals in monkey visual cortex: implications for functional connectivity at rest. *Hum. Brain Mapp.* 29, 751–761.

Skudlarski, P., Jagannathan, K., Calhoun, V. D., Hampson, M., Skudlarska, B. A., and Pearlson, G. (2008). Measuring brain connectivity: diffusion tensor imaging validates resting state temporal correlations. *Neuroimage* 43, 554–561.

Smith, P. L., and Ratcliff, R. (2004). Psychology and neurobiology of simple decisions. *Trends Neurosci.* 27, 161–168.

Smith, S. M., Fox, P. T., Miller, K. L., Glahn, D. C., Fox, P. M., Mackay, C. E., Filippini, N., Watkins, K. E., Toro, R., Laird, A. R., and Beckmann, C. F. (2009). Correspondence of the brain's functional architecture during activation and rest. *Proc. Natl. Acad. Sci. U.S.A.* 106, 13040–13045.

Sporns, O., Tononi, G., and Edelman, G. M. (2000). Theoretical neuroanatomy: relating anatomical and functional connectivity in graphs and cortical connection matrices. *Cereb. Cortex* 10, 127–141.

Sridharan, D., Levitin, D. J., and Menon, V. (2008). A critical role for the right fronto-insular cortex in switching between central-executive and default-mode networks. *Proc. Natl. Acad. Sci. U.S.A.* 105, 12569–12574.

Sterzer, P., and Kleinschmidt, A. (2010). Anterior insula activations in perceptual paradigms – often observed but barely understood. *Brain Struct. Funct.* 10.1007/s00429–010-0252–2. [Epub ahead of print].

Super, H., van der Togt, C., Spekreijse, H., and Lamme, V. A. F. (2003). Internal state of monkey primary visual cortex (V1) predicts figure-ground perception. *J. Neurosci.* 23, 3407–3414.

Sylvester, C. M., Shulman, G. L., Jack, A. I., and Corbetta, M. (2009). Anticipatory and stimulus-evoked blood oxygenation level-dependent modulations related to spatial attention reflect a common additive signal. *J. Neurosci.* 29, 10671–10682.

Tambini, A., Ketz, N., and Davachi, L. (2010). Enhanced brain correlations during rest are related to memory for recent experiences. *Neuron* 65, 280–290.

Thut, G., Nietzel, A., Brandt, S. A., and Pascual-Leone, A. (2006). Alpha-band electroencephalographic activity over occipital cortex indexes visuospatial attention bias and predicts visual target detection. *J. Neurosci.* 26, 9494–9502.

Tsodyks, M., Kenet, T., Grinvald, A., and Arieli, A. (1999). Linking spontaneous activity of single cortical neurons and the underlying functional architecture. *Science* 286, 1943–1946.

Tsuda, I. (2001). Toward an interpretation of dynamic neural activity in terms of chaotic dynamical systems. *Behav. Brain Sci.* 24, 793–810.

van Dijk, H., Schoffelen, J.-M., Oostenveld, R., and Jensen, O. (2008). Prestimulus oscillatory activity in the alpha band predicts visual discrimination ability. *J. Neurosci.* 28, 1816–1823.

Vanhatalo, S., Palva, J. M., Holmes, M. D., Miller, J. W., Voipio, J., and Kaila, K. (2004). Infraslow oscillations modulate excitability and interictal epileptic activity in the human cortex during sleep. *Proc. Natl. Acad. Sci. U.S.A.* 101, 5053–5057.

Vanhaudenhuyse, A., Noirhomme, Q., Tshibanda, L. J. F., Bruno, M.-A., Boveroux, P., Schnakers, C., Soddu, A., Perlbarg, V., Ledoux, D., Brichant, J. -. F., Moonen, G., Maquet, P., Greicius, M. D., Laureys, S., and Boly, M. (2010). Default network connectivity reflects the level of consciousness in non-communicative brain-damaged patients. *Brain* 133, 161–171.

Varoquaux, G., Sadaghiani, S., Pinel, P., Kleinschmidt, A., Poline, J. B., and Thirion, B. (2010). A group model for stable multi-subject ICA on fMRI datasets. *Neuroimage* 51, 288–299.

Vincent, J. L., Kahn, I., Snyder, A. Z., Raichle, M. E., and Buckner, R. L. (2008). Evidence for a frontoparietal control system revealed by intrinsic functional connectivity. *J. Neurophysiol.* 100, 3328–3342.

Vincent, J. L., Patel, G. H., Fox, M. D., Snyder, A. Z., Baker, J. T., Van Essen, D. C., Zempel, J. M., Snyder, L. H., Corbetta, M., and Raichle, M. E. (2007). Intrinsic functional architecture in the anaesthetized monkey brain. *Nature* 447, 83–86.

Vyazovskiy, V. V., Cirelli, C., Pfister-Genskow, M., Faraguna, U., and Tononi, G. (2008). Molecular and electrophysiological evidence for net synaptic potentiation in wake and depression in sleep. *Nat. Neurosci.* 11, 200–208.

Wackermann, J., Lehmann, D., Michel, C. M., and Strik, W. K. (1993). Adaptive segmentation of spontaneous EEG map series into spatially defined microstates. *Int. J. Psychophysiol.* 14, 269–283.

Waites, A. B., Stanislavsky, A., Abbott, D. F., and Jackson, G. D. (2005). Effect of prior cognitive state on resting state networks measured with functional connectivity. *Hum. Brain Mapp.* 24, 59–68.

Wyart, V., and Tallon-Baudry, C. (2009). How ongoing fluctuations in human visual cortex predict perceptual awareness: baseline shift versus decision bias. *J. Neurosci.* 29, 8715–8725.

Zarahn, E., Aguirre, G. K., and D'Esposito, M. (1997). Empirical analyses of BOLD fMRI statistics. I. Spatially unsmoothed data collected under null-hypothesis conditions. *Neuroimage* 5, 179–197.

Conflict of Interest Statement: The authors declare that the research was conducted in the absence of any commercial or financial relationships that could be construed as a potential conflict of interest.

Received: 05 February 2010; paper pending published: 07 March 2010; accepted: 12 May 2010; published online: 23 June 2010.

*Citation: Sadaghiani S, Hesselmann G, Friston KJ and Kleinschmidt A (2010) The relation of ongoing brain activity, evoked neural responses, and cognition. Front. Syst. Neurosci. **4**:20. doi: 10.3389/fnsys.2010.00020*

frontiers in
SYSTEMS NEUROSCIENCE

REVIEW ARTICLE
published: 21 May 2010
doi: 10.3389/fnsys.2010.00021

Typical and atypical development of functional human brain networks: insights from resting-state fMRI

Lucina Q. Uddin[1,2]*, Kaustubh Supekar[3] and Vinod Menon[1,2,4]*

[1] *Stanford Cognitive and Systems Neuroscience Laboratory, Department of Psychiatry and Behavioral Sciences, Stanford University School of Medicine, Stanford, CA, USA*
[2] *Program in Neuroscience, Stanford University School of Medicine, Stanford, CA, USA*
[3] *Graduate Program in Biomedical Informatics, Stanford University School of Medicine, Stanford, CA, USA*
[4] *Department of Neurology and Neurological Sciences, Stanford University School of Medicine, Stanford, CA, USA*

Edited by:
Silvia A. Bunge, University of California Berkeley, USA

Reviewed by:
Damien Fair, Oregon Health and Science University, USA
Moriah E. Thomason, Stanford University, USA

****Correspondence:***
Lucina Q. Uddin, Stanford Cognitive and Systems Neuroscience Laboratory, Department of Psychiatry and Behavioral Sciences, Stanford University School of Medicine, 780 Welch Road, Room 201, Stanford, CA 94304, USA.
e-mail: lucina@stanford.edu;
Vinod Menon, Stanford Cognitive and Systems Neuroscience Laboratory, Department of Psychiatry and Behavioral Sciences, Stanford University School of Medicine, 780 Welch Road, Room 201, Stanford, CA 94304, USA.
e-mail: menon@stanford.edu

Over the past several decades, structural MRI studies have provided remarkable insights into human brain development by revealing the trajectory of gray and white matter maturation from childhood to adolescence and adulthood. In parallel, functional MRI studies have demonstrated changes in brain activation patterns accompanying cognitive development. Despite these advances, studying the maturation of functional brain networks underlying brain development continues to present unique scientific and methodological challenges. Resting-state fMRI (rsfMRI) has emerged as a novel method for investigating the development of large-scale functional brain networks in infants and young children. We review existing rsfMRI developmental studies and discuss how this method has begun to make significant contributions to our understanding of maturing brain organization. In particular, rsfMRI has been used to complement studies in other modalities investigating the emergence of functional segregation and integration across short and long-range connections spanning the entire brain. We show that rsfMRI studies help to clarify and reveal important principles of functional brain development, including a shift from diffuse to focal activation patterns, and simultaneous pruning of local connectivity and strengthening of long-range connectivity with age. The insights gained from these studies also shed light on potentially disrupted functional networks underlying atypical cognitive development associated with neurodevelopmental disorders. We conclude by identifying critical gaps in the current literature, discussing methodological issues, and suggesting avenues for future research.

Keywords: functional connectivity, brain maturation, resting-state fMRI, cognitive development, autism spectrum disorders, attention-deficit/hyperactivity disorder

INTRODUCTION

Over the past several decades, refinements in neuroimaging methods have enabled significant insights into human brain development. It is now known that the human brain undergoes a protracted period of development during which changes occur at both the structural and functional levels. Structural neuroimaging studies have shown that while gray matter volume follows a regionally specific inverted U-shaped trajectory, white matter volume shows protracted increases with development (Lenroot and Giedd, 2006). This general principle affects sensorimotor and higher-order association cortices at different time points in development (Gogtay et al., 2004). These regressive (gray matter loss) and progressive (white matter increases) changes are related to cognitive development (Casey et al., 2005). Age-related changes in cortical thickness have also been reported to show regional specificity (Sowell et al., 2004). Exactly how these structural changes impact functional brain maturation is less well understood.

In general, functional brain maturation is much more difficult to study than structural maturation because differences in observed brain activation can arise from differences in cognitive effort, experience, and strategy (Casey et al., 2005). This presents a significant challenge for understanding the development of functional brain networks. The existing literature suggests that brain activation during a particular cognitive task tends to progress from more diffuse to more focal with age. Durston et al. (2006) were the first to describe this notion of diffuse-to-focal changes in activation patterns in a longitudinal study of cognitive control. They demonstrated that over time, participants revealed an increase of magnitude of activation in key frontal areas with concomitant attenuation of activation in more widespread, nonspecific brain regions. They interpreted this to reflect development of more efficient processing. There is also evidence to suggest that with development, there are decreased demands on prefrontal cortex, with increased reliance on posterior brain regions (Rivera et al., 2005). However, there is often a complex relationship between changes in brain activation related to performance differences versus those related to brain maturation, and it is often difficult to match children on performance (Tamm et al., 2002). Even in cases where children, adolescents and adults are matched on accuracy,

Abbreviations: fMRI, functional magnetic resonance imaging; rsfMRI, resting-state fMRI; ICA, independent component analysis; ReHO, regional homogeneity; ADHD, attention-deficit/hyperactivity disorder; ASD, autism spectrum disorder; TS, Tourette syndrome; DMN, default mode network; DTI, diffusion tensor imaging.

it is often impossible to control for differences in reaction time (Kwon et al., 2002). Thus, while researchers typically attempt to control for performance-related issues in their studies, this is not always readily accomplished. The complex relationships between learning, experience, and development therefore make it difficult to uncover principles governing functional brain development, and complicate the interpretation of reported differences in brain activation between children and adults.

Resting-state fMRI (rsfMRI) offers a novel framework for studying the development of functional brain circuits, and in particular for better understanding the large-scale organization of the developing brain. This method is now increasingly used to complement traditional task-based fMRI. rsfMRI involves collecting functional imaging data from participants as they lay in the MRI scanner, typically fixating gaze on a cross-hair or with eyes closed, and refraining from engaging in any specific cognitive task. Since initial reports of coherent spontaneous low-frequency fluctuations in BOLD signal within the somatomotor system in the absence of a specific task (Biswal et al., 1995), it has been widely demonstrated that brain networks that are engaged during cognitive tasks can also be reliably identified during resting states (Smith et al., 2009, see Fox and Raichle, 2007 for review). Resting-state functional connectivity uses spontaneous synchronized fluctuations in BOLD signal to determine tightly coupled functional brain networks independent of task-induced correlations. These spontaneous fluctuations are posited to act to organize, coordinate, and maintain functional brain systems (Fox and Raichle, 2007; Raichle, 2010), and bias information processing (Greicius and Menon, 2004). The advantages of using rsfMRI in pediatric and clinical populations are that functional brain organization can be examined independent of task performance, and a full dataset can be collected in as little as 5 min (Van Dijk et al., 2009). Functional connectivity measures derived from rsfMRI data are particularly useful in studying age-related changes in the wiring of neural networks (Stevens, 2009; Supekar et al., 2009). Within- and between-subject measures computed from rsfMRI are quite consistent and reproducible (Damoiseaux et al., 2006; Shehzad et al., 2009). Because the resting-state scanning procedure places a minimal cognitive burden on the participant, and requires relatively little time in the scanner compared to task fMRI studies, data can be collected from low-functioning and very young populations. A recent study of the fMRI success rate of children and adolescents reports that the success rate for completing an entire battery of experimental fMRI runs varied between 50 and 59% in patient populations such as attention-deficit/hyperactivity disorder (ADHD) and autism spectrum disorder (ASD), and 69% for typically developing children (Yerys et al., 2009). As every pediatric neuroimaging researcher knows, excessive motion and floor task performance are issues that hinder successful scanning of young children, and account for significant data loss. The use of rsfMRI data obviates the need for long scan sessions as well as concerns regarding task performance, thus is particularly well suited for studies of typical and atypical brain development. In addition, certain widely adopted methodological approaches to analyzing rsfMRI data [e.g., independent component analysis (ICA), discussed below] are quite successful at removing motion artifacts, resulting in significantly less data loss.

The first study to use rsfMRI to study brain development was conducted in 2000. Curiously, subsequent rsfMRI studies in children did not appear until 2006. The use of rsfMRI in developmental studies is clearly still in its infancy, and our review of the emerging literature is necessarily constrained by this limitation. **Table 1** summarizes current studies that have used rsfMRI to examine the typical and atypical development of functional brain networks. We begin with summaries of major findings regarding brain maturation from rsfMRI studies in neurotypical infants, children and adolescents. Within each section of the review, studies are grouped by analysis method employed, as the specific methods can have important implications for the interpretation of findings. We next review contributions of rsfMRI to the study of neurodevelopmental disorders, focusing primarily on ADHD and ASD. Next, methodological issues related to the acquisition and analyses of rsfMRI data for developmental studies are discussed. We conclude by highlighting outstanding issues in the field and suggesting avenues for future research.

TYPICAL DEVELOPMENT: STUDIES IN INFANTS AND YOUNG CHILDREN

ROI SEED-BASED ANALYSIS

Region-of-interest (ROI) seed-based analysis is one of the two most widely used methods in analysis of rsfMRI data. The method is a hypothesis-driven approach that typically involves choosing one or more ROIs and examining their whole-brain functional connectivity, often using a regression or correlation model. Kiviniemi et al. (2000) used this method in the first reported study of developing functional networks using rsfMRI. The authors studied children between 3 months and 10 years of age. During the scan participants were sedated with thiopental. Using one representative voxel time course from primary visual cortex, the authors demonstrated correlated activity within striate and extrastriate cortex as well as occipital cortices adjacent to primary visual cortex. This study demonstrated that children as young as 3 months of age have stable visual networks, and that they can be detected in rsfMRI data.

Ethical concerns preclude the use of sedation in studies of typical development. The first study to take advantage of natural sleep as a method to study brain function in young children was conducted by Redcay et al. (2007). The authors used an ROI-based approach and reported functional connectivity between superior temporal gyrus and medial and lateral prefrontal regions, as well as between occipital and parietal regions, in 2- to 4-year-old typically developing children during low-level auditory and visual stimulation. The extent to which these results reflect task-related versus intrinsic functional connectivity is at present unclear. Nonetheless, this study highlights the utility of imaging during natural sleep to obtain high quality fMRI data from very young children, which would otherwise be impossible to collect in this age range.

Lin et al. (2008) took advantage of rsfMRI during natural sleep to study functional connectivity of primary motor, sensory, and visual areas in children between 2 weeks and 2 years of age while they were asleep. This study found that the percentage of brain volume exhibiting resting functional connectivity, and the strength of resting functional connectivity, increased non-uniformly from 2 weeks to 2 years of age. The percentage of brain volume that showed resting functional connectivity in sensorimotor cortices was larger than that

Table 1 | Summary of resting-state fMRI studies in infants, children and adolescents, including neurodevelopmental disorders.

Ages studied	Authors	Population	Analyses	Brain regions examined
4.29 ± 2.56 years	Kiviniemi et al. (2000)	Typically developing	ROI-based FC	Visual cortex
Neonates 2–4 weeks of age, 1-year-olds, 2-year-olds	Lin et al. (2008)	Typically developing	ROI-based FC	Motor, sensory, and visual networks
Visual experiment: 46.4 ± 6.7 months; Auditory experiment: 46.9 ± 9.7 months	Redcay et al. (2007)	Typically developing	ROI-based FC	Superior temporal gyrus, occipital cortex
Range: 39 weeks and 1 day to 44 weeks and 2 days (gestational age at MRI: 41 weeks)	Fransson et al. (2007)	Typically developing	ICA	Somatosensory and motor cortices, temporal/inferior parietal cortex, posterior lateral and midline parietal cortex/lateral aspects of the cerebellum, medial and lateral sections of anterior prefrontal cortex
12.8 months	Liu et al. (2008)	Typically developing	ICA	Sensorimotor network
Neonates (24 ± 12 days); 1-year-olds (13 ± 1 month); 2-year-olds (25 ± 1 month)	Gao et al. (2009)	Typically developing	ICA, graph theory	Default mode network
7–9 years; 10–15 years; 19–31 years	Fair et al. (2008)	Typically developing	ROI-based FC, graph theory	Default mode network
Children: 10.6 ± 1.5 years; Adolescents: 15.4 ± 1.2 years; Adults: 22.4 ± 1.2 years	Kelly et al. (2009)	Typically developing	ROI-based FC	Cingulate-based networks
12–30 years	Stevens et al. (2009)	Typically developing	ICA, causality estimates	Whole-brain
Working memory: 7–11 years; Rest: 9–12 years	Thomason et al. (2008)	Typically developing	ICA	Default mode network
Children: 7–9 years, mean 8.6; Adolescents: 10–15 years, mean 11.9; Adults: 20–31 years, mean 24.1	Fair et al. (2007)	Typically developing	Graph theory	Thirty-nine putative task-control regions within fronto-parietal and cingulo-opercular networks
Children: 7–9 years; Adult: 19–22 years	Supekar et al. (2009)	Typically developing	Graph theory, white matter fiber tracking	Whole-brain
7–31 years	Fair et al. (2009)	Typically developing	Graph theory	Cingulo-opercular, fronto-parietal, cerebellar, and default mode networks
Children: 7–9 years; Adult: 19–22 years	Supekar et al. (2010)	Typically developing	ICA, white matter fiber tracking	Default mode network
ADHD: 13.91 ± 0.35 years; Control: 13.20 ± 0.56 years	Tian et al. (2006)	ADHD	ROI-based FC	Dorsal anterior cingulate cortex
ADHD: 13.37 ± 1.49 years; Control: 13.32 ± 0.95 years	Cao et al. (2006)	ADHD	ReHo	Whole-brain
ADHD: 13.34 ± 1.44 years; Control: age-matched within 0.5 year	Zhu et al. (2008)	ADHD	ReHo, Fisher discriminative analysis	Whole-brain
ADHD: 13.0 ± 1.4 years; Control: 13.1 ± 0.6 years	Zang et al. (2007)	ADHD	ALFF	Whole-brain
ADHD: 13.48 ± 1.11 years; Control: 13.19 ± 0.49 years	Tian et al. (2008)	ADHD	RSAI	Whole-brain
ADHD: 13.3 ± 1.4 years; Control: 13.2 ± 1.0 years	Cao et al. (2009)	ADHD	ROI-based FC	Putamen
ADHD: 34.9 ± 9.9 years; Control: 31.2 ± 9.0 years	Castellanos et al. (2008)	ADHD	ROI-based FC	Cingulate-based networks

(Continued)

Table 1 | *(Continued)*

Ages studied	Authors	Population	Analyses	Brain regions examined
ADHD: 34.9 ± 9.9 years; Control: 31.2 ± 9.0 years	Uddin et al. (2008)	ADHD	NetHo	Default mode network
ASD: 24 ± 10.6 years; control: 24 ± 9.0 years	Cherkassky et al. (2006)	ASD	ROI-based FC	Posterior cingulate cortex, ventral anterior cingulate cortex, precuneus, paracentral lobule, bilateral medial/middle prefrontal cortex, bilateral inferior parietal cortex, bilateral parahippocampal gyrus, bilateral inferolateral temporal cortex (insula)
ASD: 26.5 ± 12.8 years; Control: 27.5 ± 10.9 years	Kennedy et al. (2008)	ASD	ROI-based FC	Task-positive (dorsal attention) network, task-negative (default mode) network
ASD: 26 ± 5.93 years; TD: 27 ± 6.1 years	Monk et al. (2009)	ASD	ROI-based FC	Default mode network
ASD: 15 ± 1.45 years; TD: 16 ± 1.44 years	Weng et al. (2010)	ASD	ROI-based FC	Default mode network
8 years	Paakki et al. (2010)	ASD	ReHo	Whole-brain
TS: 12.70 years (9.92–15.83); TD: 12.69 years (10.42–15.75)	Church et al. (2009)	Tourette syndrome	ROI-based FC	Thirty-nine putative task control regions within fronto-parietal and cingulo-opercular networks
MDD: 16.5 ± 0.95 years; TD: 16.8 ± 1.5 years	Cullen et al. (2009)	Depression	ROI-based FC	Subgenual ACC, amygdala, supragenual ACC
12.2 ± 2.1 years	Thomason et al. (2009)	BDNF met-allele carriers	ROI-based FC	Default mode network, executive control network, salience network

ADHD, attention-deficit/hyperactivity disorder; ALFF, amplitude of low-frequency fluctuation; ASD, autism spectrum disorder; FC, functional connectivity; ICA, independent component analysis; MDD, major depressive disorder; NetHo, network homogeneity; ReHo, regional homogeneity; ROI, region-of-interest; RSAI, resting-state activity index; TD, typically developing.

in the visual cortex for subjects 2 weeks of age and for 1-year-olds, but not for the 2-year-olds, suggesting that functional connectivity in sensorimotor networks precedes that in the visual networks. This study highlights the utility of rsfMRI for examining development of specific functional systems in infants and very young children. The findings shed light on different developmental trajectories of distinct cortical networks underlying sensorimotor and visual processing.

ICA-BASED ANALYSIS

ICA, unlike ROI-based analysis, is a model-free, data-driven approach whereby four-dimensional fMRI data is decomposed into a set of independent one-dimensional time series and associated three-dimensional spatial maps which describe the temporal and spatial characteristics of the underlying signals or components (Beckmann et al., 2005). ICA is currently a widely used method for analyzing rsfMRI data (Calhoun et al., 2008).

In 2007, Fransson et al. studied resting-state activity in the brains of sedated sleeping infants under 1 year of age. Using ICA, five distinct networks were identified in the infant brain. These consistent networks comprised (1) primary visual areas, (2) bilateral somatosensory and motor cortices, (3) bilateral temporal/inferior parietal cortex including primary auditory cortex, (4) posterior lateral and midline parts of the parietal cortex and lateral aspects of the cerebellum, and (5) medial and lateral sections of anterior prefrontal cortex. Intriguingly, these networks represent a subset of those previously demonstrated to exist in the adult brain (Damoiseaux et al., 2006; De Luca et al., 2006), with the notable exception that the infant brain appeared to lack a component along the anterior–posterior direction, despite the fact that transcallosal functional connectivity was intact at this very young age. The authors specifically noted that they did not detect an equivalent of the default mode network (DMN) in infants (Fransson et al., 2007). The DMN is so named due to its uniquely high metabolic resting activity (Raichle et al., 2001) and characteristic deactivation during challenging cognitive tasks (Shulman et al., 1997). The network includes posterior cingulate cortex (PCC), medial prefrontal cortex (MPFC), and bilateral inferior parietal lobule (IPL, Raichle et al., 2001). While the functions of this network are widely debated, there is growing evidence that it is involved in high level self-related (e.g., autobiographical and prospective memory) (Buckner and Carroll, 2007) or social cognitive (e.g., theory of mind and moral cognition) processes (Harrison et al., 2008). Fransson et al. (2007) suggest that the absence of this network in infants may be related to both immature anterior–posterior white matter connectivity and immature development of these cognitive processes.

In another study, Liu et al. (2008) studied functional connectivity of somatomotor areas in 1-year-old infants. They used ICA to detect a sensorimotor network, and reported greater intrahemispheric connectivity than interhemispheric connectivity within sensorimotor areas. This finding is in line with the Fransson et al. (2007)

study. This suggests a universal principle guiding development of large-scale brain systems, namely that the development of intrahemispheric connectivity within local functional circuits precedes the development of interhemispheric connectivity.

GRAPH THEORETICAL AND NETWORK ANALYSIS

Graphs are data structures which have nodes and edges between the nodes (Bondy and Murty, 1976). Graph theoretical metrics such as clustering coefficient, path length, degree, and centrality provide quantitative measures to characterize large-scale networks represented as a graph (see Bullmore and Sporns, 2009 for a detailed review of various graph metrics and their interpretation). In a graphical representation of a brain network, a node corresponds to a brain region while an edge corresponds to the functional interactions between two brain regions. In recent years, there has been increasing interest in the use and application of graph metrics to characterize large-scale brain networks. This is in part due to the emergence and availability of rsfMRI data. In addition to the advantages described above, resting-state data allow, for the first time, simultaneous *in vivo* examination of all brain regions and the intrinsic interactions among them. More importantly, patterns of resting-state correlations are thought to reflect functional architecture of the brain (Hagmann et al., 2008; Margulies et al., 2009; van den Heuvel et al., 2009). Several studies have used graph theoretical approaches to characterize large-scale brain networks using rsfMRI. In adults, converging evidence from studies suggests that the adult brain has a robust and efficient small-world architecture comprised of hubs with a high degree connectivity and a modular structure (see Bullmore and Sporns, 2009 for a comprehensive review). Developmental studies are beginning to examine how these network metrics change with age and cognitive skill.

In a developmental context, Gao et al. (2009) used a combination of graph theoretical analyses and ICA to examine a large-scale brain network (DMN) in healthy 2-week to 2-year-old sleeping children. They found a primitive and incomplete DMN in 2-week-olds, followed by an increase in the number of brain regions exhibiting connectivity at 1 year of age. The DMN at 2 years of age began to resemble that observed in adults, in that it included MPFC, PCC/retrosplenial (PCC/Rsp), IPL, lateral temporal cortex, and hippocampus. As previously discussed, this network is thought to subserve self-related and social cognitive processes (Uddin et al., 2007; Spreng et al., 2009). The authors then used a measure called "betweenness" centrality, a graph theoretical measure of node importance, to show that the PCC/Rsp nodes showed the most elevated centrality measure for all age groups. The PCC/Rsp node was consistently observed in both age groups, suggesting that this region may form a "hub" even at the earliest developmental stage. They also found that the MPFC showed elevated centrality measures, though not as high as the PCC/Rsp. They suggest that the MPFC emerges as a potential secondary hub starting at the age of 1.

TYPICAL DEVELOPMENT: STUDIES IN OLDER CHILDREN, ADOLESCENTS AND YOUNG-ADULTS

ROI SEED-BASED ANALYSIS

Fair et al. (2008) used ROI-based analyses to examine differential connectivity of the ventromedial prefrontal cortex (vmPFC) in a group of 7- to 9-year-old children compared to 21- to 31-year-old adults. Children showed marked decreases in connectivity along the anterior–posterior dimension, between the vmPFC and PCC, compared to adults. To further examine differences in brain network structure between children and adults, the time series associated with 13 nodes within the DMN (such as left and right lateral parietal cortex, left and right parahippocampal gyrus, MPFC, and retrosplenial cortex) were correlated with each other. Comparison of correlation matrices generated from child and adult rsfMRI data revealed that nodes within the DMN were sparsely connected in children, and strongly functionally connected in adults. Interestingly, in this age range, interhemispheric functional connections between homotopic regions were reported to be strong in children, as in adults.

In addition to providing detailed information about the connectivity profiles of individual nodes, ROI-based analyses have aided in delineating regionally specific developmental changes within functionally heterogeneous brain regions. In a recent study, Kelly et al. (2009) examined the development of five functionally distinct cingulate-based networks in children (age 11 years), adolescents (age 15) and young-adults (age 22). These networks have been previously characterized in adults (Margulies et al., 2007), and underscore the heterogeneous connectivity of subregions within the cingulate cortex. This study found that children demonstrated a more diffuse pattern of correlation with voxels proximal to the seed ROI, whereas adults exhibited more focal patterns of functional connectivity, as well as a greater number of correlated voxels at long distances from the seed ROI. Adolescents exhibited intermediate patterns of connectivity between the children and adults. Interestingly, connectivity of networks associated with social and emotional functions [based in subgenual anterior cingulate cortex (ACC) and vmPFC] exhibited the greatest developmental effects, while connectivity of networks associated with motor control and conflict monitoring (dorsal ACC) did not differ greatly between the three groups (Kelly et al., 2009). This study demonstrates that rsfMRI data recapitulates two organizational principles of development that have previously been proposed, namely the shift from diffuse to focal activity with age (Durston et al., 2006), and the development of motor systems preceding the development of systems underlying higher cognition (Chugani et al., 1987).

ICA-BASED ANALYSIS

Using an ICA analysis in conjunction with "causal density" estimates, Stevens et al. (2009) characterized functional networks in 100 participants ranging in age from 12 to 30 years. The authors identified 13 components of interest and used Granger causality estimates to examine interactions between these networks. They report that mutual influences among networks decreased with age, and speculate that this reflects stronger within-network connectivity and more efficient between-network influences with development. Interestingly, they also found age-related reductions in the strength of interaction between lateral prefrontal-parietal (executive control) circuits and networks identified as resembling the DMN. They suggest that more segregated functioning of these sets of networks may allow greater processing flexibility.

Thomason et al. (2008) identified the DMN in 7- to 12-year-old children using both rsfMRI and examination of task-induced deactivations. They report overlap between brain regions comprising the DMN as identified by ICA applied to rsfMRI data, and regions

comprising the DMN as identified by load-dependent deactivation during a working memory task. These DMN regions identified by two methods overlapped with the regions previously reported in adults. They also found that cognitive measures collected outside the scanner correlated with BOLD decreases during the working memory tasks.

GRAPH THEORETICAL AND NETWORK ANALYSIS

In order to understand functional brain development, it is critical to investigate and characterize the underlying developmental processes that produce systematic changes in functional brain organization. Fair et al. (2008) were the first to examine this developmental process using rsfMRI. In a related study, they focused on a larger network comprised of 39 cortical regions involved in task-control (Fair et al., 2007a). This study reported a developmental process trend towards "segregation" (general decrease in connectivity strength) between regions close in anatomical space and "integration" (increased connectivity strength) between specific regions distant in Euclidean space, within the 39-node network. More generally, the authors of these two studies argue that the organization of large-scale functional brain networks shifts from a local anatomical emphasis in children to a more distributed architecture in young-adults (Fair et al., 2009).

In contrast to examining developmental process within circumscribed network nodes, Supekar et al. (2009) investigated age-related functional connectivity changes across 90 cortical and subcortical regions that spanned the entire brain. More specifically, they analyzed inter-regional functional connectivity changes within this 90-node whole-brain network in relation to distance between the regions. The inter-regional distance was measured using quantitative diffusion tensor imaging-based white matter tractography, rather than Euclidean distance between regions as used in the studies by Fair et al. (2007a). Additional analyses further revealed that adults have weaker short-range functional connectivity and stronger long-range functional connectivity than do children. Taken together, the studies by Fair et al. (2007a, 2009), Kelly et al. (2009), and Supekar et al. (2009) suggest a developmental process of greater functional segregation in children and greater functional integration in adults at the whole-brain level, as well as in specific networks such as the attentional control network and the DMN.

Understanding how the functional organization of the human brain matures and evolves from childhood to adolescence to adulthood is fundamentally important for gaining insights into the maturation of brain function. As described earlier, the graph theoretical approach is well suited for characterizing functional organization of the brain at multiple levels of granularity. At the global "whole-brain" level, Supekar et al. (2009) reported that both 7- to 9-year-old children and 19- to 22-year-old adults exhibit small-world architecture characterized by high clustering and short path lengths. A small-world architecture was also revealed in a study of multiple functional networks involving distributed nodes conducted by Fair et al. (2009). These studies indicate that at the global level, the human brain is comprised of sub-networks of densely connected nodes, mostly connected by short path lengths. More importantly, these studies indicate that this robust organization is conserved from early childhood to adulthood. At the sub-network level, however, Supekar et al. (2009) found significant differences in inter-regional connectivity patterns between children and adults. Notably, in children, subcortical areas were more strongly connected with primary sensory, association, and paralimbic areas, whereas adults showed greater cortico-cortical connectivity between paralimbic, limbic, and association areas (**Figure 1**). This finding is in line with previous work demonstrating greater reliance on subcortical structures in children during cognitive tasks (Luna et al., 2001; Thomas et al., 2004). Taken together these studies indicate that while the global functional organization of the human brain is similar in 7- to 9-year-old children and adults, at the sub-network level, brain connectivity undergoes significant reorganization with development.

In summary, studies examining functional brain organization in infants, children, and adolescents have revealed consistent findings with respect to the development of long distance connectivity and regional functional specialization. The ability to study very young children at critical developmental milestones is an advantage of the rsfMRI approach, which allows for the *in vivo* examination of intrinsic functional architecture across the entire brain. However, most of these studies have been conducted in older children, adolescents and adults, and thus to date there is little known regarding how global or local network organization changes during the important developmental period from infancy to young childhood.

NEURODEVELOPMENTAL DISORDERS: STUDIES IN CHILDREN AND ADULTS

OVERVIEW

In addition to enabling unique insights into typical brain development, rsfMRI has been used to explore potentially altered functional connectivity associated with neurodevelopmental disorders. Unfortunately, the majority of these studies have not focused on infants and young children, an issue that is particularly pressing in early impact disorders such as ASD. Nonetheless, the theoretical and methodological progress that has resulted from studies of older children and adults is paving the way for similar studies in younger populations.

ATTENTION-DEFICIT/HYPERACTIVITY DISORDER

Several recent studies have focused on ADHD, although few consistent findings have emerged. An early study in adolescents found that patients with ADHD showed more significant resting-state functional connectivity between dorsal ACC and thalamus, cerebellum, insula, and brainstem (Tian et al., 2006). Using an approach termed "regional homogeneity" (ReHo), which measures the similarity of a voxel's time series to its neighbors, it was reported that children with ADHD showed decreased ReHo in frontal–striatal–cerebellar circuits and increased ReHo in the occipital cortex (Cao et al., 2006), suggesting disordered functional organization in circuits previously implicated in structural brain imaging studies of ADHD (Giedd et al., 2001). Classifiers based on ReHo measures have been used to discriminate children with ADHD from controls with 85% accuracy (Zhu et al., 2008). Zang et al. (2007) showed that children with ADHD had decreased amplitude of low-frequency fluctuations (ALFF: 0.01–0.08 Hz) in the right inferior frontal cortex, left sensorimotor cortex, and bilateral cerebellum, and increased ALFF in the right ACC, left sensorimotor cortex, and bilateral brainstem. Using a measure incorporating ReHo and variance of LFF, Tian et al. (2008) found that adolescents with ADHD showed greater

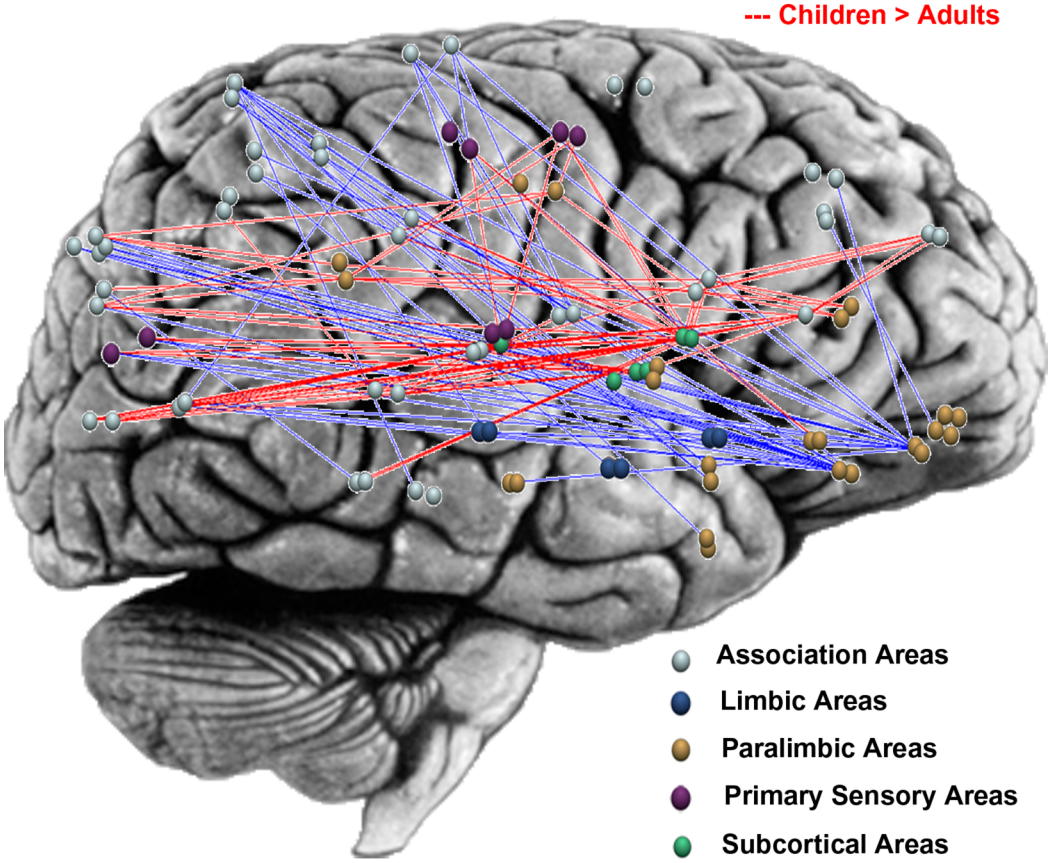

FIGURE 1 | Graphical representation of developmental changes in functional connectivity along the posterior–anterior and ventral–dorsal axes, highlighting higher subcortical connectivity (subcortical nodes are shown in green) and lower paralimbic connectivity (paralimbic nodes are shown in gold) in children, compared to young-adults. Brain regions are plotted using the *y* and *z* coordinates of their centroids (in millimeter) in the MNI space. Four hundred and thirty pairs of anatomical regions showed significantly higher correlations in children and 321 pairs showed significantly higher correlations in young-adults ($p < 0.005$, FDR corrected). For illustration purposes, the plot shows differential connectivity that was most significant, 105 pairs higher in children (indicated in red) and 53 higher in young-adults (indicated in blue) ($p < 0.0001$, FDR corrected). Adapted from Supekar et al. (2009).

resting-state activity than controls in basic sensory areas (bilateral BA 17/18/19, left BA 3, left BA 22, and bilateral thalamus). Yet another study reported putamen-specific functional connectivity abnormalities in ADHD, with group differences in putamen and cortical–striatal–thalamic circuits (Cao et al., 2009). Though intriguing, very few replicable findings have emerged from these studies, perhaps due to the relatively small sample sizes and heterogeneity of symptomatology in the patients examined.

ADHD is known to be associated with attentional lapses (Castellanos et al., 2005), thus recent studies have begun to focus on understanding how circuitry within the ACC may contribute to the symptoms of the disorder. A study of 20 adults with ADHD and 20 matched controls found decreases in negative correlations between the anterior cingulate and precuneus/ PCC regions as well as decreases in connectivity between precuneus and other default mode network components, including vmPFC (Castellanos et al., 2008). This finding was bolstered by similar results utilizing a different measure on the same dataset, which found reduced "network homogeneity" within the DMN in ADHD, particularly between the precuneus and other DMN regions (Uddin et al., 2008). These findings are in line with a theory positing that spontaneous patterns of very low frequency coherence within the DMN may intrude into periods of active task-specific processing, producing periodic fluctuations in attention that compete with goal-directed activity in ADHD (Sonuga-Barke and Castellanos, 2007).

AUTISM SPECTRUM DISORDERS

Autism is another major neurodevelopmental disorder that has long been associated with disruptions in brain connectivity (Frith, 2004). Surprisingly, to date there have been no published reports of rsfMRI studies in children with ASD. However, a few studies have used this method to study adolescents and adults with ASD. Cherkassky et al. (2006) used an ROI-based approach to demonstrate functional underconnectivity in anterior–posterior connections in ASD. ASD is associated with altered socioemotional responses, which have been linked to the DMN. Kennedy and Courchesne (2008) showed, in a mixed group of adolescents and adults, disrupted intrinsic connectivity in the DMN, but not the executive control network. Another

recent study replicated this finding of reduced DMN connectivity, and further demonstrated that restricted and repetitive behaviors in ASD were correlated with the degree of connectivity between the PCC and right parahippocampal gyrus (Monk et al., 2009). This group went on to examine DMN connectivity in adolescents with ASD. They also found that relative to controls, adolescents with ASD showed weaker connectivity in nine of the eleven areas of the DMN that were analyzed. Additionally, poorer social skills and increases in restricted and repetitive behaviors and interests correlated with weaker connectivity, whereas poorer verbal and non-verbal communication correlated with stronger connectivity in multiple areas of the DMN. Compared to their study of adults with ASD, these findings indicate that adolescents with ASD show even weaker connectivity in the DMN (Weng et al., 2010). Paakki et al. (2010) used the ReHo approach to study adolescents with ASD, and found that compared with the controls, the subjects with ASD had significantly decreased ReHo in right superior temporal sulcus region, right inferior and middle frontal gyri, right insula and right postcentral gyrus. Significantly increased ReHo was shown in left inferior frontal and anterior subcallosal gyrus (Paakki et al., 2010). A study in neurotypical adults found that functional connectivity between the anterior insula and ACC was related to social responsiveness (Di Martino et al., 2009). Future research is needed to examine how reduced functional connectivity between specific brain regions impacts symptom severity in young children and adolescents with ASD, and how these reductions influence deficits in performance on tasks involving social information processing.

While rsfMRI studies relevant to understanding the neural basis of ASD are still in their infancy, they highlight the utility and value of this approach. In addition, these studies have identified previously understudied candidate brain regions and large-scale networks of interest. In particular, we believe that the study of relationships between networks involved in self-related and social cognition (DMN), externally oriented attention (executive control) and switching between them should be particularly prioritized in future studies of ASD (Uddin and Menon, 2009).

OTHER NEURODEVELOPMENTAL DISORDERS AND GENETIC EFFECTS

Tourette syndrome (TS) is another pediatric disorder that has recently been studied using rsfMRI methods. Church et al. (2009) found that a fronto-parietal network involved in rapid, adaptive online control was weaker in adolescents with TS. Adolescents with major depressive disorder have decreased functional connectivity in a subgenual ACC-based neural network that includes the supragenual ACC, right medial frontal cortex, the left inferior and superior frontal cortex, superior temporal gyrus, and the insular cortex, areas involved in mediating emotion processing (Cullen et al., 2009).

Intriguingly, specific genetic polymorphisms have also been shown to affect resting-state functional connectivity measures in children (Thomason et al., 2009). BDNF gene variants, associated with alterations in brain anatomy and memory, appear to affect functional connectivity. Thomason et al. (2009) found a reduction in hippocampal and parahippocampal to cortical connectivity in met-allele carriers within each of three resting networks (the default mode, executive, and paralimbic networks), as well as increased connectivity to amygdala, insula and striatal regions in met-carriers, within the paralimbic network. Thus, genetic differences can contribute to functional connectivity differences at the systems-level. How these differences in functional connectivity influence memory function remains to be investigated.

METHODOLOGICAL ISSUES AND CHALLENGES

One of the primary challenges in pediatric neuroimaging is the fact that the procedure requires participants to remain motionless for an extended period of time. As this is particularly difficult for young children, especially for clinical populations such as children with ADHD or ASD, fMRI data often contains significant motion artifacts, resulting in up to 50% data loss in some cases (Yerys et al., 2009). Two main solutions to this problem are currently implemented, one at the data collection level and one at the data processing level. Data acquisition protocols often include a "mock scanner" training session, during which children practice lying still in a scanner-like mockup. Post data acquisition, artifact correction algorithms can also be implemented to remove motion-related spikes in the data (Mazaika et al., 2007, 2009). Currently, these procedures are not universally utilized, and considerable variability exists between research centers with respect to criteria for inclusion of data containing motion artifacts. As previously discussed, one advantage of rsfMRI is that it requires very little time in the scanner, and thus can be more easily collected from young participants. In addition, resting-state data is often analyzed using ICA, as summarized in the studies reviewed above. This analysis method may be helpful in effectively isolating motion-related artifacts as distinct independent components (Beckmann et al., 2005).

A second issue concerns the use of varied instructions to the participant during acquisition of rsfMRI data. By definition, resting-state signal reflects activity during a task-free ("rest") state. Accordingly, most of the developmental studies reviewed here have used data collected while the participants were not performing any task. Although these data indeed reflect resting conditions, a closer look indicates that participants were either instructed to fixate on a cross-hair, or keep their eyes open while viewing a blank screen, or keep their eyes closed for the duration of the scan. A recent study, however, indicated that resting-state connectivity within the DMN and attention network was significantly diminished in participants with eyes closed, compared to eyes open or a fixation condition (Van Dijk et al., 2009).

An important related issue is the use of "rest blocks" within task data to conduct analyses typically performed on pure resting-state data. Fair et al. (2007b) used rest blocks extracted from interleaved experimental task data in studies investigating developmental changes in intrinsic functional connectivity. Cherkassky et al. (2006) used a similar approach to investigate resting-state functional connectivity in autism, as reviewed. Another group used residual signal obtained by regressing out task-evoked effects from an event-related task to study functional connectivity within fronto-parietal resting-state networks (He et al., 2007). Given the inherent resting-state connectivity differences even within various resting states, it is more than of academic interest to investigate how well these datasets relate to pure rsfMRI data. Fair et al. (2007b) investigated this issue by comparing resting-state functional connectivity measures from data obtained from (1) residual data from event-related designs, (2) continuous resting-state data, (3) resting

data that was interleaved between task blocks, and (4) simulated interleaved resting data that was created using the continuous resting data set. They reported that the residual data set, the interleaved dataset, and the simulated interleaved dataset were mostly similar to the continuous resting state dataset, with some differences. The greatest caveats on interpretation of functional connectivity results were placed on the use of event-related data residuals (Fair et al., 2007b).

Another issue concerns the current lack of studies examining test–retest reliability of resting-state data collected for developmental studies. While the patterns of resting-state functional connectivity have been shown to be reproducible across adult participants and scans (van de Ven et al., 2004; Damoiseaux et al., 2006), there is limited evidence about their test–retest reliability, particularly for the pediatric populations. In adults, Shehzad et al. (2009) reported that the test–retest reliability of resting-state functional connectivity was high for significant positive correlations and relatively low for non-significant and negative correlations. Furthermore, they showed that the reliability for DMN connectivity was higher compared to task positive networks. Meindl et al. (2009) reported similar reproducibility results. They observed, across three scan sessions, higher reliability for DMN correlations and lower for non-DMN correlations. These results were further confirmed by Zuo et al. (2010a,b). Although the results of these studies appear promising, Honey et al. (2009) recently raised concerns about the test–retest reliability of rsfMRI data. For individual participants, they observed overall low reproducibility across scans for resting-state correlations between 998 ROIs. All of these previous studies have been conducted in adults, therefore it is not at all known to what extent this issue affects studies of development.

Yet another issue pertains to statistical power or lack thereof in pediatric resting-state studies. Most studies to date have had included relatively small numbers of participants. Although analyses of power and sample sizes have been reported for conventional task-based functional neuroimaging studies (Desmond and Glover, 2002), similar power analyses have not yet been applied to rsfMRI. This is particularly important for studies of typical and atypical pediatric populations, which are inherently highly heterogeneous. Ideally, along with statistical power analyses, a clinical pediatric resting-state study should be comprised of a relatively homogenous group, as well as a homogenous well-matched control group for meaningful interpretations and better comparability of findings across studies.

Finally, it is now well documented that raw rsfMRI data is contaminated by motion artifacts, scanner artifacts, and physiological noise (Biswal et al., 1995; Lowe et al., 1998; Cordes et al., 2000, 2001). To remove this noise, researchers have used a gamut of techniques including, but not limited to, spatial smoothing (to improve signal-to-noise ratio), temporal filtering (to remove signal contributed by physiological sources such as cardiac and respiratory cycles) (De Luca et al., 2006; Supekar et al., 2009), whole-brain signal regression (to account for noise sources such as motion, cardiac, and respiratory signals that globally influence the signal) (Desjardins et al., 2001), and regressing out cardiac and respiratory signals acquired in the scanner (to minimize unwanted physiological variations) (Birn et al., 2008; Chang and Glover, 2009; Chang et al., 2009). Although these techniques are fairly effective in removing noise, they raise some concerns regarding the interpretation of the preprocessed data. For example, regressing out whole-brain signal has shown to introduce negative correlations (Murphy et al., 2009; Smith et al., 2009; Van Dijk et al., 2009), though there is no reason to believe that all reported negative correlations are artifactual (Fox et al., 2009). Preprocessing including global signal correction has been shown to increase connection specificity. However, as negative correlations can be induced by this procedure, there is reason to interpret the directionality of these relations with caution especially when global regression is used (Weissenbacher et al., 2009). While these issues are a concern for all rsfMRI studies, not just those exploring developmental issues, the field has not yet reached a consensus as to how to best minimize the effects of noise on these analyses.

SUMMARY AND FUTURE DIRECTIONS

In this review, we have summarized the current status of research utilizing rsfMRI to examine the typical and atypical development of functional brain circuits. Several key principles of human brain development are beginning to emerge from this literature. In particular, these studies suggest that intrahemispheric connectivity develops before interhemispheric connectivity (Fransson et al., 2007; Liu et al., 2008), and that anterior–posterior connectivity is slowest to develop (Kelly et al., 2009). Sensorimotor networks emerge early in infancy and appear to develop well before visual networks (Lin et al., 2008). Whether this applies to other sensory systems remains to be investigated. Such investigations may provide important insights and have implications for cognitive development, specifically with respect to an infant's early exploration of the world.

Beyond infancy, there is converging evidence from multiple studies suggesting that by age 7–9 children manifest a similar "small world" type of functional architecture at the whole-brain level as adults (Fair et al., 2009; Supekar et al., 2009). However, the organization of individual functional sub-networks as well as their interactions have a protracted developmental time course. This process is characterized by a number of developmental features. First, children have stronger and more abundant connections between subcortical and cortical regions, while in young-adults, connections among cortical regions were more prominent. Second, the brains of young-adults are more hierarchically organized, with more regions involved in larger and longer-distance clusters of activity. Third, the development of large-scale brain networks is characterized by weakening of short-range functional connectivity and strengthening of long-range functional connectivity. Taken together, these findings suggest that the dynamic process of over-connectivity followed by pruning, which rewires connectivity at the neuronal level, also operates at the systems level and helps reconfigure and rebalance cortical and subcortical connectivity in the developing brain (Supekar et al., 2009).

Several methodological issues remain to be addressed before the field can move forward. These are thoroughly discussed and reviewed in another contribution to this Special Issue (Cole et al., 2010). It is our belief that the two main methodological approaches discussed here (ICA and seed-ROI based correlation) each make important contributions to the study of intrinsic brain architecture, and can be used in a complementary fashion to understand global and local functional properties of the developing brain.

At present, it is unknown how and to what extent changes in functional connectivity are related to structural brain maturation. Directions for future research include integrating rsfMRI with diffusion tensor imaging (DTI) to investigate how the maturity of specific fiber tracts relates to the maturation of cognitive function and skill acquisition. A recent study examined developmental changes in DMN connectivity using a multimodal imaging approach by combining rsfMRI, voxel-based morphometry and diffusion tensor imaging-based tractography. The authors found that the DMN undergoes significant developmental changes in functional and structural connectivity, but these changes are not uniform across all DMN nodes. Critically, this study found that functional connectivity in children can reach adult-like levels despite weak structural connectivity (Supekar et al., 2010). Improved multimodal analysis of anatomy and connectivity will allow us to better characterize the heterogeneous development and maturation of functional brain networks.

It has recently been demonstrated that one possible function of resting-state functional connectivity is to support the consolidation of previous experience. Lewis et al. (2009) showed that visual perceptual learning, an example of adult neural plasticity, modified the resting covariance structure of spontaneous activity between networks engaged by the task, and that the observed changes correlated with the degree of perceptual learning. The complex relationships between cognitive performance and integrity of resting-state networks is only beginning to be explored, and future work in this area will have particular significance for developmental psychologists and neuroscientists.

Additional future directions include incorporating knowledge of genetics into rsfMRI studies, as well as continued investigations into relationships between functional connectivity and cognition and behavior. The field would particularly benefit from longitudinal studies that would allow tracking of development of connectivity within individuals. Mapping the developmental trajectory of functional brain organization will be greatly facilitated by a longitudinal approach. Lastly, elucidating brain organization related to neurodevelopmental disorders is perhaps the arena in which rsfMRI can make the greatest contributions. Very young and low-functioning children who might not otherwise be able to tolerate the scanner environment may be able to participate in a resting-state scan with a 5-min duration. Such data can be used to derive brain-based biomarkers that may in the future lead to early diagnosis and thus the development of more efficient and targeted treatments and therapies.

The use of rsfMRI for studying typical and atypical brain development is still in its infancy. Critically, its potential for synthesis and uncovering general organizational principles underlying functional brain development remain largely untapped. Current efforts to pool resources and data across multiple sites will in the future result in larger sample sizes, which are particularly critical for addressing clinical developmental questions. These data-sharing efforts have already produced interesting insights into brain organization in typically developing adults (Biswal et al., 2010). With rapid methodological improvements in rsfMRI, and the use of larger, more refined samples, we can expect to see rapid progress in the use of rsfMRI for addressing important research questions in developmental systems neuroscience.

ACKNOWLEDGMENTS

This work was supported by a Mosbacher Postdoctoral Fellowship and a National Institute of Mental Health Career Development Award (K01MH092288) to Lucina Q. Uddin, as well as grants from the National Institutes of Health (NS058899, HD047520, HD059205, HD057610) to Vinod Menon, and the National Science Foundation (BCS/DRL 0449927) to Vinod Menon. The content is solely the responsibility of the authors and does not necessarily represent the official views of the NIMH or the NIH.

REFERENCES

Beckmann, C. F., DeLuca, M., Devlin, J. T., and Smith, S. M. (2005). Investigations into resting-state connectivity using independent component analysis. *Philos. Trans. R. Soc. Lond., B, Biol. Sci.* 360, 1001–1013.

Birn, R. M., Smith, M. A., Jones, T. B., and Bandettini, P. A. (2008). The respiration response function: the temporal dynamics of fMRI signal fluctuations related to changes in respiration. *Neuroimage* 40, 644–654.

Biswal, B., Yetkin, F. Z., Haughton, V. M., and Hyde, J. S. (1995). Functional connectivity in the motor cortex of resting human brain using echo-planar MRI. *Magn. Reson. Med.* 34, 537–541.

Biswal, B. B., Mennes, M., Zuo, X. N., Gohel, S., Kelly, C., Smith, S. M., Beckmann, C. F., Adelstein, J. S., Buckner, R. L., Colcombe, S., Dogonowski, A. M., Ernst, M., Fair, D., Hampson, M., Hoptman, M. J., Hyde, J. S., Kiviniemi, V. J., Kötter, R., Li, S. J., Lin, C. P., Lowe, M. J., Mackay, C., Madden, D. J., Madsen, K. H., Margulies, D. S., Mayberg, H. S., McMahon, K., Monk, C. S., Mostofsky, S. H., Nagel, B. J., Pekar, J. J., Peltier, S. J., Petersen, S. E., Riedl, V., Rombouts, S. A., Rypmam B., Schlaggar, B. L., Schmidt, S., Seidler, R. D., Siegle, G. J., Sorg, C., Teng, G. J., Veijola, J., Villringer, A., Walter, M., Wang, L., Weng, X. C., Whitfield-Gabrieli, S., Williamson, P., Windischberger, C., Zang, Y. F., Zhang, H. Y., Castellanos, F. X., and Milham, M. P. (2010). Toward discovery science of human brain function. *Proc. Natl. Acad. Sci. U.S.A.* 107, 4734–4739.

Bondy, J. A., and Murty, U. S. R. (1976). *Graph Theory with Applications*. New York: American Elsevier Pub. Co.

Buckner, R. L., and Carroll, D. C. (2007). Self-projection and the brain. *Trends Cogn. Sci.* 11, 49–57.

Bullmore, E., and Sporns, O. (2009). Complex brain networks: graph theoretical analysis of structural and functional systems. *Nat. Rev. Neurosci.* 10, 186–198.

Calhoun, V. D., Kiehl, K. A., and Pearlson, G. D. (2008). Modulation of temporally coherent brain networks estimated using ICA at rest and during cognitive tasks. *Hum. Brain Mapp.* 29, 828–838.

Cao, Q., Zang, Y., Sun, L., Sui, M., Long, X., Zou, Q., and Wang, Y. (2006). Abnormal neural activity in children with attention deficit hyperactivity disorder: a resting-state functional magnetic resonance imaging study. *Neuroreport* 17, 1033–1036.

Cao, X., Cao, Q., Long, X., Sun, L., Sui, M., Zhu, C., Zuo, X., Zang, Y., and Wang, Y. (2009). Abnormal resting-state functional connectivity patterns of the putamen in medication-naïve children with attention deficit hyperactivity disorder. *Brain Res.* 1303, 195–206.

Casey, B. J., Galvan, A., and Hare, T. A. (2005). Changes in cerebral functional organization during cognitive development. *Curr. Opin. Neurobiol.* 15, 239–244.

Castellanos, F. X., Margulies, D. S., Kelly, C., Uddin, L. Q., Ghaffari, M., Kirsch, A., Shaw, D., Shehzad, Z., Di Martino, A., Biswal, B., Sonuga-Barke, E. J. S., Rotrosen, J., Adler, L. A., and Milham, M. P. (2008). Cingulate-precuneus interactions: a new locus of dysfunction in adult attention-deficit/hyperactivity disorder. *Biol. Psychiatry* 63, 332–337.

Castellanos, F. X., Sonuga-Barke, E. J., Scheres, A., Di Martino, A., Hyde, C., and Walters, J. R. (2005). Varieties of attention-deficit/hyperactivity disorder-related intra-individual variability. *Biol. Psychiatry* 57, 1416–1423.

Chang, C., Cunningham, J. P., and Glover, G. H. (2009). Influence of heart rate on the BOLD signal: the cardiac response function. *Neuroimage* 44, 857–869.

Chang, C., and Glover, G. H. (2009). Effects of model-based physiological noise correction on default mode network anti-correlations and correlations. *Neuroimage* 47, 1448–1459.

Cherkassky, V. L., Kana, R. K., Keller, T. A., and Just, M. A. (2006). Functional connectivity in a baseline resting-state network in autism. *Neuroreport* 17, 1687–1690.

Chugani, H. T., Phelps, M. E., and Mazziotta, J. C. (1987). Positron emission tomography study of human brain functional development. *Ann. Neurol.* 22, 487–497.

Church, J. A., Fair, D. A., Dosenbach, N. U., Cohen, A. L., Miezin, F. M., Petersen, S. E., and Schlaggar, B. L. (2009). Control networks in paediatric Tourette syndrome show immature and anomalous patterns of functional connectivity. *Brain* 132(Pt. 1), 225–238.

Cole, D. M., Smith, S. M., and Beckmann, C. F. (2010). Advances and pitfalls in the analysis and interpretation of resting-state FMRI data. *Front. Syst. Neurosci.* 4:8. doi:10.3389/fnsys.2010.00008.

Cordes, D., Haughton, V. M., Arfanakis, K., Carew, J. D., Turski, P. A., Moritz, C. H., Quigley, M. A., and Meyerand, M. E. (2001). Frequencies contributing to functional connectivity in the cerebral cortex in "resting-state" data. *AJNR Am. J. Neuroradiol.* 22, 1326–1333.

Cordes, D., Haughton, V. M., Arfanakis, K., Wendt, G. J., Turski, P. A., Moritz, C. H., Quigley, M. A., and Meyerand, M. E. (2000). Mapping functionally related regions of brain with functional connectivity MR imaging. *AJNR Am. J. Neuroradiol.* 21, 1636–1644.

Cullen, K. R., Gee, D. G., Klimes-Dougan, B., Gabbay, V., Hulvershorn, L., Mueller, B. A., Camchong, J., Bell, C. J., Houri, A., Kumra, S., Lim, K. O., Castellanos, F. X., and Milham, M. P. (2009). A preliminary study of functional connectivity in comorbid adolescent depression. *Neurosci. Lett.* 460, 227–231.

Damoiseaux, J. S., Rombouts, S. A., Barkhof, F., Scheltens, P., Stam, C. J., Smith, S. M., and Beckmann, C. F. (2006). Consistent resting-state networks across healthy subjects. *Proc. Natl. Acad. Sci. U.S.A.* 103, 13848–13853.

De Luca, M., Beckmann, C. F., De Stefano, N., Matthews, P. M., and Smith, S. M. (2006). fMRI resting state networks define distinct modes of long-distance interactions in the human brain. *Neuroimage* 29, 1359–1367.

Desjardins, A. E., Kiehl, K. A., and Liddle, P. F. (2001). Removal of confounding effects of global signal in functional MRI analyses. *Neuroimage* 13, 751–758.

Desmond, J. E., and Glover, G. H. (2002). Estimating sample size in functional MRI (fMRI) neuroimaging studies: statistical power analyses. *J. Neurosci. Methods* 118, 115–128.

Di Martino, A., Shehzad, Z., Kelly, C., Roy, A. K., Gee, D. G., Uddin, L. Q., Gotimer, K., Klein, D. F., Castellanos, F. X., and Milham, M. P. (2009). Relationship between cingulo-insular functional connectivity and autistic traits in neurotypical adults. *Am. J. Psychiatry* 166, 891–899.

Durston, S., Davidson, M. C., Tottenham, N., Galvan, A., Spicer, J., Fossella, J. A., and Casey, B. J. (2006). A shift from diffuse to focal cortical activity with development. *Dev. Sci.* 9, 1–8.

Fair, D. A., Cohen, A. L., Dosenbach, N. U., Church, J. A., Miezin, F. M., Barch, D. M., Raichle, M. E., Petersen, S. E., and Schlaggar, B. L. (2008). The maturing architecture of the brain's default network. *Proc. Natl. Acad. Sci. U.S.A.* 105, 4028–4032.

Fair, D. A., Cohen, A. L., Power, J. D., Dosenbach, N. U., Church, J. A., Miezin, F. M., Schlaggar, B. L., and Petersen, S. E. (2009). Functional brain networks develop from a "local to distributed" organization. *PLoS Comput. Biol.* 5(5), e1000381. doi:10.1371/journal.pcbi.1000381.

Fair, D. A., Dosenbach, N. U., Church, J. A., Cohen, A. L., Brahmbhatt, S., Miezin, F. M., Barch, D. M., Raichle, M. E., Petersen, S. E., and Schlaggar, B. L. (2007a). Development of distinct control networks through segregation and integration. *Proc. Natl. Acad. Sci. U.S.A.* 104, 13507–13512.

Fair, D. A., Schlaggar, B. L., Cohen, A. L., Miezin, F. M., Dosenbach, N. U., Wenger, K. K., Fox, M. D., Snyder, A. Z., Raichle, M. E., and Petersen, S. E. (2007b). A method for using blocked and event-related fMRI data to study "resting state" functional connectivity. *Neuroimage* 35, 396–405.

Fox, M. D., and Raichle, M. E. (2007). Spontaneous fluctuations in brain activity observed with functional magnetic resonance imaging. *Nat. Rev. Neurosci.* 8, 700–711.

Fox, M. D., Zhang, D., Snyder, A. Z., and Raichle, M. E. (2009). The global signal and observed anticorrelated resting state brain networks. *J. Neurophysiol.* 101, 3270–3283.

Fransson, P., Skiold, B., Horsch, S., Nordell, A., Blennow, M., Lagercrantz, H., and Aden, U. (2007). Resting-state networks in the infant brain. *Proc. Natl. Acad. Sci. U.S.A.* 104, 15531–15536.

Frith, C. (2004). Is autism a disconnection disorder? *Lancet Neurol.* 3, 577.

Gao, W., Zhu, H., Giovanello, K. S., Smith, J. K., Shen, D., Gilmore, J. H., and Lin, W. (2009). Evidence on the emergence of the brain's default network from 2-week-old to 2-year-old healthy pediatric subjects. *Proc. Natl. Acad. Sci. U.S.A.* 106, 6790–6795.

Giedd, J. N., Blumenthal, J., Molloy, E., and Castellanos, F. X. (2001). Brain imaging of attention deficit/hyperactivity disorder. *Ann. N. Y. Acad. Sci.* 931, 33–49.

Gogtay, N., Giedd, J. N., Lusk, L., Hayashi, K. M., Greenstein, D., Vaituzis, A. C., Nugent III, T. F., Herman, D. H., Clasen, L. S., Toga, A. W., Rapoport, J. L., and Thompson, P. M. (2004). Dynamic mapping of human cortical development during childhood through early adulthood. *Proc. Natl. Acad. Sci. U. S. A.* 101, 8174–8179.

Greicius, M. D., and Menon, V. (2004). Default-mode activity during a passive sensory task: uncoupled from deactivation but impacting activation. *J. Cogn. Neurosci.* 16, 1484–1492.

Hagmann, P., Cammoun, L., Gigandet, X., Meuli, R., Honey, C. J., Wedeen, V. J., and Sporns, O. (2008). Mapping the structural core of human cerebral cortex. *PLoS Biol.* 6, e159. doi:10.1371/journal.pbio.0060159.

Harrison, B. J., Pujol, J., Lopez-Sola, M., Hernandez-Ribas, R., Deus, J., Ortiz, H., Soriano-Mas, C., Yucel, M., Pantelis, C., and Cardoner, N. (2008). Consistency and functional specialization in the default mode brain network. *Proc. Natl. Acad. Sci. U.S.A.* 105, 9781–9786.

He, B. J., Snyder, A. Z., Vincent, J. L., Epstein, A., Shulman, G. L., and Corbetta, M. (2007). Breakdown of functional connectivity in frontoparietal networks underlies behavioral deficits in spatial neglect. *Neuron* 53, 905–918.

Honey, C. J., Sporns, O., Cammoun, L., Gigandet, X., Thiran, J. P., Meuli, R., and Hagmann, P. (2009). Predicting human resting-state functional connectivity from structural connectivity. *Proc. Natl. Acad. Sci. U.S.A.* 106, 2035–2040.

Kelly, A. M., Di Martino, A., Uddin, L. Q., Shehzad, Z., Gee, D. G., Reiss, P. T., Margulies, D. S., Castellanos, F. X., and Milham, M. P. (2009). Development of anterior cingulate functional connectivity from late childhood to early adulthood. *Cereb. Cortex* 19, 640–657.

Kennedy, D. P., and Courchesne, E. (2008). The intrinsic functional organization of the brain is altered in autism. *Neuroimage* 39, 1877–1885.

Kiviniemi, V., Jauhiainen, J., Tervonen, O., Paakko, E., Oikarinen, J., Vainionpaa, V., Rantala, H., and Biswal, B. (2000). Slow vasomotor fluctuation in fMRI of anesthetized child brain. *Magn. Reson. Med.* 44, 373–378.

Kwon, H., Reiss, A. L., and Menon, V. (2002). Neural basis of protracted developmental changes in visuo-spatial working memory. *Proc. Natl. Acad. Sci. U.S.A.* 99, 13336–13341.

Lenroot, R. K., and Giedd, J. N. (2006). Brain development in children and adolescents: insights from anatomical magnetic resonance imaging. *Neurosci. Biobehav. Rev.* 30, 718–729.

Lewis, C. M., Baldassarre, A., Committeri, G., Romani, G. L., and Corbetta, M. (2009). Learning sculpts the spontaneous activity of the resting human brain. *Proc. Natl. Acad. Sci. U.S.A.* 106, 17558–17563.

Lin, W., Zhu, Q., Gao, W., Chen, Y., Toh, C. H., Styner, M., Gerig, G., Smith, J. K., Biswal, B., and Gilmore, J. H. (2008). Functional connectivity MR imaging reveals cortical functional connectivity in the developing brain. *AJNR Am. J. Neuroradiol.* 29, 1883–1889.

Liu, W. C., Flax, J. F., Guise, K. G., Sukul, V., and Benasich, A. A. (2008). Functional connectivity of the sensorimotor area in naturally sleeping infants. *Brain Res.* 1223, 42–49.

Lowe, M. J., Mock, B. J., and Sorenson, J. A. (1998). Functional connectivity in single and multislice echoplanar imaging using resting-state fluctuations. *Neuroimage* 7, 119–132.

Luna, B., Thulborn, K. R., Munoz, D. P., Merriam, E. P., Garver, K. E., Minshew, N. J., Keshavan, M. S., Genovese, C. R., Eddy, W. F., and Sweeney, J. A. (2001). Maturation of widely distributed brain function subserves cognitive development. *Neuroimage* 13, 786–793.

Margulies, D. S., Kelly, A. M., Uddin, L. Q., Biswal, B. B., Castellanos, F. X., and Milham, M. P. (2007). Mapping the functional connectivity of anterior cingulate cortex. *Neuroimage* 37, 579–588.

Margulies, D. S., Vincent, J. L., Kelly, C., Lohmann, G., Uddin, L. Q., Biswal, B. B., Villringer, A., Castellanos, F. X., Milham, M. P., and Petrides, M. (2009). Precuneus shares intrinsic functional architecture in humans and monkeys. *Proc. Natl. Acad. Sci. U.S.A.* 106, 20069–20074.

Mazaika, P., Hoeft, F., Glover, G. H., and Reiss, A. L. (2009). Methods and software for fMRI analysis for clinical subjects. Paper presented at the Annual Meeting of the Organization for Human Brain Mapping.

Mazaika, P., Whitfield-Gabrieli, S., and Reiss, A. L. (2007). Artifact repair for fMRI data from high motion clinical subjects. Paper presented at the Annual Meeting of the Organization for Human Brain Mapping.

Meindl, T., Teipel, S., Elmouden, R., Mueller, S., Koch, W., Dietrich, O., Coates, U., Reiser, M., and Glaser, C. (2009). Test–retest reproducibility of the default-mode network in healthy individuals. *Hum. Brain Mapp.* 31, 237–46.

Monk, C. S., Peltier, S. J., Wiggins, J. L., Weng, S. J., Carrasco, M., Risi, S., and Lord, C. (2009). Abnormalities of intrinsic functional connectivity in autism spectrum disorders. *Neuroimage* 47, 764–772.

Murphy, K., Birn, R. M., Handwerker, D. A., Jones, T. B., and Bandettini, P. A. (2009). The impact of global signal

regression on resting state correlations: are anti-correlated networks introduced? *Neuroimage* 44, 893–905.

Paakki, J. J., Rahko, J., Long, X. Y., Moilanen, I., Tervonen, O., Nikkinen, J., Starck, T., Remes, J., Tuula, H., Haapsamo, H., Jussila, K., Kuusikko-Gauffin, S., Mattila, M., Zang, Y., and Kiviniemi, V. (2010). Alterations in regional homogeneity of resting-state brain activity in autism spectrum disorders. *Brain Res.* 1321, 169–179.

Raichle, M. E. (2010). Two views of brain function. *Trends Cogn. Sci.* 14, 180–190.

Raichle, M. E., MacLeod, A. M., Snyder, A. Z., Powers, W. J., Gusnard, D. A., and Shulman, G. L. (2001). A default mode of brain function. *Proc. Natl. Acad. Sci. U.S.A.* 98, 676–682.

Redcay, E., Kennedy, D. P., and Courchesne, E. (2007). fMRI during natural sleep as a method to study brain function during early childhood. *Neuroimage* 38, 696–707.

Rivera, S. M., Reiss, A. L., Eckert, M. A., and Menon, V. (2005). Developmental changes in mental arithmetic: evidence for increased functional specialization in the left inferior parietal cortex. *Cereb. Cortex* 15, 1779–1790.

Shehzad, Z., Kelly, A. M., Reiss, P. T., Gee, D. G., Gotimer, K., Uddin, L. Q., Lee, S., Margulies, D. S., Roy, A. K., Biswal, B. B., Petkova, E., Castellanos, F. X., and Milham, M. P. (2009). The resting brain: unconstrained yet reliable. *Cereb. Cortex* 19, 2209–2229.

Shulman, G. L., Fiez, J. A., Corbetta, M., Buckner, R. L., Miezen, F. M., Raichle, M. E., and Petersen, S. E. (1997). Common blood flow changes across visual tasks: II. Decreases in cerebral cortex. *J. Cogn. Neurosci.* 9, 648–663.

Smith, S. M., Fox, P. T., Miller, K. L., Glahn, D. C., Fox, P. M., Mackay, C. E., Filippini, N., Watkins, K. E., Toro, R., Laird, A. R., and Beckmann, C. F. (2009). Correspondence of the brain's functional architecture during activation and rest. *Proc. Natl. Acad. Sci. U.S.A.* 106, 13040–13045.

Sonuga-Barke, E. J., and Castellanos, F. X. (2007). Spontaneous attentional fluctuations in impaired states and pathological conditions: a neurobiological hypothesis. *Neurosci. Biobehav. Rev.* 31, 977–986.

Sowell, E. R., Thompson, P. M., Leonard, C. M., Welcome, S. E., Kan, E., and Toga, A. W. (2004). Longitudinal mapping of cortical thickness and brain growth in normal children. *J. Neurosci.* 24, 8223–8231.

Spreng, R. N., Mar, R. A., and Kim, A. S. (2009). The common neural basis of autobiographical memory, prospection, navigation, theory of mind, and the default mode: a quantitative meta-analysis. *J. Cogn. Neurosci.* 21, 489–510.

Stevens, M. C. (2009). The developmental cognitive neuroscience of functional connectivity. *Brain Cogn.* 70, 1–12.

Stevens, M. C., Pearlson, G. D., and Calhoun, V. D. (2009). Changes in the interaction of resting-state neural networks from adolescence to adulthood. *Hum. Brain Mapp.* 30, 2356–2366.

Supekar, K., Musen, M., and Menon, V. (2009). Development of large-scale functional brain networks in children. *PLoS Biol.* 7, e1000157. doi:10.1371/journal.pbio.1000157.

Supekar, K., Uddin, L. Q., Prater, K., Amin, H., Greicius, M. D., and Menon, V. (2010). Development of functional and structural connectivity within the default mode network in young children. *Neuroimage* (in press).

Tamm, L., Menon, V., and Reiss, A. L. (2002). Maturation of brain function associated with response inhibition. *J. Am. Acad. Child Adolesc. Psychiatry* 41, 1231–1238.

Thomas, K. M., Hunt, R. H., Vizueta, N., Sommer, T., Durston, S., Yang, Y., and Worden, M. S. (2004). Evidence of developmental differences in implicit sequence learning: an fMRI study of children and adults. *J. Cogn. Neurosci.* 16, 1339–1351.

Thomason, M. E., Chang, C. E., Glover, G. H., Gabrieli, J. D., Grecius, M. D., and Gotlib, I. H. (2008). Default-mode function and task-induced deactivation have overlapping brain substrates in children. *Neuroimage* 41, 1493–1503.

Thomason, M. E., Yoo, D. J., Glover, G. H., and Gotlib, I. H. (2009). BDNF genotype modulates resting functional connectivity in children. *Front. Hum. Neurosci.* 3:55. doi: 10.3389/neuro.09.055.2009.

Tian, L., Jiang, T., Liang, M., Zang, Y., He, Y., Sui, M., and Wang, Y. (2008). Enhanced resting-state brain activities in ADHD patients: a fMRI study. *Brain Dev.* 30, 342–348.

Tian, L., Jiang, T., Wang, Y., Zang, Y., He, Y., Liang, M., Sui, M., Cao, Q., Hu, S., Peng, M., and Zhou, Y. (2006). Altered resting-state functional connectivity patterns of anterior cingulate cortex in adolescents with attention deficit hyperactivity disorder. *Neurosci. Lett.* 400, 39–43.

Uddin, L. Q., Iacoboni, M., Lange, C., and Keenan, J. P. (2007). The self and social cognition: the role of cortical midline structures and mirror neurons. *Trends Cogn. Sci.* 11, 153–157.

Uddin, L. Q., Kelly, A. M. C., Biswal, B. B., Margulies, D. S., Shehzad, Z., Shaw, D., Ghaffari, M., Rotrosen, J., Adler, L. A., Castellanos, F. X., and Milham, M. P. (2008). Network homogeneity reveals decreased integrity of default-mode network in ADHD. *J. Neurosci. Methods* 169, 249–254.

Uddin, L. Q., and Menon, V. (2009). The anterior insula in autism: under-connected and under-examined. *Neurosci. Biobehav. Rev.* 33, 1198–1203.

van den Heuvel, M. P., Mandl, R. C., Kahn, R. S., and Hulshoff Pol, H. E. (2009). Functionally linked resting-state networks reflect the underlying structural connectivity architecture of the human brain. *Hum. Brain Mapp.* 30, 3127–3141.

van de Ven, V. G., Formisano, E., Prvulovic, D., Roeder, C. H., and Linden, D. E. (2004). Functional connectivity as revealed by spatial independent component analysis of fMRI measurements during rest. *Hum. Brain Mapp.* 22, 165–178.

Van Dijk, K. R., Hedden, T., Venkataraman, A., Evans, K. C., Lazar, S. W., and Buckner, R. L. (2009). Intrinsic functional connectivity as a tool for human connectomics: theory, properties, and optimization. *J. Neurophysiol.* 103, 297–321.

Weissenbacher, A., Kasess, C., Gerstl, F., Lanzenberger, R., Moser, E., and Windischberber, C. (2009). Correlations and anticorrelations in resting-state functional connectivity MRI: a quantitative comparison of preprocessing strategies. *Neuroimage* 47, 1408–1416.

Weng, S. J., Wiggins, J. L., Peltier, S. J., Carrasco, M., Risi, S., Lord, C., and Monk, C. S. (2010). Alterations of resting state functional connectivity in the default network in adolescents with autism spectrum disorders. *Brain Res.* 1313, 202–214.

Yerys, B. E., Jankowski, K. F., Shook, D., Rosenberger, L. R., Barnes, K. A., Berl, M. M., Ritzl, E. K., VanMeter, J., Vaidya, C. J., and Gaillard, W. D. (2009). The fMRI success rate of children and adolescents: typical development, epilepsy, attention deficit/hyperactivity disorder, and autism spectrum disorders. *Hum. Brain Mapp.* 30, 3426–3435.

Zang, Y. F., Yong, H., Chao-Zhe, Z., Qing-Jiu, C., Man-Qiu, S., Meng, L., Li-Xia, T., Tian-Zi, J., and Yu-Feng, W. (2007). Altered baseline brain activity in children with ADHD revealed by resting-state functional MRI. *Brain Dev.* 29, 83–91.

Zhu, C. Z., Zang, Y. F., Cao, Q. J., Yan, C. G., He, Y., Jiang, T. Z., Sui, M., and Wang, Y. (2008). Fisher discriminative analysis of resting-state brain function for attention-deficit/hyperactivity disorder. *Neuroimage* 40, 110–120.

Zuo, X. N., Di Martino, A., Kelly, C., Shehzad, Z. E., Gee, D. G., Klein, D. F., Castellanos, F. X., Biswal, B. B., and Milham, M. P. (2010a). The oscillating brain: complex and reliable. *Neuroimage* 49, 1432–1445.

Zuo, X. N., Kelly, C., Adelstein, J. S., Klein, D. F., Castellanos, F. X., and Milham, M. P. (2010b). Reliable intrinsic connectivity networks: test–retest evaluation using ICA and dual regression approach. *Neuroimage* 49, 2163–2177.

Conflict of Interest Statement: The authors declare that the research was conducted in the absence of any commercial or financial relationships that could be construed as a potential conflict of interest.

Received: 10 February 2010; paper pending published: 10 March 2010; accepted: 16 April 2010; published online: 21 May 2010.

*Citation: Uddin LQ, Supekar K and Menon V (2010) Typical and atypical development of functional human brain networks: insights from resting-state fMRI. Front. Syst. Neurosci. **4**:21. doi: 10.3389/fnsys.2010.00021*

frontiers in
SYSTEMS NEUROSCIENCE

REVIEW ARTICLE
published: 07 June 2010
doi: 10.3389/fnsys.2010.00016

Graph-based network analysis of resting-state functional MRI

*Jinhui Wang[1], Xinian Zuo[2] and Yong He[1]**

[1] State Key Laboratory of Cognitive Neuroscience and Learning, Beijing Normal University, Beijing, China
[2] Phyllis Green and Randolph Cōwen Institute for Pediatric Neuroscience, New York University Langone Medical Center, New York, NY, USA

Edited by:
Lucina Q. Uddin,
Stanford University, USA

Reviewed by:
Sophie Achard,
University of Cambridge, UK
Edward T. Bullmore,
University of Cambridge, UK
Alex Fornito,
University of Melbourne, Australia

****Correspondence:***
Yong He, State Key Laboratory of Cognitive Neuroscience and Learning, Beijing Normal University, Beijing, China.
e-mail: yong.he@bnu.edu.cn

In the past decade, resting-state functional MRI (R-fMRI) measures of brain activity have attracted considerable attention. Based on changes in the blood oxygen level-dependent signal, R-fMRI offers a novel way to assess the brain's spontaneous or intrinsic (i.e., task-free) activity with both high spatial and temporal resolutions. The properties of both the intra- and inter-regional connectivity of resting-state brain activity have been well documented, promoting our understanding of the brain as a complex network. Specifically, the topological organization of brain networks has been recently studied with graph theory. In this review, we will summarize the recent advances in graph-based brain network analyses of R-fMRI signals, both in typical and atypical populations. Application of these approaches to R-fMRI data has demonstrated non-trivial topological properties of functional networks in the human brain. Among these is the knowledge that the brain's intrinsic activity is organized as a small-world, highly efficient network, with significant modularity and highly connected hub regions. These network properties have also been found to change throughout normal development, aging, and in various pathological conditions. The literature reviewed here suggests that graph-based network analyses are capable of uncovering system-level changes associated with different processes in the resting brain, which could provide novel insights into the understanding of the underlying physiological mechanisms of brain function. We also highlight several potential research topics in the future.

Keywords: resting-state, functional connectivity, human connectome, small-world, functional MRI, graph theory, brain, network

INTRODUCTION

As a novel, non-invasive way to measure spontaneous neural activity in the human brain, resting-state functional magnetic resonance imaging (R-fMRI) has attracted considerable attention (Biswal et al., 1995; Fox and Raichle, 2007). R-fMRI measures the endogenous or spontaneous brain activity as low-frequency fluctuations in blood oxygen level-dependent (BOLD) signals. This low-frequency fluctuation phenomenon is vital for a better understanding of human brain function because extremely disproportionate energy consumption appears within the regions showing high resting metabolisms (Raichle et al., 2001; Raichle, 2006). Beginning with a seminal demonstration of highly coherent low-frequency fluctuations within the brain motor system (Biswal et al., 1995), R-fMRI has been extensively used to investigate normal brain function (Greicius et al., 2003; Beckmann et al., 2005; Fox et al., 2005; Margulies et al., 2007; Di Martino et al., 2008; Roy et al., 2009; Smith et al., 2009; Yan et al., 2009b), trait variability and behavioral characteristics (Hampson et al., 2006; Fox et al., 2007; Hesselmann et al., 2008; Kelly et al., 2008; Di Martino et al., 2009; Yan et al., 2009a), as well as various clinical populations (for reviews, see Greicius, 2008; Broyd et al., 2009; Zhang and Raichle, 2010). To date, many R-fMRI methods have been developed to explore the nature of resting-state brain.

Currently, there are two main types of R-fMRI methods used to characterize spontaneous brain activity. One measures specific regional characteristics of R-fMRI signals within a brain region (e.g., voxels or parcellation units), such as regional homogeneity (Zang et al., 2004), network homogeneity (Uddin et al., 2008), amplitude of low-frequency fluctuations (ALFF) (Zang et al., 2007), fractional ALFF (Zou et al., 2008) and fractal complexity (Wink et al., 2006). In contrast, the other measures the relationship between different brain units (i.e., highly coherent spontaneous fluctuations or functional connectivity), such as seed-based functional connectivity analysis (Biswal et al., 1995), clustering (Cordes et al., 2002) and independent component analysis (ICA) (van de Ven et al., 2004). Connectivity-based methods have been widely used to detect functionally connected brain networks, including motor (Biswal et al., 1995), auditory (Cordes et al., 2001), visual (Lowe et al., 1998), language (Hampson et al., 2002), default-mode (Greicius et al., 2003), and attention systems (Fox et al., 2006). These brain networks have demonstrated high consistency and reproducibility across subjects and sessions (Damoiseaux et al., 2006; Chen et al., 2008a; Meindl et al., 2009; Zuo et al., 2010a), high test–retest reliability (Shehzad et al., 2009; Zuo et al., 2010a), high reproducibility across different analytic approaches (Long et al., 2008; Franco et al., 2009) and a striking correspondence to task activation maps (Smith et al., 2009). More recently, using novel graph theory-based approaches, these identified biologically plausible brain networks were found to topologically organize in a non-trivial manner (e.g., small-world architecture and modular structure) that support efficient information processing of the brain.

Graph theory-based approaches model the brain as a complex network represented graphically by a collection of nodes and edges. In the virtual graph, nodes indicate anatomical elements

(e.g., brain regions), and edges represent the relationships between nodes (e.g., connectivity). After the network modeling procedure, various graph theoretical metrics can be used to investigate the organizational mechanism underlying the relevant networks. In contrast to those widely used R-fMRI analytic methods (e.g., ALFF, seed-based functional connectivity and ICA), the graph-based network analyses allow us not only to visualize the overall connectivity pattern among all the elements of the brain (e.g., brain regions) but also to quantitatively characterize the global organization. In addition, this approach also gives insight into the topological reconfiguration of the brain in response to external task modulation (Eguiluz et al., 2005; Pachou et al., 2008; Bassett et al., 2009; Micheloyannis et al., 2009; Wang et al., 2010) or pathological attacks (for reviews, see Bassett and Bullmore, 2009 and He et al., 2009a). Moreover, it provides a vital framework to elucidate the relationship between brain structure and function (Honey et al., 2010). Both structural and functional brain networks have been demonstrated to organize intrinsically as highly modular small-world architectures capable of efficiently transferring information at a low wiring cost as well as formatting highly connected hub regions (Salvador et al., 2005; Achard et al., 2007; He et al., 2007, 2009b; Chen et al., 2008b; Hagmann et al., 2008; Gong et al., 2009a). Furthermore, the utility of graph-based techniques has been proven by an increasing number of studies to probe potential mechanisms involved in normal development (Fair et al., 2007, 2008, 2009; Supekar et al., 2009), aging (Achard and Bullmore, 2007; Gong et al., 2009b; Meunier et al., 2009a; Micheloyannis et al., 2009; Wang et al., 2010), and various brain disorders (Stam et al., 2007; He et al., 2008, 2009c; Liu et al., 2008; Supekar et al., 2009; Wang et al., 2009b; Buckner et al., 2009). Given the lack of relevant reviews that focus exclusively on graph-based brain network research using R-fMRI, the purpose of the present review is to increase multi-discipline appreciation and cooperation on this burgeoning field. In addition, this work provides the opportunity to revolutionize our view of brain organization and function by re-examining the progress made in this field.

In this review, we will summarize the recent progress made in the study of functional brain networks constructed by intrinsic brain activity measured by R-fMRI. The paper is organized to three main sections. First, some basic concepts regarding brain connectivity and graph theoretical approaches are introduced, along with a review of recent graph-based work on revealing the normal topological architecture and underlying organization of functional brain networks. Then, we survey various R-fMRI applications of graph-based approaches to uncover changes in the network properties of brain development, aging and disorders. Finally, we highlight some technical challenges and future directions in this rapidly emerging research area.

BASIC CONCEPTIONS

BRAIN CONNECTIVITY NETWORKS

A network is a collection of nodes and edges, where nodes indicate basic elements within the system of interest and edges indicate the associations among those elements. An accurate method for defining the most essential elements of a network (i.e., nodes and edges) is vital for network construction. Specifically, for brain networks, they can be described at different spatial levels, such as microscale, mesoscale, and macroscale or large-scale (Sporns et al., 2005). Given technical limitations and computational demand, most current studies focus on the macroscale or large-scale brain networks. In this review, we will also concentrate on the macroscale brain networks.

In a macroscale brain network, nodes can be defined as EEG electrodes, MEG channels, or regions of interest (ROI) derived from anatomical atlases in MRI. After the definition of nodes, the edges among nodes can be defined by the functional or structural associations among different neuronal elements of the brain. To date, functional associations are measured by either the temporal correlation between spatially remote neurophysiological events, often referred to as the functional connectivity, or the influence that one neural system exerts over another, also termed effective connectivity (Friston et al., 1993). Structural associations can be measured by examining either direct diffusion-based anatomical connectivity or indirect morphology-based statistical interdependencies across populations (Bullmore and Sporns, 2009; He and Evans, 2010). Once these two basic elements of a network, nodes and edges, are extracted from the dataset, the constructed brain connectivity network can be further characterized using graph theoretical approaches. **Figure 1** illustrates the schematic representation of network constructions using R-fMRI.

GRAPH THEORETICAL APPROACHES

Graph theory is the natural framework for the exact mathematical representation of complex networks. Formally, a complex network can be represented as a graph by G(N, K), with N denoting the number of nodes and K the number of edges in graph G. Graphs can be classified as directed or undirected based on whether the edges have sense of direction information. Likewise, graphs can also be divided into unweighted (binary) graphs if every edge in the graph has an equal weight of 1 or weighted graphs if its edges are assigned with different strengths. In this review, we will only focus on undirected and unweighted graphs. The descriptions for other types of graphs can be found in previous literature (Boccaletti et al., 2006; Bang-Jensen and Gutin, 2008).

For an undirected and unweighted graph G(N, K), the connectivity pattern can be completely described by an N × N symmetric square matrix named adjacency matrix A whose entry a_{ij} ($i,j = 1,\ldots,N$) is 1 if there exists an edge between node i and j or 0 if one does not. Now we will list some important metrics that are frequently used in the field of neuroscience.

Degree and degree distribution

In a graph G(N, K), the degree of node i is the number of edges linked to it and is calculated as $k_i = \sum_{j \in G} a_{ij}$, where a_{ij} is the ith row and jth column element of adjacency matrix A. Degree is a simple measurement for the connectivity of a node with the rest of the nodes in a network. The mean of degrees over all the nodes in G, referred to as the average degree, measures the extent to which the graph is connected. The degree distribution $P(k)$ is defined as the probability that a node chosen uniformly at random has degree k or, equivalently, as the fraction of nodes in the graph having degree k. In terms of the form of degree distribution,

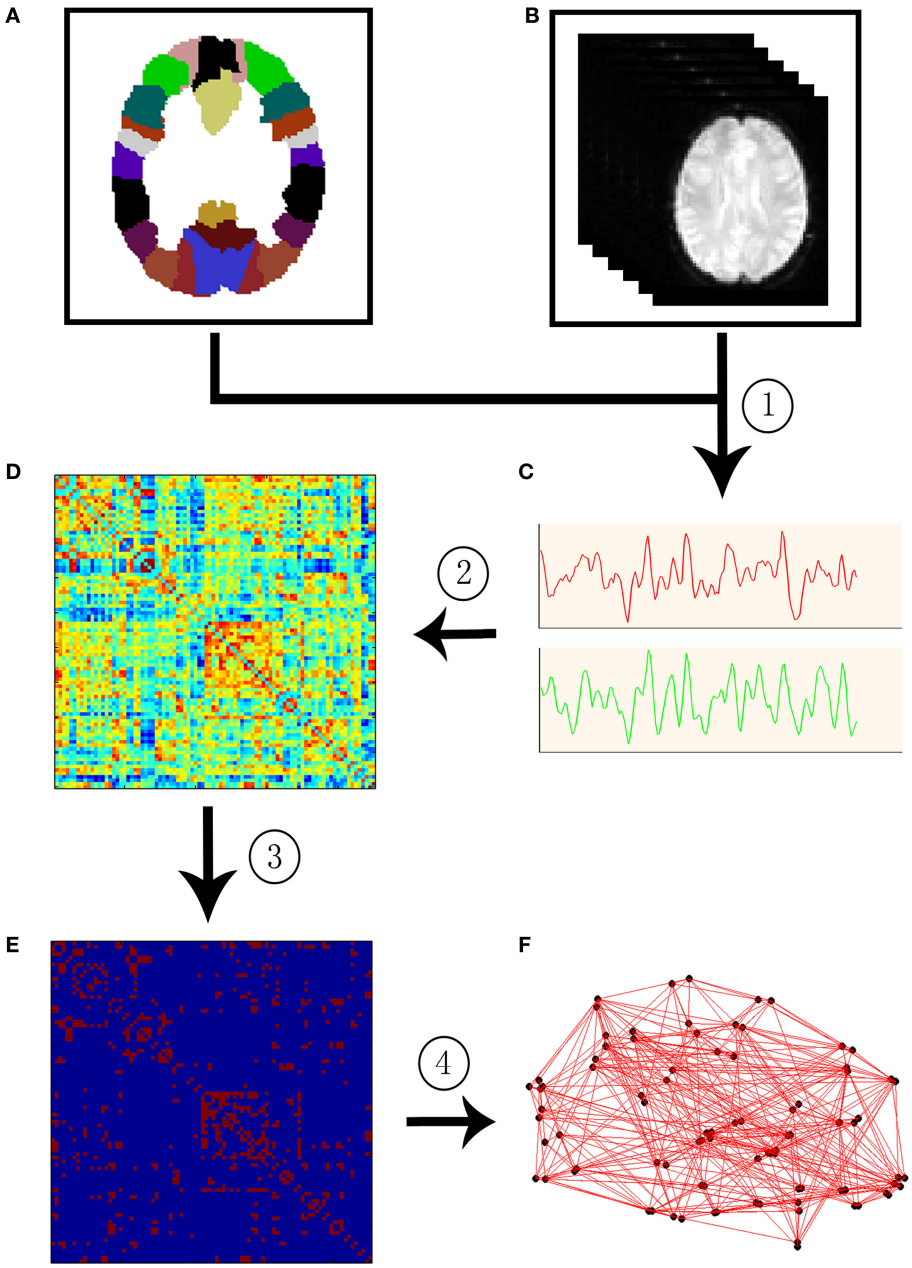

FIGURE 1 | A flowchart for the construction of functional brain network in the human brain by R-fMRI. (1) Extraction of the time course **(C)** from R-fMRI data **(B)** within each anatomical unit (i.e., network node). **(B)** Anatomical units are obtained according to a prior brain atlas **(A)** or voxels; (2) Calculation of a functional connectivity (i.e., network edge) correlation matrix **(D)** between any pairs of nodes; (3) Thresholding the correlation matrix into a binary connectivity matrix (i.e., association matrix, **E**); (4) Visualization of the association matrix as a graph **(F)**.

networks can be classified into different categories (e.g., power law or scale-free networks where nodal degrees are extremely heterogeneous) that possess distinct resilience to the removal of nodes. For example, networks of exponentially truncated power law degree were demonstrated to be equally resilient to random failures (random removal of nodes) but more resilient to targeted attacks (selective removal of nodes, such as those with the highest degrees) compared with the scale-free network in spontaneous human brain functional networks (Achard et al., 2006).

Small-world

The small-world (Watts and Strogatz, 1998) is an important model to characterize the organization principles that govern a remarkable variety of social, economic, and biological complex networks. A small-world network can be described by high local clustering, characterized by a high clustering coefficient, C_p, and low minimum path length between any pair of nodes, characterized by a low characteristic path length, L_p (Watts and Strogatz, 1998). The C_p of a network is defined as the average of the clustering coefficients

over all nodes in the network where the clustering coefficient C_i of a node i is calculated as $C(i) = 2E/k_i \times (k_i - 1)$, with E denoting the number of existing connections among the node i's neighbors and k_i representing the degree of node i. C_p quantifies the extent of local interconnectivity or cliquishness of a network. The L_p is defined as the average of the shortest path lengths (minimum number of edges needed to link one node to another) between any pair of nodes in the network. L_p measures the distance (i.e., number of edges) between any pair of nodes in a network or the extent of overall communication efficiency of a network. A shorter distance means higher routing efficiency because information is exchanged via fewer steps. Notably, this original definition of L_p is problematic in networks with multiple components where there exist nodal pairs that have no connecting path. The shortest path lengths for such disconnected node pairs are infinite. To avoid this problem, L_p can be measured by using a "harmonic mean" distance between any pairs of network nodes as proposed by Newman (2003), that is, the reciprocal of the average of the reciprocals. Notably, L_p calculated by "harmonic mean" distance is numerically the inverse of global efficiency (see below for the definition of global efficiency). Mathematically, a real network would be considered as small-world if it meets the following two conditions: $\gamma = C_p/C_{p-rand} > 1$ and $\lambda = L_p/L_{p-rand} \approx 1$, where C_{p-rand} and L_{p-rand} are the mean clustering coefficient and characteristic path length of the matched random networks (random networks have low C_p and short L_p), respectively. These two conditions can also be summarized into a simple quantitative measurement, small-worldness, $\sigma = \gamma/\lambda > 1$ (Humphries et al., 2005). Small-world is an attractive model for the description of complex brain networks because it not only supports both specialized/modularized and integrated/distributed information processing but also maximizes the efficiency of information transfer at a relatively low wiring cost (Sporns et al., 2004; Bassett and Bullmore, 2006). Using these measurements, small-world topology has been recently demonstrated in many complex brain networks across multiple species in both healthy and diseased states (for reviews, see Stam and Reijneveld, 2007; Bassett and Bullmore, 2009; Bullmore and Sporns, 2009; He et al., 2009a).

Network efficiency

Efficiency is a more biologically relevant metric to describe brain networks from the perspective of information flow, which can deal with the disconnected graphs, nonsparse graphs or both (Latora and Marchiori, 2001; Bassett and Bullmore, 2006). For a graph $G(N,K)$, the global efficiency is defined as $E_{glob}(G) = 1/N(N-1)\Sigma_{i \neq j \in G} \frac{1}{d_{ij}}$, where d_{ij} is the shortest path length between node i and node j in G. The local efficiency of G is measured as $E_{loc}(G) = \frac{1}{N}\Sigma_{i \in G} E_{glob}(G_i)$, where $E_{glob}(G_i)$ is the global efficiency of G_i, the sub-graph composed of the neighbors of node i. Global efficiency and local efficiency measure the ability of a network to transmit information at the global and local level, respectively (Latora and Marchiori, 2001, 2003). An important metric that concisely couples with network efficiency is network cost, which measures how expensive it is to build a network. For an unweighted and undirected network, network cost can be defined as the ratio of the existing number of edges to the number of all possible edges in the network. Using these measurements, networks with high efficiency, both local and global, and low cost are said to be economic small-world networks (Achard et al., 2007; Wang et al., 2009b).

Nodal centrality

Nodal centrality quantifies how important a node is within a network. Several different metrics exist for measuring nodal centrality, such as degree centrality, nodal efficiency (Achard and Bullmore, 2007), closeness centrality (Freeman, 1979), and betweenness centrality (Freeman, 1977). For a node i in a network $G(N,K)$, the degree is defined as the number of edges linked directly to it. The nodal efficiency of node i is computed as $E_i = 1/N - 1\Sigma_{j \neq i \in G} \frac{1}{d_{ij}}$. Nodal efficiency measures the ability of a node to propagate information with the other nodes in a network. The closeness centrality of node i is computed as $C_i = \frac{N-1}{\Sigma_{j \neq i \in G} d_{ij}}$, and it reflects the average distance from a node to all the other nodes in a network. The betweenness centrality captures the influence that one node has over the flow of information between all other nodes in the network and can be calculated as $B_i = \Sigma_{m \neq i \neq n \in G} \frac{\sigma_{mn}(i)}{\sigma_{mn}}$, where σ_{mn} is the total number of shortest paths from node m to node n and $\sigma_{mn}(i)$ is the number of shortest paths from node m to node n that pass through node i. A node with high centrality is considered a hub in the network (Sporns et al., 2007; He et al., 2008; Buckner et al., 2009).

Modularity

Modularity reflects the degree to which a network is organized into a modular or community structure. Modules refer to a set of nodes with denser links among them but sparser links with the rest of the network (Newman, 2006). Detection and characterization of modular structure in the brain system can help us to identify groups of anatomically and/or functionally associated components that perform specific biological functions. Several optimization algorithms are currently available, each with different advantages (Clauset et al., 2004). Based on the identified modular structure, hubs can be further subdivided in terms of their roles in maintaining intra- or inter-module connectivity. Provincial hubs are connected mainly to nodes in their own modules, whereas connector hubs are connected to nodes in other modules (Guimera et al., 2005; Chen et al., 2008; He et al., 2009b).

Hierarchy

Hierarchical structure is a fundamental characteristic of many social and biological networks (Ravasz et al., 2002; Ravasz and Barabasi, 2003; Sales-Pardo et al., 2007). In a hierarchical network, highly connected nodes (hubs) are connected predominantly to nodes that are not otherwise connected to each other. That is, the larger the degree, the lower the clustering coefficient. Such a hierarchical organization favors top-down relationships between nodes and minimizes wiring costs, but it is vulnerable to attacks on hubs (Ravasz and Barabasi, 2003; Sakata et al., 2005). Mathematically, this phenomenon can be quantified by the β value, an exponent of the power law relationship between clustering coefficient, C_i, and degree, k_i, of the nodes in the network: $C \approx k^{-\beta}$. A large positive value of β signifies a typical hierarchical structure. Such a hierarchy has been found to exist in both structural (Bassett et al., 2008) and functional (Supekar et al., 2009) human brain networks.

For more details regarding the construction of brain networks, frequently used graph-based metrics in brain networks, and the final interpretations of results, see (Bullmore and Sporns, 2009; He et al., 2009a; Rubinov and Sporns, 2009).

RESTING-STATE FUNCTIONAL BRAIN NETWORKS

Spontaneous neural activity can be recorded by multiple imaging techniques, such as EEG, MEG, and R-fMRI, each with different advantages. Several studies have successfully used EEG or MEG to construct intrinsic brain connectivity networks and further investigated state-dependent alterations in network topological properties (Stam and Reijneveld, 2007; Bassett and Bullmore, 2009). More recently, R-fMRI-based network analysis has gained popularity because of its high spatial and temporal resolution. This review will primarily focus on graph-based brain network studies using R-fMRI. **Table 1** presents the relevant literature reviewed here.

NORMAL POPULATION

Region-based resting-state brain networks

Salvador et al. (2005) were the first to utilize R-fMRI to investigate the whole brain functional network. Based on a prior Automated Anatomical Labeling (AAL) atlas, a 90-node group-level network generated from 12 healthy volunteers was constructed. Graph theoretical methods revealed that the brain functional network showed a small-world topology characterized by high local clustering and short path lengths linking different brain regions. Further hierarchical clustering and multidimensional scaling analyses demonstrated that the network included several major functional clusters corresponding to four neocortical lobes (frontal, temporal, parietal-(pre)motor, and occipital), the medial temporal lobe and subcortical nuclei. In a following study that also utilized the AAL atlas, Achard et al. (2006) investigated frequency-dependent spontaneous brain networks in five healthy volunteers. They found that the small-world topology was most salient in the low-frequency (0.03–0.06 Hz) brain network. Furthermore, several heteromodal association cortex regions were found to act as hubs in the brain network. The authors also found that the network obeys an exponentially truncated power law degree distribution, which appears to confer a distinctive tolerance against random failures and target attacks compared with scale-free or power law distribution. Recently, Wang et al. (2009a) investigated the topological organization of functional brain networks constructed from two different brain atlases [AAL atlas (90 parcellation units) and Automatic Nonlinear Imaging Matching and Anatomical Labeling (ANIMAL) atlas (70 parcellation units)]. They found that the spontaneous functional brain networks exhibited robust small-world topology and a common form of exponentially truncated power law degree distribution regardless of parcellation strategies. This suggests a stable intrinsic architecture in the resting human brain.

Table 1 | Graph-based brain functional network studies by R-fMRI.

Study	Clinical state	Node definition	*N*	Correlation metrics	Network type
Salvador et al. (2005)	Normal	Regions (AAL)	90	Partial correlation	B
Achard et al. (2006)	Normal	Regions (AAL)	90	Wavelet correlation	B, W
Wang et al. (2009a)	Normal	Regions (AAL, ANIMAL)	90, 70	Pearson correlation	B
He et al. (2009b)	Normal	Regions (AAL)	90	Pearson correlation	B
Meunier et al. (2009b)	Normal	Regions (AAL-based)	1808	Wavelet correlation	B
Ferrarini et al. (2009)	Normal	Regions (AAL)	90	Partial correlation	B
Dosenbach et al. (2007)	Normal	ROIs	39	Pearson correlation	B
Van den Heuvel et al. (2008a)	Normal	Voxels	~10000	Pearson correlation	B
Van den Heuvel et al. (2008b)	Normal	Voxels	8500~9500	Pearson correlation	W
Valencia et al. (2009)	Normal	Voxels	20898	Pearson correlation	B, W
Laurienti et al. (2009)	Normal	Voxels	~20000	Pearson correlation	B
Hayasaka and Laurienti (2009)	Normal	Regions (AAL), voxels	90~16000	Pearson correlation	B
van den Heuvel et al. (2009b)	Normal (IQ)	Voxels	~9500	Pearson correlation	B
Park et al. (2008)	Normal	Regions (AAL)	73	Pearson correlation	B
Fair et al. (2007)	Development	ROIs	39	Pearson correlation	B
Fair et al. (2008)	Development	ROIs	13	Pearson correlation	B
Fair et al. (2009)	Development	ROIs	34	Pearson correlation	B
Supekar et al. (2009)	Development	Regions (AAL)	90	Wavelet correlation	B
Achard et al. (2007)	Aging	Regions (AAL)	90	Wavelet correlation	B, W
Meunier et al. (2009a)	Aging	Regions (AAL)	90	Wavelet correlation	B
Supekar et al. (2008)	AD	Regions (AAL)	90	Wavelet correlation	B
Buckner et al. (2009)	AD	Voxels	None	Pearson correlation	B
Liu et al. (2008)	Schizophrenia	Regions (AAL)	90	Partial correlation	B
Wang et al. (2009b)	ADHD	Regions (AAL)	90	Pearson correlation	B
Liao et al. (2010)	Epilepsy	Regions (AAL)	90	Pearson correlation	B
Nakamura et al. (2009)	TBI	None	112	Partial correlation	B, W
Liu et al. (2009)	Drug (heroin)	Regions (AAL)	90	Partial correlation	B

AD, Alzheimer's disease; ADHD, attention-deficit hyperactivity disorder; TBI, traumatic brain injury; AAL, Automated Anatomical Labeling; ANIMAL, Automatic Nonlinear Imaging Matching and Anatomical Labeling; ROI, region of interest; N, the number of network nodes; B, binarized; W, weighted.

More importantly, they observed significant parcellation-related differences in multiple network topological parameters (e.g., small-worldness and network efficiency) between the two sets of networks. For example, the global efficiency of networks based on the AAL atlas was higher than those based on the ANIMAL atlas. Given that most current studies construct the brain networks using prior brain templates, this work has important implications for the consideration of parcellation-related effects in future brain network studies.

Using R-fMRI, He et al. (2009b) demonstrated modular structures of intrinsic functional brain networks (**Figure 2**). A group-level brain connectivity network was obtained and fed into a simulated annealing algorithm to detect the modular structure. The results showed that the resting-state brain network was modularly configured and optimally organized into five modules: somatosensory/motor and auditory, vision, attention, default-mode, and limbic/paralimbic and sub-cortical systems. Interestingly, when the modularity detection algorithm was iteratively applied to those identified modules, several more segregated sub-modules were observed, suggesting a hierarchical modularity. Furthermore, they demonstrated significant differences in the network structure between modules and the whole brain network, suggesting module-specific organization patterns. In a more detailed exploration, specific sets of connector nodes and bridge edges that were involved in different modules were shown to be important for maintaining the connectivity and stability of the functional brain networks. Another similar study from Meunier et al. (2009b) also demonstrated the hierarchical modularity in resting-state functional networks of the human brain. In this case, a larger brain network, consisting of 1808 regional nodes, was constructed for each of the 18 right-handed healthy volunteers and was fed into a multi-level method for detecting the hierarchical modularity. The results indicated a significant hierarchical modularity of the resting-state brain functional network, with the five largest modules observed at the highest level of the hierarchy: medial occipital, lateral occipital, central, parieto-frontal, and fronto-temporal systems. Intriguingly, the occipital modules showed less sub-modular organization in comparison with other modules, implying that distinctive organizational principles exist in function-specific sub-systems, which is consistent with previous findings (He et al., 2009b). Additionally, the nodal roles analysis indicated that connector nodes and inter-modular connections were largely concentrated in posterior modules that contain regions of association cortex. In addition to the studies mentioned above, Ferrarini et al. (2009) also validated small-world properties and hierarchical modularity by focusing on revising a clustering algorithm to detect the modularity of resting-state functional networks of the human brain.

Beyond the region-level explorations of the intrinsic topology mentioned above, brain network analyses have been done at the voxel-level. Although some intriguing results were demonstrated in intrinsic large-scale (region-level) functional brain networks, these findings may be biased by the fact that all of the analyses were restricted to predefined anatomical structures. Specifically, at the region-level, inter-regional connectivity was routinely evaluated in terms of representative time courses obtained by averaging the signals within predefined parcellation structures. However, despite the simplicity, the averaging process may simultaneously lead to a possible blurring out of some local specific information, particularly for those functionally heterogeneous parcellation units. The high spatial resolution (e.g., 4 mm) provided by R-fMRI allows investigation of the topological properties of brain networks at a finer-grained voxel-level, which is beneficial to our understanding of brain organization at a more refined level (e.g., 20,000 nodes). The next section will be devoted to reviewing some work in this area.

Voxel-based resting-state brain networks

Eguiluz et al. (2005) conducted the first study of human brain functional networks constructed at the voxel-level and found general scale-free small-world architecture under multiple task conditions. Focusing on the same features, van den Heuvel et al. (2008a) first examined the resting-state functional network of the human brain at voxel-level. After constructing individual brain networks for 28 participants, the graph theoretical analysis confirmed the small-world organization in spontaneous brain network consistent with previous region-level network analyses. This finding suggests that small-world topology is a robust organizational principle governing the global pattern of coherent fluctuations in spontaneous neural activity across multiple spatial scales (i.e., region-level and voxel-level). However, in contrast to the exponentially truncated power law degree distribution observed frequently in region-level brain networks, the voxel-level brain network exhibited a scale-free or power law form. This discrepancy implies that intrinsic functional networks of the human brain may organize differently at different spatial scales, at least in some features, therefore pointing out the need to elucidate how the organization of brain networks depends on the scale in which they are constructed.

Instead of global small-world architecture, several groups have focused on the identification of intrinsic modular/community structure in resting-state brain networks at voxel-level. Using a normalized cut graph clustering algorithm, van den Heuvel et al. (2008b) found seven resting-state networks, such as default-mode network, parietal-frontal network and motor and visual network, resembling those sub-networks or components revealed by ICA studies on R-fMRI datasets. This consistency of modularity structure or sub-systems in intrinsic functional brain networks across analytical methods was also validated by more recent voxel-level network studies (Laurienti et al., 2009; Valencia et al., 2009). Valencia et al. (2009) constructed voxel-level functional brain networks for seven healthy subjects and then investigated the modular architecture of these networks using a random-walk-based method. It is not surprising that all individuals exhibited significant modular structure with moderate stability. Refreshingly, the authors compared the spatial distribution of retrieved modules with a prior anatomical AAL atlas and found that some modules aligned well with certain brain systems. For example, 75% of the primary visual area, V1, was gathered into one module. More importantly, some modules included functionally related but spatially distant regions. These results imply that the modular organization has an underlying basis of neural functions, rather than being a consequence of vascular processes or local physiological activities. Another notable finding from this work is the exponentially truncated power law model of degree distribution for intrinsic brain networks, which contrasts with the observation of power law form by van den Heuvel

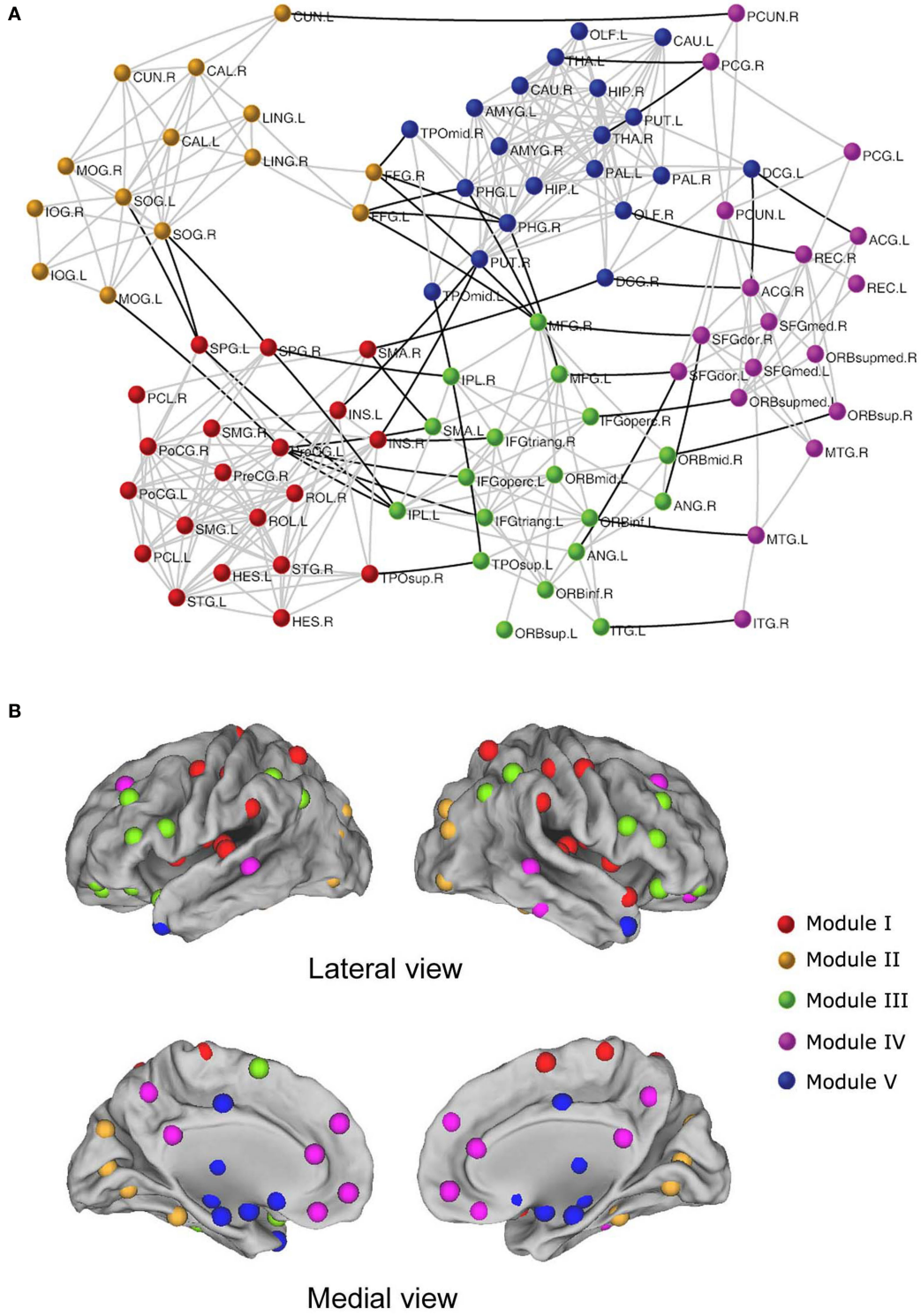

FIGURE 2 | The modular architecture of resting-state functional brain network (He et al., 2009b). (A) Five modules were identified in a functional network of the human brain, represented by five different colors. The geometric distance between brain regions on the drawing space approximates the shortest path length between them. The network is visualized with Pajek (http://vlado.fmf.uni-lj.si/pub/networks/pajek/). The intra-module and inter-module connections are shown in gray and dark lines, respectively. For the abbreviations of the regions, see He et al. (2009b). **(B)** Surface representation of modular architecture of a functional brain network. All 90 brain regions are marked by using different colored spheres (different colors represent distinct network modules) and further mapped onto the cortical surfaces in the lateral and medial views, respectively. Notably, the regions are located according to their centroid stereotaxic coordinates. For visualization purposes, the subcortical regions are projected to the medial cortical surface according to their y and z centroid stereotaxic coordinates.

et al. (2008b). This discrepancy may be attributed to the different network construction methods (i.e., network nodes were abstracted from gray matter voxels by van den Heuvel et al. vs. whole brain by Valencia et al.) given the findings of tissue specific organization that networks constructed from white matter and cerebral spinal fluid voxels did not exhibited typical power law degree distribution (van den Heuvel et al., 2008b). Almost simultaneously, Laurienti et al. (2009) combined R-fMRI and graph theory to explore the modular structure of resting-state brain networks derived from six normal young adults. Modular architecture was again uncovered in spite of the use of a different module detection algorithm of QCut. It is noteworthy that the default-mode network was separated into three primary modules: the module of the medial frontal cortex, the module of sections from the parietal lobe and parahippocampal gyrus and the module of portions from the cuneus gyrus, parietal cortex and middle frontal gyrus. This was consistent with the finding of functional brain networks (He et al., 2009b). The split of the default-mode network into multiple sub-networks is also observed in previous ICA studies (Zuo et al., 2010a) and could imply functional segregation or heterogeneity within the default-mode network (Buckner et al., 2008; Harrison et al., 2008; Kiviniemi et al., 2009; Uddin et al., 2009). Given the high sensitivity of the default-mode network to numerous mental disorders (Broyd et al., 2009), studies that focus on the pattern within and between these sub-modules may lead to new insights into the pathophysiology of these disorders.

Rather than work with whole brain network studies, Dosenbach et al. (2007) concentrated exclusively on a putative task-control network. Thirty-nine ROIs associated with task-control were selected as the network nodes, and a group-level network from 74 young adults was formed. Analogous to the whole brain network, the sub-network of task-control system also exhibited small-world features. Further visualization of the network connectivity pattern revealed eight disconnected components, including the fronto-parietal component and cingulo-opercular component, which were clearly associated with task control. More importantly, the authors found that the wiring patterns of the fronto-parietal and cingulo-opercular components to other parts of the brain were obviously different. The fronto-parietal component preferentially connected with cerebellar regions, whereas the cingulo-opercular component tended to connect firstly with putative downstream sensory regions in the occipital cortex. Inspired by this phenomenon, the authors proposed a "dual-network" hypothesis to model task control, in which the fronto-parietal network supports adaptive control function and the cingulo-opercular network handles stable set-maintenance function.

DEVELOPMENT/AGING

The mature human brain has been optimally organized into a collection of specialized functional networks that flexibly interact in rapid response to various cognitive demands. Studying the formation of the architecture in a maturing brain from a global level may provide more insights into the organizing principle that guides the maturation process. In this topic, Fair and colleagues carried out a series of experiments to explore the mechanisms of development using R-fMRI and modern network techniques. They first studied a task control related network (Fair et al., 2007), containing 39 nodes (i.e., task control regions). Three group-level networks covering different ages were generated: 49 children (7–9 years; mean 8.6), 43 adolescents (10–15 years; mean 11.9), and 47 adults (20–31 years; mean 24.1). Visualization analysis showed a clear dynamic reorganization of brain network structure over the course of development. For example, the interconnected fronto-parietal and cingulo-opercular components in children gradually became two disconnected networks in adults. Using similar methods, the authors also demonstrated a more densely connected network structure in the adult default-mode network when compared with children, implying an increased functional integration during development (Fair et al., 2008). Moving beyond a single functional network, the authors expanded their interests to a wide system that included four functional networks: cingulo-opercular, fronto-parietal, default-mode and cerebellar. Based on large R-fMRI datasets (210 subjects: 66 aged 7–9; 53 aged 10–15; 91 aged 19–31), they studied the dynamic developmental trajectory of functional brain network organization using a sliding boxcar grouping method (Fair et al., 2009). The most important finding was the observation of concurrent segregation and integration in brain networks during development, which was revealed by both qualitative and quantitative analyses. This dichotomy of development was further found to be related to a general decrease in short-range connections and an increase in long-range connections. Another interesting result in this study was the comparable small-world topology observed across the entire range of ages examined, from 8 to 25 years old, as indicated by very little changes in path lengths and clustering coefficients. This suggests a largely conserved architecture over age. All the aforementioned studies focused on some specific brain functional systems, such as the default network or control network, leaving development effects on whole brain network organization unclear. Filling this gap, Supekar et al. (2009) assessed development-related alterations in brain functional networks in great detail using R-fMRI and graph theoretical techniques. After the construction of brain networks for each of 23 children (7–9 years) and 22 IQ-matched young-adult subjects (19–22 years), obvious differences were found in both global and local properties of functional brain networks between children and young adults. For example, children showed a globally lower level of hierarchical organization in the whole network and locally higher efficiency in sub-cortical division. Of particular importance, combining with DTI-based fiber tracking, the authors found a pattern of simultaneous emergence of decreased functional segregation and increased functional integration with development, characterized by lower short-range and higher long-range functional connectivity in young adults when compared with children. Taken together, these results show that development is strongly related to a weakening of short-range functional segregation and a strengthening of long-range functional integration, which suggests a general developmental principle for intrinsic functional brain architecture.

In addition to development-related changes, some groups have also investigated the effects of normal aging on the functional organization of large-scale brain networks during rest (Achard et al., 2007; Meunier et al., 2009a). Using graph theoretical approaches, Achard et al. (2007) tested the hypothesis that resting-state functional brain networks have economical small-world properties and that their performance would be disrupted by normal aging. R-fMRI data were collected from 11 old and 15 young healthy volunteers, and

individual brain networks were constructed using the methods from Achard et al. (2006). The results confirmed the economic small-world configuration hypothesis of intrinsic functional brain networks in both young and old people. However, normal aging significantly reduced the global and local efficiency of parallel information processing. Furthermore, regional efficiency analysis found that the detrimental effects of aging were mainly localized to frontal and temporal cortical and sub-cortical regions. Notably, in this study the authors also successfully detected alterations in the overall performance of economical small-world properties in intrinsic functional brain networks associated with the pharmacological blockade of dopamine neurotransmission. This finding highlights the potential value of graph theoretical tools for characterizing the mechanisms involved in different pathophysiological processes, such as the role of dopamine transmission system. In another study of normal aging, Meunier et al. (2009a) studied aging-related changes in the module or community structure of resting-state brain functional networks from two groups: 17 younger participants (18–33 years, mean age = 24.3 years) and 13 older participants (62–76 years, mean age = 67.3 years). The module structure analyses showed that both age groups exhibited significant, non-random, and robust modularity. However, both module size and composition differed between the age groups. For instance, five modules were detected in young brain functional networks, whereas six were seen in the older group. Interestingly, the authors found a trend for modules to segregate into multiple components in the brain networks of older people compared with younger people. For example, the dorsal fronto-cingulo-parietal module in the young brain network was segregated into two smaller and more local modules in the old brain network, a dorsal prefronto-striato-thalamic module and a medial posterior module. Thereby, tracing the profile of modular architecture throughout both development and aging will be an important topic.

Overall, the use of R-fMRI and graph theoretical approaches has demonstrated that normal development and aging are associated with alterations of brain organization, particularly in the modular architecture. The reconfiguration of network structure may allow for more flexibility to meet the demands during different states of life, such as high plasticity and fast learning at young ages. Future longitudinal studies could help address this question.

APPLICATIONS IN CLINICAL POPULATION

To date, the combination of R-fMRI and graph theory-based network approaches has proven to be a powerful tool to investigate the abnormalities in the organization of intrinsic brain networks under different pathological conditions (Bassett and Bullmore, 2009; Bullmore and Sporns, 2009; He et al., 2009a).

Alzheimer's disease

Supekar et al. (2008) were the first to study Alzheimer's disease (AD)-related changes in the coordination of large-scale brain functional networks using R-fMRI. After constructing functional brain networks for each of 21 AD patients and 18 age-matched controls, they found that AD patients showed deterioration of the small-world network properties, characterized by a significantly lower normalized clustering coefficient, implying disrupted local network connectivity. Furthermore, the differences in the normalized clustering coefficient can distinguish the AD participants from the controls with a sensitivity of 72% and a specificity of 78%, suggesting that these network measures could serve as an imaging-based biomarker in AD diagnosis. These findings suggested that AD is associated with disrupted functional integrity in the intrinsic spontaneous neuronal activity of the brain functional system. In a relevant large- and multiple-datasets study, Buckner et al. (2009) performed another AD-related study using graph theoretical approaches and R-fMRI to address the spatial distribution and stability of hub regions in intrinsic functional brain networks of human. They also assessed whether the identified hubs had a preferential vulnerability to AD pathology. One hundred twenty-seven healthy young adults participated in MRI sessions, and 39 older adults (29 controls and 10 AD patients) participated in PET sessions. The results showed that hub regions were dominated mainly by heteromodal areas of the association cortex, such as the posterior cingulate and medial/lateral prefrontal cortices, consistent with previous studies (Achard et al., 2006). Of more importance, the pattern of hubs was highly consistent between datasets and activity states (passive fixation vs. semantic classification task), suggesting that this is a stable property of cortical network architecture. Finally, the authors demonstrated a striking overlap and strong correlation ($r = 0.68$) between the pattern of cortical hubs derived from young subjects and the $A\beta$ deposition map in AD patients. The results imply a dual role for hubs in brain networks. On one hand, they act as critical stations for information processing, and on the other hand, they are preferential candidates of pathology.

Schizophrenia

Using R-fMRI, Liu et al. (2008) utilized graph-based network analysis to characterize networks in schizophrenia patients. Individual brain networks were built for 31 schizophrenia patients and 31 age- and gender-matched healthy subjects. Subsequent graph theoretical analysis revealed that schizophrenia patients showed abnormalities in multiple network attributes, including lower absolute clustering coefficients, normalized clustering coefficient, small-worldness and network efficiency, as well as longer absolute path length. In addition, multiple nodal characteristics were altered in several specific regions predominately located in prefrontal, parietal and temporal lobes in schizophrenia patients. Collectively, these abnormalities suggest a dysfunctional organization of the intrinsic functional brain network in schizophrenia. It is worth noting that multiple network metrics, such as the absolute clustering coefficient and local network efficiency, were found to have a significant negative correlation with the duration of illness and the dose of medication, suggesting a potential use of the graph theoretical tool in monitoring the progression and therapy evaluation of schizophrenia.

Attention-deficit hyperactivity disorder

Wang et al. (2009b) were the first to apply graph theoretical approaches to explore the spontaneous brain networks in patients with attention-deficit hyperactivity disorder (ADHD). Based upon R-fMRI datasets from 29 ADHD and 27 control boys, the authors found that the functional brain networks in both groups exhibited economic small-world behaviors. However, the ADHD group exhibited significant increases in local efficiency but statistically unchanged global efficiency in comparison with the control subjects, suggesting a shift toward regular networks in ADHD children. In

addition, the authors also tested regional nodal efficiency and found decreased nodal efficiency in the medial prefrontal, temporal, and occipital cortex regions and increased nodal efficiency in the inferior frontal cortex and sub-cortical regions. These differences imply a loss of the optimal organization pattern in ADHD children.

Epilepsy

The first study of mesial temporal lobe epilepsy (mTLE) to use graph theoretical approaches was performed by Liao et al. (2010). They constructed endogenous brain connectivity networks for 18 mTLE patients and 27 healthy controls using R-fMRI signals. A direct between-group comparison in functional connectivity revealed significantly increased connectivity within the medial temporal lobes but decreased connectivity within the frontal and parietal lobes and between frontal and parietal lobes in mTLE patients relative to controls. Subsequent graph theoretical analyses demonstrated that regions showing a significantly decreased number of connections were mainly from components of default-mode networks in mTLE patients. In addition, normalized path length was also found to be significantly lower in mTLE patients. These alterations in functional connectivity and topological properties may be used to define tentative disease markers for mTLE after the validation of repeatability.

Others

In addition to the application of this approach to neuropsychopathic diseases, graph theoretical approaches have also been used to explore the changes in intrinsic functional brain networks during recovery from traumatic brain injury (Nakamura et al., 2009) and in drug addicts (Liu et al., 2009). Nakamura et al. (2009) studied the changes of intrinsic coordinated brain connectivity networks in six subjects in recovery from severe traumatic brain injury. They found that high-value functional connections decreased with recovery but the overall number of connections maintained relatively stable. Further analyses revealed multiple altered topological indices during the recovery timeline, such as a significant reduction of global and local efficiency in brain networks at 6 months post injury compared with those at 3 months post injury. These results suggest that graph-based network techniques could be useful in evaluating the adaptation of intrinsic brain networks to neural disruption during recovery. Liu et al. (2009) concentrated on a specific population of chronic heroin users and evaluated the impairments of their brain functions from a functional integration perspective. The results demonstrated a typical small-world configuration in the brain networks constructed from 12 chronic heroin users; however, the extent of small-worldness (i.e., σ) was much smaller than that of non-drug users. Furthermore, some regions in the prefrontal cortex, ventral striatum, and limbic/paralimbic area were found to have dysfunctional connectivity, which may be responsible for the decreased self-control, impaired inhibitory function and deficits in stress regulation observed in chronic heroin users.

Taken together, these results demonstrate the utility of the combination of R-fMRI and graph theoretical techniques in capturing the abnormal alterations in topological organization of spontaneous brain networks caused by different brain disorders. Further studies are needed to ascertain whether this kind of topology-based approach could be used as a novel way to identify biomarkers for the diagnosis and monitoring of these diseases.

TECHNICAL CHALLENGE AND FUTURE PERSPECTIVES

In this review, we summarized the recent advances in the application of modern graph theory-based network analysis techniques to study the intrinsic or spontaneous human brain functional networks derived from R-fMRI. Several consistent characteristics are demonstrated in the normal population, such as small-world topology, modular structure, and core regions, some of which are sensitive to normal development, aging and neuropsychiatric disease. These findings provide novel insights into the functional architecture of the human brain and its adaptive reconfiguration in brain maturing, aging and against pathological attacks. However, we should acknowledge that the studies of complex brain networks formed by spontaneous activity, even in normal subjects, are still in the early stages. There are still a number of unanswered questions in this research field.

First, given that the human brain is a complex network at multiple spatial and time scales, how to appropriately represent the brain as a network that can precisely reflect the natural state of the brain is a considerable task. For instance, what are the nodes and edges in a brain network? Which time scale is best suited for the brain network? As Butts (2009) stated, the inappropriate representation of nodes and edges in a network and failure to consider the dynamics of the system of interest will lead to misleading conclusions and generally poor results. Recent evidence has demonstrated the meaningful influence of node choice on the properties of resulting networks (Hayasaka and Laurienti, 2009; Wang et al., 2009a; Zalesky et al., 2009). For example, Hayasaka and Laurienti constructed functional brain networks at multiple resolutions (90~160,000 nodes) using the same R-fMRI dataset from 10 normal subjects and found more prominent small-worldness and robustness against network fragmentation in networks at the voxel-level compared with the region-level. In parallel with the definition of nodes, how to determine the functional connectivity-based edges in functional brain networks is another important issue. Multiple choices are currently available for estimating the functional connectivity between brain areas, such as partial correlation, Pearson correlation and mutual information that depict the functional associations from different angles. Our recent work (not published) demonstrates significant connectivity-related differences in the architecture of resting brain networks, implying that different organization patterns can be generated using different functional connectivity measures. Therefore, a combined analysis of multiple connectivity metrics could be more fruitful for brain network studies. In addition to intuitively conceivable nodes and edges, the human brain is a dynamic system over multiple time scales with ongoing and adaptive functional activities (Honey et al., 2009). Therefore, capturing the dynamic network behaviors at different time scales is an important topic in future.

Second, although graph theoretical brain network analysis based on R-fMRI attracts a great deal of attention, the reliability and reproducibility of network measurements, both across subjects and over time, needs to be addressed. R-fMRI has shown reliability in local low-frequency fluctuations (Zuo et al., 2010b), ROI-based functional connectivity (Shehzad et al., 2009) and ICA components (Zuo et al., 2010a). However, the reliability of topological structures has not yet been validated in R-fMRI brain networks. Nonetheless, a recent magnetoencephalography study has shown that graph metrics exhibited sufficient reliability both in resting-state and during performance of the n-back working memory task, though greater

reliability was seen in the performance of the n-back task compared with resting-state (Deuker et al., 2009). We speculate that graph-based metrics in R-fMRI may also have acceptable reliability and reproducibility, but this hypothesis needs to be tested directly by multi-center and longitudinal datasets.

Third, how do resting-state functional brain networks relate to individual traits and genetic factors? The answer to these questions may provide new insights into brain function. Smit et al. (2008) demonstrated that individual differences in the topological properties of resting-state functional brain networks constructed using EEG signals are heritable. van den Heuvel et al. (2009b) found that the overall organization of spontaneous functional brain networks had a strong association with intelligence quotient (IQ) as characterized by a negative correlation between the normalized characteristic path length and IQ, consistent with the findings from a recent structural brain network study (Li et al., 2009). Accordingly, it is of great interest to further investigate the relationship between network organization and individual characteristics, such as genotype and education level.

Fourth, only a few articles concentrate on the topological architecture of neuronal networks during the performance of tasks. Eguiluz et al. demonstrated scale-free small-world topology in human brain networks across different task conditions. Bassett et al. (2006) indicated that behavioral state in a finger-tapping task did not strongly influence the global topology of the human brain network derived from MEG signals during rest but was associated with emergence of some long-range connections. Their subsequent work (Bassett et al., 2009) further demonstrated that the superior task performance of work memory was positively correlated with the cost-efficiency (the difference between the global efficiency and cost of a network) of the β-band brain networks. More recently, Wang et al. (2010) investigated the age-related changes of functional brain networks during memory encoding and recognition, and they found longer path length in older adults due to the loss of long-range connections. Consequently, studying the brain networks under both resting and task conditions as well as the transition between these states may offer new insights into the rapid adaptive reconfiguration of neuronal assemblies that underlie the change between cognitive states.

Finally, the relationship between brain structure and function, both how brain function emerges from its structural substrate and inversely how experience-related functional plasticity reshapes brain structure, is an important future topic. The current review mainly focused on recent studies of R-fMRI based brain networks. It has been demonstrated that brain networks can also be constructed by using other imaging modalities (e.g., structural MRI, diffusion MRI, and EEG/MEG). For instance, researchers have been capable of constructing structural brain networks by measuring inter-regional correlations of cortical thickness or gray matter volume across populations (He et al., 2007, 2008, 2009c; Bassett et al., 2008), and found that the resultant networks had small-world properties. Several diffusion MRI studies have utilized deterministic or probabilistic white-matter tractography approaches to build structural brain networks, and also showed small-world topology and high connected hubs in the medial parietal and frontal regions. Of note, the brain networks derived from different imaging modalities have been found to show many common topological properties such as the small-world attributes and network hubs but specific features for each modality such as network modules (Hagmann et al., 2008; Chen et al., 2009; He et al., 2009b). Moreover, several studies have directly compared DTI-based structural connectivity and R-fMRI based functional connectivity, and largely convergent results were found that the strength of resting-state functional connectivity correlated positively with structural connectivity strength (for a review, see Damoiseaux and Greicius, 2009). This implies that functionally linked resting brain networks likely reflect underlying structural connectivity (Greicius et al., 2009; van den Heuvel et al., 2009a; Teipel et al., 2010). In particular, by focusing on the whole brain connectivity pattern, previous studies have demonstrated overall, though imperfect, agreement between functional and structural connectivity at different spatial levels (Skudlarski et al., 2008; Honey et al., 2009). In spite of these efforts, the exact nature of the bi-directional interaction between brain structure and function, especially in the global topological organization remains unclear. Concentrating on this point, Park et al. (2008) demonstrated significantly distinct topological features between structural and functional brain networks. For example, structural brain networks showed higher efficiency than the functional brain networks. Collectively, by combining multiple imaging modalities (e.g., fMRI, sMRI, and DTI), direct comparisons of the network properties using large-sample neuroimaging data would be vital to address these issues. Specifically, we need to point out that the public release of the "1000 Functional Connectomes Project" dataset (1200+ resting-state R-fMRI and structural MRI datasets independently collected at 35 sites, http://www.nitrc.org/projects/fcon_1000/) (Biswal et al., 2010) will be extremely important for the exploration and refinement of topological organization and relevant approaches to structural and functional networks in the human brain.

CONCLUSION

Through the combination of R-fMRI and graph theory-based network analysis techniques, intrinsic functional networks of the human brain have been generated and demonstrate converging and highly conserved topological organization over different scales and types of measurement, such as small-world and modular structures. More importantly, some of these features exhibit specific changes associated with normal development, aging and various pathological attacks, which indicates the potential value of these approaches in capturing and monitoring the brain organization under different mental states. With the advances in brain imaging techniques (e.g., higher spatiotemporal resolution) and the maturity and perfection of multiple analytical approaches on complex system in parallel, we can expect important progress in our understanding of how the brain works and how it interacts with other systems of the body.

ACKNOWLEDGMENTS

The work was supported by the National Natural Science Foundation of China (Grant No. 30870667), Beijing Natural Science Foundation (Grant No. 7102090) and the Scientific Research Foundation for the Returned Overseas Chinese Scholars (State Education Ministry). We thank American Journal Experts (http://www.journalexperts.com/) for English editing and proofreading.

REFERENCES

Achard, S., and Bullmore, E. T. (2007). Efficiency and cost of economical brain functional networks. *PLoS Comput. Biol.* 3, e17. doi:10.1371/journal.pcbi.0030017.

Achard, S., Salvador, R., Whitcher, B., Suckling, J., and Bullmore, E. T. (2006). A resilient, low-frequency, small-world human brain functional network with highly connected association cortical hubs. *J. Neurosci.* 26, 63–72.

Bang-Jensen, J., and Gutin, G. Z. (2008). *Digraphs: Theory, Algorithms and Applications*. Berlin: Springer-Verlag Press.

Bassett, D. S., and Bullmore, E. T. (2006). Small-world brain networks. *Neuroscientist.* 12, 512–523.

Bassett, D. S., and Bullmore, E. T. (2009). Human brain networks in health and disease. *Curr. Opin. Neurol.* 22, 340–347.

Bassett, D. S., Bullmore, E. T., Meyer-Lindenberg, A., Apud, J. A., Weinberger, D. R., and Coppola, R. (2009). Cognitive fitness of cost-efficient brain functional networks. *Proc. Natl. Acad. Sci. U.S.A.* 106, 11747–11752.

Bassett, D. S., Bullmore, E. T., Verchinski, B. A., Mattay, V. S., Weinberger, D. R., and Meyer-Lindenberg, A. (2008). Hierarchical organization of human cortical networks in health and schizophrenia. *J. Neurosci.* 28, 9239–9248.

Bassett, D. S., Meyer-Lindenberg, A., Achard, S., Duke, T., and Bullmore, E. T. (2006). Adaptive reconfiguration of fractal small-world human brain functional networks. *Proc. Natl. Acad. Sci. U.S.A.* 103, 19518–19523.

Beckmann, C. F., DeLuca, M., Devlin, J. T., and Smith, S. M. (2005). Investigations into resting-state connectivity using independent component analysis. *Philos. Trans. R. Soc. Lond. B Biol. Sci.* 360, 1001–1013.

Biswal, B. B., Mennes, M., Zuo, X. N., Gohel, S., Kelly, C., Smith, S. M., Beckmann, C. F., Adelstein, J. S., Buckner, R. L., Colcombe, S., Dogonowski, A. M., Ernst, M., Fair, D., Hampson, M., Hoptman, M. J., Hyde, J. S., Kiviniemi, V. J., Kotter, R., Li, S. J., Lin, C. P., Lowe, M. J., Mackay, C., Madden, D. J., Madsen, K. H., Margulies, D. S., Mayberg, H. S., McMahon, K., Monk, C. S., Mostofsky, S. H., Nagel, B. J., Pekar, J. J., Peltier, S. J., Petersen, S. E., Riedl, V., Rombouts, S. A., Rypma, B., Schlaggar, B. L., Schmidt, S., Seidler, R. D., Siegle, G. J., Sorg, C., Teng, G. J., Veijola, J., Villringer, A., Walter, M., Wang, L., Weng, X. C., Whitfield-Gabrieli, S., Williamson, P., Windischberger, C., Zang, Y. F., Zhang, H. Y., Castellanos, F. X., and Milham, M. P. (2010). Toward discovery science of human brain function. *Proc Natl Acad Sci U.S.A.* 107, 4734–4739.

Biswal, B., Yetkin, F. Z., Haughton, V. M., and Hyde, J. S. (1995). Functional connectivity in the motor cortex of resting human brain using echo-planar MRI. *Magn. Reson. Med.* 34, 537–541.

Boccaletti, S., Latora, V., Moreno, Y., Chavez, M., and Hwang, D. U. (2006). Complex networks: Structure and dynamics. *Phys. Rep.* 424, 175–308.

Broyd, S. J., Demanuele, C., Debener, S., Helps, S. K., James, C. J., and Sonuga-Barke, E. J. (2009). Default-mode brain dysfunction in mental disorders: a systematic review. *Neurosci. Biobehav. Rev.* 33, 279–296.

Buckner, R. L., Andrews-Hanna, J. R., and Schacter, D. L. (2008). The brain's default network: anatomy, function, and relevance to disease. *Ann. N. Y. Acad. Sci.* 1124, 1–38.

Buckner, R. L., Sepulcre, J., Talukdar, T., Krienen, F. M., Liu, H., Hedden, T., Andrews-Hanna, J. R., Sperling, R. A., and Johnson, K. A. (2009). Cortical hubs revealed by intrinsic functional connectivity: mapping, assessment of stability, and relation to Alzheimer's disease. *J. Neurosci.* 29, 1860–1873.

Bullmore, E., and Sporns, O. (2009). Complex brain networks: graph theoretical analysis of structural and functional systems. *Nat. Rev. Neurosci.* 10, 186–198.

Butts, C. T. (2009). Revisiting the foundations of network analysis. *Science* 325, 414–416.

Chen, S., Ross, T. J., Zhan, W., Myers, C. S., Chuang, K. S., Heishman, S. J., Stein, E. A., and Yang, Y. (2008a). Group independent component analysis reveals consistent resting-state networks across multiple sessions. *Brain Res.* 1239, 141–151.

Chen, Z. J., He, Y., Rosa-Neto, P., Germann, J., and Evans, A. C. (2008b). Revealing modular architecture of human brain structural networks by using cortical thickness from MRI. *Cereb. Cortex* 18, 2374–2381.

Cordes, D., Haughton, V., Carew, J. D., Arfanakis, K., and Maravilla, K. (2002). Hierarchical clustering to measure connectivity in fMRI resting-state data. *Magn. Reson. Imaging* 20, 305–317.

Cordes, D., Haughton, V. M., Arfanakis, K., Carew, J. D., Turski, P. A., Moritz, C. H., Quigley, M. A., and Meyerand, M. E. (2001). Frequencies contributing to functional connectivity in the cerebral cortex in "resting-state" data. *AJNR Am. J. Neuroradiol.* 22, 1326–1333.

Damoiseaux, J. S., and Greicius, M. D. (2009). Greater than the sum of its parts: a review of studies combining structural connectivity and resting-state functional connectivity. *Brain Struct. Funct.* 213, 525–533.

Damoiseaux, J. S., Rombouts, S. A., Barkhof, F., Scheltens, P., Stam, C. J., Smith, S. M., and Beckmann, C. F. (2006). Consistent resting-state networks across healthy subjects. *Proc. Natl. Acad. Sci. U.S.A.* 103, 13848–13853.

de Haan, W., Pijnenburg, Y. A., Strijers, R. L., van der Made, Y., van der Flier, W. M., Scheltens, P., and Stam, C. J. (2009). Functional neural network analysis in frontotemporal dementia and Alzheimer's disease using EEG and graph theory. *BMC Neurosci.* 10, 101.

Deuker, L., Bullmore, E. T., Smith, M., Christensen, S., Nathan, P. J., Rockstroh, B., and Bassett, D. S. (2009). Reproducibility of graph metrics of human brain functional networks. *Neuroimage* 47, 1460–1468.

Di Martino, A., Scheres, A., Margulies, D. S., Kelly, A. M., Uddin, L. Q., Shehzad, Z., Biswal, B., Walters, J. R., Castellanos, F. X., and Milham, M. P. (2008). Functional connectivity of human striatum: a resting state FMRI study. *Cereb. Cortex* 18, 2735–2747.

Di Martino, A., Shehzad, Z., Kelly, C., Roy, A. K., Gee, D. G., Uddin, L. Q., Gotimer, K., Klein, D. F., Castellanos, F. X., and Milham, M. P. (2009). Relationship between cingulo-insular functional connectivity and autistic traits in neurotypical adults. *Am. J. Psychiatry* 166, 891–899.

Dosenbach, N. U., Fair, D. A., Miezin, F. M., Cohen, A. L., Wenger, K. K., Dosenbach, R. A., Fox, M. D., Snyder, A. Z., Vincent, J. L., Raichle, M. E., Schlaggar, B. L., and Petersen, S. E. (2007). Distinct brain networks for adaptive and stable task control in humans. *Proc. Natl. Acad. Sci. U.S.A.* 104, 11073–11078.

Eguiluz, V. M., Chialvo, D. R., Cecchi, G. A., Baliki, M., and Apkarian, A. V. (2005). Scale-free brain functional networks. *Phys. Rev. Lett.* 94, 018102.

Fair, D. A., Cohen, A. L., Dosenbach, N. U., Church, J. A., Miezin, F. M., Barch, D. M., Raichle, M. E., Petersen, S. E., and Schlaggar, B. L. (2008). The maturing architecture of the brain's default network. *Proc. Natl. Acad. Sci. U.S.A.* 105, 4028–4032.

Fair, D. A., Cohen, A. L., Power, J. D., Dosenbach, N. U., Church, J. A., Miezin, F. M., Schlaggar, B. L., and Petersen, S. E. (2009). Functional brain networks develop from a "local to distributed" organization. *PLoS Comput. Biol.* 5, e1000381. doi:10.1371/journal.pcbi.1000381.

Fair, D. A., Dosenbach, N. U., Church, J. A., Cohen, A. L., Brahmbhatt, S., Miezin, F. M., Barch, D. M., Raichle, M. E., Petersen, S. E., and Schlaggar, B. L. (2007). Development of distinct control networks through segregation and integration. *Proc. Natl. Acad. Sci. U.S.A.* 104, 13507–13512.

Ferrarini, L., Veer, I. M., Baerends, E., van Tol, M. J., Renken, R. J., van der Wee, N. J., Veltman, D. J., Aleman, A., Zitman, F. G., Penninx, B. W., van Buchem, M. A., Reiber, J. H., Rombouts, S. A., and Milles, J. (2009). Hierarchical functional modularity in the resting-state human brain. *Hum. Brain Mapp.* 30, 2220–2231.

Fox, M. D., Corbetta, M., Snyder, A. Z., Vincent, J. L., and Raichle, M. E. (2006). Spontaneous neuronal activity distinguishes human dorsal and ventral attention systems. *Proc. Natl. Acad. Sci. U.S.A.* 103, 10046–10051.

Fox, M. D., and Raichle, M. E. (2007). Spontaneous fluctuations in brain activity observed with functional magnetic resonance imaging. *Nat. Rev. Neurosci.* 8, 700–711.

Fox, M. D., Snyder, A. Z., Vincent, J. L., Corbetta, M., Van Essen, D. C., and Raichle, M. E. (2005). The human brain is intrinsically organized into dynamic, anticorrelated functional networks. *Proc. Natl. Acad. Sci. U.S.A.* 102, 9673–9678.

Fox, M. D., Snyder, A. Z., Vincent, J. L., and Raichle, M. E. (2007). Intrinsic fluctuations within cortical systems account for intertrial variability in human behavior. *Neuron* 56, 171–184.

Franco, A. R., Pritchard, A., Calhoun, V. D., and Mayer, A. R. (2009). Interrater and intermethod reliability of default mode network selection. *Hum. Brain Mapp.* 30, 2293–2303.

Freeman, L. C. (1977). A set of measures of centrality based on betweenness. *Sociometry* 40, 35–41.

Freeman, L. C. (1979). Centrality in social networks conceptual clarification. *Soc. Networks* 1, 215–239.

Friston, K. J., Frith, C. D., Liddle, P. F., and Frackowiak, R. S. (1993). Functional connectivity: the principal-component analysis of large (PET) data sets. *J. Cereb. Blood Flow Metab.* 13, 5–14.

Gong, G., He, Y., Concha, L., Lebel, C., Gross, D. W., Evans, A. C., and Beaulieu, C. (2009a). Mapping anatomical connectivity patterns of human cerebral cortex using in vivo diffusion tensor imaging tractography. *Cereb. Cortex* 19, 524–536.

Gong, G., Rosa-Neto, P., Carbonell, F., Chen, Z. J., He, Y., and Evans, A. C. (2009b). Age- and gender-related differences in the cortical anatomical network. *J. Neurosci.* 29, 15684–15693.

Greicius, M. (2008). Resting-state functional connectivity in neuropsychiatric disorders. *Curr. Opin. Neurol.* 21, 424–430.

Greicius, M. D., Krasnow, B., Reiss, A. L., and Menon, V. (2003). Functional connectivity in the resting brain: a network analysis of the default mode hypothesis. *Proc. Natl. Acad. Sci. U.S.A.* 100, 253–258.

Greicius, M. D., Supekar, K., Menon, V., and Dougherty, R. F. (2009). Resting-state functional connectivity reflects structural connectivity in the default mode network. *Cereb. Cortex* 19, 72–78.

Guimera, R., Mossa, S., Turtschi, A., and Amaral, L. A. (2005). The worldwide air transportation network: anomalous centrality, community structure, and cities' global roles. *Proc. Natl. Acad. Sci. U.S.A.* 102, 7794–7799.

Hagmann, P., Cammoun, L., Gigandet, X., Meuli, R., Honey, C. J., Wedeen, V. J., and Sporns, O. (2008). Mapping the structural core of human cerebral cortex. *PLoS Biol.* 6, e159. doi:10.1371/journal.pbio.0060159.

Hampson, M., Driesen, N. R., Skudlarski, P., Gore, J. C., and Constable, R. T. (2006). Brain connectivity related to working memory performance. *J. Neurosci.* 26, 13338–13343.

Hampson, M., Peterson, B. S., Skudlarski, P., Gatenby, J. C., and Gore, J. C. (2002). Detection of functional connectivity using temporal correlations in MR images. *Hum. Brain Mapp.* 15, 247–262.

Harrison, B. J., Pujol, J., Lopez-Sola, M., Hernandez-Ribas, R., Deus, J., Ortiz, H., Soriano-Mas, C., Yucel, M., Pantelis, C., and Cardoner, N. (2008). Consistency and functional specialization in the default mode brain network. *Proc. Natl. Acad. Sci. U.S.A.* 105, 9781–9786.

Hayasaka, S., and Laurienti, P. J. (2009). Comparison of characteristics between region-and voxel-based network analyses in resting-state fMRI data. *Neuroimage* 2, 499–508.

He, Y., and Evans, A. (2010). Graph theoretical modeling of brain connectivity. *Curr. Opin. Neurol.*, in press.

He, Y., Chen, Z., and Evans, A. (2008). Structural insights into aberrant topological patterns of large-scale cortical networks in Alzheimer's disease. *J. Neurosci.* 28, 4756–4766.

He, Y., Chen, Z. J., and Evans, A. C. (2007). Small-world anatomical networks in the human brain revealed by cortical thickness from MRI. *Cereb. Cortex* 17, 2407–2419.

He, Y., Chen, Z., Gong, G., and Evans, A. (2009a). Neuronal networks in Alzheimer's disease. *Neuroscientist.* 15, 333–350.

He, Y., Wang, J., Wang, L., Chen, Z. J., Yan, C., Yang, H., Tang, H., Zhu, C., Gong, Q., Zang, Y., and Evans, A. C. (2009b). Uncovering intrinsic modular organization of spontaneous brain activity in humans. *PLoS ONE* 4, e5226. doi:10.1371/journal.pone.0005226.

He, Y., Dagher, A., Chen, Z., Charil, A., Zijdenbos, A., Worsley, K., and Evans, A. (2009c). Impaired small-world efficiency in structural cortical networks in multiple sclerosis associated with white matter lesion load. *Brain* 132, 3366–3379.

Hesselmann, G., Kell, C. A., Eger, E., and Kleinschmidt, A. (2008). Spontaneous local variations in ongoing neural activity bias perceptual decisions. *Proc. Natl. Acad. Sci. U.S.A.* 105, 10984–10989.

Honey, C. J., Sporns, O., Cammoun, L., Gigandet, X., Thiran, J. P., Meuli, R., and Hagmann, P. (2009). Predicting human resting-state functional connectivity from structural connectivity. *Proc. Natl. Acad. Sci. U.S.A.* 106, 2035–2040.

Honey, C. J., Thivierge, J. P., and Sporns, O. (2010). Can structure predict function in the human brain? *NeuroImage* [Epub ahead of print].

Kelly, A. M., Uddin, L. Q., Biswal, B. B., Castellanos, F. X., and Milham, M. P. (2008). Competition between functional brain networks mediates behavioral variability. *Neuroimage* 39, 527–537.

Kiviniemi, V., Starck, T., Remes, J., Long, X., Nikkinen, J., Haapea, M., Veijola, J., Moilanen, I., Isohanni, M., Zang, Y. F., et al. (2009). Functional segmentation of the brain cortex using high model order group PICA. *Hum. Brain Mapp.* 30, 3865–3886.

Latora, V., and Marchiori, M. (2001). Efficient behavior of small-world networks. *Phys. Rev. Lett.* 87, 198701.

Latora, V., and Marchiori, M. (2003). Economic small-world behavior in weighted networks. *Eur. Phys. J. B Condens Matter Complex Syst V* 32, 249–263.

Laurienti, P., Hugenschmidt, C. E., and Hayasaka, S. (2009). "Modularity maps reveal community structure in the resting human brain," in *Nature Precedings*. http://hdl.handle.net/10101/npre.2009.3069.1

Li, Y., Liu, Y., Li, J., Qin, W., Li, K., Yu, C., and Jiang, T. (2009). Brain anatomical network and intelligence. *PLoS Comput. Biol.* 5, e1000395. doi:10.1371/journal.pcbi.1000395.

Liao, W., Zhang, Z., Pan, Z., Mantini, D., Ding, J., Duan, X., Luo, C., Lu, G., and Chen, H. (2010). Altered functional connectivity and small-world in mesial temporal lobe epilepsy. *PLoS ONE* 5, e8525. doi:10.1371/journal.pone.0008525.

Liu, J., Liang, J., Qin, W., Tian, J., Yuan, K., Bai, L., Zhang, Y., Wang, W., Wang, Y., Li, Q., et al. (2009). Dysfunctional connectivity patterns in chronic heroin users: an fMRI study. *Neurosci. Lett.* 460, 72–77.

Liu, Y., Liang, M., Zhou, Y., He, Y., Hao, Y., Song, M., Yu, C., Liu, H., Liu, Z., and Jiang, T. (2008). Disrupted small-world networks in schizophrenia. *Brain* 131, 945–961.

Long, X. Y., Zuo, X. N., Kiviniemi, V., Yang, Y., Zou, Q. H., Zhu, C. Z., Jiang, T. Z., Yang, H., Gong, Q. Y., Wang, L., et al. (2008). Default mode network as revealed with multiple methods for resting-state functional MRI analysis. *J. Neurosci. Methods* 171, 349–355.

Lowe, M. J., Mock, B. J., and Sorenson, J. A. (1998). Functional connectivity in single and multislice echoplanar imaging using resting-state fluctuations. *Neuroimage* 7, 119–132.

Margulies, D. S., Kelly, A. M. C., Uddin, L. Q., Biswal, B. B., Castellanos, F. X., and Milham, M. P. (2007). Mapping the functional connectivity of anterior cingulate cortex. *Neuroimage* 37, 579–588.

Meindl, T., Teipel, S., Elmouden, R., Mueller, S., Koch, W., Dietrich, O., Coates, U., Reiser, M., and Glaser, C. (2009). Test–retest reproducibility of the default-mode network in healthy individuals. *Hum. Brain Mapp.* 31, 237–246.

Meunier, D., Achard, S., Morcom, A., and Bullmore, E. T. (2009a). Age-related changes in modular organization of human brain functional networks. *Neuroimage* 44, 715–723.

Meunier, D., Lambiotte, R., Fornito, A., Ersche, K. D., and Bullmore, E. T. (2009b). Hierarchical modularity in human brain functional networks. *Front. Neuroinformatics* 3, 37.

Micheloyannis, S., Vourkas, M., Tsirka, V., Karakonstantaki, E., Kanatsouli, K., and Stam, C. J. (2009). The influence of ageing on complex brain networks: a graph theoretical analysis. *Hum. Brain Mapp.* 30, 200–208.

Nakamura, T., Hillary, F. G., and Biswal, B. B. (2009). Resting network plasticity following brain injury. *PLoS ONE* 4, e8220. doi:10.1371/journal.pone.0008220.

Newman, M. E. (2006). Modularity and community structure in networks. *Proc. Natl. Acad. Sci. U.S.A.* 103, 8577–8582.

Newman, M. E. J. (2003). The structure and function of complex networks. *SIAM Rev.* 45, 167–256.

Pachou, E., Vourkas, M., Simos, P., Smit, D., Stam, C. J., Tsirka, V., and Micheloyannis, S. (2008). Working memory in schizophrenia: an EEG study using power spectrum and coherence analysis to estimate cortical activation and network behavior. *Brain Topogr.* 21, 128–137.

Park, C.-H., Kim, S. Y., Kim, Y.-H., and Kim, K. (2008). Comparison of the small-world topology between anatomical and functional connectivity in the human brain. *Phys. A. Stat. Mech. Appl.* 387, 5958–5962.

Raichle, M. E. (2006). Neuroscience. The brain's dark energy. *Science* 314, 1249–1250.

Raichle, M. E., MacLeod, A. M., Snyder, A. Z., Powers, W. J., Gusnard, D. A., and Shulman, G. L. (2001). A default mode of brain function. *Proc. Natl. Acad. Sci. U.S.A.* 98, 676–682.

Ravasz, E., and Barabasi, A. L. (2003). Hierarchical organization in complex networks. *Phys. Rev. E. Stat. Nonlin. Soft Matter Phys.* 67, 026112.

Ravasz, E., Somera, A. L., Mongru, D. A., Oltvai, Z. N., and Barabasi, A. L. (2002). Hierarchical organization of modularity in metabolic networks. *Science* 297, 1551–1555.

Roy, A. K., Shehzad, Z., Margulies, D. S., Kelly, A. M., Uddin, L. Q., Gotimer, K., Biswal, B. B., Castellanos, F. X., and Milham, M. P. (2009). Functional connectivity of the human amygdala using resting state fMRI. *Neuroimage* 45, 614–626.

Rubinov, M., and Sporns, O. (2009). Complex network measures of brain connectivity: uses and interpretations. *Neuroimage* [Epub ahead of print].

Sakata, S., Komatsu, Y., and Yamamori, T. (2005). Local design principles of mammalian cortical networks. *Neurosci. Res.* 51, 309–315.

Sales-Pardo, M., Guimera, R., Moreira, A. A., and Amaral, L. A. (2007). Extracting the hierarchical organization of complex systems. *Proc. Natl. Acad. Sci. U.S.A.* 104, 15224–15229.

Salvador, R., Suckling, J., Coleman, M. R., Pickard, J. D., Menon, D., and Bullmore, E. (2005). Neurophysiological architecture of functional magnetic resonance images of human brain. *Cereb. Cortex* 15, 1332–1342.

Shehzad, Z., Kelly, A. M., Reiss, P. T., Gee, D. G., Gotimer, K., Uddin, L. Q., Lee, S. H., Margulies, D. S., Roy, A. K., Biswal, B. B., et al. (2009). The resting brain: unconstrained yet reliable. *Cereb. Cortex* 19, 2209–2229.

Skudlarski, P., Jagannathan, K., Calhoun, V. D., Hampson, M., Skudlarska, B. A., and Pearlson, G. (2008). Measuring brain connectivity: diffusion tensor imaging validates resting state temporal correlations. *Neuroimage* 43, 554–561.

Smit, D. J., Stam, C. J., Posthuma, D., Boomsma, D. I., and de Geus, E. J. (2008). Heritability of "small-world" networks in the brain: a graph theoretical analysis of resting-state EEG functional connectivity. *Hum. Brain Mapp.* 29, 1368–1378.

Smith, S. M., Fox, P. T., Miller, K. L., Glahn, D. C., Fox, P. M., Mackay, C. E., Filippini, N., Watkins, K. E., Toro, R., Laird, A. R., et al. (2009). Correspondence of the brain's functional architecture during activation and rest. *Proc. Natl. Acad. Sci. U.S.A.* 106, 13040–13045.

Sporns, O., Chialvo, D. R., Kaiser, M., and Hilgetag, C. C. (2004). Organization, development and function of complex brain networks. *Trends Cogn. Sci. (Regul. Ed.)* 8, 418–425.

Sporns, O., Honey, C. J., and Kotter, R. (2007). Identification and classification of hubs in brain networks. *PLoS ONE* 2, e1049. doi:10.1371/journal.pone.0001049.

Sporns, O., Tononi, G., and Kotter, R. (2005). The human connectome: a structural description of the human brain. *PLoS Comput. Biol.* 1, e42. doi:10.1371/journal.pcbi.0010042.

Stam, C. J., Jones, B. F., Nolte, G., Breakspear, M., and Scheltens, P. (2007). Small-world networks and functional connectivity in Alzheimer's disease. *Cereb. Cortex* 17, 92–99.

Stam, C. J., and Reijneveld, J. C. (2007). Graph theoretical analysis of complex networks in the brain. *Nonlinear Biomed. Phys.* 1, 3. doi:10.1186/1753-4631-1-3

Supekar, K., Menon, V., Rubin, D., Musen, M., and Greicius, M. D. (2008). Network analysis of intrinsic functional brain connectivity in Alzheimer's disease. *PLoS Comput. Biol.* 4, e1000100. doi:10.1371/journal.pcbi.1000100.

Supekar, K., Musen, M., and Menon, V. (2009). Development of large-scale functional brain networks in children. *PLoS Biol.* 7, e1000157. doi:10.1371/journal.pbio.1000157.

Teipel, S. J., Bokde, A. L., Meindl, T., Amaro, E. Jr., Soldner, J., Reiser, M. F., Herpertz, S. C., Moller, H. J., and Hampel, H. (2010). White matter microstructure underlying default mode network connectivity in the human brain. *Neuroimage* 49, 2021–2032.

Uddin, L. Q., Kelly, A. M., Biswal, B. B., Margulies, D. S., Shehzad, Z., Shaw, D., Ghaffari, M., Rotrosen, J., Adler, L. A., Castellanos, F. X., and Milham, M. P. (2008). Network homogeneity reveals decreased integrity of default-mode network in ADHD. *J. Neurosci. Methods* 169, 249–254.

Uddin, L. Q., Kelly, A. M., Biswal, B. B., Xavier Castellanos, F., and Milham, M. P. (2009). Functional connectivity of default mode network components: correlation, anticorrelation, and causality. *Hum. Brain Mapp.* 30, 625–637.

Valencia, M., Pastor, M. A., Fernandez-Seara, M. A., Artieda, J., Martinerie, J., and Chavez, M. (2009). Complex modular structure of large-scale brain networks. *Chaos* 19, 023119.

van den Heuvel, M. P., Stam, C. J., Boersma, M., and Hulshoff Pol, H. E. (2008a). Small-world and scale-free organization of voxel-based resting-state functional connectivity in the human brain. *Neuroimage* 43, 528–539.

van den Heuvel, M., Mandl, R., and Hulshoff Pol, H. (2008b). Normalized cut group clustering of resting-state FMRI data. *PLoS ONE* 3, e2001. doi:10.1371/journal.pone.0002001.

van den Heuvel, M. P., Mandl, R. C., Kahn, R. S., and Hulshoff Pol, H. E. (2009a). Functionally linked resting-state networks reflect the underlying structural connectivity architecture of the human brain. *Hum. Brain Mapp.* 30, 3127–3141.

van den Heuvel, M. P., Stam, C. J., Kahn, R. S., and Hulshoff Pol, H. E. (2009b). Efficiency of functional brain networks and intellectual performance. *J. Neurosci.* 29, 7619–7624.

van de Ven, V. G., Formisano, E., Prvulovic, D., Roeder, C. H., and Linden, D. E. (2004). Functional connectivity as revealed by spatial independent component analysis of fMRI measurements during rest. *Hum. Brain Mapp.* 22, 165–178.

Wang, J., Wang, L., Zang, Y., Yang, H., Tang, H., Gong, Q., Chen, Z., Zhu, C., and He, Y. (2009a). Parcellation-dependent small-world brain functional networks: a resting-state fMRI study. *Hum. Brain Mapp.* 30, 1511–1523.

Wang, L., Zhu, C., He, Y., Zang, Y., Cao, Q., Zhang, H., Zhong, Q., and Wang, Y. (2009b). Altered small-world brain functional networks in children with attention-deficit/hyperactivity disorder. *Hum. Brain Mapp.* 30, 638–649.

Wang, L., Li, Y., Metzak, P., He, Y., and Woodward, T. S. (2010). Age-related changes in topological patterns of large-scale brain functional networks during memory encoding and recognition. *Neuroimage* 50, 862–872.

Watts, D. J., and Strogatz, S. H. (1998). Collective dynamics of 'small-world' networks. *Nature* 393, 440–442.

Wink, A. M., Bernard, F., Salvador, R., Bullmore, E. T., and Suckling, J. (2006). Age and cholinergic effects on hemodynamics and functional coherence of human hippocampus. *Neurobiol. Aging* 27, 1395–1404.

Yan, C., Liu, D., He, Y., Zou, Q., Zhu, C., Zuo, X., Long, X., and Zang, Y. (2009a). Spontaneous brain activity in the default mode network is sensitive to different resting-state conditions with limited cognitive load. *PLoS ONE* 4, e5743. doi:10.1371/journal.pone.0005743.

Yan, H., Zuo, X. N., Wang, D., Wang, J., Zhu, C., Milham, M. P., Zhang, D., and Zang, Y. (2009b). Hemispheric asymmetry in cognitive division of anterior cingulate cortex: a resting-state functional connectivity study. *Neuroimage* 47, 1579–1589.

Zalesky, A., Fornito, A., Harding, I. H., Cocchi, L., Yucel, M., Pantelis, C., and Bullmore, E. T. (2010). Whole-brain anatomical networks: does the choice of nodes matter? *Neuroimage* 50, 970–983.

Zang, Y., Jiang, T., Lu, Y., He, Y., and Tian, L. (2004). Regional homogeneity approach to fMRI data analysis. *Neuroimage* 22, 394–400.

Zang, Y., Yong, H., Chao-Zhe, Z., Qing-Jiu, C., Man-Qiu, S., Meng, L., Li-Xia, T., Tian-Zi, J., and Yu-Feng, W. (2007). Altered baseline brain activity in children with ADHD revealed by resting-state functional MRI. *Brain Dev.* 29, 83–91.

Zhang, D., and Raichle, M. E. (2010). Disease and the brain's dark energy. *Nat Rev Neurol* 6, 15–28.

Zou, Q. H., Zhu, C. Z., Yang, Y., Zuo, X. N., Long, X. Y., Cao, Q. J., Wang, Y. F., and Zang, Y. F. (2008). An improved approach to detection of amplitude of low-frequency fluctuation (ALFF) for resting-state fMRI: fractional ALFF. *J. Neurosci. Methods* 172, 137–141.

Zuo, X. N., Kelly, C., Adelstein, J. S., Klein, D. F., Castellanos, F. X., and Milham, M. P. (2010a). Reliable intrinsic connectivity networks: Test–retest evaluation using ICA and dual regression approach. *Neuroimage* 49, 2163–2177.

Zuo, X. N., Di Martino, A., Kelly, C., Shehzad, Z. E., Gee, D. G., Klein, D. F., Castellanos, F. X., Biswal, B. B., and Milham, M. P. (2010b). The oscillating brain: complex and reliable. *Neuroimage* 49, 1432–1445.

Conflict of Interest Statement: The authors declare that the research was conducted in the absence of any commercial or financial relationships that could be construed as a potential conflict of interest.

Received: 04 February 2010; paper pending published: 27 February 2010; accepted: 11 May 2010; published online: 07 June 2010.

*Citation: Wang J, Zuo X and He Y (2010) Graph-based network analysis of resting-state functional MRI. Front. Syst. Neurosci. **4**:16. doi: 10.3389/fnsys.2010.00016*

frontiers in
SYSTEMS NEUROSCIENCE

METHODS ARTICLE
published: 06 August 2010
doi: 10.3389/fnsys.2010.00034

A novel model-free data analysis technique based on clustering in a mutual information space: application to resting-state fMRI

Simon Benjaminsson[1,4], Peter Fransson[2,4]* and Anders Lansner[1,3,4]

[1] *Royal Institute of Technology, Stockholm, Sweden*
[2] *Department of Clinical Neuroscience, Karolinska Institute, Stockholm, Sweden*
[3] *Stockholm University, Stockholm, Sweden*
[4] *Stockholm Brain Institute, Stockholm, Sweden*

Edited by:
Lucina Q. Uddin, Stanford University, USA

Reviewed by:
Vince D. Calhoun, University of New Mexico, USA
Martin McKeown, The University of British Columbia, Canada

****Correspondence:***
Peter Fransson, Department of Clinical Neuroscience, Karolinska Institute, S-171 77 Stockholm, Sweden.
e-mail: peter.fransson@ki.se

Non-parametric data-driven analysis techniques can be used to study datasets with few assumptions about the data and underlying experiment. Variations of independent component analysis (ICA) have been the methods mostly used on fMRI data, e.g., in finding resting-state networks thought to reflect the connectivity of the brain. Here we present a novel data analysis technique and demonstrate it on resting-state fMRI data. It is a generic method with few underlying assumptions about the data. The results are built from the statistical relations between all input voxels, resulting in a whole-brain analysis on a voxel level. It has good scalability properties and the parallel implementation is capable of handling large datasets and databases. From the mutual information between the activities of the voxels over time, a distance matrix is created for all voxels in the input space. Multidimensional scaling is used to put the voxels in a lower-dimensional space reflecting the dependency relations based on the distance matrix. By performing clustering in this space we can find the strong statistical regularities in the data, which for the resting-state data turns out to be the resting-state networks. The decomposition is performed in the last step of the algorithm and is computationally simple. This opens up for rapid analysis and visualization of the data on different spatial levels, as well as automatically finding a suitable number of decomposition components.

Keywords: data analysis, resting-state, functional magnetic resonance imaging, clustering, mutual information, parallel algorithm

INTRODUCTION

Conventional methodology of fMRI analysis has favored model-based approaches, where the fMRI signal is correlated with an estimated functional response model or where a statistical comparison between the control and activated states is performed (Chuang et al., 1999). The prime example is the general linear model used in the popular software packages SPM (Friston et al., 1995) and FSL (Smith et al., 2004). The construction and parametric fitting of a model inevitably involves limitations stemming from the adopted assumptions. Consequently, the analysis and its outcomes are restricted with respect to feasible experimental conditions and the complexity of the estimated response signals (Chuang et al., 1999).

On the other hand, the model-free approach provides scope for unsupervised, purely data-driven, and bias-free ways of investigating neuroimaging data. Its potential lies in the concept of exploratory multivariate search for specific signal features without imposing rigid limitations on their spatio-temporal form. Thus, since no assumed model of functional response is needed, more complex experimental paradigms and non-standard fMRI activation patterns can be studied.

One such non-standard fMRI experiment is the study of so-called resting-state networks. These originate from the fluctuations in brain activity when the subject is at rest and are thought to reflect the underlying connectivity of the brain (Smith et al., 2009). There have been a number of model-free methods suggested for this type of fMRI data analysis, where we distinguish between three different classes of methods below.

First, independent component analysis (ICA) is commonly used in fMRI data analysis and it assumes a predefined number of components of the activity patterns to be linearly statistically independent (McKeown et al., 1998). Also, to cope with the computational complexity the dimensionality of the input data is typically reduced by PCA (Beckmann et al., 2005). Second, in various partial correlation whole-brain analysis methods and seed voxel-based methods (Salvador et al., 2005), a number of areas of the brain are specified and correlations between these are calculated. Clustering can then be performed on the correlation relations between these small numbers of areas. Third, in clustering techniques, a predefined number of clusters are adapted to the data according to some statistical distance metric (Chuang et al., 1999), either directly on the input data (Golland et al., 2008) or on the frequency spectra (Mezer et al., 2009).

The method presented here uses a general statistical dependency measure, mutual information, to create distance relations between voxels. Contrary to a covariance measure it also takes higher-order statistics into account, which is important in certain applications

(Hinrichs et al., 2006). Using multidimensional scaling (MDS), the voxels can be put in a lower-dimensional space, with their positions based on the distance relations. Clustering in this space can find the strong statistical regularities in the data. As seen in Section "Results", on resting-state data this will turn out to be the resting-state networks.

We do not assume a predefined number of clusters, or components. Similarly to the partial correlation methods, the clustering is performed after the statistics have been calculated. But instead of reducing the computational complexity by specifying a number of areas and thus decreasing the dimensions to perform the correlation analysis over, the whole-brain analysis is over all input voxels. This is similar to approaches where graphs are constructed from region of interest (ROI)-activities (Salvador et al., 2007). But where these are typically built up from a small number of regions, in our case each voxel is one region. A reduction of the data dimension is done by the MDS step after all statistical dependencies have been calculated; when the data clearly shows what statistical relations are strong. The resulting reduced matrix allows for rapid decomposition and exploration of the statistics of the dataset on multiple spatial scales.

The computational demands from using all voxels are coped with by a parallel implementation, which allows us to handle large data sizes and datasets. The parallelization of a run on a database, e.g., a collection of datasets, can be viewed on two different levels. Firstly, all parts of the algorithm have been parallelized. In this way, to handle a dataset with greater resolution or more time steps will only need more memory and compute power, such as a larger computer cluster. No additional changes to the underlying algorithm are needed. Secondly, the statistics for each individual dataset in a database can be run independently and then combined with other datasets via the generated distance matrices. Depending on the data source and what we are interested in, we may combine them in different ways. Since we for multiple datasets are combining the relations between the voxels, the individual datasets can come from different data sources, such as different studies or even different domains. This is contrary to methods that work on the absolute values.

In this paper, the proposed method is evaluated on a previously published functional MRI dataset acquired during rest in 10 subjects (Fransson, 2006). A large number of decompositions are created; one is selected, visualized, and compared to other resting-state studies. We show how the method also finds other dependencies in the data and how it can be applied to study hierarchical topology of resting-state networks in the human brain.

METHOD

ALGORITHM

We start by giving a step-by-step account for the mutual-information based clustering algorithm on fMRI data, illustrated in **Figure 1**. The distances between all voxels according to a distance measure determined by the mutual information is calculated from the input data. Multidimensional scaling is used to create a map from the distances, reflecting how different voxels are related in a mutual information-determined space. Clusters in this space correspond to high statistical regularities. To derive the positions of all voxels in this space is a computationally expensive operation, while the exploration of the structure of the space is computationally inexpensive. This opens up for rapid visualization of the statistics on different spatial scales. For multiple datasets from different subjects or/and from different domains, the distance matrices can be combined.

Distance matrix

Mutual information is used as a general dependence measure between input voxels i and j,

$$I_{ij} = \sum_{k \in i} \sum_{l \in j} p_{kl} \log \frac{p_{kl}}{p_k p_l}. \quad (1)$$

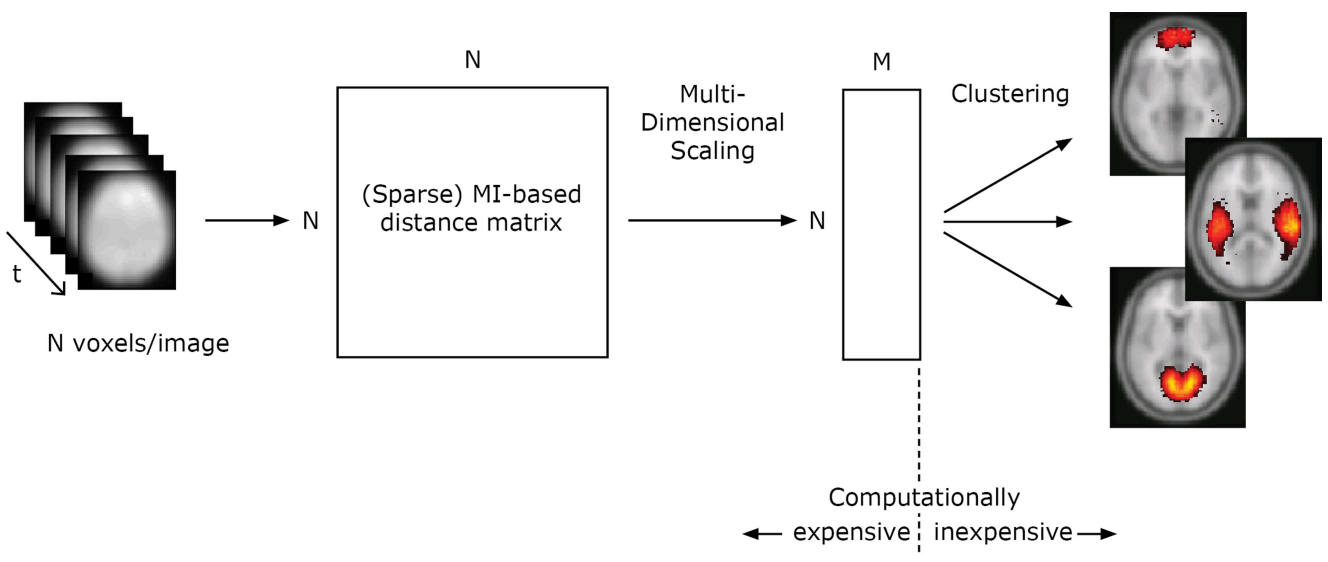

FIGURE 1 | Illustration of the algorithm for one dataset. In this study (Section "Results"), the total number of voxels in each timestep $N = 121247$ and M was set to 50. The distance matrices from 10 different datasets are combined using an average operation.

The values of the voxels are discretized by an interval code. The binning used for the interval code can be determined from a vector quantization run using the values of the dataset (as in Section "Clustering"). This will result in intervals adapted to the data, with more intervals where the distribution of values is dense and fewer where it is sparse.

The probabilities of certain values for a single voxel are estimated from the V image volumes as $p_k = 1/P \sum_{v=1}^{V} Y_k^V$ and $p_{kl} = 1/P \sum_{v=1}^{V} Y_k^V Y_l^V$. Y_k^V is set as a binary value in the interval k, but it could also have a continuous distribution. For value u_i of voxel i and value u_j of voxel j, p_k is the probability of u_i in the interval k, p_l is the probability of u_j in the interval l and p_{kl} is the probability of u_i in interval k and u_j in the interval l.

A distance measure in [0,1] is created from the mutual information (Kraskov and Grassberger, 2009) as

$D_{ij} = 1 - I_{ij}/J_{ij}$, where the joint entropy is used, $J_{ij} = -\sum_{k \in i} \sum_{l \in j} p_{kl} \log p_{kl}$.

The number of bins selected will have an effect on the resolution of the final result as visualized in **Figure 2**. A representative part of the distance matrix is shown for four different chosen numbers of intervals for the first subject in the dataset described in the Section "Experimental". The values have been thresholded at a distance of 0.9. A lower number of intervals will result in lower resolution of the distance matrix. The voxels with the strongest relations will still maintain a low distance between each other. A risk in using many bins is that the probabilities in the mutual information calculation are not calculated correctly because the sample size is small. The adaptive bin sizes used should handle this to some degree since it will result in few bins where the sample size is small.

Multidimensional scaling

The high-dimensional space given by the mutual information over all voxel values is reduced using metric multidimensional scaling (Young, 1985), where the statistical distance relations between the voxels from the distance matrix are used to build up a new, and lower-dimensional space still preserving the distance relations. Here, each voxel is represented by a point, initialized at a random position, and the optimization procedure aims to find a suitable set of positions by iteratively adjusting according to the distance relations by gradient descent until convergence: The difference in a Euclidean distance measure between a pair of voxels in the distance matrix and in their corresponding lower-dimensional space, the stress, was used as a target function to minimize.

Figure 3 shows the average stress for all voxel pairs after convergence for different selections of dimensions for the 60-bin distance matrix from one subject in the previous subsection. A low number of dimensions may have difficulties maintaining the distances in the new space, resulting in a high final stress. If a high enough dimensionality is selected little is gained by adding an additional dimension, seen by the low decrease in stress after 20 dimensions.

Clustering

The voxel positions in the M-dimensional space created from multidimensional scaling reflects the statistical regularities as described by the mutual information. Clustering in this space will join the voxels showing strong statistical dependency as they will have a short distance. We built a parallel implementation of the vector

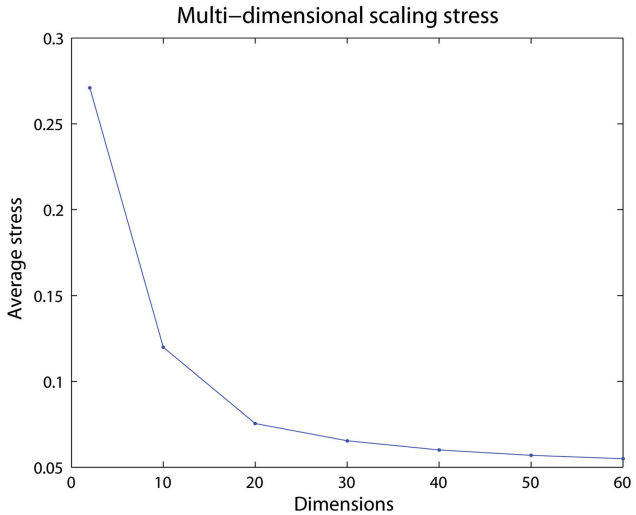

FIGURE 3 | The average stress for different number of dimensions. Here a selected dimensionality over 20 will only give small differences in how well the voxels in the created space are positioned.

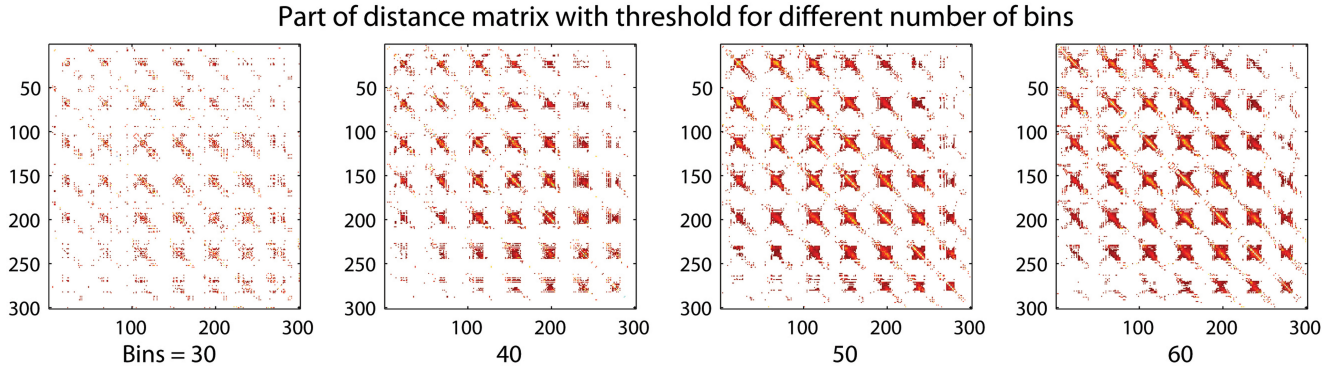

FIGURE 2 | A region of a distance matrix where 30, 40, 50, and 60 discretization intervals, or bins, in the mutual information calculation have been used. The number of bins changes the resolution of the result. A small number of bins still allow the strong relations to be captured.

quantization technique competitive selective learning (CSL) (Ueda and Nakano, 1994) both for the clustering into cluster components reflecting the strong statistical regularities and the interval coding division mentioned previously. However, any other clustering algorithm could have been used.

In the same way as traditional competitive learning, CSL uses voxel position x_i to update the position of the closest, by a Euclidean measure, cluster center y by

$$y = y + \varepsilon(x_i - y). \quad (2)$$

Here, ε determines the amount of change for the cluster center position in each iteration, and is typically gradually decreased during the training phase. In addition, CSL reinitializes cluster centers in order to avoid local minima using a selection mechanism according to the equidistortion principle (Ueda and Nakano, 1994).

The distortion measure gives an estimate of how well the cluster centers describe the original data. Using Euclidean distances, the distortion from one cluster center can be defined over all data points belonging to cluster center m as

$$D_m = \sum_{v \in m} || x_v - y ||. \quad (3)$$

A measure of the average distortion over all C cluster centers in the M-dimensional space, $D = 1/M \sum_{m=1}^{C} D_m$ (Ueda and Nakano, 1994), can be used to describe how suitable a given number of clusters are for the data distribution, as seen in the Section "Results".

INTEGRATING MULTIPLE DATASETS

The distance matrix is independent from the value distribution of the original data and the source of the data. Contrary to methods that work with the absolute values, using the relations allows us to combine distance matrices that could be from different datasets or even different data sources. Depending on what we want to evaluate, we can combine the individual distance matrices in various ways. For the multiple subject resting-state data in the Section "Results", we want to add together the individual results to get a more reliable averaged result. To this end, each distance matrix element was set to the average value over all the individual distance matrices. That is, each dataset was weighted the same. In other applications, where the individual datasets may have different sources, they could be weighted differently. Other operations could also be considered, i.e., a comparison between datasets could be implemented by a subtraction operation between distance matrices.

EXPERIMENTAL

MR DATA ACQUISITION AND DATA PRE-PROCESSING

Input to the algorithm consisted of 300 MR echo-planar image volumes sensitized to blood oxygenation level dependent (BOLD) signal changes acquired during 10 min of continuous rest (fixating on a cross-hair) in 10 subjects (Fransson, 2006). Functional MR images were acquired on a Signa Horizon Echospeed 1.5 Tesla General Electric MR scanner (FOV = 220 × 220 mm, 64 × 64 matrix size, TR/TE = 2000/40 ms, flip = 80°; number of slices = 29). Further details can be found in a previous paper by Fransson (2006). All images were realigned, normalized to the MNI template within SPM (Statistical Parametrical Mapping, Welcome Trust Center for Neuroimaging, London, Friston et al., 1995) and spatially smoothed with a FWHM = 12 mm. As a final pre-processing step, a rough cropping of the data was performed, for which the non-brain voxels were excluded from further analysis, removing 21% of the data and resulting in a total of 121247 brain voxels.

MR DATA ANALYSIS

For each of the 10 resting-state fMRI datasets the original voxel values were interval coded using vector quantization into 60 intervals based on the 1/3 first time steps. Separate distance matrices were calculated for all of the 10 subjects and combined by an average operation, where the mean was taken for each matrix element over all distance matrices. This resulted in a combined distance matrix of dimensions 121247 × 121247. Multidimensional scaling used the distance matrix to create a lower-dimensional map reflecting the statistical relations. In accordance with the discussion in Section "Multidimensional scaling" and **Figure 3**, the map dimension was set to a number that would clearly be able to maintain the distances in the new space, 50. This gave a total matrix size of 12147 × 50. The clustering algorithm was used to create all possible decompositions between 5 and 115 components. The distance determining which voxels should belong to a group when visualizing the results was specified by a threshold parameter set to 0.4. A voxel can belong to multiple components given the high-dimensional space. For instance, in some dimensions it could be close to one cluster and in others another.

RESULTS

Figure 4 shows the main results from applying the mutual-information based algorithm to the 10 resting-state fMRI datasets for 60 components. Apart from components that showed a very strong spatial resemblance to the patterns typically caused by cardio/respiratory pulsations, susceptibility-movement related effects, subject movements as well as components that were mainly located in cerebro-spinal fluid and white matter areas, 12 components showed connectivity patterns that were located in gray matter. **Figures 4A,B** show the resting-state networks typically associated with the left and right dorso-lateral parietal-frontal attention network, respectively. Further, **Figure 4C** shows a bilateral connectivity pattern that encloses the left and right auditory cortex whereas **Figure 4D** shows a resting-state network that includes the medial and lateral aspects of the sensorimotor cortex. The precuneus/posterior cingulate cortex together with the lateral parietal cortex and a small portion of the medial prefrontal cortex is included in the network shown in **Figure 4E**. The most anterior part of the medial prefrontal cortex is depicted in **Figure 4F**. The occipital cortex is by the algorithm divided into three sub-networks that encompasses the anterior/inferior (**Figure 4G**), posterior (**Figure 4H**) as well the primary visual cortex (**Figure 4K**). **Figure 4I** shows a network that includes the precuneus/posterior cingulate cortex, lateral parietal cortex as well as the medial prefrontal cortex. The network depicted in **Figure 4J** involves the bilateral temporal pole/insula region. Finally, the cerebellum was included in the network shown in **Figure 4L**.

NETWORKS AND SUB-NETWORKS

The distortion derived from the clustering algorithm can be used as a measure of how well various decompositions into resting-state networks suit the data. **Figure 5A** shows the mean

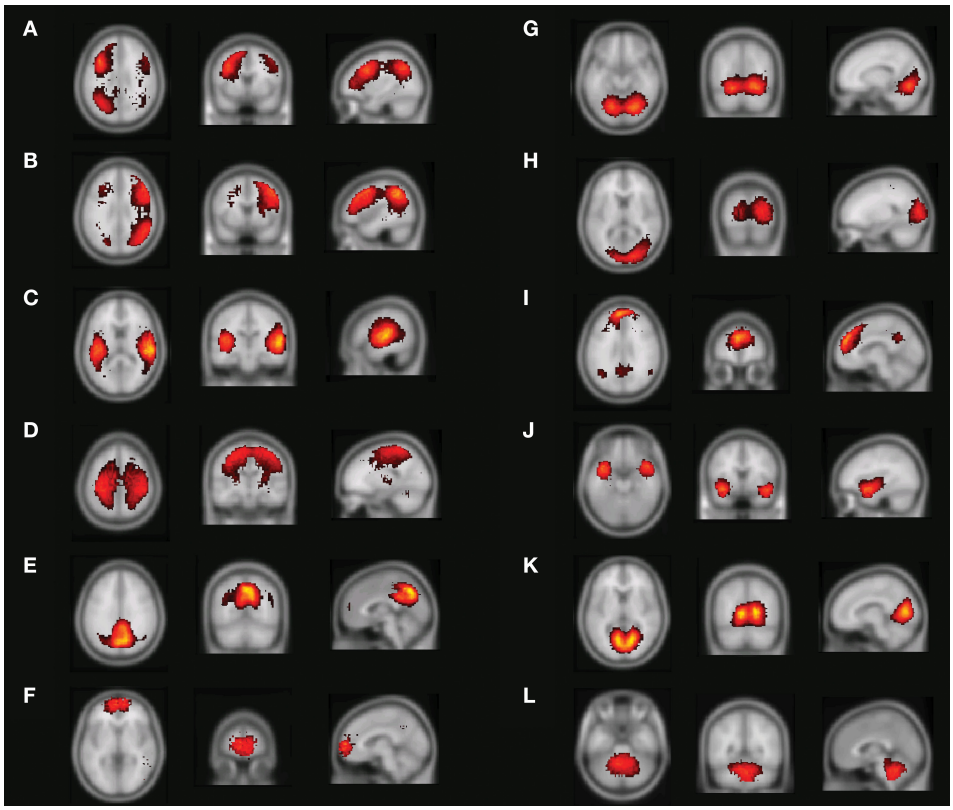

FIGURE 4 | Resting-state networks from a 60-part decomposition: (A, B) Left/right fronto-parietal attention network, (C) primary auditory cortex, (D) lateral and medial sensorimotor cortex, (E) posterior cingulate cortex/precuneus, (F) medial prefrontal cortex, (G) anterior/inferior visual cortex, (H) lateral/posterior visual cortex, (I) default network, (J) temporal pole/insula, (K) primary visual cortex (L), and the cerebellum. The color coding shows how far from the cluster center a given voxel is where brighter red-yellowness indicates a shorter distance to the cluster center.

distortion as defined in Section "Clustering" for each network in all decompositions between 5 and 115. The rapid decline for a small number of decompositions tells us that each addition of another cluster will explain the data better. The mean distortion is not changed as much after 30–40 clusters. Additional clustering will result in splitting of the statistically strong networks into their corresponding sub-networks.

Examples of this can be seen in **Figure 5B**. The left and right fronto-parietal attention networks are grouped together in the 40 clusters decomposition. At 60 they are separated into their left and right part. Increasing the number of clusters will result in further decomposition into their sub-networks as in the 80 decomposition. A similar splitting is seen for the default network.

COMPUTATIONAL COSTS

The calculation of the distance matrices is the computationally most expensive operation in the algorithm – when run on the entire dataset it scales with the number of voxels as N^2 and linearly with the number of time steps and individual datasets. The memory usage can be kept low also on much larger datasets than used here by treating the distance matrix as a sparse matrix in the parallel implementation. The calculation of a distance matrix is trivially parallelizable and involves no expensive communication between the nodes involved in the computation, contrary to parallel implementations of ICA (Keith et al., 2006).

For the resting-state data where the number of voxels was 121247, each distance matrix, one for each subject, took about 30 min to calculate on 512 nodes on a Blue Gene/L machine. However, they could have been run in parallel as each distance matrix is independent from the others. The iterative implementation of multidimensional scaling was run for about 4 h, until convergence. The MDS scales only with the number of voxels and dimensions of the resulting matrix, not with the number of datasets or time steps. These times could most likely be reduced significantly; both by optimizing the code and by considering alternative implementations of the algorithm steps.

The decomposition into different components or clusters is entirely separated from the calculation of the statistics, and since the matrix produced by the MDS is quite small, this is computationally an inexpensive step. All decompositions between 5 and 115 took about 1 h to create on 128 nodes. This is an advantage in certain applications over methods where the number of components to decompose the statistics into has to be manually predetermined. Computationally inexpensive decomposition allows for rapid visualization of the statistics on different spatial scales. Depending on what one is interested in, different decompositions may be of interest.

DISCUSSION

We have described a novel data-driven fMRI cluster analysis method based on multidimensional scaling and mutual information based clustering and shown its applicability for analysis of

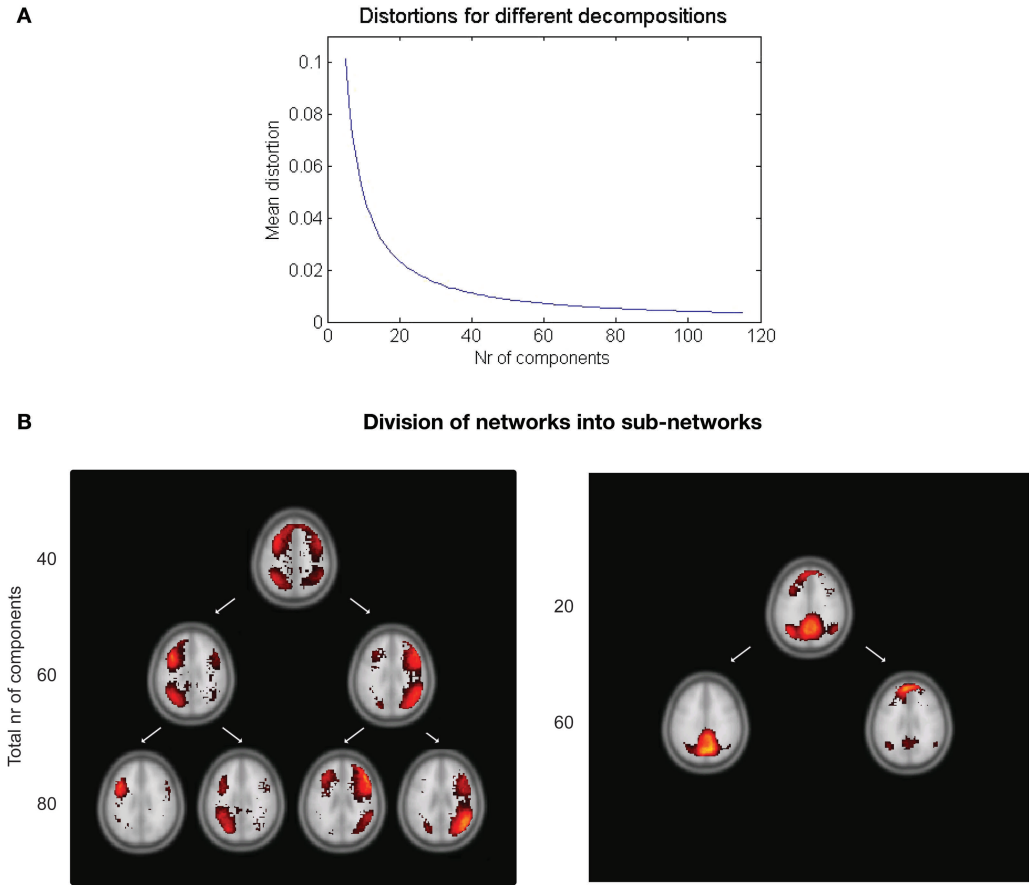

FIGURE 5 | (A) Mean distortion for various decompositions. The distortion measure can be used to predict a suitable number of clusters. **(B)** Example of the decomposition depending on the total number of clusters chosen. Left: The fronto-parietal attention networks shown in a 40, 60, and 80 decomposition. Right: A splitting of the default network occurs between the 20 and 60 decomposition.

multi-subject resting-state fMRI data sets. It is relevant to compare the present findings of resting-state networks driven by intrinsic BOLD signal changes during rest with previous investigations that have used other data-driven approaches. The studies of Beckmann et al. (2005), De Luca et al. (2006), and Damoiseaux et al. (2006) as well as the recent study by Smith et al. (2009) all used ICA based approaches to study resting-state functional connectivity, whereas the study by van den Heuvel et al. (2008) used an approach based on a normalized cut graph clustering technique.

On a general level, our results are in good agreement with the findings reported by all four previous investigations. The networks that covered the left and right fronto-parietal cortex (**Figures 4A,B**) were also detected by all previous investigations, although the left and right network was merged into a single network in the Beckmann et al.'s study (2005) (see also discussion below regarding merging/division of networks and its potential significance). Similarly, the networks that encompassed the auditory cortex (**Figure 4C**) and the sensorimotor areas (**Figure 4D**) showed a good spatial congruence with all four previously reported investigations. The network that foremost targeted the primary visual cortex (**Figure 4G**) shows a large degree of similarity to the networks shown by the De Luca, Damoiseaux, and Smith studies, whereas the primary visual cortex network was merged with the sensorimotor network in the van den Heuvel study (however, an additional explorative analysis revealed separate visual and motor networks, see van den Heuvel et al., 2008 for further information). The network that included the ventro-medial part of prefrontal cortex (**Figure 4F**) was apparent in all previous studies except the De Luca study. Further, the split of the occipital cortex into a lateral/posterior part (**Figure 4H**) and an inferior/anterior part (**Figure 4G**) was also detected by the recent Smith study, but the two networks were merged in a single network in the De Luca study. The network that involves the bilateral temporal pole/insula region (**Figure 4J**) was similarly detected in the Damoiseaux as well as in the van den Heuvel study. The cerebellar network (**Figure 4L**) was also found in the Smith study whereas the default mode network (DMN) (**Figure 4I**) has been reported by all four previous investigations. Finally, the network depicted in **Figure 4E** that encloses the posterior part of the default network was also found in the van den Heuvel study.

An important aspect of our methodology to cluster the data into resting-state networks and noise-related components is the distortion quantity that provides a measure of how well a specific cluster decomposition fits the data. By examining the degree of distortion as a function of the number of decompositions chosen, information regarding the topological hierarchy of resting-state networks in the

brain can be obtained. In the present analysis, this was exemplified for the fronto-parietal network (**Figure 5B** left) as well as for the default network (**Figure 5B** right). Regarding the fronto-parietal attention network, previous studies using data-driven methods (De Luca et al., 2006) as well as ROI seed-region based investigations (Fox et al., 2005; Fransson, 2005) have described this collection of brain regions as a single network, whereas other studies have described the collection of the brain regions typically attributed to the fronto-parietal attention network as two separate, lateralized networks that are largely left–right mirrors of each other (Damoiseaux et al., 2006; van den Heuvel et al., 2008; Smith et al., 2009). Indeed, it has previously been noted that the fronto-parietal attention network is often bilaterally activated in tasks that require top–down modulated attention (Corbetta and Shulman, 2002) whereas a unilateral activation is commonly observed for tasks that contain elements of language (left) or pain/perception (right) (Smith et al., 2009). In addition, a recent study has shown that the left side of the fronto-parietal attention network (**Figures 4A and 5B**) is conjunctively activated by intrinsic, resting-state activity as well as for language related tasks (Lohmann et al., 2009). Taken together, these results speaks to the notion that there are aspects of attention-driven cognitive processes that involve both the left and right parts of the network, and at the same time, a left–right division of cognitive labor exist at a sublevel within the same network.

In a similar vein, we observed a putative division of the DMN into an anterior and posterior sub-network (**Figures 4E,I**), respectively. Similar to the division of the fronto-parietal network, the spatial separation of the DMN was not complete. A small degree of activity of the posterior part, e.g., the precuneus/PCC, is present in the anterior sub-default network (**Figure 4I**) and vice versa for the medial prefrontal cortex in the posterior sub-default network (**Figure 4E**). Our finding of a potential anterior/posterior topographical hierarchy are in line with previous reports that have suggested that the precuneus/PCC region constitute a network hub in the DMN (Buckner et al., 2008; Fransson and Marrelec, 2008) as well as the MPFC (Buckner et al., 2008). The cognitive interpretation of a putative anterior/posterior division of the DMN is at present not clear. Speculatively, the split of the DMN observed here could reflect the fact that the anterior sub-network of the DMN, including a hub in the MPFC, is tentatively preferentially more involved in the self-referential aspects of mental processing (Gusnard et al., 2001), whereas the posterior part in which the precuneus/PCC region acts as a hub is oriented towards tasks that contains elements of retrieval of episodic memory and recognition (Dörfel et al., 2009).

The method could be extended in various ways. The MDS step could be extended to better conserve non-linear relationships as in the Isomap algorithm (Tenenbaum et al., 2000). More explicit hierarchical clustering algorithms may be used to further characterize the statistical relationships between clusters of different spatial scales (Meunier et al., 2009). The resulting MDS matrix could also be studied by other means than clustering algorithms, such as using PCA. Measurements other than mutual information could be used to study other aspects of the data, such as causal relations as determined by Granger causality (Roebroeck et al., 2005). A change of statistical expression to evaluate would generally involve no more changes than replacing the calculation determining an element value in the distance matrix. The method described here was partly based on a cortical information processing model (Lansner et al., 2009) which also included a classification step. Incorporating classification as a final step in the method would make it a good candidate for applications such as "brain reading" (Eger et al., 2009).

CONCLUSION

The generic method proposed brings a number of new properties to a model-free analysis of fMRI data: The separation of the computationally demanding calculation of the statistics and the decomposition step, which is computationally inexpensive, allows for rapid visualization and exploration of the statistics on multiple spatial scales. Input data can be handled independently and weighted together in various ways depending on the application, both for data from different subjects and data from different sources. The algorithm has been implemented completely in parallel code; this means that we can calculate the statistics over all of the input data, without any dimensionality reduction, which allows for whole-brain analysis on a voxel level. It can handle datasets with large input sizes as well as large collections of datasets in databases. Some of its properties for exploratory data analysis and its applicability to fMRI have been demonstrated on resting-state data and shown to be in agreement with findings from studies using other methods.

Our method is generic and does not use any specific properties of fMRI data. It may therefore also be applicable to completely different kinds of data. We are currently exploring its use in, e.g., PET data analysis. It further remains to optimize the method, possibly taking advantage of GPU implementation of certain steps in the algorithm.

ACKNOWLEDGMENTS

This work was partly supported by grants from the Swedish Science Council (Vetenskapsrådet, VR-621-2004-3807; www.vr.se), the European Union (FACETS project, FP6-2004-IST-FETPI-015879; http://facets.kip.uni-heidelberg.de) and the Swedish Foundation for Strategic Research (through the Stockholm Brain Institute; www.stockholmbrain.se).

REFERENCES

Beckmann, C. F., DeLuca, M., Devlin, J. T., and Smith, S. M. (2005). Investigations into resting-state connectivity using independent component analysis. *Philos. Trans. R. Soc. Lond., B, Biol. Sci.* 360, 1001–1013.

Buckner, R. L., Andrews-Hanna, J. R. , and Schacter, D. L. (2008). The brain's default network: anatomy, function and relevance to disease. *Ann. N Y Acad. Sci.* 1, 1124–1138.

Chuang, K. H., Chiu, M. J., Lin, C. C., and Chen, J. H. (1999). Model-free functional MRI analysis using Kohonen clustering neural network and fuzzy C-means. *IEEE Trans. Med. Imaging* 18, 1117–1128.

Corbetta, M., and Shulman, G. M. (2002). Control of goal-driven and stimulus-driven attention in the brain. *Nat. Rev. Neurosci.* 3, 201–215.

Damoiseaux, J. S., Rombouts, S. A. R. B., Barkhof, F., Scheltens, P., Stam, C. J., Smith, S. M., and Beckmann, C. F. (2006). Consistent resting-state networks across healthy subjects. *Proc. Natl. Acad. Sci. U.S.A.* 103, 13848–13853.

De Luca, M., Beckmann, C. F., De Stefano, N., Matthews, P. M., and Smith, S. M. (2006). fMRI resting-state networks define modes of long-distance interactions in the human brain. *Neuroimage* 29, 1359–1367.

Dörfel, D., Werner, A., Schaefer, M., von Kummer, R., and Karl, A. (2009). Distinct brain networks in recognition memory share a defined region

in the precuneus. *Eur. J. Neurosci.* 30, 1947–1959.

Eger, E., Michel, V., Thirion, B., Amadon, A., Dehaene, S., and Kleinschmidt, A. (2009). Deciphering cortical number coding from human brain activity patterns. *Curr. Biol.* 19, 1608–1615.

Fox, M. D., Snyder, A. Z., Vincent, J. L., Corbetta, M., Van Essen, D. C., and Raichle, M. E. (2005). The human brain is intrinsically organized into dynamic, anticorrelated functional networks. *Proc. Natl. Acad. Sci. U.S.A.* 102, 9673–9678.

Fransson, P. (2005). Spontaneous low-frequency BOLD signal fluctuations – an fMRI investigation of the resting-state default mode of brain function hypothesis. *Hum. Brain Mapp.* 26, 15–29.

Fransson, P. (2006). How default is the default mode of brain function? Further evidence from intrinsic BOLD fluctuations. *Neuropsychologia* 44, 2836–2845.

Fransson, P., and Marrelec, G. (2008). The precuneus/posterior cingulate cortex plays a pivotal role in the default network. Evidence from a partial correlation network analysis. *Neuroimage* 42, 1178–1184.

Friston, K. J., Holmes, A. P., Worsley, K. J., Poline, J. P., Frith, C. D., and Frackowiak, R. S. J. (1995). Statistical parametric maps in functional imaging: a general linear approach. *Hum. Brain Mapp.* 2, 189–210.

Gusnard, D. A., Akbudak, E., Shulman, G. L., and Raichle, M. E. (2001). Medial prefrontal cortex and self-referential mental activity: relation to a default mode of brain function. *Proc. Natl. Acad. Sci. U.S.A.* 98, 4259–4264.

Golland, Y., Golland, P., Bentin, S., and Malach, R. (2008). Data-driven clustering reveals a fundamental subdivision of the human cortex into two global systems. *Neuropsychologia* 46, 540–553.

Hinrichs, H., Heinze, H. J., and Schoenfeld, M. A. (2006). Causal visual interactions as revealed by an information theoretic measure and fMRI. *Neuroimage* 31, 1051–1060.

Keith, D. B. Hoge, C. C. Frank, R. M., and Malony, A. D. (2006). Parallel ICA methods for EEG neuroimaging. *Parallel and Distributed Processing Symposium*, 10–20.

Kraskov, A., and Grassberger, P. (2009). MIC: mutual information based hierarchical clustering. Inform. *Theory Stat. Learn*. 101–123.

Lansner, A., Benjaminsson, S., and Johansson, C. (2009). "From ANN to biomimetic information processing," in *Studies in Computational Intelligence* 188, eds A. Gutierrez and S. Marco. (Heidelberg: Springer Berlin), 33–43.

Lohmann, G., Hoehl, S., Brauer, J., Danielmeier, C., Bornkessel-Schlesewsky, I., Bahlmann, J., Turner, R., and Friederici, A. (2009). Setting the frame: the human brain activates a basic low-frequency network for language processing. *Cereb. Cortex,* PMID 19783579.

McKeown, M. J., Makeig, S., Brown, G. G., Jung, T.-P., Kindermann, S. S., Bell, A. J., and Sejnowski, T. J. (1998). Analysis of fMRI data by blind separation into independent spatial components. *Hum. Brain Mapp.* 6, 160–188.

Meunier, D., Lambiotte, R., Fornito, A., Ersche, K., and Bullmore, E. T. (2009). Hierarchical modularity in human brain functional networks. *Front. Neuroinform.* 3, 37. doi:10.3389/neuro.11.037.2009.

Mezer, A., Yovel, Y., Pasternak, O., Gorfine, T., and Assaf, Y. (2009). Cluster analysis of resting-state fMRI time series. *Neuroimage* 45, 1117–1125.

Roebroeck, A., Formisano, E., and Goebel, R. (2005). Mapping directed influence over the brain using granger causality and fMRI. *Neuroimage* 25, 230–242.

Salvador, R., Martínez, A., Pomarol-Clotet, E., Sarró, S., Suckling, J., and Bullmore, E. (2007). Frequency based mutual information measures between clusters of brain regions in functional magnetic resonance imaging. *Neuroimage* 35, 83–88.

Salvador, R., Suckling, J., Coleman, M. R., Pickard, J. D., Menon, D., and Bullmore, E. (2005). Neurophysiological architecture of functional magnetic resonance images of human brain. *Cereb. Cortex* 15, 1332–1342.

Smith, S. M., Fox, P. T., Miller, K. L., Glahn, D. C., Fox, P. M., Mackay, C. E., Filippini, N., Watkins, K. E., Toro, R., Laird, A. R., and Beckmann, C. F. (2009). Correspondence of the brain's functional architecture during activation and rest. *Proc. Natl. Acad. Sci. U.S.A.* 106, 13040–13045.

Smith, S. M., Jenkinson, M., Woolrich, M., Beckmann, C., Behrens, T., Johansenberg, H., Bannister, P., DeLuca, M., Drobnjak, I., and Flitney, D. (2004). Advances in functional and structural MR image analysis and implementation as FSL. *Neuroimage* 23, 208–219.

Tenenbaum, J. B., Silva, V., and Langford, J. C. (2000). A global geometric framework for nonlinear dimensionality reduction. *Science* 290, 2319–2323.

Ueda, N., and Nakano, R. (1994). A new competitive learning approach based on an equidistortion principle for designing optimal vector quantizers. *Neural Networks* 7, 1211–1227.

van den Heuvel, M., Mandl, R., and Hulshoff Pol, H. (2008). Normalized cut group clustering of resting-state fMRI data. *PLoS One* 3, e2001. doi:10.1371/journal.pone.0002001.

Young, F. W. (1985). "Multidimensional scaling," in *Encyclopedia of Statistical Sciences*, *Vol. 5*, eds S. Kotz, N. L. Johnson, and C. B. Read (New York, NY: Wiley), 649–659.

Conflict of Interest Statement: The authors declare that the research was conducted in the absence of any commercial or financial relationships that could be construed as a potential conflict of interest.

Received: 18 December 2009; paper pending published: 25 March 2010; accepted: 18 June 2010; published online: 06 August 2010.
*Citation: Benjaminsson S, Fransson P and Lansner A (2010) A novel model-free data analysis technique based on clustering in a mutual information space: application to resting-state fMRI. Front. Syst. Neurosci. **4**:34. doi: 10.3389/fnsys.2010.00034*

frontiers in
SYSTEMS NEUROSCIENCE

METHODS ARTICLE
published: 17 June 2010
doi: 10.3389/fnsys.2010.00024

Using coherence to measure regional homogeneity of resting-state fMRI signal

Dongqiang Liu[1], Chaogan Yan[1], Juejing Ren[1], Li Yao[1], Vesa J. Kiviniemi[2] and Yufeng Zang[1]*

[1] *State Key Laboratory of Cognitive Neuroscience and Learning, Beijing Normal University, Beijing, China*
[2] *Department of Diagnostic Radiology, Oulu University Hospital, Oulu, Finland*

Edited by:
Lucina Q. Uddin, Stanford University, USA

Reviewed by:
Yihong Yang, National Institutes of Health, USA
Michael Milham, New York University Langone Medical Center, USA

****Correspondence:***
Yufeng Zang, State Key Laboratory of Cognitive Neuroscience and Learning, Beijing Normal University, Beijing 100875, People's Republic of China.
e-mail: zangyf@bnu.edu.cn

In this study, we applied coherence to voxel-wise measurement of regional homogeneity of resting-state functional magnetic resonance imaging (RS-fMRI) signal. We compared the current method, regional homogeneity based on coherence (Cohe-ReHo), with previously proposed method, ReHo based on Kendall's coefficient of concordance (KCC-ReHo), in terms of correlation and paired *t*-test in a large sample of healthy participants. We found the two measurements differed mainly in some brain regions where physiological noise is dominant. We also compared the sensitivity of these methods in detecting difference between resting-state conditions [eyes open (EO) vs. eyes closed (EC)] and in detecting abnormal local synchronization between two groups [attention deficit hyperactivity disorder (ADHD) patients vs. normal controls]. Our results indicated that Cohe-ReHo is more sensitive than KCC-ReHo to the difference between two conditions (EO vs. EC) as well as that between ADHD and normal controls. These preliminary results suggest that Cohe-ReHo is superior to KCC-ReHo. A possible reason is that coherence is not susceptible to random noise induced by phase delay among the time courses to be measured. However, further investigation is still needed to elucidate the sensitivity and specificity of these methods.

Keywords: resting-state fMRI, local feature, regional homogeneity, coherence

INTRODUCTION

Biswal et al. (1995) found that during rest, low-frequency (0.01–0.08 Hz) fluctuations in blood oxygenation level-dependent (BOLD) signal are highly synchronous throughout the sensorimotor cortex. Since then, resting-state fMRI (RS-fMRI) has gained increasing popularity, particularly in recent years. In addition to the motor network, a multitude of functional systems have been examined using RS-fMRI approaches, including visual (Lowe et al., 1998), auditory (Cordes et al., 2001), emotional (Lowe et al., 1998), attentional (Fox et al., 2006), language (Hampson et al., 2002), reading (Koyama et al., 2010) and default mode (Greicius et al., 2003) networks.

The vast majority of RS-fMRI studies have adopted functional connectivity to examine their data, i.e. investigating temporal relationships between fluctuations observed in spatially distinct brain regions. However, functional connectivity provides little information about local features of spontaneous brain activity observed in individual regions, as the methods employed are typically relational. Several existing local measurements are complementary to functional connectivity approaches. For example, regional homogeneity (ReHo) (Zang et al., 2004) measures the similarity or synchronization of timeseries of nearest neighboring voxels (usually 27 voxels). It has been shown that the major regions of DMN have higher ReHo than other brain regions during resting state (Long et al., 2008). In addition, ReHo method has been applied to the detection of local abnormality in some brain disorders, e.g., attention deficit hyperactivity disorder (ADHD) (Cao et al., 2006), Alzheimer's disease (He et al., 2007), depression (Yuan et al., 2008), Parkinson disease (Wu et al., 2009), and autism (Paakki et al., 2010).

The previous ReHo method uses Kendall's coefficient of concordance (KCC) (Kendall and Gibbons, 1990) (KCC-ReHo) to measure the local synchronization of timeseries. KCC is based on temporal information (particularly rank information) of timeseries. However, the KCC value of timeseries will be reduced if there is time lag among the timeseries even though they share similar shapes. Coherence is a method for measuring synchronization in frequency domain. One characteristic of coherence is that it is insensitive to phase variability across measured timeseries. In an event-related study (Sun et al., 2004), coherence was used to measure the functional connectivity between remote brain regions. They proposed that coherence was more suitable when phase difference varied largely across brain regions (Miezin et al., 2000; Saad et al., 2001), as coherence should be less sensitive to such variability. To the best of our knowledge, coherence has not been used to measure local synchronization of BOLD signal. The aim of the current study was to use coherence-based ReHo (Cohe-ReHo) to measure the local synchronization of RS-fMRI signal. We investigated the consistency between Cohe-ReHo and KCC-ReHo from the following aspects:

(1) It has been reliably shown that the KCC-ReHo was higher in the major regions of DMN than in other brain areas (Long et al., 2008). We predicted that Cohe-ReHo value in these regions was also higher than other brain regions;
(2) Since both Cohe-ReHo and KCC-ReHo measure local synchronization, the two measurements would be highly correlated in most brain areas across participants;

(3) However, correlation analysis is not effective enough to characterize the difference between these two methods. Paired *t*-test was performed between these two measurements to reveal their difference (Zuo et al., 2010);
(4) Eyes open (EO) and eyes closed (EC) are two resting conditions. A few studies have reported differences between EO and EC in some brain regions including the visual area (Marx et al., 2003; Yang et al., 2007), the auditory cortex (Marx et al., 2003), and DMN (Yan et al., 2009). Therefore, we are interested in which of the two measurements is more sensitive to the differences between EO and EC.
(5) To examine which of the two measurements is more sensitive to abnormal local activity, we applied KCC-ReHo and Cohe-ReHo to detect differences between ADHD patients and normal controls.

MATERIALS AND METHODS

PARTICIPANTS AND DATA ACQUISITION

Dataset-1 and Dataset-2

From our previous large resting-state fMRI dataset[1] (See also Biswal et al., 2010), we chose 80 right-handed healthy participants (aged 18–26 years, 40 females). Participants with head motion larger than 3 mm or 3° in any of the 6 parameters were not included (See Data preprocessing). Written informed consent was obtained from each participant. This study was approved by the Institutional Review Board of Beijing Normal University Imaging Center for Brain Research. For validation purpose in the correlation analysis and paired *t*-test between methods, the 80 participants were randomly divided into two groups (Dataset-1 and Dataset-2), each containing 40 (20 females) participants, matched for their age and IQ. The participants lay supine with the head snugly fixed by straps and foam pads to minimize head movement. A SIEMENS 3T Trio scanner was used. Functional images were obtained using an echo-planar imaging sequence with the following parameters: 33 axial slices, thickness/gap = 3.0/0.6 mm, in-plane resolution = 64 × 64, TR = 2000 ms, TE = 30 ms, flip angle = 90°, FOV = 200 × 200 mm^2. During RS-fMRI scanning, participants were instructed to keep as motionless as possible, to keep their eyes closed, not to think of anything in particular, and not to fall asleep. In addition, a T1-weighted sagittal three-dimensional magnetization-prepared rapid gradient echo (MP-RAGE) sequence was acquired, covering the entire brain: 128 slices, TR = 2530 ms, TE = 3.39 ms, slice thickness = 1.33 mm, flip angle = 7°, inversion time = 1100 ms, FOV = 256 × 256 mm^2, and in-plane resolution = 256 × 192.

Dataset-3

Dataset-3 was from a study of within-group design (Zou et al., 2009). Twenty healthy right-handed participants (10 males and 10 females, 18- to 24-years old) underwent two RS-fMRI conditions, eyes open (EO) and eyes closed (EC). The order of the two conditions was counterbalanced across participants (See details in Zou et al., 2009). Written informed consent was obtained from each participant. This study was approved by the Institutional Review Board of Beijing Normal University Imaging Center for Brain Research. The participants lay supine with the head snugly fixed by straps and foam pads to minimize head movement. During resting-state scanning, participants were instructed to keep as motionless as possible with eyes closed for EC condition or open (with no fixation) for EO condition, not to think of anything in particular and not to fall asleep. The parameters for functional images and structural images were the same as Dataset-1 and Dataset-2 (Also see Zou et al., 2009 for detailed parameters).

Dataset-4

Dataset-4 was from a study of between-group design (Cao et al., 2009). Participants included 23 stimulant-naïve boys diagnosed with ADHD and 25 age-matched healthy boys. The participants were 11- to-16-years old. There were 19 participants in the ADHD group and 23 in the control group after excluding those who had excessive head motion (See Data Preprocessing). During resting-state scanning, participants were instructed to keep as motionless as possible with eyes closed, not to think of anything in particular and not to fall asleep. Images were acquired using a SIEMENS TRIO 3-Tesla scanner in the Institute of Biophysics, Chinese Academy of Sciences. The resting-state functional data was acquired using an echo-planar imaging sequence with the following parameters: 30 axial slices, TR = 2000 ms, TE = 30 ms, flip angle = 90°, thickness/skip = 4.5/0.0 mm, FOV = 220 × 220 mm^2, in-plane resolution = 64 × 64, 240 volumes. A high resolution T1-weighted anatomical image was acquired in a sagittal orientation using a spoiled gradient-recalled sequence covering the whole brain (See Cao et al., 2009 for detailed parameters).

DATA PROCESSING

Data preprocessing

The first 10 volumes of each session was discarded to make the longitudinal magnetization reach a steady state and for participants to get used to the scanning environment. Then slice timing, head motion correction, and spatial normalization were performed by statistical parametric mapping (SPM5)[2]. Linear trend removing and band-pass (0.01–0.08 Hz) filtering were performed by our built-in-lab software REST[3].

Algorithms

Cohe-ReHo analysis. The algorithm for calculating Cohe-ReHo included the following three steps:

Step 1: Power spectrum and cross spectrum estimation

For any two timeseries [e.g. $x(t)$ and $y(t)$] in a given cluster, we used Welch's modified periodogram averaging methods to estimate their power spectrums and cross spectrum: we divided each timeseries into N (here $N = 8$) segments of length T (here $T = 51$ time points, with 50% overlapping for neighboring segments) to make each segment approximately stationary. Because we focused on the low-frequency (0.01–0.08 Hz) components, the length of each segment should be more than 100s (0.01 Hz) to make the frequency resolution of power spectrum is high enough. To reduce the variance of power estimation, timeseries should be divided into as many segments as possible. Therefore we set the number of segments to be eight. Each resulting segment was then mean-centered and

[1]http://www.nitrc.org/projects/fcon_1000

[2]http://www.fil.ion.ucl.ac.uk/spm

[3]http://www.restfmri.net

weighted by a Hanning window of the same length to reduce spectrum leakage caused by segmentation (Welch, 1967). We estimated cross spectrum of timeseries $x(t)$ and $y(t)$:

$$\hat{f}_{xy}^{(T)}(\lambda) = \frac{1}{N}\sum_{n=1}^{N} X_n^{(T)}(\lambda)\cdot Y_n^{*(T)}(\lambda) \quad (1)$$

where $X_n^{(T)}(\lambda)$ is the discrete Fourier transform of the n_{th} segment of timeseries $x(t)$. Likewise, we can estimate the power spectrums of timeseries $x(t)$ and $y(t)$, respectively:

$$\hat{f}_{x}^{(T)}(\lambda) = \frac{1}{N}\sum_{n=1}^{N} |X_n^{(T)}(\lambda)|^2 \quad (2)$$

Step 2: Estimation of coherence across low-frequency band

For timeseries $x(t)$ and $y(t)$ in Step 1, we estimated their coherence across the low-frequency (0.01–0.08 Hz) band with their band-averaged estimates of the cross spectrum and power spectrums (Andrew and Pfurtscheller, 1996):

$$\hat{C}oh_{xy}(\bar{\lambda}) = \frac{|\sum_{\lambda}\hat{f}_{xy}(\bar{\lambda})|^2}{\sum_{\lambda}\hat{f}_{x}(\bar{\lambda})\cdot\sum_{\lambda}\hat{f}_{y}(\bar{\lambda})} \quad (3)$$

Step 3: Calculation of the Cohe-ReHo within the given cluster

To assess the overall synchronization within that cluster, we averaged the $\hat{C}oh_{xy}(\bar{\lambda})$ across all pairs of voxels in that cluster:

$$\bar{Coh} = \frac{2}{K(K-1)}\sum_{x=1}^{K-1}\sum_{y=x+1}^{K}\hat{C}oh_{xy}(\bar{\lambda}) \quad (4)$$

where K is the number of voxels within a cluster (here $K = 27$, one center voxel plus the number of its neighbors), and $\hat{C}oh_{xy}(\bar{\lambda})$ is the band-averaged coherence estimated in Step 2. We assigned the averaged coherence coefficient $\bar{Coh}$ of the cluster to its center voxel to represent Cohe-ReHo of the cluster.

An individual Cohe-ReHo map was obtained in a voxel-wise way. The Cohe-ReHo program was coded in MATLAB (The MathWorks, Inc., Natick, MA, USA).

KCC-ReHo analysis. Kendall's coefficient of concordance (KCC) was calculated to measure the KCC-based ReHo of timeseries of voxels within a cluster,

$$W = \frac{\sum_{i=1}^{n}(R_i)^2 - n(\bar{R})^2}{\frac{1}{12}K^2(n^3-n)} \quad (5)$$

where W is KCC among timeseries of given voxels, ranging from 0 to 1; R_i is the sum rank of the i_{th} time point; $\bar{R}$ is the mean of the R_is; K is number of voxels within measured cluster (here $K = 27$, one center voxel plus the number of its neighbors); n is the number of ranks (here $n = 230$ time points). The KCC value was assigned to the center voxel of this cluster. The individual KCC-ReHo map was obtained in a voxel-wise way for all dataset groups. The procedures for KCC-ReHo analysis were performed by REST.

STATISTICAL ANALYSIS

Before statistical analysis, an intersection brain mask was made for each dataset by using all individual spatially normalized EPI images of each dataset and an intracranial mask in REST. These intersection masks would be used for standardization purpose (See below) because the 33 axial slices do not cover the whole brain for some of the adult participants. The individual ReHo maps were smoothed with a Gaussian kernel of 6 mm full width at half-maximum (FWHM). In previous studies (e.g., Long et al., 2008), the KCC-ReHo value was standardized by being divided by the global mean. This procedure was the same as that in PET studies (Raichle et al., 2001). However, it has been recently suggested that transformation into standard Z value (subtracting the global mean, then being divided by standard deviation. See Zuo et al., 2010) improved the normality of distribution. Accordingly, we transformed Cohe-ReHo and KCC-ReHo value into Z value for each dataset by using its own intersection mask. The term "global" in the following text will be constrained in each intersection mask. For multiple comparison correction, Monte Carlo simulation was performed by AlphaSim command in AFNI (Cox, 1996).

One-sample t-tests

To test which brain areas have significantly higher Cohe-ReHo or KCC-ReHo value than global mean, one-sided one-sample t-tests were performed on the Z maps in Dataset-1 and Dataset-2 separately. Voxels with p value less than 1.0×10^{-12} were considered significant.

Correlation analysis between Cohe-ReHo and KCC-ReHo

To test the similarity of Cohe-ReHo and KCC-ReHo maps, linear correlation analysis was performed in a voxel-wise way across participants. Considering that Z transformation might bias the correlation results, the linear correlation was performed on the original Cohe-ReHo and KCC-ReHo maps in Dataset-1 and Dataset-2.

Paired t-test: Cohe-ReHo vs. KCC-ReHo

Linear correlation can only measure the similarity between these two measurements. For a voxel, whether its Cohe-ReHo and KCC-ReHo values are highly correlated or not, the two measurements may have different proportion to their own global mean value. Hence, paired t-test was performed between Z score of Cohe-ReHo and KCC-ReHo maps for Dataset-1 and Dataset-2, respectively.

Paired t-tests: eyes open (EO) vs. eyes closed (EC)

Paired t-tests were performed on the Z maps to reveal the differences between EO and EC. The clusters with single voxel's p value less than 0.01 and cluster size greater than 1080 mm^3 were considered significantly different between conditions ($p < 0.05$, corrected). By visual inspection, we could find both consistency and discrepancy between the results of Cohe-ReHo and KCC-ReHo (See Results). To test if there is statistically significant difference in the sensitivity of the two measurements, we calculated the ratio of the two measurements for each participant. Then, paired t-test was performed on the ratio. Multiple comparison correction was constrained within

brain areas showing significant differences between EO and EC by either Cohe-ReHo or KCC-ReHo (i.e., conjunction map). For one voxel in the conjunction map, if (1) there was no significant difference in the ratio and (2) both methods detected between-conditions differences, we considered the two measurements were equally sensitive to the between-condition differences in this voxel. However, if the difference was significant, then we further compared the absolute value of *t* value for the two measurements, particularly, we considered the measurement whose absolute value of *t* value was larger was more sensitive than the other measurement at the given voxel.

Two-sample t-tests: ADHD vs. control participants

This procedure is almost the same as the between-condition paired *t*-tests mentioned above, except that two-sample *t*-tests between ADHD and control groups rather than paired *t*-tests between two conditions were performed. The clusters with single voxel's *p* value less than 0.05 and cluster size greater than 6075 mm^3 were considered significantly different between groups ($p < 0.05$, corrected). Accordingly, two-sample *t*-test on the ratio of Cohe-ReHo to KCC-ReHo was performed. The corresponding multiple comparison correction was constrained within the brain areas showing significant difference between ADHD and control groups by either Cohe-ReHo or KCC-ReHo (i.e., conjunction map).

RESULTS AND DISCUSSION

ONE-SAMPLE *t*-TESTS

Results of one-sample *t*-tests showed that the major regions of DMN (including posterior cingulate cortex/precuneus, medial prefrontal cortex and bilateral inferior parietal lobule) had higher Cohe-ReHo as well as KCC-ReHo than the global mean (**Figure 1**). The pattern of one-sample *t*-test results is highly consistent with our previous findings (Long et al., 2008). The results of Dataset-1 and Dataset-2 are quite similar.

The DMN is of particular interest because it was found that regions in DMN have significantly higher glucose metabolism than other brain regions (Raichle et al., 2001) and these regions show task-independent or task-unspecific deactivation in the goal directed tasks (Shulman et al., 1997; Binder et al., 1999; Mazoyer et al., 2001; McKiernan et al., 2003), suggesting these regions may have important function during resting state. The current results suggest that the higher metabolism in the major regions of DMN during resting state is associated with higher local synchronization of spontaneous activity.

CORRELATION ANALYSIS

The correlation coefficients between Cohe-ReHo and KCC-ReHo were quite high in most part of brain regions, suggesting that the two indices were very similar there (**Figure 2**). In the suprasellar cistern and ventricles, their correlation coefficients were relatively low compared with other brain areas. The two measurements of some voxels in the supersellar cistern even showed negative correlation. The lower correlation between the two measurements indicates that the physiological noise has different effects on different measurements.

PAIRED *t*-TEST BETWEEN COHE-ReHo AND KCC-ReHo

Paired *t*-test between Cohe-ReHo and KCC-ReHo demonstrated that the *Z* score of Cohe-ReHo was significantly greater than that of KCC-ReHo in some cisterns and ventricles, as well as a few regions

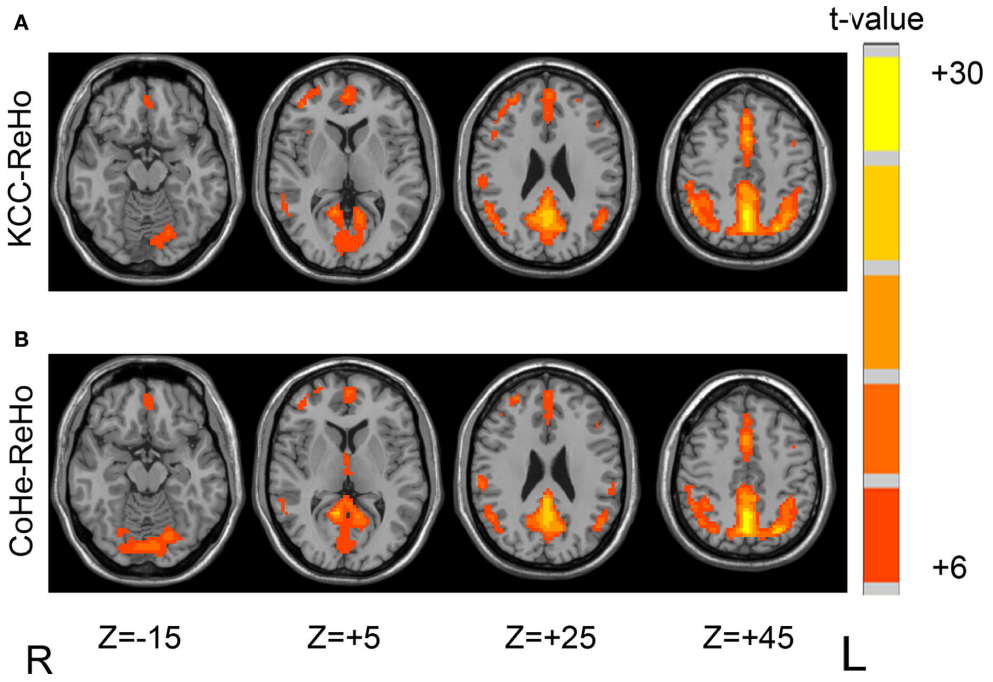

FIGURE 1 | One-sample *t*-test results of two methods on Dataset-1 showed that major regions of DMN had higher KCC-ReHo (A) and Cohe-ReHo (B) than the global mean. The left side of the image corresponds to the right side of brain.

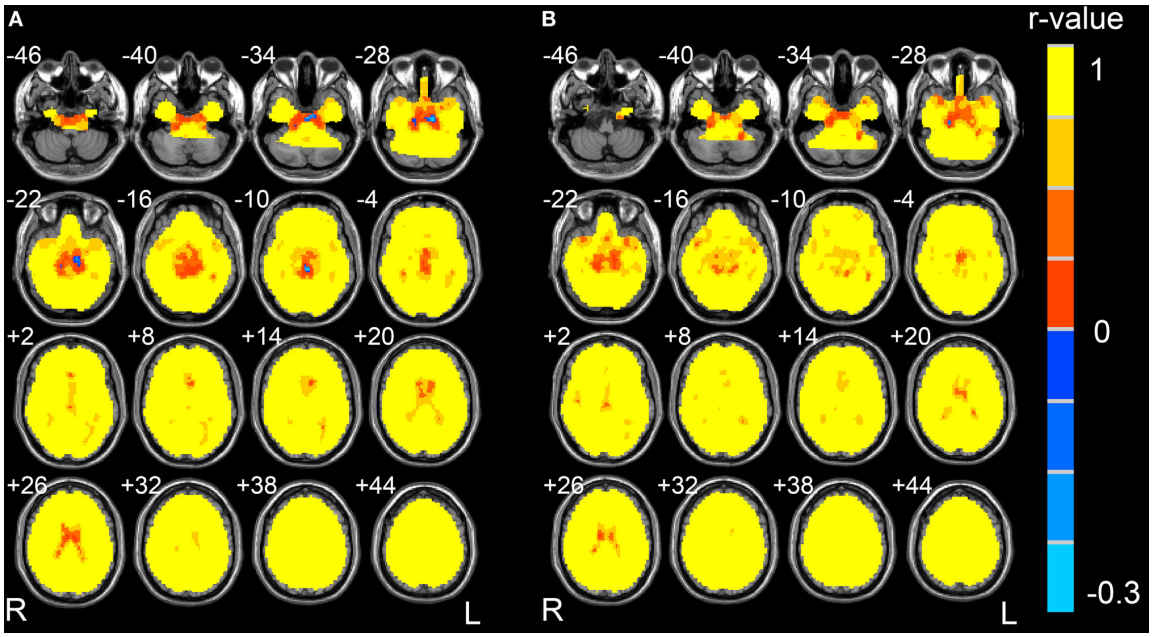

FIGURE 2 | Correlation map between Cohe-ReHo and KCC-ReHo of Dataset-1 (A) and Dataset-2 (B), respectively. The left side of the image corresponds to the right side of brain.

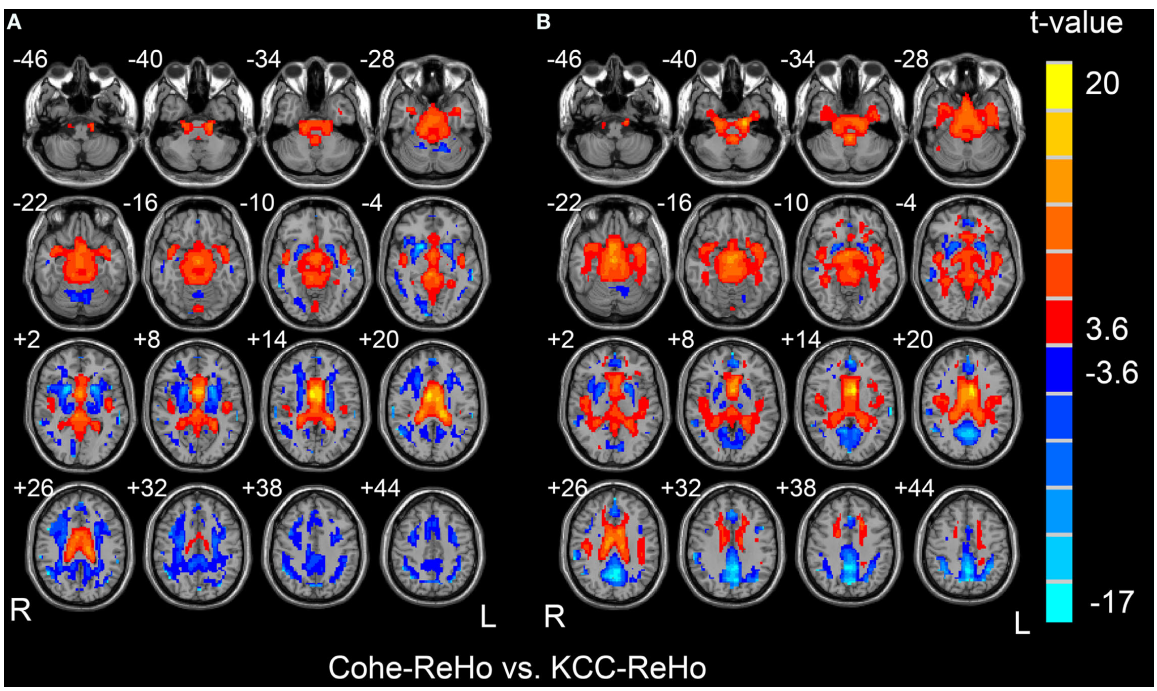

FIGURE 3 | Results of paired *t*-tests between *Z* maps of Cohe-ReHo and KCC-ReHo for Dataset-1 (A) and Dataset-2 (B). The left side of the image corresponds to the right side of brain.

in the white matter (**Figure 3**, $p < 0.05$, corrected). The Z score of Cohe-ReHo was significantly smaller than that of KCC-ReHo in a few regions in the white matter and gray matter. The results were very similar for the two datasets.

In the supersellar cisterns and ventricles, both linear correlation (See Section Correlation analysis) and paired t-test showed that Cohe-ReHo and KCC-ReHo were different from each other. All these results indicated that the physiological noise may have

different effects on the measurements. However, paired *t*-test showed that the two measurements were also significantly different in a few gray matter regions. It should be noted that, for the purpose of direct comparison between two measurements, we performed *Z* transformation to the two measurements previous to paired *t*-test. The *Z* score is a standardized value across brain. The difference shown by paired *t*-test is difference of the relative value against the global mean. Therefore, the difference found by paired *t*-test in the gray matter may be due to the fact that *Z* score is partially biased by the standardization procedure. Nevertheless, from different aspects, linear correlation and paired *t*-test revealed both similarity and discrepancy between the Cohe-ReHo and KCC-ReHo.

COMPARISON OF SENSITIVITY BETWEEN COHE-ReHo AND KCC-ReHo

Paired t-test results for Dataset-3

Paired t-test revealed that the Cohe-ReHo was significantly higher in the right middle occipital gyrus, anterior cingulate cortex (ACC), bilateral precuneus, bilateral middle frontal gyrus, bilateral inferior frontal gyrus, bilateral inferior parietal lobule, right superior frontal gyrus, and right caudate in EO resting state than in EC. It also revealed that Cohe-ReHo was significantly lower in the bilateral sensorimotor cortex, bilateral supplementary motor cortex, bilateral superior temporal gyrus, bilateral middle temporal gyrus, and bilateral thalamus in EO resting-state than in EC (**Figure 4**, $p < 0.05$, corrected). Paired t-test on KCC-ReHo maps yielded similar between-condition differences as on the Cohe-ReHo maps by visual inspection.

The brain areas showing significant between-condition differences by either Cohe-ReHo or KCC-ReHo were taken as a mask (i.e., conjunction mask). Then paired *t*-test was performed within this mask to reveal the differences of the ratio of Cohe-ReHo to KCC-ReHo between EO and EC resting states. Some of the brain areas in the conjunction mask showed significant difference on the ratio ($p < 0.05$, corrected) (See yellow and green color in **Figure 5**), indicating that the two measurements have significantly different sensitivity in detecting between-conditions differences. Taking paired *t*-test results by Cohe-ReHo (**Figure 4A**) and KCC-ReHo (**Figure 4B**) into account, it could be found that most of the areas showing significant difference on the ratio were significantly contributed by Cohe-ReHo (Yellow color in **Figure 5**). It means that, in these areas, the between-condition difference is significantly higher in Cohe-ReHo than in KCC-ReHo. Only a very small proportion was significantly contributed by KCC-ReHo (Green color in **Figure 5**). It could be concluded that Cohe-ReHo may be more sensitive to differences between EO and EC. One possible interpretation is that physiological noise may result in phase delay across time courses of the neighboring voxels in these brain areas. This phase delay may give rise to additional variance or "random noise", and hence reduce

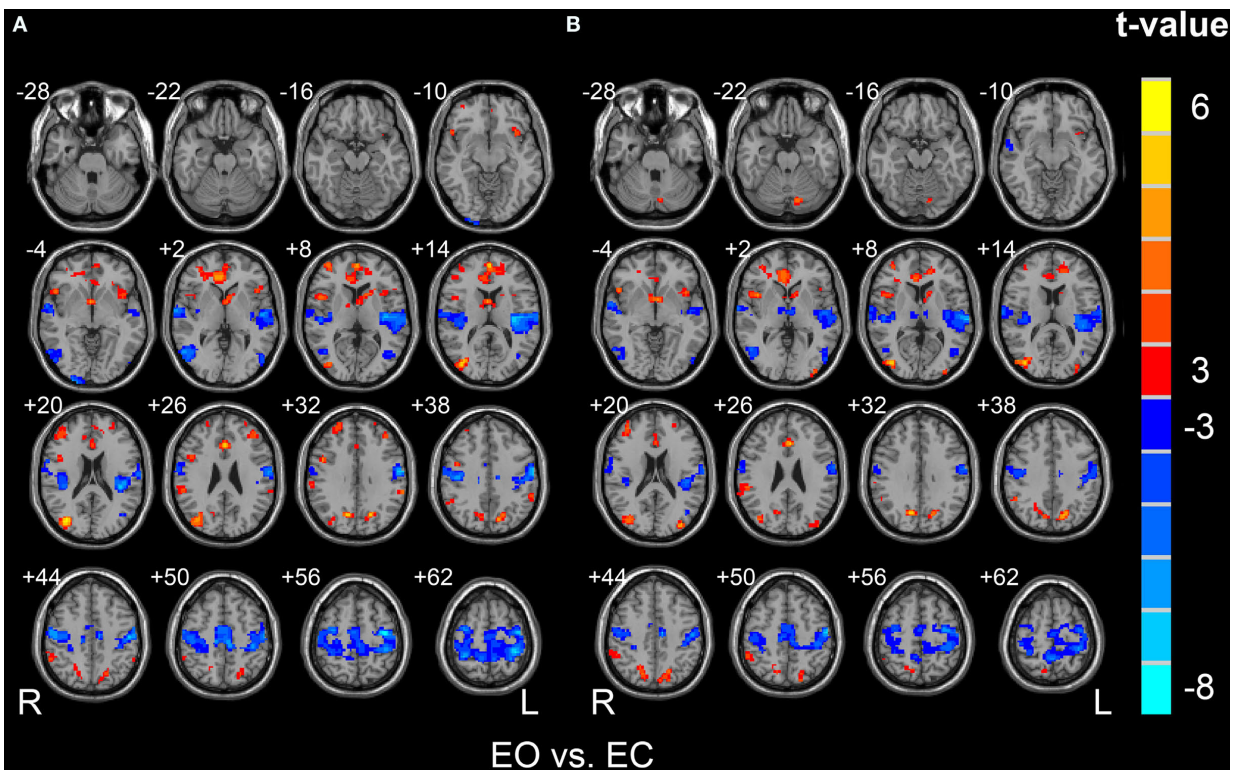

FIGURE 4 | Brain regions showing significantly different Cohe-ReHo (A) and KCC-ReHo (B) between EO and EC resting states. The left side of the image corresponds to the right side of brain.

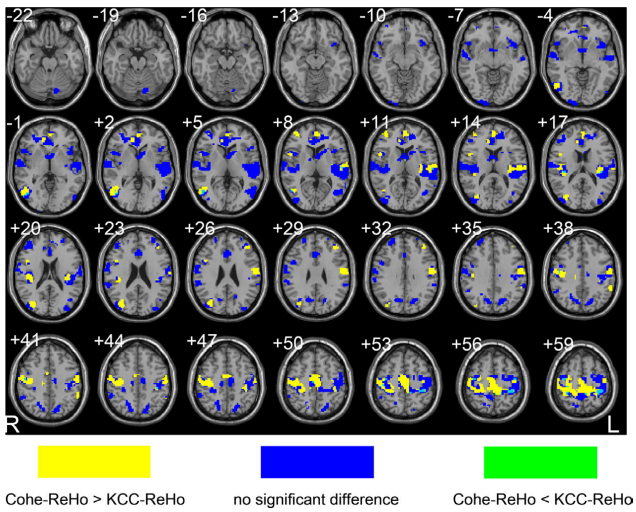

FIGURE 5 | Cohe-ReHo and KCC-ReHo have different sensitivity to the difference of local synchronization between EO and EC resting states. Yellow color means Cohe-ReHo is more sensitive than KCC-ReHo. The green color means the opposite. The blue color means that the two measurements have no significant differences in their sensitivity in detecting differences between EC and EO. The left side of the image corresponds to the right side of brain.

the possibility of difference between EO and EC resting states. However, this interpretation remains speculative and needs further investigation.

Two-sample t-test results for Dataset-4

In comparison with normal controls, the ADHD patients displayed significantly increased Cohe-ReHo in the bilateral lingual gyrus and decreased Cohe-ReHo in bilateral cerebellum and ventral ACC. Significantly increased KCC-ReHo was discovered in bilateral lingual gyrus and dorsal ACC and significantly decreased KCC-ReHo was found in bilateral cerebellum (**Figure 6**, $p < 0.05$, corrected). The pattern looks similar for the two measurements by visual inspection.

As did in the above section, to reveal the statistical difference between the sensitivity of these methods in detecting abnormal local synchronization of spontaneous activity, we performed two-sample *t*-test on the ratio map of Cohe-ReHo to KCC-ReHo. Multiple comparison correction was constrained in the conjunction map where significant differences between ADHD and control groups were found by either Cohe-ReHo or KCC-ReHo. In the right lingual gyrus and ventral ACC, Cohe-ReHo yielded more prominently between-group difference than KCC-ReHo (See yellow color in **Figure 7**). KCC-ReHo yielded almost no higher sensitivity than Cohe-ReHo. Although KCC-ReHo detected significantly between-group difference in the dorsal ACC but not Cohe-ReHo, their sensitivity in detecting abnormal local synchronization was not different enough to reach a significant level.

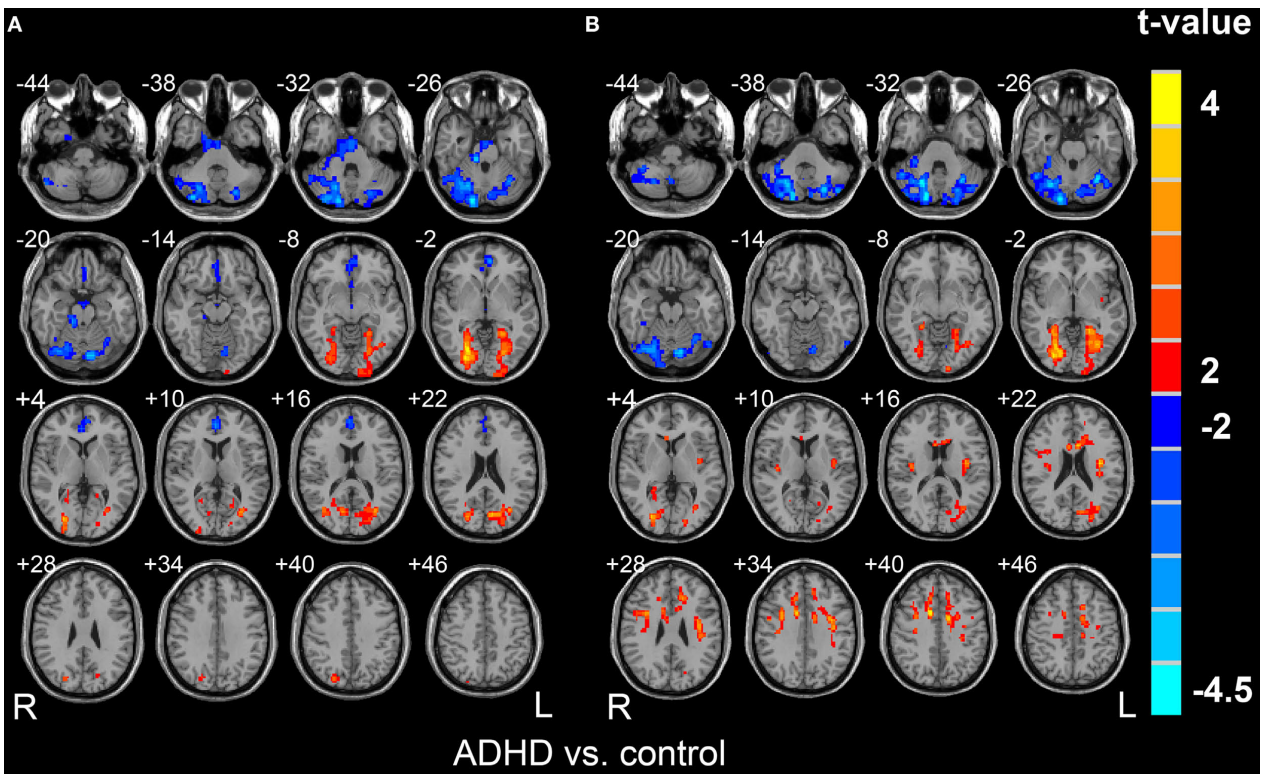

FIGURE 6 | Brain regions showing significantly different Cohe-ReHo (A) and KCC-ReHo (B) between ADHD group and control group ($p < 0.05$, corrected). The left side of the image corresponds to the right side of brain.

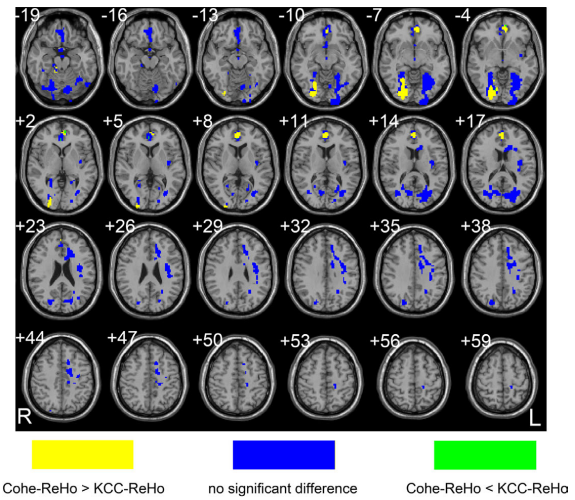

FIGURE 7 | Cohe-ReHo and KCC-ReHo had different sensitivity to the difference in local synchronization between ADHD and control groups. Yellow color means Cohe-ReHo is more sensitive than KCC-ReHo. The green color means the opposite direction. The blue color means that the two measurements have no significant difference in their sensitivity in detecting differences between the two groups. The left side of the image corresponds to the right side of brain.

SUMMARY

We applied coherence to measure the regional homogeneity or local synchronization of resting-state fMRI BOLD signal. Cohe-ReHo detected similar pattern of DMN as KCC-ReHo did. Results of correlation analysis and paired *t*-test between the two measurements indicated that physiological noise might have different effects on them. The results of between-condition paired *t*-test (EO vs. EC in Dataset 3) and between-group two-sample *t*-test (ADHD group vs. control group in Dataset 4) showed that Cohe-ReHo and KCC-ReHo yielded similar patterns. However, in-depth statistical comparison on the ratio of Cohe-ReHo to KCC-ReHo indicated that Cohe-ReHo is more sensitive to the differences of spontaneous activity between different conditions (EO vs. EC) and between different groups. One putative interpretation is that Cohe-ReHo is less susceptible to confounds from phase delay among time courses. However, we have not found an index to compare their specificity. Further investigation is necessary to elucidate their sensitivity and specificity.

ACKNOWLEDGMENTS

This work was supported by the NSFC (30770594, Chinese-Finnish NEURO Program 30621130074), the National High Technology Program of China (863 Project, No. 2008AA02Z405), and Program for Changjiang Scholars and Innovative Research Team in University (PCSIRT).

REFERENCES

Andrew, C., and Pfurtscheller, G. (1996). Event-related coherence as a tool for studying dynamic interaction of brain regions. *Electroencephalogr. Clin. Neurophysiol.* 98, 144–148.

Binder, J. R., Frost, J. A., Hammeke, T. A., Bellgowan, P. S., Rao, S. M., and Cox, R. W. (1999). Conceptual processing during the conscious resting state. A functional MRI study. *J. Cogn. Neurosci.* 11, 80–95.

Biswal, B., Yetkin, F. Z., Haughton, V. M., and Hyde, J. S. (1995). Functional connectivity in the motor cortex of resting human brain using echo-planar MRI. *Magn. Reson. Med.* 34, 537–541.

Biswal, B. B., Mennes, M., Zuo, X. N., Gohel, S., Kelly, C., Smith, S. M., Beckmann, C. F., Adelstein, J. S., Buckner, R. L., Colcombe, S., Dogonowski, A. M., Ernst, M., Fair, D., Hampson, M., Hoptman, M. J., Hyde, J. S., Kiviniemi, V. J., Kötter, R., Li, S. J., Lin, C. P., Lowe, M. J., Mackay, C., Madden, D. J., Madsen, K. H., Margulies, D. S., Mayberg, H. S., McMahon, K., Monk, C. S., Mostofsky, S. H., Nagel, B. J., Pekar, J. J., Peltier, S. J., Petersen, S. E., Riedl, V., Rombouts, S. A., Rypma, B., Schlaggar, B. L., Schmidt, S., Seidler, R. D., Siegle, G. J., Sorg, C., Teng, G. J., Veijola, J., Villringer, A., Walter, M., Wang, L., Weng, X. C., Whitfield-Gabrieli, S., Williamson, P., Windischberger, C., Zang, Y. F., Zhang, H. Y., Castellanos, F. X., and Milham, M. P. (2010). Toward discovery science of human brain function. *Proc. Natl. Acad. Sci. U.S.A.* 107, 4734–4739.

Cao, Q., Zang, Y., Sun, L., Sui, M., Long, X., Zou, Q., and Wang, Y. (2006). Abnormal neural activity in children with attention deficit hyperactivity disorder: a resting-state functional magnetic resonance imaging study. *Neuroreport* 17, 1033–1036.

Cao, X., Cao, Q., Long, X., Sun, L., Sui, M., Zhu, C., Zuo, X., Zang, Y., and Wang, Y. (2009). Abnormal resting-state functional connectivity patterns of the putamen in medication-naive children with attention deficit hyperactivity disorder. *Brain Res.* 1303, 195–206.

Cordes, D., Haughton, V. M., Arfanakis, K., Carew, J. D., Turski, P. A., Moritz, C. H., Quigley, M. A., and Meyerand, M. E. (2001). Frequencies contributing to functional connectivity in the cerebral cortex in "resting-state" data. *AJNR Am. J. Neuroradiol.* 22, 1326–1333.

Cox, R. W. (1996). AFNI: software for analysis and visualization of functional magnetic resonance neuroimages. *Comput. Biomed. Res.* 29, 162–173.

Fox, M. D., Corbetta, M., Snyder, A. Z., Vincent, J. L., and Raichle, M. E. (2006). Spontaneous neuronal activity distinguishes human dorsal and ventral attention systems. *Proc. Natl. Acad. Sci. U.S.A.* 103, 10046–10051.

Greicius, M. D., Krasnow, B., Reiss, A. L., and Menon, V. (2003). Functional connectivity in the resting brain: a network analysis of the default mode hypothesis. *Proc. Natl. Acad. Sci. U.S.A.* 100, 253–258.

Hampson, M., Peterson, B. S., Skudlarski, P., Gatenby, J. C., and Gore, J. C. (2002). Detection of functional connectivity using temporal correlations in MR images. *Hum. Brain Mapp.* 15, 247–262.

He, Y., Wang, L., Zang, Y., Tian, L., Zhang, X., Li, K., and Jiang, T. (2007). Regional coherence changes in the early stages of Alzheimer's disease: a combined structural and resting-state functional MRI study. *Neuroimage* 35, 488–500.

Kendall, M., and Gibbons, J. D. (1990). *Rank Correlation Methods.* Oxford: Oxford University Press.

Koyama, M. S., Kelly, C., Shehzad, Z., Penesetti, D., Castellanos, F. X., and Milham, M. P. (2010). Reading networks at rest. *Cereb. cortex*. [Epub ahead of print].

Long, X. Y., Zuo, X. N., Kiviniemi, V., Yang, Y., Zou, Q. H., Zhu, C. Z., Jiang, T. Z., Yang, H., Gong, Q. Y., Wang, L., Li, K. C., Xie, S., and Zang, Y. F. (2008). Default mode network as revealed with multiple methods for resting-state functional MRI analysis. *J. Neurosci. Methods* 171, 349–355.

Lowe, M. J., Mock, B. J., and Sorenson, J. A. (1998). Functional connectivity in single and multislice echoplanar imaging using resting-state fluctuations. *Neuroimage* 7, 119–132.

Marx, E., Stephan, T., Nolte, A., Deutschlander, A., Seelos, K. C., Dieterich, M., and Brandt, T. (2003). Eye closure in darkness animates sensory systems. *Neuroimage* 19, 924–934.

Mazoyer, B., Zago, L., Mellet, E., Bricogne, S., Etard, O., Houde, O., Crivello, F., Joliot, M., Petit, L., and Tzourio-Mazoyer, N. (2001). Cortical networks for working memory and executive functions sustain the conscious resting state in man. *Brain Res. Bull.* 54, 287–298.

McKiernan, K. A., Kaufman, J. N., Kucera-Thompson, J., and Binder, J. R. (2003). A parametric manipulation of factors affecting task-induced deactivation in functional neuroimaging. *J. Cogn. Neurosci.* 15, 394–408.

Miezin, F. M., Maccotta, L., Ollinger, J. M., Petersen, S. E., and Buckner, R. L. (2000). Characterizing the hemodynamic response: effects of presentation rate, sampling procedure, and the possibility of ordering brain activity based on relative timing. *Neuroimage* 11, 735–759.

Paakki, J. J., Rahko, J., Long, X., Moilanen, I., Tervonen, O., Nikkinen, J., Starck, T., Remes, J., Hurtig, T., Haapsamo, H., Jussila, K., Kuusikko-Gauffin, S., Mattila, M. L., Zang, Y., and Kiviniemi, V. (2010). Alterations in regional homogeneity of resting-state brain activity in autism spectrum disorders. *Brain Res.* 1321, 169–179.

Raichle, M. E., MacLeod, A. M., Snyder, A. Z., Powers, W. J., Gusnard, D. A., and Shulman, G. L. (2001). A default mode of brain function. *Proc. Natl. Acad. Sci. U.S.A.* 98, 676–682.

Saad, Z. S., Ropella, K. M., Cox, R. W., and DeYoe, E. A. (2001). Analysis and use of FMRI response delays. *Hum. Brain Mapp.* 13, 74–93.

Shulman, G. L., Fiez, J. A., Corbetta, M., Buckner, R. L., Miezin, F. M., Raichle, M. E., and Petersen, S. E. (1997). Common blood flow changes across visual tasks: II. Decrease in cerebral cortex. *J. Cogn. Neurosci.* 9, 648–663.

Sun, F. T., Miller, L. M., and D'Esposito, M. (2004). Measuring interregional functional connectivity using coherence and partial coherence analyses of fMRI data. *Neuroimage* 21, 647–658.

Welch, P. D. (1967). The use of fast fourier transform for the estimation of power spectra: a method based on time averaging over short, modified periodograms. *IEEE Trans. Audio Electroacoust.* AU-15, 70–73.

Wu, T., Long, X., Zang, Y., Wang, L., Hallett, M., Li, K., and Chan, P. (2009). Regional homogeneity changes in patients with Parkinson's disease. *Hum. Brain Mapp.* 30, 1502–1510.

Yan, C. G., Liu, D. Q., He, Y., Zou, Q. H., Zhu, C. Z., Zuo, X. N., Long, X. Y., and Zang, Y. F. (2009). Spontaneous brain activity in the default mode network is sensitive to different resting-state conditions with limited cognitive load. *PLoS ONE* 4, e5743. doi:10.1371/journal.pone.0005743.

Yang, H., Long, X. Y., Yang, Y., Yan, H., Zhu, C. Z., Zhou, X. P., Zang, Y. F., and Gong, Q. Y. (2007). Amplitude of low frequency fluctuation within visual areas revealed by resting-state functional MRI. *Neuroimage* 36, 144–152.

Yuan, Y., Zhang, Z., Bai, F., Yu, H., Shi, Y., Qian, Y., Liu, W., You, J., Zhang, X., and Liu, Z. (2008). Abnormal neural activity in the patients with remitted geriatric depression: a resting-state functional magnetic resonance imaging study. *J. Affect. Disord.* 111, 145–152.

Zang, Y., Jiang, T., Lu, Y., He, Y., and Tian, L. (2004). Regional homogeneity approach to fMRI data analysis. *Neuroimage* 22, 394–400.

Zou, Q. H., Long, X. Y., Zuo, X. N., Yan, C. G., Zhu, C. Z., Yang, Y. H., Liu, D. Q., He. Y., and Zang, Y. F. (2009). Functional connectivity between the thalamus and visual cortex under eyes closed and eyes open conditions: a resting-state fMRI study. *Hum. Brain Mapp.* 30, 3066–3078.

Zuo, X. N., Di Martino, A., Kelly, C., Shehzad, Z. E., Gee, D. G., Klein, D. F., Castellanos, F. X., Biswal, B. B., and Milham, M. P. (2010). The oscillating brain: complex and reliable. *Neuroimage* 49, 1432–1445.

Conflict of Interest Statement: The authors declare that the research was conducted in the absence of any commercial or financial relationships that could be construed as a potential conflict of interest.

Received: 05 February 2010; paper pending published: 10 March 2010; accepted: 23 May 2010; published online: 17 June 2010.

*Citation: Liu D, Yan C, Ren J, Yao L, Kiviniemi VJ and Zang Y (2010) Using coherence to measure regional homogeneity of resting-state fMRI signal. Front. Syst. Neurosci. **4**:24. doi: 10.3389/fnsys.2010.00024*

frontiers in
SYSTEMS NEUROSCIENCE

METHODS ARTICLE
published: 14 May 2010
doi: 10.3389/fnsys.2010.00013

DPARSF: a MATLAB toolbox for "pipeline" data analysis of resting-state fMRI

Yan Chao-Gan* and Zang Yu-Feng*

State Key Laboratory of Cognitive Neuroscience and Learning, Beijing Normal University, Beijing, China

Edited by:
Lucina Q. Uddin, Stanford University, USA

Reviewed by:
Martin Walter, Otto-von-Guericke-Universität Magdeburg, Germany
Srikanth Ryali, Stanford University, USA

****Correspondence:***
Yan Chao-Gan, State Key Laboratory of Cognitive Neuroscience and Learning, Beijing Normal University, Beijing 100875, China.
e-mail: ycg.yan@gmail.com;
Zang Yu-Feng, State Key Laboratory of Cognitive Neuroscience and Learning, Beijing Normal University, Beijing 100875, China.
e-mail: zangyf@bnu.edu.cn

Resting-state functional magnetic resonance imaging (fMRI) has attracted more and more attention because of its effectiveness, simplicity and non-invasiveness in exploration of the intrinsic functional architecture of the human brain. However, user-friendly toolbox for "pipeline" data analysis of resting-state fMRI is still lacking. Based on some functions in Statistical Parametric Mapping (SPM) and Resting-State fMRI Data Analysis Toolkit (REST), we have developed a MATLAB toolbox called Data Processing Assistant for Resting-State fMRI (DPARSF) for "pipeline" data analysis of resting-state fMRI. After the user arranges the Digital Imaging and Communications in Medicine (DICOM) files and click a few buttons to set parameters, DPARSF will then give all the preprocessed (slice timing, realign, normalize, smooth) data and results for functional connectivity, regional homogeneity, amplitude of low-frequency fluctuation (ALFF), and fractional ALFF. DPARSF can also create a report for excluding subjects with excessive head motion and generate a set of pictures for easily checking the effect of normalization. In addition, users can also use DPARSF to extract time courses from regions of interest.

Keywords: data analysis, DPARSF, REST, resting-state fMRI, SPM

INTRODUCTION

Resting-state functional magnetic resonance imaging (fMRI) has been more and more widely used since Biswal et al. (1995) firstly reported the presence of spatially coherent activity in the resting-state blood oxygen level-dependent (BOLD) fMRI signal. Resting-state fMRI is considered as a powerful tool for investigating the spontaneous neuronal activity which consumes most of the brain's energy (Fox and Raichle, 2007). In addition, resting-state fMRI is also a convenient way for clinical studies since it has advantages of reasonable spatial and temporal resolution and non-invasiveness, as well as its simplicity that does not need to set complicated cognitive tasks.

Functional connectivity (FC) is widely used in resting-state fMRI studies (Biswal et al., 1995; Lowe et al., 1998; Xiong et al., 1999; Cordes et al., 2000; Greicius et al., 2003; Fox et al., 2005, 2006; Fransson, 2005; Vincent et al., 2006). While FC measures the signal synchrony among remote brain areas, the regional spontaneous activity could be examined by several metrics, such as the regional homogeneity (ReHo, Zang et al., 2004), the amplitude of low-frequency fluctuation (ALFF, Zang et al., 2007) and the fractional ALFF (fALFF, Zou et al., 2008). All the aforementioned methods could be calculated by a toolbox *Resting-State fMRI Data Analysis Toolkit*[1] (REST). As an easy-to-use MATLAB toolbox, REST is compatible with Statistical Parametric Mapping[2] (SPM). The data could be preprocessed by SPM and then entered into REST's analysis. Although SPM is a powerful tool, lots of complicated and time-consuming operations are needed when analyzing large sample data set. In SPM, the parameters need to be set step-by-step and subject-by-subject. These manual procedures may be time-consuming and may increase the possibility of inadvertent mistakes. Hence, user-friendly toolbox for "pipeline" data analysis of resting-state fMRI would be very necessary.

Here, we have developed a MATLAB toolbox called Data Processing Assistant for Resting-State fMRI (DPARSF) for "pipeline" data analysis of resting-state fMRI. DPARSF is based on some functions in SPM and REST. After the user arranges the Digital Imaging and Communications in Medicine (DICOM) files and click a few buttons to set parameters, DPARSF will then give all the preprocessed (slice timing, realign, normalize, smooth) data and results for FC, ReHo, ALFF, and fALFF. DPARSF can also create a report for excluding subjects with excessive head motion and generate a set of pictures for easily checking the effect of normalization. In addition, users also can use DPARSF to extract time courses from regions of interest.

PROCEDURE OF DPARSF

DPARSF is a user-friendly software. Popup tips tell users what will be done when clicking on the buttons (**Figure 1**). It was developed in MATLAB (MathWorks, Inc.). It is an open source package and designed to use existing routines in the MATLAB distribution with freely available toolbox SPM and our REST toolkit. Here, we will introduce the data analysis procedures of DPARSF in details.

CONVERT DICOM FILES TO NIfTI IMAGES

Most scanners produce data in DICOM format. Before data analysis, the DICOM format is usually transformed into other formats, e.g., Neuroimaging Informatics Technology Initiative (NIfTI) file format (Cox et al., 2004). NIfTI files contain affine coordinate definitions relating voxel index to spatial location, especially the

[1]http://www.restfmri.net

[2]http://www.fil.ion.ucl.ac.uk/spm

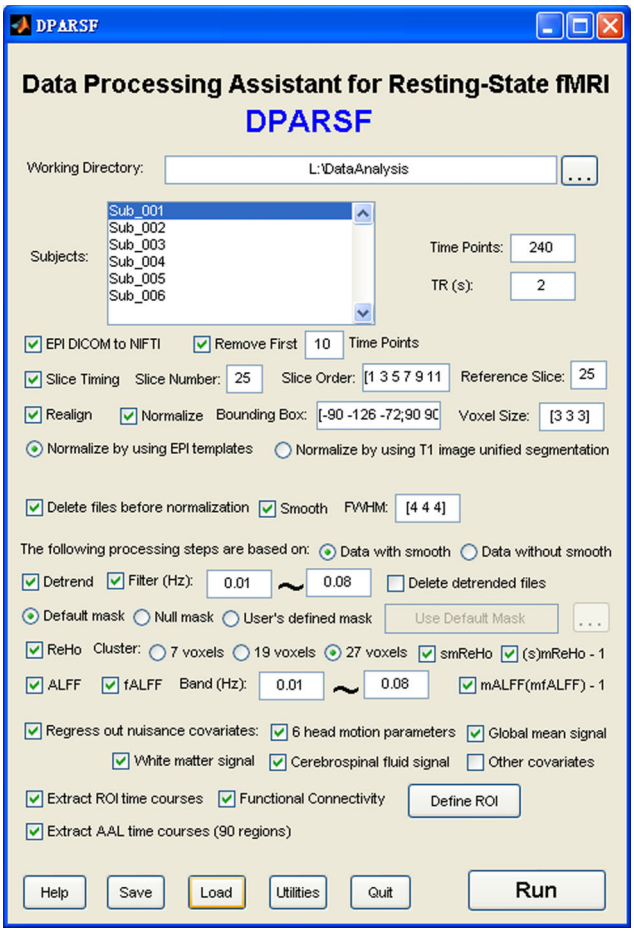

FIGURE 1 | Graphical user interface of DPARSF.

important information of left hemisphere and right hemisphere. If this converting option is checked, DPARSF will convert the data by calling dcm2nii in MRIcroN software[3]. If users have converted the data previously, this option is not needed.

REMOVE FIRST 10 (MORE OR LESS) TIME POINTS

The first few volumes of the functional images are often discarded for signal equilibrium and to allow the participants' adaptation to the scanning noise. If this option is checked, DPARSF will delete the specified number of time points for each participant.

SLICE TIMING

Most fMRI data are acquired using two-dimensional pulse sequences that acquire images one slice at a time, thus all slices are acquired at different time within a repeat time (TR). Timing differences are especially problematic for longer TR. Hence the differences in image acquisition time between slices need to be corrected. The number of slices, slice order and reference slice need to be specified, then DPARSF will do slice timing by calling functions in SPM.

[3]http://www.mricro.com

HEAD MOTION CORRECTION

The goal of motion correction is to adjust the time series of images so that the brain is in the same position in every image (Huettel et al., 2004). If this option is checked, the time-series of images will be motion-corrected by calling functions in SPM. Since excessive head motion may induce large artifact in fMRI time-series, participants with excessive head motion need to be excluded from further analysis. DPARSF will create a report of head motion based on the realign parameters estimated by SPM (as shown in "ExcludeSubjects.txt" in the "RealignParameter" directory).

NORMALIZATION

The brain size, shape, orientation, and gyral anatomy vary largely across participants. For inter-subject comparison to be feasible, the individual brain is usually transformed or spatially normalized into a standardized template. SPM provides two optional ways to normalize the functional images into the Montreal Neurological Institute (MNI) space: (1) using echo-planar imaging (EPI) template (Ashburner and Friston, 1999) and (2) using unified segmentation on T1 image (Ashburner and Friston, 2005). The latter way could improve the accuracy of spatial normalization (Ashburner and Friston, 2005) but is a little complicated in SPM. It contains three steps – coregistration, segmentation and writing normalization parameters. DPARSF has integrated these three steps into one. It's important to check the effect of normalization of each individual since some data may meet problem in normalization. DPARSF can generate a set of pictures (**Figure 2**) for easily checking the effect of normalization. It should be noted that DPARSF provides a very simple way for visual inspection. Users should check the effect of spatial normalization carefully.

SMOOTHING

Smoothing is used as a preprocessing step to suppress noise and effects due to residual differences in functional and gyral anatomy during inter-subject averaging. The most common smoothing technique is the Gaussian filter which has the shape of a normal distribution. DPARSF will smooth the data with the specified width at half of the maximum value (full-width-half-maximum, or FWHM) by calling functions in SPM.

REMOVE LINEAR TREAD

Long-term physiological shifts, movement related noise remaining after realignment or instrumental instability may contribute to a systematic increase or decrease in the signal with time (Turner et al., 1997; Lowe and Russell, 1999). The exact cause for the drift of the baseline signal is not completely understood (Smith et al., 1999), and how this structured trend affect further analysis is an interesting issue. If this option is checked, DPARSF will remove the systematic drift or trend using linear model as does in Analysis of Functional Neuroimage (AFNI) (Cox, 1996) by calling functions in REST.

FILTERING

Low frequency (0.01–0.08 Hz) fluctuations (LFFs) of the resting-state fMRI signal were reported to be of physiological importance (Biswal et al., 1995) and also were suggested to reflect spontaneous neuronal activity (Lu et al., 2007). Zuo et al. (2010) also reported low frequency oscillations (0.01–0.073 Hz) were primarily detected

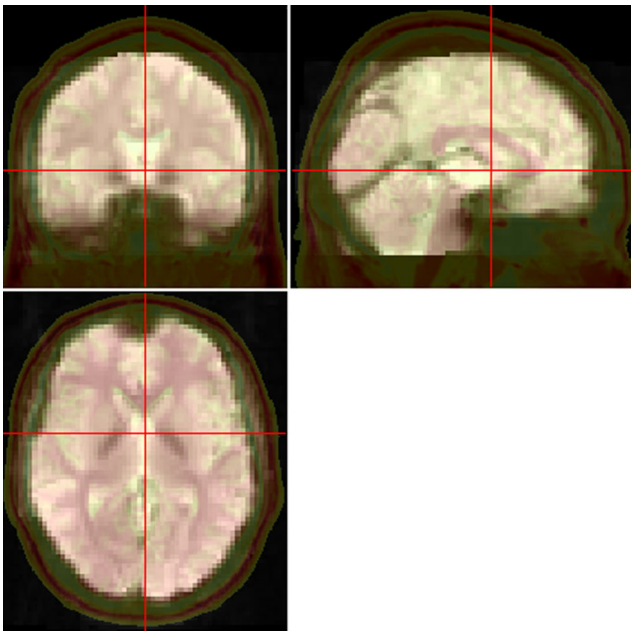

FIGURE 2 | Pictures for checking normalization. The normalized functional image was overlaid on a high resolution 3D anatomical image (the opaque one with skull. From "Colin Holmes," http://imaging.mrc-cbu.cam.ac.uk/downloads/Colin/, also distributed with MRIcroN as ch2) in the MNI space. Users can easily check the accuracy of spatial normalization by visual inspection.

within gray matter. In contrast, relatively high frequency oscillations (0.073–0.25) were primarily restricted to white matter. It's reported that respiratory and aliased cardiac signals fall in the range of relatively high frequency band (Cordes et al., 2001). Thus, the data is usually bandpass (e.g., 0.01–0.08 Hz) filtered to reduce the effect of very low frequency and high frequency physiological noise. Of note, the data should not to be filtered when calculating fALFF, because fALFF is a ratio of low frequency amplitude to full band amplitude. If this option is checked, DPARSF will filter the data by calling ideal filter functions in REST (which is in accordance with AFNI).

REGIONAL HOMOGENEITY

While FC analysis measures the signal synchrony of LFF activity among different brain areas, it does not provide information of regional spontaneous activity. The ReHo method (Zang et al., 2004), unlike the connectivity-based methods typically used in most resting-state fMRI studies, is suitable for exploring regional brain activity by examining the degree of regional synchronization of fMRI time courses. This is accomplished on a voxel-by-voxel basis by calculating Kendall's coefficient of concordance (KCC, Kendall and Gibbons, 1990) of time series of a given voxel with those of its nearest neighbors. A larger value of ReHo indicates a higher regional synchronization. In order to reduce the global effects of variability across participants, as did in PET studies (Raichle et al., 2001), the ReHo of each voxel was divided by the global mean ReHo value within the whole-brain mask (default brain mask provided in REST which was thresholded at 50% on the SPM5's *a priori* brain mask). It needs to be noted that, smoothing before ReHo calculation will largely increase the regional similarity. We recommend that the smoothing procedure is performed after ReHo calculation. However, it is still an open issue. If this option is checked, DPARSF will calculate ReHo and then smooth the ReHo results by calling functions in REST and SPM.

ALFF AND fALFF

The regional spontaneous activities can be examined by the ALFF. Biswal et al. (1995) found that the root mean square of the LFF in the white matter was reduced by about 60% relative to the gray matter. The power spectrum of the LFF (equivalent to the square of the ALFF) has been used to indicate the magnitude of neural activity (Kiviniemi et al., 2000; He et al., 2007; Hoptman et al., 2010; Zhang et al., in press). However, it has been shown that ALFF is significantly higher than the global mean ALFF in cisterns and vicinity of large blood vessels (Zang et al., 2007). That was apparently induced by the large fluctuations of high frequency physiological noise. Thus an improved measure fALFF (Zou et al., 2008) is defined as the ratio of total amplitude within the low-frequency range (0.01–0.08 Hz) to the total amplitude of the entire detectable frequency range. It was found that fALFF can better reveal the default mode network (DMN) within groups (i.e., by one-sample *t*-test). However, which of the two measures (ALFF vs. fALFF) is better for between-groups studies is still unknown. Of note, ALFF measures have higher test–retest reliability in gray matter regions than fALFF, while more susceptible to possible artifactual findings in the vicinity of blood vessels and the cerebral ventricles (Zuo et al., 2010). Similar to standardization procedure of ReHo analysis, the ALFF or fALFF of each voxel was divided by the global mean ALFF or fALFF value within the whole-brain mask.

In addition, different frequency bands are considered to be generated by distinct oscillators, each with specific properties and physiological functions, as the neuronal oscillation classes are arrayed linearly when plotted on the natural logarithmic scale (Penttonen and Buzsáki, 2003; Buzsáki and Draguhn, 2004). Thus, ALFF or fALFF of different frequency bands could also be investigated. For example, ALFF and fALFF of four frequency bands, namely slow-5 (0.01–0.027 Hz), slow-4 (0.027–0.073 Hz), slow-3 (0.073–0.198 Hz), and slow-2 (0.198–0.25 Hz), were examined, and the results showed that fALFF in the slow-4 (0.027–0.073 Hz) band is relatively specific to the basal ganglia (Zuo et al., 2010). If these options are checked, DPARSF will calculate ALFF and/or fALFF of the specified frequency band by calling functions in REST.

REMOVE EFFECT OF NUISANCE COVARIATES

In the past few years, there has been increased attention to the anti-correlation phenomenon of resting-state fMRI. A typical case is that, while the global (whole-brain) signal was removed, many researchers consistently observed that there were significant anti-correlations between the components of the default-mode and attention networks (Greicius et al., 2003; Fox et al., 2005; Fransson, 2005). Recently, the global signal has been found to be associated with respiration-induced fMRI signal (Birn et al., 2006). To reduce the effect of the physiological artifacts, the whole-brain signal would be removed by a regression analysis before FC analysis (Greicius et al., 2003; Fox et al., 2005; Fransson, 2005). Of note, it

is still an ongoing controversy since removal of the global brain signal causes the re-distribution of correlation coefficients and the interpretation of biological mechanisms of negative correlations is ambiguous (Murphy et al., 2009). In addition to the global mean signal, six motion parameters, the cerebrospinal fluid (CSF), and the white matter signals would also be removed as nuisance variables to reduce the effects of head motion and non-neuronal BOLD fluctuations (Fox et al., 2005; Kelly et al., 2008). It is still an open issue that where the ROIs should be located to represent the white matter and CSF. REST provided a few default masks made from SPM5's *a priori* masks, i.e., the whole brain mask (brainmask.nii) thresholded at 50%, the white matter mask (white.nii) thresholded at 90%, and the CSF mask (csf.nii) thresholded at 70%. It should be noted that the removal of nuisance covariates is not for ReHo and ALFF analysis. It is not clear yet how the nuisance covariates affect the ReHo or ALFF results.

FUNCTIONAL CONNECTIVITY

FC is widely used in resting-state fMRI (Biswal et al., 1995; Lowe et al., 1998; Xiong et al., 1999; Cordes et al., 2000; Greicius et al., 2003; Fox et al., 2005, 2006; Fransson, 2005; Vincent et al., 2006). The correlations in spontaneous BOLD fluctuations may reflect the inter-regional correlations in neuronal variability (Friston et al., 1993; Horwitz, 2003). If this option is checked, the averaged time course will be obtained from a specified seed region and the correlation analysis will be performed in a voxel-wise way to generate the FC map. The correlation coefficient map will be converted into *z* map by Fisher's *r*-to-*z* transform to improve the normality (Rosner, 2006) by calling functions in REST.

ILLUSTRATIONS

To validate and illustrate the usage of DPARSF, we performed the ReHo, ALFF, fALFF and FC analyses.

DATA

Data were selected from a large sample resting-state fMRI dataset of our group, which has been publicly released in the "1000 Functional Connectomes" Project[4]. We selected 86 young healthy volunteers (48 females: 20.8 ± 1.6 years old, range 18–25; and 38 males: 20.7 ± 1.7 years old, range 17–25) with head motion less than 2.0 mm displacement in any of the *x*, *y*, or *z* directions or 2.0° of any angular motion throughout the resting-state scan. All are right-handed and had no history of neurological and psychiatric disorders. Written informed consent was obtained from each participant, and the study was approved by the Institutional Review Board of Beijing Normal University Imaging Center for Brain Research.

MRI data were acquired using a SIEMENS TRIO 3-Tesla scanner in the Beijing Normal University Imaging Center for Brain Research. The participants lay supine with the head snugly fixed by straps and foam pads to minimize head movement. During the resting-state session, the participants were instructed to keep as motionless as possible and not to think systematically. The functional images were obtained using an EPI sequence with the following parameters: 33 axial slices, thickness/gap = 3/0.6 mm, in-plane resolution = 64 × 64, TR = 2000 ms, TE = 30 ms, flip angle = 90°, FOV = 200 × 200 mm. In addition, a T1-weighted sagittal three-dimensional magnetization-prepared rapid gradient echo (MPRAGE) sequence was acquired, covering the entire brain: 128 slices, TR = 2530 ms, TE = 3.39 ms, slice thickness = 1.33 mm, flip angle = 7°, inversion time = 1100 ms, FOV = 256 mm × 256 mm, and in-plane resolution = 256 × 192.

PREPROCESSING

Data were processed by using DPARSF pipeline analysis as introduced in the last section. Briefly, after converting DICOM files to NIFTI images, the first 10 time points were discarded. Then slice timing and head motion correction were performed. The data were then normalized to MNI space by using unified segmentation of T1 image and re-sampled to 3-mm isotropic voxels. After smoothing with a 4 mm FWHM Gaussian kernel (for ALFF, fALFF, FC except for ReHo), the linear trend of time courses were removed and then temporally band-pass filtering (0.01–0.08 Hz) (with an exception of fALFF) was performed.

ReHo, ALFF, fALFF AND FC

As indicated in the corresponding sections, spatial smoothing was performed after ReHo calculation, but for the other three (ALFF, fALFF and FC) methods, spatial smoothing was performed before their calculation. fALFF was calculated based on preprocessed data without filtering since fALFF is the value divided by the total power in the entire detectable frequency range. The ReHo, ALFF or fALFF of each voxel was divided by the global mean value within the whole-brain mask.

Before FC calculation, nine nuisance covariates including six head motion parameters, the global signal, the white matter signal and the CSF signal were removed from the preprocessed data. A sphere (radius = 6 mm) in the posterior cingulate cortex (PCC) (−5, −49, 40) were defined as the seed region for each participant in line with a previous study (Fox et al., 2005). The averaged time course was then obtained from the sphere ROI and the correlation analysis was performed in a voxel-wise way to generate the FC of the PCC, called the PCC-FC map. Finally, the correlation coefficient map was converted into *z* maps by Fisher's *r*-to-*z* transform to improve the normality (Rosner, 2006).

STATISTICAL ANALYSIS

To explore the within-group patterns, one-sample *t*-tests were performed on the ReHo, ALFF, fALFF, and FC maps, respectively, in a voxel-wise way by using SPM. For ReHo, ALFF and fALFF maps, the one-sample *t*-tests were to find regions showing significantly higher ReHo, ALFF and fALFF, respectively, than the global mean value. After being divided by the global mean value, each individual ReHo, ALFF and fALFF map has a "new" global mean of "1". Thus the one-sample *t*-tests were performed against "1" other than "0". Since the module for one-sample t test in SPM just can compare values with base "0", we subtracted "1" from the ReHo, ALFF and fALFF maps which had been divided by global mean value of the whole brain, and then perform one-tailed one-sample *t*-tests on the subtracted maps in SPM. For FC maps, two-tailed one sample *t*-test was performed on the *z* maps to show both the DMN and its anti-correlated network patterns. The within-condition statistical threshold was set at $t > 3.89$ ($P < 0.0001$) for one-tailed *t*-tests (for ReHo, ALFF and

[4]http://www.nitrc.org/projects/fcon_1000/

fALFF) and $|t| > 4.08$ ($P < 0.0001$) for two-tailed *t*-test (for FC) and cluster size >135 mm^3, which corresponds to a corrected $P < 0.0001$. This correction was confined within the whole-brain mask (size: 1912437 mm^3) and was determined by Monte Carlo simulations (Ledberg et al., 1998) that were performed by the program REST AlphaSim (which is based on AlphaSim in AFNI[5]).

RESULTS AND DISCUSSION

One-sample *t*-tests showed that the DMN which included PCC/precuneus, medial prefrontal cortex and bilateral inferior parietal lobule, exhibited significantly higher ReHo, ALFF and fALFF than the global mean (**Figures 3A–C**). This pattern was consistent with that in previous studies which showed high ReHo (Long et al., 2008), ALFF and fALFF (Zang et al., 2007; Zou et al., 2008; Zuo et al., 2010) within the DMN. Previous studies have consistently demonstrated that the DMN regions show task-independent deactivation across a wide range of cognitive tasks compared with the resting-state (Shulman et al., 1997; Binder et al., 1999; Mazoyer et al., 2001), and these areas had significantly higher blood flow and oxygen consumption than the global mean value (Raichle et al., 2001). The current results that DMN showed high activity is consistent with the conclusion that these regions represent the functional core underlying resting brain dynamics (Ghosh et al., 2008; Honey et al., 2009; Zuo et al., 2010). In line with previous studies (Zou et al., 2008; Zuo et al., 2010), we also found ALFF measure may be more susceptible to possible artifactual effect in the vicinity of blood vessels and the cerebral ventricles than fALFF. However, which of the two measures, ALFF vs. fALFF, is better for between-groups studies or sensitive to abnormal spontaneous brain activity needs to be further investigated.

FC analysis showed that the medial prefrontal cortex and bilateral inferior parietal lobule had significantly positive correlation with PCC (**Figure 3D**). The dorsal anterior cingulate cortex, bilateral insula, bilateral middle temporal cortex and bilateral dorsolateral

[5]http://afni.nimh.nih.gov/pub/dist/doc/manual/AlphaSim.pdf

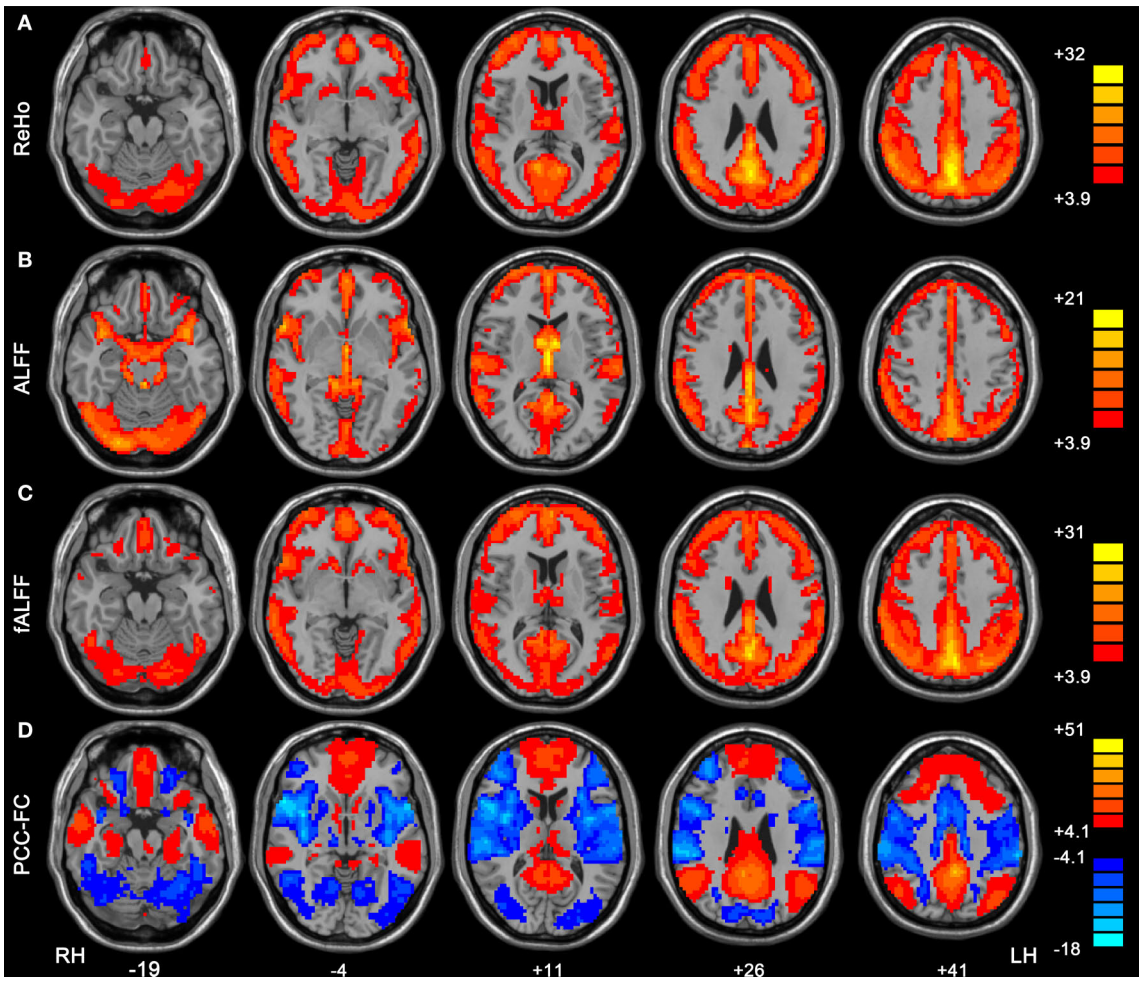

FIGURE 3 | Within-condition patterns of ReHo (A), ALFF (B), fALFF (C) and PCC-FC (D). All these methods revealed the pattern of the default mode network. The numbers below the images refer to the MNI *z* coordinates. The statistical threshold was set at $t > 3.89$ ($P < 0.0001$) for one-tailed *t*-tests (for ReHo, ALFF and fALFF) and $|t| > 4.08$ ($P < 0.0001$) for two-tailed *t*-test (for FC) and cluster size >135 mm^3, which corresponds to a corrected $P < 0.0001$. LH, left hemisphere; RH, right hemisphere.

prefrontal cortex showed negative correlation with PCC. These results are consistent with previous studies that suggested a competitive relationship between the DMN and the anti-correlated network (Fox et al., 2005; Fransson, 2005; Long et al., 2008; Yan et al., 2009).

The illustrations of ReHo, ALFF, fALFF and FC analyses by using DPARSF pipeline analysis validated its correctness and demonstrated its effectiveness.

CONCLUSIONS

Based on some functions in SPM and REST, DPARSF is a user-friendly toolbox for "pipeline" data analysis of resting-state fMRI. It can help the users to save time for data processing and reduce errors in cumbersome setting of parameters. DPARSF can also create a report for excluding subjects with excessive head motion and generate a set of pictures for easily checking the effect of normalization. This toolbox is freely available at http://www.restfmri.net. We hope this user-friendly toolbox could make the relatively novel technique of resting-state fMRI easier to study, especially for clinical studies.

ACKNOWLEDGMENTS

This work was supported by the NSFC (30770594, 30621130074), the National High Technology Program of China (863 Project, No. 2008AA02Z405), Program for Changjiang Scholars and Innovative Research Team in University (PCSIRT), and Funds for Outstanding Doctoral Dissertation, Beijing Normal University (08046).

REFERENCES

Ashburner, J., and Friston, K. J. (1999). Nonlinear spatial normalization using basis functions. *Hum. Brain Mapp.* 7, 254–266.

Ashburner, J., and Friston, K. J. (2005). Unified segmentation. *Neuroimage* 26, 839–851.

Binder, J. R., Frost, J. A., Hammeke, T. A., Bellgowan, P. S., Rao, S. M., and Cox, R. W. (1999). Conceptual processing during the conscious resting state. A functional MRI study. *J. Cogn. Neurosci.* 11, 80–95.

Birn, R. M., Diamond, J. B., Smith, M. A., and Bandettini, P. A. (2006). Separating respiratory-variation-related fluctuations from neuronal-activity-related fluctuations in fMRI. *Neuroimage* 31, 1536–1548.

Biswal, B., Yetkin, F. Z., Haughton, V. M., and Hyde, J. S. (1995). Functional connectivity in the motor cortex of resting human brain using echo-planar MRI. *Magn. Reson. Med.* 34, 537–541.

Buzsáki, G., and Draguhn, A. (2004). Neuronal oscillations in cortical networks. *Science* 304, 1926–1929.

Cordes, D., Haughton, V. M., Arfanakis, K., Carew, J. D., Turski, P. A., Moritz, C. H., Quigley, M. A., and Meyerand, M. E. (2001). Frequencies contributing to functional connectivity in the cerebral cortex in "resting-state" data. *AJNR Am. J. Neuroradiol.* 22, 1326–1333.

Cordes, D., Haughton, V. M., Arfanakis, K., Wendt, G. J., Turski, P. A., Moritz, C. H., Quigley, M. A., and Meyerand, M. E. (2000). Mapping functionally related regions of brain with functional connectivity MR imaging. *AJNR Am. J. Neuroradiol.* 21, 1636–1644.

Cox, R., Ashburner, J., Breman, H., Fissell, K., Haselgrove, C., Holmes, C., Lancaster, J., Rex, D., Smith, S., Woodward, J., and Strother, S. (2004). "A (sort of) new image data format standard: Nifti-1," in *10th Annual Meeting of the Organization for Human Brain Mapping (OHBM 2004)*, Vol. 25, Budapest, Hungary, June 13–17. Available at: http://nifti.nimh.nih.gov/nifti-1/documentation/hbm_nifti_2004.pdf

Cox, R. W. (1996). AFNI: software for analysis and visualization of functional magnetic resonance neuroimages. *Comput. Biomed. Res.* 29, 162–173.

Fox, M., Corbetta, M., Snyder, A., Vincent, J., and Raichle, M. (2006). Spontaneous neuronal activity distinguishes human dorsal and ventral attention systems. *Proc. Natl. Acad. Sci. U.S.A.* 103, 10046–10051.

Fox, M. D., and Raichle, M. E. (2007). Spontaneous fluctuations in brain activity observed with functional magnetic resonance imaging. *Nat. Rev. Neurosci.* 8, 700–711.

Fox, M. D., Snyder, A. Z., Vincent, J. L., Corbetta, M., Van Essen, D. C., and Raichle, M. E. (2005). The human brain is intrinsically organized into dynamic, anticorrelated functional networks. *Proc. Natl. Acad. Sci. U.S.A.* 102, 9673–9678.

Fransson, P. (2005). Spontaneous low-frequency BOLD signal fluctuations: an fMRI investigation of the resting-state default mode of brain function hypothesis. *Hum. Brain Mapp.* 26, 15–29.

Friston, K. J., Frith, C. D., Liddle, P. F., and Frackowiak, R. S. (1993). Functional connectivity: the principal-component analysis of large (PET) data sets. *J. Cereb. Blood Flow Metab.* 13, 5–14.

Ghosh, A., Rho, Y., McIntosh, A. R., Kotter, R., and Jirsa, V. K. (2008). Noise during rest enables the exploration of the brain's dynamic repertoire. *PLoS Comput. Biol.* 4, e1000196. doi: 10.1371/journal.pcbi.1000196.

Greicius, M., Krasnow, B., Reiss, A., and Menon, V. (2003). Functional connectivity in the resting brain: A network analysis of the default mode hypothesis. *Proc. Natl. Acad. Sci. U.S.A.* 100, 253–258.

He, Y., Wang, L., Zang, Y., Tian, L., Zhang, X., Li, K., and Jiang, T. (2007). Regional coherence changes in the early stages of Alzheimer's disease: a combined structural and resting-state functional MRI study. *Neuroimage* 35, 488–500.

Honey, C. J., Sporns, O., Cammoun, L., Gigandet, X., Thiran, J. P., Meuli, R., and Hagmann, P. (2009). Predicting human resting-state functional connectivity from structural connectivity. *Proc. Natl. Acad. Sci. U.S.A.* 106, 2035–2040.

Hoptman, M. J., Zuo, X. N., Butler, P. D., Javitt, D. C., D'Angelo, D., Mauro, C. J., and Milham, M. P. (2010). Amplitude of low-frequency oscillations in schizophrenia: a resting state fMRI study. *Schizophr. Res.* 117, 13–20.

Horwitz, B. (2003). The elusive concept of brain connectivity. *Neuroimage* 19, 466–470.

Huettel, S., Song, A., and McCarthy, G. (2004). *Functional Magnetic Resonance Imaging.* Sunderland, MA: Sinauer Associates.

Kelly, A. M., Uddin, L. Q., Biswal, B. B., Castellanos, F. X., and Milham, M. P. (2008). Competition between functional brain networks mediates behavioral variability. *Neuroimage* 39, 527–537.

Kendall, M., and Gibbons, J. D. R. (1990). *Correlation Methods.* Oxford: Oxford University Press.

Kiviniemi, V., Jauhiainen, J., Tervonen, O., Pääkkö, E., Oikarinen, J., Vainionpää, V., Rantala, H., and Biswal, B. (2000). Slow vasomotor fluctuation in fMRI of anesthetized child brain. *Magn. Reson. Med.* 44, 373–378.

Ledberg, A., Akerman, S., and Roland, P. E. (1998). Estimation of the probabilities of 3D clusters in functional brain images. *Neuroimage* 8, 113–128.

Long, X. Y., Zuo, X. N., Kiviniemi, V., Yang, Y., Zou, Q. H., Zhu, C. Z., Jiang, T. Z., Yang, H., Gong, Q. Y., Wang, L., Li, K. C., Xie, S., and Zang, Y. F. (2008). Default mode network as revealed with multiple methods for resting-state functional MRI analysis. *J. Neurosci. Methods* 171, 349–355.

Lowe, M. J., Mock, B. J., and Sorenson, J. A. (1998). Functional connectivity in single and multislice echoplanar imaging using resting-state fluctuations. *Neuroimage* 7, 119–132.

Lowe, M. J., and Russell, D. P. (1999). Treatment of baseline drifts in fMRI time series analysis. *J. Comput. Assist. Tomogr.* 23, 463–473.

Lu, H., Zuo, Y., Gu, H., Waltz, J. A., Zhan, W., Scholl, C. A., Rea, W., Yang, Y., and Stein, E. A. (2007). Synchronized delta oscillations correlate with the resting-state functional MRI signal. *Proc. Natl. Acad. Sci. U.S.A.* 104, 18265–18269.

Mazoyer, B., Zago, L., Mellet, E., Bricogne, S., Etard, O., Houde, O., Crivello, F., Joliot, M., Petit, L., and Tzourio-Mazoyer, N. (2001). Cortical networks for working memory and executive functions sustain the conscious resting state in man. *Brain Res. Bull.* 54, 287–298.

Murphy, K., Birn, R. M., Handwerker, D. A., Jones, T. B., and Bandettini, P. A. (2009). The impact of global signal regression on resting state correlations: are anti-correlated networks introduced? *Neuroimage* 44, 893–905.

Penttonen, M., and Buzsáki, G. (2003). Natural logarithmic relationship between brain oscillators. *Thalamus Relat. Syst.* 2, 145–152.

Raichle, M. E., MacLeod, A. M., Snyder, A. Z., Powers, W. J., Gusnard, D. A., and Shulman, G. L. (2001). A default mode of brain function. *Proc. Natl. Acad. Sci. U.S.A.* 98, 676–682.

Rosner, B. A. (2006). *Fundamentals of Biostatistics*, 6th Edn. Belmont, CA: Thomson-Brooks/Cole.

Shulman, G. L., Fiez, J. A., Corbetta, M., Buckner, R. L., Miezin, F. M., Raichle, M. E., and Petersen, S. E. (1997). Common blood flow changes across visual tasks: II. Decreases in cerebral cortex. *J. Cogn. Neurosci.* 9, 648–663.

Smith, A. M., Lewis, B. K., Ruttimann, U. E., Ye, F. Q., Sinnwell, T. M., Yang, Y., Duyn, J. H., and Frank, J. A. (1999). Investigation of low frequency drift in fMRI signal. *Neuroimage* 9, 526–533.

Turner, R., Howseman, A., Rees, G., and Josephs, O. (1997). "Functional imaging with magnetic resonance," in *Human Brain Function*, ed. R. S. J. Frackowiak (San Diego: Academic Press), 467–486.

Vincent, J. L., Snyder, A. Z., Fox, M. D., Shannon, B. J., Andrews, J. R., Raichle, M. E., and Buckner, R. L. (2006). Coherent spontaneous activity identifies a hippocampal-parietal memory network. *J. Neurophysiol.* 96, 3517–3531.

Xiong, J., Parsons, L. M., Gao, J. H., and Fox, P. T. (1999). Interregional connectivity to primary motor cortex revealed using MRI resting state images. *Hum. Brain Mapp.* 8, 151–156.

Yan, C., Liu, D., He, Y., Zou, Q., Zhu, C., Zuo, X., Long, X., and Zang, Y. (2009). Spontaneous brain activity in the default mode network is sensitive to different resting-state conditions with limited cognitive load. *PLoS ONE* 4, e5743. doi: 10.1371/journal.pone.0005743.

Zang, Y. F., He, Y., Zhu, C. Z., Cao, Q. J., Sui, M. Q., Liang, M., Tian, L. X., Jiang, T. Z., and Wang, Y. F. (2007). Altered baseline brain activity in children with ADHD revealed by resting-state functional MRI. *Brain Dev.* 29, 83–91.

Zang, Y. F., Jiang, T. Z., Lu, Y. L., He, Y., and Tian, L. X. (2004). Regional homogeneity approach to fMRI data analysis. *Neuroimage* 22, 394–400.

Zhang Z., Lu, G., Zhong, Y., Tan, Q., Chen, H., Liao, W., Tian, L., Li, Z., Shi, J., and Liu, Y. (in press). fMRI study of mesial temporal lobe epilepsy using amplitude of low-frequency fluctuation analysis. *Hum. Brain Mapp.* [Epub ahead of print].

Zou, Q. H., Zhu, C. Z., Yang, Y., Zuo, X. N., Long, X. Y., Cao, Q. J., Wang, Y. F., and Zang, Y. F. (2008). An improved approach to detection of amplitude of low-frequency fluctuation (ALFF) for resting-state fMRI: fractional ALFF. *J. Neurosci. Methods* 172, 137–141.

Zuo, X. N., Di Martino, A., Kelly, C., Shehzad, Z. E., Gee, D. G., Klein, D. F., Castellanos, F. X., Biswal, B. B., and Milham, M. P. (2010). The oscillating brain: complex and reliable. *Neuroimage* 49, 1432–1445.

Conflict of Interest Statement: The authors declare that the research was conducted in the absence of any commercial or financial relationships that could be construed as a potential conflict of interest.

Received: 30 January 2010; paper pending published: 24 February 2010; accepted: 15 April 2010; published online: 14 May 2010.

Citation: Yan C and Zang Y (2010) DPARSF: a MATLAB toolbox for "pipeline" data analysis of resting-state fMRI. Front. Syst. Neurosci. ***4****:13. doi: 10.3389/fnsys.2010.00013*

frontiers in
SYSTEMS NEUROSCIENCE

PERSPECTIVE ARTICLE
published: 28 June 2010
doi: 10.3389/fnsys.2010.00027

Exploring the electrophysiological correlates of the default-mode network with intracerebral EEG

Karim Jerbi[1,2]*†, Juan R. Vidal[1,2†], Tomas Ossandon[1,2], Sarang S. Dalal[1,2], Julien Jung[1,2], Dominique Hoffmann[3], Lorella Minotti[3], Olivier Bertrand[1,2], Philippe Kahane[3] and Jean-Philippe Lachaux[1,2]

[1] *Institut National de la Santé et de la Recherche Médicale, U821, Brain Dynamics and Cognition, Lyon, France*
[2] *Université Claude Bernard, Lyon 1, Lyon, France*
[3] *Neurology Department, Grenoble Hospital, Grenoble, France*

Edited by:
Lucina Q. Uddin, Stanford University, USA

Reviewed by:
Biyu J. He, Washington University School of Medicine, USA
Helmut Laufs, Johann Wolfgang Goethe-University, Germany

***Correspondence:**
Karim Jerbi, Institut National de la Santé et de la Recherche Médicale, U821, Brain Dynamics and Cognition, Centre Hospitalier Le Vinatier, Bâtiment 452, 95 Boulevard Pinel, 69500 Lyon, France.
e-mail: karim.jerbi@inserm.fr

†Karim Jerbi and Juan R. Vidal have contributed equally to this work.

While functional imaging studies allow for a precise spatial characterization of resting state networks, their neural correlates and thereby their fine-scale temporal dynamics remain elusive. A full understanding of the mechanisms at play requires input from electrophysiological studies. Here, we discuss human and non-human primate electrophysiological data that explore the neural correlates of the default-mode network. Beyond the promising findings obtained with non-invasive approaches, emerging evidence suggests that invasive recordings in humans will be crucial in order to elucidate the neural correlates of the brain's default-mode function. In particular, we contend that stereotactic-electroencephalography, which consists of implanting multiple depth electrodes for pre-surgical evaluation in drug-resistant epilepsy, is particularly suited for this endeavor. We support this view by providing rare data from depth recordings in human posterior cingulate cortex and medial prefrontal cortex that show transient neural deactivation during task-engagement.

Keywords: default-mode network, electrophysiology, gamma-band activity, stereotactic-electroencephalography, intracranial EEG

INTRODUCTION

The fact that parts of our brain are active even when we are not overtly engaged with the external world may not appear to be that much of a surprise *per se*. The fact that thoughts and inner mental processes are ongoing, and that they are certainly more prominent when we are not processing stimuli from the outside world, makes the concept of ongoing brain activity not only plausible but crucial. By contrast, what is definitely striking is the significant discrepancy between how much we have learned about the spatial characteristics of the so-called "default-mode" of brain function (Raichle et al., 2001) and how little we know about the precise neural mechanisms underlying its modulations and the fine-scale temporal dynamics thereof.

Over recent years, the default-mode network (DMN) (Gusnard and Raichle, 2001; Raichle et al., 2001) has been examined in the light of its putative relationship to self-cognition (Gusnard et al., 2001) and mind wandering (Mason et al., 2007). Deactivation of the DMN has been implicated in attention and task-engagement (Corbetta and Shulman, 2002) and its dysfunction has been linked to various mental disorders (Greicius, 2008; Broyd et al., 2009). A steady flow of seminal findings advancing our understanding of intrinsic brain activity continues to emerge from neuroimaging studies. Current important topics include the use of functional magnetic resonance imaging (fMRI) to investigate intrinsic network dynamics and connectivity patterns (Greicius et al., 2003; Fox et al., 2005; Uddin et al., 2009) and the putative relationship between DMN deactivations and behavioral performance (Weissman et al., 2006; Shulman et al., 2007; Anticevic et al., 2010). Nevertheless, the quest to fully elucidate the function of intrinsic brain networks also requires a solid understanding of the link between neuroimaging findings and their electrophysiological underpinnings.

In this paper we provide perspectives on the necessity, feasibility, and limitations of tackling the electrophysiological properties of DMN dynamics. We will discuss the utility and limitations of non-invasive electrophysiological techniques such as electroencephalography (EEG) and magnetoencephalography (MEG) in this endeavor. Most importantly, we will focus on the potential of direct electrophysiological recordings in humans to unravel the spectral and temporal properties of task-related changes of population activity in DMN structures.

A parallel stream of research in humans has revealed that blood-oxygenation level-dependent (BOLD) signal increases are tightly coupled with task-related power increases in the high-frequency range (broad-band gamma, 50–150 Hz) of the intracranial EEG signal (Mukamel et al., 2005; Lachaux et al., 2007a; Nir et al., 2007). It is therefore tempting to ask whether task-related BOLD deactivations, typical for DMN areas, are in turn associated with suppressions of high gamma power. While human studies of gamma power increases are abundant (e.g., Lachaux et al., 2005; Crone et al., 2006; Jensen et al., 2007; Jerbi et al., 2009a), little is known about task-related gamma power suppression. Intracerebral studies from our group were the first to provide direct evidence in humans for task-related decreases of broad-band gamma (>50 Hz) power during performance of attention-demanding cognitive tasks (Lachaux et al., 2005, 2008). More recent studies (Mainy et al., 2008; Miller et al., 2009; Jung et al., 2010) provide further evidence for the co-occurrence of

task-related increases and decreases of broad-band gamma activity in distinct brain areas during goal-directed behavior. As a matter of fact, because direct recordings from the cortex are not affected by physiological noise (e.g., breathing or cardiac changes), such studies are critical to refute claims that DMN observations constitute an epiphenomenon not of neuronal origin (Birn et al., 2008). Besides, we argue that depth recordings in humans will be key to probing the temporal properties of DMN deactivation and to unraveling the role of gamma activity therein. To further support this claim, we present rare human intracerebral stereotactic-EEG (SEEG) data recorded directly from two prominent DMN areas, namely the posterior cingulate cortex (PCC) and the medial prefrontal cortex (MPFC). Using time-frequency analysis we computed temporal and spectral profiles of population-level activity depicting task-related gamma-band deactivation in these areas during performance of attention-demanding tasks. Finally, we discuss some implications of our findings and we outline directions for future research in this challenging and rapidly growing field.

INVESTIGATING DMN WITH ANIMAL ELECTROPHYSIOLOGY

Unfortunately, our knowledge of the neural correlates of DMN remains elusive. This is in part due to the fact that investigating the electrophysiological correlates of the BOLD signal is a technically challenging endeavor and acquiring electrophysiological signals from human DMN structures faces multiple challenges. So what have electrophysiological approaches taught us about the neural correlates of DMN and what are their current limitations? Let us address this question first of all from the perspective of animal studies. A highly interesting study by Hayden et al. (2009) has reported significant task-related suppression of neuronal firing rate in macaque PCC a region considered to be a prominent component of DMN. As in previous reports of task-related BOLD deactivation, the reduction in neuronal firing in macaque PCC occurred during task performance and was followed by a return to higher baseline levels between trials. Most importantly, the firing-rate suppression reported by Hayden et al. (2009) was predictive of performance (errors and reaction times). Despite the fact that the BOLD signal was not recorded in this study, the authors argue that the relationship to fMRI findings is strengthened by the fact that the activity of lateral intraparietal (LIP) neurons was enhanced during the task, i.e., LIP showed the inverse effect observed in PCC. Such non-human primate studies hold the potential to advance our understanding of the neural correlates of the DMN. The degree to which animal data can be generalized to humans may be restricted by the limits of anatomo-functional cross-species comparison. However, a more serious limitation to the study of DMN function with animal recordings arises if we want to test specific hypotheses about its putative role in mediating internally oriented mental processes (e.g., self-cognition, episodic and prospective memory, covert speech, etc.). Nevertheless, by contrast to electrophysiology, imaging studies in anesthetized animal can provide insights into the large-scale functional architecture of the DMN. As a matter of fact, the detection of spontaneous BOLD correlations (typical of resting state networks) in anesthetized monkeys (Vincent et al., 2007) has direct implications on the ongoing debate on the correlations between DMN connectivity and levels of consciousness (Greicius et al., 2008).

NON-INVASIVE INVESTIGATION OF DMN WITH EEG

Non-invasive electrophysiological techniques such as EEG or MEG provide whole-head coverage at a high temporal (millisecond-range) resolution and thus carry the potential to unravel the fine-temporal dynamics of the brain's intrinsic activity. Several EEG studies suggest various relationships between resting state networks and multiple spatial and spectral properties of the EEG. In particular, combining EEG and fMRI recordings provides a powerful framework for the comparison between various electrophysiological components and the BOLD responses during resting states (Laufs et al., 2003; Debener et al., 2005; Mantini et al., 2007; Laufs, 2008; Scheeringa et al., 2008; Jann et al., 2009). A first step toward assessing the EEG correlates of DMN is to decipher the way non-invasive surface measurements relate to the BOLD response. This question has been addressed by correlating BOLD with EEG power in various frequency bands. For instance, the BOLD signal has been shown to correlate negatively with EEG power in the alpha band (Goldman et al., 2002; Moosmann et al., 2003) and a recent study found positive correlations between BOLD and MEG high gamma power (Zumer et al., 2010). Numerous studies found correlations between DMN activity patterns and the power in traditional EEG frequency bands including theta (4–7 Hz), alpha (8–12 Hz), beta (13–30Hz), and low-gamma (30–50 Hz) bands (Laufs et al., 2003; Mantini et al., 2007; Chen et al., 2008; Scheeringa et al., 2008; Jann et al., 2009). In contrast, putative links between BOLD responses and components in the lower end of the EEG frequency spectrum, namely delta oscillations (1–4 Hz), slow cortical potentials (SCPs), and infra-slow fluctuations (0.01–0.1 Hz) have proven harder to establish (Khader et al., 2008). Infra-slow EEG fluctuations (e.g., Monto et al., 2008) and SCPs have been proposed to reflect slow fluctuations in fMRI spontaneous activity (He and Raichle, 2009).

More generally, attempts to use non-invasive electrophysiological methods such as EEG or MEG to elucidate the neural mechanisms of intrinsic brain networks are challenged by two main limitations: the poor spatial resolution of MEG/EEG and the relatively limited signal-to-noise ratio of surface measurements especially with regards to detecting higher frequency components of the signal, namely the high gamma-band (~60–200 Hz). Advanced MEG/EEG source reconstruction techniques yield cortical activation maps that are physiologically easier to interpret than sensor-level topographies (e.g., Baillet et al., 2001; Dalal et al., 2008). Nevertheless, the estimation of deeper sources in MEG/EEG is less reliable than the localization of activity from sources close to the sensors. This could be a severe limitation when it comes to detecting activity from deep regions of the default-mode such as the PCC. Moreover, the fact that high-frequency activity in the gamma-range is less easily detected with surface recordings (Pfurtscheller and Cooper, 1975; Jerbi et al., 2009a) might also be considered a further obstacle in this endeavor. As mentioned earlier, high gamma activity is an important target signal for DMN investigations because of its putative coupling with the BOLD signal (Logothetis et al., 2001; Niessing et al., 2005; Nir et al., 2007; Lachaux et al., 2008). Recently a number of studies have shown that MEG and EEG can, under certain circumstances, be used to detect task-related activity above 60 Hz (e.g., Ball et al., 2008; Cheyne et al., 2008; Dalal et al., 2008, 2009; Tecchio et al., 2008; Waldert et al., 2008; Van Der Werf et al., 2010; Zumer et al., 2010).

INTRACEREBRAL RECORDINGS: CLINICAL SETTING AND TECHNICAL FEATURES

Fortunately, access to high resolution spatial and temporal signals through direct recordings from the human brain is sometimes possible in some clinical settings. Various types of invasive recordings from cortical and subcortical structures are used in conjunction with several clinical conditions (Engel et al., 2005). The surgical treatment of drug-resistant epilepsy requires intracranial recordings in multiple brain areas in order to localize the epileptic tissue (Kahane et al., 2004, 2006). During this pre-surgical evaluation period, electrical cortical stimulation and task-related functional mapping (Crone et al., 2006; Jerbi et al., 2009a) are used to map out healthy and eloquent cortex that should be spared during surgery. The two main invasive recording techniques used in the field of epilepsy consist of grid electrode placement over the cortex, a procedure known as Electrocorticography (ECoG) and of multi-lead depth electrode implantation known as SEEG (reviewed in Jerbi et al., 2009a). From the point of view of functional mapping, a major advantage of the multi-lead depth electrode implantation used in SEEG is the fact that the recordings are not limited to the cortical surface. An SEEG electrode consists of upto 15 contacts that probe multiple sites from lateral structures all the way through to medial wall regions (see **Figure 1A**). This represents a major advantage when it comes to the investigation of DMN structures such as PCC, MPFC that are rarely probed by other electrophysiological techniques. Nevertheless, ECoG does occasionally involve placement of electrode strips on the surface of the medial wall and could in these cases be used for DMN investigations. Previous ECoG findings point toward SCP and gamma-range power as two types of electrical signals that display correlation patterns that mirror those observed in spontaneous fMRI BOLD signals (He et al., 2008; He and Raichle, 2009).

DETECTION OF TASK-RELATED NEURAL DEACTIVATION WITH SEEG

Given that a defining property of DMN is its task-related deactivation (i.e., negative BOLD response) during exteroceptive goal-directed behavior, the natural question that comes to mind is whether the DMN also displays task-related deactivations detectable in the electrophysiological signal. Robust SEEG deactivations in such regions may represent a putative neural correlate of task-related BOLD deactivations.

In the following, we further make the case for SEEG recordings as a particularly promising approach to study DMN deactivation, by providing samples of direct recordings from two regions of the

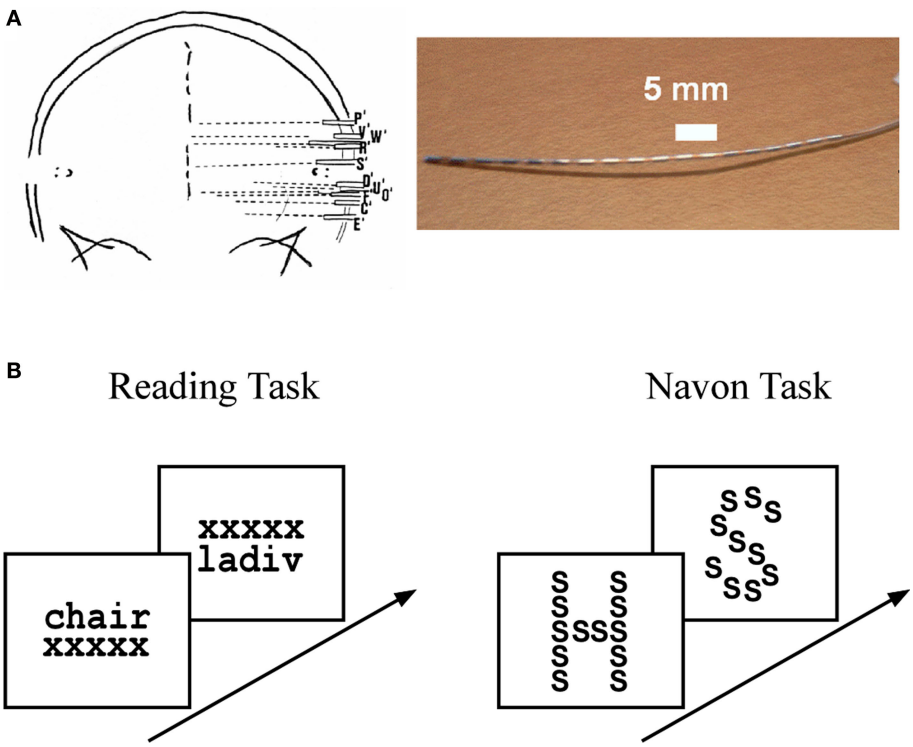

FIGURE 1 | Intracerebral stereotactic-EEG (SEEG) setting and cognitive paradigms. (A) SEEG recording procedure showing a typical implantation sketch based on a post-implantation X-ray scan (left panel) and a typical SEEG depth electrode array (right panel). See Materials and Methods in Supplementary Material for a detailed description of SEEG data acquisition. **(B)** Reading task (left panel): subjects were presented with stimuli that consisted of words and pseudowords. To ensure both categories were read, the subjects had to indicate whether the word represented a living or non-living item and, in the case of a pseudoword, whether it was made up of two syllables or not. Navon task (right panel): subjects were presented with a large letter ("global letter"), which was itself composed of repeated smaller letters ("local letter"). The global and local letters could be either the letter "H" or the letter "S," leading to four types of global-to-local stimulus configurations. At the beginning of a trial the subjects were cued to focus either on the global or the local level of the upcoming stimulus. The task consisted in identifying, as fast as possible, the stimulus letter at the level indicated by the cue. In both experiments the stimuli were presented for a maximum of 3 s and disappeared as soon as the subject responded.

human DMN: the posterior cingulate cortex (PCC) and the MPFC. We then report, for the sake of comparison, electrode data acquired in the same subjects but from sites not assumed to be part of the DMN. The data presented here were acquired from subjects with SEEG depth electrodes implanted at multiple locations of the brain as part of their pre-surgical evaluation period (see supplementary material for details of the experimental procedures). The subjects participated in routine localizer experiments including a series of attention-demanding tasks such as a classical "global versus local" attention task (Navon, 1977) and a "word versus pseudoword" reading task (**Figure 1B**). Subsequent data analysis was strictly restricted to recording sites that showed no pathological activity. **Figures 2 and 3** show results obtained with data recorded directly in PCC and MPFC respectively. Using time-frequency analysis of bipolar

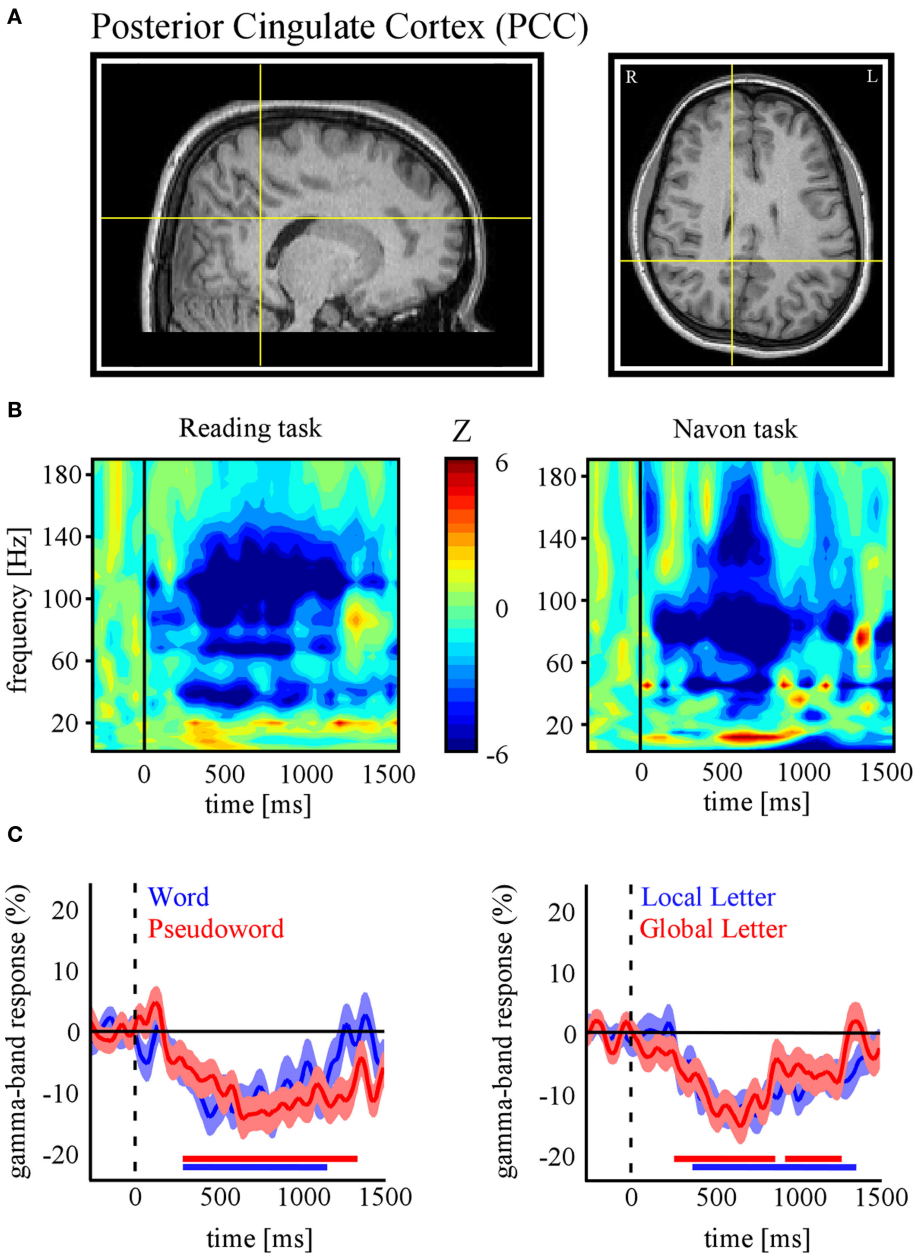

FIGURE 2 | Task-related gamma-band power suppressions in posterior cingulate cortex (PCC). (A) Anatomical location of the SEEG recording site in PCC of subject 1 (Talairach coordinates: $x = 10$, $y = -38$, $z = 35$). **(B)** Time-frequency representations of PCC activity for the reading (left panel) and Navon (right panel) tasks. Values represent task-related power modulations across time and frequency, compared with average baseline activity during fixation (Wilcoxon test). In both tasks strong decreases in PCC gamma power were found (indicated by negative Z values). **(C)** Time profile of percent power decreases (below baseline levels) at this electrode site for the conditions of each task (Left: Reading, Right: Navon). All conditions show significant gamma suppression in this region of DMN. The red/blue horizontal lines indicate statistical significance ($p < 0.05$) based on a Wilcoxon signed rank test and confidence intervals represent ± s.e.m. (See Materials and Methods in Supplementary Material for more details).

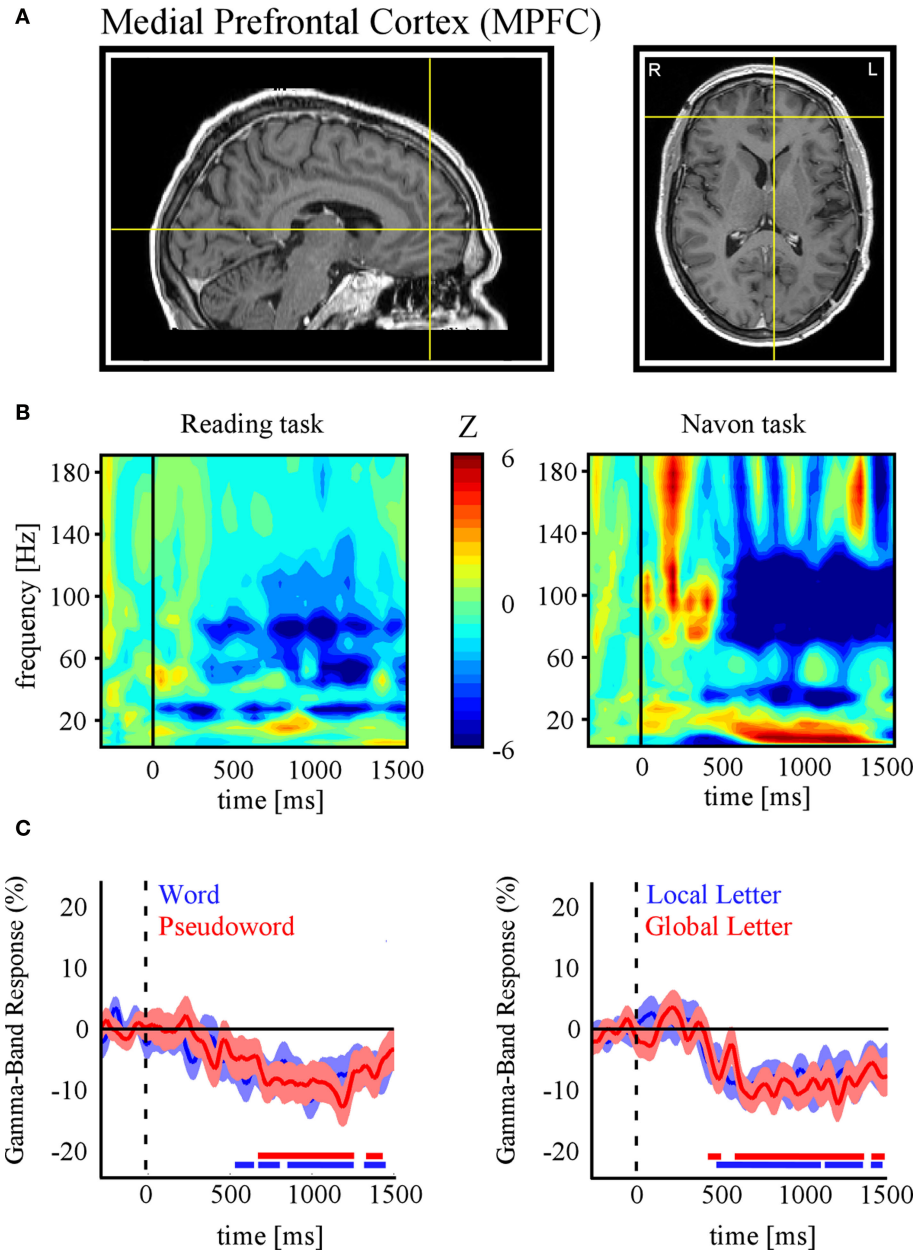

FIGURE 3 | Task-related gamma-band power suppressions in Medial Prefrontal Cortex (MPFC). (A) Anatomical location of the SEEG recording site in MPFC of subject 2 (Talairach coordinates: $x = -4$, $y = -46$, $z = -3$). **(B)** Time-frequency representations of MPFC activity for the reading (left panel) and Navon (right panel) tasks. Strong decreases in MPFC gamma power were found in both tasks. **(C)** Time profile of percent power decreases (below baseline levels) at this electrode site for the conditions of each task (Left: Reading, Right: Navon). As for PCC (**Figure 2**), gamma activity in MPFC is significantly suppressed for all conditions. Display conventions and methods used are identical to those of **Figure.2**.

recordings in these areas we derive task-related maps that depict modulations of power across time and frequency, as compared to baseline levels (methods as in Jerbi et al., 2009a). Strikingly, compared to pre-stimulus baseline levels (during which subject simply fixate a cross), the Reading and the Navon tasks were associated with strong suppressions of power in the high gamma (~50–150 Hz) observed in both PCC and MPFC sites (**Figures 2B and 3B**). Most importantly, as shown in **Figures 2C and 3C**, the gamma-band deactivations were systematically present for all experimental conditions in both tasks. In addition to this task non-specificity, the fact that these intracranially recorded gamma suppressions occur in two regions known to be part of the DMN is in agreement with a putative link between SEEG gamma power deactivation and BOLD deactivation reported in the human fMRI DMN literature (Raichle et al., 2001). Importantly, this view is further supported by the fact that task-related gamma suppressions were not ubiquitous across recording sites. Applying the same spectral analysis to the data acquired in the same subjects but at other recording sites which

are not part of DMN shows the inverse effect, i.e., task-related increases in the gamma-range and in both experiments (**Figure 4**). This was the case for recording sites in the fusiform gyrus (S1) and in the insula (S2). Moreover, it is noteworthy that the time course of gamma power suppression (**Figures 2C and 3C**) suggests that significant gamma-band deactivation starts on average around 250 ms in the PCC and then around 500 ms in MPFC. The deactivations are sustained in time lasting beyond 1000 ms post stimulus presentation. However, the data presented here are based only on two subjects. Clearly, more subjects will be needed to reliably estimate the temporal dynamics of gamma suppression and its relationship to behavior.

DISCUSSION AND PERSPECTIVES

A number of studies have established a tight relationship between BOLD activations and task-related increases in the gamma-range of the LFP signal in the same areas (Logothetis et al., 2001; Mukamel et al., 2005; Niessing et al., 2005; Lachaux et al., 2007a; Nir et al., 2007). Such observations lead to the corollary prediction that negative BOLD activity may also be correlated with gamma-band power suppressions. This has been shown to be indeed the case in monkey primary visual area (V1) (Shmuel et al., 2006). Task-related decreases in high gamma power have also been reported with intracerebral recordings in human V1 during processing of complex visual stimuli (Lachaux et al., 2005). More generally, it is tempting to ask whether the so-called task-positive networks and task-negative networks revealed by the fMRI literature (Fox et al., 2005), are spatially coincident with task-related gamma power enhancement networks and task-related gamma power suppression networks respectively. This view implies that DMN areas would exhibit less gamma power during execution of attention-demanding tasks than during resting baseline periods. Support for this hypothesis has been reported in monkey PCC (Hayden et al., 2009). However, so far, equivalent findings in humans have been scarce. The frequency range of the high gamma-band (~40–160 Hz) falls beyond the reach of most EEG studies that have been performed so far with the aim to assess the neural correlates of the DMN (e.g., Laufs et al., 2003; Mantini et al., 2007). This limitation, as well as source localization uncertainty (i.e., limited spatial resolution), can be in part overcome by the high signal-to-noise ratio and spatio-temporal resolution of intracerebral recordings. Although there have been a few reports of task-related gamma deactivations in some specific components of

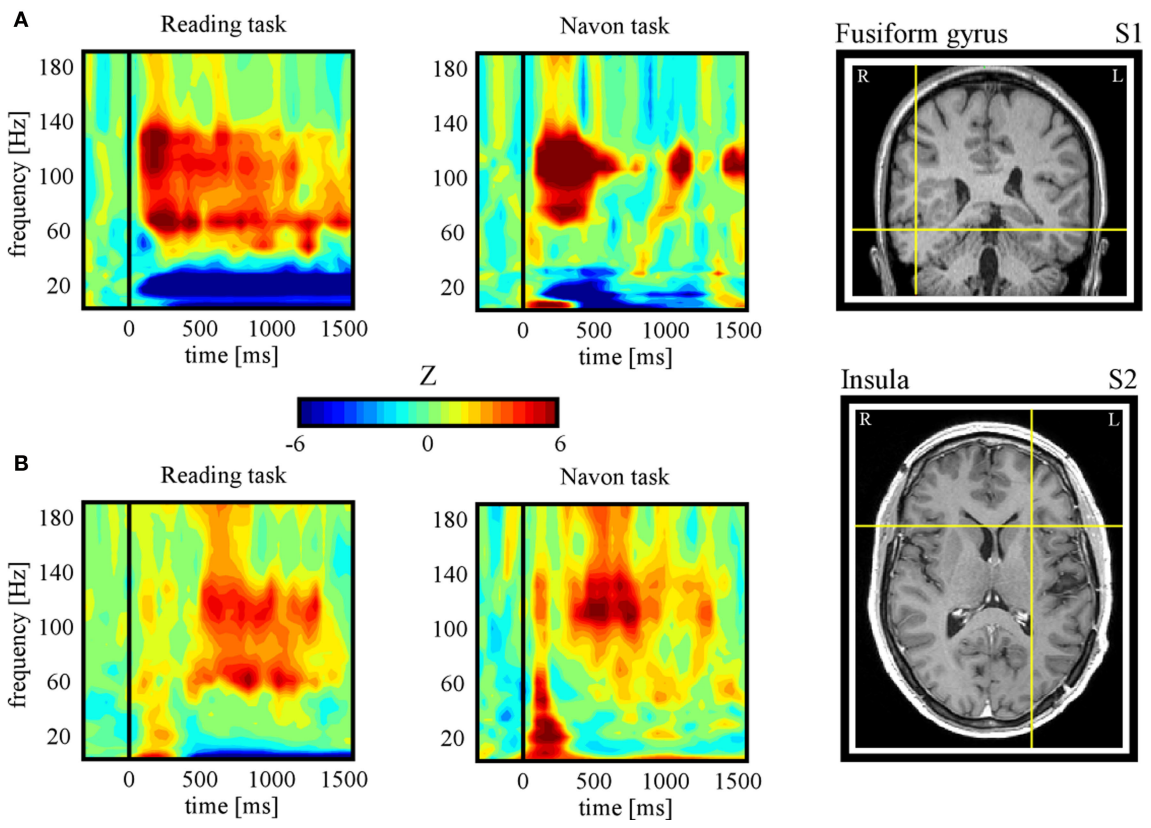

FIGURE 4 | Task-related gamma-band power increases. (A) Subject 1: time-frequency representations during Reading (condition: pseudoword) (left panel) and Navon (condition: local) (central panel) tasks for an electrode located in the fusiform gyrus (right panel, Tailarach coordinates: $x = 46$, $y = -43$, $z = -13$). Strong increases in gamma power were found in both tasks, in contrast to the decreases found for the same subject in PCC (see **Figure 2**). **(B)** Subject 2: time-frequency representations during Reading (condition: pseudoword) (left panel) and Navon (condition: local) (central panel) tasks for an electrode located in the fusiform gyrus (right panel, Tailarach coordinates: $x = -26$, $y = 16$, $z = 8$). The task-related enhancement of gamma power found here in both tasks is concurrent with task-related suppression in MPFC in the same subject (see **Figure 3**). Note that the full temporal profile of task-related gamma increases for the two conditions of each task for both subjects is provided in **Figure S1** in Supplementary Material.

human DMN using intracerebral recordings (Lachaux et al., 2008; Miller et al., 2009; Jung et al., 2010), an exhaustive investigation of all DMN structures and their fine-temporal dynamics using such techniques is hard to achieve and is still lacking.

The SEEG data presented here provides evidence for suppression of high-frequency activity in the human PCC and MPFC during task-engagement. This gamma-band deactivation (40–150 Hz) was task-related and occurred systematically across all experimental conditions. It is noteworthy that the Navon task we implemented (local versus global visual processing) induced significant gamma power suppressions in PCC, a region that has previously been shown to display negative BOLD in responses to the same paradigm performed with fMRI (Weissman et al., 2006). Remarkably, the high gamma suppression, found in the DMN, co-occurred with task-related enhancement outside the DMN (**Figure 4**). Elevated gamma power in the fusiform gyrus and in the anterior insula may reflect visual processing of the stimulus and intrinsic alertness activity respectively. Interestingly, increases in anterior insular gamma activity could be related to its role as part of the putative core task-set system (Dosenbach et al., 2006). Our observation of concurrent positive and negative high gamma responses, outside and inside the DMN respectively, is in line with the hypothesis that gamma modulations represent an electrical correlate of BOLD signal modulations. Critically, the population-level deactivation presented here extends a number of electrophysiological studies of DMN deactivation (e.g., Hayden et al., 2009; Miller et al., 2009) and strongly argues against the DMN being an epiphenomenon (Birn et al., 2008). Further studies across large populations of implanted patients are needed to strengthen and fine-tune these physiological interpretations. The illustrative data we report in PCC and MPFC highlight the potential of SEEG recordings as a tool to investigate the neurophysiology of DMN, and more generally speaking, of the resting state networks. Our group is actively pursuing the detection of brain-wide spatial distributions of gamma power decreases and increases in attention-demanding tasks as well as the investigation of correlation patterns within the involved networks (Ossandon et al., 2009).

More generally, if we assume that broad-band gamma power suppressions observed in the default-mode areas reflect *de facto* neural disengagement, then we should also expect a concurrent reduction in local neuronal firing. An assessment of this hypothesis in the light of the tight relationship between spiking activity and broad-band gamma (Mukamel et al., 2005; Niessing et al., 2005; Manning et al., 2009; Whittingstall and Logothetis, 2009), leads to the hypothesis that default-mode areas may be characterized by task-related suppression of neuronal firing during attentive states. Although there is some recent evidence for this in monkey PCC (Hayden et al., 2009), little is known about task-related modulations of spiking activity specifically in default-mode structures of the human brain. This is primarily due to the rarity of unit recordings in human cortex and may change in the future if microelectrode recordings are used more often in clinical settings to probe DMN structures. Until then, various hypotheses about spike firing-rate modulations in human DMN may be inferred indirectly from the analysis of the broad-band gamma-range component of the EEG.

Furthermore, combining fMRI and EEG in simultaneous recordings will undoubtedly continue to provide unique insights into the links between electrophysiological and BOLD signals in resting state networks (Debener et al., 2005; Mantini et al., 2007; Scheeringa et al., 2008). The advent of simultaneous fMRI and intracranial EEG in the near future will move the multimodal investigations in this field a major step forward (Carmichael et al., 2010). However, the important impact that intracerebral recordings are expected to have on the study of the electrophysiological correlates of the DMN does not lessen the need for non-invasive electrophysiological approaches for this endeavor. Indeed, the precision of EEG and MEG will continue to improve thanks to the use of advanced source localization techniques (e.g., Baillet et al., 2001; Gross et al., 2001; Dalal et al., 2008) and signal decomposition tools such as independent component analysis (Mantini et al., 2007). Besides, given the putatively prominent role of high-frequency activity, improving the sensitivity of surface recordings to high gamma activity will be a critical issue (Jerbi et al., 2009a). Results of our recent study using simultaneously acquired MEG and intracerebral EEG data suggest that source imaging can indeed enhance our ability to detect the cortical generator of gamma activity with MEG (Dalal et al., 2009). In addition, several studies have shown that EEG signals can be contaminated by signals in the gamma-range that originate from eye muscles rather than cortical tissue (Reva and Aftanas, 2004; Trujillo et al., 2005; Yuval-Greenberg et al., 2008). Therefore, ruling out the effect of such saccade-related artifacts is a prerequisite for a reliable assessment of cortical gamma-band power using non-invasive techniques and constitutes an important topic for future research. As a matter of fact, we have recently shown that gamma-range saccadic artifacts might, in some cases, even contaminate intracranial EEG recordings (Jerbi et al., 2009b).

Investigating the connectivity properties of intrinsic brain networks is clearly a topic where the input from electrophysiological recordings will be critical. Correlation and anti-correlation phenomena appear to be fundamental concepts surrounding resting state networks (Fox et al., 2005). Much still needs to be learned about how connectivity properties revealed with fMRI relate to brain-wide neural interactions revealed by MEG, EEG, and iEEG. Slow fluctuations in baseline activity observed with fMRI may be indirectly linked to higher frequency amplitude modulations via slow-to-fast cross-frequency interactions (Jensen and Colgin, 2007). Previous studies have shown that SCP can modulate higher frequency EEG activity (Vanhatalo et al., 2004), but also behavioral performance (Birbaumer et al., 1990; He et al., 2008; He and Raichle, 2009). Interestingly, in a recent study, Monto et al. (2008) used *infra-slow* EEG to provide evidence for very slow EEG fluctuations (~0.01 Hz) that were correlated with slow perceptual performance modulations. The authors reported phase-amplitude coupling between these slow fluctuations and patterns of faster cortical oscillations. The use of within and cross-frequency coupling measures to assess local and long-range interactions in scalp-EEG, MEG, and intracranial EEG data is a rapidly growing field of research, yet its potential contribution to understanding the mechanisms of DMN is still largely underexploited.

Real-time monitoring of the electrophysiological activity within the DMN may open up the exciting perspective of performing online monitoring of vigilance or attention. What's more, real-time monitoring of DMN neuronal populations may allow for novel experimental designs with stimulation parameters that adapt online to the subjects state. While several challenges still

need to be dealt with in order to achieve this with non-invasive measurements, real-time monitoring of high gamma activity in humans is readily achieved using depth SEEG recordings. We have implemented an online system for the estimation and visualization of power modulations in various frequency bands (including the high gamma-band) in conjunction with depth recording in epilepsy patients (Lachaux et al., 2007b). In addition to performing online functional mapping, this interface (dubbed *Brain TV*) could be seen as a window to the patient's ongoing and spontaneous brain activity. Therefore, with electrodes implanted in DMN areas, the Brain TV set-up could be used to monitor real-time modulations of power across the EEG spectrum during various states such as mind wandering or focused attention. Besides, the online monitoring of DMN activity could be beneficial to investigations into the functional role of DMN. For example, it may be possible to define online the timing of target or distractor stimulus presentation to correspond to specific states of the DMN. Ultimately, performing attention monitoring in real-time and non-invasively could have numerous clinical applications. Overall, a better understanding of the neural underpinnings and correlation dynamics within the DMN and, more globally, within resting state networks could have strong implications on the development of novel diagnostic and rehabilitation solutions for numerous neurological impairments.

ACKNOWLEDGMENTS

Support provided in part by the Fondation pour la Recherche Médicale (FRM) to Karim Jerbi, BrainSync FP7 European Project (Grant HEALTH-F2-2008-200728) to Juan R. Vidal, Marie Curie Fellowship (FP7-221097) from the European Commission to Sarang S. Dalal, and a doctoral fellowship from the Ministère de l'Education Nationale et la Recherche (France) to Tomas Ossandon.

SUPPLEMENTARY MATERIAL

The Supplementary Material for this article can be found online at http://www.frontiersin.org/neuroscience/systemsneuroscience/paper/10.3389/fnsys.2010.00027/

REFERENCES

Anticevic, A., Repovs, G., Shulman, G. L., and Barch, D. M. (2010). When less is more: TPJ and default network deactivation during encoding predicts working memory performance. *Neuroimage* 49, 2638–2648.

Baillet, S., Mosher, J. C., and Leahy, R. M. (2001). Electromagnetic brain mapping. *IEEE Signal Process. Mag.* 18, 14–30.

Ball, T., Demandt, E., Mutschler, I., Neitzel, E., Mehring, C., Vogt, K., Aertsen, A., and Schulze-Bonhage, A. (2008). Movement related activity in the high gamma range of the human EEG. *Neuroimage* 41, 302–310.

Birbaumer, N., Elbert, T., Canavan, A. G., and Rockstroh, B. (1990). Slow potentials of the cerebral cortex and behavior. *Physiol. Rev.* 70, 1–41.

Birn, R. M., Murphy, K., and Bandettini, P. A. (2008). The effect of respiration variations on independent component analysis results of resting state functional connectivity. *Hum. Brain Mapp.* 29, 740–750.

Broyd, S. J., Demanuele, C., Debener, S., Helps, S. K., James, C. J., and Sonuga-Barke, E. J. (2009). Default-mode brain dysfunction in mental disorders: a systematic review. *Neurosci. Biobehav. Rev.* 33, 279–296.

Carmichael, D. W., Thornton, J. S., Rodionov, R., Thornton, R., McEvoy, A. W., Ordidge, R. J., Allen, P. J., and Lemieux, L. (2010). Feasibility of simultaneous intracranial EEG-fMRI in humans: a safety study. *Neuroimage* 49, 379–390.

Chen A. C., Feng, W., Zhao, H., Yin, Y., and Wang, P. (2008). EEG default mode network in the human brain: spectral regional field powers. *Neuroimage* 41, 561–574.

Cheyne, D., Bells, S., Ferrari, P., Gaetz, W., and Bostan, A. C. (2008). Self-paced movements induce high-frequency gamma oscillations in primary motor cortex. *Neuroimage* 42, 332–342.

Corbetta, M., and Shulman, G. L. (2002). Control of goal-directed and stimulus-driven attention in the brain. *Nat. Rev. Neurosci.* 3, 201–215.

Crone, N. E., Sinai, A., and Korzeniewska, A. (2006). High-frequency gamma oscillations and human brain mapping with electrocorticography. *Prog. Brain Res.* 159, 275–295.

Dalal, S. S., Baillet, S., Adam, C., Ducorps, A., Schwartz, D., Jerbi, K., Bertrand, O., Garnero, L., Martinerie, J., and Lachaux, J.-P. (2009). Simultaneous MEG and intracranial EEG recordings during attentive reading. *Neuroimage* 45, 1289–1304.

Dalal, S. S., Guggisberg, A. G., Edwards, E., Sekihara, K., Findlay, A. M., Canolty, R. T., Berger, M. S., Knight, R. T., Barbaro, N. M., Kirsch, H. E., and Nagarajan, S. S. (2008). Five-dimensional neuroimaging: localization of the time-frequency dynamics of cortical activity. *Neuroimage* 40, 1686–1700.

Debener, S., Ullsperger, M., Siegel, M., Fiehler, K., von Cramon, D. Y., and Engel, A. K. (2005). Trial-by-trial coupling of concurrent electroencephalogram and functional magnetic resonance imaging identifies the dynamics of performance monitoring. *J. Neurosci.* 25, 11730–11737.

Dosenbach, N. U., Visscher, K. M., Palmer, E. D., Miezin, F. M., Wenger, K. K., Kang. H. C., Burgund, E. D., Grimes, A. L., Schlaggar, B. L., and Petersen, S. E. (2006). A core system for the implementation of task sets. *Neuron* 50, 799–812.

Engel, A. K., Moll, C. K., Fried, I., and Ojemann, G. A. (2005). Invasive recordings from the human brain: clinical insights and beyond. *Nat. Rev. Neurosci.* 6, 35–47.

Fox, M. D., Snyder, A. Z., Vincent, J. L., Corbetta, M., Van Essen, D. C., and Raichle, M. E. (2005). The human brain is intrinsically organized into dynamic, anticorrelated functional networks. *Proc. Natl. Acad. Sci. U.S.A.* 102, 9673–9678.

Goldman, R. I., Stern, J. M., Engel, J. Jr., and Cohen, M. S. (2002). Simultaneous EEG and fMRI of the alpha rhythm. *Neuroreport* 13, 2487–2492.

Greicius, M. (2008). Resting-state functional connectivity in neuropsychiatric disorders. *Curr. Opin. Neurol.* 21, 424–430.

Greicius, M. D., Kiviniemi, V., Tervonen, O., Vainionpaa, V., Alahuhta, S., Reiss, A. L., and Menon, V. (2008). Persistent default-mode network connectivity during light sedation. *Hum. Brain Mapp.* 29, 839–847.

Greicius, M. D., Krasnow, B., Reiss, A. L., and Menon, V. (2003). Functional connectivity in the resting brain: a network analysis of the default mode hypothesis. *Proc. Natl. Acad. Sci. U.S.A.* 100, 253–258.

Gross, J., Kujala, J., Hamalainen, M., Timmermann, L., Schnitzler, A., and Salmelin, R. (2001). Dynamic imaging of coherent sources: studying neural interactions in the human brain. *Proc. Natl. Acad. Sci. U.S.A.* 98, 694–699.

Gusnard, D. A., Akbudak, E., Shulman, G. L., and Raichle, M. E. (2001). Medial prefrontal cortex and self-referential mental activity: relation to a default mode of brain function. *Proc. Natl. Acad. Sci. U.S.A.* 98, 4259–4264.

Gusnard, D. A., and Raichle, M. E. (2001). Searching for a baseline: functional imaging and the resting human brain. *Nat. Rev. Neurosci.* 2, 685–694.

Hayden, B. Y., Smith, D. V., and Platt, M. L. (2009). Electrophysiological correlates of default-mode processing in macaque posterior cingulate cortex. *Proc. Natl. Acad. Sci. U.S.A.* 106, 5948–5953.

He, B. J., and Raichle, M. E. (2009). The fMRI signal, slow cortical potential and consciousness. *Trends Cogn. Sci. (Regul. Ed.)* 13, 302–309.

He, B. J., Snyder, A. Z., Zempel, J. M., Smyth, M. D., and Raichle, M. E. (2008). Electrophysiological correlates of the brain's intrinsic large-scale functional architecture. *Proc. Natl. Acad. Sci. U.S.A.* 105, 16039–16044.

Jann, K., Dierks, T., Boesch, C., Kottlow, M., Strik, W., and Koenig, T. (2009). BOLD correlates of EEG alpha phase-locking and the fMRI default mode network. *Neuroimage* 45, 903–916.

Jensen, O., and Colgin, L. L. (2007). Cross-frequency coupling between neuronal oscillations. *Trends Cogn. Sci. (Regul. Ed.)* 11, 267–269.

Jensen, O., Kaiser, J., and Lachaux, J. P. (2007). Human gamma-frequency oscillations associated with attention and memory. *Trends Neurosci.* 30, 317–324.

Jerbi, K., Ossandon, T., Hamame, C. M., Senova, S., Dalal, S. S., Jung, J., Minotti, L., Bertrand, O., Berthoz, A., Kahane, P., and Lachaux, J. P. (2009a). Task-related gamma-band dynamics from an intracerebral perspective: review and implications for surface EEG and MEG. *Hum. Brain Mapp.* 30, 1758–1771.

Jerbi, K., Freyermuth, S., Dalal, S., Kahane, P., Bertrand, O., Berthoz, A., and

Lachaux, J. P. (2009b). Saccade related gamma-band activity in intracerebral EEG: dissociating neural from ocular muscle activity. *Brain Topogr.* 22, 18–23.

Jung, J., Jerbi, K., Ossandon, T., Ryvlin, P., Isnard, J., Bertrand, O., Guénot, M., Mauguière, F., and Lachaux, J. P. (2010). Brain responses to success and failure: direct recordings from human cerebral cortex. *Hum. Brain Mapp.* (in press) doi: 10.1002/hbm.20930.

Kahane, P., Landre, E., Minotti, L., Francione, S., and Ryvlin, P. (2006). The Bancaud and Talairach view on the epileptogenic zone: a working hypothesis. *Epileptic Disord.* 8(Suppl. 2), S16–S26.

Kahane, P., Minotti, L., Hoffmann, D., Lachaux, J., and Ryvlin, P. (2004). "Invasive EEG in the definition of the seizure onset zone: depth electrodes," in *Handbook of Clinical Neurophysiology. Pre-Surgical Assessment of the Epilepsies with Clinical Neurophysiology and Functional Neuroimaging*, eds F. Rosenow and H. O. Lüders, (Amsterdam, Boston: Elsevier Science), 109–133.

Khader, P., Schicke, T., Röder, B., and Rösler, F. (2008). On the relationship between slow cortical potentials, and BOLD signal changes in humans. *Int. J. Psychophysiol.* 67, 252–261.

Lachaux, J. P., Fonlupt, P., Kahane, P., Minotti, L., Hoffmann, D., Bertrand, O., and Baciu, M. (2007a). Relationship between task-related gamma oscillations and BOLD signal: new insights from combined fMRI and intracranial EEG. *Hum. Brain Mapp.* 28, 1368–1375.

Lachaux, J. P., Jerbi, K., Bertrand, O., Minotti, L., Hoffmann, D., Schoendorff, B., and Kahane, P. (2007b). A blueprint for real-time functional mapping via human intracranial recordings. *PLoS ONE* 2, e1094. doi: 10.1371/journal.pone.0001094.

Lachaux, J. P., George, N., Tallon-Baudry, C., Martinerie, J., Hugueville, L., Minotti, L., Kahane, P., and Renault, B. (2005). The many faces of the gamma band response to complex visual stimuli. *Neuroimage* 25, 491–501.

Lachaux, J. P., Jung, J., Mainy, N., Dreher, J. C., Bertrand, O., Baciu, M., Minotti, L., Hoffmann, D., and Kahane, P. (2008). Silence is golden: transient neural deactivation in the prefrontal cortex during attentive reading. *Cereb. Cortex* 18, 443–450.

Laufs, H. (2008). Endogenous brain oscillations and related networks detected by surface EEG-combined fMRI. *Hum. Brain Mapp.* 29, 762–769.

Laufs, H., Krakow, K., Sterzer, P., Eger, E., Beyerle, A., Salek-Haddadi, A., and Kleinschmidt, A. (2003). Electroencephalographic signatures of attentional and cognitive default modes in spontaneous brain activity fluctuations at rest. *Proc. Natl. Acad. Sci. U.S.A.* 100, 11053–11058.

Logothetis, N. K., Pauls, J., Augath, M., Trinath, T., and Oeltermann, A. (2001). Neurophysiological investigation of the basis of the fMRI signal. *Nature* 412, 150–157.

Mainy, N., Jung, J., Baciu, M., Kahane, P., Schoendorff, B., Minotti, L., Hoffmann, D., Bertrand, O., and Lachaux, J. P. (2008). Cortical dynamics of word recognition. *Hum. Brain Mapp.* 29, 1215–1230.

Manning, J. R., Jacobs, J., Fried, I., and Kahana, M. J. (2009). Broadband shifts in local field potential power spectra are correlated with single-neuron spiking in humans. *J. Neurosci.* 29, 13613–13620.

Mantini, D., Perrucci, M. G., Del Gratta, C., Romani, G. L., and Corbetta, M. (2007). Electrophysiological signatures of resting state networks in the human brain. *Proc. Natl. Acad. Sci. U.S.A.* 104, 13170–13175.

Mason, M. F., Norton, M. I., Van Horn, J. D., Wegner, D. M., Grafton, S. T., and Macrae, C. N. (2007). Wandering minds: the default network and stimulus-independent thought. *Science* 315, 393–395.

Miller, K. J., Weaver, K. E., and Ojemann, J. G. (2009). Direct electrophysiological measurement of human default network areas. *Proc. Natl. Acad. Sci. U.S.A.* 106, 12174–12177.

Monto, S., Palva, S., Voipio, J., and Palva, J. M. (2008). Very slow EEG fluctuations predict the dynamics of stimulus detection and oscillation amplitudes in humans. *J. Neurosci.* 28, 8268–8272.

Moosmann, M., Ritter, P., Krastel, I., Brink, A., Thees, S., Blankenburg, F., Taskin, B., Obrig, H., and Villringer, A. (2003). Correlates of alpha rhythm in functional magnetic resonance imaging and near infrared spectroscopy. *Neuroimage* 20, 145–158.

Mukamel, R., Gelbard, H., Arieli, A., Hasson, U., Fried, I., and Malach, R. (2005). Coupling between neuronal firing, field potentials, and FMRI in human auditory cortex. *Science* 309, 951–954.

Navon, D. (1977). Forest before trees: the precedence of global features in visual perception. *Cogn. Psychol.* 9, 353–383.

Niessing, J., Ebisch, B., Schmidt, K. E., Niessing, M., Singer, W., and Galuske, R. A. (2005). Hemodynamic signals correlate tightly with synchronized gamma oscillations. *Science* 309, 948–951.

Nir, Y., Fisch, L., Mukamel, R., Gelbard-Sagiv, H., Arieli, A., Fried, I., and Malach, R. (2007). Coupling between neuronal firing rate, gamma LFP, and BOLD fMRI is related to interneuronal correlations. *Curr. Biol.* 17, 1275–1285.

Ossandon, T., Jerbi, K., Bayle, D., Bertrand, O., Kahane, P., and Lachaux, J.-P. (2009). Task-related gamma band suppressions: a plausible electrophysiological correlate of the default-mode network? *Soc. Neurosci.* Abstract 2009 (Program No 804.10) SfN 2009, Chicago, IL.

Pfurtscheller, G., and Cooper, R. (1975). Frequency dependence of the transmission of the EEG from cortex to scalp. *Electroencephalogr. Clin. Neurophysiol.* 38, 93–96.

Raichle, M. E., MacLeod, A. M., Snyder, A. Z., Powers, W. J., Gusnard, D. A., and Shulman, G. L. (2001). A default mode of brain function. *Proc. Natl. Acad. Sci. U.S.A.* 98, 676–682.

Reva, N. V., and Aftanas, L. I. (2004). The coincidence between late nonphase-locked gamma synchronization response and saccadic eye movements. *Int. J. Psychophysiol.* 51, 215–222.

Scheeringa, R., Bastiaansen, M. C., Petersson, K. M., Oostenveld, R., Norris, D. G., and Hagoort, P. (2008). Frontal theta EEG activity correlates negatively with the default mode network in resting state. *Int. J. Psychophysiol.* 67, 242–251.

Shmuel, A., Augath, M., Oeltermann, A., and Logothetis, N. K. (2006). Negative functional MRI response correlates with decreases in neuronal activity in monkey visual area V1. *Nat. Neurosci.* 9, 569–577.

Shulman, G. L., Astafiev, S. V., McAvoy, M. P., d'Avossa, G., and Corbetta, M. (2007). Right TPJ deactivation during visual search: functional significance and support for a filter hypothesis. *Cereb. Cortex* 17, 2625–2633.

Tecchio, F., Zappasodi, F., Porcaro, C., Barbati, G., Assenza, G., Salustri, C., and Rossini, P. M. (2008). High-gamma band activity of primary hand cortical areas: a sensorimotor feedback efficiency index. *Neuroimage* 40, 256–264.

Trujillo, L. T., Peterson, M. A., Kaszniak, A. W., and Allen, J. J. (2005). EEG phase synchrony differences across visual perception conditions may depend on recording and analysis methods. *Clin. Neurophysiol.* 116, 172–189.

Uddin, L. Q., Kelly, A. M., Biswal, B. B., Xavier Castellanos, F., and Milham, M. P. (2009). Functional connectivity of default mode network components: correlation, anticorrelation, and causality. *Hum. Brain Mapp.* 30, 625–637.

Van Der Werf, J., Jensen, O., Fries, P., and Medendorp, W. P. (2010). Neuronal synchronization in human posterior parietal cortex during reach planning. *J. Neurosci.* 30, 1402–1412.

Vanhatalo, S., Palva, J. M., Holmes, M. D., Miller, J. W., and Voipio, J, Kaila, K. (2004). Infraslow oscillations modulate excitability and interictal epileptic activity in the human cortex during sleep. *Proc. Natl. Acad. Sci. U.S.A.* 101, 5053–5057.

Vincent, J. L., Patel, G. H., Fox, M. D., Snyder, A. Z., Baker, J. T., Van Essen, D. C., Zempel, J. M., Snyder, L. H., Corbetta, M., and Raichle, M. E. (2007). Intrinsic functional architecture in the anaesthetized monkey brain. *Nature* 447, 83–86.

Waldert, S., Preissl, H., Demandt, E., Braun, C., Birbaumer, N., Aertsen, A., and Mehring, C. (2008). Hand movement direction decoded from MEG and EEG. *J. Neurosci.* 28, 1000–1008.

Weissman, D. H., Roberts, K. C., Visscher, K. M., and Woldorff, M. G. (2006). The neural bases of momentary lapses in attention. *Nat. Neurosci.* 9, 971–978.

Whittingstall, K., and Logothetis, N. K. (2009). Frequency-band coupling in surface EEG reflects spiking activity in monkey visual cortex. *Neuron* 64, 281–289.

Yuval-Greenberg, S., Tomer, O., Keren, A. S., Nelken, I., and Deouell, L. Y. (2008). Transient induced gamma-band response in EEG as a manifestation of miniature saccades. *Neuron* 58, 429–441.

Zumer, J. M., Brookes, M. J., Stevenson, C. M., Francis, S. T., and Morris, P. G. (2010). Relating BOLD fMRI and neural oscillations through convolution and optimal linear weighting. *Neuroimage* 49, 1479–1489.

Conflict of Interest Statement: The authors declare that the research was conducted in the absence of any commercial or financial relationships that could be construed as a potential conflict of interest.

Received: 09 February 2010; paper pending published: 28 March 2010; accepted: 04 June 2010; published online: 28 June 2010.
Citation: Jerbi K, Vidal JR, Ossandon T, Dalal SS, Jung J, Hoffmann D, Minotti L, Bertrand O, Kahane P and Lachaux J-P (2010) Exploring the electrophysiological correlates of the default-mode network with intracerebral EEG. Front. Syst. Neurosci. 4:27. doi: 10.3389/fnsys.2010.00027